

*The Design, Development and Characterisation of a new  
Biosensor for In-vivo Neurochemical Monitoring of D-Serine*

A Thesis submitted by

**Kenneth W. Pierce, B.Sc. (Honours)**

To the

*National University of Ireland Maynooth*



for the degree of

**Doctor of Philosophy**

**October 2012**

*Based on research carried out in the Department of Chemistry, N.U.I. Maynooth*

*Under the supervision of Prof. John P. Lowry (N.U.I.M.)  
and Dr. Mark Tricklebank (Eli Lilly)*

## *Declaration*

I hereby declare that this thesis has not been submitted as an exercise for a degree at this or any other university and that it is entirely my own work.

I agree that the Library may lend or copy this thesis upon request.

Signed

---

## *Abstract*

The desire to monitor important neurotransmitters in the *in vivo* environment, in real-time and in conscious subjects has been the driving force behind the continued development over the last 40 years of a range of biosensor devices. This is a none too difficult task considering the milieu of substances that are present *in vivo*, particularly in the brain where there also exists a wide range of electroactive species, and where foreign objects are treated as hostile and subject to severe biological strain. Nevertheless, the rewards for developing a selective and sensitive biosensor are worth the effort. Today they are used, have been used and will increasingly be used for extremely important medical processes, including developing an understanding of disease etiology, determination of key intercession points in these pathologies, preclinical and clinical testing of proposed new treatments, and earlier diagnosis of medical conditions. With this in mind this thesis focused on the development and characterisation of a D-serine biosensor based around the flavin enzyme D-amino acid oxidase. In the recent past D-serine has been elevated from an “unnatural” amino acid to be recognised as a very important neurotransmitter that could be responsible for the regulation of a large portion of glutamate signalling in the forebrain. It has been highly implicated in a number a severe and widely occurring neurodegenerative diseases, ranging from schizophrenia to amyotrophic lateral sclerosis.

Initial groundwork and development of a biosensor was underway when this thesis began. Extensive investigation and characterisation of this sensor, conducted at the start of this thesis, found that the biosensor displayed satisfactory sensitivity and selectivity properties. However, for the purposes of this project, to develop a biosensor suitable for chronic *in vivo* monitoring of D-serine, it was deemed unfit. This was due to an uneconomical and difficult to reproduce production methodology. Thus, from a solid starting point, from which much useful information had been gleamed, an entirely new biosensor was designed with the underlining principal of reproducibility and economic viability added to the need for sensitivity and selectivity. The final design involved the use of the cross-linking agent glutaraldehyde in conjunction with methyl methacrylate to immobilise the D-amino acid oxidase on to the surface of the electrode. To achieve effective interference rejection the dual use of Nafion<sup>®</sup> followed by an electropolymerised layer of poly-*o*-phenylenediamine was utilised. The electrode surface was a 125 µm Pt/Ir wire that was 0.5 mm in length.

The design achieved a sensitivity of  $16.47 \pm 0.18 \mu\text{A}\cdot\text{cm}^{-2}\cdot\text{mM}^{-1}$ . It was found that the response was oxygen independent up to  $100 \mu\text{M}$  D-serine. The limit of detection was determined to be  $0.425 \pm 0.005 \mu\text{M}$  and the biosensor has a response time of  $5.95 \pm 0.75$  s. In the *in vivo* environment it was demonstrated that the biosensor could detect both increases and decreases in the endogenous concentration of D-serine, particularly in response to typical and traditional N-methyl-D-aspartate receptor antagonists like MK-801.

Our device will make it possible to monitor, *in vivo* in real-time and without interference, the concentration of, and changes that occur in D-serine in a conscious subject. This could have a major impact on medical processes, both normal and pathological, whereby the metabolism of D-serine is of interest, including the development and testing of potential new drugs.

## ***Acknowledgements***

*To begin with I must thank my supervisor, Professor John Lowry, for offering me the amazing opportunity to embark on this voyage. For your guidance, help, advice, and patience over the last five years, you have been there whenever I needed you, but equally as important have been all the laughs and friendships, the nights out and trips to conferences and the many jokes (usually revolving around my hair, or lack thereof!). You have been a wonderful supervisor and have made the experience a great and happy one.*

*To the staff of the Chemistry Department in N.U.I.M., from top to bottom you have made all gone out of your way to make this as pain-free a time as possible. Thanks to Noel, for the supplies for the lab and elsewhere, and in particular for constructing and helping me to construct all the equipment I have needed over the last six and half years, you have been invaluable. Thanks to all the technical, academic and executive staff who have always been there to offer a helping hand. Thanks is also due to Dr. Mark Tricklebank and Eli Lilly & Company, Science Foundation Ireland and the Centre of Applied Science under PRTL Cycle 4, for supporting and funding this project.*

*To those I have shared a lab with over the last five years, you have all been a joy to work with and your contribution in this endeavour cannot be underestimated. Firstly, to Dr's Bolger and Finnerty (Messers Fi and Finno), I most certainly would not have found the light at the end of the tunnel without both of you. Your advice, knowledge, experience, guidance and timely kicks in the derrière have been invaluable and I want to thank you both most sincerely. To Rachel and Saidhbhe, my almost partners in crime, and my first "students", I think you have taught me more than I taught you, thank you for everything, the highs and lows, the laughs and the tears, it wouldn't have been the same without you (Dublin hasn't been the same since we showed them "our legs Pat"!).*Benji, I wouldn't have made it through without you. Emma, thank you for the guidance and constant cheer during my first few months lost in the wilderness, you're next and don't let it go. I would also like to thank Colin and Stephen who began with me in the lab. Jack, you've been puntastic, a level head and source of constant hilarity and stimulating discussion, thank you. Keeley and Andrea (Andy), the newbies (not), and Michele, the real newbie, I hope I haven't frightened you too much and I know anytime I did you put me back in my box, you added new levels of craic to my experience, thank

*you. And to all the fourth years and summer students who have contributed to the lab and the fun times, thanks.*

*Now to the other students in the department who have been part of this enjoyable experience. To Niamh and Paul who started with me down this path 5 years ago, (what did we get ourselves into?) thanks for all the chats and venting! Theresa (my lab mother, still minding me 6 years later!), Robert, Tammy, Martin, Maryanne, Owen, Ciarán and Paddy, all long since gone now, but who made a lasting and very important impression, thank you all for your wisdom and the 11 o'clock tea break crosswords. Thank you to all those, past and present, too many to mention, who have been in the department with me, you are all part of this endeavour, in particular for the sanctity of the tea room! To those who were involved in the sports orientated venting, be it football, hockey, tag rugby or rounders, thanks (especially Johnny C for our combined impromptu evacuation of the canteen!).*

*Thanks to all of those who have nothing to do with chemistry, you have been vital in maintaining my sanity (or insanity) throughout this time. To Finbarr, for the chats, timeouts, and unconditional friendship, thank you. The Friday footballers, so many of you over the years who have brought a focal point to every week regardless of how it was going in the lab, thank you. All the friends I have made in the amateur and professional world of musical theatre and opera, thank you for the much needed, though sometimes too distracting, distraction! And to the Rockits, for bringing untold quantities of happiness usually right when I need it, in particular Eamo.*

*To Rachel, I can't put it into words except to say thank you, your belief and encouragement and love has been a huge part of me and this project. Lucy, Jimmy and Carol, your encouragement has been wonderful, thank you.*

*Lastly, and most importantly, I must thank my family. David and Catherine, for always reminding me there are other things than college! Mam and Dad, I love you both, and this would not have been possible without you*

---

*Kenneth W. Pierce*

*To Mam and Dad,*

*Thank you for your unwavering love and support,*

*And affording me every opportunity that anyone could ask for.*

***“For small beings such as we, the vastness is only bearable through love”***

*Carl Sagan*

***“Try not to become a man of success, but rather try to become a man of value”***

*Albert Einstein*

## TABLE OF CONTENTS

<b>1.</b>	<b>INTRODUCTION.....</b>	<b>1</b>
1.1	Introduction .....	2
1.2	<i>In Vivo</i> Neurochemical Analysis.....	4
1.3	IVV Biosensors .....	7
1.4	D-Serine in the Brain .....	9
1.4.1	Serine Racemase and the Metabolism of D-serine.....	11
1.4.2	The Relevance of D-serine to Schizophrenia.....	14
1.4.3	D-Serine in Relation to other Disease States .....	15
1.5	D-Amino Acid Oxidase .....	16
1.6	Existing Work.....	18
1.7	Thesis Overview.....	18
<b>2.</b>	<b>THEORY .....</b>	<b>42</b>
2.1	Introduction .....	43
2.2	Charge Distribution at the Active Surface.....	44
2.3	Mass Transport.....	45
2.3.1	Diffusion .....	46
2.4	Amperometry.....	49
2.5	Cyclic Voltammetry .....	50
2.6	Microdialysis.....	52
2.7	Enzymes.....	54
2.7.1	Introduction .....	54
2.7.2	Enzyme Kinetics .....	55
2.8	Structures and Reactions.....	59
2.8.1	D-Serine .....	59
2.8.2	Flavin Adenine Dinucleotide .....	59
2.8.3	Hydrogen Peroxide.....	60
2.8.4	Electropolymerisation of <i>o</i> -Phenylenediamine .....	61
2.8.5	Ascorbic Acid.....	63
2.9	Data Analysis .....	64
2.9.1	Linear and Non-Linear Regression .....	65
2.9.2	Statistical Analysis .....	65

2.9.2.1	t-Tests .....	65
2.9.2.2	P-values .....	65
2.9.2.3	R <sup>2</sup> values.....	66
2.9.2.4	One-Way ANOVA .....	66
2.9.3	Current Density .....	66
2.9.4	Linear Region Slope.....	67
<b>3.</b>	<b>EXPERIMENTAL .....</b>	<b>72</b>
<b>3.1</b>	<b>Chemicals .....</b>	<b>73</b>
3.1.1	Enzymes .....	73
3.1.2	Interferent Species.....	73
3.1.3	Amino-Acids .....	73
3.1.4	Electrode Fabrication Chemicals.....	74
3.1.5	<i>In Vitro</i> Chemicals .....	74
3.1.6	<i>In Vivo</i> chemicals .....	74
<b>3.2</b>	<b>Solutions .....</b>	<b>75</b>
3.2.1	Enzyme Solutions.....	75
3.2.2	Electrode Fabrication Solutions .....	76
3.2.3	<i>In Vivo</i> Solutions .....	77
<b>3.3</b>	<b>Computer – Based Instrumentation and Software.....</b>	<b>78</b>
3.3.1	Potentiostat, Data Acquisition Hardware and CPU.....	79
3.3.2	Computer Software .....	79
<b>3.4</b>	<b>Ancillary Equipment.....</b>	<b>80</b>
3.4.1	Cylinder Electrode Spinner .....	80
3.4.2	Other Equipment .....	81
<b>3.5</b>	<b>Electrode Preparation .....</b>	<b>82</b>
3.5.1	<i>In vitro</i> Electrodes .....	82
3.5.1.1	Disc Working Electrodes.....	82
3.5.1.2	Cylinder Working Electrodes .....	82
3.5.2	<i>In vivo</i> Electrodes .....	83
3.5.2.1	Working Electrodes .....	83
3.5.2.2	Auxiliary Electrode .....	83
3.5.2.3	Reference Electrode .....	84
3.5.3	Electropolymerisation of <i>o</i> -PD.....	84
3.5.4	Dipping Procedures .....	84
3.5.5	Structured Naming of Designs .....	85
<b>3.6</b>	<b><i>In Vitro</i> Experimental Cell.....</b>	<b>86</b>
3.6.1	General Calibration Method.....	87

3.6.2	Repeated Calibrations Methodology .....	87
3.6.3	Full-Scope Amino Acid and Electroactive Interferent Calibration Methods .....	88
3.6.4	Oxygen Dependence Calibration Method .....	88
<b>3.7</b>	<b>Surgical Procedures .....</b>	<b>89</b>
3.7.1	Animal Subjects .....	89
3.7.2	Surgery Setup and Equipment.....	89
3.7.3	Surgery Protocol.....	90
3.7.4	Post-Operative Care .....	92
<b>3.8</b>	<b><i>In Vivo</i> Experimental Procedures .....</b>	<b>93</b>
<b>4.</b>	<b>AN INVESTIGATION INTO IMMOBILISATION MATRIX FREE D-SERINE BIOSENSOR DESIGNS.....</b>	<b>96</b>
<b>4.1</b>	<b>Introduction .....</b>	<b>97</b>
<b>4.2</b>	<b>Biosensor Configuration .....</b>	<b>98</b>
<b>4.3</b>	<b>Circumstantial Functioning of the Biosensor .....</b>	<b>99</b>
<b>4.4</b>	<b>Nafion<sup>®</sup> interactions and Effect on Biosensor Sensitivity .....</b>	<b>103</b>
<b>4.5</b>	<b>Contribution of Glutaraldehyde to Biosensor Sensitivity .....</b>	<b>106</b>
<b>4.6</b>	<b>Variations of the Enzyme Solution .....</b>	<b>111</b>
4.6.1	Different Suppliers of DAAO .....	111
4.6.2	Effect of Additives in the Enzyme Solution on Biosensor Sensitivity.....	114
<b>4.7</b>	<b>Combined Alterations to the Biosensor Recipe .....</b>	<b>121</b>
4.7.1	Enzyme Solution pH Changes Combined with GA Changes .....	121
4.7.2	Different Polymer Growth Methods Combined with an Altered GA % and Enzyme Solution Changes .....	123
<b>4.8</b>	<b>Variations to the Biosensor Formulation Based on Previously Designed Biosensors.....</b>	<b>126</b>
4.8.1	Alternative Methods for Primary Binding of DAAO .....	127
4.8.1.1	Duplication of Layering .....	127
4.8.1.2	Use of PEI as a Binding Agent.....	128
4.8.1.3	Binding DAAO using PEI and BSAGA.....	130
4.8.2	Further Alterations Including FAD .....	133
<b>4.9</b>	<b>Conclusions .....</b>	<b>135</b>
<b>5.</b>	<b>AN INVESTIGATION OF BIOSENSOR DESIGNS UTILISING STYRENE AS AN IMMOBILISATION MATRIX.....</b>	<b>140</b>
<b>5.1</b>	<b>Introduction .....</b>	<b>141</b>
<b>5.2</b>	<b>Basic Constructs of a Biosensor .....</b>	<b>142</b>

5.2.1	Adsorption of $\alpha$ AAO.....	142
5.2.2	The Use of GA as a Binding Agent.....	144
5.2.3	Styrene as a Primary Binding Agent.....	147
5.2.4	Water and PBS in the Enzyme Solution.....	150
<b>5.3</b>	<b>A Comprehensive Study of the Binding Properties of GA .....</b>	<b>154</b>
5.3.1	Ten Dips into GA.....	155
5.3.2	Five Dips into GA.....	158
5.3.3	Two Dips into GA.....	160
5.3.4	One Dip into GA.....	162
5.3.5	Discussion of the Trends in GA Alterations .....	164
<b>5.4</b>	<b>A Comprehensive Study of the Binding Properties of BSAGA.....</b>	<b>166</b>
5.4.1	Ten Dips into BSAGA .....	167
5.4.2	Five Dips into BSAGA .....	171
5.4.3	Two Dips into BSAGA .....	173
5.4.4	Conclusions of the GA and BSAGA study .....	175
<b>5.5</b>	<b>An Extensive Study of PEI Included With Styrene.....</b>	<b>179</b>
5.5.1	PEI 1% Included After Styrene .....	179
5.5.2	PEI 0.1% Included After Styrene.....	181
5.5.3	PEI 5% Included After Styrene.....	183
5.5.3.1	PEI 5% Used In Conjunction with PEI 1.0% .....	183
5.5.3.2	PEI 5% Used In Conjunction with PEI 0.1% .....	185
<b>5.6</b>	<b>The Incorporation of FAD into Selected Designs .....</b>	<b>187</b>
5.6.1	FAD Included Before $\alpha$ AAO .....	187
5.6.2	FAD Included After $\alpha$ AAO.....	189
<b>5.7</b>	<b>Conclusion.....</b>	<b>191</b>
<b>6.</b>	<b>CYLINDER ELECTRODES, METHYL METHACRYLATE AS AN IMMOBILISATION MATRIX AND <i>IN VITRO</i> CHARACTERISATION</b>	<b>198</b>
<b>6.1</b>	<b>Introduction .....</b>	<b>199</b>
<b>6.2</b>	<b>Cylinder Electrodes and MMA – Protocol Improvements.....</b>	<b>200</b>
6.2.1	The Use of Electrodes with a Cylindrical Surface .....	200
6.2.2	MMA as an Immobilisation Matrix.....	203
<b>6.3</b>	<b>Further Examination of MMA Based Recipes .....</b>	<b>206</b>
6.3.1	Previous Best Recipes Re-Examined .....	206
6.3.2	Addition of FAD to the GA 1% Recipes.....	208
6.3.3	An Additional Layer of MMA .....	210
<b>6.4</b>	<b>Interference Rejection Strategies.....</b>	<b>212</b>

6.4.1	Hydrogen Peroxide and AA without Interference Rejection Layers.....	213
6.4.2	P- <i>o</i> -PD Grown by CV and CPA.....	214
6.4.3	Naf before CV and CPA Grown P- <i>o</i> PD.....	216
6.4.4	Effects on Electrode Sensitivity of Interferent Layers .....	218
<b>6.5</b>	<b><i>In Vitro</i> Characterisation – Stability.....</b>	<b>220</b>
6.5.1	Repeated Calibration Stability – Short Term .....	221
6.5.2	Repeated Calibration Stability – Long Term .....	223
6.5.3	Long Term Stability – Shelf Life Study.....	226
<b>6.6</b>	<b><i>In Vitro</i> Characterisation – Bio-Compatibility .....</b>	<b>227</b>
6.6.1	BSA 1% Treatment .....	228
6.6.2	BSA 10% Treatment .....	230
6.6.3	PEA 1% Treatment.....	233
6.6.4	PEA 10% Treatment.....	235
6.6.5	Brain Tissue Treatment .....	237
<b>6.7</b>	<b><i>In Vitro</i> Characterisation – pH and Temperature Effects.....</b>	<b>240</b>
6.7.1	pH Changes .....	240
6.7.2	Temperature Changes.....	242
<b>6.8</b>	<b><i>In Vitro</i> Characterisation – Interference Studies .....</b>	<b>244</b>
6.8.1	Amino-Acids and Glycine.....	244
6.8.2	D-Alanine.....	246
6.8.3	Native Electroactive Species .....	248
<b>6.9</b>	<b><i>In Vitro</i> Characterisation – Oxygen Dependency Studies.....</b>	<b>251</b>
6.9.1	Oxygen Dependence at 10 $\mu$ M D-serine.....	251
6.9.2	Oxygen Dependence at 20 $\mu$ M D-serine.....	254
6.9.3	Oxygen Dependence at 50 $\mu$ M D-serine.....	256
6.9.4	Oxygen Dependence at 100 $\mu$ M D-serine.....	257
<b>6.10</b>	<b><i>In Vitro</i> Characterisation – Other Parameters .....</b>	<b>259</b>
6.10.1	Limit of Detection .....	259
6.10.2	Response Time .....	260
<b>6.11</b>	<b>Conclusions .....</b>	<b>262</b>
<b>7.</b>	<b>A PRELIMINARY <i>IN VIVO</i> STUDY OF THE BIOSENSOR FUNCTIONALITY.....</b>	<b>271</b>
<b>7.1</b>	<b>Introduction .....</b>	<b>272</b>
<b>7.2</b>	<b>aCSF Perfusion.....</b>	<b>273</b>
<b>7.3</b>	<b>Serine Perfusions .....</b>	<b>274</b>

7.3.1	D-serine perfusions .....	274
7.3.1.1	10 $\mu$ M D-serine .....	274
7.3.1.2	20 $\mu$ M D-serine .....	275
7.3.1.3	100 $\mu$ M D-serine .....	276
7.3.1.4	1000 $\mu$ M D-serine .....	277
7.3.1.5	D-serine Perfusions Conclusions.....	278
7.3.2	L-serine perfusion .....	279
<b>7.4</b>	<b>Veratridine Perfusion.....</b>	<b>280</b>
<b>7.5</b>	<b>Mg.ATP Perfusion.....</b>	<b>282</b>
<b>7.6</b>	<b>EDTA Perfusions.....</b>	<b>287</b>
<b>7.7</b>	<b>NO Perfusion.....</b>	<b>289</b>
<b>7.8</b>	<b>L-NAME Perfusion.....</b>	<b>291</b>
<b>7.9</b>	<b>AA Perfusion.....</b>	<b>292</b>
<b>7.10</b>	<b>Saline Injection .....</b>	<b>294</b>
<b>7.11</b>	<b>MK-801 Injection .....</b>	<b>294</b>
<b>7.12</b>	<b>Conclusions .....</b>	<b>297</b>
<b>8.</b>	<b>GENERAL CONCLUSIONS .....</b>	<b>304</b>
<b>8.1</b>	<b>General Conclusions.....</b>	<b>305</b>
<b>8.2</b>	<b>Publications, Conferences and Funding Acknowledgements.....</b>	<b>309</b>
8.2.1	Publications .....	309
8.2.2	Conferences Attended .....	310
8.2.3	Awards .....	310
8.2.4	Funding Acknowledgements.....	310
8.2.5	In Preparation .....	310
<b>9.</b>	<b>APPENDIX 1: MEAN AND SEM DATA FOR CHAPTER 4.....</b>	<b>311</b>
<b>10.</b>	<b>APPENDIX 2: MEAN AND SEM DATA FOR CHAPTER 5.....</b>	<b>320</b>
<b>11.</b>	<b>APPENDIX 3: MEAN AND SEM DATA FOR CHAPTER 6.....</b>	<b>334</b>

## *List of Abbreviations*

5-Hydroxyindole 3-Acetic Acid	5-HIAA
5-Hydroxytyptamine	5-HT
Ascorbic Acid	AA
Artificial Cerebro-Spinal Fluid	aCSF
Alzheimer's Disease	AD
Adenine diphosphate	ADP
Alanine	Ala
Amyotrophic Lateral Sclerosis	ALS
Adenine Monophosphate	AMP
2-Amino-3-(3-hydroxy-5-methyl-isoxazol-4-yl)propanoic Acid	AMPA
One-Way Analysis of Variance	ANOVA
Anterior-Posterior	A-P
Arginine	Arg
Alanine-Serine-Cysteine Transporter	ASCT2
Amino Acid Transporter 1	ASC1
Aspartic Acid	Asp
Adenosine Triphosphate	ATP
Adenosine 5'-Triphosphate Magnesium Salt	Mg.ATP
Blood-Oxygen-Level-Dependant	BOLD
Bovine Serum Albumin	BSA
Bovine Serum Albumin & Glutaraldehyde solution	BSAGA
Calibration	Cal
Constant Potential Amperometry	CPA
Computed Tomography	CT
Cyclic Voltammetry	CV
Cysteine	Cys
Dopamine	DA
D-Amino Acid Oxidase	dAAO
Dehydroascorbic Acid	DHAA
3,4-dihydroxyphenyl-acetic Acid	DOPAC
Dorsal-Ventral	D-V
Extracellular Fluid	ECF
Ethylenediaminetetraacetic Acid	EDTA
Electroencephalography	EEG
Electromotive Force	e.m.f.
Flavin Adenine Dinucleotide	FAD
Flavin Adenine Dinucleotide	FADH <sub>2</sub>
Foreign Body Response	FBR
Fast Cyclic Voltammetry	FCV
Glutaraldehyde	GA
Glutamic acid	Glu
Glutathione	Gluta
Glycine	Gly
Hydrogen Peroxide	H <sub>2</sub> O <sub>2</sub>
Histidine	His
High Performance Liquid Chromatography	HPLC
Homovanillic Acid	HVA
Intraperitoneal	i.p.
<i>In Vivo</i> Voltammetry	IVV

Current Density	J
Maximum Current Density	$J_{\max}$
Potassium Chloride	KCl
Michaelis Constant	$K_M$
<i>N</i> - $\omega$ -nitro-L-argininemethylester hydrochloride	L-NAME
Linear Region Slope	LRS
Long-Term Depression	LTD
Long-Term Potentiation	LTP
Lysine	Lys
Magnetoencephalography	MEG
Medial-Lateral	M-L
Michaelis-Menten	MM
Methyl methacrylate	MMA
Michaelis-Menten Hill	MMH
Magnetic Resonance Imaging	MRI
Nafion <sup>®</sup>	Naf
<i>N</i> -methyl-D-aspartate	NMDA
<i>N</i> -methyl-D-aspartate Receptor	NMDAr
Nuclear Magnetic Resonance	NMR
Nitrogen	$N_2$
Nitric Oxide	NO
Oxygen	$O_2$
Phosphate Buffered Solution	PBS
Parkinson's Disease	PD
3-sn-Phosphatidylethanolamine	PEA
Polyethyleneimine	PEI
Positron-emission-tomography	PET
Phenylalanine	Phe
Protein Interacting c-Kinase 1	PICK1
Phosphatidylinositol-(4,5)-biphosphate	PIP2
Poly- <i>o</i> -phenylenediamine	P- <i>o</i> -PD
Poly- <i>o</i> -phenylenediamine Grown by CPA	PPD
Poly- <i>o</i> -phenylenediamine Grown by CV	PPD <sub>CV</sub>
Proline	Pro
Platinum	Pt
Platinum Cylinder Electrode	Pt <sub>C</sub>
Platinum Disk Electrode	Pt <sub>D</sub>
Platinum/Iridium	Pt/Ir
Subcutaneous	s.c.
Saturated Calomel Electrode	SCE
Standard Deviation	SD
Standard Error of Mean	SEM
Serine	Ser
Single-photon-emission-computed-tomography	SPECT
Serine Racemase	SR
Styrene	Sty
Tetracyanoquinodimethane	TCNQ
Tryptophan	Trp
Tetrathiafulvalene	TTF
Tyrosine	Tyr
Uric Acid	UA
Ultra-violet Visible Spectroscopy	UV-Vis

Voltage  
Maximum Voltage

$V$   
 $V_{\max}$

---

---

# **1. INTRODUCTION**

---

---

## 1.1 Introduction

The primary aim of this thesis is the development of a sensor that can detect, with appropriate sensitivity and selectivity, the excitatory amino-acid D-serine, which is both a neurotransmitter and a gliotransmitter, in a physiological environment. It is hoped that such a device will be an invaluable tool to help bring some clarity to the major discussions ongoing at present in the field of neuroscience about the role of D-serine in some of the major degenerative diseases that are increasingly afflicting the human race.

It is only in the last 20 years that D-serine (D-ser) has become interesting to the neuroscience community. This occurred as evidence mounted that it could act as a coagonist, with glutamate, at the “glycine”-site of an *N*-methyl-D-aspartate receptor (NMDAr) (Fadda *et al.*, 1988; Wood *et al.*, 1989). Since then a large body of evidence has grown to suggest that many important neuromodulatory processes are controlled by the presence of D-ser and not glycine. Indeed, had these discoveries been made 10 or 20 years earlier the glycine-site would possibly be named the D-serine-site.

The human brain, while only responsible for 2% of body weight, consumes 20% of oxygen and 25% of glucose used overall in the body. It is larger, when compared to body weight, than that of any other mammal. The brain is comprised of two different types of matter, grey and white, and two types of cells, neurons and glial cells. Neurons are the cells that conduct signalling and are the main working units, numbering  $\sim 10^{11}$  in a human brain. The neurons could not function without the glial cells which insulate, physically support, provide nutrition and oxygen, destroy pathogens, and remove dead neurons. In other words the glial cells maintain homeostasis for the neurons. Both of these cells form the grey matter of the brain. White matter consists of the dendrites and axons which connect the neurons to each other. A schematic diagram of neuron is shown in Figure 1-1:

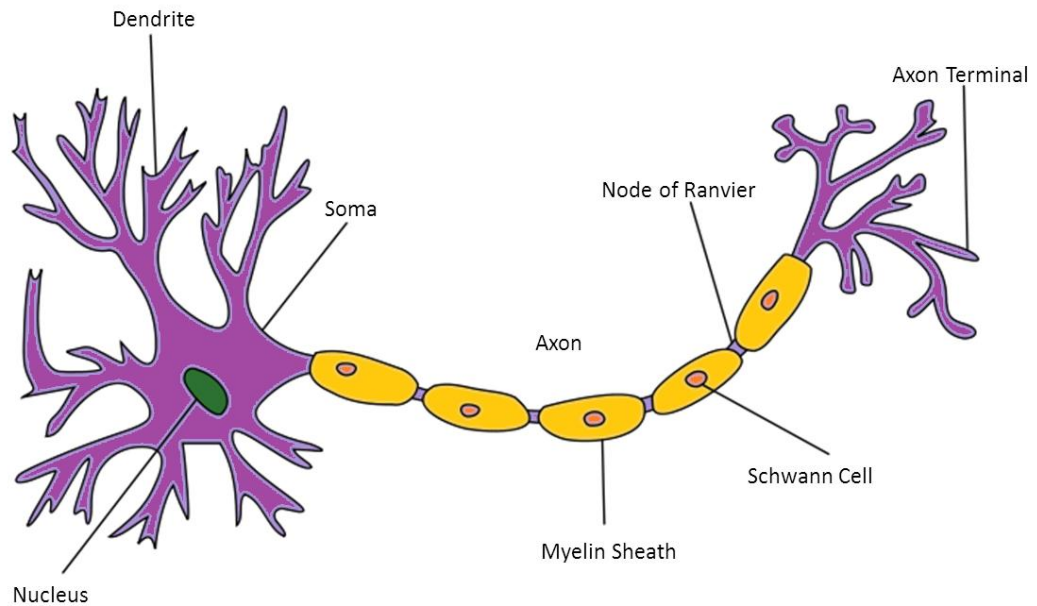


**Figure 1-1**

**A neuron.**

The release of neurotransmitters at a synapse is triggered by an action potential. This action potential is created when an initial stimulus causes an electrical impulse, consisting of  $K^+$  or  $Na^+$ , to form. This impulse travels down the axon of a neuron to the dendrites at the axon terminal where neurotransmitters are released from the pre-synaptic neurons. The neurotransmitters diffuse across the synaptic cleft where they stimulate action from either surrounding astrocytes or a post-synaptic neuron. This stimulation can lead to the creation of an action potential in the post-synaptic neuron or be inhibitory and prevent any further signal transmission.

The largest component of the brain is the cerebrum, or the telencephalon. Together with the diencephalon it forms the forebrain or prosencephalon. The midbrain (mesencephalon) and hindbrain (rhombencephalon) form the brain stem. The cerebrum is divided into four areas; frontal lobe, parietal lobe, temporal lobe and occipital lobe. It is these areas which have evolved massively over time to be responsible for the many higher order functions that distinguish humans from other mammals.

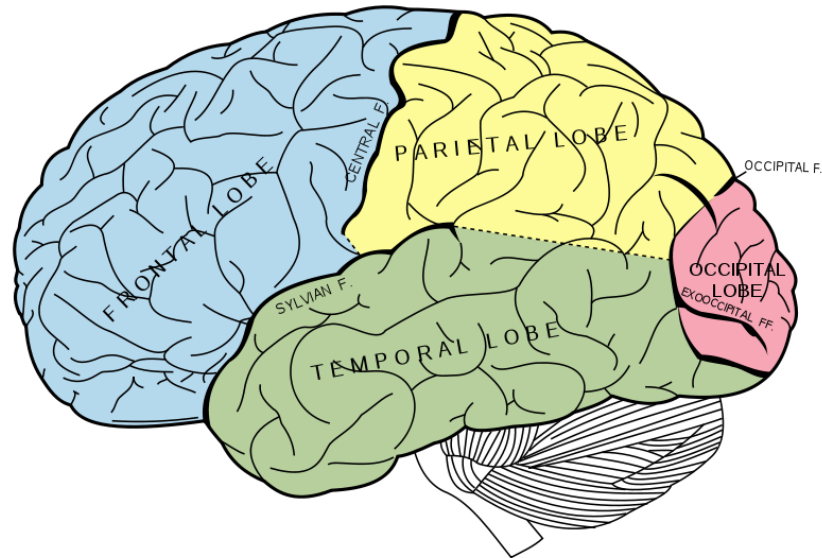


**Figure 1-2**  
The lobes of the cerebrum.

The cerebral cortex is the general term for all of the grey matter of the cerebrum. Underneath the grey matter exists the white matter and basal ganglia. It is in the basal ganglia that the striatum is found (see Section 7.1). With glutamate being an excitatory neurotransmitter at over 90% of synapses in grey matter, and the NMDA the most dominant device for controlling synaptic plasticity and memory, the study of a coagonist of glutamate, which not only has a greater affinity than glycine for the glycine site, but also increases the affinity of the glutamate site towards glutamate (Fuchs *et al.*, 2011), is vitally important to better understand the functioning of the signalling processes taking place at synapses.

## 1.2 *In Vivo* Neurochemical Analysis

As it became clear that the brain could not be treated as a uniform unit, with different processes occurring in different areas, different localisations of cells and specific areas being responsible for different tasks, methodologies for analysing neurochemicals *in vivo* evolved to allow determination and closer examination of these features. This has led to the development of a wide range of techniques.

Electroencephalography (EEG) measures, using a series of electrodes placed on the outside of the scalp, the voltage changes that occur in the cerebral cortex due to activity or ion flow. It measures the summation of the synchronous activity of millions of neurons at any one point, and while it has poor spatial resolution it has good temporal

resolution. Magnetoencephalography (MEG) works in much the same way as EEG but it monitors the changing magnetic flux created in the brain by the flow of ions. While it has similar temporal resolution as EEG, MEG has a superior spatial resolution. It has the disadvantage however of only being able to monitor the fields produced by dendrites that are orientated in a certain way due to technological limitations.

Techniques that measure the three-dimensional changes in blood flow began with single-photon emission computed tomography (SPECT) and positron emission tomography (PET). Both techniques require the injection of a radionuclide containing substance into the bloodstream. X-ray computed tomography (CT) can also involve the use of a contrast agent but it is not necessary. All three of these techniques provide good spatial resolution but very poor temporal resolution. An important technological advance came with the advent of 3-D magnetic resonance imaging (MRI), which utilises the principals of NMR (nuclear magnetic resonance). Unlike CT it does not use ionising radiation and provides better resolution than the previously mentioned techniques, especially in relation to slight variation in tissue types. Contrast agents can be used in MRI to further enhance its identification of features. The most recent advancement in this technology has been the advent of functional magnetic resonance imaging, fMRI. This is a very important technique developed to elucidate functional variations in the brain. It utilises blood-oxygen-level-dependant (BOLD) contrast to determine the difference between arterial and venous blood, and hence map activity. It is by far the most widely used brain imaging technique as it does not require injection of radiomarkers or contrast agents or involve exposure to radiation.

Alongside the development of these non-invasive techniques has also been the development of two very important surgically invasive techniques – microdialysis and *in vivo* voltammetry (IVV). With a lot of the processes that are interesting to neuroscientists occurring in the synaptic cleft these two methods allow sampling of chemicals in the extracellular fluid (ECF) of the brain (microdialysis) or real-time monitoring of the concentration of particular analytes (IVV). Recently, certain IVV techniques have even been likened to, or developed to be analogous to fMRI, an important advance which increases the variety of experiments (*i.e.* behavioural and freely moving) that can be conducted as bulky machinery and anaesthetics (for rodent work) are not required (Lowry *et al.*, 2010).

Microdialysis is a technique whereby a probe with a semi-permeable membrane is surgically implanted into a region of interest. The membrane allows the diffusion of molecules, small enough to pass through the pores, from the ECF into the fluid being pumped through the probe (called the perfusate when it is pumped into the probe and dialysate when it is collected) or the diffusion of molecules from the perfusate into the brain, a targeted method of delivery known as retrodialysis. Substances collected in the dialysate can then be analysed post-collection and quantisation of a large variety of substances is possible by high-performance liquid chromatography and mass spectrometry. A full discussion of the microdialysis method can be found in Section 2.6.

First demonstrated as a feasible method of monitoring oxygen and ascorbic acid by Clark (Clark *et al.*, 1953; Clark *et al.*, 1958; Clark & Lyons, 1965) IVV, as it is currently understood, did not become a mainstream neuroanalytical technique until 1973 when pioneering work by Adams *et al.* established modern methodologies for its use (Kissinger *et al.*, 1973). This is despite the fact that Clark demonstrated its efficacy during surgical procedures (Clark & Lyons, 1962), and indeed a lot of modern sensors are based on the platinum electrode that Clark first described. The general principle behind IVV is the application of a suitable potential, or potential profile, to an electrode and the monitoring of the current produced as species of interest are reduced or oxidised on the surface of the transducer. Potentials applied can vary greatly; fixed pulse amplitude and time intervals of chronoamperometry, continually changing the applied voltage which is swept between two voltages (linear sweep voltammetry), away from and back to the starting voltage at a slow (cyclic voltammetry) or fast scan rate (e.g. fast cyclic voltammetry, FCV). Voltages can be stepped between two points by fixed amounts at fixed intervals (staircase voltammetry), and techniques can be combined, like differential pulse voltammetry which is a combination of chronoamperometry and the sweep technique, or double pulse amperometry which is like chronoamperometry also but with two voltages used in each pulse. There is also constant potential amperometry (CPA) where the voltage is held constant at a level which causes continual reaction. Amperometry is a subset of IVV techniques.

Sensors have been developed which when used with IVV are capable of detecting a myriad of different, interesting substances found in the ECF. These include ascorbic acid (AA) (O'Neill *et al.*, 1984; Hasebe *et al.*, 1998), oxygen (Bolger & Lowry, 2005; Bazzu *et al.*, 2009; Bolger *et al.*, 2011), nitric oxide (Bedioui *et al.*, 1997; Chang *et al.*,

2005; Brown *et al.*, 2009), dopamine and/or serotonin and/or homovanillic acid (O'Neill *et al.*, 1982; Forni & Nieoullon, 1984; Crespi *et al.*, 1989; Rice *et al.*, 1994; Kulagina *et al.*, 2001; Al Mulla *et al.*, 2009), noradrenaline, uric acid (O'Neill & Lowry, 1995), and many others (O'Neill, 1994). However, all of these substances are electroactive at various potentials. Thus, the difficult part in producing a selective sensor is developing a technique which blocks or selectively removes the other electroactive species by the addition of choice thin films and choice of a potential profile. What happens though when it is a non-electroactive substance, like an amino-acid neurotransmitter, that is the target molecule for detection by electrochemical methods?

### 1.3 IVV Biosensors

When the target molecule of interest for a sensor is not electroactive, it becomes necessary to include a substance which produces an electroactive species or a current in response to the presence of this non-electroactive species. This sensor is then known as a biosensor, as the recognition element takes the form of a biomolecule. This biorecognition element can have many forms – enzyme, tissue, organelle, microbes and antibodies – and be mounted on a multitude of transducers (O'Neill *et al.*, 1998; Cooper & Cass, 2004). Clark and Lyons were again pioneers in the field of biosensors, utilising glucose oxidase to detect glucose in the first reported fabrication and utilisation of a biosensor (Clark & Lyons, 1962). Subsequently, biosensors have been designed for glutamate (Belay *et al.*, 1999; Karyakin *et al.*, 2000; Burmeister & Gerhardt, 2001; McMahon *et al.*, 2006; Pauliukaite *et al.*, 2006; Qin *et al.*, 2008; Tian *et al.*, 2009), glucose (Boutelle *et al.*, 1986; Lowry *et al.*, 1994; Karyakin *et al.*, 1995; Hu & Wilson, 1997a; Lowry *et al.*, 1998; Garjonyte & Malinauskas, 1999), lactate (Hu & Wilson, 1997b; de Keijzer *et al.*, 1999; Yang *et al.*, 1999), choline and/or acetylcholine (Kano *et al.*, 1994; Garguilo & Michael, 1995b; Tsafack *et al.*, 2000; Burmeister *et al.*, 2008), aspartate (Haughton, pending publication), hydrogen peroxide (Kulagina & Michael, 2003; O'Brien *et al.*, 2007), pyruvate and ascorbate (Fernandes *et al.*, 1999; Chauhan *et al.*, 2011).

Two important components of a biosensor are the biological element which responds to the desired substrate and how this recognition event is converted into a current in the transducer. The bio-recognition element can be bound by a number of processes including physical adsorption, cross-linking, entrapment in or under a membrane,

covalent bonding, or a combination of these processes (O'Neill *et al.*, 1998). However, it is the method of transferring the information of the biological event occurring to the surface of the transducer that has led to the general classification system for voltammetric biosensors. First generation biosensors are of the type first developed by Clark in the 50's and 60's. They monitor substrate concentration by observing the consumption of O<sub>2</sub> or the production of H<sub>2</sub>O<sub>2</sub> (Clark & Lyons, 1962; Updike & Hicks, 1967). This is achieved by the use of a large over-current in the case of H<sub>2</sub>O<sub>2</sub>, which creates interference from species such as ascorbic acid (AA), or a negative potential for O<sub>2</sub>. A constant drawback for first generation biosensors is that they suffer from variable oxygen tension *in vivo* (see Section 6.9), yet they remain the most common type. Second generation biosensors utilise a mediator as an electron transfer agent. This removes the need for a large current to successfully operate the biosensor, and removes oxygen from the reaction mechanism. A problem is created however in that a lot of mediators are highly toxic and have the potential of leeching from the surface (Gründig & Krabisch, 1989) and causing unknown quantities of damage in the *in vivo* environment (Beh *et al.*, 1991), as well as reactivity towards organic molecules (Wilson & Turner, 1992). Third generation biosensors are based on the principle of direct electron transfer between the redox site in the enzyme and the transducer, achieved using organic salts such as tetrathiafulvalene (TTF) and tetracyanoquinodimethane (TCNQ) (Albery *et al.*, 1985), although these have been shown to be quasi-second generation in function utilising charged species (e.g. TCNQ<sup>-</sup>) to transfer charge (Centonze *et al.*, 1997). Development of “wired” third generation biosensors, utilising functionalised surfaces with electron transfer arrays (Heller, 1990), remains the most promising in overcoming the problems highlighted. First-generation biosensors are the area of interest to our group and work.

Regardless of the generation of biosensor a constant issue is that of electroactive interference from endogenous molecules. Even in second generation biosensors, with their lower operating potential, this problem is not totally mitigated (Lowry & O'Neill, 1992b) Many methods have been utilised to overcome this issue, which is particularly important in the physiological environment (Wilson & Gifford, 2005). Generally, the methodology involves the deposition of a thin-film of a polymeric substance onto the surface of the transducer which is thick enough to reject interference species from the surface, but also thin enough so as not to hinder the arrival of the H<sub>2</sub>O<sub>2</sub> or O<sub>2</sub> molecule, in the case of first generation biosensors, at the reactive surface. The use of Nafion<sup>®</sup>

(which also repels species by electrostatic interaction) and poly-amines are quite common in this regard (Kunimura *et al.*, 1988; Malitesta *et al.*, 1990; Lowry & O'Neill, 1992a; Lowry *et al.*, 1994; Garguilo & Michael, 1995a; Friedemann *et al.*, 1996; Jezkova *et al.*, 1997; Malinauskas *et al.*, 1998; Brown & Lowry, 2003; Craig & O'Neill, 2003; Dai *et al.*, 2006; Kirwan *et al.*, 2007; McMahon *et al.*, 2007; Brown *et al.*, 2009; Rothwell *et al.*, 2009; Rothwell *et al.*, 2010; Bilal *et al.*, 2011), and both are discussed further in this thesis (see Sections 2.8.4, 4.4 and 6.4).

## 1.4 D-Serine in the Brain

Although they were known to be present in bacteria for several decades, D-amino acids have only recently become interesting. The initial discovery of high levels of D-aspartate (D-asp) in both rat and human brains (Dunlop *et al.*, 1986) led to further investigations by other groups. The discovery of unusually high quantities of D-ser (Hashimoto *et al.*, 1992) and D-aspartate (D-asp) (Hashimoto *et al.*, 1993c) has led to a whole new direction in neuroscientific research, with growing implications for several complex disease states.

This interest began due to the discovery that D-ser has an identical or higher affinity for the historical “glycine-site” of the NMDAR (Danysz *et al.*, 1990; Matsui *et al.*, 1995; Priestley *et al.*, 1995). This increased affinity is possibly explained by the ability of D-ser to displace water from the binding pocket of NR1 and form three additional hydrogen bonds in comparison to glycine (Furukawa & Gouaux, 2003). The glycine-site is situated on the NR1 subunit (Johnson & Ascher, 1987), one of four components of the NMDAR. Thus, it was proposed that D-ser is an endogenous ligand of the NMDAR (Hashimoto *et al.*, 1993b), which is released by glutamate to work in the synapse with glutamate (Cull-Candy, 1995). In order to test this hypothesis several groups began to look at the distribution of NMDAR's, D-ser and glycine in the brain. It was discovered that D-ser was found to be most concentrated in astrocytes in the grey matter and white matter (Schell *et al.*, 1995; Schell *et al.*, 1997) with the highest levels found in the forebrain, in the cerebral cortex, the hippocampus and the striatum in particular (Chouinard *et al.*, 1993; Hashimoto *et al.*, 1993b; Hashimoto *et al.*, 1995b). There is no reported difference between concentrations in the grey and white matter (Kumashiro *et al.*, 1995). The concentration decreases as one travels from the telencephalon to the diencephalon, to the midbrain and finally the brain stem and cerebellum in the

hindbrain. More interesting still is the fact that this distribution pattern is almost the exact same as NMDAr's and the opposite of glycine distribution (Schell *et al.*, 1997). Furthermore because of a strong uptake and transporter system the concentration of glycine at the synapse is well below the saturation level and D-ser is up to 100 times more efficient at moderating NMDAr synaptic currents (Berger *et al.*, 1998; Bergeron *et al.*, 1998).

With all of this physical evidence mounting more in-depth studies of the relationship between D-ser and the NMDAr were inevitable, and they added to a growing body of evidence that D-ser is very important in neurotransmission. This includes the discovery of D-ser immunoreactivity in neurons (Yasuda *et al.*, 2001b; Kartvelishvily *et al.*, 2006; Rosenberg *et al.*, 2010), dendrites and axons (Yasuda *et al.*, 2001b) and microglia (Williams *et al.*, 2006). Glutamate released from neurons is found to stimulate AMPA and/or kainite receptors on glial cells and neurons (Ribeiro *et al.*, 2002; Mothet *et al.*, 2005; Kartvelishvily *et al.*, 2006; Martineau *et al.*, 2008), which in turn releases D-ser into the synaptic cleft. Recent reports all appear to favour D-ser as the favoured coagonist and not glycine (Shleper *et al.*, 2005; Panatier *et al.*, 2006; Stevens *et al.*, 2010a) at NMDAr's, with blockade of the glycine GlyT1 transporter leading to full occupancy of binding sites, and blockade of GlyT2 having no effect on NMDAr currents or sensitivity to exogenous D-ser (Stevens *et al.*, 2010a; Stevens *et al.*, 2010b). Locally high concentrations of GlyT1 around NMDAr's thus serves to demonstrate that glycine content is kept low allowing D-ser to regulate the majority of activity.

It has also been shown that glutamate and NMDAr elicited neurotoxicity is regulated by D-ser and not gly (Shleper *et al.*, 2005). Perhaps some of the strongest evidence of this link is provided by a study which shows that selective degradation of D-ser and not gly adversely affects NMDAr mediated neurotransmission (Mothet *et al.*, 2000). A hypothesis has also been offered that both glutamate and D-ser are stored in astrocytic vesicles allowing for the release of a potent NMDAr activating cocktail (Oliet & Mothet, 2009). It has been shown that neuronal D-ser mediates NMDAr activation and controls its extracellular concentration (Rosenberg *et al.*, 2010), and that serine racemase protein and mRNA is higher in neurons than in astrocytes (Takeyama *et al.*, 2006; Yoshikawa *et al.*, 2007). This and other evidence points to different roles for glial and neuronal D-ser (Wolosker, 2007), especially in development as relative concentrations change over time (Hashimoto *et al.*, 1993a; Hashimoto *et al.*, 1993d;

Schell *et al.*, 1997; Koike & Ninomiya, 2000; Wang & Zhu, 2003; Balu & Coyle, 2012).

A general requirement for the classification of a substance is that it must have a transport mechanism. Although two transporters capable of transporting D-ser have been identified, the alanine-serine-cysteine transporter (ASCT2) and a general amino acid transporter (Asc-1) (Helboe *et al.*, 2003; Matsuo *et al.*, 2004; Sikka *et al.*, 2010), no D-ser specific transporter has been identified. A final twist in the complicated, and still not fully understood, pathway has come with the very recent elucidation of differing activation methods for NMDAr's in different locations. It now appears that synaptic NMDAr's are potentiated by D-ser, while extrasynaptic NMDAr's are activated by gly (Papouin *et al.*, 2012).

#### **1.4.1 Serine Racemase and the Metabolism of D-serine**

All of this theorising around the function of D-ser would be purely speculative without a method to synthesise it, an important property for any putative neurotransmitter to possess. For many years it was believed that D-amino acids did not have a synthetic pathway in mammals. The synthesis of D-ser was first reported in 1965 in eukaryotes and 33 years later in silkworms, where serine racemase was found to synthesise D-ser from L-serine (L-ser) (Srinivasan *et al.*, 1965; Uo *et al.*, 1998).

Further developments were to follow rapidly, particularly from Wolosker *et al.* who discovered enriched quantities of serine racemase (SR) in glial cells, and that it is responsible for endogenous D-ser and thus activation of the NMDAr (Wolosker *et al.*, 1999a; Wolosker *et al.*, 1999b; Wolosker *et al.*, 2002; Xia *et al.*, 2004). Combining this information with evidence that L-ser concentration changes affects the levels of D-ser (Dunlop & Neidle, 1997; Takahashi *et al.*, 1997), and the similar to D-ser glial distribution of L-ser and the mechanism to synthesise L-ser (Yamasaki *et al.*, 2001; Yasuda *et al.*, 2001a) provided a strong case for the presentation of D-ser as a neurotransmitter. This information also cleared up the debate on whether gly or L-ser was the precursor for D-ser (Iwama *et al.*, 1997). More recently it has been established that SR is found predominantly in neurons and not glia (Yoshikawa *et al.*, 2007; Miya *et al.*, 2008). With an increasing number of neurotransmitter criteria being fulfilled by D-

ser investigations into the functionality of SR and the metabolism of D-ser were conducted.

Early on it was established that mammalian SR requires the cofactor pyridoxal 5'-phosphate (serine/threonine dehydratases also require this cofactor) and is highly selective for L-ser, it does not racemise any other amino acids (Wolosker *et al.*, 1999b; de Miranda *et al.*, 2000). The fact that SR could also degrade L-ser and D-ser by an  $\alpha,\beta$ -elimination reaction (de Miranda *et al.*, 2002; Foltyn *et al.*, 2005) into pyruvate and water was unexpected but provides a local mechanism for the degradation and control of D-ser levels, and indeed approximately three times more pyruvate is synthesised compared to D-ser under normal conditions. Cofactors for the improved activation of SR were determined to be  $Mg^{2+}$ ,  $Ca^{2+}$  and an Mg.ATP complex, although ADP and AMP work just as well (Cook *et al.*, 2002; de Miranda *et al.*, 2002).

Physiologically SR is found to be regulated in many different ways. Mainly this occurs through two proteins, positively via a glutamate receptor interacting protein GRIP-1 (Kim *et al.*, 2005; Baumgart *et al.*, 2007) and negatively by Golga3 (Dumin *et al.*, 2006). Another protein, the scaffold protein interacting with C-kinase-1 (PICK1) is also implicated in, but not directly responsible for, the activation of SR (Fujii *et al.*, 2006; Hikida *et al.*, 2008). The association of SR with Golga3 has also shown that SR is often bound to intracellular and dendritic membranes, which inactivates it towards D-ser production (Dumin *et al.*, 2006). This mechanism is regulated by phosphatidylinositol-(4,5)-biphosphate (PIP2) and a feedback mechanism initiated by the activation of NMDAr's which is responsible for the translocation of SR (Balan *et al.*, 2009; Mustafa *et al.*, 2009). Phosphorylation of SR in general is also required for effective production of D-ser (Foltyn *et al.*, 2010), and a second feedback mechanism, also instigated by NMDAr activation, via neuronally derived nitric oxide (NO) also inhibits the action of SR. These two feedback mechanisms have lead to the theory that it is actually tight regulation of D-ser levels, the coagonist, which prevents glutamatergic over-potential and neurotoxicity. This complex metabolic pathway is summarised below in Figure 1-3;



### 1.4.2 The Relevance of D-serine to Schizophrenia

Aside from its role in basic neurotransmission processes, D-ser has been a target of much research in relation to schizophrenia. Traditionally there are two hypotheses that describe the pathology of schizophrenia, the GABA/dopaminergic hypofunction theory and the NMDAR/glutamatergic theory (Lisman *et al.*, 2008). The NMDAR model has particular relevance for D-ser, especially when considered in the now evolving context of D-ser being the primary control mechanism of glutamatergic neurotransmission. Affecting approximately 1% of the population worldwide, schizophrenia is a severely debilitating disease with three classes of symptoms; positive, negative and cognitive. Modern medical interventions are not particularly efficacious in treating the negative and cognitive symptoms, illustrating that the diseases etiology is still not particularly well understood. Thus, further investigation and identification of new treatment points is very important.

There is a lot of pathophysiological evidence for the involvement of D-ser in schizophrenia (Javitt, 2012; Labrie *et al.*, 2012). Genetic risk factors for schizophrenia are difficult to identify and there is only a tentative link between the genealogy of D-ser (specifically for SR and DAAO) and schizophrenia. Not disregarding this, NMDAR antagonists produce schizophrenic like symptoms without further deterioration by dopaminergic agonists (Javitt & Zukin, 1991; Krystal *et al.*, 1994; Krystal *et al.*, 2005). A reduced D-ser to total serine ratio has been found when drug naive schizophrenic patients were examined (Hashimoto *et al.*, 2005b; Bendikov *et al.*, 2007), there are reduced levels of D-ser in the serum of patients (Hashimoto *et al.*, 2003; Yamada *et al.*, 2005) and there is a correlation between improved symptoms and increased plasma D-ser levels (Ohnuma *et al.*, 2008). There is also strong evidence for increased DAAO expression in the cerebellum (Kapoor *et al.*, 2006; Verrall *et al.*, 2007; Burnet *et al.*, 2008; Madeira *et al.*, 2008; Ono *et al.*, 2009) with more unclear results in other parts of the brain.

Perhaps the more compelling arguments are found when animal models of schizophrenia are considered. Animal models are created using specific drugs, genetic alterations or through the isolation model. Pharmacological models whereby NMDAR antagonists, and modulation of their effects, are used have been shown to cause in particular the negative and cognitive symptoms (Lipina *et al.*, 2005; Almond *et al.*, 2006; Takeyama *et al.*, 2006; Hashimoto *et al.*, 2007a; Gozzi *et al.*, 2008; Hashimoto *et*

*al.*, 2008b; Labrie *et al.*, 2008; Hashimoto *et al.*, 2009; Abou El-Magd *et al.*, 2010; Vardigan *et al.*, 2010). Genetically altered animals, where SR or DAAO has been removed or been made inactive also show many promising results in terms of characterisation of schizophrenic behaviours (Hashimoto *et al.*, 2005a; Almond *et al.*, 2006; Hashimoto *et al.*, 2008a; Labrie *et al.*, 2009a; Labrie *et al.*, 2009b; Konno *et al.*, 2010; Labrie *et al.*, 2010). Finally, D-ser has been shown to be effective in the attenuation of schizophrenic symptoms both as an add-on and individual therapy

### 1.4.3 D-Serine in Relation to other Disease States

The interest in D-ser is not only limited to schizophrenia. It is implicated in many other important and prevalent diseases. These implications begin at the most basic level, memory formation, synaptic plasticity and long-term-potential (LTP). Here it has been shown that D-ser and neuronal SR are essential for LTP to occur, particularly in the hippocampus and medial prefrontal cortex (Turpin *et al.*, 2011; Fossat *et al.*, 2012), and how age related deficits and spatial learning and recall are mediated by these two substances (Maekawa *et al.*, 2005; Turpin *et al.*, 2011; Benneyworth *et al.*, 2012). Both LTP and long-term-depression (LTD) are very important targets for pharmaceutical treatment (Zhang *et al.*, 2008; Collingridge *et al.*, 2013). D-aspartate, another highly prevalent D-amino acid, has also been shown to have a link to LTD and schizophrenia in a drug model of the disease (Errico *et al.*, 2008). On the other side of this coin, abnormalities in levels of D-ser have been shown to be highly implicated in cell death, both in the brain and in peripheral organs. Global ischemia and perinatal asphyxia are both mediated by increased levels of D-ser and glutamate which leads to over-activation of NMDAr's and thus excitotoxicity (Katsuki *et al.*, 2004; Katsuki *et al.*, 2007; Dhawan *et al.*, 2011; Fuchs *et al.*, 2012). Excitotoxicity induced by D-ser can occur anywhere from the hippocampus to the kidney (Shleper *et al.*, 2005; Soto *et al.*, 2008).

Strong links have also been found between increased D-ser and glutamate levels and bipolar disorder and major depression, with D-ser also shown to block the effect of common anti-depressants (Hashimoto *et al.*, 2007b; Wlaz *et al.*, 2011). Drug addictions are also linked to the glutamatergic pathway, with D-ser reducing drug-seeking behaviour in cocaine addiction treatment (Hammond *et al.*, 2013), the NMDAr being linking to  $\mu$ -opioid receptor systems and morphine shown to increase SR and D-ser levels (Yoshikawa *et al.*, 2008). There is tentative evidence for a link between the

NMDAr and neurodegenerative disorders such as Alzheimer's, Parkinson's and vascular dementia, all of which have been extensively reviewed (Danysz & Parsons, 2012; Malinow, 2012; Olivares *et al.*, 2012). Finally, the most common adult-onset neuromuscular disease, motor neuron disease or amyotrophic lateral sclerosis (ALS) has been extensively reviewed and examined in the context of the involvement of  $\alpha$ -AAO, SR and D-ser (Crow *et al.*, 2012; Paul & de Belleruche, 2012).

## 1.5 D-Amino Acid Oxidase

A flavin dependant oxidase enzyme,  $\alpha$ -AAO was first discovered in 1935 by Hans Krebs (Krebs, 1935) and has become a model FAD-dependant oxidase for study, as indicated by a nine paper study of its various properties which was undertaken in the 60's and 70's (Yagi *et al.*, 1967; Yagi *et al.*, 1975). Much of this work has occurred in relation to  $\alpha$ -AAO derived from pig kidney, as with Yagi *et al.*, or the yeast *Rhodotorula Gracilis* (Pilone, 2000), as until recently it has been very difficult to express human  $\alpha$ -AAO and thus has only recently been characterised (Molla *et al.*, 2006). It has a very broad substrate specificity producing the relevant imino acid and hydrogen peroxide from the metabolism of a number of neutral, hydrophobic, polar and basic D-amino acids. The reaction occurs at the centralised FAD moiety (see Figure 1-4) and is discussed further in Section 2.8.2.

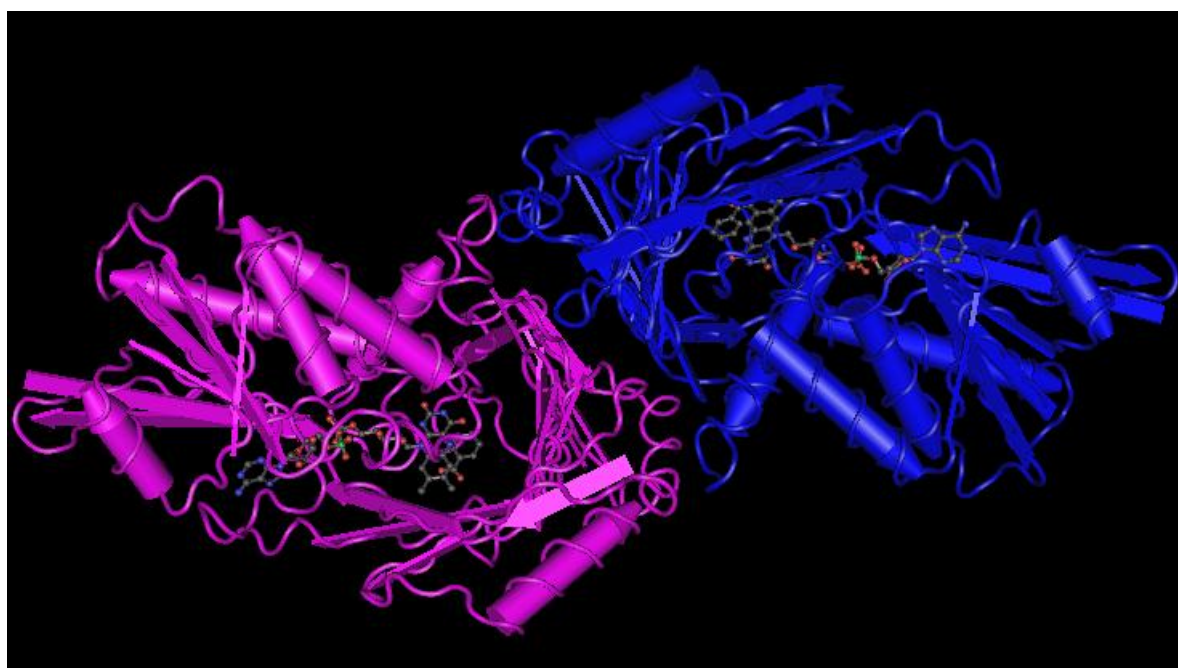


Figure 1-4

A human  $\alpha$ -AAO dimer, showing the position of the FAD units in the interior. The FAD unit is complexed to benzoic acid. Source : (Kawazoe *et al.*, 2006)

Although the presence of enriched DAAO in mammalian brains has been acknowledged for nearly 50 years (Neims *et al.*, 1966), it was not until large quantities of D-amino acids such as D-ser, D-ala and D-proline were detected that its purpose began to become clear. The distribution of DAAO tells a story of its own, it is inversely correlated with the distribution of D-ser (Horiike *et al.*, 1987; Horiike *et al.*, 1994), where it is highly concentrated in the hindbrain and midbrain and virtually absent in the forebrain. It also undergoes development changes in distribution with its levels in the cerebellum (hindbrain), medulla and pons (midbrain) only beginning to increase at postnatal day 10 in rodents, about the time that D-ser levels significantly decrease in these regions (Weimar & Neims, 1977; Hashimoto *et al.*, 1995a). This indicates that it has a role in the metabolism of D-ser, and that the two have a developmental regulative role. Indeed, DAAO protein and presence is detected in the forebrain (Bendikov *et al.*, 2007; Verrall *et al.*, 2007; Sacchi *et al.*, 2008), but it appears that its activity is down-regulated by some negative effector (Molla *et al.*, 2006). This lends further strength to the case for D-ser as an important neurotransmitter in the forebrain; its main degrading mechanism is disabled in this region.

In relation to disease states there are several important links which have been drawn. DAAO inhibitors have been strongly linked to the attenuation of psychotic and schizophrenic symptoms (Adage *et al.*, 2008; Hashimoto *et al.*, 2009; Smith *et al.*, 2009; Abou El-Magd *et al.*, 2010; Smith *et al.*, 2010) through the induced alteration of D-ser levels. Furthermore, mice lacking DAAO activity have been shown to exhibit schizophrenic-like behaviours (Almond *et al.*, 2006; Labrie *et al.*, 2009a; Labrie *et al.*, 2010). The gene G72 has been tentatively linked to schizophrenia and one of its spliced isoforms pLG72 is responsible for the inactivation of DAAO (Sacchi *et al.*, 2008).

DAAO is used in this thesis as a means to detect the presence of D-ser. This is based/duel in part to the success of other work carried out in using this enzyme for this purpose, and also because in our area of interest, the forebrain, there are many interesting ways to manipulate the levels of D-ser without impacting on the activity of DAAO. This is in direct contrast to the hind and midbrain where DAAO activity is the primary route for the metabolism of D-ser.

## 1.6 Existing Work

To our knowledge there have been two published electrochemical D-ser biosensors designed before which could be suitable for *in vivo* use. The first published biosensor (Pernot *et al.*, 2008) utilised yeast DAAO, which was recombined and purified to a concentration of 55 U/mg before utilisation. It achieved a detection limit of 16 nM and a response time of 2 seconds and a sensitivity of 9.2 pA.mM<sup>-1</sup>. Using a poly-*m*-phenylenediamine layer it achieved an interference rejection rate of 97%. The biosensor was constructed on a platinum fibre 25 µm in diameter and 150 µm long.

The second biosensor, designed by Z.M. Zain and based on the same Pt/Ir 125 µm diameter wire that this thesis is based on is discussed in further detail in Chapter 4. It is the basis on which this body of work was conducted and provided a solid foundation for the development described later in this thesis. It reports a detection limit of 20 nM and a response time of 0.7 seconds with sensitivity of  $61 \pm 7 \mu\text{A}\cdot\text{cm}^{-2}\cdot\text{mM}^{-1}$ .

Previous to the development of biosensors D-ser content has been detected in a number of ways. These include HPLC and gas chromatography in combination with microdialysis (Hashimoto *et al.*, 1992; Hashimoto *et al.*, 1995b). Capillary electrophoresis (CE) has also been utilised (Zhao *et al.*, 2005) and expanded on in the form of microdialysis-CE-laser induced fluorescence (Ciriacks & Bowser, 2006). Both D-ser immunoreactivity staining (Schell *et al.*, 1997) and monitoring via an enzymatic array constructed using D-ser dehydratase have also been reported (Ito *et al.*, 2007). Finally, in the food industry D- and L- amino acids are key indicators of nutritional value and ripeness and as such general D-amino acid biosensors have been developed to aid their use in this area (Rosini *et al.*, 2008).

## 1.7 Thesis Overview

This thesis begins with a brief outline of some of the theoretical aspects utilised in the body of research and a description of the experiment conditions and process utilised during the work in Chapters 2 and 3 respectively. Chapter 4 will take an in depth look at the biosensor designed by Zain as discussed in Section 1.6 and explore its construction and component parts. This information will feed into Chapter 5 where the design of a new D-ser biosensor will begin. This design process will be concluded in the early part of Chapter 6, with the rest of the chapter dedicated to the further *in vitro*

characterisation of the new biosensor's properties. A brief *in vivo* investigation into the correct functioning and validation of the operation of the biosensor will be explored in Chapter 7, before final conclusions are drawn in Chapter 8.

## References

- Abou El-Magd RM, Park HK, Kawazoe T, Iwana S, Ono K, Chung SP, Miyano M, Yorita K, Sakai T & Fukui K. (2010). The effect of risperidone on D-amino acid oxidase activity as a hypothesis for a novel mechanism of action in the treatment of schizophrenia. *Journal of Psychopharmacology* **24**, 1055-1067.
- Adage T, Trillat AC, Quattropiani A, Perrin D, Cavarec L, Shaw J, Guerassimenko O, Giachetti C, Greco B, Chumakov I, Halazy S, Roach A & Zaratin P. (2008). In vitro and in vivo pharmacological profile of AS057278, a selective D-amino acid oxidase inhibitor with potential anti-psychotic properties. *European Neuropsychopharmacology* **18**, 200-214.
- Al Mulla I, Lowry JP, Serra PA & O'Neill RD. (2009). Development of a voltammetric technique for monitoring brain dopamine metabolism: compensation for interference caused by DOPAC electrogenerated during homovanillic acid detection. *Analyst* **134**, 893-898.
- Albery WJ, Bartlett PN & Craston DH. (1985). Amperometric enzyme electrodes: Part II. Conducting salts as electrode materials for the oxidation of glucose oxidase. *Journal of Electroanalytical Chemistry and Interfacial Electrochemistry* **194**, 223-235.
- Almond SL, Fradley RL, Armstrong EJ, Heavens RB, Rutter AR, Newman RJ, Chiu CS, Konno R, Hutson PH & Brandon NJ. (2006). Behavioral and biochemical characterization of a mutant mouse strain lacking D-amino acid oxidase activity and its implications for schizophrenia. *Molecular and Cellular Neurosciences* **32**, 324-334.
- Balan L, Foltyn VN, Zehl M, Dumin E, Dikopoltsev E, Knoch D, Ohno Y, Kihara A, Jensen ON, Radzishewsky IS & Wolosker H. (2009). Feedback inactivation of D-serine synthesis by NMDA receptor-elicited translocation of serine racemase to the membrane. *Proceedings of the National Academy of Sciences* **106**, 7589-7594.
- Balu DT & Coyle JT. (2012). Neuronal D-serine regulates dendritic architecture in the somatosensory cortex. *Neuroscience Letters* **517**, 77-81.
- Baumgart F, Mancheno JM & Rodriguez-Crespo I. (2007). Insights into the activation of brain serine racemase by the multi-PDZ domain glutamate receptor interacting protein, divalent cations and ATP. *The FEBS Journal* **274**, 4561-4571.

- Bazzu G, Puggioni GG, Dedola S, Calia G, Rocchitta G, Migheli R, Desole MS, Lowry JP, O'Neill RD & Serra PA. (2009). Real-time monitoring of brain tissue oxygen using a miniaturized biotelemetric device implanted in freely moving rats. *Analytical Chemistry* **81**, 2235-2241.
- Bedioui F, Trevin S, Devynck J, Lantoine F, Brunet A & Devynck MA. (1997). Elaboration and use of nickel planar macrocyclic complex-based sensors for the direct electrochemical measurement of nitric oxide in biological media. *Biosensors & Bioelectronics* **12**, 205-212.
- Beh SK, Moody GJ & Thomas JDR. (1991). Studies on enzyme electrodes with ferrocene and carbon paste bound with cellulose triacetate. *Analyst* **116**, 459-462.
- Belay A, Collins A, Ruzgas T, Kissinger PT, Gorton L & Csoregi E. (1999). Redox hydrogel based bienzyme electrode for L-glutamate monitoring. *Journal of Pharmaceutical & Biomedical Analysis* **19**, 93-105.
- Bendikov I, Nadri C, Amar S, Panizzutti R, De Miranda J, Wolosker H & Agam G. (2007). A CSF and postmortem brain study of D-serine metabolic parameters in schizophrenia. *Schizophrenia Research* **90**, 41-51.
- Benneyworth MA, Li Y, Basu AC, Bolshakov VY & Coyle JT. (2012). Cell selective conditional null mutations of serine racemase demonstrate a predominate localization in cortical glutamatergic neurons. *Cellular & Molecular Neurobiology* **32**, 613-624.
- Berger AJ, Dieudonne S & Ascher P. (1998). Glycine uptake governs glycine site occupancy at NMDA receptors of excitatory synapses. *Journal of Neurophysiology* **80**, 3336-3340.
- Bergeron R, Meyer TM, Coyle JT & Greene RW. (1998). Modulation of N-methyl-D-aspartate receptor function by glycine transport. *Proceedings of the National Academy of Sciences USA* **95**, 15730-15734.
- Bilal S, Ali Shah A-u-H & Holze R. (2011). Spectroelectrochemistry of poly(*o*-phenylenediamine): Polyaniline-like segments in the polymer structure. *Electrochimica Acta* **56**, 3353-3358.
- Bolger FB, Bennett R & Lowry JP. (2011). An *in vitro* characterisation comparing carbon paste and Pt microelectrodes for real-time detection of brain tissue oxygen. *Analyst* **136**, 4028-4035.

- Bolger FB & Lowry JP. (2005). Brain tissue oxygen: *In vivo* monitoring with carbon paste electrodes. *Sensors* **5**, 473-487.
- Boutelle MG, Stanford C, Fillenz M, Albery WJ & Bartlett PN. (1986). An amperometric enzyme electrode for monitoring brain glucose in the freely moving rat. *Neuroscience Letters* **72**, 283-288.
- Brown FO, Finnerty NJ & Lowry JP. (2009). Nitric oxide monitoring in brain extracellular fluid: characterisation of Nafion-modified Pt electrodes *in vitro* and *in vivo*. *Analyst* **134**, 2012-2020.
- Brown FO & Lowry JP. (2003). Microelectrochemical sensors for *in vivo* brain analysis: An investigation of procedures for modifying Pt electrodes using Nafion®. *Analyst* **128**, 700-705.
- Burmeister JJ & Gerhardt GA. (2001). Self-referencing ceramic-based multisite microelectrodes for the detection and elimination of interferences from the measurement of L-glutamate and other analytes. *Analytical Chemistry* **73**, 1037-1042.
- Burmeister JJ, Pomerleau F, Huettl P, Gash CR, Werner CE, Bruno JP & Gerhardt GA. (2008). Ceramic-based multisite microelectrode arrays for simultaneous measures of choline and acetylcholine in CNS. *Biosensors and Bioelectronics* **23**, 1382-1389.
- Burnet PW, Eastwood SL, Bristow GC, Godlewska BR, Sikka P, Walker M & Harrison PJ. (2008). D-amino acid oxidase activity and expression are increased in schizophrenia. *Molecular Psychiatry* **13**, 658-660.
- Centonze D, Losito I, Malitesta C, Palmisano F & Zamboni PG. (1997). Electrochemical immobilisation of enzymes on conducting organic salt electrodes: characterisation of an oxygen independent and interference-free glucose biosensor. *Journal of Electroanalytical Chemistry* **435**, 103-111.
- Chang SC, Pereira-Rodrigues N, Henderson JR, Cole A, Bedioui F & McNeil CJ. (2005). An electrochemical sensor array system for the direct, simultaneous *in vitro* monitoring of nitric oxide and superoxide production by cultured cells. *Biosensors & Bioelectronics* **21**, 917-922.
- Chauhan N, Narang J & Pundir CS. (2011). Fabrication of multiwalled carbon nanotubes/polyaniline modified Au electrode for ascorbic acid determination. *Analyst* **136**, 1938-1945.

- Chouinard ML, Gaitan D & Wood PL. (1993). Presence of the N-methyl-D-aspartate-associated glycine receptor agonist, D-serine, in human temporal cortex: comparison of normal, Parkinson, and Alzheimer tissues. *Journal of Neurochemistry* **61**, 1561-1564.
- Ciriacks CM & Bowser MT. (2006). Measuring the effect of glutamate receptor agonists on extracellular D-serine concentrations in the rat striatum using online microdialysis-capillary electrophoresis. *Neuroscience Letters* **393**, 200-205.
- Clark LC, Jr. & Lyons C. (1962). Electrode systems for continuous monitoring in cardiovascular surgery. *Annals of the New York Academy of Sciences* **102**, 29-45.
- Clark LC, Jr. & Lyons C. (1965). Studies of a glassy carbon electrode for brain polarography with observations on the effect of carbonic anhydrase inhibition. *The Alabama Journal of Medical Sciences* **2**, 353-359.
- Clark LC, Jr., Misrahy G & Fox RP. (1958). Chronically implanted polarographic electrodes. *Journal of Applied Physiology* **13**, 85-91.
- Clark LC, Jr., Wolf R, Granger D & Taylor Z. (1953). Continuous recording of blood oxygen tensions by polarography. *Journal of Applied Physiology* **6**, 189-193.
- Collingridge GL, Volianskis A, Bannister N, France G, Hanna L, Mercier M, Tidball P, Fang G, Irvine MW, Costa BM, Monaghan DT, Bortolotto ZA, Molnár E, Lodge D & Jane DE. (2013). The NMDA receptor as a target for cognitive enhancement. *Neuropharmacology* **64**, 13-26.
- Cook SP, Galve-Roperh I, Martinez del Pozo A & Rodriguez-Crespo I. (2002). Direct calcium binding results in activation of brain serine racemase. *Journal of Biological Chemistry* **277**, 27782-27792.
- Cooper J & Cass T. (2004). *Biosensors*. Oxford University Press, USA.
- Craig JD & O'Neill RD. (2003). Comparison of simple aromatic amines for electrosynthesis of permselective polymers in biosensor fabrication. *Analyst* **128**, 905-911.
- Crespi F, Martin KF, Heal DJ, Marsden CA, Buckett WR & Sanghera MK. (1989). Measurement of 3-methoxytyramine by in vivo voltammetry: evidence for differences in central dopamine function in BALB/c and CBA mice. *Brain Research* **500**, 241-246.

- Crow JP, Marecki JC & Thompson M. (2012). D-Serine Production, Degradation, and Transport in ALS: Critical Role of Methodology. *Neurology Research International* **2012**, 625245.
- Cull-Candy S. (1995). Neurotransmitters. NMDA receptors: do glia hold the key? *Current Biology* **5**, 841-843.
- Dai Y-Q, Zhou D-M & Shiu K-K. (2006). Permeability and permselectivity of polyphenylenediamine films synthesized at a palladium disk electrode. *Electrochimica Acta* **52**, 297-303.
- Danysz W, Fadda E, Wroblewski JT & Costa E. (1990). [3H]D-serine labels strychnine-insensitive glycine recognition sites of rat central nervous system. *Life Sciences* **46**, 155-164.
- Danysz W & Parsons CG. (2012). Alzheimer's disease, beta-amyloid, glutamate, NMDA receptors and memantine - searching for the connections. *British Journal of Pharmacology* **167**, 324-352.
- de Keijzer MH, Brandts RW & Brans PG. (1999). Evaluation of a biosensor for the measurement of lactate in whole blood. *Clinical Biochemistry* **32**, 109-112.
- de Miranda J, Panizzutti R, Foltyn VN & Wolosker H. (2002). Cofactors of serine racemase that physiologically stimulate the synthesis of the N-methyl-D-aspartate (NMDA) receptor coagonist D-serine. *Proceedings of the National Academy of Sciences* **99**, 14542-14547.
- de Miranda J, Santoro A, Engelender S & Wolosker H. (2000). Human serine racemase: molecular cloning, genomic organization and functional analysis. *Gene* **256**, 183-188.
- Dhawan J, Benveniste H, Luo Z, Nawrocky M, Smith SD & Biegon A. (2011). A new look at glutamate and ischemia: NMDA agonist improves long-term functional outcome in a rat model of stroke. *Future Neurology* **6**, 823-834.
- Dumin E, Bendikov I, Foltyn VN, Misumi Y, Ikehara Y, Kartvelishvily E & Wolosker H. (2006). Modulation of D-serine levels via ubiquitin-dependent proteasomal degradation of serine racemase. *Journal of Biological Chemistry* **281**, 20291-20302.
- Dunlop DS & Neidle A. (1997). The origin and turnover of D-serine in brain. *Biochemical & Biophysical Research Communications* **235**, 26-30.

- Dunlop DS, Neidle A, McHale D, Dunlop DM & Lajtha A. (1986). The presence of free D-aspartic acid in rodents and man. *Biochemical & Biophysical Research Communications* **141**, 27-32.
- Errico F, Rossi S, Napolitano F, Catuogno V, Topo E, Fisone G, D'Aniello A, Centonze D & Usiello A. (2008). D-aspartate prevents corticostriatal long-term depression and attenuates schizophrenia-like symptoms induced by amphetamine and MK-801. *Journal of Neuroscience* **28**, 10404-10414.
- Fadda E, Danysz W, Wroblewski JT & Costa E. (1988). Glycine and D-serine increase the affinity of N-methyl-D-aspartate sensitive glutamate binding sites in rat brain synaptic membranes. *Neuropharmacology* **27**, 1183-1185.
- Fernandes JCB, Kubota LT & Neto GdO. (1999). Potentiometric biosensor for L-ascorbic acid based on ascorbate oxidase of natural source immobilized on ethylene-vinylacetate membrane. *Analytica Chimica Acta* **385**, 3-12.
- Foltyn VN, Bendikov I, De Miranda J, Panizzutti R, Dumin E, Shleper M, Li P, Toney MD, Kartvelishvily E & Wolosker H. (2005). Serine racemase modulates intracellular D-serine levels through an  $\alpha,\beta$ -elimination activity. *Journal of Biological Chemistry* **280**, 1754-1763.
- Foltyn VN, Zehl M, Dikopoltsev E, Jensen ON & Wolosker H. (2010). Phosphorylation of mouse serine racemase regulates D-serine synthesis. *FEBS Letters* **584**, 2937-2941.
- Forni C & Nieoullon A. (1984). Electrochemical detection of dopamine release in the striatum of freely moving hamsters. *Brain Research* **297**, 11-20.
- Fossat P, Turpin FR, Sacchi S, Dulong J, Shi T, Rivet JM, Sweedler JV, Pollegioni L, Millan MJ, Oliet SH & Mothet JP. (2012). Glial D-serine gates NMDA receptors at excitatory synapses in prefrontal cortex. *Cerebral Cortex* **22**, 595-606.
- Friedemann MN, Robinson SW & Gerhardt GA. (1996). *o*-Phenylenediamine-modified carbon fiber electrodes for the detection of nitric oxide. *Analytical Chemistry* **68**, 2621-2628.
- Fuchs S, Peeters-Scholte C, de Barse M, Roeleveld M, Klomp L, Berger R & de Koning T. (2012). Increased concentrations of both NMDA receptor co-agonists D-serine and glycine in global ischemia: a potential novel treatment target for perinatal asphyxia. *Amino Acids* **43**, 355-363.

Fuchs SA, Berger R & de Koning TJ. (2011). D-Serine: The right or wrong isoform? *Brain Research* **1401**, 104-117.

Fujii K, Maeda K, Hikida T, Mustafa AK, Balkissoon R, Xia J, Yamada T, Ozeki Y, Kawahara R, Okawa M, Haganir RL, Ujike H, Snyder SH & Sawa A. (2006). Serine racemase binds to PICK1: potential relevance to schizophrenia. *Molecular Psychiatry* **11**, 150-157.

Furukawa H & Gouaux E. (2003). Mechanisms of activation, inhibition and specificity: crystal structures of the NMDA receptor NR1 ligand-binding core. *The EMBO Journal* **22**, 2873-2885.

Garguilo MG & Michael AC. (1995a). Enzyme-modified electrodes for peroxide, choline, and acetylcholine. *Trends in Analytical Chemistry* **14**, 164-169.

Garguilo MG & Michael AC. (1995b). Optimization of amperometric microsensors for monitoring choline in the extracellular fluid of brain-tissue. *Analytica Chimica Acta* **307**, 291-299.

Garjonyte R & Malinauskas A. (1999). Amperometric glucose biosensor based on glucose oxidase immobilized in poly(*o*-phenylenediamine) layer. *Sensors and Actuators B: Chemical* **56**, 85-92.

Gozzi A, Herdon H, Schwarz A, Bertani S, Crestan V, Turrini G & Bifone A. (2008). Pharmacological stimulation of NMDA receptors via co-agonist site suppresses fMRI response to phencyclidine in the rat. *Psychopharmacology* **201**, 273-284.

Gründig B & Krabisch C. (1989). Electron mediator-modified electrode for the determination of glucose in fermentation media. *Analytica Chimica Acta* **222**, 75-81.

Hammond S, Seymour CM, Burger A & Wagner JJ. (2013). D-Serine facilitates the effectiveness of extinction to reduce drug-primed reinstatement of cocaine-induced conditioned place preference. *Neuropharmacology* **64**, 464-471.

Hasebe Y, Akiyama T, Yagisawa T & Uchiyama S. (1998). Enzyme-less amperometric biosensor for L-ascorbate using poly-L-histidine-copper complex as an alternative biocatalyst. *Talanta* **47**, 1139-1147.

Hashimoto A, Konno R, Yano H, Yoshikawa M, Tamaki R, Matsumoto H & Kobayashi H. (2008a). Mice lacking D-amino acid oxidase activity exhibit marked reduction of methamphetamine-induced stereotypy. *European Journal of Pharmacology* **586**, 221-225.

- Hashimoto A, Kumashiro S, Nishikawa T, Oka T, Takahashi K, Mito T, Takashima S, Doi N, Mizutani Y, Yamazaki T & et al. (1993a). Embryonic development and postnatal changes in free D-aspartate and D-serine in the human prefrontal cortex. *Journal of Neurochemistry* **61**, 348-351.
- Hashimoto A, Nishikawa T, Hayashi T, Fujii N, Harada K, Oka T & Takahashi K. (1992). The presence of free D-serine in rat brain. *FEBS Letters* **296**, 33-36.
- Hashimoto A, Nishikawa T, Konno R, Niwa A, Yasumura Y, Oka T & Takahashi K. (1993b). Free D-serine, D-aspartate and D-alanine in central nervous system and serum in mutant mice lacking D-amino acid oxidase. *Neuroscience Letters* **152**, 33-36.
- Hashimoto A, Nishikawa T, Oka T, Hayashi T & Takahashi K. (1993c). Widespread distribution of free D-aspartate in rat periphery. *FEBS Letters* **331**, 4-8.
- Hashimoto A, Nishikawa T, Oka T & Takahashi K. (1993d). Endogenous D-serine in rat brain: N-methyl-D-aspartate receptor-related distribution and aging. *Journal of Neurochemistry* **60**, 783-786.
- Hashimoto A, Oka T & Nishikawa T. (1995a). Anatomical distribution and postnatal changes in endogenous free D-aspartate and D-serine in rat brain and periphery. *European Journal of Neuroscience* **7**, 1657-1663.
- Hashimoto A, Oka T & Nishikawa T. (1995b). Extracellular concentration of endogenous free D-serine in the rat brain as revealed by in vivo microdialysis. *Neuroscience* **66**, 635-643.
- Hashimoto A, Yoshikawa M, Andoh H, Yano H, Matsumoto H, Kawaguchi M, Oka T & Kobayashi H. (2007a). Effects of MK-801 on the expression of serine racemase and D-amino acid oxidase mRNAs and on the D-serine levels in rat brain. *European Journal of Pharmacology* **555**, 17-22.
- Hashimoto A, Yoshikawa M, Niwa A & Konno R. (2005a). Mice lacking D-amino acid oxidase activity display marked attenuation of stereotypy and ataxia induced by MK-801. *Brain Research* **1033**, 210-215.
- Hashimoto K, Engberg G, Shimizu E, Nordin C, Lindström LH & Iyo M. (2005b). Reduced D-serine to total serine ratio in the cerebrospinal fluid of drug naive schizophrenic patients. *Progress in Neuro-Psychopharmacology and Biological Psychiatry* **29**, 767-769.

- Hashimoto K, Fujita Y, Horio M, Kunitachi S, Iyo M, Ferraris D & Tsukamoto T. (2009). Co-administration of a D-amino acid oxidase inhibitor potentiates the efficacy of D-serine in attenuating prepulse inhibition deficits after administration of dizocilpine. *Biological Psychiatry* **65**, 1103-1106.
- Hashimoto K, Fujita Y, Ishima T, Chaki S & Iyo M. (2008b). Phencyclidine-induced cognitive deficits in mice are improved by subsequent subchronic administration of the glycine transporter-1 inhibitor NFPS and D-serine. *European Neuropsychopharmacology* **18**, 414-421.
- Hashimoto K, Fukushima T, Shimizu E, Komatsu N, Watanabe H, Shinoda N, Nakazato M, Kumakiri C, Okada S, Hasegawa H, Imai K & Iyo M. (2003). Decreased serum levels of D-serine in patients with schizophrenia: evidence in support of the N-methyl-D-aspartate receptor hypofunction hypothesis of schizophrenia. *Archives of General Psychiatry* **60**, 572-576.
- Hashimoto K, Sawa A & Iyo M. (2007b). Increased levels of glutamate in brains from patients with mood disorders. *Biological Psychiatry* **62**, 1310-1316.
- Haughton E. (pending publication). Real-time Neurochemical Analysis of Excitatory Amino Acids: Enzyme-modified Microelectrochemical Biosensors for Aspartate and Glutamate. In *Department of Chemistry*. National University of Ireland, Maynooth, (pending publication).
- Helboe L, Egebjerg J, Møller M & Thomsen C. (2003). Distribution and pharmacology of alanine-serine-cysteine transporter 1 (asc-1) in rodent brain. *European Journal of Neuroscience* **18**, 2227-2238.
- Heller A. (1990). Electrical wiring of redox enzymes. *Accounts of Chemical Research* **23**, 128-134.
- Hikida T, Mustafa AK, Maeda K, Fujii K, Barrow RK, Saleh M, Haganir RL, Snyder SH, Hashimoto K & Sawa A. (2008). Modulation of D-serine levels in brains of mice lacking PICK1. *Biological Psychiatry* **63**, 997-1000.
- Horiike K, Tojo H, Arai R, Nozaki M & Maeda T. (1994). D-Amino-acid oxidase is confined to the lower brain stem and cerebellum in rat brain: regional differentiation of astrocytes. *Brain Research* **652**, 297-303.
- Horiike K, Tojo H, Arai R, Yamano T, Nozaki M & Maeda T. (1987). Localization of D-amino acid oxidase in Bergmann glial cells and astrocytes of rat cerebellum. *Brain Research Bulletin* **19**, 587-596.

- Hu Y & Wilson GS. (1997a). Rapid changes in local extracellular rat brain glucose observed with an *in vivo* glucose sensor. *Journal of Neurochemistry* **68**, 1745-1752.
- Hu Y & Wilson GS. (1997b). A temporary local energy pool coupled to neuronal activity: fluctuations of extracellular lactate levels in rat brain monitored with rapid-response enzyme-based sensor. *Journal of Neurochemistry* **69**, 1484-1490.
- Ito T, Takahashi K, Naka T, Hemmi H & Yoshimura T. (2007). Enzymatic assay of D-serine using D-serine dehydratase from *Saccharomyces cerevisiae*. *Analytical Biochemistry* **371**, 167-172.
- Iwama H, Takahashi K, Kure S, Hayashi F, Narisawa K, Tada K, Mizoguchi M, Takashima S, Tomita U & Nishikawa T. (1997). Depletion of cerebral D-serine in non-ketotic hyperglycinemia: possible involvement of glycine cleavage system in control of endogenous D-serine. *Biochemical & Biophysical Research Communications* **231**, 793-796.
- Javitt DC. (2012). Twenty-five years of glutamate in schizophrenia: Are we there yet? *Schizophrenia Bulletin* **38**, 911-913.
- Javitt DC & Zukin SR. (1991). Recent advances in the phencyclidine model of schizophrenia. *American Journal of Psychiatry* **148**, 1301-1308.
- Jezkova J, Iwuoha EI, Smyth MR & Vytras K. (1997). Stabilization of an osmium bis-bipyridyl polymer-modified carbon paste amperometric glucose biosensor using polyethyleneimine. *Electroanalysis* **9**, 978-984.
- Johnson JW & Ascher P. (1987). Glycine potentiates the NMDA response in cultured mouse brain neurons. *Nature* **325**, 529-531.
- Kano K, Morikage K, Uno B, Esaka Y & Goto M. (1994). Enzyme microelectrodes for choline and acetylcholine and their applications. *Analytica Chimica Acta* **299**, 69-74.
- Kapoor R, Lim KS, Cheng A, Garrick T & Kapoor V. (2006). Preliminary evidence for a link between schizophrenia and NMDA-glycine site receptor ligand metabolic enzymes, D-amino acid oxidase (DAAO) and kynurenine aminotransferase-1 (KAT-1). *Brain Research* **1106**, 205-210.
- Kartvelishvily E, Shleper M, Balan L, Dumin E & Wolosker H. (2006). Neuron-derived D-serine release provides a novel means to activate N-methyl-D-aspartate receptors. *Journal of Biological Chemistry* **281**, 14151-14162.

- Karyakin AA, Gitelmacher OV & Karyakina EE. (1995). Prussian blue-based first-generation biosensor. A sensitive amperometric electrode for glucose. *Analytical Chemistry* **67**, 2419-2423.
- Karyakin AA, Karyakina EE & Gorton L. (2000). Amperometric biosensor for glutamate using prussian blue-based “artificial peroxidase” as a transducer for hydrogen peroxide. *Analytical Chemistry* **72**, 1720-1723.
- Katsuki H, Nonaka M, Shirakawa H, Kume T & Akaike A. (2004). Endogenous D-serine is involved in induction of neuronal death by N-methyl-D-aspartate and simulated ischemia in rat cerebrocortical slices. *Journal of Pharmacology and Experimental Therapeutics* **311**, 836-844.
- Katsuki H, Watanabe Y, Fujimoto S, Kume T & Akaike A. (2007). Contribution of endogenous glycine and D-serine to excitotoxic and ischemic cell death in rat cerebrocortical slice cultures. *Life Sciences* **81**, 740-749.
- Kawazoe T, Tsuge H, Piloni MS & Fukui K. (2006). Crystal structure of human D-amino acid oxidase: Context-dependent variability of the backbone conformation of the VAAGL hydrophobic stretch located at the si-face of the flavin ring. *Protein Science* **15**, 2708-2717.
- Kim PM, Aizawa H, Kim PS, Huang AS, Wickramasinghe SR, Kashani AH, Barrow RK, Haganir RL, Ghosh A & Snyder SH. (2005). Serine racemase: activation by glutamate neurotransmission via glutamate receptor interacting protein and mediation of neuronal migration. *Proceedings of the National Academy of Sciences* **102**, 2105-2110.
- Kirwan SM, Rocchitta G, McMahon CP, Craig JD, Killoran SJ, O'Brien KB, Serra PA, Lowry JP & O'Neill RD. (2007). Modifications of poly(*o*-phenylenediamine) permselective layer on Pt-Ir for biosensor application in neurochemical monitoring. *Sensors* **7**, 420-437.
- Kissinger PT, Hart JB & Adams RN. (1973). Voltammetry in brain tissue-a new neurophysiological measurement. *Brain Research* **55**, 209-213.
- Koike T & Ninomiya T. (2000). Alteration of veratridine neurotoxicity in sympathetic neurons during development in vitro. *Neuroreport* **11**, 151-155.
- Konno R, Hamase K, Maruyama R & Zaitsev K. (2010). Mutant mice and rats lacking D-amino acid oxidase. *Chemistry & Biodiversity* **7**, 1450-1458.

- Krebs HA. (1935). Metabolism of amino-acids: Deamination of amino-acids. *The Biochemical Journal* **29**, 1620-1644.
- Krystal JH, Karper LP, Seibyl JP, Freeman GK, Delaney R, Bremner JD, Heninger GR, Bowers MB, Jr. & Charney DS. (1994). Subanesthetic effects of the noncompetitive NMDA antagonist, ketamine, in humans. Psychotomimetic, perceptual, cognitive, and neuroendocrine responses. *Archives of General Psychiatry* **51**, 199-214.
- Krystal JH, Perry EB, Jr., Gueorguieva R, Belger A, Madonick SH, Abi-Dargham A, Cooper TB, Macdougall L, Abi-Saab W & D'Souza DC. (2005). Comparative and interactive human psychopharmacologic effects of ketamine and amphetamine: implications for glutamatergic and dopaminergic model psychoses and cognitive function. *Archives of General Psychiatry* **62**, 985-994.
- Kulagina NV & Michael AC. (2003). Monitoring hydrogen peroxide in the extracellular space of the brain with amperometric microsensors. *Analytical Chemistry* **75**, 4875-4881.
- Kulagina NV, Zigmond MJ & Michael AC. (2001). Glutamate regulates the spontaneous and evoked release of dopamine in the rat striatum. *Neuroscience* **102**, 121-128.
- Kumashiro S, Hashimoto A & Nishikawa T. (1995). Free D-serine in post-mortem brains and spinal cords of individuals with and without neuropsychiatric diseases. *Brain Research* **681**, 117-125.
- Kunimura S, Ohsaka T & Oyama N. (1988). Preparation of thin polymeric films on electrode surfaces by electropolymerization of *o*-aminophenol. *Macromolecules* **21**, 894-900.
- Labrie V, Clapcote SJ & Roder JC. (2009a). Mutant mice with reduced NMDA-NR1 glycine affinity or lack of D-amino acid oxidase function exhibit altered anxiety-like behaviors. *Pharmacology, Biochemistry & Behaviour* **91**, 610-620.
- Labrie V, Duffy S, Wang W, Barger SW, Baker GB & Roder JC. (2009b). Genetic inactivation of D-amino acid oxidase enhances extinction and reversal learning in mice. *Learning & Memory* **16**, 28-37.
- Labrie V, Lipina T & Roder JC. (2008). Mice with reduced NMDA receptor glycine affinity model some of the negative and cognitive symptoms of schizophrenia. *Psychopharmacology (Berlin)* **200**, 217-230.

- Labrie V, Wang W, Barger SW, Baker GB & Roder JC. (2010). Genetic loss of D-amino acid oxidase activity reverses schizophrenia-like phenotypes in mice. *Genes, Brain & Behaviour* **9**, 11-25.
- Labrie V, Wong AHC & Roder JC. (2012). Contributions of the D-serine pathway to schizophrenia. *Neuropharmacology* **62**, 1484-1503.
- Lipina T, Labrie V, Weiner I & Roder J. (2005). Modulators of the glycine site on NMDA receptors, D-serine and ALX 5407, display similar beneficial effects to clozapine in mouse models of schizophrenia. *Psychopharmacology (Berlin)* **179**, 54-67.
- Lisman JE, Coyle JT, Green RW, Javitt DC, Benes FM, Heckers S & Grace AA. (2008). Circuit-based framework for understanding neurotransmitter and risk gene interactions in schizophrenia. *Trends in Neurosciences* **31**, 234-242.
- Lowry JP, Griffin K, McHugh SB, Lowe AS, Tricklebank M & Sibson NR. (2010). Real-time electrochemical monitoring of brain tissue oxygen: A surrogate for functional magnetic resonance imaging in rodents. *Neuroimage* **52**, 549-555.
- Lowry JP, Mcateer K, Elatrash SS, Duff A & O'Neill RD. (1994). Characterization of glucose oxidase-modified poly(phenylenediamine)-coated electrodes *in vitro* and *in vivo* - Homogeneous interference by ascorbic-acid in hydrogen-peroxide detection. *Analytical Chemistry* **66**, 1754-1761.
- Lowry JP, Miele M, O'Neill RD, Boutelle MG & Fillenz M. (1998). An amperometric glucose-oxidase/poly(*o*-phenylenediamine) biosensor for monitoring brain extracellular glucose: *In vivo* characterisation in the striatum of freely-moving rats. *Journal of Neuroscience Methods* **79**, 65-74.
- Lowry JP & O'Neill RD. (1992a). Homogeneous mechanism of ascorbic-acid interference in hydrogen-peroxide detection at enzyme-modified Electrodes. *Analytical Chemistry* **64**, 453-456.
- Lowry JP & O'Neill RD. (1992b). Strategies for reducing ascorbate interference at glucose-oxidase modified conducting organic salt electrodes. *Journal of Electroanalytical Chemistry* **334**, 183-194.
- Madeira C, Freitas ME, Vargas-Lopes C, Wolosker H & Panizzutti R. (2008). Increased brain D-amino acid oxidase (DAAO) activity in schizophrenia. *Schizophrenia Research* **101**, 76-83.

- Maekawa M, Watanabe M, Yamaguchi S, Konno R & Hori Y. (2005). Spatial learning and long-term potentiation of mutant mice lacking D-amino-acid oxidase. *Neuroscience Research* **53**, 34-38.
- Malinauskas A, Bron M & Holze R. (1998). Electrochemical and Raman spectroscopic studies of electrosynthesized copolymers and bilayer structures of polyaniline and poly(*o*-phenylenediamine). *Synthetic Metals* **92**, 127-137.
- Malinow R. (2012). New developments on the role of NMDA receptors in Alzheimer's disease. *Current Opinion in Neurobiology* **22**, 559-563.
- Malitesta C, Palmisano F, Torsi L & Zambonin PG. (1990). Glucose fast-response amperometric sensor based on glucose oxidase immobilized in an electropolymerized poly(*o*-phenylenediamine) film. *Analytical Chemistry* **62**, 2735-2740.
- Martineau M, Galli T, Baux G & Mothet J-P. (2008). Confocal imaging and tracking of the exocytotic routes for D-serine-mediated gliotransmission. *Glia* **56**, 1271-1284.
- Matsui T, Sekiguchi M, Hashimoto A, Tomita U, Nishikawa T & Wada K. (1995). Functional comparison of D-serine and glycine in rodents: the effect on cloned NMDA receptors and the extracellular concentration. *Journal of Neurochemistry* **65**, 454-458.
- Matsuo H, Kanai Y, Tokunaga M, Nakata T, Chairoungdua A, Ishimine H, Tsukada S, Ooigawa H, Nawashiro H, Kobayashi Y, Fukuda J & Endou H. (2004). High affinity D- and L-serine transporter Asc-1: cloning and dendritic localization in the rat cerebral and cerebellar cortices. *Neuroscience Letters* **358**, 123-126.
- McMahon CP, Rocchitta G, Kirwan SM, Killoran SJ, Serra PA, Lowry JP & O'Neill RD. (2007). Oxygen tolerance of an implantable polymer/enzyme composite glutamate biosensor displaying polycation-enhanced substrate sensitivity. *Biosensors & Bioelectronics* **22**, 1466-1473.
- McMahon CP, Rocchitta G, Serra PA, Kirwan SM, Lowry JP & O'Neill RD. (2006). Control of the oxygen dependence of an implantable polymer/enzyme composite biosensor for glutamate. *Analytical Chemistry* **78**, 2352-2359.
- Miya K, Inoue R, Takata Y, Abe M, Natsume R, Sakimura K, Hongou K, Miyawaki T & Mori H. (2008). Serine racemase is predominantly localized in neurons in mouse brain. *The Journal of Comparative Neurology* **510**, 641-654.

- Molla G, Sacchi S, Bernasconi M, Pilone MS, Fukui K & Pollegioni L. (2006). Characterization of human D-amino acid oxidase. *FEBS Letters* **580**, 2358-2364.
- Mothet J-P, Parent AT, Wolosker H, Brady RO, Linden DJ, Ferris CD, Rogawski MA & Snyder SH. (2000). D-Serine is an endogenous ligand for the glycine site of the N-methyl-D-aspartate receptor. *Proceedings of the National Academy of Sciences* **97**, 4926-4931.
- Mothet J-P, Pollegioni L, Ouanounou G, Martineau M, Fossier P & Baux G. (2005). Glutamate receptor activation triggers a calcium-dependent and SNARE protein-dependent release of the gliotransmitter D-serine. *Proceedings of the National Academy of Sciences* **102**, 5606-5611.
- Mustafa AK, van Rossum DB, Patterson RL, Maag D, Ehmsen JT, Gazi SK, Chakraborty A, Barrow RK, Amzel LM & Snyder SH. (2009). Glutamatergic regulation of serine racemase via reversal of PIP2 inhibition. *Proceedings of the National Academy of Sciences* **106**, 2921-2926.
- Neims AH, Zieverink WD & Smilack JD. (1966). Distribution of D-amino acid oxidase in bovine and human nervous tissues. *Journal of Neurochemistry* **13**, 163-168.
- O'Brien KB, Killoran SJ, O'Neill RD & Lowry JP. (2007). Development and characterization *in vitro* of a catalase-based biosensor for hydrogen peroxide monitoring. *Biosensors & Bioelectronics* **22**, 2994-3000.
- O'Neill RD. (1994). Microvoltammetric techniques and sensors for monitoring neurochemical dynamics *in vivo*. A review. *Analyst* **119**, 767-779.
- O'Neill RD, Fillenz M & Albery WJ. (1982). Circadian changes in homovanillic acid and ascorbate levels in the rat striatum using microprocessor-controlled voltammetry. *Neuroscience Letters* **34**, 189-193.
- O'Neill RD, Fillenz M, Sundstrom L & Rawlins JN. (1984). Voltammetrically monitored brain ascorbate as an index of excitatory amino acid release in the unrestrained rat. *Neuroscience Letters* **52**, 227-233.
- O'Neill RD & Lowry JP. (1995). On the significance of brain extracellular uric acid detected with *in-vivo* monitoring techniques: a review. *Behavioural Brain Research* **71**, 33-49.
- O'Neill RD, Lowry JP & Mas M. (1998). Monitoring brain chemistry *in vivo*: Voltammetric techniques, sensors, and behavioral applications. *Critical Reviews in Neurobiology* **12**, 69-127.

- Ohnuma T, Sakai Y, Maeshima H, Hatano T, Hanzawa R, Abe S, Kida S, Shibata N, Suzuki T & Arai H. (2008). Changes in plasma glycine, L-serine, and D-serine levels in patients with schizophrenia as their clinical symptoms improve: Results from the Juntendo University Schizophrenia Projects (JUSP). *Progress in Neuro-Psychopharmacology and Biological Psychiatry* **32**, 1905-1912.
- Oliet SHR & Mothet JP. (2009). Regulation of N-methyl-D-aspartate receptors by astrocytic D-serine. *Neuroscience* **158**, 275-283.
- Olivares D, Deshpande VK, Shi Y, Lahiri DK, Greig NH, Rogers JT & Huang X. (2012). N-methyl-D-aspartate (NMDA) receptor antagonists and memantine treatment for Alzheimer's disease, vascular dementia and Parkinson's disease. *Current Alzheimer Research* **9**, 746-758.
- Ono K, Shishido Y, Park HK, Kawazoe T, Iwana S, Chung SP, Abou El-Magd RM, Yorita K, Okano M, Watanabe T, Sano N, Bando Y, Arima K, Sakai T & Fukui K. (2009). Potential pathophysiological role of D-amino acid oxidase in schizophrenia: immunohistochemical and in situ hybridization study of the expression in human and rat brain. *Journal of Neural Transmission* **116**, 1335-1347.
- Panatier A, Theodosis DT, Mothet J-P, Touquet B, Pollegioni L, Poulain DA & Oliet SHR. (2006). Glia-derived D-serine controls NMDA receptor activity and synaptic memory. *Cell* **125**, 775-784.
- Papouin T, Ladépêche L, Ruel J, Sacchi S, Labasque M, Hanini M, Groc L, Pollegioni L, Mothet J-P & Oliet Stéphane HR. (2012). Synaptic and extrasynaptic NMDA receptors are gated by different endogenous coagonists. *Cell* **150**, 633-646.
- Paul P & de Belleruche J. (2012). The role of D-amino acids in amyotrophic lateral sclerosis pathogenesis: A review. *Amino Acids* **43**, 1823-1831.
- Pauliukaite R, Zhylyak G, Citterio D & Spichiger-Keller U. (2006). D-Glutamate biosensor for estimation of the taste of tomato specimens. *Analytical & Bioanalytical Chemistry* **386**, 220-227.
- Pernot P, Mothet J-P, Schuvailo O, Soldatkin A, Pollegioni L, Pilone M, Adeline M-T, Cespluglio R & Marinesco S. (2008). Characterization of a yeast D-amino acid oxidase microbiosensor for D-serine detection in the central nervous system. *Analytical Chemistry* **80**, 1589-1597.

- Pilone MS. (2000). D-Amino acid oxidase: New findings. *Cellular & Molecular Life Sciences* **57**, 1732-1747.
- Priestley T, Laughton P, Myers J, Le Bourdelles B, Kerby J & Whiting PJ. (1995). Pharmacological properties of recombinant human N-methyl-D-aspartate receptors comprising NR1a/NR2A and NR1a/NR2B subunit assemblies expressed in permanently transfected mouse fibroblast cells. *Molecular Pharmacology* **48**, 841-848.
- Qin S, Van der Zeyden M, Oldenzien W, Cremers T & Westerink B. (2008). Microsensors for in vivo measurement of glutamate in brain tissue. *Sensors* **8**, 6860-6884.
- Ribeiro CS, Reis M, Panizzutti R, de Miranda J & Wolosker H. (2002). Glial transport of the neuromodulator D-serine. *Brain Research* **929**, 202-209.
- Rice ME, Richards CD, Nedergaard S, Hounsgaard J, Nicholson C & Greenfield SA. (1994). Direct monitoring of dopamine and 5-HT release in substantia nigra and ventral tegmental area in vitro. *Experimental Brain Research* **100**, 395-406.
- Rosenberg D, Kartvelishvily E, Shleper M, Klinker CMC, Bowser MT & Wolosker H. (2010). Neuronal release of D-serine: a physiological pathway controlling extracellular D-serine concentration. *The FASEB Journal* **24**, 2951-2961.
- Rosini E, Molla G, Rossetti C, Pilone MS, Pollegioni L & Sacchi S. (2008). A biosensor for all D-amino acids using evolved D-amino acid oxidase. *Journal of Biotechnology* **135**, 377-384.
- Rothwell SA, Kinsella ME, Zain ZM, Serra PA, Rocchitta G, Lowry JP & O'Neill RD. (2009). Contributions by a novel edge effect to the permselectivity of an electrosynthesized polymer for microbiosensor applications. *Analytical Chemistry* **81**, 3911-3918.
- Rothwell SA, McMahon CP & O'Neill RD. (2010). Effects of polymerization potential on the permselectivity of poly(*o*-phenylenediamine) coatings deposited on Pt-Ir electrodes for biosensor applications. *Electrochimica Acta* **55**, 1051-1060.
- Sacchi S, Bernasconi M, Martineau M, Mothet J-P, Ruzzene M, Pilone MS, Pollegioni L & Molla G. (2008). pLG72 modulates intracellular D-serine levels through its interaction with D-amino acid oxidase. *Journal of Biological Chemistry* **283**, 22244-22256.

- Schell MJ, Brady Jr RO, Molliver ME & Snyder SH. (1997). D-Serine as a neuromodulator: Regional and developmental localizations in rat brain glia resemble NMDA receptors. *The Journal of Neuroscience* **17**, 1604-1615.
- Schell MJ, Molliver ME & Snyder SH. (1995). D-Serine, an endogenous synaptic modulator: Localization to astrocytes and glutamate-stimulated release. *Proceedings of the National Academy of Sciences* **92**, 3948-3952.
- Shleper M, Kartvelishvily E & Wolosker H. (2005). D-Serine Is the dominant endogenous coagonist for NMDA receptor neurotoxicity in organotypic hippocampal slices. *The Journal of Neuroscience* **25**, 9413-9417.
- Sikka P, Walker R, Cockayne R, Wood MJA, Harrison PJ & Burnet PWJ. (2010). D-Serine metabolism in C6 glioma cells: Involvement of alanine-serine-cysteine transporter (ASCT2) and serine racemase (SRR) but not D-amino acid oxidase (DAAO). *Journal of Neuroscience Research* **88**, 1829-1840.
- Smith SM, Uslaner JM & Hutson PH. (2010). The therapeutic potential of D-amino acid oxidase (DAAO) inhibitors. *The Open Medicinal Chemistry Journal* **4**, 3-9.
- Smith SM, Uslaner JM, Yao L, Mullins CM, Surles NO, Huszar SL, McNaughton CH, Pascarella DM, Kandebo M, Hinchliffe RM, Sparey T, Brandon NJ, Jones B, Venkatraman S, Young MB, Sachs N, Jacobson MA & Hutson PH. (2009). The behavioral and neurochemical effects of a novel D-amino acid oxidase inhibitor compound 8 [4H-thieno [3,2-b]pyrrole-5-carboxylic acid] and D-serine. *Journal of Pharmacology and Experimental Therapeutics* **328**, 921-930.
- Soto A, DelRaso NJ, Schlager JJ & Chan VT. (2008). D-Serine exposure resulted in gene expression changes indicative of activation of fibrogenic pathways and down-regulation of energy metabolism and oxidative stress response. *Toxicology* **243**, 177-192.
- Srinivasan NG, Corrigan JJ & Meister A. (1965). Biosynthesis of D-serine in the silkworm, *bombyx mori*. *Journal of Biological Chemistry* **240**, 796-800.
- Stevens ER, Gustafson EC & Miller RF. (2010a). Glycine transport accounts for the differential role of glycine vs. D-serine at NMDA receptor coagonist sites in the salamander retina. *European Journal of Neuroscience* **31**, 808-816.
- Stevens ER, Gustafson EC, Sullivan SJ, Esguerra M & Miller RF. (2010b). Light-evoked NMDA receptor-mediated currents are reduced by blocking D-serine synthesis in the salamander retina. *Neuroreport* **21**, 239-244.

- Takahashi K, Hayashi F & Nishikawa T. (1997). In vivo evidence for the link between L- and D-serine metabolism in rat cerebral cortex. *Journal of Neurochemistry* **69**, 1286-1290.
- Takeyama K, Yoshikawa M, Oka T, Kawaguchi M, Suzuki T & Hashimoto A. (2006). Ketamine enhances the expression of serine racemase and D-amino acid oxidase mRNAs in rat brain. *European Journal of Pharmacology* **540**, 82-86.
- Tian F, Gourine AV, Huckstepp RTR & Dale N. (2009). A microelectrode biosensor for real time monitoring of L-glutamate release. *Analytica Chimica Acta* **645**, 86-91.
- Tsafack VC, Marquette CA, Leca B & Blum LJ. (2000). An electrochemiluminescence-based fibre optic biosensor for choline flow injection analysis. *Analyst* **125**, 151-155.
- Turpin FR, Potier B, Dulong JR, Sinet PM, Alliot J, Oliet SH, Dutar P, Epelbaum J, Mothet JP & Billard JM. (2011). Reduced serine racemase expression contributes to age-related deficits in hippocampal cognitive function. *Neurobiology of Aging* **32**, 1495-1504.
- Uo T, Yoshimura T, Shimizu S & Esaki N. (1998). Occurrence of pyridoxal 5'-phosphate-dependent serine racemase in silkworm, *bombyx mori*. *Biochemical & Biophysical Research Communications* **246**, 31-34.
- Uptake SJ & Hicks GP. (1967). The enzyme electrode. *Nature* **214**, 986-988.
- Vardigan JD, Huszar SL, McNaughton CH, Hutson PH & Uslaner JM. (2010). MK-801 produces a deficit in sucrose preference that is reversed by clozapine, D-serine, and the metabotropic glutamate 5 receptor positive allosteric modulator CDPPB: Relevance to negative symptoms associated with schizophrenia? *Pharmacology Biochemistry and Behavior* **95**, 223-229.
- Verleysdonk S & Hamprecht B. (2000). Synthesis and release of L-serine by rat astroglia-rich primary cultures. *Glia* **30**, 19-26.
- Verrall L, Walker M, Rawlings N, Benzel I, Kew JNC, Harrison PJ & Burnet PWJ. (2007). D-Amino acid oxidase and serine racemase in human brain: normal distribution and altered expression in schizophrenia. *European Journal of Neuroscience* **26**, 1657-1669.
- Wang LZ & Zhu XZ. (2003). Spatiotemporal relationships among D-serine, serine racemase, and D-amino acid oxidase during mouse postnatal development. *Acta Pharmacologica Sinica* **24**, 965-974.

- Weimar WR & Neims AH. (1977). The development of D-amino acid oxidase in rat cerebellum. *Journal of Neurochemistry* **29**, 649-656.
- Williams SM, Diaz CM, Macnab LT, Sullivan RKP & Pow DV. (2006). Immunocytochemical analysis of D-serine distribution in the mammalian brain reveals novel anatomical compartmentalizations in glia and neurons. *Glia* **53**, 401-411.
- Wilson GS & Gifford R. (2005). Biosensors for real-time in vivo measurements. *Biosensors & Bioelectronics* **20**, 2388-2403.
- Wilson R & Turner APF. (1992). Glucose oxidase: an ideal enzyme. *Biosensors & Bioelectronics* **7**, 165-185.
- Wlaz P, Kasperek R, Wlaz A, Szumilo M, Wrobel A, Nowak G & Poleszak E. (2011). NMDA and AMPA receptors are involved in the antidepressant-like activity of tianeptine in the forced swim test in mice. *Pharmacological Reports* **63**, 1526-1532.
- Wolosker H. (2007). NMDA receptor regulation by D-serine: New findings and perspectives. *Molecular Neurobiology* **36**, 152-164.
- Wolosker H. (2011). Serine racemase and the serine shuttle between neurons and astrocytes. *Biochimica et Biophysica Acta* **1814**, 1558-1566.
- Wolosker H, Blackshaw S & Snyder SH. (1999a). Serine racemase: A glial enzyme synthesizing D-serine to regulate glutamate-N-methyl-D-aspartate neurotransmission. *Proceedings of the National Academy of Sciences* **96**, 13409-13414.
- Wolosker H, Panizzutti R & Miranda JD. (2002). Neurobiology through the looking-glass: D-serine as a new glial-derived transmitter. *Neurochemistry International* **41**, 327-332.
- Wolosker H, Sheth KN, Takahashi M, Mothet J-P, Brady RO, Ferris CD & Snyder SH. (1999b). Purification of serine racemase: Biosynthesis of the neuromodulator D-serine. *Proceedings of the National Academy of Sciences* **96**, 721-725.
- Wood PL, Emmett MR, Rao TS, Mick S, Cler J & Iyengar S. (1989). In vivo modulation of the N-methyl-D-aspartate receptor complex by D-serine: potentiation of ongoing neuronal activity as evidenced by increased cerebellar cyclic GMP. *Journal of Neurochemistry* **53**, 979-981.

Xia M, Liu Y, Figueroa DJ, Chiu C-S, Wei N, Lawlor A-M, Lu P, Sur C, Koblan KS & Connolly TM. (2004). Characterization and localization of a human serine racemase. *Molecular Brain Research* **125**, 96-104.

Yagi K, Naoi M, Harada M, Okamura K, Hidaka H, Ozawa T & Kotaki A. (1967). Structure and function of D-amino acid oxidase: I. Further purification of hog kidney D-amino acid oxidase and its hydrodynamic and optical rotatory properties. *The Journal of Biochemistry* **61**, 580-597.

Yagi K, Tanaka F & Ohishi N. (1975). Structure and function of D-amino acid oxidase: IX. Changes in the fluorescence polarization of FAD upon complex formation. *The Journal of Biochemistry* **77**, 463-468.

Yamada K, Ohnishi T, Hashimoto K, Ohba H, Iwayama-Shigeno Y, Toyoshima M, Okuno A, Takao H, Toyota T, Minabe Y, Nakamura K, Shimizu E, Itokawa M, Mori N, Iyo M & Yoshikawa T. (2005). Identification of multiple serine racemase (SRR) mRNA isoforms and genetic analyses of SRR and DAO in schizophrenia and D-serine levels. *Biological Psychiatry* **57**, 1493-1503.

Yamasaki M, Yamada K, Furuya S, Mitoma J, Hirabayashi Y & Watanabe M. (2001). 3-Phosphoglycerate dehydrogenase, a key enzyme for L-serine biosynthesis, is preferentially expressed in the radial glia/astrocyte lineage and olfactory ensheathing glia in the mouse brain. *Journal of Neuroscience* **21**, 7691-7704.

Yang Q, Atanasov P & Wilkins E. (1999). Needle-type lactate biosensor. *Biosensors & Bioelectronics* **14**, 203-210.

Yasuda E, Ma N & Semba R. (2001a). Immunohistochemical demonstration of L-serine distribution in the rat brain. *NeuroReport* **12**, 1027-1030.

Yasuda E, Ma N & Semba R. (2001b). Immunohistochemical evidences for localization and production of D-serine in some neurons in the rat brain. *Neuroscience Letters* **299**, 162-164.

Yoshikawa M, Shinomiya T, Takayasu N, Tsukamoto H, Kawaguchi M, Kobayashi H, Oka T & Hashimoto A. (2008). Long-term treatment with morphine increases the D-serine content in the rat brain by regulating the mRNA and protein expressions of serine racemase and D-amino acid oxidase. *Journal of Pharmacological Sciences* **107**, 270-276.

Yoshikawa M, Takayasu N, Hashimoto A, Sato Y, Tamaki R, Tsukamoto H, Kobayashi H & Noda S. (2007). The serine racemase mRNA is predominantly expressed in rat brain neurons. *Archives of Histology and Cytology* **70**, 127-134.

Zhang Z, Gong N, Wang W, Xu L & Xu T-L. (2008). Bell-shaped D-serine actions on hippocampal long-term depression and spatial memory retrieval. *Cerebral Cortex* **18**, 2391-2401.

Zhao S, Song Y & Liu Y-M. (2005). A novel capillary electrophoresis method for the determination of D-serine in neural samples. *Talanta* **67**, 212-216.

---

## **2. THEORY**

---

## 2.1 Introduction

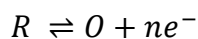
The *in vitro* development and characterisation of a D-ser biosensor which is suitable for *in vivo* characterisation and use is the primary goal of this thesis. Two voltammetric electrochemical techniques were utilised in this work and their theories will be described in this chapter. The first, constant potential amperometry is discussed in Section 2.4, and the second, cyclic voltammetry is discussed in Section 2.5.

The effectiveness and suitability of the various electrode designs are described and compared by their response to the target substrate and interferent species using current density ( $J$ ,  $\mu\text{A}\cdot\text{cm}^{-2}$ ) and other statistical analyses described in Section 2.9. The theory of Michaelis-Menten kinetics, and the important parameters  $K_M$  and  $J_{\text{max}}$ , which are used to describe the activity of enzymes towards a substrate, is detailed in Section 2.7.

Microdialysis, an analytical method which is both complementary to and an alternative of biosensor technology, is detailed in Section 2.6. This technique was used in the modified format of retrodialysis to carry out preliminary *in vivo* characterisation and verification of the final biosensor design.

The theory of mass transport governs a major parameter in all of these techniques, the motion of reactants and products to and from the active surface of the electrode. This theory details the processes which take place in the bulk liquid medium; it is described in Section 2.3.

A second process which underlies all electrochemical techniques is the electron transfer which takes place as a species is oxidised or reduced at the active surface. The general reaction for this process is detailed in Equation 2-1.



**Equation 2-1**

$O$  and  $R$  are the oxidised and reduced species respectively and  $n$  is the number of electrons transferred in the reaction. Distribution of charge on the active surface of the electrode and its interaction with the bulk media also play a role, as it is the applied potential which drives this process, and are detailed briefly in Section 2.2.

## 2.2 Charge Distribution at the Active Surface

Voltammetry involves the application of an electric potential (e.m.f.), with respect to a fixed potential, to an electrode in order for the desired reduction or oxidation processes to take place at its surface. It is well known that due to electrostatic repulsion all charge in a conductor resides on its outside surface. This charge on the surface of the electrode will induce a charge distribution in the electrolyte. The distribution of charge within the electrolyte is complex, depending on several factors including electrode potential and background electrolyte concentration among other things.

There are three classical models to describe how the space-charge region behaves; the Helmholtz model, the Gouy-Chapman model and the Stern model. In all of these models the interface between the electrode and the electrolyte may be considered as a two dimensional space, regardless of the geometry of the interface. The following is a brief description of more detailed discussions (Brett & Brett, 1993; Bard & Faulkner, 2001; Monk, 2001; Gileadi & Urbakh, 2003).

The Helmholtz model envisages the interface region as planes of charge containing the electrons of the applied potential and the counter-ions in the electrolyte separated by an ion-free solvent layer. This is sometimes called the ‘compact layer’ or Helmholtz layer and is indicative of the closest distance of approach by surface-inactive ions. It does however not take into account electrolyte concentration which can have profound effects at lower concentrations.

Gouy and Chapmann independently proposed a treatment based on a non-linear distribution of charge extending into the electrolyte, based around the Poisson-Boltzmann equation for a system of electric charges. This ‘diffuse’ model took into account applied potential and electrolyte concentration, however experimental results and its predictions varied greatly.

Stern proposed a combination of both of these models. This model had a compact layer of charge and a diffusion of charge into the electrolyte. It is most commonly used in a form later proposed by Grahame which describes the potential drop across the interface as a sum of the compact and diffuse layer. This is most successful in experimental prediction as it treats the compact layer as independent of the concentration of the

inactive electrolyte layer while the diffuse layer is dependent on the background electrolyte concentration.

For the purposes of the experiments described within this thesis the background electrolyte concentration was kept as a sufficiently high level ( $> 100$  mM, (Brett & Brett, 1993)) so as to negate the predictive inaccuracies of the Helmholtz model. Thus, all charge transfer processes can be treated as taking place at the outer Helmholtz plane. The diffuse layer is considered negligible and the potential drop occurs in a linear fashion across the Helmholtz layer.

### 2.3 Mass Transport

As a particular reduction or oxidation reaction occurs, at the Helmholtz plane, a concentration differential is created. This is due to the formation of products and usage of reactants which produces a spatial concentration difference with the bulk solution. The solution will act to address this concentration imbalance, and three different transport mechanisms can be effected, which are summarised in the following discussion (Brett & Brett, 1993; Bard & Faulkner, 2001; Monk, 2001; Calvo, 2003). Expanding Equation 2-1 and examining the expression for the rate of an electrode reaction (Equation 2-5) we can see the importance of this imbalance and the transport mechanisms.

$$R_{bulk} \rightarrow R_{electrode}$$

**Equation 2-2**

$$R_{electrode} \rightarrow ne^{-} + O_{electrode}$$

**Equation 2-3**

$$O_{electrode} \rightarrow O_{bulk}$$

**Equation 2-4**

$$rate = k_a[R]_{electrode} - k_c[O]_{electrode}$$

Equation 2-5

The transport mechanisms are diffusion, convection and migration. Diffusion is the movement of species down a concentration gradient, convection is the bulk movement of the solution due to an applied mechanical force or thermodynamic effect, and migration is the movement of ions down a potential gradient. Migration was negated for this work due to the presence of a large amount of background electrolyte and can thus be discounted. All measurements, unless otherwise specified were taken in quiescent solutions and this convection effects were also negligible. This leaves diffusion as the primary means of transport of species within the bulk solution.

### 2.3.1 Diffusion

Diffusion is a natural movement of species from an area of high concentration to an area of low concentration and applies to neutral or charged species. The phenomenon of diffusion is described by Fick's 1<sup>st</sup> Law (see Equation 2-6). This states that the flux of the species,  $J$ , is proportional to the change in the concentration,  $c$ , with respect to the direction  $x$ , which is also called the concentration gradient,  $\frac{\partial c}{\partial x}$ . They are related by the proportionality constant  $D$ , the diffusion coefficient, and this can be determined experimentally or estimated by using a variety of relations.

$$J = -D \frac{\partial c}{\partial x}$$

Equation 2-6

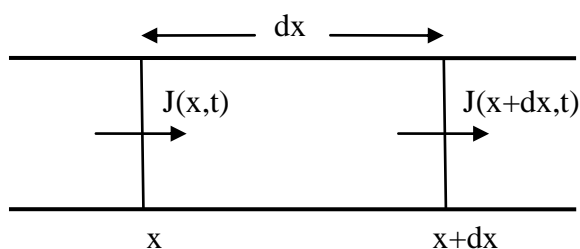


Figure 2-1

A volume segment  $dx$  of solution with a concentration gradient, where a flux  $J$  is flowing from the area of higher concentration to the area of lower concentration.

By considering Fick's 1<sup>st</sup> Law (Equation 2-6) and Figure 2-1 we can derive Fick's 2<sup>nd</sup> Law (see Equation 2-7) which elucidates the change in concentration with respect to time.

$$\frac{\partial c}{\partial t} = D \frac{\partial^2 c}{\partial x^2}$$

**Equation 2-7**

As a reaction proceeds it is usual for the concentration of the reactants to decrease in time. However, in the case of microelectrodes (diameters in the range 5 to 300  $\mu\text{m}$ ) where only minimal substrate is consumed and currents are small a steady state response is achieved and there is no change in concentration over time, i.e.  $\frac{\partial c}{\partial t} = 0$  (O'Neill *et al.*, 1998). However, the microelectrodes used in this project were not of the size, 0.1 to 50  $\mu\text{m}$ , where their diffusion properties were altered and planar diffusion became mixed with hemispherical diffusion.

Thus, for the purposes of calculating the variation of current with time, the disk electrodes may be considered to be planar and uniformly accessible to the bulk solution. This results, from Fick's 2<sup>nd</sup> Law, in the Cottrell equation (see Equation 2-8)

$$I = nFAJ = \frac{nFAD^{\frac{1}{2}}c_{\infty}}{(\pi t)^{\frac{1}{2}}}$$

**Equation 2-8**

where  $I$  is the current measured at time  $t$  at the electrode of surface area  $A$ ,  $n$  is the number of electrons,  $F$  is the Faraday constant,  $J$  is the flux and  $D$  is the diffusion coefficient.  $I$  is directly proportional to the concentration of the substrate in the bulk solution  $c_{\infty}$ .

When considering cylinder electrodes it is necessary to change the coordinate system from the simple one dimensional system previously considered for planar electrode surfaces. To do this Fick's 1<sup>st</sup> Law is altered, allowing inclusion of the Laplacian Operator,  $\nabla$ (see Equation 2-9). This operator, in the appropriate form, allows one to

change coordinate systems freely. As a consequence Fick's second law is also altered to the form shown in Equation 2-10.

$$J = -D\nabla^2 c$$

**Equation 2-9**

$$\frac{\partial c}{\partial t} = D\nabla^2 c$$

**Equation 2-10**

For an electrode of a cylindrical shape with a diameter greater than 50  $\mu\text{m}$  the Laplacian Operator takes the form of (Brett & Brett, 1993)

$$\frac{\partial}{\partial r} + \left(\frac{1}{r}\right)\left(\frac{\partial}{\partial \varphi}\right) + \frac{\partial}{\partial x}$$

**Equation 2-11**

In order to solve Fick's 2<sup>nd</sup> Law, and thus find the flux variation in time and the diffusion limited current, it is necessary to define conditions for the system to obey. These conditions specify concentration and/or spatial characteristics, and are defined in relation to time, i.e. at  $t=0$ .

Solving Fick's 1<sup>st</sup> Law for a species  $R$  at the surface of an electrode it is found that the flux,  $J_R(0,t)$ , is proportional to the current density,  $\frac{i}{A}$ . This is because the total number of electrons transferred per unit time must be proportional to the quantity of  $R$  reaching the surface in that time  $t$ , i.e.

$$-J_R(0,t) = \frac{i}{nFA} = D_R \left[ \frac{\partial c_R(x,t)}{\partial x} \right]_{x=\infty}$$

**Equation 2-12**

$A$  is the surface area of the electrode,  $F$  is the Faraday constant,  $n$  is the number of electrons transferred per molecule that reacts at the surface and  $i$  is the current.

The solutions to Equation 2-12 and Equation 2-10 can determine the current flowing across the electrode-solution interface as a function of time, concentration or other parameters for any electrode geometry.

## 2.4 Amperometry

The most frequently utilised electrochemical method in this project, constant potential amperometry (CPA) is the recording of the current produced by the oxidation or reduction of an analyte under the conditions of a fixed applied potential. Diffusion is the only form of mass transport considered to be occurring within the system (see Section 2.3). After the initial application of a fixed voltage the capacitance currents associated with the setup of the charged layers at the active surface (see Section 2.2) decay to almost zero, resulting in steady-state currents. The potentials used in the project were chosen such that all substrate reaching the surface was oxidised, also known as overpotential. Thus, the amperometric current measured is directly proportional to analyte concentration at all times. This current is the sum of two different contributing factors; see Equation 2-13, the Cottrell current and the steady-state current.

$$I_{amp} = i_{cot} + i_{ss}$$

**Equation 2-13**

The Cottrell component disappears for large values of time,  $t$ , and the steady-state current predominates. It is these diffusion-limited steady-state currents which are reported in this work and for a reversible or irreversible reaction they are given by Equation 2-14 (Forster, 1994)

$$i_{ss} = \frac{nFADc}{r}$$

**Equation 2-14**

where  $n$  is the number of electrons transferred,  $F$  is the Faraday constant,  $A$  is the surface area,  $D$  is the diffusion coefficient,  $c$  is the concentration and  $r$  is the radius of the electrode.

However,  $i_{ss}$  is influenced by many subtleties of the system (Dayton *et al.*, 1980) including, for instance, the thickness of insulation. As such a geometric correction factor,  $G$ , is included to take account of these influences resulting in the modified Equation 2-15

$$i_{ss} = G \frac{nFADc}{r}$$

**Equation 2-15**

Despite theoretical reports of true steady-state behaviour not being reached by microelectrodes, a quasi-steady-state is achieved (Aoki, 1993). This is dependent on, and proportional to, the radius of the electrode. The results reported in this thesis demonstrate effective steady-state currents within a certain time frame.

## 2.5 Cyclic Voltammetry

Cyclic voltammetry (CV) involves the application of a triangular waveform potential profile (see Figure 2-2). Starting at an initial potential,  $E_i$ , where no oxidation occurs the potential is increased at a constant rate,  $v$ , to a maximum value,  $E_{max}$ , before being decreased at the same rate until the initial potential is reached.

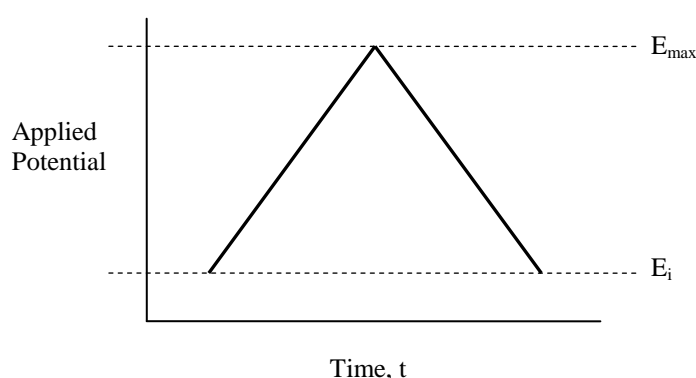


**Figure 2-2**

**A cyclic voltammogram potential waveform.**

As the potential is decreased back to the initial starting potential any species that was oxidised on the forward sweep is reduced. There is a delay between scans to prevent the

previous scan influencing the next scan and measurements are performed in quiescent solution meaning, as with CPA, all mass transport is diffusion controlled.

Similar to CPA, CV produces two kinds of current at the active surface. However, in the case of CV the capacitance current never dissipates as the applied e.m.f. is continuously varied. This results in constant changes to the double layer charge. As a result it is necessary to subtract the background current, taken before addition of an analyte to the solution, from the overall current. This enables observation of the Faradaic current resultant from any electrochemical processes and the characteristic CV of a particular analyte.

Figure 2-2 describes a reversible system, which when applied to CV results in a current-potential profile similar to that illustrated in Figure 2-3. At  $E_i$  only  $R$  is present in the system and no electron transfer is taking place. As the potential is swept forward electron transfer is induced once appropriate potential values are reached. Initially the rate of transfer, or the rate of oxidation, is limited by the potential. Once a sufficient potential is reached then all  $R$  reaching the surface is oxidised to  $O$ . Further increases in potential from this point do not result in an increased rate of reaction, and hence larger currents, as the process is now being controlled by diffusion. This is the case until the point is reached where potential inversion begins. The maximum anodic current,  $i_{pa}$ , is a balance between the increasing electrochemical rate constant,  $k_{ox}$ , and decreasing surface concentration of  $R$ . Before  $E_{pa}$  is reached a rapidly increasing  $k_{ox}$  controls  $i$ , and at potentials higher than  $E_{pa}$  diffusion controls the rate of reaction.

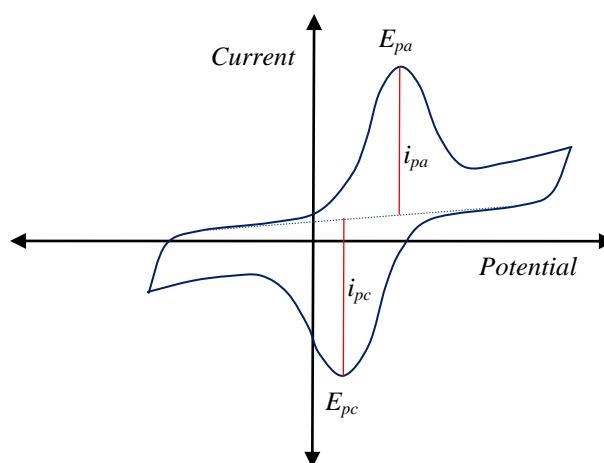


Figure 2-3

A typical current-potential profile for a CV of a reversible redox substrate.

On the reverse sweep, the electroactive species is reduced from  $O$  back to  $R$  in a manner similar to the oxidation process.

## 2.6 Microdialysis

A technique first carried out by Prof. Urban Ungerstedt in the Karolinska Institut in Sweden (Ungerstedt & Pycock, 1974), microdialysis involves the implantation of a probe into the living brain or tissue. Based on dialysis theory the probe has a semi-permeable membrane at its tip. The membrane is manufactured to allow passage of water and small solutes up to a specified cut-off point, usually 10 – 30 kD molecular weight. The passage of molecules through the membrane allows sampling of metabolites, neurotransmitters and other analytes of interest from the living brain. Perfused with artificial cerebrospinal fluid (aCSF), designed to mimic the ionic concentration of the brain, the perfusate equilibrates with the extracellular fluid (ECF) by osmotic diffusion across the membrane. The dialysate can then be collected and analysed using, for example, high performance liquid chromatography (HPLC).

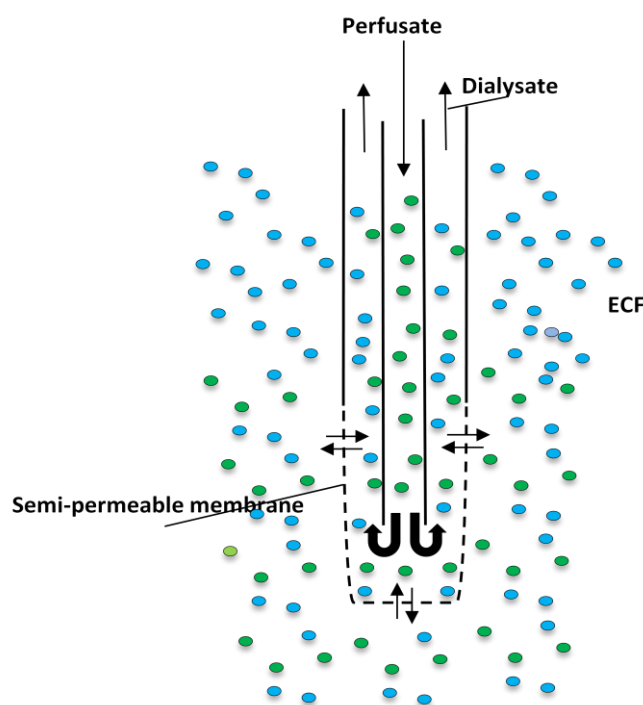


Figure 2-4

A microdialysis probe, showing the flow of molecules out of the perfusate into the ECF and vice versa.

The most important use of microdialysis has been its employment in preclinical neuropsychopharmacology, which has been extensively reviewed (Darvesh *et al.*, 2011; Zhang *et al.*, 2012), where it has been used widely in rodents. It is used to study the

concentration of neurotransmitters and transporter molecules, and consequent changes following the delivery of drugs of interest to the brain environment. Of particular interest is the study of monoamines, like dopamine, norepinephrine and serotonin, and amino acids, including glutamate and acetylcholine. The study of the altered concentrations of these molecules following treatment with psychostimulants and potential/existing treatments for diseases such as AD, PD and schizophrenia has become an industry of its own.

Microdialysis is utilised in the measurement of various analytes where brain trauma has occurred (Hillered & Persson, 1999) in order to monitor surgical procedures (Bhatia *et al.*, 2006), recovery and post incident changes in certain analytes (Feuerstein *et al.*, 2010) which can indicate secondary ischemia and deterioration in the patient's condition. However, it does have disadvantages, the primary one being damage caused to tissues peripheral to the probe as a result of fibrosis (Mathy *et al.*, 2003) and damage to the blood brain barrier (Grabb *et al.*, 1998; Groothuis *et al.*, 1998). Attempts are being made to incorporate sensor technology in-line with microdialysis in order to remove the need for coupled HPLC monitoring as this means analysis is often several minutes behind the real-time events which sensors would be able to detect (Rogers *et al.*, 2011).

For this project microdialysis was used for the delivery of substances into the environment of a biosensor. The two devices were co-implanted with proximity of less than 1 mm (Yang *et al.*, 1998). As explained in Section 1.2, this distance is normally required to ensure the electrode was not enveloped in the region of brain injury caused by the probe (Kadota *et al.*, 1994). However for the purposes of the experiments carried out within this project there was little interest in the natural response of analyte levels and the brain to the procedures carried out. Rather perfusions were carried out in order to elicit a response indicative of a correctly functioning biosensor. Requiring only this ability to create a change in response did not require normal probe-electrode spacing to be adhered to as saturation of the area around the electrode was generally sufficient for the experiments performed.

## 2.7 Enzymes

### 2.7.1 Introduction

Enzymes are biological catalysts; they increase the rate of reaction without themselves being used up in the reaction. They achieve this by lowering the activation energy of the particular reaction of interest, but they do not change the position of equilibrium. Highly complex in nature and structure, enzymes are usually highly specific, reacting with generally only one substrate and having minimal affinity for other species. Due to this specificity they are extremely desirable substances for incorporation into biosensor designs. The immobilisation of a stable enzyme on a biosensor allows its corresponding substrates concentration to be monitored indirectly by electrochemical means. The use of the enzyme D-amino acid oxidase is central to this thesis and the fabrication of a D-ser biosensor.

Enzymes are constructed from long chains of amino acids which are folded into complex structures to produce the active site where the substrate specific reaction takes place. The combination of their size and multiple amino acid segments enable an enzyme to bind very specifically, via multiple active sites, to its particular substrate. It is the flavin moiety which binds molecular oxygen and converts the enzyme back to its original form so that it may interact with another molecule of substrate. D-amino acid oxidase, as already discussed, is an oxidoreductase enzyme which incorporates a flavin moiety, FAD, acts on the CH-NH<sub>2</sub> group and must have O<sub>2</sub> present as an accepting group. The general scheme of an oxidase enzyme reaction process at the surface of a first generation biosensor is illustrated in Figure 2-5. Hydrogen peroxide, produced when the FAD is oxidised, reacts at the electrode surface to produce a current and is thus called the signalling molecule.

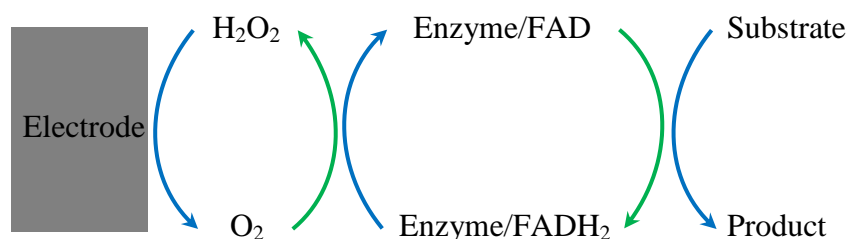
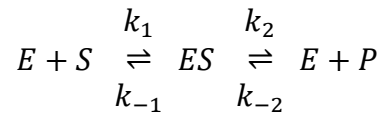


Figure 2-5

Generalised reaction mechanism of an oxidase enzyme on a first generation biosensor. The green arrows represent reduction and blue arrows indicate oxidation.

### 2.7.2 Enzyme Kinetics

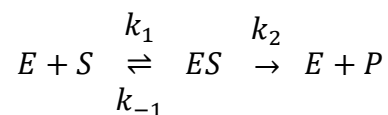
The highly complex nature of the active site of an enzyme is what allows it to selectively react with only one or a limited number of substrates. The complex structure leads to complex reaction mechanisms with many variables. It is, however, possible to treat these reactions in a generalised fashion in order to determine the overall kinetic parameters of a specific reaction.



**Equation 2-16**

Equation 2-16 is the general enzymatic kinetic equation, where  $E$  is the enzyme,  $S$  is the substrate,  $ES$  is the enzyme-substrate complex,  $P$  is the product and  $k$  represents the rate constant for each of the reactions.

Initially it is found in a reaction that the concentration of the product is low and thus the reverse reaction of product to the enzyme-substrate complex, indicated by  $k_2$  is negligible. This yields the result shown in Equation 2-17:



**Equation 2-17**

It was in 1913 that Michaelis and his student Menten formulated a method of applying the steady-state approximation to the formation and destruction of  $ES$ , and subsequently derive a rate equation for an enzymatic catalysis process (Michaelis & Menten, 1913). The rate of change of  $ES$  is of primary importance to this process. This rate and an expression for the total enzyme concentration,  $[E]_0$ , are indicated in Equation 2-18 and Equation 2-19 respectively:

$$\frac{d[ES]}{dt} = k_1[E][S] - k_{-1}[ES] - k_2[ES]$$

**Equation 2-18**

$$[E] = [E]_0 - [ES]$$

**Equation 2-19**

where [ ] indicates concentration. Combining these two equations and applying the steady-state approximation, where  $\frac{d[ES]}{dt} = 0$ , it is found:

$$k_1[E]_0[S] - k_1[ES][S] - k_{-1}[ES] - k_2[ES] = 0$$

**Equation 2-20**

From Equation 2-20 it is possible to isolate the concentration of the enzyme-substrate complex, giving Equation 2-21:

$$[ES] = \frac{[E]_0[S]}{[S] + \frac{k_{-1} + k_2}{k_1}}$$

**Equation 2-21**

Michaelis and Menten replaced the constants,  $\frac{k_{-1} + k_2}{k_1}$ , with the Michaelis constant  $K_M$  to further simplify the equation to:

$$[ES] = \frac{[E]_0[S]}{[S] + K_M}$$

**Equation 2-22**

But the overall rate of reaction,  $v$ , is solely dependent on the concentration of the enzyme-substrate complex and the rate of formation of products,  $k_2$ , thus:

$$v = k_2[ES]$$

**Equation 2-23**

and therefore,

$$v = \frac{k_2[E]_0[S]}{[S] + K_M}$$

**Equation 2-24**

If the concentration of the substrate is very high compared to the enzyme then the enzyme will only exist as the complex  $ES$  and the rate of reaction can reach its maximal initial velocity,  $V_{max}$ . Thus since  $[S] \gg K_M$

$$V_{max} = k_2[E]_0$$

**Equation 2-25**

Further assuming that substrate is actually present in much higher concentration than the enzyme, then the initial substrate concentration,  $[S]_0$ , is much greater than the initial enzyme concentration,  $[E]_0$ , and therefore we can say  $[S] \cong [S]_0$ . All together, combining this assumption with Equation 2-24 and Equation 2-25 we arrive at the Michaelis-Menten equation:

$$v = \frac{V_{max}[S]_0}{[S]_0 + K_M}$$

**Equation 2-26**

where  $v$  is the rate of reaction,  $V_{max}$  is the maximal rate of reaction,  $[S]_0$  is the initial substrate concentration and  $K_M$  is the Michaelis constant.

When experimental values of  $v$  are plotted against  $[S]_0$ , as shown in Figure 2-6, we observe a rectangular hyperbola. From this graph both  $V_{max}$  and  $K_M$  can be obtained as shown, with  $K_M$  being  $[S]$  where  $v = \frac{V_{max}}{2}$ .

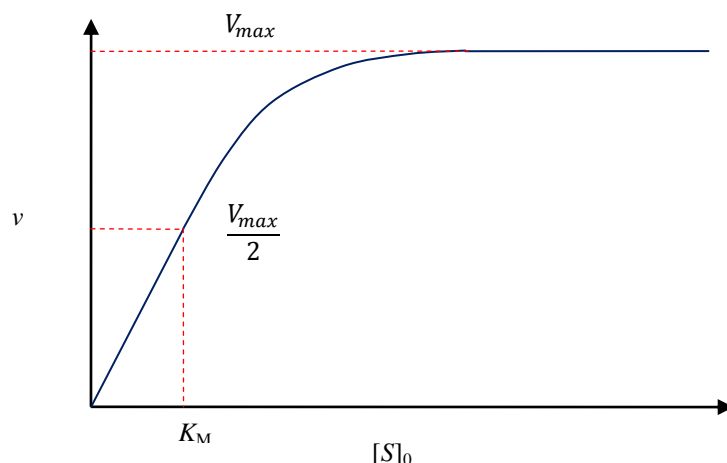


Figure 2-6

Graph of the reaction rate,  $v$ , against substrate concentration,  $[S]_0$ , for an enzyme concentration,  $[E]_0$  for a single substrate enzyme catalysed reaction resulting from the Michaelis-Menten equation (Equation 2-26).

While Michaelis-Menten kinetics (M-M) is a very useful tool, in its simplicity and approximations it does fail to take account of certain circumstances that do occur. One of these situations is where more than one molecule of substrate binds to a single molecule of enzyme. Where all enzyme sites are similar and independent the response will still be the hyperbolic curve illustrated. However, in circumstances where the phenomenon of cooperativity is present, the binding of a substrate to one active site on the enzyme increases the affinity of other sites on the enzyme to bind more molecules of substrate (Ricard & Cornish-Bowden, 1987). In this case an altered version of the Michaelis-Menten equation is used to quantify the deviation from hyperbolic, idealised kinetics. This constant  $\alpha$  was introduced following the work of Hill on the aggregation of haemoglobin and oxygen (Hill, 1910; Stryer, 1988). The new form of the equation is called Michaelis-Menten Hill-type kinetics (M-M-H) and is described as follows:

$$i = \frac{V_{max}}{1 + \left(\frac{K_M}{[S]}\right)^\alpha}$$

Equation 2-27

Here  $i$  indicates the current observed from the oxidation of hydrogen peroxide at the surface of the electrode. Values of  $\alpha$  that are smaller than 1 indicates negative cooperativity. Conversely an  $\alpha$  value  $>1$  means there is positive cooperativity which means a larger change in rate of reaction with  $[S]$  and thus increased sensitivity, if only over a particular range of  $[S]$ .

## 2.8 Structures and Reactions

### 2.8.1 D-Serine

D-amino acids are oxidised by D-amino acid oxidase into the corresponding imino acid. The imino acid then reacts with a water molecule to produce an  $\alpha$ -keto acid and ammonia. In the case of D-ser the imino acid produced is imino-pyruvic acid, and the  $\alpha$ -keto acid is  $\beta$ -hydroxypyruvic acid. The reaction is illustrated in Figure 2-7:

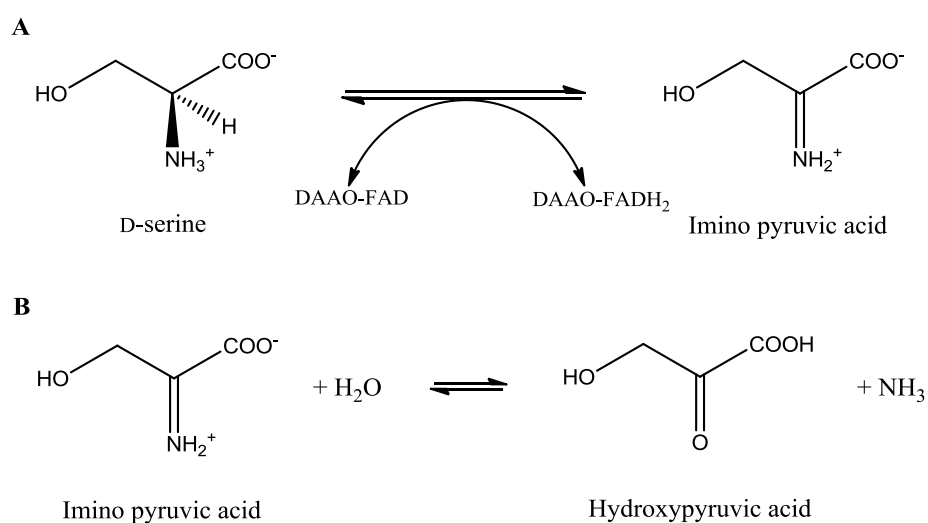


Figure 2-7

Mechanism for the oxidation of D-ser to A) its imino acid and B) further to its correspond  $\alpha$ -keto acid with the production of ammonia. The FAD moiety attached to D-amino acid oxidase is also reduced to FADH<sub>2</sub> in the first step.

### 2.8.2 Flavin Adenine Dinucleotide

A large molecule (Figure 2-8) located at the heart of the structure D-amino acid oxidase, it is actually the FAD unit which is reduced as a D-ser molecule is oxidised. The FAD is then re-oxidised by molecular oxygen with accompanying production of hydrogen peroxide, see Figure 2-9:

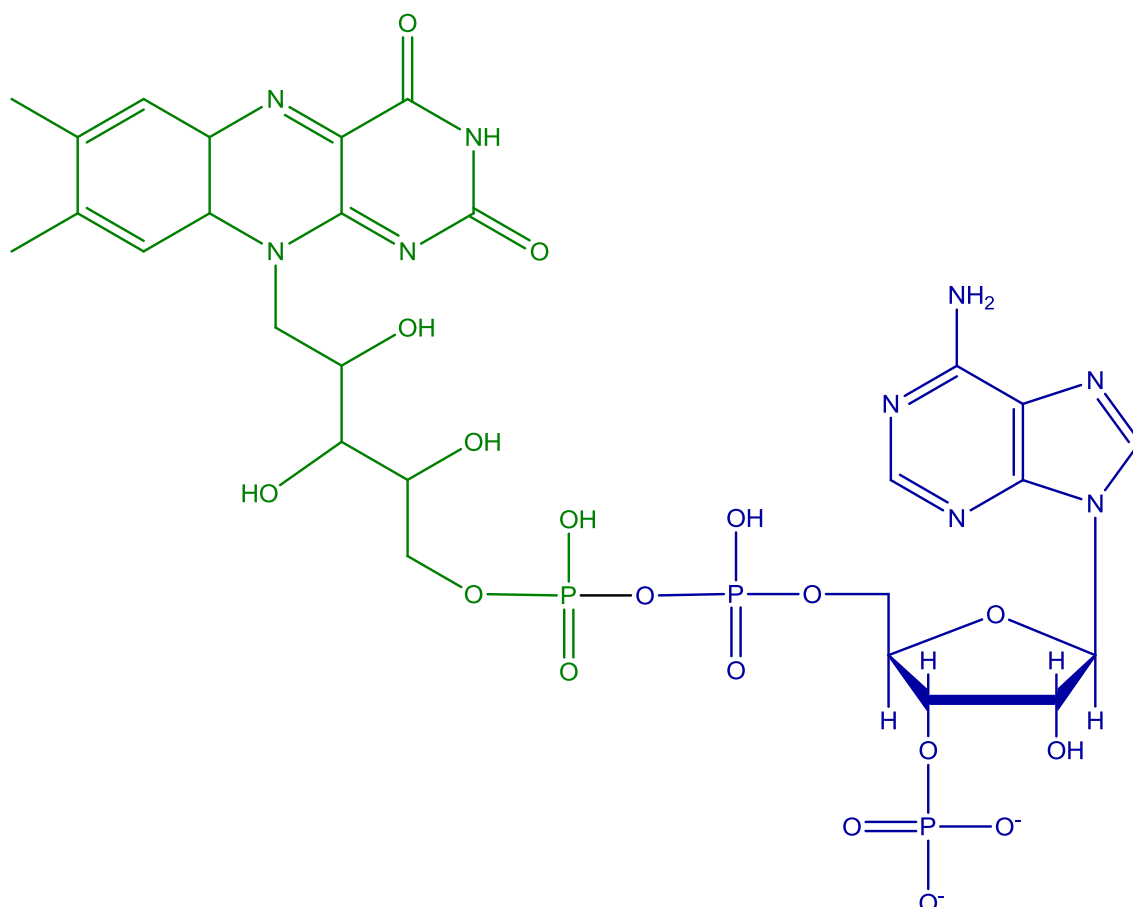


Figure 2-8

Structure of the entire FAD molecule, showing the flavin mononucleotide (FMN) unit in green and the adenine monophosphate (AMP) group in blue (Stryer, 1988).

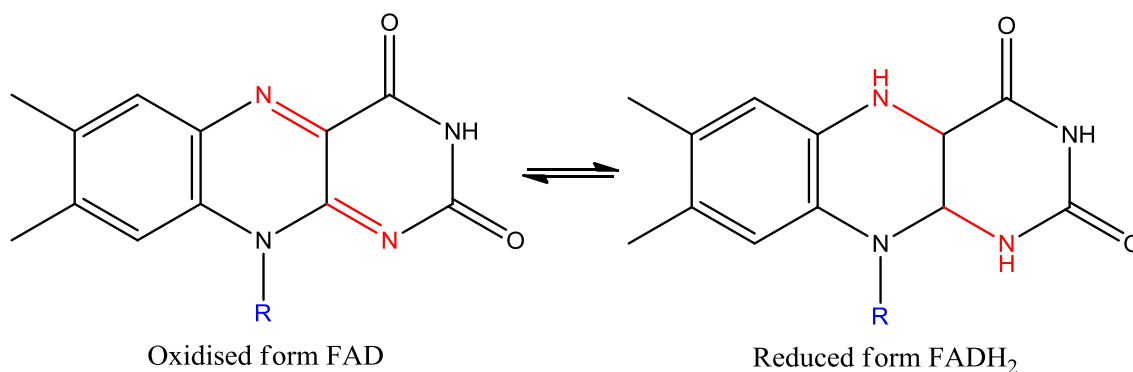


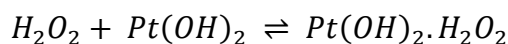
Figure 2-9

Structures of the reactive parts of the FAD and FADH<sub>2</sub> moieties (Stryer, 1988).

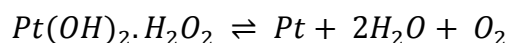
### 2.8.3 Hydrogen Peroxide

First generation biosensors utilising enzymes produce stoichiometrically equivalent amounts of hydrogen peroxide as substrates react with the enzyme. The electrode material widely used for the detection of this hydrogen peroxide is platinum (Hall *et al.*, 1998a). The process is well known and characterised as a two-electron transfer that was first proposed by Hickling and Wilson and then backed up with further evidence by

Lingane and Lingane. (Hickling & Wilson, 1951; Lingane *et al.*, 1963). It is based on a thin oxide film forming on the surface of the platinum, with which the  $H_2O_2$  interacts, similar to that proposed for palladium (Gorton, 1985). The mechanism for the oxidation is outlined below in three equations (Hall *et al.*, 1998b):



Equation 2-28



Equation 2-29



Equation 2-30

The complex formation between the oxide film and hydrogen peroxide is described in Equation 2-28. Equation 2-29 describes the breakdown of this complex releasing water and oxygen and leaving behind an unoxidised metal surface. Finally in Equation 2-30 it is seen that the water recombines with the platinum surface to release two protons and two electrons. It is these electrons which produce the current that is measured and related directly to the concentration of substrate in solution.

#### 2.8.4 Electropolymerisation of *o*-Phenylenediamine

*o*-phenylenediamine is the most widely studied polymer, of the phenylenediamine derivatives, for use as an interference rejection layer in biosensor design (Rothwell *et al.*, 2010). It functions on a size exclusion principle whereby the pores within its structure are small enough for  $H_2O_2$  and gaseous molecules can pass freely through the pores but electroactive substances are blocked because of their substantially larger size. Yet despite extensive research (Li *et al.*, 2002) little is still known about the structure of poly-*o*-phenylenediamine (PPD) and the mechanism by which it occurs, particularly under neutral conditions as in this work. However, two proposed structures have emerged which appear to be dependent on the conditions the polymerisation is carried out under. Under conditions of low pH (<1) it is believed that the structure is a

phenazine-like ‘ladder’ structure, see Figure 2-10. This is the most commonly reported structure, supported by work on infrared, Raman and UV-Vis spectroscopy, quartz microcrystal balance studies, radiometry and electrochemical techniques (Bilal *et al.*, 2011).

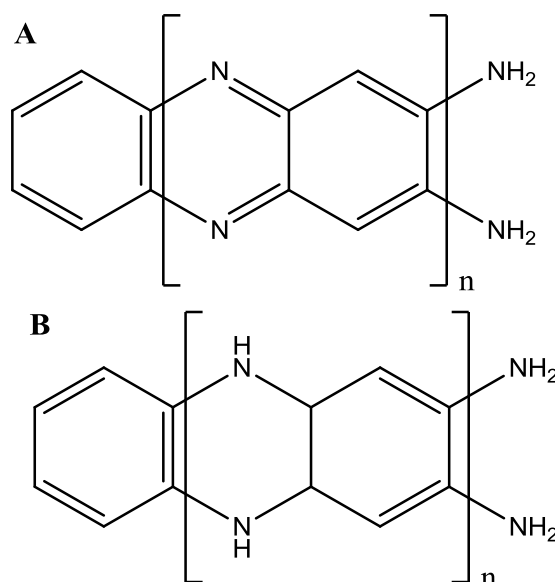


Figure 2-10

Proposed phenazine “ladder” like structures of PPD where A is the oxidised form (Sayyah *et al.*, 2009) and B has not been oxidised at all (Bilal *et al.*, 2011).

With increasing pH the extent of conjugation decreases as more free amino groups are detected on the surface (Losito *et al.*, 2003). The presence of these ‘defects’ in the phenazine-like structure possibly as main repeating units could give an indication of the material produced under slightly acidic or neutral condition, although there is no or very limited information available (Losito *et al.*, 2001). The more ‘open’ or polyaniline-like 1,4-substituted benzenoid-quinoid structure (Yano, 1995) can be seen in Figure 2-11.

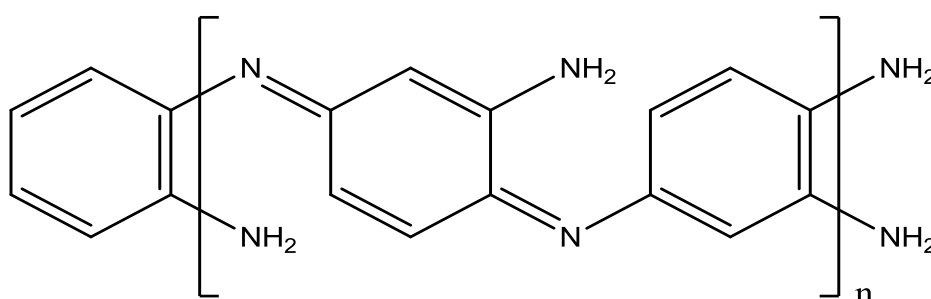


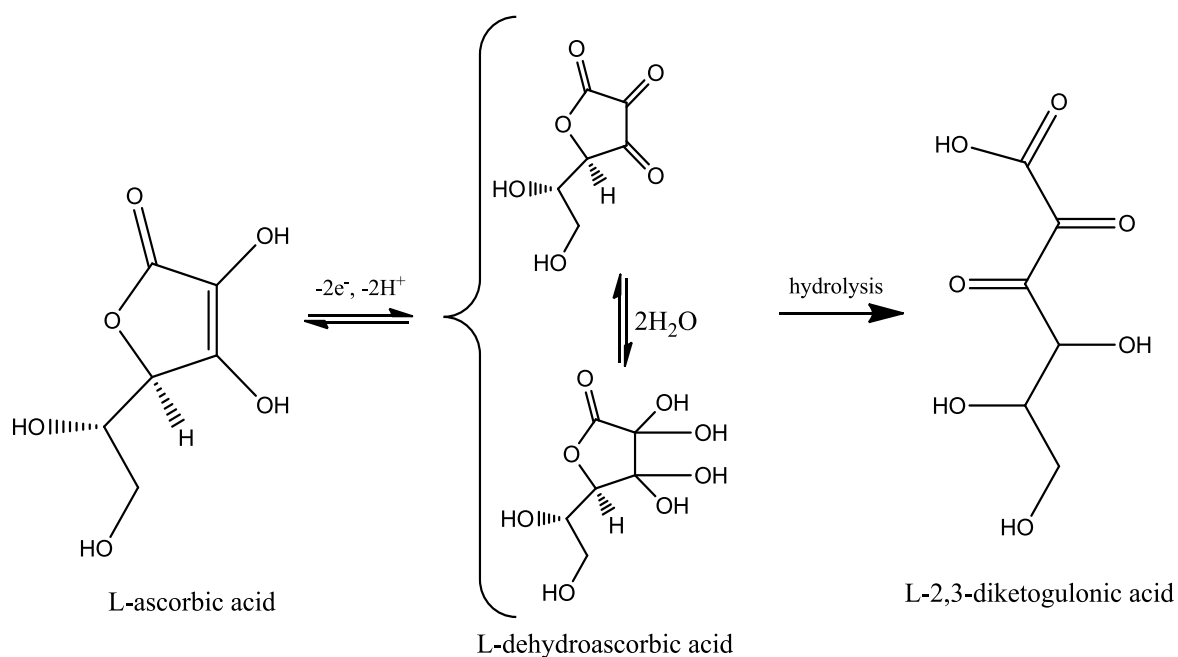
Figure 2-11

Proposed 1,4-substituted benzenoid-quinoid structure of PPD, ‘open’ structure (Losito *et al.*, 2001).

A mechanism for the polymerisation of *o*-PD to PPD with the ‘open’ structure has been proposed (Sayyah *et al.*, 2009) and it is illustrated below in Figure 2-12:



(O'Neill *et al.*, 1998). As such it is used as a model interferent species in biosensor design. The reaction mechanism is described in Figure 2-12.



Reaction mechanism for the oxidation of AA to the electro-inactive product L-2,3-diketogulonic acid

## 2.9 Data Analysis

Experimental calibrations in this project were carried out using CPA. Analysis of the data collected began with the smoothing of data using an in-built function in LabChart 6. This function used a Bartlett Triangular Window method to filter the data and reduce noise which was inherent in the system. The triangular window is resultant from the convolution of two rectangular *sinc* windows, and is an apodisation function. Thus, the Bartlett window is a  $sinc^2$  function which reduces an interferogram smoothly to zero at the edges of the sampled region. The width of the window that the function was applied to was  $2n+1$ , where  $n$  was the number of readings taken per second during the calibration.

Post smoothing a time averaged response was extracted using LabChart 6. This sample was taken from a steady-state response period over a time period of *ca.* 20 seconds. The extracted data samples were then brought into GraphPad Prism 5 for further analysis.

## 2.9.1 Linear and Non-Linear Regression

Regression fitting involves finding a line or a curve which minimises the sum of the squares of the perpendicular distances of the points to the fitted line or curve. Linear regression fits were applied to calibrations for response to AA and H<sub>2</sub>O<sub>2</sub>. Non-linear regression fits taking the form of the Michaelis-Menten equation and the modified Hill-Type equation (see Section 2.7.2) were applied to enzymatic calibrations for response to D-ser. Upon fitting of a regression to a particular set of data various other forms of statistical analyses were used to glean further information from the data and to enable comparisons to be drawn.

## 2.9.2 Statistical Analysis

### 2.9.2.1 *t*-Tests

Parametric *t*-tests allow the comparison of two pieces of information with a quantitative examination of the statistical difference between the results. Two types of *t*-test were used during this work. Where possible it was favourable to use paired *t*-tests, which examined electrodes that differed only by post production intervention, for example time or protein treatment. Otherwise unpaired *t*-tests were used for electrodes which differed by production treatment, for example the application of different substances or layers. When conducting unpaired *t*-tests Welch correction was used where deemed necessary. GraphPad InStat was used for all *t*-tests.

### 2.9.2.2 *P*-values

The assigned *P*-value is a probability, thus its value is  $0 \leq P \leq 1$ . It describes the statistical difference between two values and allows one to decide whether or not it is significantly different. The smaller the *P*-value the more likely it is to be significantly different, small values indicate that the sampled values have a difference that is unlikely due to chance. A confidence interval of 95 % was used throughout this project meaning a *p*-value of  $< 0.0500$  was required to indicate a significant difference between the two data sets involved. It was denoted graphically by \*. However, confidence values of 99 %,  $p < 0.0100^{**}$  and 99.9 %,  $p < 0.0010^{***}$ , were also used in various instances to indicate differences of even greater significance.

### 2.9.2.3 $R^2$ values

Known as the coefficient of correlation, the  $R^2$  value is a measure of the goodness of fit of a data set to a regression (linear and non-linear). Like the  $P$ -value it is a unit-less value with the range  $0 \leq R^2 \leq 1$ . A value of 1 indicates a perfect fit, where all points lie directly on the line or curve which is proposed as the fit. A value of 0 indicates that there is no relationship between the X and Y values in the data set and that it is not possible to ascribe the chosen trend, linear or non-linear, to them.

### 2.9.2.4 One-Way ANOVA

One-way Analysis of Variance (ANOVA) with standard Tukey-Kramer Multiple Comparison tests was used to compare results of treatment. In this case the electrodes have not been modified since fabrication save a ‘treatment’ of time, being stored in a particular substance, or multiple calibrations. The multiple calibrations could be conducted as per normal (see Section 3.6) or with, for instance, an altered temperature or pH. This is a better form of analysis as it takes into account that the same electrodes are being examined and each result is dependent on previous results and the ‘treatments’ applied. Results analysed by this method will only be displayed as  $p > 0.0500$ ,  $p < 0.0500^*$ ,  $p < 0.0100^{**}$  and  $p < 0.0010^{***}$ .

## 2.9.3 Current Density

In this project electrodes of varying sizes and geometries are used and it is important to be able to compare them on an equal footing. In order to do that in this thesis all current values were converted to current densities,  $J$ . This is a process of normalising the currents to the surface area of the electrode from which these currents were attained, see Equation 2-31:

$$J = \frac{I}{A}$$

Equation 2-31

where  $J$  is the current density,  $I$  is the current flowing and  $A$  is the active surface area of the electrode. Thus current per unit area,  $J$  ( $\mu\text{A}\cdot\text{cm}^{-2}$ ), were compared across electrode types and allow comparison to other work.

### 2.9.4 Linear Region Slope

Sensitivity to a particular analyte is an important characteristic to define for a biosensor. Calculation of the linear region slope was the method used to determine sensitivity within this project. The linear region of the response to an analyte is generally considered to extend as far as  $\frac{K_M}{2}$ . For a substrate like D-ser, whose concentration *in vivo* is low, the extent of the linear region is not of particular importance, rather high sensitivity within the linear region is critical. The linear region slope (LRS) is approximately equal to  $\frac{J_{max}}{K_M}$ , see Equation 2-32 (O'Neill *et al.*, 2008) which is derived from Equation 2-26:

$$\lim_{[S] \rightarrow 0} J(S) = \frac{J_{max}}{1 + \frac{K_M}{[S]}} = \frac{J_{max}[S]}{[S] + K_M} \approx \frac{J_{max}}{K_M} [S]$$

Equation 2-32

## References

- Aoki K. (1993). Theory of ultramicroelectrodes. *Electroanalysis* **5**, 627-639.
- Bard AJ & Faulkner LR. (2001). *Electrochemical Methods: Fundamentals and Applications*. Wiley, U.S.A.
- Bhatia R, Hashemi P, Razzaq A, Parkin MC, Hopwood SE, Boutelle MG & Strong AJ. (2006). Application of rapid-sampling, online microdialysis to the monitoring of brain metabolism during aneurysm surgery. *Neurosurgery* **58**, ONS-313-320; discussion ONS-321.
- Bilal S, Ali Shah A-u-H & Holze R. (2011). Spectroelectrochemistry of poly(*o*-phenylenediamine): Polyaniline-like segments in the polymer structure. *Electrochimica Acta* **56**, 3353-3358.
- Brett CMA & Brett AMO. (1993). *Electrochemistry: Principles, Methods, and Applications*. Oxford University Press, New York.
- Calvo EJ. (2003). *Encyclopedia of Electrochemistry, Volume 2: Interfacial Kinetics and Mass Transport*. Wiley - VCH, Weinheim.
- Chiba K, Ohsaka T, Ohnuki Y & Oyama N. (1987). Electrochemical preparation of a ladder polymer containing phenazine rings. *Journal of Electroanalytical Chemistry* **219**, 117-124.
- Darvesh AS, Carroll RT, Geldenhuys WJ, Gudelsky GA, Klein J, Meshul CK & Van der Schyf CJ. (2011). *In vivo* brain microdialysis: Advances in neuropsychopharmacology and drug discovery. *Expert Opinion on Drug Discovery* **6**, 109-127.
- Dayton MA, Brown JC, Stutts KJ & Wightman RM. (1980). Faradaic electrochemistry at micro-voltammetric electrodes. *Analytical Chemistry* **52**, 946-950.
- Feuerstein D, Manning A, Hashemi P, Bhatia R, Fabricius M, Toliás C, Pahl C, Ervine M, Strong AJ & Boutelle MG. (2010). Dynamic metabolic response to multiple spreading depolarizations in patients with acute brain injury: an online microdialysis study. *Journal of Cerebral Blood Flow and Metabolism* **30**, 1343-1355.
- Forster RJ. (1994). Microelectrodes - new dimensions in electrochemistry. *Chemical Society Reviews* **23**, 289-297.

- Gileadi E & Urbakh M. (2003). *Encyclopedia of Electrochemistry, Volume 1: Thermodynamics and Electrified Interfaces*. Wiley - VCH, Weinheim.
- Gorton L. (1985). A carbon electrode sputtered with palladium and gold for the amperometric detection of hydrogen peroxide. *Analytica Chimica Acta* **178**, 247-253.
- Grabb MC, Sciotti VM, Gidday JM, Cohen SA & van Wylen DG. (1998). Neurochemical and morphological responses to acutely and chronically implanted brain microdialysis probes. *Journal of Neuroscience Methods* **82**, 25-34.
- Groothuis DR, Ward S, Schlageter KE, Itskovich AC, Schwerin SC, Allen CV, Dills C & Levy RM. (1998). Changes in blood-brain barrier permeability associated with insertion of brain cannulas and microdialysis probes. *Brain Research* **803**, 218-230.
- Grunewald RA, O'Neill RD, Fillenz M & Albery WJ. (1983). The origin of circadian and amphetamine-induced changes in the extracellular concentration of brain ascorbate. *Neurochemistry International* **5**, 773-778.
- Hall SB, Khudaish EA & Hart AL. (1998a). Electrochemical oxidation of hydrogen peroxide at platinum electrodes. Part I: An adsorption-controlled mechanism. *Electrochimica Acta* **43**, 579-588.
- Hall SB, Khudaish EA & Hart AL. (1998b). Electrochemical oxidation of hydrogen peroxide at platinum electrodes. Part II: Effect of potential. *Electrochimica Acta* **43**, 2015-2024.
- Hickling A & Wilson WH. (1951). The anodic decomposition of hydrogen peroxide. *Journal of the Electrochemical Society* **98**, 425-433.
- Hill AV. (1910). Proceedings of the Physiological Society: January 22, 1910. *Journal of Physiology-London* **40**, i-vii.
- Hillered L & Persson L. (1999). Neurochemical monitoring of the acutely injured human brain. *Scandinavian Journal of Clinical & Laboratory Investigation Supplementum* **229**, 9-18.
- Kadota E, Nonaka K, Karasuno M, Nishi K, Nakamura Y, Namikawa K, Okazaki Y, Teramura K & Hashimoto S. (1994). Experimental quantitative evaluation of

transvascular removal of unnecessary substances in brain edema fluid. *Acta Neurochirurgica Supplementum (Wien)* **60**, 162-164.

Li XG, Huang MR, Duan W & Yang YL. (2002). Novel multifunctional polymers from aromatic diamines by oxidative polymerizations. *Chemical Reviews* **102**, 2925-3030.

Lingane JJ, Lingane PJ & Morris MD. (1963). Gravimetric determination of cobalt as presumed  $K_3CO(NO_2)_6$ . *Analytica Chimica Acta* **29**, 10-&.

Losito I, De Giglio E, Cioffi N & Malitesta C. (2001). Spectroscopic investigation on polymer films obtained by oxidation of *o*-phenylenediamine on platinum electrodes at different pHs. *Journal of Materials Chemistry* **11**, 1812-1817.

Losito I, Palmisano F & Zambonin PG. (2003). *o*-Phenylenediamine electropolymerization by cyclic voltammetry combined with electro spray ionization-ion trap mass spectrometry. *Analytical Chemistry* **75**, 4988-4995.

Malitesta C, Palmisano F, Torsi L & Zambonin PG. (1990). Glucose fast-response amperometric sensor based on glucose oxidase immobilized in an electropolymerized poly(*o*-phenylenediamine) film. *Analytical Chemistry* **62**, 2735-2740.

Mathy FX, Denet AR, Vroman B, Clarys P, Barel A, Verbeeck RK & Preat V. (2003). *In vivo* tolerance assessment of skin after insertion of subcutaneous and cutaneous microdialysis probes in the rat. *Skin Pharmacology & Applied Skin Physiology* **16**, 18-27.

Michaelis L & Menten ML. (1913). Die kinetik der invertinwirkung. *Biochemische Zeitschrift* **49**, 333-369.

Monk PMS. (2001). *Fundamentals of Electroanalytical Chemistry*. Wiley, Chichester.

O'Neill RD, Lowry JP & Mas M. (1998). Monitoring brain chemistry *in vivo*: Voltammetric techniques, sensors, and behavioral applications. *Critical Reviews in Neurobiology* **12**, 69-127.

O'Neill RD, Rocchitta G, McMahon CP, Serra PA & Lowry JP. (2008). Designing sensitive and selective polymer/enzyme composite biosensors for brain monitoring *in vivo*. *Trends in Analytical Chemistry* **27**, 78-88.

Ricard J & Cornish-Bowden A. (1987). Co-operative and allosteric enzymes: 20 years on. *European Journal of Biochemistry* **166**, 255-272.

Rogers M, Leong C, Niu X, de Mello A, Parker KH & Boutelle MG. (2011). Optimisation of a microfluidic analysis chamber for the placement of microelectrodes. *Physical Chemistry Chemical Physics* **13**, 5298-5303.

Rothwell SA, McMahon CP & O'Neill RD. (2010). Effects of polymerization potential on the permselectivity of poly(*o*-phenylenediamine) coatings deposited on Pt–Ir electrodes for biosensor applications. *Electrochimica Acta* **55**, 1051-1060.

Sayyah SM, El-Deeb MM, Kamal SM & Azooz RE. (2009). Electropolymerization of *o*-phenylenediamine on Pt-electrode from aqueous acidic solution: Kinetic, mechanism, electrochemical studies and characterization of the polymer obtained. *Journal of Applied Polymer Science* **112**, 3695-3706.

Stryer L. (1988). *Biochemistry*. W.H. Freeman and Co., New York.

Ungerstedt U & Pycock C. (1974). Functional correlates of dopamine neurotransmission. *Bulletin der Schweizerischen Akademie der Medizinischen Wissenschaften* **30**, 44-55.

Yang H, Peters JL & Michael AC. (1998). Coupled effects of mass transfer and uptake kinetics on *in vivo* microdialysis of dopamine. *Journal of Neurochemistry* **71**, 684-692.

Yano J. (1995). Electrochemical and structural studies on soluble and conducting polymer from *o*-phenylenediamine. *Journal of Polymer Science Part A-Polymer Chemistry* **33**, 2435-2441.

Zhang X, Liu L, Zhang X, Ma K, Rao Y, Zhao Q & Li F. (2012). Analytical methods for brain targeted delivery system *in vivo*: Perspectives on imaging modalities and microdialysis. *Journal of Pharmaceutical & Biomedical Analysis* **59**, 1-12.

---

---

### **3. EXPERIMENTAL**

---

---

### 3.1 Chemicals

#### 3.1.1 Enzymes

D-Amino Acid Oxidase (porcine kidney) (DAAO)	BBI Enzymes Ltd.
D-Amino Acid Oxidase (porcine kidney)	Fluka Chemie GmbH.
D-Amino Acid Oxidase (porcine kidney)	Sigma Chemical Co.

#### 3.1.2 Interferent Species

Ascorbic Acid (AA)	Sigma-Aldrich Chemical Co.
3-Hydroxytyramine (Dopamine), (DA)	Sigma Chemical Co.
Uric Acid (UA)	Sigma Chemical Co.
L-Tryptophan (L-trp)	Aldrich Chemical Co.
5-Hydroxyindole 3-Acetic Acid (5-HIAA)	Sigma Chemical Co.
Dehydroascorbic Acid (DHAA)	Aldrich Chemical Co.
3,4-Dihydroxyphenyl-acetic Acid (DOPAC)	Aldrich Chemical Co.
L-Glutathione, oxidised form 90% (L-gluta)	Aldrich Chemical Co.
Homovanillic Acid (HVA)	BioChemika Ltd.
L-Tyrosine (L-tyr)	Aldrich Chemical Co.
L-Cysteine (L-cys)	Aldrich Chemical Co.
5-Hydroxytryptamine (Serotonin), (5-HT)	Sigma Chemical Co.

#### 3.1.3 Amino-Acids

D-Serine (D-ser)	Sigma Chemical Co.
D-Aspartic Acid (D-asp)	Aldrich Chemical Co.
D-Alanine (D-ala)	Aldrich Chemical Co.
D-Proline (D-pro)	Fluka Chemie GmbH
D-Phenylalanine (D-phe)	Aldrich Chemical Co.
D-Tyrosine (D-tyr)	Aldrich Chemical Co.
D-Glutamic Acid (D-glu)	Lancaster Synthesis Ltd.
D-Arginine (D-arg)	Fluka Chemie GmbH
D-Histidine (D-his)	Fluka Chemie GmbH
D-Lysine (D-lys)	Aldrich Chemical Co.
Glycine (gly)	Alpha Aesar Ltd.

L-Serine (L-ser)	Aldrich Chemical Co.
L-Aspartic Acid (L-asp)	Sigma Chemical Co.
L-Alanine (L-ala)	Aldrich Chemical Co.
L-Proline (L-pro)	Lancaster Synthesis Ltd.
L-Phenylalanine (L-phe)	Aldrich Chemical Co.
L-Glutamic Acid (L-glu)	Sigma Chemical Co.
L-Arginine (L-arg)	Sigma Chemical Co.
L-Histidine (L-his)	Fluka BioChemika

### 3.1.4 Electrode Fabrication Chemicals

Bovine Serum Albumin (Fraction V) (BSA)	Sigma Chemical Co.
Flavin Adenine Dinucleotide (FAD)	Sigma Chemical Co.
Glutaraldehyde, Grade I, 25% solution (GA)	Sigma-Aldrich Chemical Co.
Nafion <sup>®</sup> , 5% in Aliphatic Alcohol (Naf)	Aldrich Chemical Co.
Polyethylenimine, 80% ethoxylated (PEI)	Aldrich Chemical Co.
Styrene (Sty)	Aldrich Chemical Co.
Methyl Methacrylate (MMA)	Aldrich Chemical Co.
<i>o</i> -Phenylenediamine ( <i>o</i> -PD)	Sigma Chemical Co.
Glycerol	Aldrich Chemical Co.

### 3.1.5 *In Vitro* Chemicals

Oxygen Gas (Medical Grade)	BOC Gases
Nitrogen Gas	BOC Gases
Acetone	Sigma Chemical Co.
Ethanol	Sigma Chemical Co.
Hydrogen Peroxide 30% w/w ACS reagent	Sigma Chemical Co.
3-sn-phosphatidylethanolamine (PEA)	Sigma Chemical Co.
Sodium Hydroxide	Sigma-Aldrich Chemical Co.
Sodium Chloride	Sigma-Aldrich Chemical Co.
Sodium Phosphate Monohydrate	Sigma-Aldrich Chemical Co.

### 3.1.6 *In Vivo* chemicals

Ethylenediaminetetraacetic acid (EDTA)	BDH Chemicals Ltd.
--	--------------------

Veratridine	Sigma Chemical Co.
Magnesium Chloride	Sigma Chemical Co.
Calcium Chloride	Sigma Chemical Co.
Potassium Chloride	Sigma Chemical Co.
Adenosine 5'-triphosphate Magnesium salt (ATP.Mg)	Sigma Chemical Co.
<i>N</i> <sub>ω</sub> -Nitro-L-arginine methyl ester hydrochloride(L-NAME)	Sigma Chemical Co.
(+)-MK-801	Sigma Chemical Co.
L-Arginine (L-arg)	Sigma Chemical Co.

## 3.2 Solutions

All solutions were prepared with doubly distilled water which was deionised using a Milli-RO water purification system, or water from a Milli-Q Q-Pod, Millipore Integral 3 (A10) system unless otherwise stated. Both systems were supplied by Millipore Ireland BV, Tullagreen, Carrigtwohill, Co. Cork. Solutions that could be kept for more than 12 hours were stored at 4 °C or -18 °C in a Hotpoint FF220E fridge-freezer.

### 3.2.1 Enzyme Solutions

*D-Amino Acid Oxidase (porcine kidney) (DAAO) (BBI Enzymes Ltd.)*

A 600 U.mL<sup>-1</sup> solution was made by dissolving 0.00201 g of the 7.46 U.mg<sup>-1</sup> solid in 250 μL of water, PBS pH 8.5, PBS pH 7.6 or PBS pH 8.0. Alternately PBS pH 8.5 with 25 mg.mL<sup>-1</sup> BSA and 1% glycerol (w/v) was used to dissolve the enzyme.

*D-Amino Acid Oxidase (porcine kidney) (Fluka Chemie GmbH.)*

A 200 U.mL<sup>-1</sup> solution was made by dissolving 0.00263 g of the 1.9 U.mg<sup>-1</sup> solid in 250 μL of water.

*D-Amino Acid Oxidase (porcine kidney) (Sigma Chemical Co.)*

100 U.mL<sup>-1</sup>, 250 U.mL<sup>-1</sup> and 600 U.mL<sup>-1</sup> solutions of the 2.3 U.mg<sup>-1</sup> solid were obtained by dissolving 0.00109 g, 0.00272 g or 0.00652 g in 250 μL of water respectively.

### 3.2.2 Electrode Fabrication Solutions

#### *o*-Phenylenediamine (*o*-PD)

A 300 mM super saturated solution of *o*-PD was prepared under strict conditions of N<sub>2</sub> saturation by dissolving 0.324 g of monomer in 10 mL of PBS. The solution was sonicated for 2 minutes to aid dissolution. Care was taken to ensure at all times that air was excluded from the process as oxygen in solution can oxidise the monomer to varying degrees reducing the uniformity of the polymer obtained.

#### Bovine Serum Albumin 1% (BSA)

A 1% w/v solution was prepared by dissolving 0.01 g in 1 mL H<sub>2</sub>O.

#### Glutaraldehyde solutions (GA)

A 1 % v/v solution was prepared by dissolving 40  $\mu$ L 25% GA in 1 mL H<sub>2</sub>O. Alternately 0.1, 0.2, 0.5, 1.5, 2.0, 2.5, 5 and 10 % solutions were prepared by dissolving 4, 8, 20, 60, 80, 100, 200 or 400  $\mu$ L respectively in 1 mL H<sub>2</sub>O.

#### 1% BSA in 1% GA (BSAGA)

This solution was prepared by dissolving 0.01 g of BSA in 0.5 mL water. To this 40  $\mu$ L of 25% GA was added to the resulting solution and was made up to 1 ml with water to yield a 1% w/v BSA and 1% v/v GA solution. The solution was prepared in this way to limit the amount of cross-linking of the BSA and GA. This solution was altered by using 4, 8, 20, 60 or 80  $\mu$ L of 25 % GA to produce a solution with 1 % BSA and 0.1 %, 0.2 %, 0.5 %, 1.5 % and 2 % GA respectively.

#### Flavin Adenine Dinucleotide (FAD)

Two concentrations of FAD solution were used. A 0.08 mM solution of FAD was produced by dissolving 0.00314 g in 50 mL H<sub>2</sub>O. A 0.02 mM solution was produced from this by diluting 12.5 mL of the 0.08 mM solution in 50 mL of H<sub>2</sub>O.

#### Nafion<sup>®</sup> solutions (Naf)

This was used as a 5 % solution obtained from the manufacturer or diluted to 1% by making 200  $\mu$ L of the 5 % solution up to 1 mL using a 50 : 25 : 25 mixture of water : methanol : ethanol.

*Polyethylenimine (PEI)*

Three solutions of 0.1 %, 1 % and 5 % were prepared from an 80 % ethoxylated PEI (35 – 40 % solution in water) solution by dissolving 0.00313g, 0.03125 g or 0.15625 g respectively in 1 mL of water.

*Styrene (Sty)*

Styrene was used as pure 99% monomer, as received from the manufacturer.

*Methyl Methacrylate (MMA)*

MMA was used in its pure 99% monomer form from the manufacturer.

### **3.2.3 In Vivo Solutions**

*Artificial Cerebro-Spinal Fluid (aCSF)*

aCSF was prepared with 8.766 g sodium chloride (0.15 M), 0.178 g calcium chloride (0.0016 M), 0.204 g magnesium chloride (0.0021 M) and 0.298 g potassium chloride (0.004 M) dissolved in 1L of water.

*Normal Saline Solution*

0.9% normal saline solution was prepared by dissolving 0.9 g NaCl in 100 mL of water.

*Veratridine*

A 100  $\mu$ M solution of Veratridine was prepared by dissolving 0.00034 g in 5 mL of aCSF.

*Nitric Oxide Solution (NO)*

NO was synthesised by a well characterised and highly reproducible method previously described (Brown *et al.*, 2005).

*Ethylenediaminetetraacetic Acid (EDTA)*

A 1000 $\mu$ M solution of EDTA was prepared by dissolving 0.00146 g in 5 mL of aCSF.

*Adenosine Triphosphate (ATP)*

The ATP.Mg salt was certified as containing 8% w/w Mg<sup>2+</sup> on average. Thus 0.00278 g was dissolved in 5 mL water.

*L-Serine and D-Serine*

100 mM solutions were prepared by dissolving 0.2627g in 25 mL aCSF. From this two 1000  $\mu$ M solutions were formulated by diluting 50  $\mu$ L of the 100 mM solutions in 5 mL of aCSF. Further serial dilutions of D-ser were prepared by diluting 500, 200, 100, 50, 25, 10 and 5  $\mu$ L of the 1000  $\mu$ M solution in 5 mL aCSF to produce 100, 40, 20, 10, 5, 2 and 1  $\mu$ M solutions respectively.

*D-Serine and EDTA*

A combined 1000  $\mu$ M D-ser and 1000  $\mu$ M EDTA solution was prepared by dissolving 0.00372 g EDTA in 100  $\mu$ L of 100 mM D-ser solution, and making the combined solution up to 10 mL with aCSF.

*L-Serine and ATP*

A combined 1000  $\mu$ M L-ser and 1000  $\mu$ M ATP solution was prepared by dissolving 0.00556 g ATP in 100  $\mu$ L of 100 mM L-ser solution, and making the combined solution up to 10 mL with aCSF.

*N $\omega$ -Nitro-L-arginine methyl ester hydrochloride (L-NAME)*

A 100  $\mu$ M solution was prepared by dissolving 0.0013 g in 5 mL of aCSF.

*Ascorbic Acid (AA)*

A 1000  $\mu$ M solution was prepared by freshly dissolving 0.00088 g in 5 mL of N<sub>2</sub> saturated aCSF and used immediately.

*MK-801*

A 0.3 mg/kg solution of MK-801 was prepared in 1 mL of normal saline solution based on the weight of the animal.

### **3.3 Computer – Based Instrumentation and Software**

The use of computers was essential to the process of carrying out any experiment, be that a polymerisation or calibration. They allow the accurate collection, storage and analysis of vast quantities of information, and are now an integral part of bioanalytical science.

### 3.3.1 Potentiostat, Data Acquisition Hardware and CPU

All experiments were carried out using a low-noise potentiostat from ACM Instruments. This was connected to a PowerLab 400 data acquisition device from ADInstruments Ltd. (Oxford, UK) via a U2SCX cable, which allows SCSI to USB connectivity, supplied by Ratoc Systems International, California. The PowerLab was connected to a Dell Inspiron 6000 (Intel® Pentium Centrino® M 1.60 GHz processor) which stored the data and displayed it in real-time. The experimental equipment setup is displayed in Figure 3-1 and was protected by a Masterplug PowerCut surge protection device.

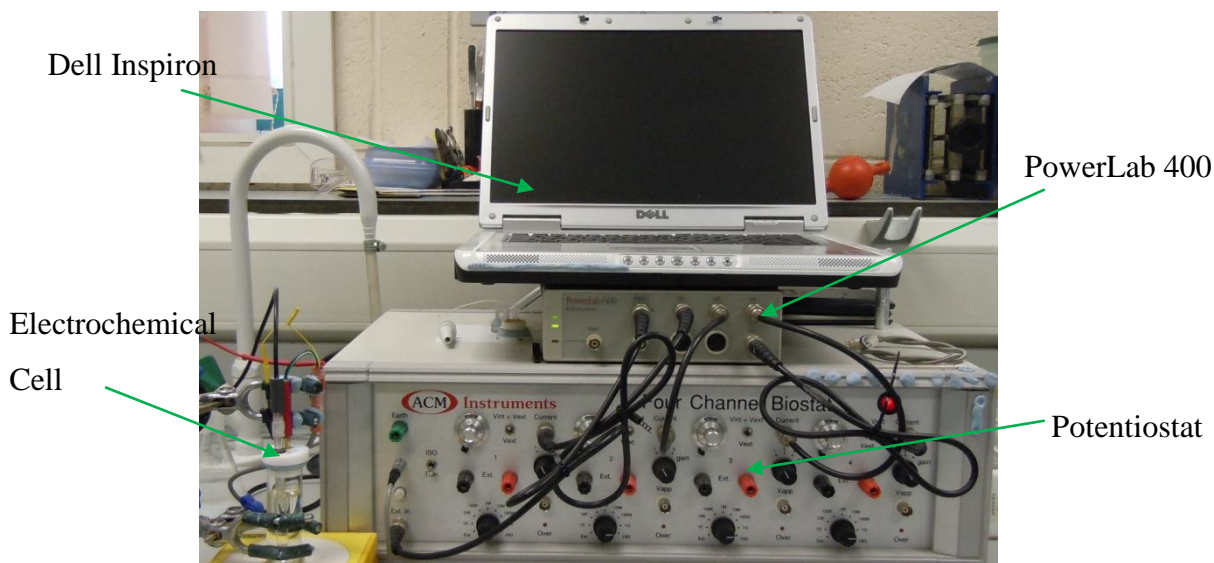


Figure 3-1

A picture of the experimental equipment setup. A Dell Inspiron 6000 sits on top of a PowerLab 400. Beneath both of these is the ACM Potentiostat. To the left can be seen an electrochemical cell.

All data generated was copied onto and analysed on an Acer Aspire 5610 (Intel® Core Duo® T2300 processor).

### 3.3.2 Computer Software

All potentiostatic experimental procedures (*e.g.* CPA) were carried out using Chart4 (Chart for Windows Version 4.2.3) from ADInstruments Ltd, Oxford, UK. They were then analysed using LabChart6, Version 6.1.1 also supplied by ADInstruments Ltd. Potentiodynamic protocols (*e.g.* CV) were carried out and analysed using EChem (EChem for Windows Version 1.5.2) also from ADInstruments Ltd. UK.

Graphical analysis and display of data, including the fitting of linear and non-linear regressions, was undertaken using GraphPad Prism Version 5.01 from GraphPad

Software Inc., California, U.S.A. This software package was also used to graph raw data obtained from *in vivo* experiments. Statistical analyses including paired and unpaired t-tests were performed using GraphPad InStat, Version 3.05, also from GraphPad Software Inc.

### 3.4 Ancillary Equipment

#### 3.4.1 Cylinder Electrode Spinner

In order to assist with the fabrication of cylinder electrodes devices were designed to rotate the electrodes in a horizontal plane. Initially an electric hotplate with a magnetic stirring mechanism was modified to allow fixing of electrodes to the rotating magnet. However after initial experiments a more suitable design was required as the rotation speed of the hotplate device was difficult to control and erratic. Thus a design was constructed using Lego<sup>®</sup> TECHNIC which was powered by a 12 V DC geared instrument motor, supplied by Mclennon Servo Supplies Ltd. UK, and a R95 12V 500mA DC power supply adapter, model number MC120S050, supplied by Mean Well Europe BV. There were two versions of this device, as shown in Figure 3-2;

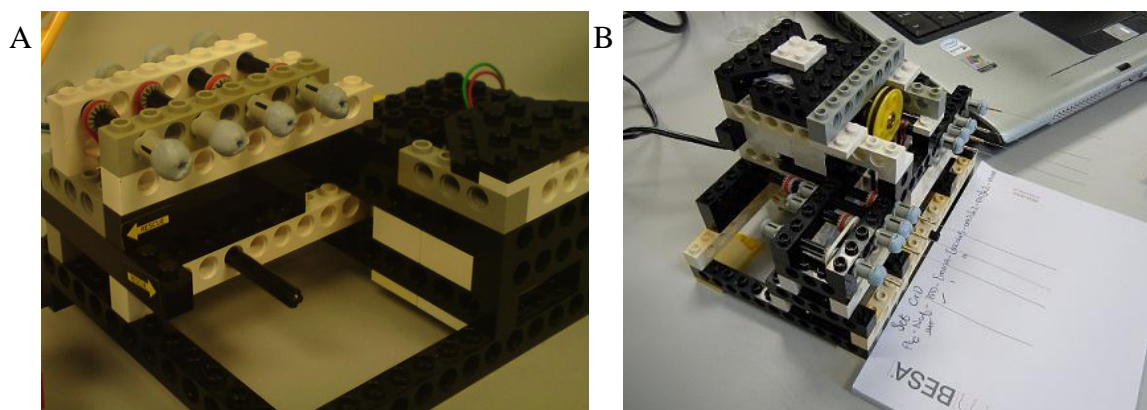


Figure 3-2

Pictures of the electrode spinning devices created primarily from Lego<sup>®</sup> TECHNIC. A was the first version and B was the second version.

where design A was the initial construction capable of handling 8 electrodes, 4 on either side, and design B had the capacity to spin the 8 electrodes all on the same side.

### 3.4.2 Other Equipment

Two types of microscope were used to carry out microscopic observations. An SM22 microscope was used in conjunction with a stereo heatless FLQ 150 light source, both manufactured by Hund<sup>®</sup> Wetzler, Germany. An Olympus SZ51 utilising a stereo Schott EasyLED RL+ light source, both supplied by Mason Technology, Dublin 8, was the second microscopy tool used.

The pH meters used were; a SevenEasy<sup>™</sup> pH Meter S20, supplied by Mettler Toledo AG, Analytical, Sonnenbergstrasse 74, CH-8603 Schwerzenbach and a PerpHecT LogR 350 meter, from Orion Research Inc., Boston, MA, U.S.A. They were calibrated using Buffer Solution pH 4.00 with fungicide and Buffer Solution pH 7.00 with fungicide, both supplied by Riedel-de-Haën, Sigma-Aldrich Laborchemikalien GmbH.

Homogenisation of solutions were carried out using a Fisherbrand<sup>®</sup> FB11002 Sonicator, manufactured by Elma<sup>®</sup>, Germany, an ULTRASONIK<sup>™</sup> 57X Cleaner from Ney Dental Inc., supplied by AGB Ireland, and a REAX Top vortex, supplied by Heidolph, Germany.

A Sartorius LA230S electronic balance, accurate to  $\pm 0.1$  mg, was used to weigh out most compounds. A Sartorius CP225D electronic balance, accurate to  $\pm 0.01$  mg, was used to weigh compounds where a greater degree of accuracy was required, for example *D*AAO. A Sartorius BP310P, accurate to  $\pm 1$ mg, was used to weigh out *o*-PD. All balances were supplied by Sartorius AG, Göttingen, Germany.

Three models of stirring magnetic stirring plate were utilised, a Yellowline MST mini, a Yellowline MSH basic S2 and a Yellowline MST basic C. The MST basic C model was also used in conjunction with a TC1 temperature probe and controller. All were supplied by IKA-Werke GmbH, Staufen, Germany.

Air pumps used during this project were the Stellar 110 Series II, from Aqua One<sup>®</sup>, UK, and the Air 100, from Rena<sup>®</sup>, France.

To accurately measure aliquots of solutions a series (1, 10, 20, 100, 1000  $\mu$ L) of Hamilton MICROLITER<sup>™</sup> Syringes were used. They were sourced from Hamilton Bonaduz AG, Switzerland.

### 3.5 Electrode Preparation

Working electrodes used in this work were all platinum based. This was due to the high sensitivity of platinum to  $\text{H}_2\text{O}_2$  (O'Neill *et al.*, 2004). They were manufactured using Teflon<sup>®</sup> coated Platinum/Iridium (90%/10%) wire (125  $\mu\text{m}$  bare diameter, 160  $\mu\text{m}$  coated diameter (5T), Advent Research Materials, Suffolk, UK), herein referred to as Pt/Ir. Approximately a 6 cm length of Pt/Ir was cut and 4 mm of Teflon<sup>®</sup> was gently removed from one end. This end was then soldered (Sn-Pb-Ag low melting point solder, Multicore, Henkel AG, Germany; Weller<sup>®</sup> WTCP51 soldering station and iron, Apex Tool Group GmbH & Co., Germany; Xytronic 426 DLX fume extractor, Xytronic Industries, Taiwan) into a gold clip (Fine Science Tools GmbH, Germany) which provided rigidity and good electrical contact for subsequent connection to a potentiostat via a flexible, screened, six-core cable (Plastics One Inc., U.S.A.). These were the basic production steps for an electrode before the disc or cylinder surfaces were produced.

#### 3.5.1 *In vitro* Electrodes

Two types of *in vitro* electrodes were fabricated during this project. These were disc and cylinder working electrodes. The auxiliary electrode was a solid strand of pure Pt wire 1 mm in diameter and the reference electrode was a saturated calomel electrode.

##### 3.5.1.1 *Disc Working Electrodes*

Disc electrodes were used during this project for the completion of the first two sections of work. A disc electrode was formed by cutting the end of the electrode transversely through the Teflon<sup>®</sup> and the metal wire inside to produce a flat surface perpendicular to the axis of the length of the wire. It is illustrated in Figure 3-3



**Figure 3-3**  
A diagram of a disc electrode

##### 3.5.1.2 *Cylinder Working Electrodes*

Cylinder electrodes were used in the latter half of this project for reasons outlined in Section 6.1. All cylinder electrodes used were 0.5 mm in length. They were fabricated

by taking the basic electrode described above (Section 3.5) and very carefully removing 1 mm of Teflon<sup>®</sup> from the end of the wire. The electrode was then placed under a microscope and the freshly exposed cylindrical surface was trimmed back to 0.5 mm guided by marks created immediately prior using a digital Vernier callipers.



**Figure 3-4**  
A schematic of a 0.5 mm cylinder electrode.

### 3.5.2 *In vivo* Electrodes

#### 3.5.2.1 *Working Electrodes*

Electrodes for use *in vivo* were prepared in the same manner as the *in vitro* electrodes, with two minor changes. Firstly, the *in vitro* gold clip was replaced with a smaller *in vivo* gold clip, which was better suited to fitting the pedestal required for making the connection between the animal and the potentiostat (see Section 3.7.4). The connection between the wire and the clip was also covered in a thin layer of 2-part-epoxy (Sigma Aldrich Co.) to ensure a secure connection and prevent the Teflon<sup>®</sup> coating from moving whilst being handled during surgery.

#### 3.5.2.2 *Auxiliary Electrode*

The auxiliary electrode was prepared from Teflon<sup>®</sup> coated Silver wire (200  $\mu\text{m}$  bare diameter, 250  $\mu\text{m}$  coated diameter (5T), Advent Research Materials, Suffolk, UK). From one end of the 4.5 cm electrode 5 mm of Teflon<sup>®</sup> was removed. This was then soldered into an *in vivo* gold clip and the joint sealed with 2-part-epoxy. 1 cm of Teflon<sup>®</sup> was removed from the opposing end and this exposed surface was then tightly wrapped around a stainless steel surgical screw (Plastics One, VA, USA). The contact of the silver wire and screw was then ensured by application of a small quantity of solder, see Figure 3-5. This also ensured that the electrode would not move during surgery.



Figure 3-5

Diagram of *in vivo* electrodes, both are made from silver wire, soldered into a gold clip and sealed with epoxy resin. *A* represents a reference electrode and *B* is an auxiliary electrode.

### 3.5.2.3 Reference Electrode

The reference electrode for surgical procedures was prepared in the same manner as the auxiliary electrode. However, the 1 cm of exposed silver was not attached to a screw - instead it was bent, first at 90 ° to the electrode axis, then in a semi-circle and finally back along the electrode axis, as shown in Figure 3-5. This bent shape allowed the electrode to make contact with tissue but prevented it from moving around or changing its depth into the tissue.

### 3.5.3 Electropolymerisation of *o*-PD

*o*-PD was polymerised by two methods. The principal one was by CPA where the electrodes were held at +700 mV *vs.* SCE in a 300 mM solution of monomer for 30 minutes. The second method of preparation was by using CV. Here the electrodes were cycled between 0 V and +1 V *vs.* SCE at a scan rate of 100 mVs<sup>-1</sup> for 15 cycles, again in a 300 mM solution of monomeric *o*-PD. After polymerisation was completed the electrodes were washed with water and allowed to dry at 4 °C before further use.

### 3.5.4 Dipping Procedures

The dipping procedure involved the immersion of a prepared electrode into the desired solution for ~ 1 second. This constituted a dip. There was often more than one dip in a layer. Dips in a single layer were separated by the minimal amount of time possible. Each layer was allowed to air dry for 5 minutes before addition of the next layer. Usually there were ten layers in a single application but there could be as many as twenty and as few as five. Applications were allowed to dry for 1 hour at 4 °C. An application could then be repeated in order to achieve a complete protocol.

### 3.5.5 Structured Naming of Designs

The multitude of designs tested in this thesis required a logical reusable naming procedure which could instantly elucidate the differences in a particular protocol. An example of this is as follows:

$$Pt_D - Na_f - PPD - \{MMA - [600UPBS \times 2 - GA2\%] \times 5 - FAD(5)\} \times 2$$

Here { } indicate a complete application and the  $\times 2$  proceeding it indicates the application was applied twice to complete the protocol.

The [ ] indicates layers that were repeated within the application, in this case a dip of 600 U DAAO in PBS pH 8.5 (this was the standard pH utilised as described later in Section 4.7.1, solutions with other pH values will be indicated within the text with appropriate naming labels) was applied on layer one and on layer two the dip into DAAO was followed by a dip of GA 2%. This process was repeated 5 times as shown by the  $\times 5$ .

The ( ) indicates a dip that was applied once on a particular layer within the application. The particular layer is indicated by the number enclosed within the brackets. Here it was a dip of FAD on the fifth layer only.

A detailed layout of the dipping procedure is described below in Table 3-1;

Application	Layer	Dip	Substance
1	1	1	MMA
		2	600U pH 8.5
	2	1	600U 8.5
		2	GA 2%
	3	1	600U 8.5
	4	1	600U 8.5
		2	GA 2%
	5	1	600U 8.5
		2	FAD
	6	1	600U 8.5
		2	GA 2%
	7	1	600U 8.5
	8	1	600U 8.5
		2	GA 2%
	9	1	600U 8.5
	10	1	600U 8.5
		2	GA 2%

Table 3-1

Complete detailed description of the dipping procedure followed for Application 1 for the protocol described by Pt<sub>D</sub> – Naf – PPD – { MMA – [600UPBS x2 – GA2%] x5 – FAD(5) }x2.

Within the application the first dip into MMA was proceeded directly by the first dip of 600UPBS constituting the first complete layer. Pt<sub>D</sub> indicates the electrodes were prepared as a Pt/Ir disc.

Naf indicates the application of Nafion layers, unless otherwise specified it was 5 layers of Nafion 5% following by drying at 4 °C for twelve hours.

PPD indicates that *o*-PD was polymerised onto the surface by CPA unless otherwise specified.

### 3.6 *In Vitro* Experimental Cell

*In vitro* calibrations were carried out in a cell, constructed in-house, at room temperature and under normal atmospheric calibrations. The cell consisted of a 25 mL glass vial to which was fitted a custom designed Teflon<sup>®</sup> lid. A standard 3-electrode set-up was used to carry out experiments. The lid had several ports to allow the insertion of these three electrode types: an auxiliary, a reference and working electrodes. There were also inlets to allow the injection of solutions into the cell and control of the gaseous atmosphere within the cell. A diagram of the experimental cell and the Teflon<sup>®</sup> cap are shown in Figure 3-6:

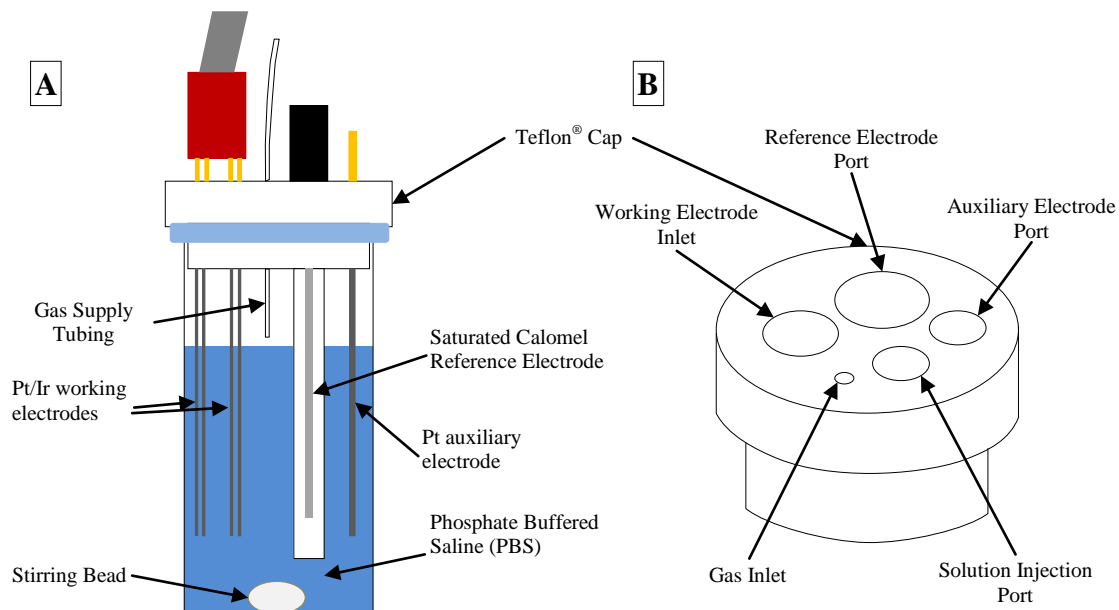


**Figure 3-6**

**Schematic of: A the 3-electrode experimental cell, and B the Teflon® cap used with the cell.**

The saturated calomel electrode provided a reference background potential against which the current flowing in the working electrodes was measured. The Pt auxiliary electrode provided a ‘well’ or ‘sink’ of electrons for the electrolyte, which ensured the electrochemical phenomena could take place at the working electrodes.

### 3.6.1 General Calibration Method

To carry out a calibration 20 mL of PBS, pH 7.4, was inserted into this cell. The reference, auxiliary and working electrodes were inserted and connected to the potentiostat. Subsequently, aliquots of substrate solution (for example 10  $\mu\text{L}$  of 100 mM D-ser solution) were injected into the cell using an appropriate syringe. Resultant current changes were monitored until a steady-state was achieved, see Section 2.4. The next aliquot of substrate was then injected. The aliquot sizes were calculated to increase the overall concentration of the solution in the cell to a predetermined level.

### 3.6.2 Repeated Calibrations Methodology

Short-term repeated calibrations were conducted by fabricating the biosensors and calibrating six times in quick succession. Between each calibration the electrodes were dried in the air for five minutes before being placed into a fresh solution of PBS for calibration again. The entire process took 2 days per set, with the electrodes being stored overnight at 4 °C between calibration 3 and 4.

Long-term repeated calibrations were conducted over a four week period. There were to be three calibrations at the start, Day 0, Day 1 and Day 3, and three calibrations spread out over the rest of the time period, Day 7, Day 21 and Day 28. Between each calibration the electrodes were stored at 4 °C.

Shelf-life tests were conducted on Day 0 and either Day 21 or Day 28. Between the Day 0 and the second calibration the electrodes were again stored at 4 °C

### **3.6.3 Full-Scope Amino Acid and Electroactive Interferent Calibration Methods**

These calibrations were carried out by setting up the experimental cell as per normal (under N<sub>2</sub> saturation for electroactive interferents). Once the electrodes had settled the calibration began with the injection of substrate into the cell. Each injection brought the level of that substrate to 10 μM in the cell. After a ten minute settling period, the next substrate was injected. This continued until all of the substrates had been added.

### **3.6.4 Oxygen Dependence Calibration Method**

An experimental method was devised to elucidate the effect that changing oxygen levels would have on the response of the sensor to D-ser. Three working electrodes and one bare Pt/Ir disk electrode, at -650 mV to monitor oxygen levels (Bolger *et al.*, 2011), were placed into a cell, setup as normal but with air being bubbled directly into the PBS. Then an aliquot of D-ser was added to the solution and allowed to settle with the air bubbling through the solution. Next, with care being taken to maintain a constant level of bubbling (to keep convective effects constant), N<sub>2</sub> was bubbled into the solution and the air was removed. Once the signals had stabilised again the process was reversed, with the N<sub>2</sub> supply being removed and the air supply being reinstated. This process was continued with the level of D-ser being increased with each cycle of decreasing and increasing the dissolved O<sub>2</sub> content. This method of calibration was devised to best replicate the short term changes in dissolved oxygen that might occur in the physiological environment.

## 3.7 Surgical Procedures

### 3.7.1 Animal Subjects

Out-bred Wistar rats (an albino strain of the species *Rattus norvegicus*) were acquired from Charles River UK Ltd. (Kent, UK), weighing between 200 and 250 g at the time of delivery. Animals were housed in a temperature, (17 - 23 °C), humidity and light (08:00 on and 20:00 off cycle) controlled environment. They were supplied with water and food *ad libitum*. All animals were regularly handled prior to surgery and subsequently commencement of the experimental procedures. In this period they were group housed, with a maximum of 3 animals per cage.

### 3.7.2 Surgery Setup and Equipment

Prior to the surgical procedure a number of items of equipment had to be setup and checked. The first checks and setup procedures were conducted on the anaesthetic units. Pre-operative anaesthesia was provided by a vaporiser for induction (Univentor 400 Anaesthesia Unit) with a Stellar S3 air pump (both supplied by Agnθος, Sweden) and a 1.4 L capacity Induction Chamber. Anaesthesia during the surgery was provided by the same vaporising system and a stereotaxic inhalation mask, again supplied by Agnθος. The stereotaxic frame was sourced from Kopf, CA, USA. The frame was located in a bench-top laminar flow unit, and a surgical drill was setup. An incubation chamber, Thermacage MKII, supplied by Datasand Ltd, UK, was turned on and set to 27 °C. A thermal plate was also placed in the stereotaxic frame, for the rat to be placed on and a steady body temperature maintained throughout the procedure.

Surgical screws and Teflon<sup>®</sup> pedestals were supplied by Plastics One Inc., VA, USA and were used in conjunction with dental acrylate cement (Sigma Aldrich) to secure the biosensors and a microdialysis probe (CMA Microdialysis, Sweden) to the skull of the subject. Previous to this, all electrodes were prepared. Biosensors were made according to the *in vivo* protocols in Section 3.5.2, and then pre-calibrated for response to AA and D-ser. A reference and auxiliary electrode were also fabricated. One biosensor was attached to the microdialysis probe with the active surface of the biosensor positioned less than 1 mm to the side of and centrally to the dialysis membrane (see Section 2.6). Attachment was achieved using the two part epoxy along most of the length of the insulated part of the biosensor and the probe shaft.

### 3.7.3 Surgery Protocol

Rats were anaesthetised by volatile anaesthetic, Isoflurane (using the vaporiser and induction chamber), at a flow rate of 700 – 800 mL.min<sup>-1</sup> and a concentration of 4%. Upon attaining successful anaesthesia the animal was weighed and had its hair removed from the skull using an electric razor. The animal was then secured in the stereotaxic frame where anaesthesia was maintained using the inhalation mask under a flow rate of 400 – 500 mL.min<sup>-1</sup> and a concentration of 3% initially to ensure complete anaesthesia post transfer but then reduced to 1.8 – 2.2% for the duration of the procedure, depending on the weight of the rat. During the incision and drilling phases the concentration was raised to 2.5 – 3.0% but lowered again once these procedures were completed. Within the stereotaxic frame the skull was held level between lambda and bregma. Lambda is where the sagittal and lambdoidal sutures intersect. Bregma is the point where the sagittal and coronal sutures intersect and is anterior to lambda. Their locations can be confirmed by applying pressure to the different skull plates and observing the junctions. Bregma was used as the zero point for calculation of coordinates for implantation.

A rectal temperature probe was inserted into the rat, to maintain a body temperature of 37 °C throughout the procedure in conjunction with the heating plate positioned underneath the subject. The animal's body and face were covered in sterile drapes and the incision area cleaned with tincture of iodine. An incision was made in the centre of the skull, along the anterior-posterior plane, from just behind the eyes to the back of the ears. The scalp was manoeuvred to the sides and held using a combination of forceps and small surgical bull clamps. This exposed the maximum surface area for the procedure to be carried out. The lipid periosteum layers were also removed and clamped to the sides, as these would prevent secure adhesion of the cement and hinder the procedure. Epidural haemorrhages were eliminated by cauterising, to prevent excessive bleeding.

The stereotaxic coordinates used were determined from the Paxinos and Watson rat atlas (Paxinos & Watson, 2007). The anterior-posterior (A-P) and medial-lateral (M-L) coordinates were referenced with respect to the zero-point (bregma), with A-P positive in the anterior and M-L positive lateral to medial on the right hemisphere. Dorsal-ventral (D-V) coordinates were calculated from the dura mater. The dura is the first of three meninges that surround the brain and spinal cord. Increasing negative coordinates

in this case indicated greater distance into the brain, *i.e.* ventral to the dura. Only one location was used for the entirety of the *in vivo* characterisation, that of the Striatum. The coordinates used were; A-P  $\pm 1.0$  mm, M-L  $\pm 2.5$  mm, D-V – 5 mm.

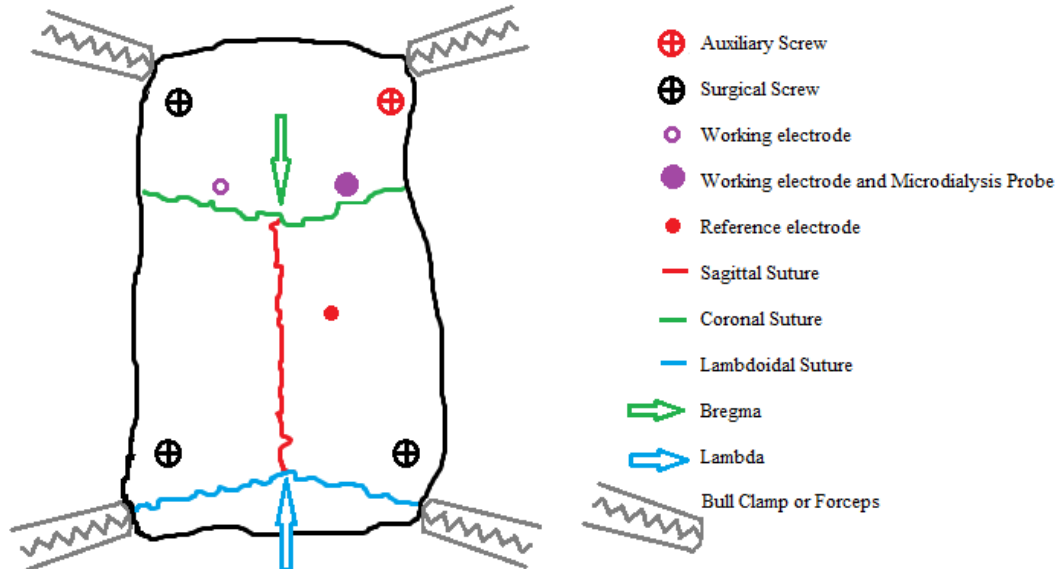


Figure 3-7

A representative diagram of the exposed area of the skull during surgery and placement of the various points of interest.

With bregma determined and the stereotaxic equipment zeroed the skull was drilled at the relevant working electrode sites. The combined microdialysis probe and biosensor were facilitated by the drilling of a 1 mm bore hole at the right hemisphere coordinates. A hole was also drilled for the reference electrode (in the cortex), the combined auxiliary electrode and screw, and the three other surgical screws. A diagram of the approximate placement of these items is shown in Figure 3-7. The surgical screws were inserted. Their main purpose was to aid the securing of the dental cement to the skull (except for the combined screw and auxiliary electrode), hence they were placed at the extremities of the procedure area. The dura mater, arachnoid and pia mater meninges were penetrated using a hypodermic needle for 5 seconds to ensure safe passage of the probe and biosensors. They were then stereotaxically inserted to the correct depth. The reference electrode was placed into its correct position and whilst all the electrodes were still attached to the stereotaxic frame a layer of dental cement was applied to the skull to secure them. With all components parts secured against ‘moving about’, they were detached from the stereotaxic frame and the electrode clips were inserted into the Teflon<sup>®</sup> headpiece according to the diagram in Figure 3-8;

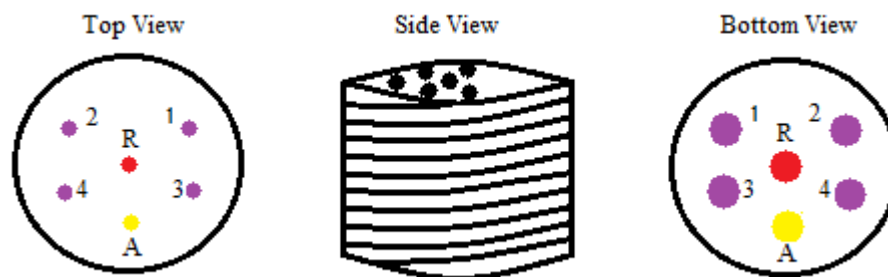


Figure 3-8

Map of the Teflon® headpiece which the electrodes were cemented into (bottom side) and to which the shielded cable screws onto (top side) to connect the subject to the potentiostat. The holes on the bottom side are larger to hold the female pins which are attached to the electrodes. The smaller holes on top accommodate the male ends of the cable. The working electrodes are numbered 1 – 4 and with the reference in R and the auxiliary A.

The electrodes were then secured into the headpiece using dental cement, taking care to ensure only the bottom few threads of the headpiece were secured in the cement and no cement got into the top of the headpiece or electrode clips. The excess wire was then folded down carefully onto the skull, the headpiece pushed down as close to the skull as possible and all exposed wires and parts of the microdialysis probe cemented over completely to ensure that they could not be damaged by scratching. Care was taken to ensure the scalp was not trapped in the cement, this would allow air to circulate around the wound better when the procedure was completed, and thus provide better healing. Once the cement had dried completely the surgical incision was closed using a suture so that the scalp came up over the bottom of the dental cement and closed around it below the headpiece. The surgical procedure was then completed and the animal was removed from the stereotaxic frame.

### 3.7.4 Post-Operative Care

Following conclusion of the surgery and prior to the placement of the rat within the incubation chamber to recover, it was administered 1.0 mL of saline containing 0.1 mg.kg<sup>-1</sup> of Tamgesic (buprenorphine hydrochloride) by subcutaneous injection (s.c.). This provided post-operative analgesia and aided the recovery of the subject while in the incubation chamber. After at least one hour recovery in the incubation chamber, and when the animal was beginning to move about again, it was transferred to its home bowl in the experimental procedure room, where it would remain until termination. It was provided with water and food *ad libitum* and allowed to recover for at least 12 hours before being connected to the potentiostat. No experiments were conducted until at least 24 hours after the conclusion of the surgical procedures and 12 hours after the

potentiostat had been connected and switched on. A photograph of the home bowl setup is shown below in Figure 3-9;



**Figure 3-9**

**The setup of the home bowl where subjects were housed post-operatively and throughout all experimental procedures.**

All animals were housed individually post-operatively to ensure the best possible protection of the electrode-containing headpiece and microdialysis probe. The housing consisted of a home bowl, with side door and lid, mounted on a Ratum system (BASi, Bioanalytical Systems Inc, Indiana, U.S.A.) which rotated automatically to prevent entanglement and to allow the animal to move around freely. The implanted electrodes were connected to the potentiostat via an insulated, flexible, screened six-core cable (supplied by Plastics One Inc., VA, USA). The animal was tethered with the cable passing through the swivel mount of the tether (positioned in the centre of the bowl above the rats head) to ensure free movement around the home bowl. The animal's health, food and drink consumption, and weight was continuously monitored and scored each day.

### **3.8 *In Vivo* Experimental Procedures**

Microdialysis solutions were prepared in aCSF, except NO which was prepared in water, and all subcutaneous (s.c.) injection solutions made up in normal saline solution. Previous to the commencement of experiments a steady baseline was observed for at least 5 minutes. At least 3 hours was left between the end of one procedure and the commencement of the next, with up to 24 hours between the more 'stressful' experiments, details within each section to follow. All solutions were freshly prepared before use.

At the beginning of each microdialysis experiment the lines were purged with 0.5 mL of biocide followed by 1 mL aCSF. Then 0.5 mL of the solution to be used was purged through the lines and connected to a syringe of the appropriate solution, being careful to avoid getting air bubbles in the tubing. The syringe was then placed into the Univentor. A flow rate of  $2 \mu\text{L}\cdot\text{min}^{-1}$  was used for all experiments. The Univentor was turned on until solution was flowing freely from the end of the tube. It was then rapidly connected to the inlet of the probe in the subject's headpiece. The dialysate was not collected for further analysis, and allowed to flow out the outlet, with the appearance of the first drop marking the beginning of the experiment.

When the signal was judged to have reached a stable new baseline the Univentor was turned off and the flow of solution discontinued. The tubing was disconnected from the outlet valve. In other experiments a liquid swivel was used to alternate between two solutions. Once each solution had been used, in the predetermined order, with each reaching its own response level, all tubing as disconnected and the syringe pump was turned off. The signal response was allowed time to recover and the new baseline noted. During all of this time the animal was free to move, eat and drink. All experiments were conducted during the 'day' period of the light cycle, beginning at least one hour after the changeover from 'night' and finished at least one hour before the next 'night'.

The specific subject which will be reported on had a full day recovery before experiments commenced. The experimental period lasted for 21 days. Termination was carried out by a lethal s.c. injection of 1 mL Euthatal. All graphs will display the biosensor with the microdialysis probe in the right striatum as a green trace. The lone biosensor in the left striatum will be a green trace and red arrows will indicate the start and end of a perfusion. All values presented in table format are gathered from the mean value of 30 second samples of the signal at each level.

References

- Bolger FB, Bennett R & Lowry JP. (2011). An *in vitro* characterisation comparing carbon paste and Pt microelectrodes for real-time detection of brain tissue oxygen. *Analyst* **136**, 4028-4035.
- Brown FO, Finnerty NJ, Bolger FB, Millar J & Lowry JP. (2005). Calibration of NO sensors for in-vivo voltammetry: laboratory synthesis of NO and the use of UV-visible spectroscopy for determining stock concentrations. *Analytical & Bioanalytical Chemistry* **381**, 964-971.
- O'Neill RD, Chang SC, Lowry JP & McNeil CJ. (2004). Comparisons of platinum, gold, palladium and glassy carbon as electrode materials in the design of biosensors for glutamate. *Biosensors & Bioelectronics* **19**, 1521-1528.
- Paxinos G & Watson C. (2007). *The Rat Brain in Stereotaxic Coordinates*. Elsevier.

---

## **4. AN INVESTIGATION INTO IMMOBILISATION MATRIX FREE D-SERINE BIOSENSOR DESIGNS**

---

## 4.1 Introduction

The project began based on work carried out by Z. M. Zain, later published (Zain *et al.*, 2010), which started the search for a sensitive and selective biosensor for D-ser using porcine D-amino acid oxidase as the bio-recognition unit. At the beginning of this project it was hoped that a suitable, stable configuration had been achieved and that after *in vitro* characterisation and reproducibility testing that the sensor already designed could be taken to the *in vivo* environment for further detailed characterisation. To be successful as a chronic *in vivo* biosensor it was deemed that a limit of detection (LOD) of less than 1  $\mu\text{M}$  and a  $K_M$  which is larger than 100  $\mu\text{M}$  and less than 1000  $\mu\text{M}$  were necessary. The biosensor would not have to be reusable after implantation, but would need to retain its sensitivity for the two calibrations that would be required to characterise the biosensor before implantation. However, shortly into the project it was determined that the sensor designed, while functional and producing satisfactory results, was quite difficult to reproduce. An investigation was then conducted into the design to study the various components in an attempt to determine the contributions of each element and if it was possible to reproduce, or enhance the reproducibility of the design. It was found that the biosensor could be fabricated, but it did not meet all of the requirements necessary for a chronic *in vivo* biosensor. This chapter will describe the investigation that took place and the results produced in attempting to improve the robustness of the biosensor.

Results presented in this chapter and subsequent chapter will be presented in three formats. A table presenting the calibration points used within individual calibration of a group of electrodes can be found in Appendix 1. This data will be a sample of the raw data recorded during the calibration which has undergone a simple transformation to a current density value appropriate for the particular geometry of the electrodes utilised. Secondly, within the following chapters there will be a table of the kinetic data calculated, in Prism, based on the raw data presented in the relevant calibration data table. The kinetic parameters are a statistical comparison for best fit between M-M and M-M-H kinetics, see Section 2.7.2, where  $p < 0.05$  is significant and indicates M-M-H kinetics. In a case where one model did not converge, denoted by n/c, the other kinetic fit was chosen. The  $R^2$ ,  $J_{\max}$ ,  $K_M$ ,  $\alpha$  and LRS are the values obtained from the best fit kinetic model.  $R^2$  indicates goodness of fit of the chosen kinetic model. Finally this information will be graphically represented with the raw data plotted as individual

points with error bars indicating the SEM. These points are then overlaid with a curve of the calculated best fit kinetic model.

The basic configuration, of most biosensors discussed within this chapter, is as depicted in Figure 4-1. All alterations discussed in this chapter centre on this design with various layers being omitted or modified or added as detailed in each section.

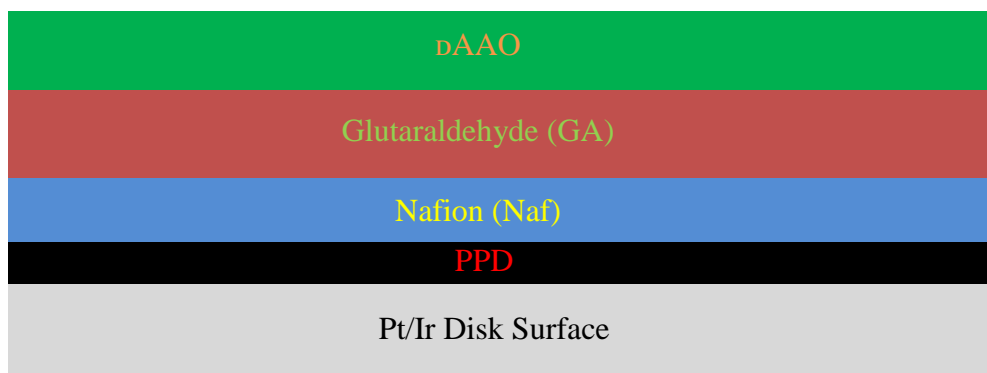


Figure 4-1

The basic configuration of biosensors discussed within Chapter 4.

## 4.2 Biosensor Configuration

At the onset of this project the working electrode design was detailed as being;

$$Pt_D - PPD - Naf\ 1\% \times 3\ (5\ sec\ dip) - GA\ 25\% \times 3\ (5\ sec\ dip) - DAAO\ (600\ U\ H_2O)$$

By the time of the publication of the design the procedure changed, by Zain, without change in the sensitivity (LRS), whereby the PPD growth was carried out using CV and the dipping regime altered.

$$Pt_D - PPD_{cv} - Naf\ 1\% \times 5\ (5\ sec\ dip) - GA\ 25\% \ (5\ min\ dip) - DAAO\ (600\ U\ H_2O)$$

This second design reported a current-density (see Section 2.9.3) transformed Michaelis–Menten non-linear regression with a  $J_{max}$  of  $91 \pm 2\ \mu\text{M}\cdot\text{cm}^{-2}$  and a  $K_M$  of  $1300 \pm 100\ \mu\text{M}$ . The linear region displayed a sensitivity of  $63 \pm 2\ \mu\text{A}\cdot\text{cm}^{-2}\cdot\text{mM}^{-1}$  ( $n = 4$ ),  $R^2 = 0.996$ . This can be seen below in Figure 4-2:

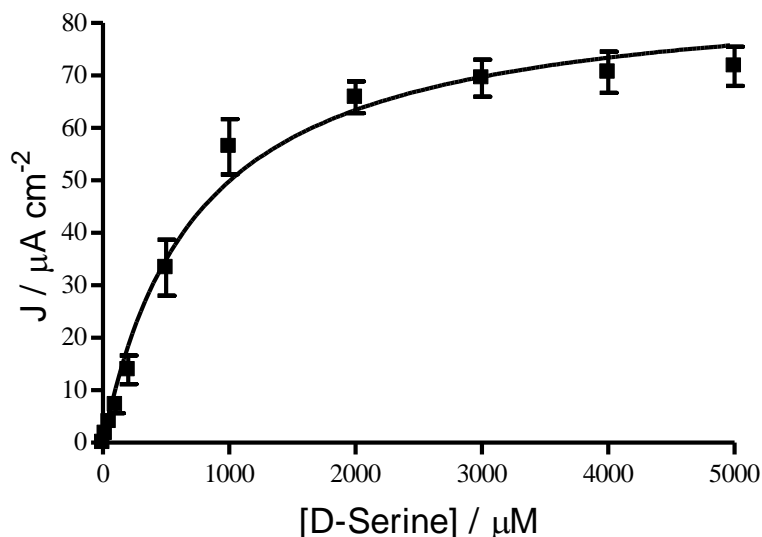


Figure 4-2

Current density – concentration plot for Pt<sub>D</sub>-PPD-Naf-GA-DAAO biosensor designed by Z.M. Zain.

These reported values were the benchmark for sensitivity with which this project began, with good sensor characteristics of a high  $J_{\text{max}}$ , low  $K_{\text{M}}$  and thus a high LRS.

### 4.3 Circumstantial Functioning of the Biosensor

Initial attempts to reproduce the biosensor designed by Z. M. Zain yielded poor results, as typified by the calibration data shown in Table 9-1 and displayed in Figure 4-3. These three initial designs were chosen as they matched most closely the methods previously described in Section 4.2. The designs were;

Pt<sub>D</sub>-PPD-Naf1% $\times$ 5-GA25%-600UH<sub>2</sub>O $\times$ 10,

Pt<sub>D</sub>-PPD-Naf1% $\times$ 3-GA25% $\times$ 3-600UH<sub>2</sub>O $\times$ 10

and Pt<sub>D</sub>-PPD-Naf1% $\times$ 3-GA25% $\times$ 3-600UH<sub>2</sub>O $\times$ 5.

It can be seen in Table 4-1 that the  $J_{\text{max}}$ ,  $K_{\text{M}}$  and LRS were all inferior to the reported values. Pt<sub>D</sub>-PPD-Naf1% $\times$ 3-GA25% $\times$ 3-600UH<sub>2</sub>O $\times$ 10 provides the highest  $J_{\text{max}}$ , Pt<sub>D</sub>-PPD-Naf1% $\times$ 3-GA25% $\times$ 3-600UH<sub>2</sub>O $\times$ 5 the lowest  $K_{\text{M}}$  and Pt<sub>D</sub>-PPD-Naf1% $\times$ 3-GA25% $\times$ 3-600UH<sub>2</sub>O $\times$ 10 the highest LRS, yet all are significantly different ( $p < 0.0001^{***}$ ,  $p = 0.0030^{**}$  and  $p < 0.0001^{***}$  respectively) and unfavourable compared to the reported values, see Section 4.2.

Electrode Design	Pt <sub>D</sub> -PPD-Naf1% $\times$ 5-GA25% $\times$ 1-600UH <sub>2</sub> O $\times$ 10, n=13	Pt <sub>D</sub> -PPD-Naf1% $\times$ 3-GA25% $\times$ 3-600UH <sub>2</sub> O $\times$ 10, n=7	Pt <sub>D</sub> -PPD-Naf1% $\times$ 3-GA25% $\times$ 3-600UH <sub>2</sub> O $\times$ 5, n=4
<b>Kinetics</b>	M-M, p = 0.6972	M-M, p = 0.7593	M-M, p = 0.2311
<b>R<sup>2</sup></b>	0.9992	0.9999	0.9940
<b>J<sub>max</sub>, <math>\mu</math>A.cm<sup>-2</sup></b>	29.03 $\pm$ 0.98	34.72 $\pm$ 0.35	18.02 $\pm$ 1.35
<b>K<sub>M</sub>, <math>\mu</math>M</b>	5936 $\pm$ 351	5486 $\pm$ 100	4409 $\pm$ 641
<b>LRS, <math>\mu</math>A.cm<sup>-2</sup>.mM<sup>-1</sup></b>	4.89 $\pm$ 0.13	6.33 $\pm$ 0.05	4.09 $\pm$ 0.31

Table 4-1

Kinetic parameters, fit, J<sub>max</sub> and K<sub>M</sub> values calculated from the calibration data in Table 9-1. J<sub>max</sub>, K<sub>M</sub> and LRS are presented as Mean  $\pm$  SEM.

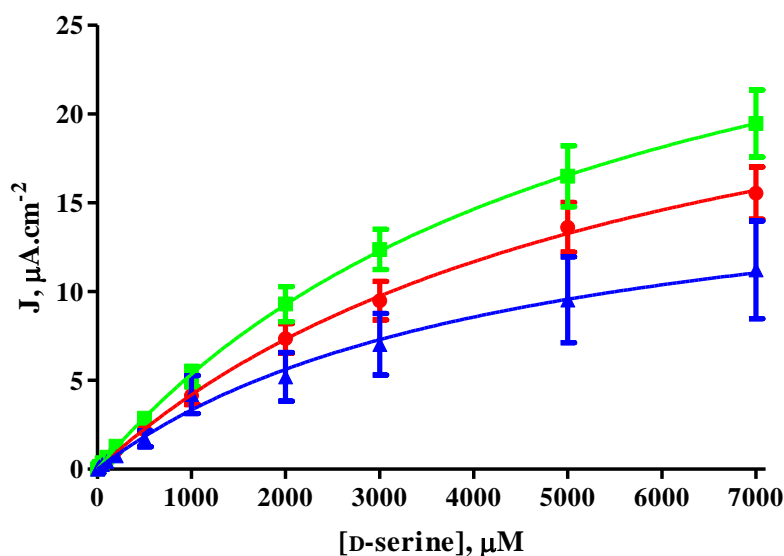


Figure 4-3

J - concentration profile of replications of sensor designed by Zain, Mean  $\pm$  SEM. Green trace Pt<sub>D</sub>-PPD-Naf1% $\times$ 3-GA25% $\times$ 3-600UH<sub>2</sub>O $\times$ 10, n = 13; red trace Pt<sub>D</sub>-PPD-Naf1% $\times$ 5-GA25% $\times$ 1-600UH<sub>2</sub>O $\times$ 10, n = 7; blue trace Pt<sub>D</sub>-PPD-Naf1% $\times$ 3-GA25% $\times$ 3-600UH<sub>2</sub>O $\times$ 5, n = 4.

Further investigation of the reported design and consultation with Z. M. Zain provided a clue as to the reason why efforts to reproduce reported sensitivity were unsuccessful. Zain's electrodes were made with solutions newly prepared before production of each set of 4 electrodes. This improved the sensitivities of the biosensors but did not ensure the desired sensitivity was achieved every time.

To investigate this further two sets of 4 electrodes were prepared simultaneously from freshly prepared solutions according to recipe Pt<sub>D</sub>-PPD-Naf1% $\times$ 3-GA25% $\times$ 3-600UH<sub>2</sub>O $\times$ 10. The electrodes were produced/dipped in the sequence E1, E2, E3.....E8. The individual response of these electrodes to D-ser is displayed in Figure 4-4. Also depicted is the grouped response of E2 - E4 and E5 - E8.

Electrodes	E1	E2 - E4	E5 - E8
Kinetics	M-M-H, $p = 0.0070$	M-M, $p = 0.8127$	M-M, n/c
$R^2$	0.9781	0.9854	0.9957
$J_{max}$ , $\mu A.cm^{-2}$	$40.97 \pm 1.60$	$32.98 \pm 2.47$	$26.63 \pm 1.30$
$K_M$ , $\mu M$	$456.3 \pm 59.1$	$3464 \pm 635$	$4724 \pm 502$
$\alpha$	$1.980 \pm 0.430$		

Table 4-2

Kinetic parameters, fit,  $J_{max}$  and  $K_M$  values calculated from the calibration data in Table 9-2.  $J_{max}$ ,  $K_M$  and  $\alpha$  are presented as Mean  $\pm$  SEM.

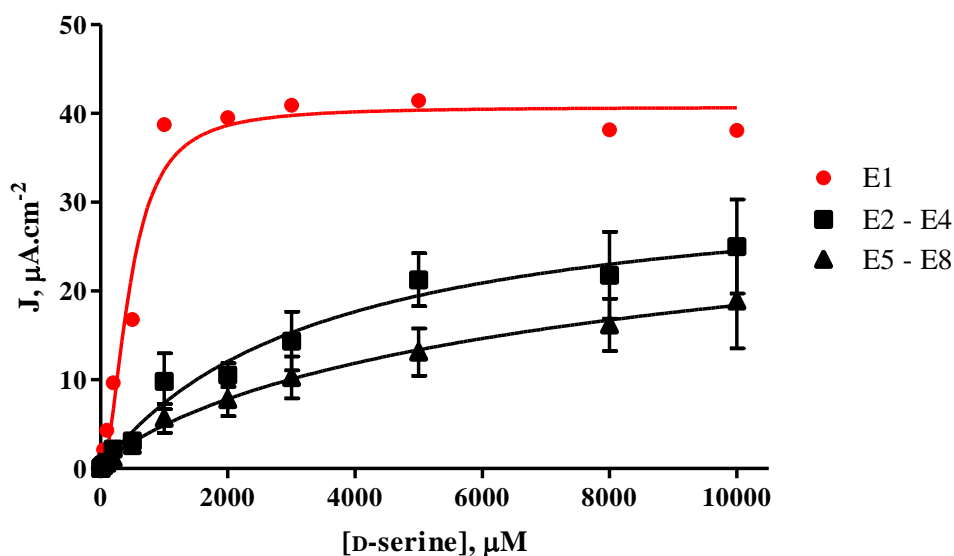


Figure 4-4

J-concentration plot for  $Pt_D$ -PPD-Naf1% $\times$ 3-GA25% $\times$ 3-600UH<sub>2</sub>O $\times$ 10 obtained when all solutions are freshly prepared immediately prior to the dipping process. Depicted are the responses of an individual electrodes, which was the first electrode prepared from the new solutions, and calibrated once the fabrication process was complete. The Mean  $\pm$  SEM of electrodes 2, 3 & 4 is indicated by black squares and of electrodes 5, 6, 7 & 8 by the black triangles.

Cursory inspection of the responses in Figure 4-4 immediately shows a discrepancy between the 1<sup>st</sup> electrode, E1, prepared in the fresh solutions and all other electrodes prepared subsequently. Examining the data presented in Table 9-2 and Table 4-2 it can be seen that E1 has a different kinetic model, M-M-H, to the rest of the electrodes, M-M. This difference was illustrated best by disparity in the  $K_M$  values. E1 has an ideal  $K_M$  of  $456.3 \pm 59.1 \mu M$ , which is much smaller than the E2 – E4 value of  $3464 \pm 635 \mu M$ , which increases again to  $4724 \pm 502 \mu M$  for E5 – E8. Contrastingly the  $J_{max}$  is seen to be decreasing, from  $40.97 \pm 1.60$ , to  $32.98 \pm 2.47$ , to  $26.63 \pm 1.30 \mu A.cm^{-2}$ , for the same electrodes respectively.

As a further effort to quantify these differences and observe changes that might take place over time, the electrodes were stored at 4 °C for 7 days and then calibrated for response to D-ser again. The results are illustrated in Figure 4-5 and listed in Table 4-3;

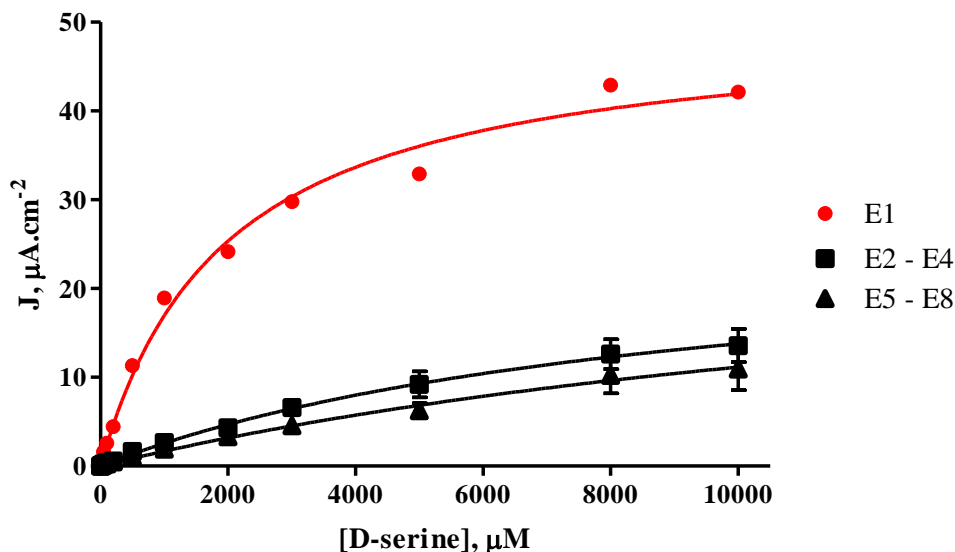


Figure 4-5

J-concentration plot for  $\text{Pt}_D\text{-PPD-Naf1}\% \times 3\text{-GA25}\% \times 3\text{-600UH}_2\text{Ox10}$  as in Figure 4-4. Depicted are the responses 7 days after that initial calibration. The Mean  $\pm$  SEM of electrodes 2, 3 & 4 is indicated by black squares and of electrodes 5, 6, 7 & 8 by the black triangles.

Electrodes	E1	E2 - E4	E5 - E8
Kinetics	M-M, $p = 0.1452$	M-M, n/c	M-M, $p = 0.2066$
$R^2$	0.9927	0.9920	0.9952
$J_{\max}$ , $\mu\text{A}\cdot\text{cm}^{-2}$	$50.12 \pm 1.94$	$26.74 \pm 1.25$	$29.97 \pm 4.20$
$K_M$ , $\mu\text{M}$	$1955 \pm 229$	$9405 \pm 757$	$16878 \pm 3383$

Table 4-3

Kinetic parameters, fit,  $J_{\max}$  and  $K_M$  values calculated from the responses elicited after the biosensors in Table 4-2 were stored for 7 days, see Table 9-3.  $J_{\max}$  and  $K_M$  are presented as Mean  $\pm$  SEM.

The  $J_{\max}$  of E2 – E4 and E5 – E8 is not significantly different after 7 days,  $p = 0.0872$  and  $p = 0.4762$  respectively. However the  $K_M$  values are significantly different for both E2 – E4,  $p = 0.0039^{**}$ , and E5 – E8,  $p = 0.0120^*$ . These two sets of statistics combine to illustrate an enzymatic response which has become linear, indeed the  $K_M$  for E2 – E4 is almost outside the calibration range and the  $K_M$  for E5 – E8 is well beyond the calibrated range and is an extrapolated value. The  $K_M$  of E1 has increased by a factor of  $\sim 4$  after 7 days and the kinetic model has changed from M-M-H to M-M, also indicating a more linear response to D-ser. It was felt that this was due to a continuing slow interaction between the enzyme and the high concentration of GA which was altering the activity of the enzyme.

From the data in Table 4-1 it was decided to continue forward with 10 dips of 600 U/ml of DAAO from this point forward as  $\text{Pt}_D\text{-PPD-Naf1}\% \times 3\text{-GA25}\% \times 3\text{-600UH}_2\text{Ox10}$  and  $\text{Pt}_D\text{-PPD-Naf1}\% \times 5\text{-GA25}\% \times 1\text{-600UH}_2\text{Ox10}$  provided a higher  $J_{\max}$  ( $p < 0.0001^{***}$  and

$p < 0.0001^{***}$ ) and LRS value ( $p < 0.0001^{***}$  and  $p = 0.0139^*$ ) than the lower number of 5 dips. Between the two 10 enzyme dip recipes there was also a significant difference in the  $J_{\max}$  values ( $p = 0.0006^{***}$ ) and LRS ( $p < 0.0001^{***}$ ). There was no significant difference between their  $K_M$  values ( $p = 0.3703$ ). It was the large  $K_M$  value ( $\sim 5000 \mu\text{M}$ ) which was seen as the main obstacle to a successful biosensor as it determined the LRS. Maintaining a large  $J_{\max}$  and reducing the  $K_M$  to between the  $456 \mu\text{M}$  of E1 and  $1300 \mu\text{M}$  reported by Zain was seen as a fundamental objective.

Taking all of the above data into account it was decided to embark on an exploration of the different components of the sensor recipe to elucidate what effect each had on the sensitivity. The results of these explorations are detailed in Sections 4.4 to 4.10. For these experiments the “freshly” prepared enzyme solution that had been utilised for the experiments in Figure 4-4 and Figure 4-5 was used throughout. It was not envisaged that fresh solutions of enzyme should have to be used each time for the sensor to be reproducible (Ryan *et al.*, 1997; O'Brien *et al.*, 2007).

#### 4.4 Nafion<sup>®</sup> interactions and Effect on Biosensor Sensitivity

The inclusion of Nafion<sup>®</sup> (Naf) in the recipe was one which was considered a little unusual and different. It has been documented that it has a detrimental effect on PPD films, possibly due to the presence of the alcohols in the Naf solution degrading the film (Friedemann *et al.*, 1996). In that study it was shown that the interferent rejection layer had less selectivity to NO (similar in size to  $\text{H}_2\text{O}_2$ , the signal molecule in this project) over AA, DA and nitrite when the Naf layer was applied after the PPD film compared to when the Naf layer was applied before the PPD layer.

The proceeding work was carried out previous to discovery and use of the second formulation by Zain, and so followed the general formulation of  $\text{Pt}_D\text{-PPD-Naf1\%x3-GA25\%x3-600UH}_2\text{Ox5}$ . The first alterations involved the removal of the PPD film (yellow trace in Figure 4-6) and the removal of the PPD and Naf 1% dips (green trace). In order to aid further understanding of the interactions of the constituents', in the sensor design, a further recipe was produced. This recipe had the PPD and GA 25% dips removed (blue trace).

The  $D$ -ser calibrations of these four new electrode recipes are presented in Table 9-4 and Table 4-4. The collected data is also graphed in Figure 4-6 along with the calibration

curve of Pt<sub>D</sub>-PPD-Naf1%<sup>x3</sup>-GA25%<sup>x3</sup>-600UH<sub>2</sub>Ox<sub>5</sub>, originally described in Table 4-1 and depicted in Figure 4-3 (blue trace). This sensor recipe is represented by the red trace in Figure 4-6.

The removal of the PPD film (yellow trace in Figure 4-6) had a significant effect on the sensitivity of the biosensor. The  $J_{\max}$  is significantly increased from  $18.02 \pm 1.35$  to  $69.23 \pm 6.04 \mu\text{A}\cdot\text{cm}^{-2}$ ,  $p = 0.0002^{***}$ , whereas the  $K_M$  changed to  $5246 \pm 836.4$  from  $4409 \pm 641 \mu\text{M}$ , a non-significant change,  $p = 0.4573$ . Absence of the PPD layer and the 3xNaf1% dips (green trace) returns the  $J_{\max}$  and  $K_M$  to levels that are not significantly different from the starting recipe,  $p = 0.1259$  and  $p = 0.0511$  respectively. Conversely removal of the PPD and 3xGA25% dips (blue trace) meant that the  $J_{\max}$  remained elevated at  $74.27 \pm 4.29 \mu\text{A}\cdot\text{cm}^{-2}$ . This is significantly higher,  $p < 0.0001^{***}$ , than the original recipe but similar to the value where only the PPD film was absent,  $p = 0.5217$ . The  $K_M$  values were not significantly different,  $p = 0.0908$  and  $p = 0.3942$ , for the same comparisons.

Examination of the designs  $J_{\max}$  and LRS values lead to a few conclusions being drawn (the differences in the  $K_M$  being largely insignificant does not allow conclusions to be drawn). The first one is that the function of the GA appears to be the tight binding of the  $\text{DAAO}$ . This is seen clearly by observing that in both Pt<sub>D</sub>-PPD-Naf1%<sup>x3</sup>-GA25%<sup>x3</sup>-600UH<sub>2</sub>Ox<sub>5</sub> and Pt<sub>D</sub>-GA25%<sup>x3</sup>-600UH<sub>2</sub>Ox<sub>5</sub> the  $J_{\max}$  and LRS are significantly lower than the other two recipes lowest. This indicates the strength of the GA has restrictively bound the  $\text{DAAO}$ , inhibiting its function and reducing turnover of  $\text{D-ser}$ . It is also possible to speculate that the Naf and PPD have also combined in a manner which has rendered it impossible for the GA to interact with. The chemical combination produced could provide a surface which is inert to both of the amine interactive carbonyl groups on the GA. At best the combination of PPD film and Naf dip layers is no different than the bare metal surface at a base surface for the GA and enzyme linking to occur on.

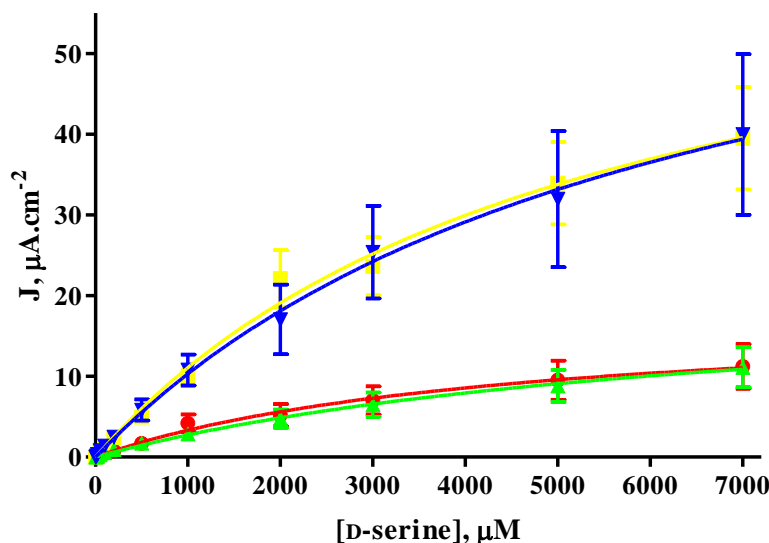


Figure 4-6

J-concentration plot for Pt<sub>D</sub>-PPD-Naf1% $\times$ 3-GA25% $\times$ 3-600UH<sub>2</sub>Ox<sub>5</sub> (red trace) and the 3 variations fabricated to elucidate the role of the Naf1% $\times$ 3 dips. Pt<sub>D</sub>-Naf1% $\times$ 3-GA25% $\times$ 3-600UH<sub>2</sub>Ox<sub>5</sub> is the yellow trace, Pt<sub>D</sub>-GA25% $\times$ 3-600UH<sub>2</sub>Ox<sub>5</sub> is the green trace, Pt<sub>D</sub>-Naf1% $\times$ 3-600UH<sub>2</sub>Ox<sub>5</sub> is the blue trace. All traces are plotted as Mean J  $\pm$  SEM with fitted kinetic curve.

Electrode Design	Pt <sub>D</sub> -Naf1% $\times$ 3-GA25% $\times$ 3-600UH <sub>2</sub> Ox <sub>5</sub> , n=4	Pt <sub>D</sub> -GA25% $\times$ 3-600UH <sub>2</sub> Ox <sub>5</sub> , n=4	Pt <sub>D</sub> -Naf1% $\times$ 3-600UH <sub>2</sub> Ox <sub>5</sub> , n=4
Kinetics	M-M, p = 0.4354	M-M, n/c	M-M, p = 0.3559
R <sup>2</sup>	0.9938	0.9974	0.9978
J <sub>max</sub> , µA.cm <sup>-2</sup>	69.23 $\pm$ 6.04	21.54 $\pm$ 1.45	74.27 $\pm$ 4.29
K <sub>M</sub> , µM	5246 $\pm$ 836.4	6844 $\pm$ 770.1	6200 $\pm$ 617.3
LRS, µA.cm <sup>-2</sup> .mM <sup>-1</sup>	13.20 $\pm$ 1.01	3.148 $\pm$ 0.151	11.98 $\pm$ 0.53

Table 4-4

Kinetic parameters, fit, J<sub>max</sub> and K<sub>M</sub> values calculated from the calibration data in Table 9-4. J<sub>max</sub>, K<sub>M</sub> and LRS are presented as Mean  $\pm$  SEM.

This is further borne out by the data provided by Pt<sub>D</sub>-Naf1% $\times$ 3-600UH<sub>2</sub>Ox<sub>5</sub> (blue trace). Here the removal of the GA25% $\times$ 3 dips has resulted in a J<sub>max</sub> significantly higher than the first two examples discussed. Interestingly the J<sub>max</sub> and LRS of Pt<sub>D</sub>-Naf1% $\times$ 3-GA25% $\times$ 3-600UH<sub>2</sub>Ox<sub>5</sub> (yellow trace) is statistically the same as Pt<sub>D</sub>-Naf1% $\times$ 3-600UH<sub>2</sub>Ox<sub>5</sub>. This could indicate that with the removal of the PPD film and the subsequent loss of any interaction between the PPD and Naf has changed how binding occurs within the recipe. Here it appears that the GA now primarily binds to the Naf and that there are only a limited number of carbonyl groups remaining to interact with the GA. It may be that one carbonyl group is bound to the Naf and one group is free to bind a dAAO or even that the majority of all groups are bound to the Naf. Either way it certainly appears that the cross-linking of dAAO to each other and even the binding of a

single GA to two sites on the same  $\alpha$ AAO is severely reduced when Naf and GA are combined without the presence of PPD. In the presence of PPD or without PPD and Naf it appears that the GA serves to restrict the shape, movement and functioning of the enzyme.

Thus it is possible to say that the Naf contributes little to the design of the sensor. It interacts, most probably in a detrimental way, with the PPD film. The GA does not appear to bind effectively to the Naf in the formulation and thus results in a recipe with two separate entities. The first is a PPD-Naf film on top of which is resting a heavily cross-linked GA- $\alpha$ AAO complex. The degree of cross-linking appears to be detrimental to the full function of the enzyme, inhibiting turnover of substrate.

#### 4.5 Contribution of Glutaraldehyde to Biosensor Sensitivity

Having demonstrated that the GA- $\alpha$ AAO complex was possibly denaturing the enzyme and reducing its ability to turnover substrate, investigating its role within the biosensor recipe was the next component to be examined. It was a component which had drawn attention of its own accord, as the use of GA at 25% concentration is unusual. It would be more typical to see GA used at concentration levels similar to 2.5% (Wang *et al.*, 1997), 1% (O'Brien *et al.*, 2007), 0.5% (Hu & Wilson, 1997) 0.13% (Burmeister & Gerhardt, 2001) and 0.01% (Sanford *et al.*, 2010). Where GA had been used as a 25% solution it was used in the context of holding the electrode in close proximity of the solution and allowing the vapours released to form the cross-links (McMahon *et al.*, 2005) and not dipping the electrode directly into the solution. Glutaraldehyde, 0.5%, has been used previously in conjunction with  $\alpha$ AAO to immobilise the enzyme onto aminated beads, and thus providing the most stable configuration (López-Gallego *et al.*, 2005b)

A further alteration was also considered across all of the biosensors fabricated. The PPD film was formed by CV rather than CPA. This yielded a PPD<sub>cv</sub> layer. The reasons for this change are found in Section 4.2 where it was stated that Zain had also utilised a CV method to form the polymer layer. Thus by forming the PPD<sub>cv</sub> layer not only is a comparison enabled between the various GA percentages but also an insight might be gained into the effect of the type of polymer formed on the biosensor sensitivity. An in-

depth examination of different polymer formation methods (in conjunction with 2% GA) and resultant effects on sensitivity are detailed in Section 4.7.2.

Thus to explore the influence of the GA on the properties of the biosensor, electrodes were prepared according to the general recipe  $\text{Pt}_D\text{-PPD}_{cv}\text{-Naf1x3\%-GA25\%x3-600UH}_2\text{Ox5}$  but with the GA 25% replaced by concentrations of 0.5%, 1.0%, 2.0%, 5.0% and 10.0% GA. The results obtained for these electrodes are listed in Table 9-5 and Table 4-5.

The results obtained are also graphically represented in Figure 4-7 and Figure 4-8. The large variation in the observed sensitivities with corresponding change in % of GA used is very apparent when considering these two diagrams.

Use of 0.5 % GA produced a biosensor with minimal response to increases in substrate concentration (red trace, Figure 4-7) with a  $J_{\max}$  of  $0.279 \pm 0.014 \mu\text{A}\cdot\text{cm}^{-2}$  and  $K_M$  of  $4312 \pm 508 \mu\text{M}$ . These were significantly different when compared to 1%, 2%, 5%, 10% and 25% GA respectively. The lower value of  $J_{\max}$  ( $p = 0.0003^{***}$ ,  $p < 0.0001^{***}$ ,  $p = 0.0004^{***}$ ,  $p = 0.0007^{***}$ ,  $p = 0.0007^{***}$ ) was unfavourable. However, the lower  $K_M$  value ( $p = 0.0058^{**}$ ,  $p = 0.0383^*$ ,  $p = 0.0009^{***}$ ,  $p = 0.0048^{**}$ ,  $p = 0.0222^*$ ) was desirable. While the lower  $K_M$  is beneficial the very small  $J_{\max}$  renders this recipe untenable.

The changes in sensitivity show the combined effect of the  $J_{\max}$  and  $K_M$  changes. The 2% GA recipe has a significantly higher LRS than the 0.5%, 5% and 10% GA recipes,  $p < 0.0001^{***}$  for all three comparisons. The LRS of the 25% recipes is significantly larger than that of the 2% recipe,  $p = 0.0042^{**}$ .

%GA used	0.5%, n = 4	1.0%, n = 3	2.0%, n = 8
<b>Kinetics</b>	M-M, n/c	M-M, p = 0.9107	M-M, p = 0.3781
<b>R<sup>2</sup></b>	0.9942	0.9997	0.9956
<b>J<sub>max</sub>, <math>\mu\text{A}\cdot\text{cm}^{-2}</math></b>	0.2794 $\pm$ 0.0146	81.26 $\pm$ 1.51	22.33 $\pm$ 1.61
<b>K<sub>M</sub>, <math>\mu\text{M}</math></b>	4312 $\pm$ 508.6	7251 $\pm$ 252.1	7993 $\pm$ 1039
<b>LRS, <math>\mu\text{A}\cdot\text{cm}^{-2}\cdot\text{mM}^{-1}</math></b>	0.0648 $\pm$ 0.0046	11.21 $\pm$ 0.19	0.9537 $\pm$ 0.0355
%GA used	5%, n = 3	10%, n = 3	25%, n = 4
<b>Kinetics</b>	M-M, n/c	M-M, n/c	M-M, n/c
<b>R<sup>2</sup></b>	0.9997	0.9995	0.9957
<b>J<sub>max</sub>, <math>\mu\text{A}\cdot\text{cm}^{-2}</math></b>	5.914 $\pm$ 0.115	3.671 $\pm$ 0.087	14.25 $\pm$ 0.95
<b>K<sub>M</sub>, <math>\mu\text{M}</math></b>	8853 $\pm$ 299.7	7500 $\pm$ 325.9	7548 $\pm$ 926.4
<b>LRS, <math>\mu\text{A}\cdot\text{cm}^{-2}\cdot\text{mM}^{-1}</math></b>	0.6680 $\pm$ 0.0102	0.4895 $\pm$ 0.0103	1.888 $\pm$ 0.112

Table 4-5

Kinetic parameters, fit, J<sub>max</sub> and K<sub>M</sub> values calculated from the calibration data in Table 9-5. J<sub>max</sub> and K<sub>M</sub> are presented as Mean  $\pm$  SEM.

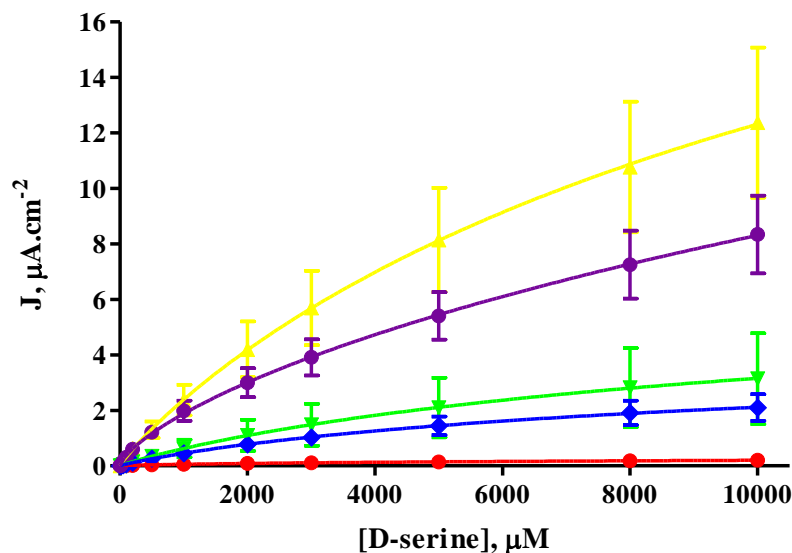


Figure 4-7

J-concentration plot for Pt<sub>D</sub>-PPD<sub>cv</sub>-Naf1% $\times$ 3-GA25% $\times$ 3-600UH<sub>2</sub>O $\times$ 5 (purple trace) and 4 of the 5 variations fabricated to elucidate the role of the GA25% $\times$ 3 dips. The blue trace is GA10% $\times$ 3, GA5% $\times$ 3 is the green trace, GA2% $\times$ 3 is the yellow trace and GA0.5% $\times$ 3 is represented by the red trace. All traces are plotted as Mean J  $\pm$  SEM with fitted kinetic curve.

Interestingly the 1% GA (orange trace in Figure 4-8) recipe produced a significantly higher J<sub>max</sub>, 81.26  $\pm$  1.51  $\mu\text{A}\cdot\text{cm}^{-2}$ , than either 2%, 5%, 10% or 25%, p < 0.0001\*\*\* for all. The J<sub>max</sub> decreases to 22.33  $\pm$  1.61  $\mu\text{A}\cdot\text{cm}^{-2}$  for 2% GA, and continues to decrease significantly, p < 0.0001\*\*\*, for 5% GA to 5.914  $\pm$  0.115  $\mu\text{A}\cdot\text{cm}^{-2}$ , and significantly further to 3.671  $\pm$  0.087  $\mu\text{A}\cdot\text{cm}^{-2}$ , p < 0.0001\*\*\*. Increasing the GA concentration used to 25% increases the J<sub>max</sub> to 14.25  $\pm$  0.95  $\mu\text{A}\cdot\text{cm}^{-2}$ , which is significantly higher than 10% GA, p = 0.0016\*\* but significantly lower than 2% GA, p = 0.0075\*\*.

Examining the  $K_M$  values there is no significant difference between 1% and 2%,  $p = 0.6832$ , 1% and 10% GA,  $p = 0.5782$ , or 1% and 25% GA,  $p = 0.8008$ . There is also no difference between 2% and 10%,  $p = 0.7862$ , 2% and 25%,  $p = 0.7903$ , or between 10% and 25% GA,  $p = 0.9677$ . The 5%  $K_M$  values are significantly higher than 1% and 10%,  $p = 0.0150^*$  and  $p = 0.0378^*$ , but not 2% or 25%,  $p = 0.6372$  and  $p = 0.2982$  respectively.

The comparison, of the LRS of the 1% GA recipes to the other five recipes, illustrates the degree of change which occurs with the use of this particular concentration of GA. It is significantly larger than all the other sensitivity values,  $p < 0.0001^{***}$  for all values. Numerically it is an order of magnitude more sensitive than the other GA recipes.

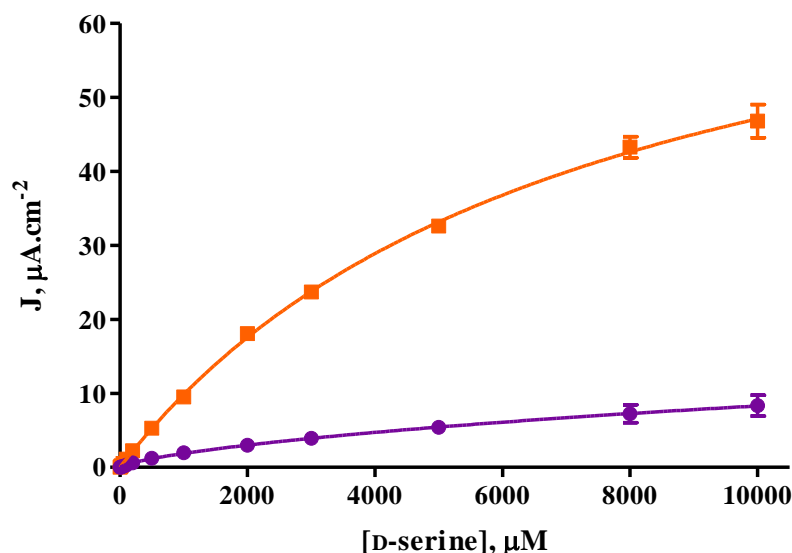


Figure 4-8

**J-concentration plot for  $\text{Pt}_D\text{-PPD}_{cv}\text{-Naf1\%GA25\%600UH}_2\text{Ox5}$  (purple trace) and its variation with  $\text{GA1\%}$ , represented by the orange trace. All traces are plotted as Mean  $J \pm \text{SEM}$  with fitted kinetic curve.**

Taken together these results indicate that the  $J_{\max}$  and  $K_M$  values change in a radical way, particularly over small changes in the % of GA used when the % of GA is kept low. Both  $K_M$  and  $J_{\max}$  appear to settle into a particular range once the GA % reaches and exceeds 5%. Below this value, particularly between 0.5% and 2% GA there does seem to be an important and radical interplay between the two kinetic parameters. This was demonstrated most obviously by the biosensors fabricated with 1% GA in the recipe. They obtained a  $J_{\max} \sim 5$  times higher than the 2% and 25% GA recipes and  $\sim 300$  times higher than the 0.5% recipe, however its  $K_M$  is the same as that of the 25% and 2%, slightly lower than 5% and almost twice the value obtained for 0.5% GA. This

complex interplay is summarised in Figure 4-9. From the plot it is quite clear that possibly the most interesting area, in terms of GA% used, for further study could be that between 0.5% and 2%. Within this region it appears that the interplay between  $K_M$  and  $J_{max}$  is most complex and could provide the solution to a biosensor with a high  $J_{max}$  and a low  $K_M$ . It also most certainly appears that using GA as a 25% solution is unlikely to provide the best solution as above 5% concentration the  $K_M$  remains high and the  $J_{max}$  low.

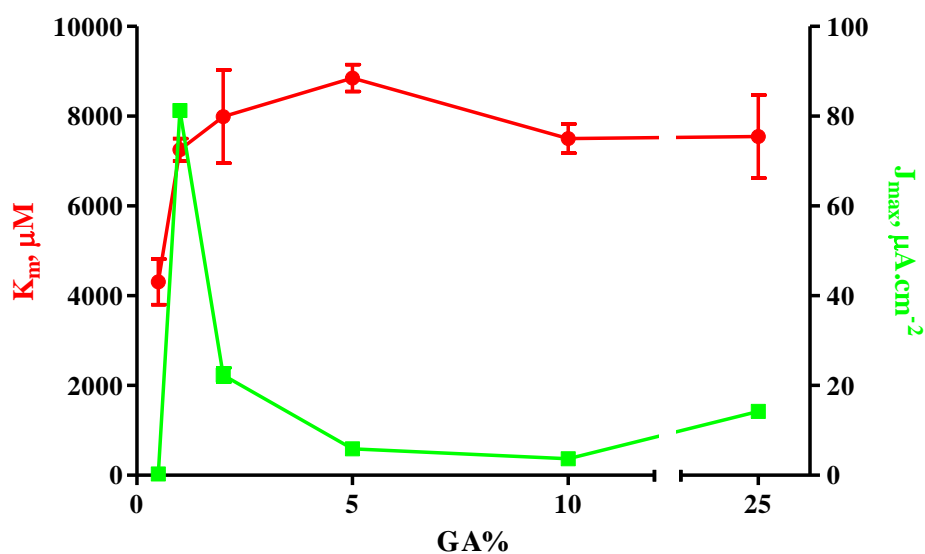


Figure 4-9

A plot of the  $K_M$  values (red points) and  $J_{max}$  (green points) obtained when the % concentration of GA used in the recipe  $\text{Pt}_D\text{-PPD}_{cv}\text{-Naf1}\% \times 3\text{-GA25}\% \times 3\text{-600UH}_2\text{O} \times 5$  was varied between 0.5% and 25%.

Larger concentrations of GA are either distorting the active site of the enzyme, rendering it inactive, providing an increased diffusional barrier or distorting the underlying films. Individually or in combination these three processes are limiting the  $J_{max}$  and increasing the  $K_M$  resulting in significantly lower sensitivities for concentrations of GA over 2%.

Briefly, turning to the difference caused by the change in polymerisation method it is necessary to compare the results here for  $\text{Pt}_D\text{-PPD}_{cv}\text{-3}\% \text{Naf1}\% \text{-3}\% \text{GA25}\% \text{-5}\% \text{600UH}_2\text{O}$  with the results for  $\text{Pt}_D\text{-PPD}\text{-3}\% \text{Naf1}\% \text{-3}\% \text{GA25}\% \text{-5}\% \text{600UH}_2\text{O}$  as obtained in Section 4.3. It is seen that there is no significant difference between the  $J_{max}$  values,  $p = 0.0625$ , but that the  $K_M$  is increased significantly for  $\text{PPD}_{cv}$ ,  $p = 0.0317^*$ . Further comparisons like this are examined in Section 4.7.2.

## 4.6 Variations of the Enzyme Solution

### 4.6.1 Different Suppliers of DAAO

Previous to work commencing on the biosensor recipe provided by Z. M. Zain preliminary methodology work had been carried out on a sample of DAAO obtained from Fluka Chemie. It was noticed that this enzyme produced differing results to the enzyme obtained from BBI Enzymes. As a result it was decided to examine the effect different enzyme samples from different suppliers would have on the sensitivity of the biosensor. Each of three suppliers, Fluka, Sigma and BBI, provided the enzyme with differing ratios of enzyme and protein,  $1.9 \text{ U.g}^{-1}$ ,  $2.3 \text{ U.g}^{-1}$  and  $7.46 \text{ U.g}^{-1}$  (units per gram of solid) respectively.

Thus different solutions were prepared from the Fluka and Sigma enzyme samples and compared to the BBI enzyme which was being used as a standard. A  $200 \text{ U.mL}^{-1}$  solution was prepared from the Fluka  $1.9 \text{ U.g}^{-1}$  enzyme. From the Sigma  $2.3 \text{ U.g}^{-1}$  enzyme  $100 \text{ U.mL}^{-1}$ ,  $250 \text{ U.mL}^{-1}$  and  $600 \text{ U.mL}^{-1}$  solutions were prepared. These solutions were then used to fabricate biosensors according to the recipe Pt<sub>D</sub>-PPD-Naf1% $\times$ 5-GA25%-Enzymex10 and were subsequently calibrated for their response to D-ser. The results of these calibrations are detailed in Table 9-6 and are directly comparable to the Pt<sub>D</sub>-PPD-Naf1% $\times$ 5-GA25%-600UH<sub>2</sub>Ox10 results detailed in Table 4-1.

It is interesting to note that electrodes fabricated with the  $600 \text{ U.mL}^{-1}$  solution, formulated from the  $2.3 \text{ U.g}^{-1}$  Sigma DAAO, could only be made with 5 dips into the enzyme solution and not 10 as per the other recipes. This was due to the very viscous nature of the solution at this high concentration and the formation of clumps of material on the electrode surface rather than a smooth film. It was for this same reason that the Fluka enzyme was only prepared in a solution of  $200 \text{ U.mL}^{-1}$ . This solution and the Sigma  $250 \text{ U.mL}^{-1}$  solution were found to be the optimum high concentration before clumping became an issue.

Electrode Design	200U.mL <sup>-1</sup> soln, 1.9U.g <sup>-1</sup> solid Fluka, n = 8	100U.mL <sup>-1</sup> soln, 2.3U.g <sup>-1</sup> solid Sigma, n = 8	250U.mL <sup>-1</sup> soln, 2.3U.g <sup>-1</sup> solid Sigma, n = 8	600U.mL <sup>-1</sup> soln, 2.3U.g <sup>-1</sup> solid Sigma, n = 3
<b>Kinetics</b>	M-M, p = 0.4354	M-M, n/c	M-M, p = 0.3559	M-M- H,p=0.0214
<b>R<sup>2</sup></b>	0.9978	0.9970	0.9981	0.9981
<b>J<sub>max</sub>, μA.cm<sup>-2</sup></b>	30.27 ± 1.40	29.46 ± 1.65	64.08 ± 4.36	33.69 ± 2.80
<b>K<sub>M</sub>, μM</b>	3929 ± 314	8881 ± 844	10274 ± 1019	3735 ± 573
<b>α</b>				1.273 ± 0.098
<b>LRS, μA.cm<sup>-2</sup>.mM<sup>-1</sup></b>	7.706 ± 0.280	3.317 ± 0.137	6.238 ± 0.207	9.020 ± 0.649

Table 4-6

Kinetic parameters, fit, J<sub>max</sub> and K<sub>M</sub> values calculated from the calibration data in Table 9-6. The values for Pt<sub>D</sub>-PPD-Naf1% $\times$ 5-GA25%-600UH<sub>2</sub>O $\times$ 10 have been omitted but can be found in Table 4-1. J<sub>max</sub>, K<sub>M</sub>, α and LRS are presented as Mean ± SEM.

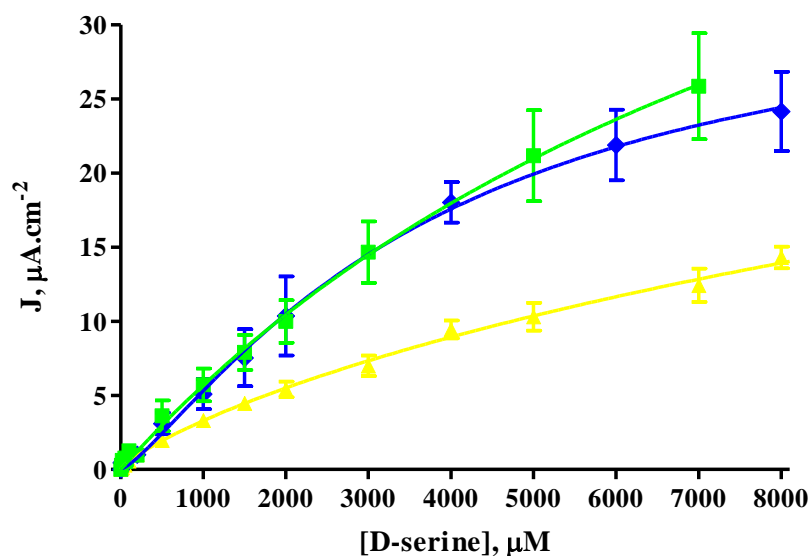


Figure 4-10

J-concentration plot for the Pt<sub>D</sub>-PPD-Naf1% $\times$ 5-GA25%-Enzymex10 recipes presented in Table 9-6. 100 U.ml<sup>-1</sup> 2.3 U.g<sup>-1</sup> is the yellow trace, 250 U.ml<sup>-1</sup> 2.3 U.g<sup>-1</sup> is the green trace and 600 U.ml<sup>-1</sup> 2.3 U.g<sup>-1</sup> is the blue trace. Kinetic curve fits are those described in Table 4-6 and Table 4-1. All traces are plotted as Mean J ± SEM with fitted kinetic curve.

It is interesting to observe from Table 4-6 and Table 4-1 that the 600 U.mL<sup>-1</sup> Sigma solution is the only one of the 5 solutions considered that conformed to Michaelis-Menten Hill-Type kinetics, a more desirable kinetic model as will produce a higher LRS and lower K<sub>M</sub> than Michaelis-Menten kinetics for the same J<sub>max</sub>. Indeed it can be seen that its K<sub>M</sub> is significantly lower than the 100 U.mL<sup>-1</sup> and 250 U.mL<sup>-1</sup> solutions made with the Sigma enzyme, p = 0.0065\*\* and p = 0.0046\*\* respectively, and significantly lower than the 600 U.mL<sup>-1</sup> solution made with the BBI enzyme, p = 0.0145\*. It is not significantly different from the 200 U.mL<sup>-1</sup> solution made from the Fluka enzyme, p = 0.7609. The benefit of this M-M-H kinetics can be seen visually in Figure 4-10 where the 250 U.ml<sup>-1</sup> 2.3 U.g<sup>-1</sup> is the green trace and 600 U.ml<sup>-1</sup> 2.3 U.g<sup>-1</sup> is the blue trace. It

can be seen that the M-M-H kinetics mean a more linear initial region of increasing  $J$  with increasing concentration of D-ser and also a more marked turning point as the enzyme reaches the limit of its ability to turn-over substrate.

The  $J_{\max}$  of various solutions are non-significantly different, except for that of the 250 U.mL<sup>-1</sup> solution formulated from the 2.3 U.g<sup>-1</sup> Sigma enzyme. This is significantly higher than the other solutions,  $p < 0.0001^{***}$  for all solutions except the 600 U.mL<sup>-1</sup> 2.3 U.g<sup>-1</sup> solution where  $p = 0.0027^{**}$ .

The LRS of the 600 U.mL<sup>-1</sup> 2.3 U.g<sup>-1</sup> Sigma solution is significantly higher than the other solutions,  $p < 0.0001^{***}$  for 100 U.mL<sup>-1</sup> 2.3 U.g<sup>-1</sup> solution,  $p < 0.0004^{***}$  for 250 U.mL<sup>-1</sup> 2.3 U.g<sup>-1</sup> solution and  $p < 0.0001^{***}$  for 600 U.mL<sup>-1</sup> 7.46 U.g<sup>-1</sup> solution. The exception to this is the 200 U.mL<sup>-1</sup> 1.9 U.g<sup>-1</sup> solution, which is not significantly lower,  $p = 0.0539$ .

Increasing the enzyme concentration for the 2.3 U.g<sup>-1</sup> solution from 250 U.ml<sup>-1</sup> to 600 U.ml<sup>-1</sup> changes the kinetics to a Hill-type which may indicate that the increasing quantity of enzyme and protein on the surface is changing the diffusional properties of the biosensor.

From Figure 4-10 it can be seen that obtaining as high a concentration of enzyme in solution can be beneficial. It appears that increased enzyme loading on the electrode surface not only increases the  $J_{\max}$  but also possibly decreases the  $K_M$  and can change the kinetic model to the more favourable M-M-H. Figure 4-11 (comparison of the highest concentration solutions before “clumps” appear on the electrode surface) elucidates the possibility that the environment the enzyme is trapped within is also important to consider. Here the ratio of active enzyme to protein as supplied demonstrates the capability of providing a more favourable environment for optimum activity. It is also possible to relate this back to the information in Sections 4.4 and 4.5 and deduce that all components of the biosensor impact its operation and need to be tuned to each other in order to obtain the most sensitive functioning possible.

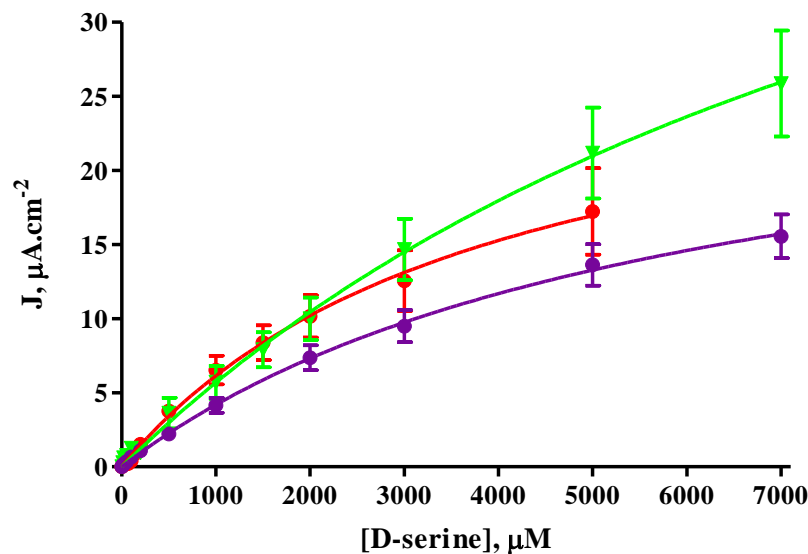


Figure 4-11

J-concentration plot for the Pt<sub>D</sub>-PPD-Naf1% $\times$ 5-GA25%-Enzymex10 recipes presented in Table 9-6 where the enzyme solutions have reached maximum useable concentration. 200 U.ml<sup>-1</sup> 1.9 U.g<sup>-1</sup> is the red trace and 250 U.ml<sup>-1</sup> 2.3 U.g<sup>-1</sup> is the green trace. Also included is the Pt<sub>D</sub>-PPD-Naf1% $\times$ 5-GA25%-10 $\times$  600 U.ml<sup>-1</sup> 7.46 U.g<sup>-1</sup> recipe from Table 4-1 (purple trace). Kinetic curve fits are those described in Table 4-6 and Table 4-1. All traces are plotted as Mean J  $\pm$  SEM with fitted kinetic curve.

The lower sensitivity of the 600 U.ml<sup>-1</sup> 7.46 U.g<sup>-1</sup> biosensor in comparison to the 600 U.ml<sup>-1</sup> 2.3 U.g<sup>-1</sup> design is particularly indicative of the importance of the delicate balance between enzyme, protein and cross-linking agent. This is further backed up by the similar  $J_{\max}$  of 200 U.ml<sup>-1</sup> 1.9 U.g<sup>-1</sup> and 100 U.ml<sup>-1</sup> 2.3 U.g<sup>-1</sup> with differing  $K_M$  and the same  $K_M$  but differing  $J_{\max}$  of the 100 U.ml<sup>-1</sup> and 250 U.ml<sup>-1</sup> 2.3 U.g<sup>-1</sup> biosensor designs.

#### 4.6.2 Effect of Additives in the Enzyme Solution on Biosensor Sensitivity

Consideration was also given to the method of formulating the enzyme solution. It was noted that previous reports of working with DAAO in a biosensor has reported using it with 25 mg.mL<sup>-1</sup> BSA and 1% glycerol in 0.02M PBS with a pH 8.5 (Pernot *et al.*, 2008). Thus an enzyme solution containing these substances was formulated with enzyme concentration remaining at 600 U.mL<sup>-1</sup> (symbolised by 600U+A in recipes). Three electrode types were initially prepared with this enzyme solution. These were analogous to those prepared initially in Section 4.3 to investigate the original reported biosensor design.

The calibration data obtained from the three Pt<sub>D</sub>-PPD-Naf1%-GA25%-600U+A electrodes is displayed in Table 9-7, and the kinetic parameters in Table 4-7. All

formulations of the 600U+A display M-M kinetics. There is no significant difference between Pt<sub>D</sub>-PPD-Naf1%<sub>x3</sub>-GA25%<sub>x3</sub>-600U+Ax5 and Pt<sub>D</sub>-PPD-Naf1%<sub>x5</sub>-GA25%-600U+Ax10 in either K<sub>M</sub> or J<sub>max</sub>, p = 0.5655 and p = 0.1295 respectively. Both curves are also M-M fit with no significant difference in the LRS value, p = 0.2830. The extra quantity of Naf in the latter appears to be counteracted by the extra quantity of 600U+A utilised and the different method of application of GA.

Electrode Design	Naf1% <sub>x5</sub> -GA25%-600U+Ax10, n=4	Naf1% <sub>x3</sub> -GA25% <sub>x3</sub> -600U+Ax10, n=3	Naf1% <sub>x3</sub> -GA25% <sub>x3</sub> -600U+Ax5, n=7
<b>Kinetics</b>	M-M, p = 0.3170	M-M, p = 0.9431	M-M, n/c
<b>R<sup>2</sup></b>	0.9984	0.9979	0.9994
<b>J<sub>max</sub>, μA.cm<sup>-2</sup></b>	29.27 ± 1.69	53.50 ± 1.49	32.08 ± 0.86
<b>K<sub>M</sub>, μM</b>	6126 ± 534	3215 ± 219	6453 ± 287
<b>LRS, μA.cm<sup>-2</sup>.mM<sup>-1</sup></b>	4.778 ± 0.152	16.64 ± 0.74	4.971 ± 0.09

Table 4-7

Kinetic parameters, fit, J<sub>max</sub> and K<sub>M</sub> values calculated from the calibration data in Table 9-7. The values are comparable to those found in Table 4-1, where the same designs are discussed excepting the enzyme solution which is made up in water. J<sub>max</sub>, K<sub>M</sub> and LRS are presented as Mean ± SEM.

There is a significant difference however between Pt<sub>D</sub>-PPD-Naf1%<sub>x3</sub>-GA25%<sub>x3</sub>-600U+Ax10 and Pt<sub>D</sub>-PPD-Naf1%<sub>x5</sub>-GA25%-600U+Ax10 or Pt<sub>D</sub>-PPD-Naf1%<sub>x3</sub>-GA25%<sub>x3</sub>-600U+Ax5. Its K<sub>M</sub> is significantly lower, p = 0.0069\*\* and p = 0.0001\*\*\* respectively. Its J<sub>max</sub> is significantly higher, p = 0.0001\*\*\* and p < 0.0001\*\*\* respectively, as is the LRS, p < 0.0040\*\* and p = 0.0040\*\* respectively. Here the higher amount of 600U+A, the lower quantity of Naf and the layering of the GA application has influenced all parameters favourably.

Thus even though it has the same number of enzyme dips as Pt<sub>D</sub>-PPD-Naf1%<sub>x5</sub>-GA25%-600U+Ax10 or the same other components as Pt<sub>D</sub>-PPD-Naf1%<sub>x3</sub>-GA25%<sub>x3</sub>-600U+Ax5, the results for Pt<sub>D</sub>-PPD-Naf1%<sub>x3</sub>-GA25%<sub>x3</sub>-600U+Ax10 are very significantly different, with all kinetic parameters significantly higher. Despite their difference in component and enzyme dips Pt<sub>D</sub>-PPD-Naf1%<sub>x5</sub>-GA25%-600U+Ax10 and Pt<sub>D</sub>-PPD-Naf1%<sub>x3</sub>-GA25%<sub>x3</sub>-600U+Ax5 show no statistical differences.

Graphed above in Figure 4-12 is a comparison of the 600UH<sub>2</sub>O and the 600U+A enzyme solution formulations of the Pt<sub>D</sub>-PPD-Naf1%<sub>x5</sub>-GA25%-Enzymex10 recipes. It can clearly be seen that there is a non-significant difference between the K<sub>M</sub> values, p = 0.7907, J<sub>max</sub> values, p = 0.9063, and LRS values, p = 0.5900. The different formulation

of the enzyme solution has no effect on the response obtained from this biosensor recipe.

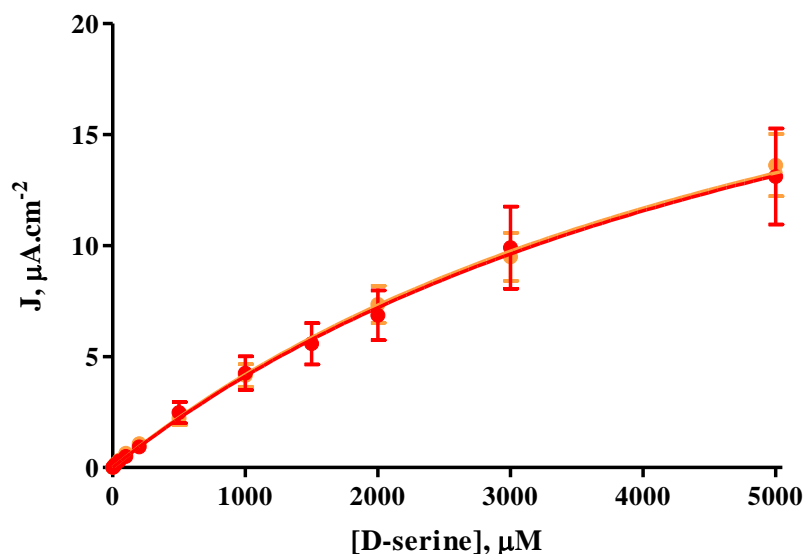


Figure 4-12

J-concentration plot for the comparison of  $Pt_D$ -PPD-Naf1% $\times$ 5-GA25%-Enzymex10. The orange trace represents the 600U+A recipe from and Table 4-7. The red trace represents the original 600UH<sub>2</sub>O recipe from and Table 4-1. Traces are plotted as Mean  $J \pm SEM$  with fitted kinetic curve.

Contrastingly, there are significant differences seen in Figure 4-13 between the 600UH<sub>2</sub>O and the 600U+A enzyme solution formulations of the  $Pt_D$ -PPD-Naf1% $\times$ 3-GA25% $\times$ 3-Enzymex10 recipes. The 600U+A solution produces a  $K_M$  that is significantly lower,  $p < 0.0001^{***}$ , a higher  $J_{max}$ ,  $p = 0.0062^{**}$ , and a higher LRS,  $p = 0.0051^{**}$ . This is a far superior result as it has increased the  $J_{max}$ , lowered the  $K_M$  and thus increased the LRS, which are all results that this exploration was attempting to achieve.

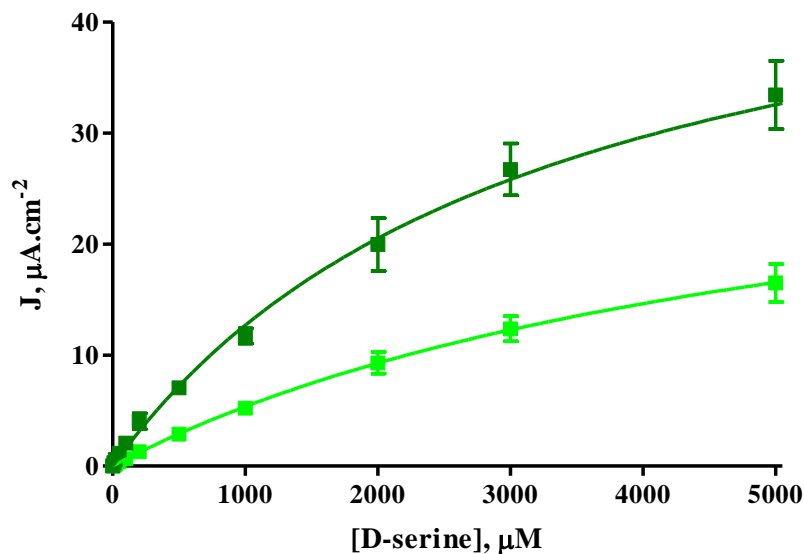


Figure 4-13

J-concentration plot comparing the Pt<sub>D</sub>-PPD-Naf1% $\times$ 3-GA25% $\times$ 3-Enzymex10 recipes. The dark green trace is the 600U+A recipe in Table 4-7. The bright green trace is the original 600UH<sub>2</sub>O recipe in Table 4-1. Traces are plotted as Mean J  $\pm$  SEM with fitted kinetic curve.

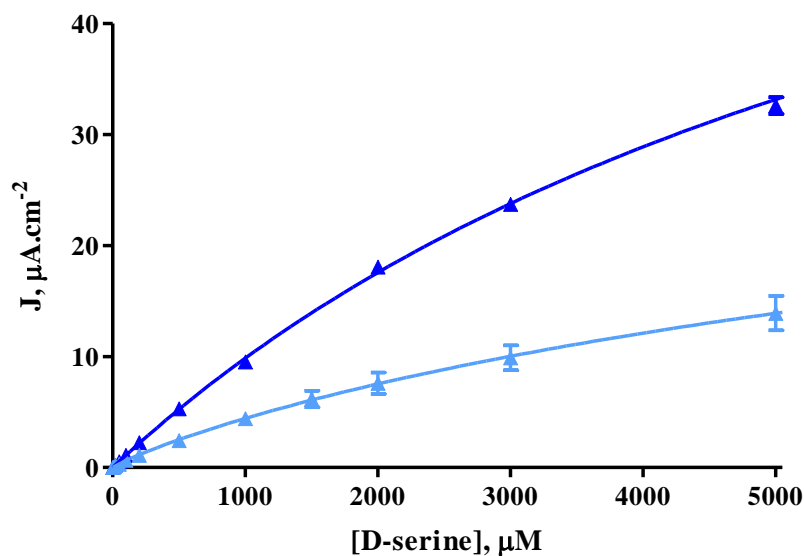


Figure 4-14

J-concentration plot comparing the Pt<sub>D</sub>-PPD-Naf1% $\times$ 3-GA25% $\times$ 3-Enzymex5 recipes. The light blue trace is the 600U+A recipe in Table 4-7. The royal blue trace is the original 600UH<sub>2</sub>O recipe in Table 4-1. Traces are plotted as Mean J  $\pm$  SEM with fitted kinetic curve.

Above in Figure 4-14 a further variance in results is seen between the 600U+A and 600UH<sub>2</sub>O solutions. In this instance, applied to the Pt<sub>D</sub>-PPD-Naf1% $\times$ 3-GA25% $\times$ 3-Enzymex5 recipe, observed is a non-significant decrease in the  $K_M$ ,  $p = 0.0960$ , a significant decrease in the  $J_{\text{max}}$ ,  $p < 0.0001^{***}$ , and a corresponding significant decrease in the LRS,  $p < 0.0001^{***}$ .

The dramatic difference between the results obtained for Pt<sub>D</sub>-PPD-Naf1%<sub>3</sub>-GA25%<sub>3</sub>-600U+A<sub>5</sub> and Pt<sub>D</sub>-PPD-Naf1%<sub>3</sub>-GA25%<sub>3</sub>-600U+A<sub>10</sub>, in comparison to their 600UH<sub>2</sub>O counterparts, demonstrates further that all changes to the biosensor recipe must be made in the context of all the component parts. Producing a significant change with one recipe by making a particular alteration will not necessarily produce a similar result even in closely related recipes. Initially, it was found that there was no difference between the water and additive solutions (Figure 4-12) when the recipe contained 5 dips into Naf and 1 dip into GA with 10 dips of enzyme solution, this could be due to the single layer of GA which allows for a finite amount of cross-linking with substances in the enzyme solution.

Next, with three dips of Naf and GA and ten dips of the enzyme solution it is found that the additive solution produces a much more sensitive biosensor than the water based enzyme solution (Figure 4-13). Upon reduction of the enzyme dips to five, in conjunction with the three dips of Naf and GA, the sensitivities are reversed with the water solution now displaying the larger LRS (Figure 4-14). This suggests that the larger number of GA dips are beneficial to the retention of the additive enzyme and resultant sensitivity increases, although this effect is lost with a reduced number of enzyme dips.

In order to further explore how slight changes to a biosensor recipe would affect the sensitivity a two further sets of electrodes were prepared with 600U+A and 600UH<sub>2</sub>O. These electrodes followed the general recipe Pt<sub>D</sub>-PPD-Naf1%<sub>3</sub>-GA25%<sub>3</sub>-Enzymex<sub>3</sub>. The calibration data obtained is displayed in Table 9-8 and the subsequently determined kinetic parameters are listed in Table 4-8 and graphed in Figure 4-15.

Initially it is necessary to note that the 600UH<sub>2</sub>O biosensor produced a significantly higher  $K_M$  than Pt<sub>D</sub>-PPD-Naf1%<sub>3</sub>-GA25%<sub>3</sub>-600UH<sub>2</sub>Ox<sub>5</sub>, the lowest  $K_M$  from Section 4.3,  $p = 0.0005^{***}$ . It has a significantly lower  $J_{max}$  than Pt<sub>D</sub>-PPD-Naf1%<sub>3</sub>-GA25%<sub>3</sub>-600UH<sub>2</sub>Ox<sub>10</sub>, the highest  $J_{max}$  from Section 4.3,  $p < 0.0001^{***}$ . Finally its LRS is significantly lower than Pt<sub>D</sub>-PPD-Naf1%<sub>3</sub>-GA25%<sub>3</sub>-600UH<sub>2</sub>Ox<sub>10</sub>, the highest LRS from Section 4.3,  $p < 0.0001^{***}$ .

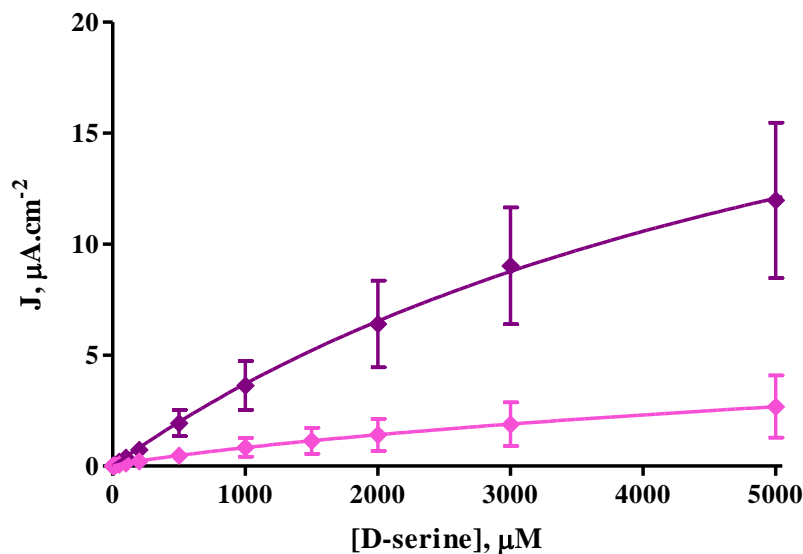


Figure 4-15

J-concentration plot for the comparison of Pt<sub>D</sub>-PPD-Naf1%<sup>x3</sup>-GA25%<sup>x3</sup>-Enzymex3. The pink trace represents the 600U+A recipe, and the purple trace represents the 600UH<sub>2</sub>O recipe. Both sets of data are taken from Table 9-8 and Table 4-8. Traces are plotted as Mean J ± SEM with fitted kinetic curve.

Electrode Design	Pt <sub>D</sub> -PPD-Naf1% <sup>x3</sup> -GA25% <sup>x3</sup> -600H <sub>2</sub> O <sup>x3</sup> n = 4	Pt <sub>D</sub> -PPD-Naf1% <sup>x3</sup> -GA25% <sup>x3</sup> -600U+A <sup>x3</sup> n = 4
Kinetics	M-M, p = 0.1476	M-M, n/c
R <sup>2</sup>	0.9997	0.9989
J <sub>max</sub> , μA.cm <sup>-2</sup>	27.79 ± 0.43	6.080 ± 0.306
K <sub>M</sub> , μM	6509 ± 194	6463 ± 485
LRS, μA.cm <sup>-2</sup> .mM <sup>-1</sup>	4.269 ± 0.066	4.971 ± 0.09

Table 4-8

Kinetic parameters, fit, J<sub>max</sub> and K<sub>M</sub> values calculated from the calibration data in Table 9-8. J<sub>max</sub>, K<sub>M</sub> and LRS are presented as Mean ± SEM.

The results between the 600U+A and 600UH<sub>2</sub>O for Pt<sub>D</sub>-PPD-Naf1%<sup>x3</sup>-GA25%<sup>x3</sup>-Enzymex3 are comparatively similar to those obtained for Pt<sub>D</sub>-PPD-Naf1%<sup>x3</sup>-GA25%<sup>x3</sup>-Enzymex5. The K<sub>M</sub> is not different, p = 0.9327. The J<sub>max</sub> and LRS are however significantly lower, both p < 0.0001\*\*\*. This results further bears out the results seen with the previous three recipes whereby the beneficial effect of the increased number of GA dips in relation to the additive enhanced enzyme solution is lost when the number of enzyme dips is also reduced, and the water based enzyme solution then becomes more efficient.

This collected and complex set of interplays for the recipe is graphically summarised in Figure 4-16. Here, as in Figure 4-9, the K<sub>M</sub> values are represented by red points and error bars. The J<sub>max</sub> values are displayed by green points and error bars. In an added

level of complexity though, the values obtained using the 600UH<sub>2</sub>O solution are connected using blue lines and the purple lines connect the 600U+A solution results.

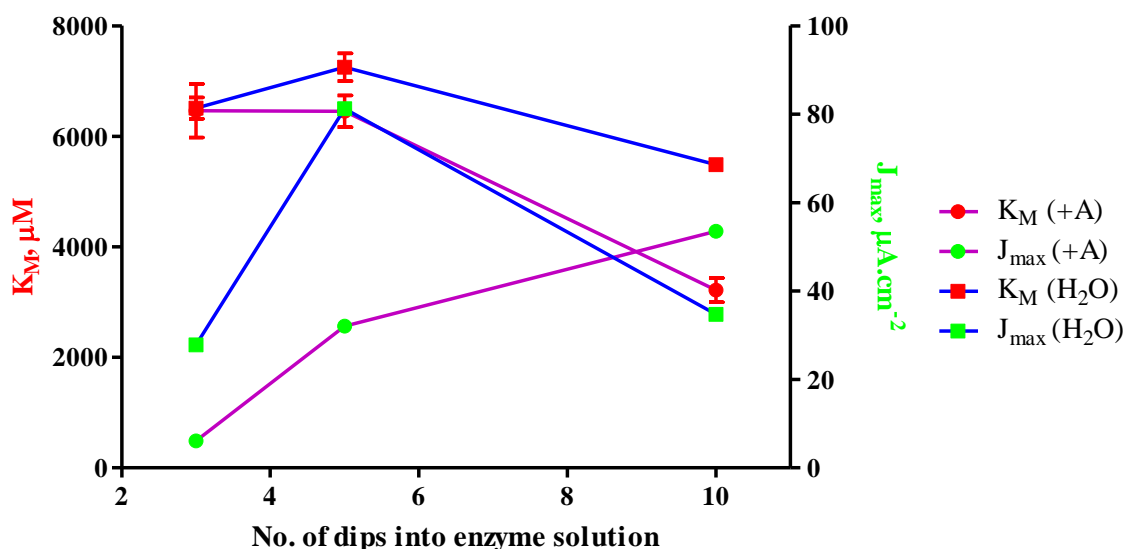


Figure 4-16

A plot of the  $K_M$  values (red points) and  $J_{\text{max}}$  (green points) obtained when the number of enzyme dips used in the recipe Pt<sub>D</sub>-PPD-Naf1% $\times$ 3-GA25% $\times$ 3-Enzymex? were varied. The enzyme solution used was also changed with the purple line connecting results obtained using a 600U+A solution and the blue line connecting results from a 600UH<sub>2</sub>O solution.

It is interesting to note, and easier to observe, that the observed  $K_M$  appears to reduce as dips of enzyme are increased for both solutions. However, the  $J_{\text{max}}$  tends to also decrease, except in the case of the 600U+A solution. This could point to a beneficial effect whereby if the enzyme is tempered or stabilised by an appropriate set of other components increasing number of dips could allow a continued decrease in  $K_M$  and increase in  $J_{\text{max}}$ .

Although the additives showed the possibility for potential benefits in biosensor design they were not found to have a pronounced effect over a large range of recipes for them to be considered for all future designs. This is especially true when one considers that the solution of  $\alpha$ AAO, PBS, glycerol and BSA “went off” after three days. Black lumps, of an undetermined nature, most likely a mould or fungus, were discovered to appear in the solution after this length of time. These lumps were also found in the PBS, glycerol and BSA solution which was prepared previous to the addition of the  $\alpha$ AAO. Taking this into account it was decided that this combination of additives was unsuitable for long term, multiple uses because of the limited shelf life of the solution and the

uncertainty in what was occurring and what effect it was having on the solution/enzyme.

## 4.7 Combined Alterations to the Biosensor Recipe

All the results from the preceding sections and experiments (from Section 4.2 to Section 4.6.2) indicated that changing one component of a biosensor recipe in isolation produced varying and unpredictable changes in sensitivity. Thus it was decided that a compound approach whereby one or more aspects of the recipe were changed simultaneously should be examined. These compound changes related to changes in; the PPD layer formed, the GA % used and the enzyme solution.

### 4.7.1 Enzyme Solution pH Changes Combined with GA Changes

The first combined change to be examined involved the alteration of the DAAO solution between 600UH<sub>2</sub>O and a 600 U.mL<sup>-1</sup> solution made up in PBS pH 8.5 (600UPBS). These solutions were used in a Pt<sub>D</sub>-PPD-Naf1%<sup>x3</sup>-GA<sup>x3</sup>-Enzymex5 recipe where the GA % used was 2% and 25%. GA 2% was chosen as it was the percentage which showed the most similar results to 25% in previous testing, see Figure 4-7 in Section 4.5. Yet, 2% is a much lower concentration and hopefully would not have a detrimental effect on the enzyme solution over time. The decision to use PBS at pH 8.5 was influenced by its use in the additives described previously in Section 4.6.2.

The results of these combined changes provide some interesting information. The first and possibly most important point is that the biosensors made with the 600UPBS solution provide significant enhancement of desired properties in the case of both 2% GA and 25% GA. This can be seen in Table 4-9 and Figure 4-17 where, in the case of 2% GA, the 600UPBS  $J_{max}$  is increased over the 600UH<sub>2</sub>O,  $p = 0.0002^{***}$ , and the  $K_M$  is not significantly different,  $p = 0.6604$ . When 25% GA was used the  $J_{max}$  increased significantly,  $p = 0.0012^{**}$ , and the  $K_M$  again was not significantly changed,  $p = 0.6345$ . Combined this meant that there was a significant increase in the LRS of both sets,  $p < 0.0001^{***}$  for 2% GA and  $p = 0.0031^{**}$  for 25% GA.

Electrode Design	GA 2%, 600UH <sub>2</sub> O, n = 4	GA 2%, 600UPBS, n = 3	GA 25%, 600UH <sub>2</sub> O, n = 4	GA 25%, 600UPBS, n = 7
<b>Kinetics</b>	M-M, p = 0.0569	M-M-H, p=0.0026	M-M, p = 0.2311	M-M, p = 0.3782
<b>R<sup>2</sup></b>	0.9979	1.000	0.9940	0.9932
<b>J<sub>max</sub>, μA.cm<sup>-2</sup></b>	20.70 ± 1.18	36.05 ± 0.84	18.02 ± 1.35	29.13 ± 1.60
<b>K<sub>M</sub>, μM</b>	9506 ± 919	10045 ± 463	4409 ± 641	3999 ± 511
<b>α</b>		0.9588 ± 0.0101		
<b>LRS, μA.cm<sup>-2</sup>.mM<sup>-1</sup></b>	2.177 ± 0.092	3.589 ± 0.083	4.086 ± 0.307	7.284 ± 0.568

Table 4-9

Kinetic parameters, fit, J<sub>max</sub>, K<sub>M</sub> and A values calculated from the calibration data in Table 9-9. J<sub>max</sub>, K<sub>M</sub>, LRS and α are presented as Mean ± SEM.

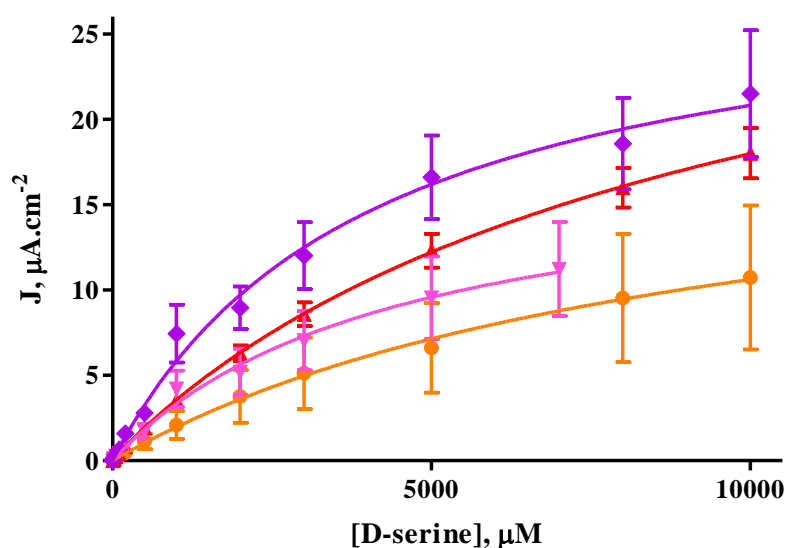


Figure 4-17

J-concentration plot for the comparison of Pt<sub>D</sub>-PPD-Naf1%<sup>x3</sup>-GA<sup>x3</sup>-Enzymex5. The purple trace represents biosensors formulated with 25% GA and 600UPBS, and the pink trace 25% GA and 600UH<sub>2</sub>O. Biosensors made with 2% GA and 600UPBS are depicted in red and the orange trace plots 2% GA and 600UH<sub>2</sub>O. Both sets of data are taken from Table 9-9 and Table 4-9. Traces are plotted as Mean J ± SEM with fitted kinetic curve.

Comparing the 2% GA 600UPBS and the 25% GA 600UPBS it is seen that the 2% GA has a significantly higher J<sub>max</sub> value, p = 0.0281\*, but that the 2% GA has a significantly higher K<sub>M</sub>, p = 0.0001\*\*\*. This results in the 25% GA 600UPBS still having significantly higher LRS than the 2% GA equivalent, p = 0.0034\*\*.

The 2% 600UPBS biosensors have a significantly higher J<sub>max</sub> compared to the 25% GA 600UH<sub>2</sub>O, p = 0.0001\*\*\*, although the K<sub>M</sub> is significantly higher, p = 0.0012\*\*. This combination results in LRS values that are non-significantly different, p = 0.2372. Thus formulation the enzyme solution with PBS pH 8.5 rather than neutral deionised water appears to increase the sensitivity of the biosensors.

Noteworthy too is the fact that the 2% GA 600UPBS is the only formulation displaying M-M-H kinetics. While this is a positive indication it is however offset by the fact that it also has the largest  $K_M$  value of the four designs. So despite this design having the largest  $J_{max}$  combined with M-M-H kinetics, it was not the result that was being searched for, as demonstrated by its poor LRS.

#### 4.7.2 Different Polymer Growth Methods Combined with an Altered GA % and Enzyme Solution Changes

Continuing with the  $Pt_D$ -PPD-Naf1% $\times$ 3-GA $\times$ 3-Enzymex5 recipe which utilised now 2% GA and not 25%, a further set of changes was examined. These changes involved the continuing examination of the 600UH<sub>2</sub>O and 600UPBS enzyme solutions. Further alterations now included examination of the PPD layer. Initial reports from Z.M. Zain discussed the use of CPA to grow the PPD layer, however as previously noted (see Section 4.2) by the time of publication (Zain *et al.*, 2010) this had changed to a CV growth method. Both methods are described in Section 3.5.3.

The polymer alterations were thus; the use of the CPA technique (PPD), the use of the CV technique (PPD<sub>cv</sub>) and a variant of the CPA technique (PPD<sub>a</sub>). This variant involved a less stringent application of the completely N<sub>2</sub> saturated process that would be normally followed. Once polymerisation had begun the solution was exposed to the atmosphere (as denoted by the <sub>a</sub> in the nomenclature) allowing a certain degree of ‘oxidised’ polymer formation to occur (see Section 2.8.4). The reason for this was that, as previously stated, the type of polymerisation that occurs and the structure of the polymer is still greatly disputed and while previous research by the group indicates that complete nitrogen saturation provides a more selective membrane, the effect of nitrogen saturation during polymerisation on sensitivity was one which was desirable to explore. It is also impossible to compare the degree of nitrogen saturation achieved by different studies and groups. Thus by comparing different controlled polymerisation methods within this study it was considered possible to discover useful comparisons. Thus four new sensor designs were created, using PPD<sub>cv</sub>/PPD<sub>a</sub>, 2% GA and 600UPBS/600UH<sub>2</sub>O. These were compared to the PPD, 2% GA, 600UPBS/600UH<sub>2</sub>O examined previously, in Section 4.7.1. Examining the data in Table 4-10 and Table 4-9 we see the continuation of the trend whereby the use of 600UPBS either increases the  $J_{max}$  or decreases the  $K_M$  substantially. This further leads to an improvement in the LRS across

the three different polymerisation methods utilised when compared to the 600UH<sub>2</sub>O alternative.

Electrode Design	PPD <sub>a</sub> , 2% GA, 600UH <sub>2</sub> O, n = 4	PPD <sub>a</sub> , 2% GA, 600UPBS, n = 4	PPD <sub>cv</sub> , 2% GA, 600UH <sub>2</sub> O, n = 8	PPD <sub>cv</sub> , 2% GA, 600UPBS, n = 4
<b>Kinetics</b>	M-M-H, p < 0.0001	M-M, p = 0.6136	M-M, p = 0.3781	M-M-H, p = 0.0001
<b>R<sup>2</sup></b>	1.000	0.9995	0.9956	0.9999
<b>J<sub>max</sub>, μA.cm<sup>-2</sup></b>	42.09 ± 1.18	36.05 ± 0.62	22.33 ± 1.61	58.98 ± 2.74
<b>K<sub>M</sub>, μM</b>	11974 ± 663	5177 ± 188	7993 ± 1039	12741 ± 1195
<b>α</b>		0.9323 ± 0.0104		0.9244 ± 0.0242
<b>LRS, μA.cm<sup>-2</sup>.mM<sup>-1</sup></b>	3.515 ± 0.096	6.964 ± 0.143	2.794 ± 0.172	4.629 ± 0.220

Table 4-10

Kinetic parameters, fit, J<sub>max</sub> and K<sub>M</sub> values calculated from the calibration data in Table 9-10. J<sub>max</sub>, K<sub>M</sub>, α and LRS are presented as Mean ± SEM.

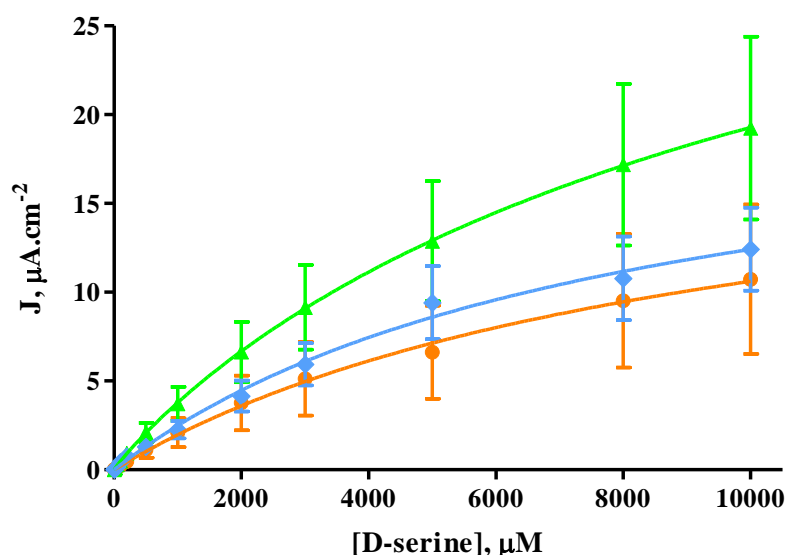


Figure 4-18

J-concentration plot for the comparison of Pt<sub>0</sub>-PPD-Naf1% $\times$ 3-GA2% $\times$ 3-600UH<sub>2</sub>O $\times$ 5. The orange trace signifies PPD (taken from Figure 4-17). The green trace represents PPD<sub>a</sub>. The blue trace represents PPD<sub>cv</sub>. Both sets of data are taken from Table 9-10 and Table 4-10. Traces are plotted as Mean J ± SEM with fitted kinetic curve.

Firstly it is necessary to analyse the 600UH<sub>2</sub>O recipes collectively. In Figure 4-18 can be seen the composite J-concentration plot for the three 2% GA and 600UH<sub>2</sub>O recipes. The most noticeable difference between the recipes is that the PPD recipe (orange trace, in keeping with that of Figure 4-17) and the PPD<sub>cv</sub> recipe (blue trace) produce significantly lower sensitivities than the PPD<sub>a</sub> alternative. This is interesting as the former PPD layers are polymerised under strict conditions of N<sub>2</sub> saturation, whereas

PPD<sub>a</sub> is exposed to the atmosphere during the polymerisation process, while all solutions were prepared under the same conditions of N<sub>2</sub> saturation.

Comparing PPD<sub>a</sub> to PPD and PPD<sub>cv</sub> it can be seen that its J<sub>max</sub> is significantly higher, both  $p < 0.0001^{***}$ , and the K<sub>M</sub> is unchanged,  $p = 0.3743$  and  $p = 0.0534$  respectively, leading to an LRS value which is also significantly higher,  $p < 0.0001^{***}$  and  $p = 0.0186^*$  respectively. The differences between PPD and PPD<sub>cv</sub> are minimal. The J<sub>max</sub> of PPD is not significantly different,  $p = 0.5233$ , and neither is the K<sub>M</sub>,  $p = 0.2176$ . However the LRS of PPD is significantly lower,  $p = 0.0368$ .

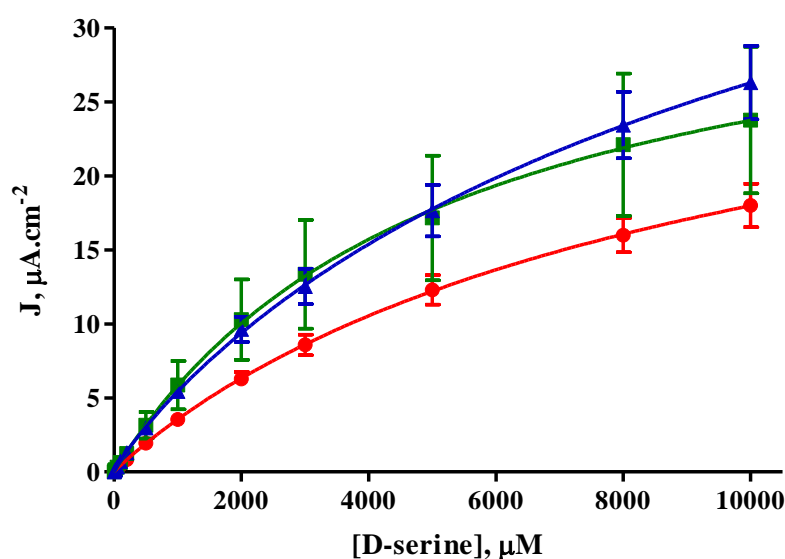


Figure 4-19

J-concentration plot for the comparison of Pt<sub>D</sub>-PPD-Naf1%GA2-600UPBSx5. The red trace signifies PPD (taken from Figure 4-17). The green trace represents PPD<sub>a</sub>. The blue trace represents PPD<sub>cv</sub>. Both sets of data are taken from Table 9-10 and Table 4-10. Traces are plotted as Mean J ± SEM with fitted kinetic curve.

Turning now to look at the three 600UPBS recipes collectively in Figure 4-19 it is possible to see similar trends. Again, it is observed that the PPD recipe (red trace as in Figure 4-17) has a lower sensitivity than the PPD<sub>a</sub> (green trace) and PPD<sub>cv</sub> (blue trace). Its J<sub>max</sub> is non-significantly different from PPD<sub>a</sub>,  $p > 0.9999$ , and significantly lower than PPD<sub>cv</sub>,  $p = 0.0010^{**}$ . The K<sub>M</sub> is significantly higher than that of PPD<sub>a</sub>,  $p = 0.0001^{***}$ , and non-significantly different from the PPD<sub>cv</sub> value,  $p = 0.1253$ . As with 600UH<sub>2</sub>O this leads the PPD 600UPBS to have a significantly lower LRS than either PPD<sub>a</sub> or PPD<sub>cv</sub>,  $p < 0.0001^{***}$  and  $p = 0.0119^*$  respectively.

As in the case of the PPD with 600UPBS and 600UH<sub>2</sub>O (see Section 4.7.1) the use of the 600UPBS with PPD<sub>a</sub> and PPD<sub>cv</sub> improves at least one kinetic parameter and thus the LRS. For PPD<sub>a</sub> it is seen that the  $J_{\max}$  is decreased for 600UPBS,  $p = 0.0040^{**}$ , however the  $K_M$  is also drastically reduced,  $p < 0.0001^{***}$ , leading to an overall increase in LRS,  $p < 0.0001^{***}$ . The  $J_{\max}$  of PPD<sub>cv</sub> is increased,  $p < 0.0001^{***}$ , the  $K_M$  is increased also,  $p = 0.0193^*$ , but together, again, they lead to a significant increase in the LRS,  $p < 0.0001^{***}$ , when 600UPBS is utilised in the recipe.

The percentage error in each of the sensors using different polymerisation method is also noted to decrease with the use of 600UPBS. For example, consider the  $J_{\max}$  values, as a percentage of the mean the SEM decreases in all cases. The PPD error reduces from 5.70% to 2.33%, the PPD<sub>a</sub> error reduces from 2.80% to 1.72%, and for PPD<sub>cv</sub> it reduces from 7.21% to 4.65%. Similar results are found for  $K_M$  and LRS values. Thus it also appears that 600UPBS produces more consistent biosensors, as it may be reducing variation in the enzyme solutions – water solutions being unbuffered are subject to pH variations.

Finally noteworthy also is the enzymatic fit differences. Unfortunately although some recipes do display a better M-M-H fit, they are blighted by high  $K_M$  values and thus no advantage is gained.

#### **4.8 Variations to the Biosensor Formulation Based on Previously Designed Biosensors**

Lastly of interest in this exploration was whether any techniques or chemicals used previously could enhance the sensitivity of the sensors or provide any useful information. This included examining different binding techniques, stabilisers and bio-molecules.

The use of PEI was one of particular interest in this broadening of parameters investigated. This is an interesting molecule as it is a polymeric substance which has polycationic structure and has been used widely in sensors before (Belay *et al.*, 1999; Patel *et al.*, 2000). It has been used to secure and stabilise substances to the surface of an electrode (Jezkova *et al.*, 1997; Cox *et al.*, 2003) and to increase efficiency of enzymes after other substances have reduced it (McMahon *et al.*, 2006; Bolger, 2007; Haughton, pending publication).

Widely used also has been either BSA on its own (Ryan *et al.*, 1997; Pernot *et al.*, 2008) or in a solution combined with glutaraldehyde, BSAGA (Hu & Wilson, 1997; Burmeister & Gerhardt, 2001; O'Brien *et al.*, 2007).

Of interest also was the FAD moiety. This molecule is the actual site within the  $\alpha$ AAO structure where the electron transfer processes take place. Addition of further quantities of FAD to biosensor designs is an approach that has been examined before with some degree of success (Haughton, pending publication)

#### 4.8.1 Alternative Methods for Primary Binding of $\alpha$ AAO

Thus it was decided to try alternative methods of binding the  $\alpha$ AAO to the surface. These methods constituted the use of both PEI and BSAGA as binding elements. In addition to this a duplication of the GA and  $\alpha$ AAO layering from the standard recipe was also considered.

##### 4.8.1.1 Duplication of Layering

It was hoped that a repetition of the layers of the cross-linking agent, GA, and the enzyme, 600UH<sub>2</sub>O could improve the sensitivity or kinetics parameters of the sensor. This effect had been observed before within the group (Haughton, pending publication). Thus the Pt<sub>D</sub>-PPD-Naf1%<sup>x3</sup>-GA2%-600UH<sub>2</sub>O<sup>x5</sup> recipe was altered to take the form Pt<sub>D</sub>-PPD-Naf1%<sup>x3</sup>-[GA2%<sup>x3</sup>-600UH<sub>2</sub>O<sup>x5</sup>]<sup>x2</sup>. 2% GA was chosen as it was hoped to provide a good level of cross-linking without the detrimental effects of 25% GA as discussed previously (Section 4.3).

The data for Pt<sub>D</sub>-PPD-Naf1%<sup>x3</sup>-GA2%<sup>x3</sup>-600UH<sub>2</sub>O<sup>x5</sup> was previously presented in Section 4.7.1 and depicted as the orange trace in Figure 4-17. It is restated here for clarity and easier comparison. It was seen previously that its sensitivity could be improved by using 600UPBS, but it was decided to utilise 600UH<sub>2</sub>O to retain consistency with the original recipes.

It is quite clear from examining the data in Table 4-11 that there is an advantage to be gained from doubling the layers of GA and 600UH<sub>2</sub>O. The  $J_{\max}$  has doubled in value, a significant difference,  $p = 0.0003^{***}$ , however the  $K_M$  has also increased,  $p = 0.0298^*$ . Overall this does lead to an improved LRS,  $p = 0.0001^{***}$ .

Electrode Design	Pt <sub>D</sub> -PPD-Naf1% $\times$ 3-[GA2% $\times$ 3-600UH <sub>2</sub> Ox5] $\times$ 2, n = 4	Pt <sub>D</sub> -PPD-Naf1% $\times$ 3-GA2%-600UH <sub>2</sub> Ox5, n = 4
Kinetics	M-M, p = 0.1964	M-M, p = 0.0569
R <sup>2</sup>	0.9996	0.9979
J <sub>max</sub> , $\mu\text{A}\cdot\text{cm}^{-2}$	42.94 $\pm$ 2.738	20.70 $\pm$ 1.18
K <sub>M</sub> , $\mu\text{M}$	13578 $\pm$ 1104	9506 $\pm$ 919
LRS, $\mu\text{A}\cdot\text{cm}^{-2}\cdot\text{mM}^{-1}$	3.162 $\pm$ 0.058	2.177 $\pm$ 0.092

Table 4-11

Kinetic parameters, fit, J<sub>max</sub> and K<sub>M</sub> values calculated from the calibration data in Table 9-11. J<sub>max</sub>, K<sub>M</sub> and LRS are presented as Mean  $\pm$  SEM.

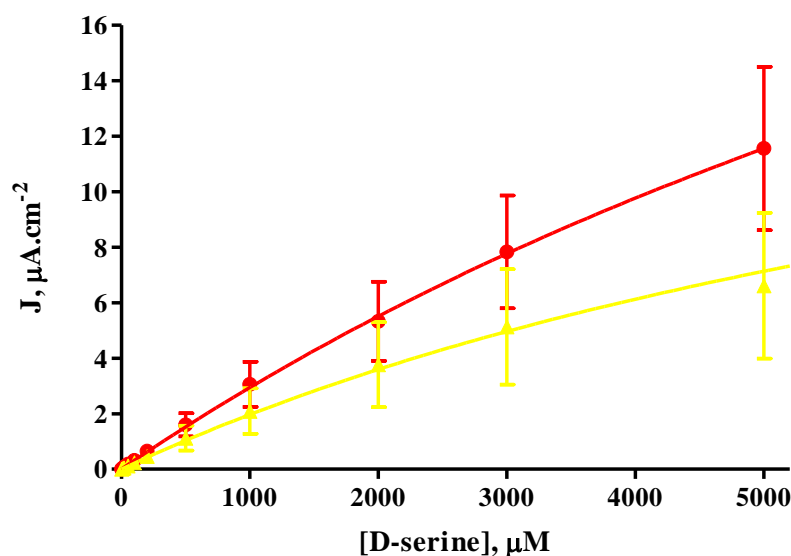


Figure 4-20

J-concentration plot for the comparison of Pt<sub>D</sub>-PPD-Naf1% $\times$ 3-GA2% $\times$ 3-600UH<sub>2</sub>Ox5 (yellow trace) and Pt<sub>D</sub>-PPD-Naf1% $\times$ 3-[GA2% $\times$ 3-600UH<sub>2</sub>Ox5] $\times$ 2 (red trace). Both sets of data are taken from Table 9-11 and Table 4-11. Traces are plotted as Mean J  $\pm$  SEM with fitted kinetic curve.

Although this was a positive result, the increased size of the linear region as denoted by the larger K<sub>M</sub> was not a desired outcome. It is also worth noticing that the J<sub>max</sub> of the double layered biosensors is not significantly different, p = 0.529, than the single layered 600UPBS biosensors in Section 4.7.1, which also has a lower K<sub>M</sub>, p = 0.0256\*, and a better LRS, p = 0.0056\*\*.

#### 4.8.1.2 Use of PEI as a Binding Agent

As a preliminary examination of the usefulness of PEI as binding agent in combination with the original recipe, 1 layer of 1% PEI was included before the enzyme dips. This resulted in the biosensor recipe Pt<sub>D</sub>-PPD-Naf1% $\times$ 3-GA25% $\times$ 3-PEI1%-600UH<sub>2</sub>Ox5. The hope was that the positive charges in the PEI structure would interact favourably with negatively charged groups (amino acid residues) on the outside of the enzyme. The

use of aminated molecules and PEI in particular has been shown to substantially increase the stability of not only DAAO but glucose oxidase and other enzymes (Alonso *et al.*, 2005; López-Gallego *et al.*, 2005a; López-Gallego *et al.*, 2005c). This was hoped would lead to a better orientation of the enzyme or a more secure binding to the surface without compromising functionality. 25% GA was used in order to keep comparisons true to the original recipe.

The calibration data for Pt<sub>D</sub>-PPD-Naf1% $\times$ 3-GA25% $\times$ 3-PEI1%-600UH<sub>2</sub>Ox5 is presented in Table 9-12 and Table 4-12 and displayed in Figure 4-21.

What is immediately clear from examining the data obtained above is that the use of PEI has had a hugely detrimental effect on all kinetic aspects of the biosensors. The  $J_{\max}$  calculated is not significantly different,  $p = 0.0919$ , however the LRS is significantly worse than the original recipe,  $p < 0.0001^{***}$ . The  $K_M$  value is difficult to consider, it is extremely large, well outside of the calibrated range and the error calculated for it is so large that, despite the mean value being nearly eight times larger than the original, there is no significant difference in the values,  $p = 0.0654$ .

Electrode Design	Pt <sub>D</sub> -PPD-Naf1% $\times$ 3-GA25% $\times$ 3-PEI1%-600UH <sub>2</sub> Ox5, n = 4	Pt <sub>D</sub> -PPD-Naf1% $\times$ 3-GA25% $\times$ 3-600UH <sub>2</sub> Ox5, n = 4
<b>Kinetics</b>	M-M-H, $p < 0.0001$	M-M, $p = 0.2311$
<b>R<sup>2</sup></b>	0.9998	0.9940
<b>J<sub>max</sub>, <math>\mu\text{A}\cdot\text{cm}^{-2}</math></b>	$11.77 \pm 2.811$	$18.02 \pm 1.35$
<b>K<sub>M</sub>, <math>\mu\text{M}</math></b>	$73601 \pm 30744$	$4409 \pm 641$
<b><math>\alpha</math></b>	$0.7815 \pm 0.0209$	
<b>LRS, <math>\mu\text{A}\cdot\text{cm}^{-2}\cdot\text{mM}^{-1}</math></b>	$0.1599 \pm 0.0287$	$4.086 \pm 0.307$

**Table 4-12**

Kinetic parameters, fit,  $J_{\max}$ ,  $A$  and  $K_M$  values calculated from the calibration data in Table 9-12.  $J_{\max}$ ,  $\alpha$  and  $K_M$  are presented as Mean  $\pm$  SEM.

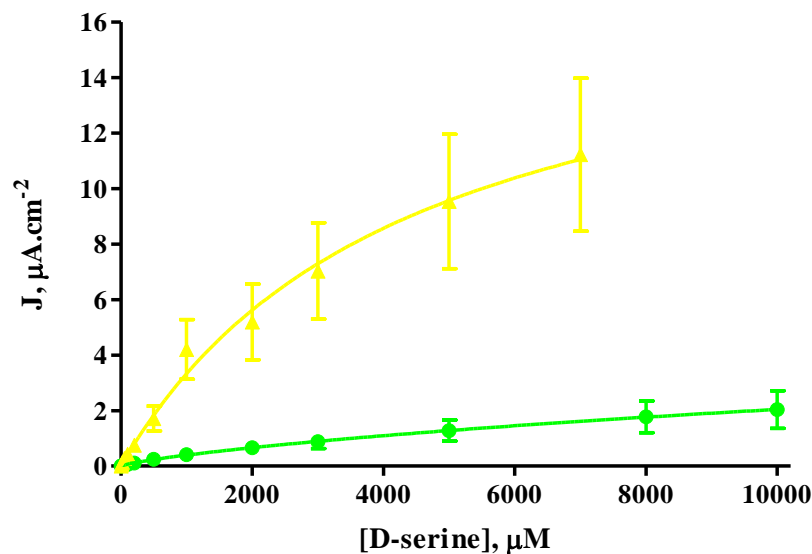


Figure 4-21

J-concentration plot of  $\text{Pt}_D\text{-PPD-Naf1}\% \times 3\text{-GA25}\% \times 3\text{-PEI1}\% \text{-600UH}_2\text{Ox5}$  (green trace), the data is taken from Table 9-12 and Table 4-12.  $\text{Pt}_D\text{-PPD-Naf1}\% \times 3\text{-GA25}\% \times 3\text{-600UH}_2\text{Ox5}$  (yellow trace) is taken from Table 9-11 and Table 4-11. Traces are plotted as Mean  $J \pm \text{SEM}$  with fitted kinetic curve.

Taken together, these parameters appear to indicate, according to best data, that there is a very large initial linear range, before the levelling off as per M-M-H kinetics. But in the linear region the current increases only very slowly. It was quite clear that adding PEI to the recipe without incorporating any other compounds was not likely to lead to a beneficial outcome; indeed incorporating it appears that the positive charges could be repelling  $\text{DAAO}$ , preventing it from binding to the surface. Furthermore it appears the PEI is preventing  $\text{D-ser}$  from reaching the enzyme in the normal diffusion-controlled manner, possibly due to its interaction with the charges which are present on  $\text{D-ser}$ , which has a zwitterionic form at neutral pH.

#### 4.8.1.3 Binding $\text{DAAO}$ using PEI and BSAGA

Having realised that PEI on its own was not likely to enhance the sensitivity of the biosensors it was decided to consider it in conjunction with other additions to the recipe. The first of these to be examined was the BSAGA combined solution (see Section 3.2.2). This solution, as previously stated at the start of Section 4.8.1, is a particular formulation of two substances that are widely used in the production of biosensors. It combines the cross-linking agent GA and the protein BSA which can serve to provide a non-severe, natural environment for an enzyme to function. This is because BSA is rich in lysine residues, residing primarily on the outside of the protein, and these are the

most favourable bonding sites for GA. Thus this solution can be a very successful stabilising agent when immobilising enzymes onto a surface.

It was decided to examine two variants of the original recipe that would incorporate PEI and BSAGA. Having previously seen that the addition of PEI before the enzyme layers had drastically reduced the efficiency of the biosensor it was decided to add it after the enzyme layers had been applied. The BSAGA solution used was made with 1% v/v GA and 1% w/v BSA. The recipes devised were Pt<sub>D</sub>-PPD-Naf1%<sup>x3</sup>-GA25%<sup>x3</sup>-600UH<sub>2</sub>Ox5-PEI1%-BSAGA and Pt<sub>D</sub>-PPD-Naf1%<sup>x3</sup>-600UH<sub>2</sub>O-PEI1%-BSAGA. It was hoped these would elucidate better the binding potential of both the PEI and BSAGA, whether using PEI after the enzyme layers could positively affect the sensitivity, and whether in combination they could securely bind the enzyme to the surface with or without the use of GA.

Upon examining the calibration data in Table 9-13 and Table 4-13 it is easy to see there is a large difference between the two recipes. Looking at the graphic in Figure 4-22 this difference becomes even more apparent. The recipe without the GA dip (red trace) is vastly inferior to the recipe with the GA included (Pt<sub>D</sub>-PPD-Naf1%<sup>x3</sup>-GA25%<sup>x3</sup>-600UH<sub>2</sub>Ox5-PEI1%-BSAGA, green trace).

Comparing the two recipes it can be seen that the  $J_{\max}$  of the recipe including GA (green trace) is significantly higher than that without GA (red trace),  $p = 0.0019^{**}$ . Similar to the PEI recipe discussed just previously it can be seen again that the  $K_M$  value has increased hugely, to a mean value that is four times the maximum concentration calibrated for an error which is twice as large. Thus statistically there is no significant difference in the  $K_M$  values,  $p = 0.2475$ .

Electrode Design	PtD-PPD-Naf1% <sup>x3</sup> -600UH <sub>2</sub> Ox5-PEI1%-BSAGA, n = 4	PtD-PPD-Naf1% <sup>x3</sup> -GA25%-600UH <sub>2</sub> Ox5-PEI1%-BSAGA, n = 4
<b>Kinetics</b>	M-M-H, $p = 0.0001$	M-M, $p = 0.9353$
<b>R<sup>2</sup></b>	0.9991	0.9901
<b>J<sub>max</sub>, <math>\mu\text{A}\cdot\text{cm}^{-2}</math></b>	$3.306 \pm 0.876$	$36.75 \pm 3.13$
<b>K<sub>M</sub>, <math>\mu\text{M}</math></b>	$30178 \pm 16880$	$5956 \pm 1014$
<b><math>\alpha</math></b>	$0.7257 \pm 0.0374$	
<b>LRS, <math>\mu\text{A}\cdot\text{cm}^{-2}\cdot\text{mM}^{-1}</math></b>	$0.110 \pm 0.032$	$6.170 \pm 0.560$

Table 4-13

Kinetic parameters, fit,  $J_{\max}$  and  $K_M$  values calculated from the calibration data in Table 9-13.  $J_{\max}$ ,  $\alpha$ ,  $K_M$  and LRS are presented as Mean  $\pm$  SEM.

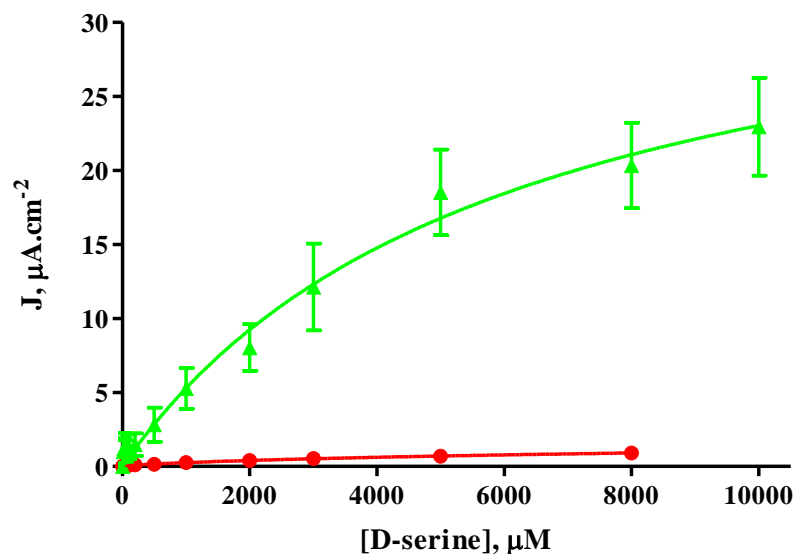


Figure 4-22

J-concentration plot of Pt<sub>D</sub>-PPD-Naf1%<sup>x3</sup>-GA25%<sup>x3</sup>-600UH<sub>2</sub>Ox5-PEI1%-BSAGA (green trace) and Pt<sub>D</sub>-PPD-Naf1%<sup>x3</sup>-600UH<sub>2</sub>Ox5-PEI1%-BSAGA (red trace). The data plotted is taken from Table 9-13 and Table 4-13. Traces are plotted as Mean J ± SEM with fitted kinetic curve.

There is a significant difference in the LRS values with the GA recipe being significantly higher,  $p < 0.0001^{***}$ . It appears that with sufficient quantities of GA the  $\alpha$ AAO will not be negatively influenced by Naf, as previously seen in the case of Pt<sub>D</sub>-PPD<sub>cv</sub>-Naf1<sup>x3</sup>%-GA0.5%<sup>x3</sup>-600UH<sub>2</sub>Ox5 in Section 4.5. It is possible that the exterior layer of BSAGA is not affecting the enzyme at all and that in fact it is cross-linking the PEI. As such for the green trace the first layer of GA is functioning to retain the enzyme and the PEI is interacting minimally with the  $\alpha$ AAO and mainly with the BSAGA. In the recipe without an initial GA layer (red trace) it is probable that the  $\alpha$ AAO will absorb onto the Naf, as seen in Section 4.4, but that the PEI layer on top of this is detrimental to the activity of the enzyme without it being stabilised by the first GA layer.

If consideration is given to the original starting recipe of Pt<sub>D</sub>-PPD-Naf1%<sup>x3</sup>-GA25%<sup>x3</sup>-600UH<sub>2</sub>Ox5, as examined in Section 4.3, and Pt<sub>D</sub>-PPD-Naf1%<sup>x3</sup>-GA25%<sup>x3</sup>-600UH<sub>2</sub>Ox5-PEI1%-BSAGA some significant changes are observed. The  $J_{\max}$  is increased,  $p = 0.0015^{**}$ , the  $K_M$  is non-significantly different,  $p = 0.2446$ . Combined, this produces a significantly higher LRS,  $p = 0.0006^{***}$ . Thus the inclusion of PEI and BSAGA can produce a significant improvement in the kinetic parameters, although it is likely to only affect diffusion of substrates and provide a further protective and retention layer on top of the  $\alpha$ AAO.

When comparing Pt<sub>D</sub>-PPD-Naf1%<sup>x3</sup>-GA25%<sup>x3</sup>-600UH<sub>2</sub>Ox5-PEI1%-BSAGA to the un-modified Pt<sub>D</sub>-PPD-Naf1%<sup>x3</sup>-GA25%<sup>x3</sup>-600UPBSx5 there are some differences to observe. The  $J_{max}$  of the PEI-BSAGA biosensors is significantly higher,  $p = 0.0380^*$ . However the  $K_M$  is non-significantly different with the PEI and BSAGA added,  $p = 0.0843$ . Overall this yields a lower, but not significantly lower LRS of  $6.170 \pm 0.560 \mu\text{A}\cdot\text{cm}^{-2}\cdot\text{mM}^{-1}$ ,  $p = 0.1012$ . The inclusion of the PEI and BSAGA can be considered a significant improvement yielding approximately the same benefit as the change from 600UH<sub>2</sub>O to 600UPBS.

#### 4.8.2 Further Alterations Including FAD

As discussed in Section 2.8.2 the FAD unit which lies at the heart of the  $\alpha$ AAO structure is the component part which undergoes reduction as the amino acid is oxidised to an imino acid. This unit is then re-oxidised by molecular oxygen. Therefore it was of interest to discover could provision of extra quantities of this unit increase the turnover rate of the enzyme and thus increase the sensitivity of the biosensors.

Two recipes were devised which were hoped would provide some indication of whether FAD could be incorporated with a beneficial effect. These recipes were Pt<sub>D</sub>-PPD-Naf1%<sup>x3</sup>-PEI1%-600UPBSx5-FAD and Pt<sub>D</sub>-PPD-Naf1%<sup>x3</sup>-GA25%<sup>x3</sup>-PEI1%-600UPBSx5-FAD. These two recipes put the PEI before the  $\alpha$ AAO again to examine would the FAD increase the sensitivities and at the GA primary binding layer.

Electrode Design	Pt <sub>D</sub> -PPD-Naf1% <sup>x3</sup> -GA25% <sup>x3</sup> -PEI1%-600UH <sub>2</sub> Ox5-FAD, n = 4	Pt <sub>D</sub> -PPD-Naf1% <sup>x3</sup> -PEI1%-600UH <sub>2</sub> Ox5-FAD, n = 4
<b>Kinetics</b>	M-M-H, $p < 0.0001$	M-M, n/c
<b>R<sup>2</sup></b>	0.9997	0.9861
<b>J<sub>max</sub>, <math>\mu\text{A}\cdot\text{cm}^{-2}</math></b>	$26.25 \pm 5.266$	$0.2520 \pm 0.0192$
<b>K<sub>M</sub>, <math>\mu\text{M}</math></b>	$46340 \pm 18831$	$4100 \pm 720$
<b><math>\alpha</math></b>	$0.7335 \pm 0.0248$	
<b>LRS, <math>\mu\text{A}\cdot\text{cm}^{-2}\cdot\text{mM}^{-1}</math></b>	$5.664 \pm 1.169$	$0.0615 \pm 0.0065$

Table 4-14

Kinetic parameters, fit,  $J_{max}$  and  $K_M$  values calculated from the calibration data in Table 9-14.  $J_{max}$ ,  $K_M$ ,  $\alpha$  and LRS are presented as Mean  $\pm$  SEM.

The calibration data and kinetic parameters obtained for the two recipes are listed in Table 9-14 and Table 4-14 respectively, and is graphically represented below in Figure 4-23;

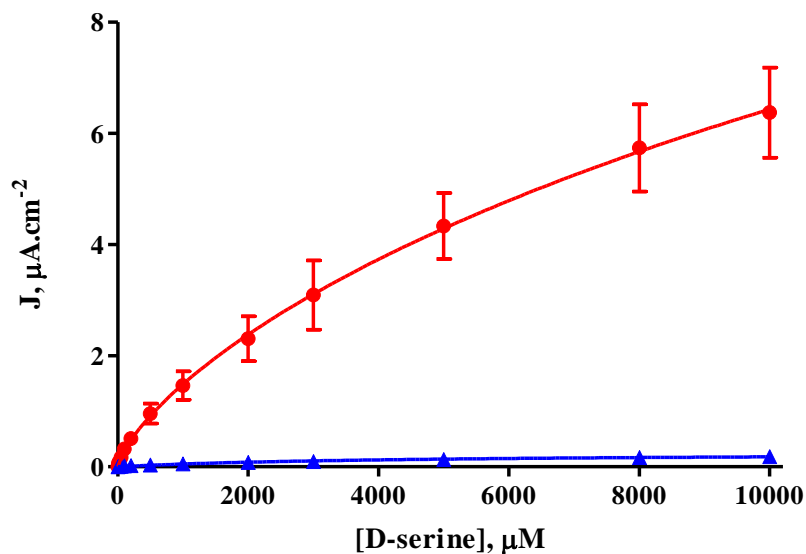


Figure 4-23

J-concentration plot of PtD-PPD-Naf1% $\times$ 3-GA-PEI1%-600UH<sub>2</sub>Ox<sub>5</sub>-FAD (red trace) and PtD-PPD-Naf1% $\times$ 3-PEI1%-600UH<sub>2</sub>Ox<sub>5</sub>-FAD (blue trace). The data plotted is taken from Table 9-14 and Table 4-14. Traces are plotted as Mean  $J \pm$  SEM with fitted kinetic curve.

Following on from the trend seen in Sections 4.5 and 4.8.1.3, it is again apparent that without sufficiently concentrated GA or in the complete absence of GA there is little or no binding of DAAO to the surface of the sensor, and that PEI could be denaturing the enzyme. This is shown by the drastically reduced current density of Pt<sub>D</sub>-PPD-Naf1% $\times$ 3-PEI1%-600UPBSx<sub>5</sub>-FAD in the above figure (blue trace). Its  $J_{\max}$  is significantly lower than the alternative with 25% GA,  $p = 0.0159^*$ . The  $K_M$  concentration again is difficult to analyse. As seen previously, when PEI was included in a recipe with GA, the  $K_M$  becomes very large and the SEM also becomes very large as a percentage of the mean. Thus there is no significant difference between the two values,  $p = 0.1108$ . The LRS of the recipe with GA does have a larger LRS,  $p = 0.0230^*$ .

Comparing Pt<sub>D</sub>-PPD-Naf1% $\times$ 3-GA25%-PEI1%-600UH<sub>2</sub>Ox<sub>5</sub>-FAD to Pt<sub>D</sub>-PPD-Naf1% $\times$ 3-GA25% $\times$ 3-PEI1%-600UH<sub>2</sub>Ox<sub>5</sub> from Section 4.8.1.2 it is possible to examine the influence of FAD on the recipe. It is clear that the FAD does have an effect, the  $J_{\max}$  is larger, although not significantly,  $p = 0.0515$ , and there is no difference in the  $K_M$  values,  $p = 0.4782$ . However the combined analysis exhibited by the LRS is significantly higher,  $p = 0.0432^*$ . Thus some marginal benefit on sensitivity was gained by the incorporation of FAD.

## **4.9 Conclusions**

The beginning of this project was aimed at replicating a biosensor that had already been designed (Zain *et al.*, 2010). However, it was quickly determined that the proposed design, while being a solid basis for the development of a chronic *in vivo* biosensor, had its problems. The main issue was reproducibility, which was attainable only by use of an entirely fresh set of solutions every time a sensor was being fabricated. This was an impractical situation as the DAAO was not easy to procure at the required activity and it was also expensive.

Preliminary examination of the proposed recipe revealed a number of potential causes of the reproducibility problem, based on previous experience within the group and from the methodologies and published results from other groups. Thus I set out to explore the construction of this biosensor with the aim of optimising it.

The first issue was the use of Naf after the PPD film had been applied, despite it being shown that Naf has strong interference rejection capabilities. It had been shown before that this approach led to a reduction in the efficiency of the interference rejection properties of biosensors. In cases where PPD is used to reject interferents it is more desirable to place the Naf layer underneath the PPD. It is hypothesised that the alcohol used in Naf solutions interacts with the polymer. This is difficult to prove however as the exact structure of PPD is yet to be elucidated (Section 2.8.4). Never the less it was an unusual formulation.

Secondly, the use of GA at a concentration of 25% was highly unusual. While not unheard of, at this concentration GA is typically applied by vapour saturation, rather than directly dipping the biosensor into the solution. As previously stated when directly applied to the surface of an electrode it is more commonly used at a concentration between 2.5% and 0.01%. Thus an investigation was conducted in all aspects of the proposed design to elucidate the contribution of each component part and discover any benefits of changes that could be considered.

Initial examination began with the Naf layers applied after the PPD and before the GA 25%. It was shown that the benefits of the Naf are questionable, beyond a possible increase in interference rejection over PPD alone. It appears to interact with the PPD to yield a self contained layer that GA appears to have little affinity for. Without the PPD

layer the Naf interacts with the GA to reduce the sensitivity of the sensors to a value less than if the DAAO was purely adsorbed onto the surface.

With regard to the GA it appears that the 25% GA is so concentrated that it denatures the enzyme, creating too many interactions between the molecules. It was shown that approximately the same, 2% GA, and much better, 1% GA, sensitivities are obtainable without compromising the enzyme solution.

Changing the supplier of the enzyme, or rather the activity it was supplied at, did not have any beneficial effects, as the original supplier supplied the highest activity form of the enzyme. However, changing the enzyme solution from 600UH<sub>2</sub>O to 600UPBS, where the PBS is at pH 8.5, significantly increases sensitivity across the board as well as possibly decreasing error and increasing reproducibility.

Using different polymer growth methods also changed the sensitivity. However, only in a situation where there was a possibility of compromising the integrity of the PPD layer by decreasing the N<sub>2</sub> saturation of the polymerisation process. The use of PEI as a binding agent only produced an improvement in the kinetic parameters of the biosensors when used in conjunction with BSAGA after the enzyme had been applied. This may be due solely to the BSAGA as using PEI before the enzyme was detrimental to sensitivity in all cases. FAD also served to improve the sensitivity of biosensors that contained PEI. Finally the duplication of layers of GA and DAAO did provide a significant increase in the LRS and shows promise.

Overall, it was possible to reproduce the desired sensitivities, but not in a manner which was robust enough for the purposes of a chronic *in vivo* biosensor. It was not possible, despite extensive investigation, to optimise the biosensor design for our needs. An alternative would have to be produced, which would be aided greatly by the information gleaned in this section of work.

References

- Alonso N, López-Gallego F, Betancor L, Hidalgo A, Mateo C, Guisan JM & Fernandez-Lafuente R. (2005). Immobilization and stabilization of glutaryl acylase on aminated sephabeads supports by the glutaraldehyde crosslinking method. *Journal of Molecular Catalysis B: Enzymatic* **35**, 57-61.
- Belay A, Collins A, Ruzgas T, Kissinger PT, Gorton L & Csoregi E. (1999). Redox hydrogel based bienzyme electrode for L-glutamate monitoring. *Journal of Pharmaceutical & Biomedical Analysis* **19**, 93-105.
- Bolger FB. (2007). The *in vitro* and *in vivo* characterisation and application of real time sensors and biosensors for neurochemical studies of brain energy metabolism. In *Department of Chemistry*. National University of Ireland, Maynooth.
- Burmeister JJ & Gerhardt GA. (2001). Self-referencing ceramic-based multisite microelectrodes for the detection and elimination of interferences from the measurement of L-glutamate and other analytes. *Analytical Chemistry* **73**, 1037-1042.
- Cox JA, Hensley PM & Loch CL. (2003). Evaluation of polycation-stabilized lactate oxidase in a silica sol-gel as a biosensor platform. *Microchimica Acta* **142**, 1-5.
- Friedemann MN, Robinson SW & Gerhardt GA. (1996). *o*-Phenylenediamine-modified carbon fiber electrodes for the detection of nitric oxide. *Analytical Chemistry* **68**, 2621-2628.
- Haughton E. (pending publication). Real-time Neurochemical Analysis of Excitatory Amino Acids: Enzyme-modified Microelectrochemical Biosensors for Aspartate and Glutamate. In *Department of Chemistry*. National University of Ireland, Maynooth, (pending publication).
- Hu Y & Wilson GS. (1997). Rapid changes in local extracellular rat brain glucose observed with an *in vivo* glucose sensor. *Journal of Neurochemistry* **68**, 1745-1752.
- Jezkova J, Iwuoha EI, Smyth MR & Vytras K. (1997). Stabilization of an osmium bis-bipyridyl polymer-modified carbon paste amperometric glucose biosensor using polyethyleneimine. *Electroanalysis* **9**, 978-984.
- López-Gallego F, Betancor L, Hidalgo A, Alonso N, Fernández-Lafuente R & Guisán JM. (2005a). Co-aggregation of Enzymes and Polyethyleneimine: A Simple

Method To Prepare Stable and Immobilized Derivatives of Glutaryl Acylase. *Biomacromolecules* **6**, 1839-1842.

López-Gallego F, Betancor L, Hidalgo A, Alonso N, Fernandez-Lorente G, Guisan JM & Fernandez-Lafuente R. (2005b). Preparation of a robust biocatalyst of d-amino acid oxidase on sepabeads supports using the glutaraldehyde crosslinking method. *Enzyme and Microbial Technology* **37**, 750-756.

López-Gallego F, Betancor L, Mateo C, Hidalgo A, Alonso-Morales N, Dellamora-Ortiz G, Guisán JM & Fernández-Lafuente R. (2005c). Enzyme stabilization by glutaraldehyde crosslinking of adsorbed proteins on aminated supports. *Journal of Biotechnology* **119**, 70-75.

McMahon CP, Killoran SJ & O'Neill RD. (2005). Design variations of a polymer-enzyme composite biosensor for glucose: Enhanced analyte sensitivity without increased oxygen dependence. *Journal of Electroanalytical Chemistry* **580**, 193-202.

McMahon CP, Rocchitta G, Serra PA, Kirwan SM, Lowry JP & O'Neill RD. (2006). The efficiency of immobilised glutamate oxidase decreases with surface enzyme loading: An electrostatic effect, and reversal by a polycation significantly enhances biosensor sensitivity. *Analyst* **131**, 68-72.

O'Brien KB, Killoran SJ, O'Neill RD & Lowry JP. (2007). Development and characterization *in vitro* of a catalase-based biosensor for hydrogen peroxide monitoring. *Biosensors & Bioelectronics* **22**, 2994-3000.

Patel NG, Erlenkötter A, Cammann K & Chemnitz GC. (2000). Fabrication and characterization of disposable type lactate oxidase sensors for dairy products and clinical analysis. *Sensors & Actuators B: Chemical* **67**, 134-141.

Pernot P, Mothet J-P, Schuvailo O, Soldatkin A, Pollegioni L, Pilone M, Adeline M-T, Cespuglio R & Marinesco S. (2008). Characterization of a yeast d-amino acid oxidase microbiosensor for d-serine detection in the central nervous system. *Analytical Chemistry* **80**, 1589-1597.

Ryan MR, Lowry JP & O'Neill RD. (1997). Biosensor for neurotransmitter L-glutamic acid designed for efficient use of L-glutamate oxidase and effective rejection of interference. *Analyst* **122**, 1419-1424.

Sanford AL, Morton SW, Whitehouse KL, Oara HM, Lugo-Morales LZ, Roberts JG & Sombers LA. (2010). Voltammetric detection of hydrogen peroxide at carbon fiber microelectrodes. *Analytical Chemistry* **82**, 5205-5210.

Wang J, Liu J & Cepra G. (1997). Thermal stabilization of enzymes immobilized within carbon paste electrodes. *Analytical Chemistry* **69**, 3124-3127.

Zain ZM, O'Neill RD, Lowry JP, Pierce KW, Tricklebank M, Dewa A & Ab Ghani S. (2010). Development of an implantable D-serine biosensor for in vivo monitoring using mammalian D-amino acid oxidase on a poly (*o*-phenylenediamine) and Nafion-modified platinum-iridium disk electrode. *Biosensors & Bioelectronics* **25**, 1454-1459.

---

---

**5. AN INVESTIGATION OF BIOSENSOR  
DESIGNS UTILISING STYRENE AS AN  
IMMOBILISATION MATRIX**

---

---

## 5.1 Introduction

Having thoroughly investigated the possibilities of altering the formulation of the Z.M. Zain D-ser biosensor it was accepted that a different approach was necessary to arrive at a recipe which would, without exorbitant costs, fulfil sensitivity requirements and be stable enough for chronic *in vivo* use. To do this it was decided to start at the very beginning of the design process and use the information previously gleaned as a rough guide.

It was decided at the beginning of this process that based on previous experience it was necessary to combine the elements of the biosensor in a more integrated manner. This would mean that different substances would be interspersed within the proposed recipes and not layered exclusively. For example the previous design applied the Naf layers first, then the GA layers and finally the enzyme. Now the approach was to place layers of different substances within the layers of enzyme.

Consideration also was given to the need to have a primary binding matrix other than GA. This was due to the fact that it had been shown that the concentrated 25% enzyme was detrimental to the enzyme and that lower percentages opened up the possibility of not binding the enzyme to the surface of the electrode with sufficient strength. Thus it was decided to use Styrene as an immobilisation matrix, within which all of the other compounds would hopefully be bound securely without sacrificing sensitivity or function of the biosensor. Styrene had previously been shown to be effective in this manner within the group during the design of lactate (Bolger, 2007), aspartate and glutamate biosensors (Haughton, pending publication). It has also been widely used by other groups where it has been used as a functionalised backbone of the sensor (Poyard *et al.*, 1999; Xu & Han, 2004), as a bonding layer (Shimizu *et al.*, 1994) or as a substance into which the enzyme was immobilised (Volotovskiy & Kim, 1998). In the case of this project it was to be used as a monomeric solution into which hopefully the other substances would be immobilised as the slow thermal/UV-initiated polymerisation takes place. Its use in such circumstances has been characterised by other group members, and the data was communicated personally. The basic configuration, of most biosensors discussed within this chapter, is as depicted in Figure 5-1. All alterations discussed in this chapter centre on this design with various layers being omitted or modified or added as detailed in each section.

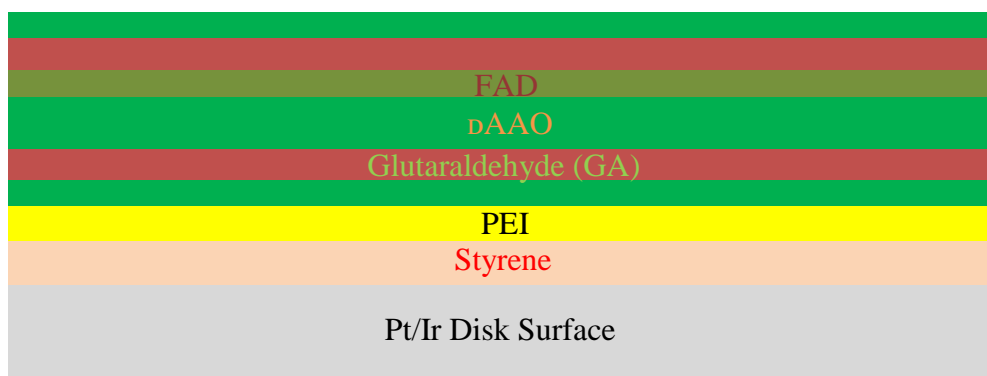


Figure 5-1

The basic configuration of biosensors discussed within Chapter 5.

## 5.2 Basic Constructs of a Biosensor

### 5.2.1 Adsorption of dAAO

The initial stage of the design of a new biosensor began with the simple physical adsorption of the enzyme onto the bare metal surface. The aim was to provide basic information on the amount of layers of enzyme that could be applied, without the addition of a binding agent, before they became self-limiting. This could happen because successive layers could block the access of the substrate to the initial layers, or because the mass of adsorbed material could pull previously applied quantities of substrate off the surface. Either method would cause the sensitivity to cease to increase, after a point, or start to decrease.

To examine this possibility four sensor recipes were examined, Pt<sub>D</sub>-600UH<sub>2</sub>O, Pt<sub>D</sub>-600UH<sub>2</sub>Ox5, Pt<sub>D</sub>-600UH<sub>2</sub>Ox10 and Pt<sub>D</sub>-600UH<sub>2</sub>Ox15. The calibration data and kinetic considerations obtained are listed in Table 10-1 and Table 5-1.

The collected calibration data and kinetic fit is plotted in Figure 5-2. The most important piece of information that can be immediately gleaned from this diagram and the above data is that without a binding agent of any sort the amount of dAAO which can be adhered to surface is minimal. The current density across the four recipes is very low.

Examining the findings in more detail another point that becomes quite obvious is that with only one dip in the enzyme solution, Pt<sub>D</sub>-600UH<sub>2</sub>O, there is very little enzyme on the surface. Comparing the four designs what is also apparent is the large degree of

error associated with creating the sensors without a binding agent. This only decreases for 15 layers of enzyme which appears to suggest that it is quantity of layers ensuring uniformity.

Electrode Design	Pt <sub>D</sub> -600UH <sub>2</sub> O n = 4	Pt <sub>D</sub> -600UH <sub>2</sub> Ox5 n = 3	Pt <sub>D</sub> -600UH <sub>2</sub> Ox10 n = 4	Pt <sub>D</sub> -600UH <sub>2</sub> Ox15 n = 4
<b>Kinetics</b>	M-M, n/c	M-M-H, p=0.0003	M-M-H, p=0.0358	M-M-H, p<0.0001
<b>R<sup>2</sup></b>	0.1443	0.9975	0.9994	0.9996
<b>J<sub>max</sub>, μA.cm<sup>-2</sup></b>	-0.1650 ± 0.0721	3.544 ± 1.271	1.818 ± 0.211	1.053 ± 0.153
<b>K<sub>M</sub>, μM</b>	157.5 ± 412.6	18555 ± 15883	8790 ± 1947	14943 ± 4253
<b>α</b>		0.6739 ± 0.0577	0.9148 ± 0.0347	0.8169 ± 0.0276
<b>LRS, μA.cm<sup>-2</sup>.mM<sup>-1</sup></b>	-1.047 ± 2.440	0.1910 ± 0.0952	0.2068 ± 0.0292	0.0705 ± 0.0099

Table 5-1

Kinetic parameters, fit, J<sub>max</sub> and K<sub>M</sub> values calculated from the calibration data in Table 10-1. J<sub>max</sub>, K<sub>M</sub>, α and LRS are presented as Mean ± SEM.

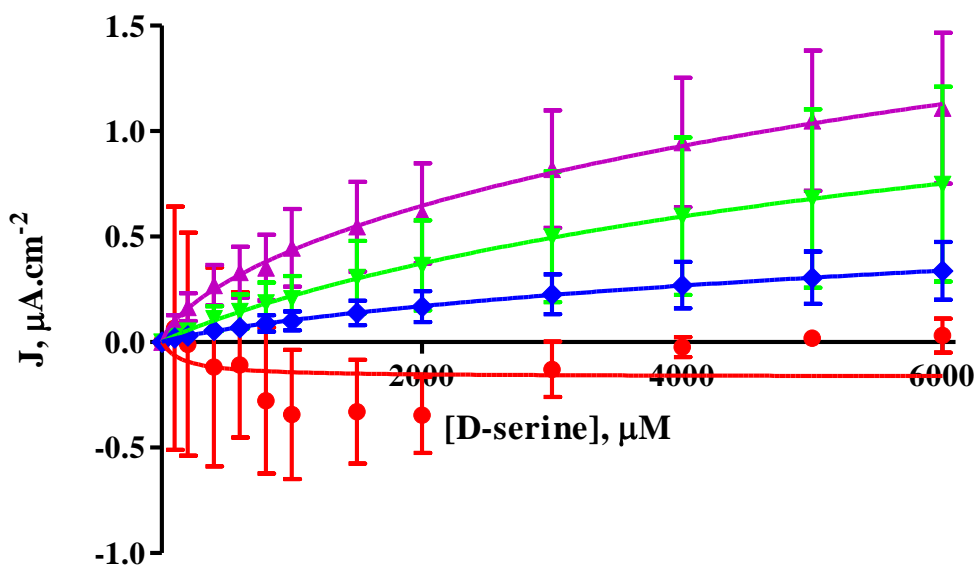


Figure 5-2

J-concentration plot of the four recipes where 600UH<sub>2</sub>O was purely adsorbed onto the surface. Depicted are Pt<sub>D</sub>-600UH<sub>2</sub>O (red trace), Pt<sub>D</sub>-600UH<sub>2</sub>Ox5 (purple trace), Pt<sub>D</sub>-600UH<sub>2</sub>Ox10 (green trace) and Pt<sub>D</sub>-600UH<sub>2</sub>Ox15 (blue trace). The data plotted is taken from Table 10-1 and Table 5-1. Traces are plotted as Mean J ± SEM with fitted kinetic curve.

Kinetically, if Pt<sub>D</sub>-600UH<sub>2</sub>Ox5 is compared to Pt<sub>D</sub>-600UH<sub>2</sub>Ox10 it is seen that there is no significant difference in J<sub>max</sub>, p = 0.3123, the K<sub>M</sub>, p = 0.6038, or LRS, p = 0.8864. Indeed there is no significant difference when any of the values of J<sub>max</sub>, K<sub>M</sub> or LRS are compared with each other for the three recipes, Pt<sub>D</sub>-600UH<sub>2</sub>Ox5, Pt<sub>D</sub>-600UH<sub>2</sub>Ox10 and Pt<sub>D</sub>-600UH<sub>2</sub>Ox15, except in one case of the LRS values of the latter two recipes, p = 0.0013\*\*, where Pt<sub>D</sub>-600UH<sub>2</sub>Ox10 has a higher sensitivity. Thus despite the visual

depiction of a decreasing sensitivity from 5 to 10 to 15 dips of enzyme this is not borne out by the statistics. Only the sensitivity of 10 and 15 dips is significantly different even though the sensitivity of 5 and 10 dips or 5 and 15 dips are not. However the lower mean of the 10 dips  $K_M$  and higher mean of  $J_{max}$  for 5 dips point to these values having most value moving forward.

### 5.2.2 The Use of GA as a Binding Agent

Having discovered very little about the quantity of layers of enzyme that would be useful in the fabrication of an electrode it was decided to consider the issue again. This time 1% GA was used to provide some binding of enzyme to the surface of the electrode and to allow cross-linking of DAAO molecules. It was applied in two general formats, Pt<sub>D</sub>-[600UH<sub>2</sub>O-GA1%] and Pt<sub>D</sub>-[GA1%-600UH<sub>2</sub>O]. The layers of GA and 600UH<sub>2</sub>O were applied 1, 5, 10 and 15 times, with no time between dips and 5 minutes drying time between layers.

The first group to be considered is the recipes where the GA was applied before the enzyme; Pt<sub>D</sub>-[GA1%-600UH<sub>2</sub>O], Pt<sub>D</sub>-[GA1%-600UH<sub>2</sub>O]<sub>x5</sub>, Pt<sub>D</sub>-[GA1%-600UH<sub>2</sub>O]<sub>x10</sub> and Pt<sub>D</sub>-[GA1%-600UH<sub>2</sub>O]<sub>x15</sub>.

From examining Figure 5-3 it is again clear that the biosensors with only 1 layer are far inferior to those with 5, 10 or 15 layers. The  $J_{max}$  is significantly lower than the 10 layer or 15 layer protocols,  $p = 0.0003^{***}$  and  $p = 0.0019^{**}$  respectively, and its  $K_M$  is significantly larger,  $p = 0.0001^{***}$  and  $p < 0.0001^{***}$ . This results in the LRS for the 1 layer recipe being significantly lower than that of either 10 or 15 layers,  $p < 0.0001^{***}$  and  $p = 0.0008^{***}$ . Although the  $K_M$  for 1 layer is less than that for 5 layers,  $p = 0.0006^{***}$ , because the  $J_{max}$  is also significantly lower,  $p < 0.0001^{***}$ , it also has an inferior LRS,  $p < 0.0001^{***}$ .

Noticing that both Pt<sub>D</sub>-[GA1%-600UH<sub>2</sub>O]<sub>x10</sub> and Pt<sub>D</sub>-[GA1%-600UH<sub>2</sub>O]<sub>x15</sub> have M-M-H kinetics rather than the M-M kinetics of the 1 and 5 layer recipes it is found that there is no significant differences between these recipes. The  $J_{max}$ ,  $K_M$  and LRS are all non-significantly different,  $p = 0.4035$ ,  $p = 0.8329$  and  $p = 0.1350$  respectively.

Electrode Design	Pt <sub>D</sub> -[GA1%-600UH <sub>2</sub> O]x1, n=4	Pt <sub>D</sub> -[GA1%-600UH <sub>2</sub> O]x5, n=4	Pt <sub>D</sub> -[GA1%-600UH <sub>2</sub> O]x10, n=4	Pt <sub>D</sub> -[GA1%-600UH <sub>2</sub> O]x15, n=4
<b>Kinetics</b>	M-M, p = 0.9390	M-M, p = 0.6346	M-M-H, p<0.0001	M-M-H, p<0.0001
<b>R<sup>2</sup></b>	0.9997	0.9999	0.9993	0.9996
<b>J<sub>max</sub>, μA.cm<sup>-2</sup></b>	18.87 ± 0.39	94.17 ± 1.14	64.30 ± 2.24	61.52 ± 1.81
<b>K<sub>M</sub>, μM</b>	6149 ± 204	7780 ± 143	2703 ± 156	2755 ± 147
<b>α</b>			1.452 ± 0.051	1.290 ± 0.035
<b>LRS, μA.cm<sup>-2</sup>.mM<sup>-1</sup></b>	3.069 ± 0.042	12.10 ± 0.08	23.79 ± 0.58	22.33 ± 0.55

Table 5-2

Kinetic parameters, fit, J<sub>max</sub> and K<sub>M</sub> values calculated from the calibration data in Table 10-2. J<sub>max</sub>, K<sub>M</sub>, α and LRS are presented as Mean ± SEM.

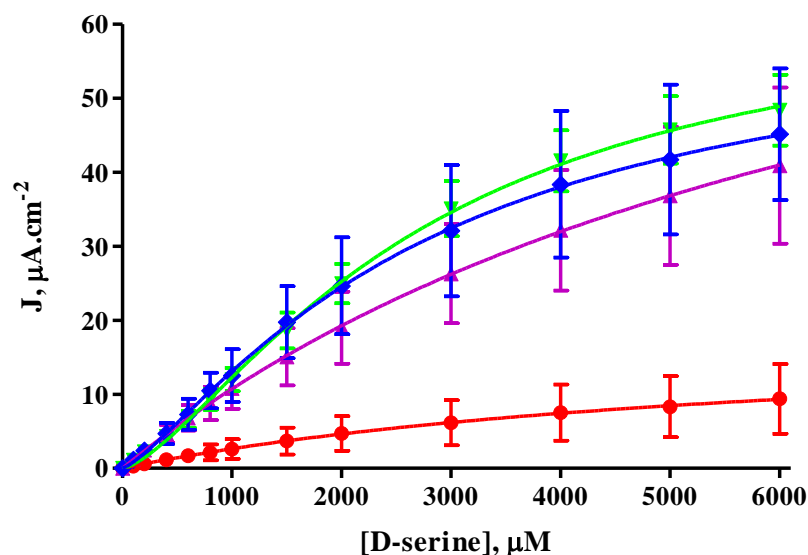


Figure 5-3

J-concentration plot of the four recipes where 600UH<sub>2</sub>O was cross-linked with GA onto the surface. Depicted are Pt<sub>D</sub>-[GA1%-600UH<sub>2</sub>O] (red trace), Pt<sub>D</sub>-[GA1%-600UH<sub>2</sub>O]x5 (purple trace), Pt<sub>D</sub>-[GA1%-600UH<sub>2</sub>O]x10 (green trace) and Pt<sub>D</sub>-[GA1%-600UH<sub>2</sub>O]x15 (blue trace). The data plotted is taken from Table 10-2 and Table 5-2. Traces are plotted as Mean J ± SEM with fitted kinetic curve.

Turning ones attention to Pt<sub>D</sub>-[GA1%-600UH<sub>2</sub>O]x5 it is noticeable that while visually in Figure 5-3 there appears to be little difference between it and the 10 and 15 layer alternatives. However, when the kinetic parameters are examined there is quite a difference, owing mainly to the difference kinetic model that fits it best, M-M. Here we see that due to this model the J<sub>max</sub> is significantly higher than the other two recipes, p < 0.0001\*\*\* for both, and its K<sub>M</sub> is also significantly higher, p < 0.0001\*\*\* in both cases. Thus while the higher J<sub>max</sub> is desirable, the higher K<sub>M</sub> is not and the resultant LRS is significantly lower, p < 0.0001\*\*\* and p = 0.0029\*\* respectively.

Overall these are promising results, as with only a very basic examination LRS values achieved for the 10 and 15 layer recipes in particular are far larger than any of those achieved by the recipes examined in Chapter 4. To further explore these results a set of alternate recipes were formulated where the order of the GA and DAAO dips were reversed within a layer. The results are presented below in Table 5-3 and Figure 5-4.

Electrode Design	Pt <sub>D</sub> -[600UH <sub>2</sub> O-GA1%]x1, n = 3	Pt <sub>D</sub> -[600UH <sub>2</sub> O-GA1%]x5, n = 4	Pt <sub>D</sub> -[600UH <sub>2</sub> O-GA1%]x10, n = 3	Pt <sub>D</sub> -[600UH <sub>2</sub> O-GA1%]x15, n = 3
<b>Kinetics</b>	M-M, p = 0.2275	M-M, n/c	M-M, p = 0.0552	M-M, p = 0.5411
<b>R<sup>2</sup></b>	0.8519	0.9979	0.9848	0.9989
<b>J<sub>max</sub>, μA.cm<sup>-2</sup></b>	91.98 ± 7.51	31.21 ± 3.26	35.52 ± 5.23	25.45 ± 1.22
<b>K<sub>M</sub>, μM</b>	322.2 ± 120.1	13869 ± 1897	6556 ± 1535	8407 ± 595.2
<b>LRS, μA.cm<sup>-2</sup>.mM<sup>-1</sup></b>	285.5 ± 89.6	2.250 ± 0.076	5.418 ± 0.500	3.027 ± 0.073

Table 5-3

Kinetic parameters, fit, J<sub>max</sub> and K<sub>M</sub> values calculated from the calibration data in Table 10-3. J<sub>max</sub>, K<sub>M</sub> and LRS are presented as Mean ± SEM.

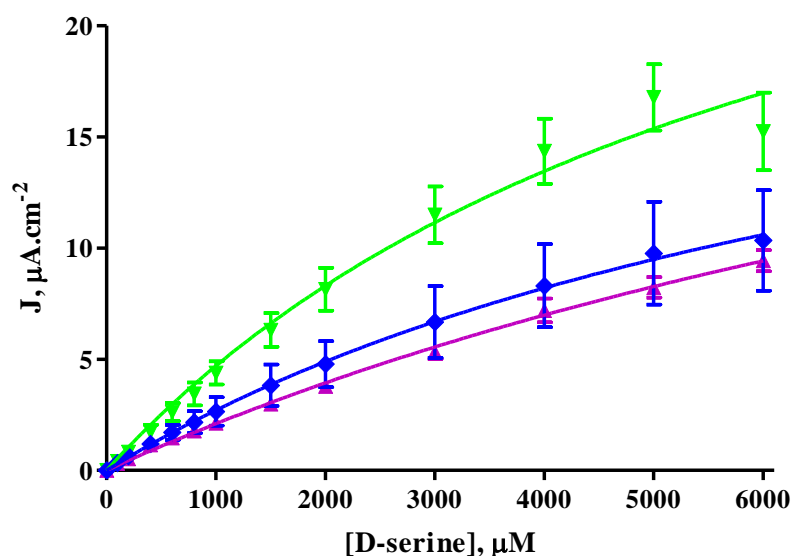


Figure 5-4

J-concentration plot of the four recipes where 600UH<sub>2</sub>O was cross-linked with GA onto the surface of the electrode. Depicted are Pt<sub>D</sub>-[600UH<sub>2</sub>O-GA1%]x5 (purple trace), Pt<sub>D</sub>-[600UH<sub>2</sub>O-GA1%]x10 (green trace) and Pt<sub>D</sub>-[600UH<sub>2</sub>O-GA1%]x15 (blue trace). The data plotted is taken from Table 10-3 and Table 5-3. Traces are plotted as Mean J ± SEM with fitted kinetic curve.

Taking a close look at the calibration data for Pt<sub>D</sub>-[600UH<sub>2</sub>O-GA1%]x1 one can see that there were very strange phenomena taking place where some electrodes were non responsive and yet others were very sensitive. This is apparent when observing that in some instances the error for a particular calibration point is almost 100% of the mean value and that this value also varies greatly across the values. This made plotting the

data difficult and as such it is omitted from Figure 5-4 below. It is also difficult to take any meaning from the statistics and as such they will not be compared to the other recipes. It is suspected that this occurs as the binding layer is added after the enzyme and as such the quantity of DAAO remaining on the surface of the electrode, as it is dipped into the GA, is quite variable and unreliable.

When consideration is given to the other three recipes it is noted that all three are M-M kinetics type biosensors. Pt<sub>D</sub>-[600UH<sub>2</sub>O-GA1%]x5 has a J<sub>max</sub> which does not differ from that of Pt<sub>D</sub>-[600UH<sub>2</sub>O-GA1%]x10,  $p = 0.4936$ , but a significantly higher K<sub>M</sub>,  $p = 0.0368^*$ , which results in an LRS that is significantly lower,  $p = 0.0007^{***}$ . Compared with Pt<sub>D</sub>- [600UH<sub>2</sub>O-GA1%]x15 the 5 layer recipe has a non-significantly different J<sub>max</sub> and K<sub>M</sub>,  $p = 0.2089$  and  $p = 0.0635$ , but together there is a difference in LRS,  $p = 0.0009^{***}$ .

Pt<sub>D</sub>-[600UH<sub>2</sub>O-GA1%]x10 produces the best results. As already seen it is significantly better than the 5 layer alternative and compared to Pt<sub>D</sub>-[600UH<sub>2</sub>O-GA1%]x15 its J<sub>max</sub> and K<sub>M</sub> are not significantly different,  $p = 0.1342$  and  $p = 0.3238$ , but together they yield a sensitivity which is significantly higher,  $p = 0.0091^{**}$ . It appears, overall, that 10 layers is about the optimum number. This is due to its higher LRS in the recipe just examined, and that it is equally as sensitive as any other recipe in the Pt<sub>D</sub>-[GA1%-600UH<sub>2</sub>O] format, as well as it having favourable M-M-H kinetics. When purely absorbed onto the surface it also yielded the lowest K<sub>M</sub> value.

It is interesting to note a general comparison between the Pt<sub>D</sub>-[600UH<sub>2</sub>O-GA1%] and the Pt<sub>D</sub>-[GA1%-600UH<sub>2</sub>O] recipes. Individually each recipe where the GA was applied first obtains a higher LRS,  $p < 0.0001^{***}$  for 5 and 10 layer recipes and  $p = 0.0008^{***}$  for the 15 layer recipe. This appears to indicate the need for there to be a binding layer or cross-linking agent applied to the surface of the electrode before any enzyme is applied. This would ensure a stable framework for the rest of the layers to build upon.

### 5.2.3 Styrene as a Primary Binding Agent

Having identified the need for a primary binding agent to ensure adequate adhesion of the enzyme to the surface of the electrode it was clear at this point that there was a need examine styrene as an agent to fulfil this role. As previously stated, Section 5.1, this polymer had been used previously with great effect and success in many different

biosensors. Thus, to form a more complete picture a layer study was also conducted with only styrene as an ‘immobilisation matrix’.

Styrene, in pure monomeric form, has a boiling point of 145.14 °C and is therefore unlikely to evaporate from the surface of the electrode. Significant surface changes have been noted by the group before upon examination by SEM of an electrode after a dip into styrene monomer. Without the addition of inhibitors the monomer will undergo spontaneous polymerisation (Mayo & Gregg, 1948; Priddy, 1994), and the rate of polymerisation can be affected by the availability of oxygen (Miller & Mayo, 1956) along with a multitude of other factors which affect the chain transfer mechanism (Mayo, 1943; Gregg & Mayo, 1947, 1948; Mayo, 1948; Mayo *et al.*, 1951; Gregg & Mayo, 1953; Mayo, 1953). Thus while the quantity and average mass of polymer on the surface is unknown there is a slow polymerisation process which occurs as the biosensor is being fabricated. Indeed temperatures over 65 °C can initiate runaway polymerisations in bulk quantities of styrene.

The styrene was applied in its 99% monomeric form in a single dip prior to application of the enzyme dips. The first dip into 600UH<sub>2</sub>O was applied immediately after the styrene to complete the first layer.

As in the previous sections four recipes with differing numbers of layers were created; Pt<sub>D</sub>-Sty-600UH<sub>2</sub>Ox5, Pt<sub>D</sub>-Sty-600UH<sub>2</sub>Ox10, Pt<sub>D</sub>-Sty-600UH<sub>2</sub>Ox15 and Pt<sub>D</sub>-Sty-600UH<sub>2</sub>Ox20. A recipe with one layer was not considered due to the previous poor results with this setup. The results obtained are presented in Table 10-4 and Table 5-4.

The set of results by these four different recipes are a bit erratic but it is possible to put meaning to them. They are depicted in Figure 5-5. At 5 layers, the kinetic parameters appear favourable, but deteriorate for 10 layers, changing to more favourable values again at 15 layers, but with an increased SEM, and finally deteriorate to undesirable values again at 20 layers.

Electrode Design	Pt <sub>D</sub> -Sty-600U H <sub>2</sub> Ox5, n=4	Pt <sub>D</sub> -Sty-600U H <sub>2</sub> Ox10, n=4	Pt <sub>D</sub> -Sty-600U H <sub>2</sub> Ox15, n=4	Pt <sub>D</sub> -Sty-600U H <sub>2</sub> Ox20, n=4
<b>Kinetics</b>	M-M, p = 0.6734	M-M, n/c	M-M, p = 0.3125	M-M, n/c
<b>R<sup>2</sup></b>	0.9270	0.9908	0.9986	0.9744
<b>J<sub>max</sub>, μA.cm<sup>-2</sup></b>	29.08 ± 3.79	13.95 ± 1.46	43.41 ± 1.31	3.729 ± 0.261
<b>K<sub>M</sub>, μM</b>	3183 ± 1180	10411 ± 2110	7813 ± 479.5	2912 ± 599
<b>LRS, μA.cm<sup>-2</sup>.mM<sup>-1</sup></b>	9.136 ± 2.370	1.340 ± 0.139	5.556 ± 0.186	1.281 ± 0.188

Table 5-4

Kinetic parameters, fit, J<sub>max</sub> and K<sub>M</sub> values calculated from the calibration data in Table 10-4. J<sub>max</sub>, K<sub>M</sub> and LRS are presented as Mean ± SEM.

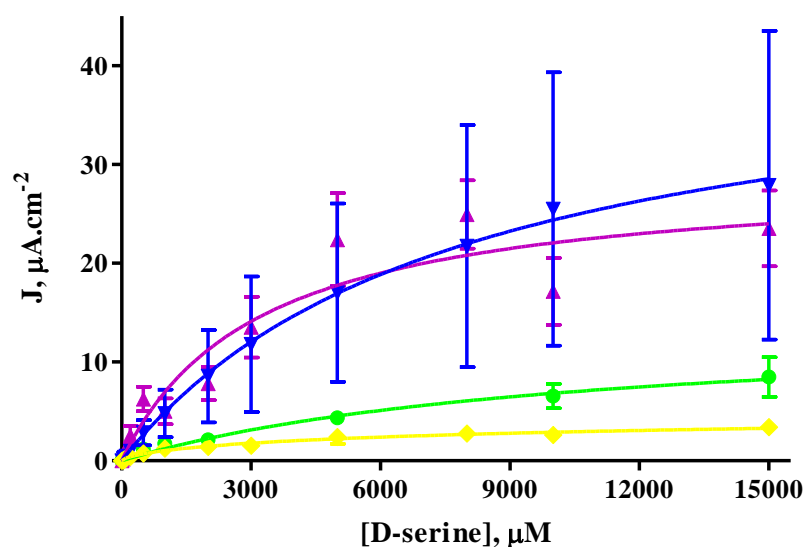


Figure 5-5

J-concentration plot of the four recipes where 600UH<sub>2</sub>O was immobilised in Styrene onto the surface of the electrode. Depicted are Pt<sub>D</sub>-Sty-600UH<sub>2</sub>Ox5 (purple trace), Pt<sub>D</sub>-Sty-600UH<sub>2</sub>Ox10 (green trace), Pt<sub>D</sub>-Sty-600UH<sub>2</sub>Ox15 (blue trace) and Pt<sub>D</sub>-Sty-600UH<sub>2</sub>Ox20 (yellow trace). The data plotted is taken from Table 10-4 and Table 5-4. Traces are plotted as Mean J ± SEM with fitted kinetic curve.

It is quite clear that 5 is the optimum amount of layers in the process of immobilising DAAO in styrene. Compared with 10 and 20 layers its J<sub>max</sub> is significantly higher, p = 0.0098\*\* and p = 0.0005\*\*\* respectively, but not the 15 layer recipe, compared to which it is significantly lower, p = 0.0117\*. The K<sub>M</sub> value is significantly lower than that of 10 or 15 layers, p = 0.0243\* and p = 0.0109\*, although not the 20 layer recipe, p = 0.8445. As a result its LRS value of 9.136 ± 2.370 μA.cm<sup>-2</sup>.mM<sup>-1</sup> is significantly larger than the 10 and 20 layer alternatives, p = 0.0167\*, p = 0.2292 and p = 0.0456\*. It is however not significantly larger than the 15 layer recipe, p = 0.2292, despite the mean values giving that impression. However when one considers the SEM of the data achieved for the 15 layer recipe it is clear that it should be discounted as a possible route forward. I believe this is due to 15 layers of enzyme to be an intermediary point

whereby the mass of adsorbed material is on the brink of falling due to its own weight. This leads to some biosensors retaining the enzyme and others losing vast quantities of it back into solution. Thus large SEM's are resultant.

What is also clear is that to obtain the best possible immobilisation and binding of DAAO to the surface of the electrode, a combination of the immobilisation in Styrene with additional cross-linking or stabilisation agents is necessary. This should enable efficient layering of component parts up to 10 layers. This will be achievable as it has now been shown that the Styrene can efficiently contain five layers of enzyme and the cross-linking agent GA can stabilise up to 10 layers effectively. A combination of these two approaches, it was hoped, would therefore yield the best results.

#### 5.2.4 Water and PBS in the Enzyme Solution

Given the results obtained previously, see Sections 4.7.1 and 4.7.2, the conclusion was reached that it was necessary to compare again 600UH<sub>2</sub>O and 600UPBS. It was hoped to make a clear distinction between the two solutions and to carry only one forward into any further investigations. Thus sensors were constructed using styrene as an immobilisation matrix and then adding 10 layers of enzyme solution, 600UH<sub>2</sub>O and 600UPBS, with different stabilising and cross-linking agents.

It was hoped that this broad approach using the other substances, that were likely to be included in the final fabrication process, would yield the most relevant results. Incorporation of these elements could change radically the outcome in comparison to a situation where only one of the immobilisation agent, cross-linking substance or stabiliser was utilised. Thus the general formulation became Pt<sub>D</sub>-Sty-[Enzyme-Stabiliser]<sub>x10</sub>. The first two stabilising substances to be examined were GA1% and BSA1%. These two substances were then combined to yield two more solutions which were also examined. They were BSAGA, the standard solution where the component parts were present in a 1% w/v and 1% v/v concentration respectively, and also BSA1%GA0.1%, where the GA was only present as 0.1% v/v concentration. The data obtained is presented in Table 10-5, with the associated calculated kinetic parameters in Table 5-5.

Electrode Design	Pt <sub>D</sub> -Sty-[600UH <sub>2</sub> O-GA1%]x10 n = 3	Pt <sub>D</sub> -Sty-[600UH <sub>2</sub> O-BSA1%]x10 n = 4	Pt <sub>D</sub> -Sty-[600UH <sub>2</sub> O-BSAGA]x10 n = 4	Pt <sub>D</sub> -Sty-[600UH <sub>2</sub> O-BSAGA0.1%]x10 , n = 6
<b>Kinetics</b>	M-M, p = 0.2300	M-M-H, p<0.0001	M-M, p = 0.9696	M-M-H,p< 0.0001
<b>R<sup>2</sup></b>	0.9953	0.9995	0.9959	0.9998
<b>J<sub>max</sub>, μA.cm<sup>-2</sup></b>	47.74 ± 2.03	1.760 ± 0.197	84.79 ± 3.82	2.904 ± 0.408
<b>K<sub>M</sub>, μM</b>	5241 ± 525	23313 ± 6291	6459 ± 636	62372 ± 19381
<b>α</b>		0.7260 ± 0.0271		0.6894 ± 0.0180
<b>LRS, μA.cm<sup>-2</sup>.mM<sup>-1</sup></b>	9.109 ± 0.566	0.07551 ± 0.01197	13.13 ± 0.75	0.04656 ± 0.00794
Electrode Design	Pt <sub>D</sub> -Sty-[600UPBS-GA1%]x10 n = 8	Pt <sub>D</sub> -Sty-[600UPBS-BSA1%]x10 n = 4	Pt <sub>D</sub> -Sty-[600UPBS-BSAGA]x10 n = 4	Pt <sub>D</sub> -Sty-[600UPBS-BSAGA0.1%]x10 , n = 4
<b>Kinetics</b>	M-M, p = 0.2646	M-M-H, p=0.0038	M-M-H, p=0.0131	M-M, p = 0.0675
<b>R<sup>2</sup></b>	0.9965	0.9968	0.9991	0.9812
<b>J<sub>max</sub>, μA.cm<sup>-2</sup></b>	90.56 ± 4.90	2.996 ± 0.775	61.28 ± 1.533	9.530 ± 0.669
<b>K<sub>M</sub>, μM</b>	3538 ± 524	19050 ± 12639	2704 ± 163	3155 ± 651
<b>α</b>		0.7068 ± 0.0690	1.129 ± 0.046	
<b>LRS, μA.cm<sup>-2</sup>.mM<sup>-1</sup></b>	25.59 ± 2.59	0.1573 ± 0.0638	22.66 ± 0.84	3.021 ± 0.449

Table 5-5

Kinetic parameters, fit, J<sub>max</sub> and K<sub>M</sub> values calculated from the calibration data in Table 10-5. J<sub>max</sub>, K<sub>M</sub>, α and LRS are presented as Mean ± SEM.

From a first examination of the calibration data and the associated kinetic model results it is clear that one of the recipes has not functioned as well as hoped. This is the recipe with the BSA1% as a stabilising agent. Despite BSA being a protein which should provide a natural environment for the enzyme to reside in, and its widespread use in enzymatic biosensors, it appears to have no ability to help retain the DAAO on the surface of the electrode.

The result is, in the case of both 600UH<sub>2</sub>O and 600UPBS, that the J<sub>max</sub> and LRS are small and the K<sub>M</sub> is high and has a very large SEM. There is no significant difference between any of the kinetic parameters of the two formulations, p = 0.2200, p = 0.7729 and p = 0.2969 for the J<sub>max</sub>, K<sub>M</sub> and LRS respectively. Taking the poor sensitivity into account these results are not graphed. The results for Pt<sub>D</sub>-Sty-[Enzyme-GA1%]x10 and Pt<sub>D</sub>-Sty-[Enzyme-BSAGA]x10 are displayed in Figure 5-6 and Figure 5-7 respectively.

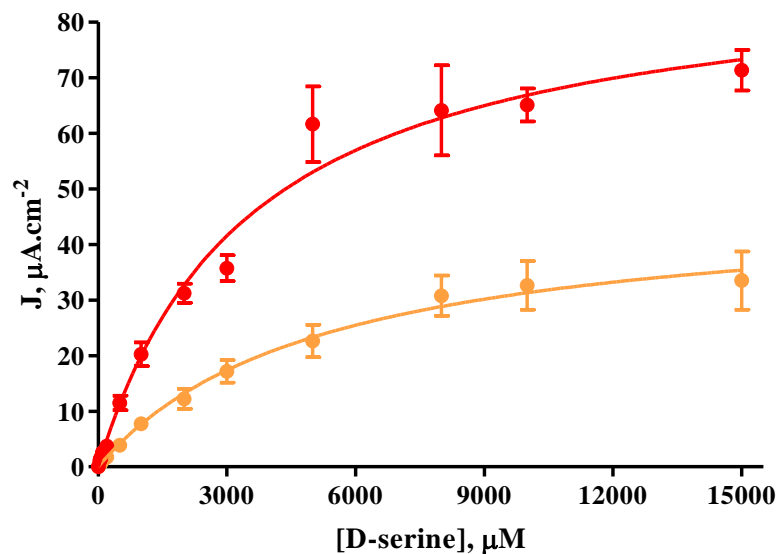


Figure 5-6

J-concentration plot of the sensors designed to elucidate the difference between 600UH<sub>2</sub>O and 600UPBS. Depicted are PtD-Sty-[600UH<sub>2</sub>O-GA1%]x10 (orange trace) and PtD-Sty-[600UPBS-GA1%]x10 (red trace). The data plotted is taken from Table 10-5 and Table 5-5.

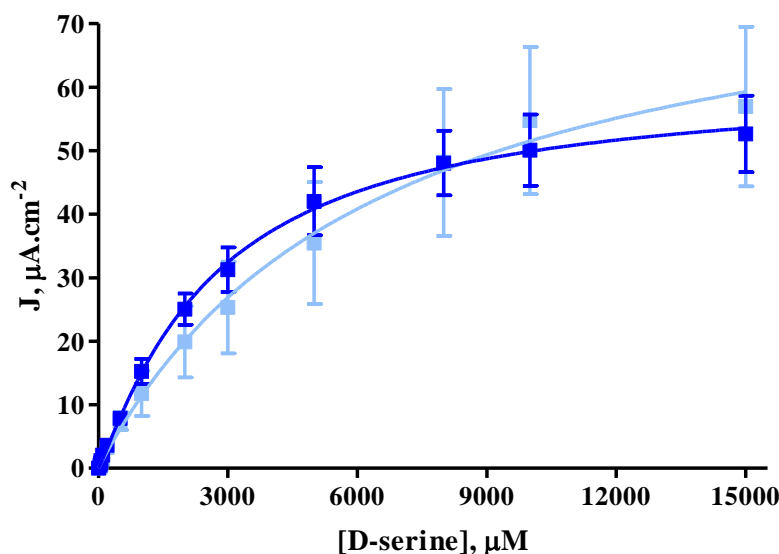


Figure 5-7

J-concentration plot of the sensors designed to elucidate the difference between 600UH<sub>2</sub>O and 600UPBS. Depicted are PtD-Sty-[600UH<sub>2</sub>O-BSAGA]x10 (light blue trace) and PtD-Sty-[600UPBS-BSAGA]x10 (royal blue trace). The data plotted is taken from Table 10-5 and Table 5-5.

In the case of Pt<sub>D</sub>-Sty-[600UH<sub>2</sub>O-GA1%]x10 and Pt<sub>D</sub>-Sty-[600UPBS-GA1%]x10 the improved results achieved with the use of PBS pH 8.5 instead of water. The  $J_{\max}$  of the 600UPBS recipe is significantly higher,  $p = 0.0006^{***}$ , the  $K_M$  is not significantly different,  $p = 0.1008$ , and the LRS of  $25.59 \pm 2.59 \mu\text{A}\cdot\text{cm}^{-2}\cdot\text{mM}^{-1}$  is significantly larger than the 600UH<sub>2</sub>O recipe,  $p = 0.0004^{***}$ .

The graph of the  $\text{Pt}_D\text{-Sty-[600UH}_2\text{O-BSAGA]x10}$  and  $\text{Pt}_D\text{-Sty-[600UPBS-BSAGA]x10}$  data (Figure 5-7) appears a little bit more complicated. However, examination of the calculated kinetic data reveals that once again 600UPBS produces significantly better results. The  $J_{\max}$  of the biosensors formulated with the PBS solution is significantly lower,  $p = 0.0012^{**}$  which is not an ideal result, however, the  $K_M$  is also significantly lower,  $p = 0.0106^*$ . However, these conflicting positive and negative changes do result in an LRS which is  $22.66 \pm 0.84 \mu\text{A}\cdot\text{cm}^{-2}\cdot\text{mM}^{-1}$  and significantly larger than the 600UH<sub>2</sub>O LRS,  $p = 0.0001^{***}$ .

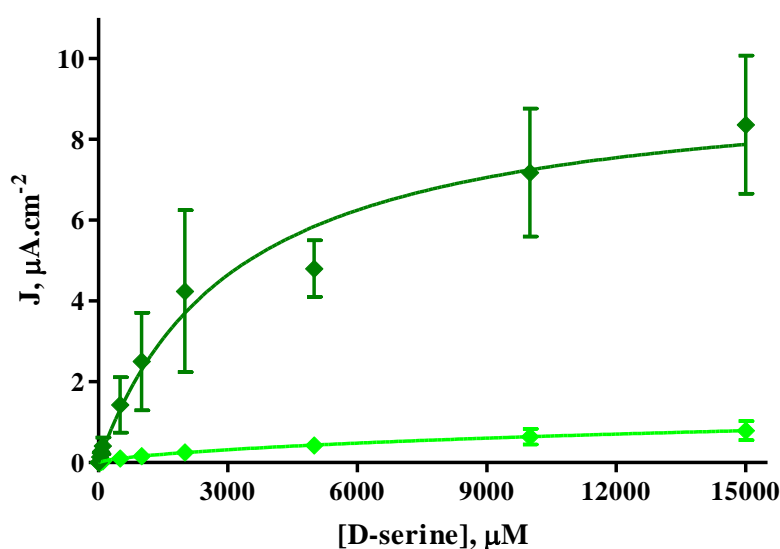


Figure 5-8

**J-concentration plot of the sensors designed to elucidate the difference between 600UH<sub>2</sub>O and 600UPBS. Depicted are  $\text{Pt}_D\text{-Sty-[600UH}_2\text{O-BSAGA0.1%]x10}$  (light green trace) and  $\text{Pt}_D\text{-Sty-[600UPBS-BSAGA0.1%]x10}$  (dark green trace). The data plotted is taken from Table 10-5 and Table 5-5. Traces are plotted as Mean  $J \pm \text{SEM}$  with fitted kinetic curve.**

Once again the benefits of using 600UPBS instead of 600UH<sub>2</sub>O are clear to see with the  $\text{Pt}_D\text{-Sty-[Enzyme-BSAGA0.1%]x10}$  recipes (Figure 5-8). It is also easy to see that the all the essential kinetic values are vastly inferior compared to the BSAGA and GA recipes. Despite this fact, it is still possible to extract useful and relevant information about the two enzyme solutions these recipes were designed to compare. Looking first at the  $J_{\max}$  the calculated value is significantly larger,  $p < 0.0001^{***}$  and the  $K_M$  value is significantly smaller,  $p = 0.0283$ . Both of these results are favourable, and as a result the LRS is also significantly larger,  $p < 0.0001^{***}$ .

The conclusion must be, and was, reached that given this set of results it is, almost without fail, better to use PBS, with a pH of 8.5, than water when formulating the

enzyme solutions. Thus from this point forward in the project only 600UPBS was used while fabricating any biosensor recipes.

### 5.3 A Comprehensive Study of the Binding Properties of GA

Having seen in many previous sections of this project that glutaraldehyde was capable of effectively binding DAAO to the surface of an electrode it was decided to undertake a comprehensive study of its abilities. Indeed GA is the most widely studied cross-linking agent across a wide variety of scientific fields (Migneault *et al.*, 2004) as well as being one of the most gentle coupling methods used in enzyme technology (Weetall, 1974). Yet despite this there is still a great deal of debate as to its structure and mechanism of cross-linking in solution, depending on pH in particular, with up to 11 different forms proposed (Aso & Aito, 1962; Richards & Knowles, 1968; Hardy *et al.*, 1969; Korn *et al.*, 1972; Monsan *et al.*, 1975; Rembaum *et al.*, 1978; Margel & Rembaum, 1980; Tashima *et al.*, 1987; Tashima *et al.*, 1991; Kawahara *et al.*, 1992). GA reacts with a variety of functional groups, primarily lysine residues on protein molecules (Weetall, 1974), and shows little reversibility between pH 7.0 and 9.0 (Okuda *et al.*, 1991). There was awareness also that too great a quantity of GA could denature the enzyme and prevent it functioning fully. It has been shown previously that there is a very delicate balance in this regard which is dependent on the nature of the enzyme (Avrameas & Ternynck, 1969; Broun, 1976) concentration of the enzyme and reagent, pH, ionic strength of the solution, temperature and reaction time (Jansen & Olson, 1969; Jansen *et al.*, 1971; Ottesen & Svensson, 1971; Tomimatsu *et al.*, 1971; Zaborsky & Co, 1973; Broun, 1976). Thus it was important not only to consider how and where the GA would be included but also to explore the effect of changing the concentration of GA utilised. The importance of these changes has already been demonstrated in Section 4.5, Section 4.8.1.1 and to a lesser extent in Section 4.4.

A general recipe was followed for these explorations; Pt<sub>D</sub>-Sty-[600UPBS-GA]. Within this the electrodes were first dipped into the 600UPBS immediately after the dip into styrene. The number, and concentration, of GA dips within the layers were then varied. There were always 10 dips into 600UPBS, each on a separate layer. The electrodes were allowed to dry for five minutes between layers. While drying they were hung vertically, with the active surface pointing downward.

To help enable comparison the colourings for the different percentages of GA are maintained throughout this section in all figures. 0.1% is red, 0.2% is yellow, 0.5% is green, 1.0% is blue, 1.5% is purple and 2.0% is purple.

### 5.3.1 Ten Dips into GA

The first set of recipes devised incorporated a full 10 dips into GA, one for each dip in 600UPBS. The general recipe took the form of Pt<sub>D</sub>-Sty-[600UPBS-GA]x10 with the concentration of GA used being varied within this. The GA concentrations used were; 0.1%, 0.2%, 0.5%, 1.0%, 1.5% and 2.0% (all v/v). The calibration data for the six recipes is presented in Table 10-6, along with the relevant kinetic data below in Table 5-6. The two least effective percentages of GA for use in this general fabrication method are quite apparent when one considers the LRS values that were calculated. Both 0.1% and 0.2% only achieve an LRS of approximately  $2 - 3 \mu\text{A}\cdot\text{cm}^{-2}\cdot\text{mM}^{-1}$ . This is about one order of magnitude below the value reached by other concentrations used. They will thus not be considered for further statistical examination.

According to the graphical representation in Figure 5-9 it appears that the 0.5% and 1.0% recipes are quite similar. Examination of the kinetic parameters backs this observation up. The  $J_{\text{max}}$  for 1.0% is significantly higher,  $p = 0.0184^*$ , but the  $K_M$  and LRS are both not significantly difference,  $p = 0.05672$  and  $p = 0.4370$  respectively. The only discernible difference is, therefore, the  $J_{\text{max}}$ , of which 1.0% GA has the better value. It appears too that there is little difference between 1.5% and 2.0% when the graph below is examined. Examining the figures though, there is a realisation that the two recipes are quite different. Firstly the 1.5% GA recipe is M-M kinetics fitted and the 2.0% GA analogue conforms to M-M-H kinetics. When the  $J_{\text{max}}$  are compared it is discovered that the 1.5% recipe has a significantly higher value,  $p = 0.0003^{***}$ . But the 2% GA yields a significantly lower  $K_M$ ,  $p = 0.0003^{***}$ . Finally it is found that the 2% also has a significantly better LRS,  $p = 0.0009^{***}$ . Thus, it is apparent that the 2% recipe is the superior of the two.

Electrode Design	Pt <sub>D</sub> -Sty-[600UPBS-GA0.1%]x10, n = 3	Pt <sub>D</sub> -Sty-[600UPBS-GA0.2%]x10, n = 4	Pt <sub>D</sub> -Sty-[600UPBS-GA0.5%]x10, n = 4
Kinetics	M-M-H, p = 0.0028	M-M, p = 0.1176	M-M, p = 0.0624
R <sup>2</sup>	1.000	1.000	0.9988
J <sub>max</sub> , μA.cm <sup>-2</sup>	31.87 ± 0.27	27.30 ± 0.22	75.11 ± 1.22
K <sub>M</sub> , μM	11126 ± 177.3	11118 ± 176	3213 ± 148
α	0.9836 ± 0.003342		
LRS, μA.cm <sup>-2</sup> .mM <sup>-1</sup>	2.864 ± 0.022	2.456 ± 0.020	23.38 ± 0.75
Electrode Design	Pt <sub>D</sub> -Sty-[600UPBS-GA1.0%]x10, n = 8	Pt <sub>D</sub> -Sty-[600UPBS-GA1.5%]x10, n = 3	Pt <sub>D</sub> -Sty-[600UPBS-GA2.0%]x10, n = 4
Kinetics	M-M, p = 0.4396	M-M, p = 0.5790	M-M-H, p = 0.0024
R <sup>2</sup>	0.9882	0.9989	0.9988
J <sub>max</sub> , μA.cm <sup>-2</sup>	90.56 ± 4.90	39.72 ± 0.52	33.05 ± 0.4989
K <sub>M</sub> , μM	3538 ± 524	1573 ± 82	816.2 ± 40.6
α			1.327 ± 0.085
LRS, μA.cm <sup>-2</sup> .mM <sup>-1</sup>	25.59 ± 2.59	25.25 ± 1.09	40.19 ± 1.64

Table 5-6

Kinetic parameters, fit, J<sub>max</sub> and K<sub>M</sub> values calculated from the calibration data in Table 10-6. J<sub>max</sub>, K<sub>M</sub>, α and LRS are presented as Mean ± SEM.

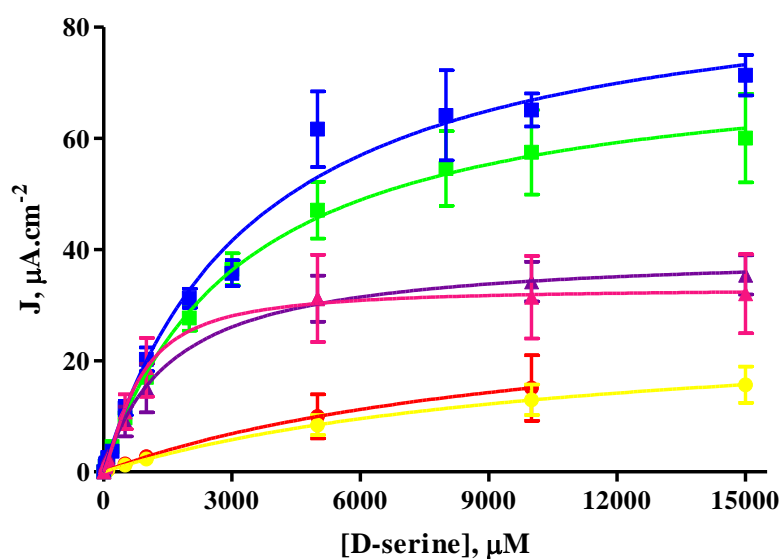


Figure 5-9

J-concentration plot of sensors created to explore the effect of different GA concentrations when applied 10 times. Depicted are Pt<sub>D</sub>-Sty-[600UPBS-GA0.1%]x10 (red trace), Pt<sub>D</sub>-Sty-[600UPBS-GA0.2%]x10 (yellow trace), Pt<sub>D</sub>-Sty-[600UPBS-GA0.5%]x10 (green trace), Pt<sub>D</sub>-Sty-[600UPBS-GA1.0%]x10 (blue trace), Pt<sub>D</sub>-Sty-[600UPBS-GA1.5%]x10 (purple trace) and Pt<sub>D</sub>-Sty-[600UPBS-GA2.0%]x10 (pink trace). The data plotted is taken from Table 10-6 and Table 5-6.

Among the four recipes of 0.5%, 1.0%, 1.5% and 2.0% different recipes present different aspects which are desirable and superior to the others. For instance the 1% has a higher J<sub>max</sub> than 0.5%, 1.5% (p < 0.0001\*\*\*) and 2.0% (p < 0.0001\*\*\*) and the 2% recipe has a lower K<sub>M</sub> than the 0.5% (p = 0.0006\*\*\*), 1.0% (p = 0.0013\*\*).

The 2% GA also produces an LRS which is higher than 0.5% ( $p < 0.0001^{***}$ ), 1.0% ( $p = 0.0035^{**}$ ) and 1.5%. However, visually, in Figure 5-9, there appears to be no difference in the initial slope. If the raw calibration data is examined, for instance at 1000  $\mu\text{M}$ , it is seen that there is no difference between 1% and 2%,  $p = 0.7628$ . Indeed the 1% value is not significantly larger than 1.5%,  $p = 0.2629$ , or 0.5%,  $p = 0.1831$ , and neither is the 2% value,  $p = 0.6300$  and  $p = 0.7621$  respectively.

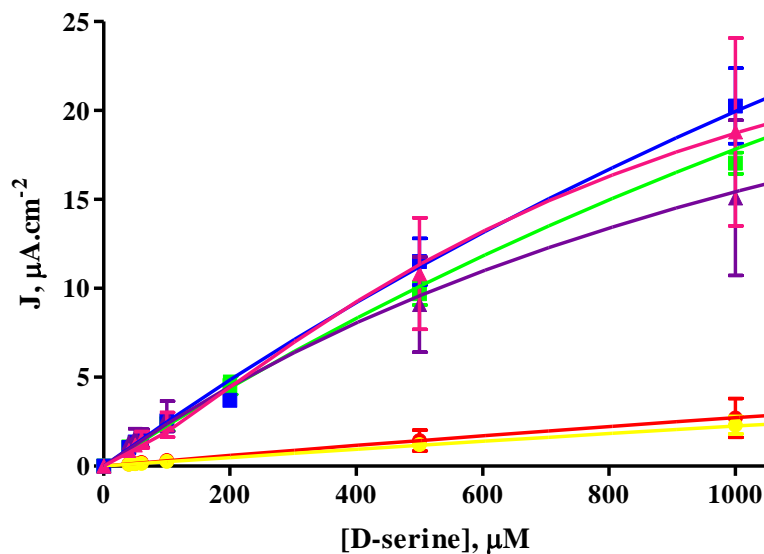


Figure 5-10

J-concentration plot of sensors created to explore the effect of different GA concentrations when applied 10 times. Depicted are  $\text{Pt}_D\text{-Sty-[600UPBS-GA0.1\%]x10}$  (red trace),  $\text{Pt}_D\text{-Sty-[600UPBS-GA0.2\%]x10}$  (yellow trace),  $\text{Pt}_D\text{-Sty-[600UPBS-GA0.5\%]x10}$  (green trace),  $\text{Pt}_D\text{-Sty-[600UPBS-GA1.0\%]x10}$  (blue trace),  $\text{Pt}_D\text{-Sty-[600UPBS-GA1.5\%]x10}$  (purple trace) and  $\text{Pt}_D\text{-Sty-[600UPBS-GA2.0\%]x10}$  (pink trace). The data plotted is taken from Table 10-6 and Table 5-6. Traces are plotted as Mean  $J \pm \text{SEM}$  with fitted kinetic curve.

To help illustrate this graphically an expanded J-concentration plot has been created over the range 0 – 1000  $\mu\text{M}$  D-ser, see Figure 5-10. Here it is possible to see how little difference there is between the four percentages, with all of their SEM bars overlapping. Closer examination does however reveal that a difference does exist between the 1% (blue) and 2% (pink) recipes, the recipes with the highest  $J_{\text{max}}$  and LRS respectively. This difference is in their shape over this concentration range. It can be seen that the 1% recipe has a very linear increase over this range. However the 2% recipe appears to change its slope several times. This is due to the M-M-H kinetic fit. As the  $\alpha$  value for this kinetic model increases above 1 and towards 2 there is increasing degree of a sigmoidal shape to the response, rather than an initial linear response. This particular 2% GA design has an  $\alpha$  value of  $1.327 \pm 0.085$ , which appears to be enough for the sigmoidal shape to begin to become evident in the plot.

### 5.3.2 Five Dips into GA

Having examined what happens to the sensitivity of the biosensors when 10 dips of GA are applied, it seemed logical to next examine the effect of five dips of GA, one every second layer. The general recipe thus became  $Pt_D\text{-Sty-[600UPBSx2-GA2.0%]}_x5$ . The same 0.1%, 0.2%, 0.5%, 1.0%, 1.5% and 2.0% GA concentrations were again examined. The calibration data is listed in Table 10-7 with the associated kinetic parameters calculated in Table 5-7. These two sets of data are then graphically displayed in Figure 5-11.

A casual perusal of the data and plot shows that the changes observed for 5 dips of GA are not as straight forwards as was found to be the case for 10 dips. The sensitivity fluctuates more radically between different percentages. The  $J_{\max}$ , in particular, appears to alternately increase and decrease for every increase in GA concentration.

Beginning with the  $J_{\max}$  value, statistically it does not change from 0.1% to 0.2%,  $p = 0.0507$ , nor does it change between 0.2% and 0.5%,  $p = 0.1203$ . This is due to the large error associated with the calculated value for 0.2%. However it does increase significantly from 0.1% and 0.5%,  $p = 0.0003^{***}$ . From this value it increases further when 1.0% is used,  $p < 0.0001^{***}$ . It then decreases significantly as the change is made to 1.5%,  $p < 0.0001^{***}$ , before finally increasing for 2.0%,  $p < 0.0001^{***}$ . The largest value of  $J_{\max}$  is found using 1% GA, it is significantly larger than all others including 2.0%,  $p = 0.0127^*$ , except 0.2% GA, which is again due to the large associated error with this value.

Electrode Design	Pt <sub>D</sub> -Sty-[600UPBSx2-GA0.1%]x5, n = 3	Pt <sub>D</sub> -Sty-[600UPBSx2-GA0.2%]x5, n = 3	Pt <sub>D</sub> -Sty-[600UPBSx2-GA0.5%]x5, n = 3
Kinetics	M-M-H, p < 0.0001	M-M-H, p = 0.0182	M-M, p = 0.2392
R <sup>2</sup>	0.9998	0.9980	0.9993
J <sub>max</sub> , μA.cm <sup>-2</sup>	16.70 ± 1.82	76.95 ± 13.99	40.30 ± 0.75
K <sub>M</sub> , μM	34824 ± 7758	13033 ± 6100	5949 ± 319
α	0.7988 ± 0.0219	0.7575 ± 0.0639	
LRS, μA.cm <sup>-2</sup> .mM <sup>-1</sup>	4.795 ± 0.055	5.905 ± 1.695	6.774 ± 0.249
Electrode Design	Pt <sub>D</sub> -Sty-[600UPBSx2-GA1.0%]x5, n = 3	Pt <sub>D</sub> -Sty-[600UPBSx2-GA1.5%]x5, n = 4	Pt <sub>D</sub> -Sty-[600UPBSx2-GA2.0%]x5, n = 4
Kinetics	M-M-H, p = 0.0021	M-M, p = 0.2406	M-M, p = 0.1621
R <sup>2</sup>	0.9990	0.9995	1.000
J <sub>max</sub> , μA.cm <sup>-2</sup>	83.64 ± 2.128	29.25 ± 0.65	64.73 ± 0.31
K <sub>M</sub> , μM	2060 ± 154	6882 ± 361	5616 ± 71
α	1.332 ± 0.078		
LRS, μA.cm <sup>-2</sup> .mM <sup>-1</sup>	40.60 ± 2.158	4.251 ± 0.135	11.53 ± 0.09

Table 5-7

Kinetic parameters, fit, J<sub>max</sub> and K<sub>M</sub> values calculated from the calibration data in Table 10-7. J<sub>max</sub>, K<sub>M</sub>, α and LRS are presented as Mean ± SEM.

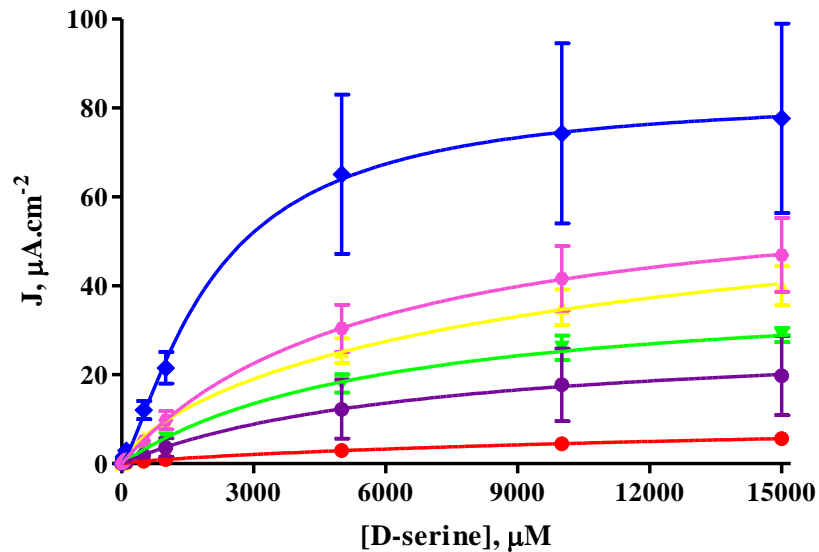


Figure 5-11

J-concentration plot of sensors created to explore the effect of different GA concentrations when applied 5 times. Depicted are Pt<sub>D</sub>-Sty-[600UPBSx2-GA0.1%]x5 (red trace), Pt<sub>D</sub>-Sty-[600UPBSx2-GA0.2%]x5 (yellow trace), Pt<sub>D</sub>-Sty-[600UPBSx2-GA0.5%]x5 (green trace), Pt<sub>D</sub>-Sty-[600UPBSx2-GA1.0%]x5 (blue trace), Pt<sub>D</sub>-Sty-[600UPBSx2-GA1.5%]x5 (purple trace) and Pt<sub>D</sub>-Sty-[600UPBSx2-GA2.0%]x5 (pink trace). The data plotted is taken from Table 10-7 and Table 5-7.

Examining the K<sub>M</sub> values reveals a similar situation. It begins with the worst value, a large K<sub>M</sub> with significant error for 0.1% GA. This results in no significant change between 0.1% and 0.2%, p = 0.0918. The same is also true when comparing 0.2% and 0.5%, p = 0.3659, owing to the large error also present with 0.2% GA; the SEM is

almost 50% of the mean. As with the  $J_{\max}$ , from 0.5% and upwards distinctions are much simpler to draw. The  $K_M$  decreases significantly with 1.0% GA applied five times,  $p = 0.0004^{***}$ , increases significantly from that value with 1.5% GA,  $p = 0.0001^{***}$  before finally decreasing again with the use of 2.0% GA,  $p = 0.0412^*$ .

Mirroring the results of the  $J_{\max}$  values, the  $K_M$  of 1% GA is found to be the best (lowest),  $p < 0.0001^{***}$  for 2%, although owing to the large errors of 0.1% and 0.2% there is no significant difference in these cases,  $p = 0.0639$  and  $p = 0.3481$  respectively.

The clearest indication of the overall changes is revealed by the LRS. There is no significant difference between 0.1% and 0.2%,  $p = 0.0854$ , 0.2% and 0.5%,  $p = 0.6624$ , although there is an increase from 0.1% to 0.5%,  $p = 0.0016^{**}$ . Increasing the GA concentration from 0.5% to 1.5% applied 5 times to the electrode produces a significant decrease in the LRS,  $p = 0.0002^{***}$ , and from 1.5% to 2.0% the LRS increase again significantly,  $p < 0.0001^{***}$ . The value for 2.0% is also significantly higher than the value for 0.5%,  $p < 0.0001^{***}$ .

With consideration of the LRS values, a definite conclusion can be reached that the 1% recipe is the most sensitive, as depicted in the J-concentration plot. It has a significantly higher LRS than that achieved while using 0.1%, 0.2%, 0.5%, 1.5% and 2.0% GA in the same general recipe,  $p = 0.0029^{**}$ ,  $p = 0.0002^{***}$ ,  $p = 0.0041^{**}$ ,  $p = 0.0035^{**}$  and  $p = 0.0055^{**}$  respectively.

### 5.3.3 Two Dips into GA

In a continuation of the examination the amount of GA within the recipes was then reduced to two dips, one on the fifth and tenth layer. The general recipe thus became  $Pt_D\text{-Sty-[600UPBSx5-GA]}_2$  and the same percentages of GA were utilised again. The gathered data from the resultant calibrations and subsequently calculated kinetic data is presented in Table 10-8 and Table 5-8. The accompanying J-concentration plot also follows the colour convention as per the last two sections, see Figure 5-12.

Electrode Design	Pt <sub>D</sub> -Sty-[600UPBSx5-GA0.1%]x2, n = 4	Pt <sub>D</sub> -Sty-[600UPBSx5-GA0.2%]x2, n = 4	Pt <sub>D</sub> -Sty-[600UPBSx5-GA0.5%]x2, n = 3
Kinetics	M-M, p = 0.3742	M-M, p = 0.7657	M-M-H, p = 0.0046
R <sup>2</sup>	0.9954	0.9968	0.9999
J <sub>max</sub> , μA.cm <sup>-2</sup>	4.046 ± 0.164	76.95 ± 13.99	30.37 ± 0.58
K <sub>M</sub> , μM	5166 ± 498.3	14089 ± 1593	7137 ± 291
α			1.068 ± 0.017
LRS, μA.cm <sup>-2</sup> .mM <sup>-1</sup>	0.7381 ± 0.0470	5.835 ± 0.279	4.256 ± 0.094
Electrode Design	Pt <sub>D</sub> -Sty-[600UPBSx5-GA1.0%]x2, n = 3	Pt <sub>D</sub> -Sty-[600UPBSx5-GA1.5%]x2, n = 3	Pt <sub>D</sub> -Sty-[600UPBSx5-GA2.0%]x2, n = 4
Kinetics	M-M-H, p = 0.0081	M-M-H, p = 0.0015	M-M-H, p = 0.0188
R <sup>2</sup>	0.9998	0.9997	0.9999
J <sub>max</sub> , μA.cm <sup>-2</sup>	178.8 ± 4.5	55.98 ± 1.80	6.451 ± 0.309
K <sub>M</sub> , μM	5049 ± 291	3619 ± 254	15078 ± 1471
α	1.109 ± 0.030	1.212 ± 0.041	0.9355 ± 0.0205
LRS, μA.cm <sup>-2</sup> .mM <sup>-1</sup>	35.41 ± 1.19	15.47 ± 0.61	0.4278 ± 0.0214

Table 5-8

Kinetic parameters, fit, J<sub>max</sub> and K<sub>M</sub> values calculated from the calibration data in Table 10-8. J<sub>max</sub>, K<sub>M</sub>, α and LRS are presented as Mean ± SEM.

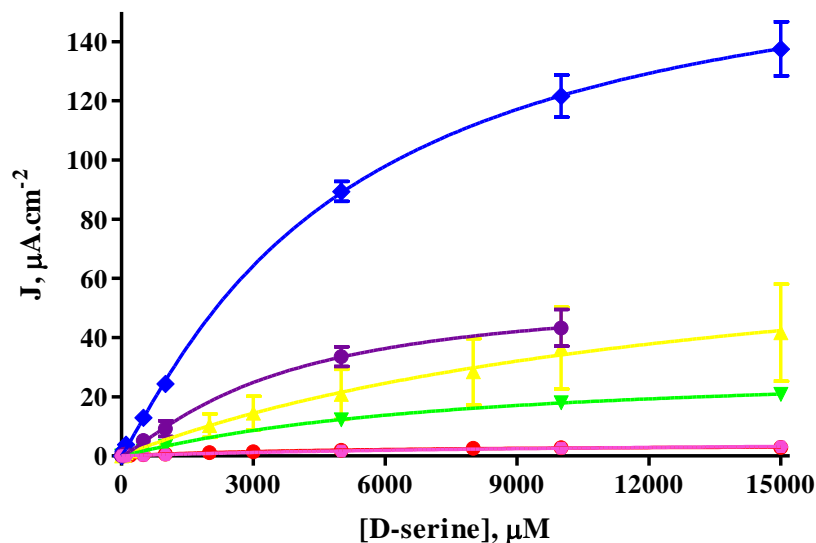


Figure 5-12

J-concentration plot of sensors created to explore the effect of different GA concentrations when applied 2 times. Depicted are Pt<sub>D</sub>-Sty-[600UPBSx5-GA0.1%]x2 (red trace), Pt<sub>D</sub>-Sty-[600UPBSx5-GA0.2%]x2 (yellow trace), Pt<sub>D</sub>-Sty-[600UPBSx5-GA0.5%]x2 (green trace), Pt<sub>D</sub>-Sty-[600UPBSx5-GA1.0%]x2 (blue trace), Pt<sub>D</sub>-Sty-[600UPBSx5-GA1.5%]x2 (purple trace) and Pt<sub>D</sub>-Sty-[600UPBSx5-GA2.0%]x2 (pink trace). The data plotted is taken from Table 10-8 and Table 5-8. Traces are plotted as Mean J ± SEM with fitted kinetic curve.

Cursory inspection of the kinetic data allows one to see that the 0.1% and 2.0% recipes were largely ineffectual. They yielded low J<sub>max</sub> values, had relatively high K<sub>M</sub>

concentrations and as a result the LRS of both are very low, as can be clearly be seen in the plot.

In detail, and beginning with the  $J_{\max}$ , starting from  $4.046 \pm 0.164 \mu\text{A}\cdot\text{cm}^{-2}$  with 0.1% it increases significantly with the change to 0.2%,  $p = 0.0008^{***}$ . From that value it increases significantly with 0.5% GA,  $p = 0.0027^{**}$ , and significantly further again with 1.0%,  $p = 0.0009^{***}$ , to reach a peak of  $178.8 \pm 4.5 \mu\text{A}\cdot\text{cm}^{-2}$ . The  $J_{\max}$  value then decreases significantly as the GA changes from 1.0% to 1.5%,  $p < 0.0001^{***}$ , and significantly further again with the use of 2.0%,  $p = 0.0014^{**}$ .

The  $K_M$  values are a more complicated picture. Initially it increases between 0.1% and 0.2%,  $p = 0.0128^*$ , before decreasing with 0.5%,  $p = 0.0232^*$ , and decreasing again with 1.0%,  $p = 0.0071^{**}$ . The  $K_M$  continues to decrease with 1.5% GA,  $p = 0.0208^*$ , before increasing again with 2.0%,  $p = 0.0046^{**}$ . However, more important, in this instance, than the changes with respect to the increasing percentage of GA, is the how the  $K_M$  of 1% GA compares to the others. It is non-significantly different from that of 0.1%,  $p = 0.8616$ , significantly larger than that of 1.5% and significantly smaller than 0.5%, both already stated. The 1.0%  $K_M$  is also significantly smaller than that of the other two recipes, 0.2% and 2.0%,  $p = 0.0113^*$  and  $p = 0.0068^{**}$  respectively.

These results combined lead to two recipes that have significantly larger LRS values than any of the other recipes. The second highest value is that of 1.5% GA. At  $15.47 \pm 0.61 \mu\text{A}\cdot\text{cm}^{-2}\cdot\text{mM}^{-1}$  it is significantly larger than 0.1%, 0.2%, 0.5% and 2.0%,  $p = 0.0017^{**}$ ,  $p < 0.0001^{***}$ ,  $p = 0.0030^{**}$  and  $p = 0.0016^{**}$  respectively. The largest LRS however is attained by the use of 1.0% GA when applying the GA only twice. Its value of  $35.41 \pm 1.19 \mu\text{A}\cdot\text{cm}^{-2}\cdot\text{mM}^{-1}$  is significantly larger than 0.1%, 0.2%, 0.5%, 1.5% and 2.0% ( $p = 0.0012^{**}$ ,  $p = 0.0017^{**}$ ,  $p = 0.0014^{**}$ ,  $p = 0.0001^{***}$  and  $p = 0.0011^{**}$ ).

### 5.3.4 One Dip into GA

The final alteration to the general recipe considered in the study of GA percentages and number of dips involved the use of GA on only one layer for one dip. This dip was applied in the final, tenth, layer of enzyme. The general recipe thus became  $\text{Pt}_D\text{-Sty-[600UPBS]}\times 10\text{-GA}$ . The data obtained from the six variants of this recipe, using 0.1%, 0.2%, 0.5%, 1.0%, 1.5% and 2.0% GA, are presented below in Table 10-9 and Table 5-9.

Electrode Design	Pt <sub>D</sub> -Sty-[600UPBS]x10-GA0.1%, n = 4	Pt <sub>D</sub> -Sty-[600UPBS]x10-GA0.2%, n = 3	Pt <sub>D</sub> -Sty-[600UPBS]x10-GA0.5%, n = 4
<b>Kinetics</b>	M-M-H, p = 0.0037	M-M-H, p < 0.0001	M-M-H, p = 0.0016
<b>R<sup>2</sup></b>	0.9970	0.9991	0.9998
<b>J<sub>max</sub>, μA.cm<sup>-2</sup></b>	1.214 ± 0.355	27.61 ± 12.51	17.07 ± 0.39
<b>K<sub>M</sub>, μM</b>	20451 ± 16379	121781 ± 128919	4536 ± 240
<b>α</b>	0.6598 ± 0.0681	0.6106 ± 0.0380	1.155 ± 0.032
<b>LRS, μA.cm<sup>-2</sup>.mM<sup>-1</sup></b>	0.05938 ± 0.03027	0.2267 ± 0.1376	3.764 ± 0.117
Electrode Design	Pt <sub>D</sub> -Sty-[600UPBS]x10-GA1.0%, n = 4	Pt <sub>D</sub> -Sty-[600UPBS]x10-GA1.5%, n = 4	Pt <sub>D</sub> -Sty-[600UPBS]x10-GA2.0%, n = 4
<b>Kinetics</b>	M-M-H, p = 0.0018	M-M-H, p = 0.0011	M-M, p = 0.0853
<b>R<sup>2</sup></b>	0.9998	0.9987	0.9812
<b>J<sub>max</sub>, μA.cm<sup>-2</sup></b>	24.87 ± 0.69	42.13 ± 1.08	75.73 ± 10.24
<b>K<sub>M</sub>, μM</b>	5471 ± 326.0	1919 ± 148	6739 ± 2184
<b>α</b>	1.161 ± 0.035	1.443 ± 0.099	
<b>LRS, μA.cm<sup>-2</sup>.mM<sup>-1</sup></b>	4.545 ± 0.150	21.96 ± 1.24	11.24 ± 2.23

Table 5-9

Kinetic parameters, fit, J<sub>max</sub> and K<sub>M</sub> values calculated from the calibration data in Table 10-9. J<sub>max</sub>, K<sub>M</sub>, α and LRS are presented as Mean ± SEM.

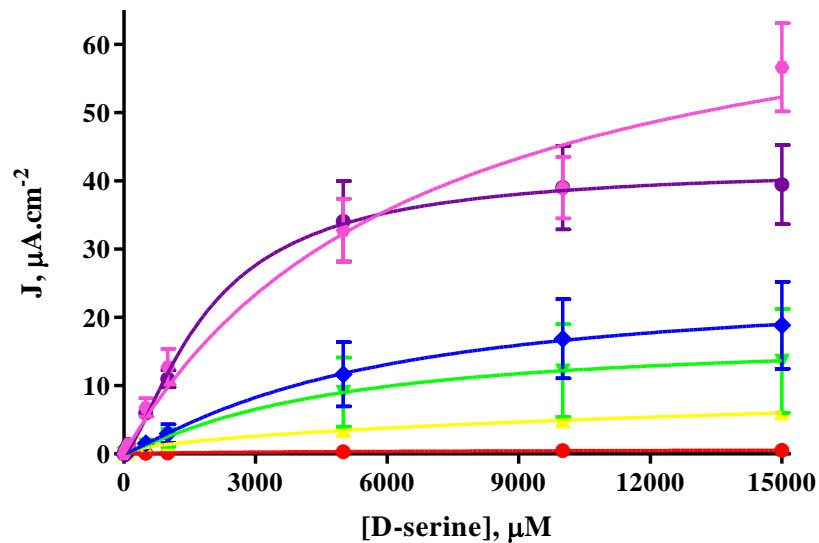


Figure 5-13

J-concentration plot of sensors created to explore the effect of different GA concentrations when applied 1 time. Depicted are Pt<sub>D</sub>-Sty-[600UPBSx5-GA0.1%]x2 (red trace), Pt<sub>D</sub>-Sty-[600UPBSx5-GA0.2%]x2 (yellow trace), Pt<sub>D</sub>-Sty-[600UPBSx5-GA0.5%]x2 (green trace), Pt<sub>D</sub>-Sty-[600UPBSx5-GA1.0%]x2 (blue trace), Pt<sub>D</sub>-Sty-[600UPBSx5-GA1.5%]x2 (purple trace) and Pt<sub>D</sub>-Sty-[600UPBSx5-GA2.0%]x2 (pink trace). The data plotted is taken from Table 10-9 and Table 5-9. Traces are plotted as Mean J ± SEM with fitted kinetic curve.

A glance at the calibration data and kinetic parameters of the 0.1% biosensors and in particular the kinetic parameters of the 0.2% indicate that they were not very successful fabrications. This is a similar situation with one dip of those GA percentages as was

found for the recipes with two dips, see Section 5.3.3. As such these two designs will not be statistically discussed. Moving on to consider the other four designs it is plain to see the effect of the lower number of GA dips. The sensitivities of 0.5% and 1.0% are quite reduced in comparison to the results seen when these concentrations were applied two, five and ten times. This is reinforced by the fact that only 1.5% and 2.0% show any decent sensitivity.

The  $J_{\max}$  of 1.0% is significantly higher than the  $J_{\max}$  of 0.5%,  $p < 0.0001^{***}$ , and the 1.5% value is significantly larger again,  $p < 0.0001^{***}$ . The highest  $J_{\max}$  is that of 2.0% GA, it is larger than the other three percentages,  $p = 0.0470^*$  for 1.5%,  $p = 0.0158^*$  for 1.0% and  $p = 0.0106^*$  for 0.5%.

The smallest  $K_M$  is that of the 1.5% recipe at  $1919 \pm 148 \mu\text{M}$ . It is significantly smaller than either 0.5% or 1.0%, both  $p < 0.0001^{***}$ . The value for 2.0% is not significantly different,  $p = 0.1150$ , although this is due in a large way to the SEM for the  $K_M$  being more than one third of the mean. The mean of the 1.5% value is less than one third of the mean for 2.0%.

This data is summarised best by considering the LRS values of the designs. The 0.5% GA LRS is smallest. The 1% value is significantly larger,  $p = 0.0063^{**}$ , the 2.0% value is not significantly different from the 1.0% value,  $p = 0.0576$ . But, the largest value is that of the 1.5% GA recipe. It is significantly larger than the LRS of 2.0%,  $p = 0.0057^{**}$ , 1.0%,  $p = 0.0008^{***}$ , and of 0.5%,  $p = 0.0007^{***}$ . Therefore in the case of one dip of GA added at the end of the 10 layers of enzyme, the use of 1.5% GA yields the most sensitive biosensors.

### 5.3.5 Discussion of the Trends in GA Alterations

Examination of the above sets of data series to attempt to elucidate overall or underlying trends is a difficult process. Figure 5-14 relates the changing GA% in the recipes to the number of times this GA is applied within the protocol.

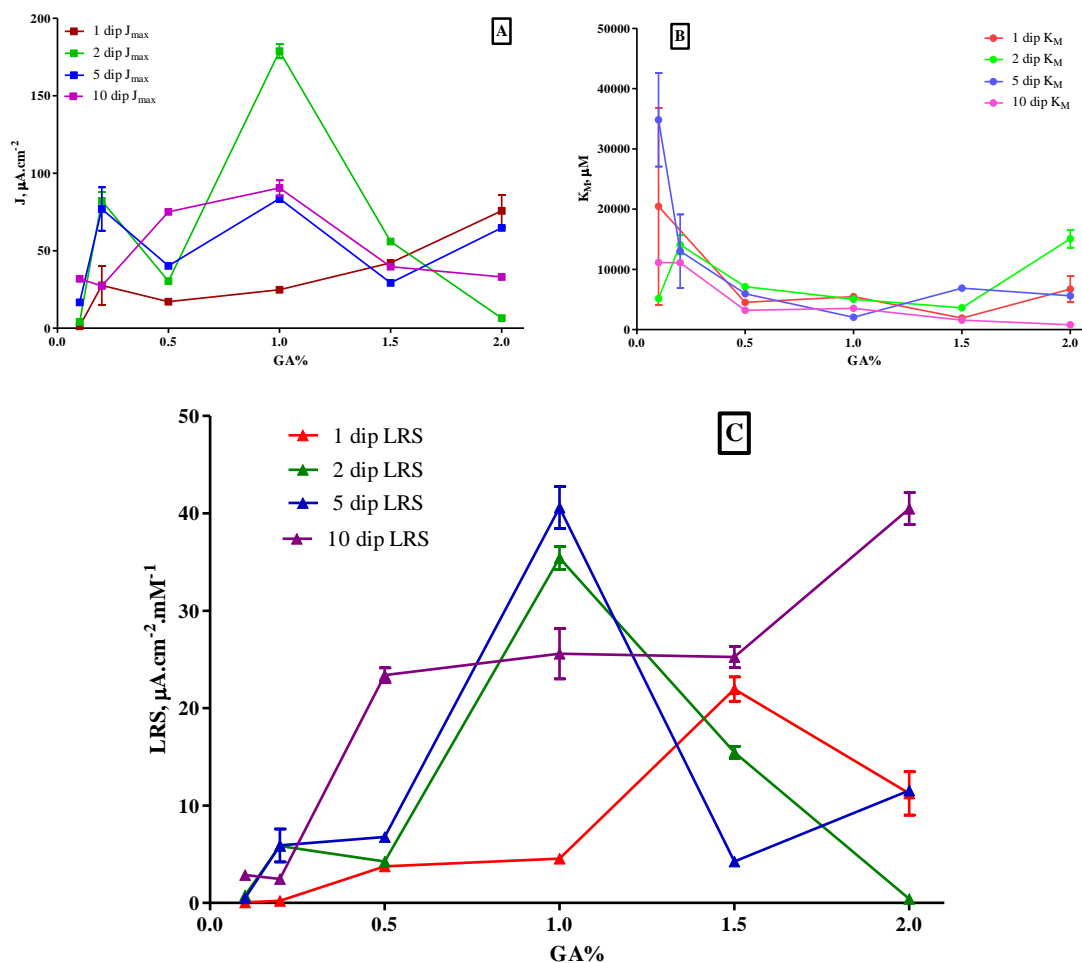


Figure 5-14

Plots of the trends occurring within the three kinetic properties of the GA dip study. *A*, displays the  $K_M$  changes, *B*, the  $J_{max}$  changes, and the main graph, *C*, their combined effect on the LRS. All graphs are plotted as a function of GA% with the 1 dip series depicted in red, the 2 dip series in blue, the 5 dip series in blue and the 10 dip series in purple.

The results in *A* for  $J_{max}$  show that overall there is no distinctly better GA%, although 1% does emerge as appearing to be the best. It results in the single highest value for the 2 dip and 10 dip protocols with an apparent parabolic increase and decrease to be observed, with the 10 dip designs displayed a significantly reduced maximum due to the vastly increased amount of cross-linking that must be occurring. This behaviour, while retaining greater quantities of enzyme, appears to be restricting the activity of the enzyme possibly due to a less flexible matrix. The results for 1 dip GA display almost a linear increase with increasing concentration. This can be treated as an expected result with the single dip of GA requiring higher and higher concentrations to retain further quantities of enzyme. The trend for the 5 dip protocol is more complex, appearing to be linear about a single value of  $J$ , with alternate recipes resulting in a  $J$  higher or lower than this fixed value.

The trends observed in **B**, the summary of the  $K_M$  data are more uniform than those of the  $J_{max}$  values. In general the values for the lower GA concentrations, 0.1% and 0.2% are higher than those of the intermediary 0.5%, 1.0% and 1.5%. There is a general trend towards increasing  $K_M$  values observed again over the 1.5% and 2.0% GA recipes, except in the case of the 10 dip protocol where the  $K_M$  continues to decrease. This trend can be attributed to the lower concentrations of GA having a more linear kinetic behaviour and thus high  $K_M$ , the high GA concentrations serving to begin to restrict the movement and shape of the enzyme, and the intermediate concentrations reaching a compromise between retention of sufficient quantities of enzyme without an overly rigid matrix which inhibits the activity of the enzyme.

The combination of these two factors results in two differing trends in the LRS graph. For the 1, 2 and 5 dip protocols, there is a period of increasing sensitivity, until a maximum is reached, at 1.0% for the 2 and 5 dip recipes and 1.5% for the 1 dip designs, followed by a subsequent decrease in the sensitivity. Only the 10 dip designs deviated from this pattern, whereby they displayed a linear increase in sensitivity as the GA% was increased.

#### **5.4 A Comprehensive Study of the Binding Properties of BSAGA**

In further pursuit of the most complete picture of how to maximise the sensitivity of the DAAO based D-ser biosensors, a second study was undertaken with BSAGA as a stabilising/cross-linking agent. The inclusion of BSA is an important element to study in a GA cross-linked enzyme application with the degree of cross-linking greatly affected by the presence of lysine in the enzyme structure (Avrameas & Ternynck, 1969) and the addition of the inert lysine rich BSA protein a long established method since its first suggestion in the 70's (Broun, 1976). The recipes examined followed the same general structure as those for the GA study, except with the GA being replaced by BSAGA.

The analogue of changing the GA percentage in the previous section was to change the percentage of GA within the BSAGA formulation. The BSA concentration was maintained at 1% w/v. The GA was altered between 0.1% and 2.0% as previously seen to create six solutions as follows; BSAGA0.1%, BSAGA0.2%, BSAGA0.5%, BSAGA1.0%, BSAGA1.5% and BSAGA2.0%. Again, the use of these solutions was examined for 10, 5, 2 and 1 dips within the 10 layers applied to the sensors and also in

keeping with the previous examination of GA the colours used in the following figures were maintained from the previous section. Thus BSAGA0.1% will be red, BSAGA0.2% yellow, BSAGA0.5% green, BSAGA1.0% blue, BSAGA1.5% purple and BSAGA2.0% will be pink.

#### 5.4.1 Ten Dips into BSAGA

The first set of recipes incorporated a full 10 dips into BSAGA, one for each dip in 600UPBS, thus each layer contained enzyme and stabilising agent. The general recipe took the form of Pt<sub>D</sub>-Sty-[600UPBS-BSAGA]x10 with the concentration of the GA used being varied within the BSAGA recipe.

For the sake of completeness, a greater set of values which are more representative of the range of BSAGA solutions used by other groups, see Section 4.5, were used. The GA concentrations used were; 0.005%, 0.01%, 0.02%, 0.05%, 0.1%, 0.2%, 0.5%, 1.0%, 1.5% and 2.0% (all v/v), while the BSA1% was always 1% w/v.

The results from the recipes with 0.005%, 0.01%, 0.02% and 0.05% will be considered first. The calibration data is presented in Table 10-10 and Table 5-10. This data is plotted in Figure 5-15. Included in this plot are also the traces for the 0.1% and 0.2% recipes to allow an easier visual comparison between the first and second set of data. The data for the 0.1%, 0.2%, 0.5%, 1.0%, 1.5% and 2.0% are presented in Table 10-10 and Table 5-11 and displayed in Figure 5-16.

Electrode Design	Pt <sub>D</sub> -Sty-[600UPBS-BSAGA0.005%] x10, n = 3	Pt <sub>D</sub> -Sty-[600UPBS-BSAGA0.01%] x10, n = 4	Pt <sub>D</sub> -Sty-[600UPBS-BSAGA0.02%] x10, n = 4	Pt <sub>D</sub> -Sty-[600UPBS-BSAGA0.05%] x10, n = 4
<b>Kinetics</b>	M-M, p = 0.7681	M-M, n/c	M-M, p = 0.1008	M-M, p = 0.0656
<b>R<sup>2</sup></b>	0.9915	0.9418	0.9995	0.9976
<b>J<sub>max</sub>, μA.cm<sup>-2</sup></b>	0.8483 ± 0.1095	0.5761 ± 0.0709	1.437 ± 0.022	4.707 ± 0.1393
<b>K<sub>M</sub>, μM</b>	10865 ± 2746	2877 ± 1200	3853 ± 182	3350 ± 318
<b>LRS, μA.cm<sup>-2</sup>.mM<sup>-1</sup></b>	0.0781 ± 0.0101	0.2003 ± 0.0631	0.3729 ± 0.0126	1.405 ± 0.098

Table 5-10

Kinetic parameters, fit, J<sub>max</sub> and K<sub>M</sub> values calculated from the calibration data in Table 10-10. J<sub>max</sub>, K<sub>M</sub> and LRS are presented as Mean ± SEM.

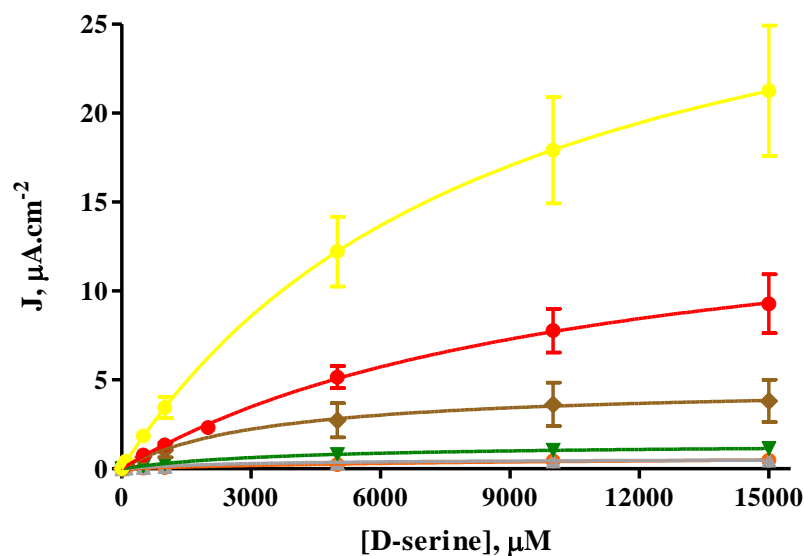


Figure 5-15

J-concentration plot of sensors created to explore the effect of different GA concentrations within a BSAGA solution and then utilised 10 times to bind DAAO to the surface of the electrode. Depicted are Pt<sub>D</sub>-Sty-[600UPBS-BSAGA0.005%]x10 (orange trace), Pt<sub>D</sub>-Sty-[600UPBS-BSAGA0.01%]x10 (grey trace), Pt<sub>D</sub>-Sty-[600UPBS-BSAGA0.02%]x10 (dark green trace), Pt<sub>D</sub>-Sty-[600UPBS-BSAGA0.05%]x10 (brown trace). The data plotted is taken from Table 10-10 and Table 5-10. Also included is Pt<sub>D</sub>-Sty-[600UPBS-BSAGA0.1%]x10 (red trace) and Pt<sub>D</sub>-Sty-[600UPBS-BSAGA0.2%]x10 (yellow trace) from Table 5-11 for clearer comparison with the data presented there.

It is quite apparent from examination of the kinetic data in Table 5-10 that the recipes with the lower percentage of GA were not very sensitive. This is reinforced when they are observed in the plot with the BSAGA0.1% and BSAGA0.2% recipes. Here it is possible to see that at these lower concentrations the sensitivity appears to increase as a direct consequence of the amount of GA incorporated in the BSAGA solution.

The most successful of these recipes was the Pt<sub>D</sub>-Sty-[600UPBS-BSAGA0.05%]x10 recipe (brown trace). Only it will be analysed statistically, as analysing the other recipes serves no purpose. Comparing the BSAGA0.05% to the BSAGA0.1% recipe it can be seen that the former's  $J_{max}$  is significantly lower,  $p = 0.0001^{***}$ , and that its  $K_M$  is also significantly lower,  $p < 0.0001^{***}$ . This results in an LRS which is not significantly different,  $p = 0.4910$ .

Analysing the BSAGA0.05% with the BSAGA0.2% it is observed that the latter has a significantly higher  $J_{max}$ ,  $p < 0.0001^{***}$  and its  $K_M$  is significantly larger too,  $p = 0.0005^{***}$ . The resultant LRS is significantly larger than the 0.05% recipe,  $p = 0.0001^{***}$ . Thus while there is no significant difference in the sensitivity of 0.05% and 0.1%, increasing the percentage further to 0.2% yields a biosensor which is more

sensitive. It was demonstrated that increasing the concentration of included GA could further increase the sensitivity. This data is presented in Table 10-10 and Table 5-11.

The first important observation to make with the data collected from the BSAGA0.1% to BSAGA2.0% biosensors is that within these six recipes, the one with the lowest  $J_{\max}$ , BSAGA0.1% has already been shown to have a higher  $J_{\max}$  than the recipes examined at the start of this section. BSAGA0.1% has significantly lower  $J_{\max}$  when compared to 0.2%, 0.5%, 1.0%, 1.5% and 2.0%,  $p < 0.0001^{***}$ ,  $p = 0.0002^{***}$ ,  $p = 0.0186^*$ ,  $p < 0.0001^{***}$  and  $p < 0.0001^{***}$  respectively. It has an LRS which is also significantly lower than the others,  $p < 0.0001^{***}$ ,  $p = 0.0048^{**}$ ,  $p = 0.0004^{***}$ ,  $p < 0.0001^{***}$  and  $p < 0.0001^{***}$  respectively. There is no trend to be observed in the  $K_M$  values.

The 0.2% and 1.5% have the second lowest  $J_{\max}$ , and are non-significantly different from each other,  $p = 0.0768$ . The 2.0% value increases significantly over these two,  $p = 0.0013^{**}$  and  $p < 0.0001^{***}$  respectively. The use of BSAGA0.5% provides a further increase,  $p = 0.0015^{***}$ , finally reaching a maximum with the use of BSAGA1.0%,  $p = 0.0003^{***}$ . The  $K_M$  values are quite erratic and all quite large. The largest appears to be found using BSAGA1.0%, although it is significantly larger than 0.1%, 0.2%, 0.5%, 1.5%,  $p = 0.0340^*$ ,  $p = 0.0169^*$ ,  $p = 0.0273^*$  and  $p = 0.0003^{***}$  respectively, it is non-significantly different than 0.5%,  $p = 0.4436$ .

Electrode Design	Pt <sub>D</sub> -Sty-[600UPBS-BSAGA0.1%]x10, n = 4	Pt <sub>D</sub> -Sty-[600UPBS-BSAGA0.2%]x10, n = 4	Pt <sub>D</sub> -Sty-[600UPBS-BSAGA0.5%]x10, n = 3
Kinetics	M-M, p = 0.5133	M-M, p = 0.0644	M-M-H, p = 0.0004
R <sup>2</sup>	0.9995	1.000	0.9999
J <sub>max</sub> , μA.cm <sup>-2</sup>	16.09 ± 0.43	33.67 ± 0.12	56.05 ± 2.07
K <sub>M</sub> , μM	10853 ± 549	8770 ± 66	12990 ± 1057
α			0.8902 ± 0.0163
LRS, μA.cm <sup>-2</sup> .mM <sup>-1</sup>	1.482 ± 0.038	3.389 ± 0.016	4.315 ± 0.193
Electrode Design	Pt <sub>D</sub> -Sty-[600UPBS-BSAGA1.0%]x10, n = 3	Pt <sub>D</sub> -Sty-[600UPBS-BSAGA1.5%]x10, n = 4	Pt <sub>D</sub> -Sty-[600UPBS-BSAGA2.0%]x10, n = 4
Kinetics	M-M-H, p = 0.0014	M-M, p = 0.1572	M-M, p = 0.7249
R <sup>2</sup>	0.9997	0.9997	0.9992
J <sub>max</sub> , μA.cm <sup>-2</sup>	99.68 ± 3.743	31.56 ± 0.79	43.55 ± 0.84
K <sub>M</sub> , μM	14341 ± 1152	10671 ± 524	6198 ± 264
α	0.9000 ± 0.0157		
LRS, μA.cm <sup>-2</sup> .mM <sup>-1</sup>	6.951 ± 0.299	2.957 ± 0.075	7.026 ± 0.177

Table 5-11

Kinetic parameters, fit, J<sub>max</sub> and K<sub>M</sub> values calculated from the calibration data in Table 10-10. J<sub>max</sub>, K<sub>M</sub>, α and LRS are presented as Mean ± SEM.

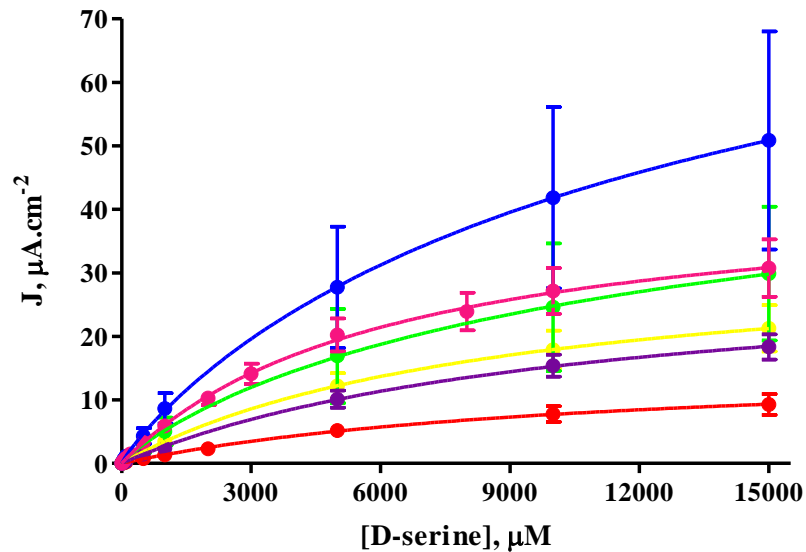


Figure 5-16

J-concentration plot of sensors created to explore the effect of different GA concentrations within a BSAGA solution and then utilised 10 times to bind DAAO to the surface of the electrode. Depicted are Pt<sub>D</sub>-Sty-[600UPBS-BSAGA0.1%]x10 (red trace), Pt<sub>D</sub>-Sty-[600UPBS-BSAGA0.2%]x10 (yellow trace), Pt<sub>D</sub>-Sty-[600UPBS-BSAGA0.5%]x10 (green trace), Pt<sub>D</sub>-Sty-[600UPBS-BSAGA1.0%]x10 (blue trace), Pt<sub>D</sub>-Sty-[600UPBS-BSAGA1.5%]x10 (purple trace) and Pt<sub>D</sub>-Sty-[600UPBS-BSAGA2.0%]x10 (pink trace). Data is taken from Table 10-10 and Table 5-11. Traces are plotted as Mean J ± SEM with fitted kinetic curve.

Considering the LRS values it is observed that, after the 0.1% recipe already examined, the 1.5% value is the smallest. The 0.2% recipe provides a significantly larger LRS again, p = 0.0014\*\*. There is no significant difference between the BSAGA0.2% and

0.5%,  $p = 0.1331$ . Further improvement is achieved with the use of BSAGA1.0% and 2.0%. They are also not significantly different from each other,  $p = 0.8360$ , but significantly more sensitive than 0.2% and 0.5%,  $p = 0.0019^{**}$  and  $p = 0.0011^{**}$  for 1.0%,  $p = 0.0004^{***}$  and  $p = 0.0002^{***}$  for 2.0% respectively. Thus the trend for recipes incorporating 1.0% GA or 2.0% GA being the most sensitive appears to continue when BSAGA solutions are used.

#### 5.4.2 Five Dips into BSAGA

As with the GA exploration, the BSAGA study then changed the number of dips to 5 of BSAGA to ten dips of 600UPBS. Thus every second layer contained enzyme and stabilising agent. The general recipe took the form of  $Pt_D\text{-Sty-[600UPBSx2-BSAGA]x5}$  with the concentration of the GA used being varied within the BSAGA recipe. The examination used the same six BSAGA solutions again. The calibration data collected, the resultant kinetic fit information and the resultant plots are displayed in Table 10-11, Table 5-12 and Figure 5-17.

Unlike other general recipes that have been explored there appears to be two distinct levels in the plot of response for  $Pt_D\text{-Sty-[600UPBSx2-BSAGA]x5}$ . The first level encompasses the BSAGA0.1%, BSAGA0.2% and BSAGA0.5% recipes and the responses are quite low. There is then a large gap, and a jump in response to D-ser for the 1.0%, 1.5% and 2.0% recipes. The J axis in Figure 5-17 had to be split in order for the three lower percentage recipes to be clearly visible.

Upon examining the figures in detail, this observation is borne out to a certain degree, particularly when the  $J_{\max}$  values are considered. The  $J_{\max}$  is a minimum with 0.1% and significantly increases with 0.2%,  $p = 0.0065^{**}$ , and remains at that level with the change to 0.5%,  $p = 0.1238$ . These  $J_{\max}$  values are all under  $6 \mu\text{A}\cdot\text{cm}^{-2}$ . With the change of BSAGA0.5% to BSAGA1.0% there is a large increase in  $J_{\max}$ , to the maximum reached, to  $77.55 \pm 2.14 \mu\text{A}\cdot\text{cm}^{-2}$ , significantly higher than the 0.5% value,  $p < 0.0001^{***}$ . This value is also significantly larger than the 1.5% and 2.0% value,  $p = 0.0009^{***}$  and  $p = 0.0001^{***}$ . However, more significant is that the 2.0%  $J_{\max}$  is still  $50.68 \pm 0.75 \mu\text{A}\cdot\text{cm}^{-2}$ , which is an order of magnitude and significantly larger than the 0.5% value,  $p < 0.0001^{***}$ . The 2.0% is significantly smaller than the 1.5% value,  $p = 0.0007^{***}$ .

Electrode Design	Pt <sub>D</sub> -Sty-[600UPBSx2-BSAGA0.1%]x5, n = 3	Pt <sub>D</sub> -Sty-[600UPBSx2-BSAGA0.2%]x5, n = 3	Pt <sub>D</sub> -Sty-[600UPBSx2-BSAGA0.5%]x5, n = 3
Kinetics	M-M-H, p = 0.0020	M-M, p = 0.6174	M-M-H, p < 0.0001
R <sup>2</sup>	0.9999	0.9981	1.000
J <sub>max</sub> , μA.cm <sup>-2</sup>	2.055 ± 0.130	4.811 ± 0.514	5.887 ± 0.206
K <sub>M</sub> , μM	17572 ± 2316	21359 ± 3500	21703 ± 1711
α	0.8883 ± 0.0227		0.7895 ± 0.0095
LRS, μA.cm <sup>-2</sup> .mM <sup>-1</sup>	0.1169 ± 0.0804	0.2252 ± 0.0134	0.2713 ± 0.0119
Electrode Design	Pt <sub>D</sub> -Sty-[600UPBSx2-BSAGA1.0%]x5, n = 4	Pt <sub>D</sub> -Sty-[600UPBSx2-BSAGA1.5%]x5, n = 4	Pt <sub>D</sub> -Sty-[600UPBSx2-BSAGA2.0%]x5, n = 3
Kinetics	M-M-H, p = 0.0097	M-M-H, p = 0.0004	M-M-H, p = 0.0001
R <sup>2</sup>	0.9998	0.9995	0.9998
J <sub>max</sub> , μA.cm <sup>-2</sup>	77.55 ± 2.14	62.53 ± 1.25	50.68 ± 0.75
K <sub>M</sub> , μM	6477 ± 384	2343 ± 131	2436 ± 101
α	1.095 ± 0.028	1.303 ± 0.053	1.244 ± 0.035
LRS, μA.cm <sup>-2</sup> .mM <sup>-1</sup>	11.97 ± 0.39	26.69 ± 1.04	20.81 ± 0.59

Table 5-12

Kinetic parameters, fit, J<sub>max</sub> and K<sub>M</sub> values calculated from the calibration data in Table 10-11. J<sub>max</sub>, K<sub>M</sub>, α and LRS are presented as Mean ± SEM.

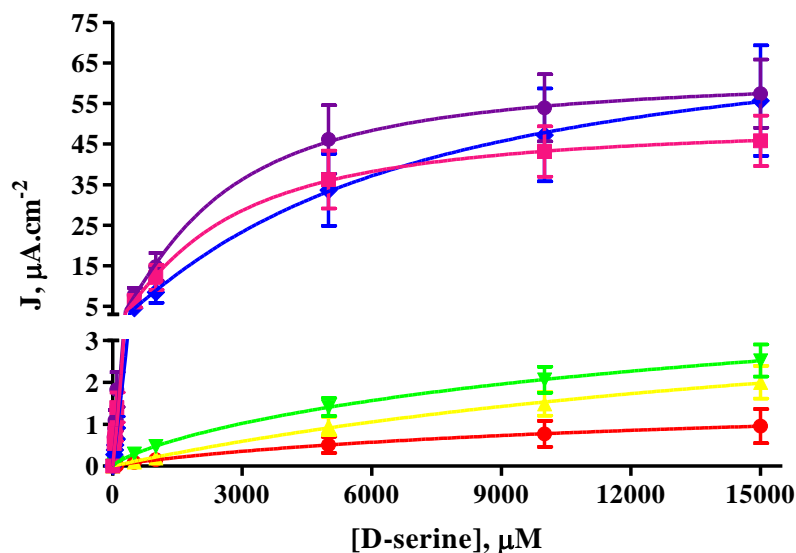


Figure 5-17

J-concentration plot of sensors created to explore the effect of different GA concentrations within a BSAGA solution and then utilised 5 times to bind nAAO to the surface of the electrode. Depicted are Pt<sub>D</sub>-Sty-[600UPBSx2-BSAGA0.1%]x5 (red trace), Pt<sub>D</sub>-Sty-[600UPBSx2-BSAGA0.2%]x5 (yellow trace), Pt<sub>D</sub>-Sty-[600UPBSx2-BSAGA0.5%]x5 (green trace), Pt<sub>D</sub>-Sty-[600UPBSx2-BSAGA1.0%]x5 (blue trace), Pt<sub>D</sub>-Sty-[600UPBSx2-BSAGA1.5%]x5 (purple trace) and Pt<sub>D</sub>-Sty-[600UPBSx2-BSAGA2.0%]x5 (pink trace). Data is taken from Table 10-11 and Table 5-12. The J axis is split into two, 0 - 3 μA.cm<sup>-2</sup> and 3 - 75 μA.cm<sup>-2</sup>.

The  $K_M$  concentrations also tell a similar story. The 0.1%, 0.2% and 0.5% value are all close to 20,000  $\mu\text{M}$ , whereas the 1.0%, 1.5% and 2.0% concentrations are an order of magnitude smaller and between 2,000 and 6,000  $\mu\text{M}$ . The  $K_M$  of 0.2% is not significantly different from the 0.1% or the 0.5% value,  $p = 0.4179$  and  $p = 0.9339$  respectively. Neither is the 0.5% value different from the 0.1% value,  $p = 0.2247$ . The smallest concentration of the three though, 0.1%, is significantly larger than the value for 1.0%,  $p = 0.0420^*$ . This is in turn significantly larger than the concentration calculated for 1.5%,  $p < 0.0001^{***}$ , which in turn is not significantly different from the  $K_M$  of BSAGA2.0%,  $p = 0.6211$ .

Looking at the calculated sensitivities the culmination of these results is quite stark. The 0.1% LRS is very small, as is the 0.2% value, although it is significantly larger,  $p = 0.0023^{**}$ . The LRS of BSAGA0.5% is not increased over 0.2%,  $p = 0.0617$ . All of these values are less than  $0.3 \mu\text{A}\cdot\text{cm}^{-2}\cdot\text{mM}^{-1}$ . The LRS then increases dramatically, by two orders of magnitude, to nearly 50 times that value for BSAGA1.0%. This is obviously significantly larger than the 0.5% value,  $p < 0.0001^{***}$ . The LRS more than doubles again for 1.5%,  $p < 0.0001^{***}$ , before decreasing slightly with the use of BSAGA2.0%,  $p = 0.0067^{**}$ . The LRS of 2.0% is still significantly larger than the 1.0% recipe,  $p < 0.0001^{***}$ .

### 5.4.3 Two Dips into BSAGA

The series of BSAGA recipes continued with the general recipe  $\text{Pt}_D\text{-Sty-[600UPBSx5-BSAGA0.2%]x2}$ . In this case the BSAGA solution was only applied on two layers. These were the fifth and tenth layers. As before the BSAGA0.1%, BSAGA0.2%, BSAGA0.5%, BSAGA1.0%, BSAGA1.5% and BSAGA2.0% solutions were all utilised. As was seen in the case of five applications, there seems to be a distinctive split in the level of response attained when two dips of BSAGA solution were utilised. This split appears in this instance between the BSAG 0.2% and the BSAG0.5% recipes. Both the 0.1% and 0.2% formulations appear to have very low sensitivity while the other four recipes have a far greater response to changes in the concentration of D-ser. This is best illustrated in the J-concentration plot which again has to have a split J axis. There is little point examining in detail the 0.1% and 0.2% recipes other than to say that the sensitivity increases with the use of 0.2%,  $p = 0.0170^*$ .

Electrode Design	Pt <sub>D</sub> -Sty-[600UPBSx5-BSAGA0.1%]x2, n = 3	Pt <sub>D</sub> -Sty-[600UPBSx5-BSAGA0.2%]x2, n = 3	Pt <sub>D</sub> -Sty-[600UPBSx5-BSAGA0.5%]x2, n = 3
Kinetics	M-M, p = 0.6156	M-M, p < 0.0001	M-M-H, p = 0.0115
R <sup>2</sup>	0.9787	0.9999	0.9990
J <sub>max</sub> , μA.cm <sup>-2</sup>	1.601 ± 0.183	8.712 ± 0.306	122.7 ± 12.0
K <sub>M</sub> , μM	4919 ± 1542	14163 ± 1109	8615 ± 2159
α		0.8634 ± 0.0140	0.8265 ± 0.0494
LRS, μA.cm <sup>-2</sup> .mM <sup>-1</sup>	0.3256 ± 0.0685	0.6151 ± 0.0267	14.24 ± 2.19
Electrode Design	Pt <sub>D</sub> -Sty-[600UPBSx5-BSAGA1.0%]x2, n = 4	Pt <sub>D</sub> -Sty-[600UPBSx5-BSAGA1.5%]x2, n = 4	Pt <sub>D</sub> -Sty-[600UPBSx5-BSAGA2.0%]x2, n = 4
Kinetics	M-M-H, p = 0.0095	M-M-H, p = 0.0005	M-M, p = 0.9749
R <sup>2</sup>	0.9988	0.9999	0.9999
J <sub>max</sub> , μA.cm <sup>-2</sup>	59.64 ± 0.95	66.57 ± 0.58	87.96 ± 0.57
K <sub>M</sub> , μM	818.0 ± 44.4	1494 ± 41	2630 ± 59
α	1.227 ± 0.073	1.135 ± 0.024	
LRS, μA.cm <sup>-2</sup> .mM <sup>-1</sup>	72.91 ± 3.19	44.55 ± 0.91	33.44 ± 0.58

Table 5-13

Kinetic parameters, fit, J<sub>max</sub> and K<sub>M</sub> values calculated from the calibration data in Table 10-12. J<sub>max</sub>, K<sub>M</sub>, α and LRS are presented as Mean ± SEM.

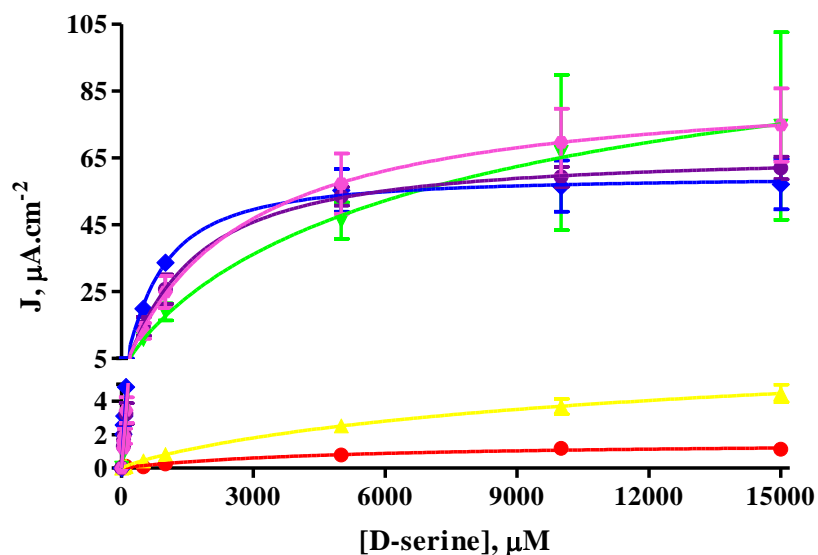


Figure 5-18

J-concentration plot of sensors created to explore the effect of different GA concentrations within a BSAGA solution and then utilised twice to bind DAAO to the surface of the electrode. Depicted are Pt<sub>D</sub>-Sty-[600UPBSx5-BSAGA0.1%]x2 (red trace), Pt<sub>D</sub>-Sty-[600UPBSx5-BSAGA0.2%]x2 (yellow trace), Pt<sub>D</sub>-Sty-[600UPBSx5-BSAGA0.5%]x2 (green trace), Pt<sub>D</sub>-Sty-[600UPBSx5-BSAGA1.0%]x2 (blue trace), Pt<sub>D</sub>-Sty-[600UPBSx5-BSAGA1.5%]x2 (purple trace) and Pt<sub>D</sub>-Sty-[600UPBSx5-BSAGA2.0%]x2 (pink trace). Data is taken from Table 10-12 and Table 5-13. Traces are plotted as Mean J ± SEM with fitted kinetic curve.

The  $J_{\max}$  of the BSAGA0.5% recipe is significantly larger than that of the 1.0% or 1.5%,  $p = 0.0344^*$  and  $p = 0.0427^*$ , but owing to the large error associated with the 0.5% value it is not significantly larger than the 2.0% value,  $p = 0.1012$ , despite the large difference in their mean value. The 2.0% recipe has the second largest  $J_{\max}$ , significantly higher than either 1.0% or 1.5%,  $p < 0.0001^{***}$  in both cases. The lowest  $J_{\max}$  is that of the 1.0% recipe, which is significantly lower than the  $J_{\max}$  of the BSAGA1.5% recipe,  $p = 0.0008^{***}$ .

Unfortunately, the largest  $K_M$  also occurs with the use of BSAGA0.5%. It does however have a large associated SEM and therefore is not significantly larger than the value for BSAGA2.0%, the second largest value when the mean value is considered,  $p = 0.1093$ . For the same reason it is also not larger than the 1.5% concentration or the 2.0% concentration,  $p = 0.0809$  and  $p = 0.0689$  respectively. The  $K_M$  produced by using BSAGA2.0% is significantly larger than the value obtained using either 1.5% or 1.0%,  $p < 0.0001^{***}$  in both cases. The smallest value of the four is that of BSAGA1.0%. It is significantly lower than that achieved using 1.5%,  $p < 0.0001^{***}$ .

Combining the  $J_{\max}$  and  $K_M$  information and looking at the LRS values provides further reinforcement of the trend that those recipes using GA1% yield the best results overall. This time 0.5% is the smallest, because of the large  $K_M$ . It is significantly smaller than the LRS of BSAGA2.0%,  $p = 0.0136^*$ , which is itself smaller than the value for 1.5%,  $p < 0.0001^{***}$ . The BSAGA1.0% LRS is larger than all of the 0.1%, 0.2%, 0.5%, 1.5% and 2.0% values,  $p = 0.0002^{***}$ ,  $p = 0.0002^{***}$ ,  $p < 0.0001^{***}$ ,  $p = 0.0034^{**}$  and  $p = 0.0012^{**}$  respectively.

#### 5.4.4 Conclusions of the GA and BSAGA study

Unlike in the GA study there were no recipes with only one dip of BSAGA considered. This decision was taken for a few reasons. The first being that for GA only there had been a marked reduction in sensitivity when only 1 dip of GA was used when compared to ten, five and two dipo. This was particularly prevalent among the biosensors with the lower percentage of GA, with only the higher percentages showing reasonable sensitivity. Secondly the additional quantity of BSA that the GA would have to bind in the BSAGA recipes would likely further reduce the sensitivity of the biosensors. Lastly, with five and two dipo of BSAGA there had already been shown how several recipes

had suffered greatly with the reduced quantity of GA being utilised. Following, in Figure 5-19, is a summary of the kinetic details gathered during the BSAGA study.

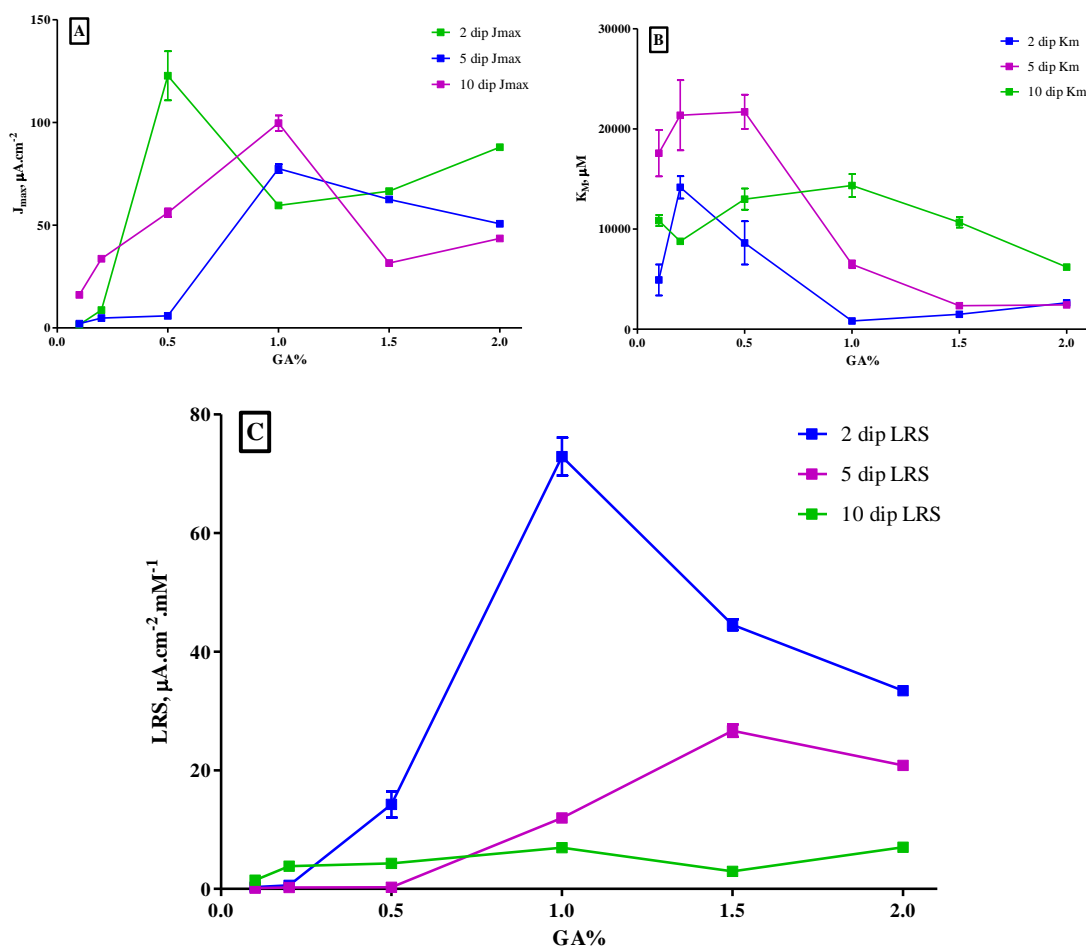


Figure 5-19

Plots of the trends occurring within the three kinetic properties of the BSA/GA dip study. *A* displays the  $K_M$  changes, *B* the  $J_{max}$  changes, and the main graph, *C*, their combined effect on the LRS. All graphs are plotted as a function of GA% with the 2 dip series in blue, the 5 dip series in purple and the 10 dip series in green.

There are marked differences, and some similarities, in the trends displayed when compared to the results for the GA study. Firstly the three sets of  $J_{max}$  results all appear to increase towards a maximum before decreasing to mid range values, with an increase registering again after the initial post-maximum drop. The maximum occurs again at 1% GA, with the exception of the 2 dip designs. The addition of the BSA has removed the linear aspect of the 5 dip protocol results, and tempered the maximum  $J$  achieved in the dip recipes. The highest  $J_{max}$  attained is now for the 2 dip BSAGA0.5% recipe, followed by the ten dip BSAGA1.0% recipe. Previously without the BSA the 2 dip recipe GA1.0% recipe had a  $J_{max}$  double that of any of the other highest values.

The addition of the BSA has also had an effect on the  $K_M$  values. For the lower GA concentrations the SEM as a percentage of the mean has been reduced. The trend of decreasing  $K_M$  concentrations as the GA concentration is increased is present again. However the is slower to take effect, with the major decreases occurring between BSAGA0.5% and BSAGA1.5%, as opposed to between GA0.1% and GA0.5% for the GA only protocol.

The overall result on the LRS is very different when the BSA is included in the recipes. The 10 dip protocol changes from a linearly increasing value, peaking at  $40 \mu\text{A}\cdot\text{cm}^{-2}\cdot\text{mM}^{-1}$ , to an unchanging value, between 5 and  $8 \mu\text{A}\cdot\text{cm}^{-2}\cdot\text{mM}^{-1}$ , over the range of GA concentrations utilised. When 5 dips of BSAGA are utilised, the maximum sensitivity is found to shift from GA1.0% to BSAGA1.5%. The peak value is also lower when BSA is incorporated. The sensitivities of the 2 dip BSAGA protocols follow the same trend as the GA only designs, both peaking at 1.0% GA, but here the inclusion of the BSA has doubled the peak LRS value. Thus it was deemed appropriate to take stock of results that had been attained and to select a few promising designs which might be taken forward for consideration and further modification. In selecting these designs overall trends and individual results were taken into account to select biosensors showing similarities and consistently good sensitivity. Overall it was judged that recipes involving GA1.0% and BSAGA1.0% were the most consistently sensitive designs and thus most suited to further examination. It was deemed that recipes where two and five dips of the GA or BSAGA was applied were more successful overall than the ten or one dip designs.

The recipes carried forth for further exploration were thus,  $\text{Pt}_D\text{-Sty-[600UPBSx5-BSAGA1.0%]x2}$ ,  $\text{Pt}_D\text{-Sty-[600UPBSx2-BSAGA1.0%]x5}$ ,  $\text{Pt}_D\text{-Sty-[600UPBSx5-GA1.0%]x2}$  and  $\text{Pt}_D\text{-Sty-[600UPBSx2-GA1.0%]x5}$ . The kinetic data for these recipes and a combined plot of them are shown below for clarity in Table 5-14 and Figure 5-20.

From looking at the J-concentration plot it is easy to see that even within this small segment of similar recipes there are large variances. This would hopefully be useful in evaluating future alterations and give a greater scope for improvements to be discovered, if not for all then at least for one or two recipes.

Electrode Design	Pt <sub>D</sub> -Sty-[600UPBSx5-BSAGA1.0%]x2, n = 4	Pt <sub>D</sub> -Sty-[600UPBSx2-BSAGA1.0%]x5, n = 4	Pt <sub>D</sub> -Sty-[600UPBSx5-GA1.0%]x2, n = 3	Pt <sub>D</sub> -Sty-[600UPBSx2-GA1.0%]x5, n = 3
<b>Kinetics</b>	M-M-H, p = 0.0095	M-M-H, p = 0.0097	M-M-H, p = 0.0081	M-M-H, p = 0.0021
<b>R<sup>2</sup></b>	0.9988	0.9998	0.9998	0.9990
<b>J<sub>max</sub>, μA.cm<sup>-2</sup></b>	59.64 ± 0.95	77.55 ± 2.14	178.8 ± 4.5	83.64 ± 2.128
<b>K<sub>M</sub>, μM</b>	818.0 ± 44.4	6477 ± 384	5049 ± 291	2060 ± 154
<b>α</b>	1.227 ± 0.073	1.095 ± 0.028	1.109 ± 0.030	1.332 ± 0.078
<b>LRS, μA.cm<sup>-2</sup>.mM<sup>-1</sup></b>	72.91 ± 3.19	11.97 ± 0.39	35.41 ± 1.19	40.60 ± 2.158

Table 5-14

Summary of the kinetic data associated with the four recipes selected for further study.

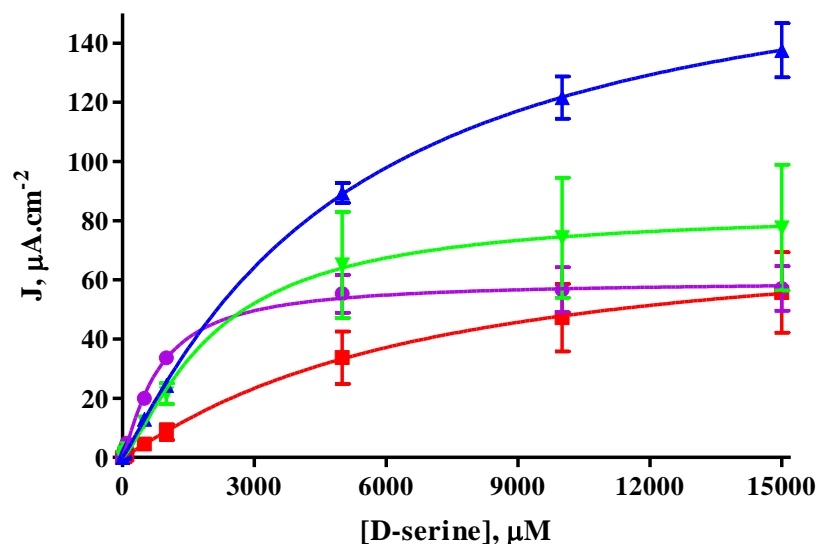


Figure 5-20

J-concentration plot of the four recipes selected for further investigation. Represented are Pt<sub>D</sub>-Sty-[600UPBSx5-BSAGA1.0%]x2 (purple trace), Pt<sub>D</sub>-Sty-[600UPBSx2-BSAGA1.0%]x5 (red trace), Pt<sub>D</sub>-Sty-[600UPBSx5-GA1.0%]x2 (blue trace) and Pt<sub>D</sub>-Sty-[600UPBSx2-GA1.0%]x5 (green trace).

A quick comparison of these recipes reveals that Pt<sub>D</sub>-Sty-[600UPBSx2-BSAGA1.0%]x5 has the lowest sensitivity. Significantly larger is the 2 dip GA1% recipe,  $p < 0.0001^{***}$ . This is not different from the 5 dip GA1% value,  $p = 0.1024$ . The 2 dip BSAGA recipe is significantly larger than either the 2 dip GA1% or 5 dip GA1% recipes,  $p = 0.0002^{***}$  and  $p = 0.0006^{***}$  respectively. Worthy of note also is that all of these recipes conform to Michaelis-Menten Hill-Type kinetics.

## 5.5 An Extensive Study of PEI Included With Styrene

The short examination conducted with PEI, in Section 4.8.1., was not very structured or comprehensive. Thus given its use and success in other biosensor designs it was decided to study the possibility of using it in a more structured way. The method of inclusion was selected as immediately after the dip into styrene, and before the first dip of enzyme solution. This was in the hope that the combination of PEI and Sty could provide a favourable and stable matrix for the retention of the enzyme. Such favourable interactions have been observed before with polyelectrolyte substances in general (Gibson *et al.*, 1996) but also for carbon paste based biosensors for detecting D- and L-amino acids (Johansson *et al.*, 1993; Kacaniklic *et al.*, 1994) and the immobilisation of biocatalyst via adsorption to solids supports (Kamath *et al.*, 1988; Senthuran *et al.*, 1997). It is known that inclusion of PEI can alter the pH in the microenvironment of the enzyme as compared to the bulk solution (Goldstein, 1976) thus while it can be of benefit, increasing stability during storage, against temperature changes and some irreversible inactivating mechanisms (Andersson & Hatti-Kaul, 1999) it also has the potential to change the position of the enzyme in relation to its iso-electric point and thus the activated charged groups in its structure. This could be a negative or positive change, and this study is required to elucidate which effect is most likely.

### 5.5.1 PEI 1% Included After Styrene

The four recipes selected at the end of the last section, as having the best prospect for high sensitivity, were altered to allow for the inclusion of the PEI. The first alteration performed was the inclusion of PEI1.0%. The four recipes thus became; Pt<sub>D</sub>-Sty-PEI1.0%-[600UPBSx5-BSAGA1.0%]x2, Pt<sub>D</sub>-Sty-PEI1.0%-[600UPBSx2-BSAGA1.0%]x5, Pt<sub>D</sub>-Sty-PEI1.0%-[600UPBSx5-GA1.0%]x2 and Pt<sub>D</sub>-Sty-PEI1.0%-[600UPBSx2-GA1.0%]x5. The calibration data for these recipes is presented in Table 10-13.

Electrode Design	Pt <sub>D</sub> -Sty-PEI1.0%-[600UPBSx5-BSAGA1.0%]x2, n=4	Pt <sub>D</sub> -Sty-PEI1.0%-[600UPBSx2-BSAGA1.0%]x5, n=4	Pt <sub>D</sub> -Sty-PEI1.0%-[600UPBSx5-GA1.0%]x2, n=4	Pt <sub>D</sub> -Sty-PEI1.0%-[600UPBSx2-GA1.0%]x5, n=4
<b>Kinetics</b>	M-M-H, p = 0.0299	M-M-H, p < 0.0001	M-M, p = 0.1212	M-M, p = 0.6255
<b>R<sup>2</sup></b>	0.9998	1.000	0.9969	0.9995
<b>J<sub>max</sub>, μA.cm<sup>-2</sup></b>	56.02 ± 1.55	25.63 ± 0.21	83.52 ± 4.19	52.80 ± 1.41
<b>K<sub>M</sub>, μM</b>	6574 ± 397	9065 ± 166	5976 ± 757	8706 ± 500
<b>α</b>	1.070 ± 0.026	0.9575 ± 0.0052		
<b>LRS, μA.cm<sup>-2</sup>.mM<sup>-1</sup></b>	8.522 ± 0.283	2.827 ± 0.029	13.98 ± 1.12	6.064 ± 0.194

Table 5-15

Kinetic parameters, fit, J<sub>max</sub> and K<sub>M</sub> values calculated from the calibration data in Table 10-13. J<sub>max</sub>, K<sub>M</sub>, α and LRS are presented as Mean ± SEM.

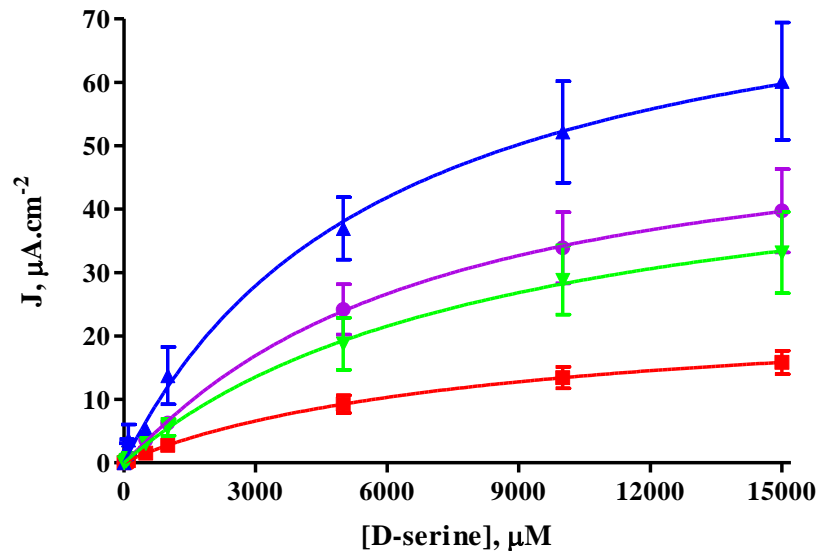


Figure 5-21

J-concentration plot of the four recipes selected for further investigation when modified with PEI1.0%. Represented are Pt<sub>D</sub>-Sty-PEI1.0%-[600UPBSx5-BSAGA1.0%]x2 (purple trace), Pt<sub>D</sub>-Sty-PEI1.0%-[600UPBSx2-BSAGA1.0%]x5 (red trace), Pt<sub>D</sub>-Sty-PEI1.0%-[600UPBSx5-GA1.0%]x2 (blue trace) and Pt<sub>D</sub>-Sty-PEI1.0%-[600UPBSx2-GA1.0%]x5 (green trace).

The kinetic fit data calculated in Table 5-15 clearly shows an overall decrease in the sensitivity of all recipes when compared to the original recipes without PEI1.0%. Comparing only with their non-PEI analogues the J<sub>max</sub> value of the 2 dip BSAGA1.0% is unchanged, p = 0.0934, the 5 dip BSAGA1.0% value is reduced, p = 0.0002\*\*\*, the 2 dip GA1.0% recipe is decreased, p < 0.0001\*\*\*, and the 5 dip GA1.0% is also reduced, p < 0.0001\*\*\*. Examining the K<sub>M</sub> values in the same manner a similar deterioration of the concentrations calculated is also observed. The 2 dip BSAGA1.0% recipe with PEI1.0% is significantly increased, p = 0.0007\*\*\*, over the value for the recipe without

the PEI. The 5 dip BSAGA1.0% design is also significantly increased,  $p = 0.0035^{**}$ , as is the 5 dip GA1.0%,  $p = 0.0001^{***}$ . The 2 dip GA1.0%  $K_M$  value is unchanged,  $p = 0.3639$ .

The overall sensitivities returned by the recipes altered with PEI1.0% are all negatively affected. The LRS of the 2 dip BSAGA1.0% design is significantly lower,  $p = 0.0003^{***}$ , so is the 5 dip BSAGA1.0%,  $p = 0.0002^{***}$ . The 2 dip GA1% and 5 dip GA1% recipes are also significantly reduced,  $p < 0.0001^{***}$ ,  $p = 0.0039^{**}$ .

In Figure 5-21 the colours and symbols used are maintained from Figure 5-20 in Section 5.4.4 for the same general recipes. Thus 2 dip BSAGA is the purple trace, 5 dip BSAGA is the red trace, 2 dip GA is the blue trace and 5 dip GA is the green trace.

An observation may also be made that the two GA1.0% recipes are no longer conforming to M-M-H kinetics. In Figure 5-21 it can be seen too that the shape of the kinetic curves are now very similar, with no dramatic change noticeable from the initial linear region into the region where the rate is limited by diffusion and the substrate has saturated the enzyme.

Overall the addition of a PEI1.0% dip after the Sty, and before the enzyme and BSAGA or GA layers were applied, was not of benefit, when compared to the recipe without PEI, to the current density,  $K_M$  concentration or the sensitivity values.

### 5.5.2 PEI 0.1% Included After Styrene

The same four recipes were next altered with PEI0.1% after the Sty dip. The four recipes thus became;  $Pt_D\text{-Sty-PEI0.1\%-[600UPBSx5-BSAGA1.0\%]x2}$ ,  $Pt_D\text{-Sty-PEI0.1\%-[600UPBSx2-BSAGA1.0\%]x5}$ ,  $Pt_D\text{-Sty-PEI0.1\%-[600UPBSx5-GA1.0\%]x2}$  and  $Pt_D\text{-Sty-PEI0.1\%-[600UPBSx2-GA1.0\%]x5}$ . The calibration data for these recipes is presented below in Table 10-14. It was hoped that a lower percentage might produce better results than the PEI1.0% designs. However, examination of the calibration data and the resultant kinetic fits, calculated and displayed in Table 5-16, shows that the results for PEI0.1% are similar to those for PEI1.0%.

Electrode Design	Pt <sub>D</sub> -Sty-PEI0.1%-[600UPBSx5-BSAGA1.0%]x2, n=4	Pt <sub>D</sub> -Sty-PEI0.1%-[600UPBSx2-BSAGA1.0%]x5, n=3	Pt <sub>D</sub> -Sty-PEI0.1%-[600UPBSx5-GA1.0%]x2, n=4	Pt <sub>D</sub> -Sty-PEI0.1%-[600UPBSx2-GA1.0%]x5, n=4
<b>Kinetics</b>	M-M, p = 0.0609	M-M, p = 0.2162	M-M, p = 0.4588	M-M-H, p = 0.0228
<b>R<sup>2</sup></b>	0.9992	0.9957	0.9998	0.9999
<b>J<sub>max</sub>, μA.cm<sup>-2</sup></b>	73.90 ± 2.41	60.57 ± 1.96	45.51 ± 0.59	37.12 ± 0.87
<b>K<sub>M</sub>, μM</b>	8104 ± 585	2287 ± 270	6260 ± 201	5795 ± 309
<b>α</b>				1.068 ± 0.024
<b>LRS, μA.cm<sup>-2</sup>.mM<sup>-1</sup></b>	9.119 ± 0.377	26.49 ± 2.45	7.270 ± 0.146	6.406 ± 0.194

Table 5-16

Kinetic parameters, fit, J<sub>max</sub> and K<sub>M</sub> values calculated from the calibration data in Table 10-14. J<sub>max</sub>, K<sub>M</sub>, α and LRS are presented as Mean ± SEM.

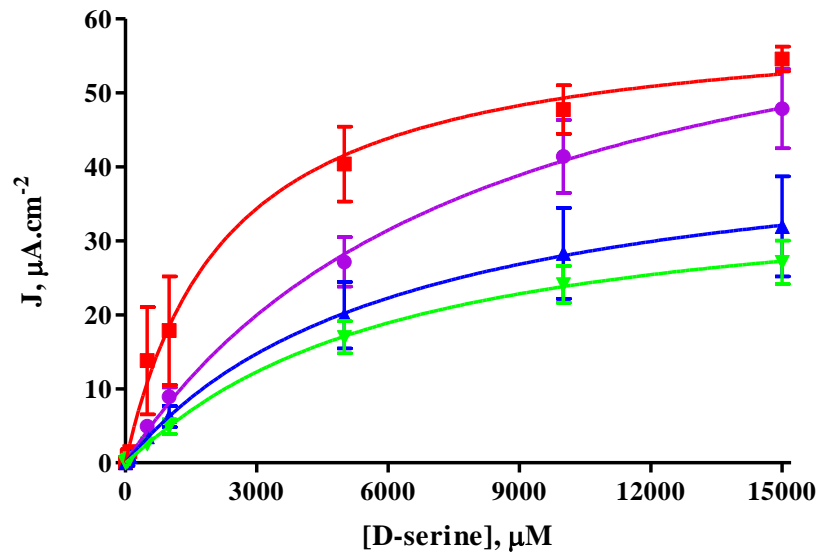


Figure 5-22

J-concentration plot of the four recipes selected for further investigation when modified with PEI0.1%. Represented are Pt<sub>D</sub>-Sty-PEI0.1%-[600UPBSx5-BSAGA1.0%]x2 (purple trace), Pt<sub>D</sub>-Sty-PEI0.1%-[600UPBSx2-BSAGA1.0%]x5 (red trace), Pt<sub>D</sub>-Sty-PEI0.1%-[600UPBSx5-GA1.0%]x2 (blue trace) and Pt<sub>D</sub>-Sty-PEI0.1%-[600UPBSx2-GA1.0%]x5 (green trace).

Comparing each result to its original form, as per Section 5.4.4, it can be seen that the J<sub>max</sub> values are often significantly poorer. The 2 dip BSAGA value is significantly higher, p = 0.0113\*. But, the 5 dip BSAGA J<sub>max</sub> is significantly lower, p = 0.0025\*\*, the 2 dip GA value is significantly lower, p = 0.0012\*\*, and the 5 dip GA value is also lower, p < 0.0001\*\*\*.

Concentrations indicative of the K<sub>M</sub> have also changed dramatically, and not in a preferable direction. The concentration at which the K<sub>M</sub> is found for the 2 dip BSAGA

design is significantly higher,  $p = 0.0011^{**}$ , as is the 5 dip BSAGA value,  $p = 0.0004^{***}$ , the 2 dip value,  $p = 0.0161^*$ , and the 5 dip GA value,  $p = 0.0002^{***}$ .

Combining  $J_{\max}$  values which are generally smaller and  $K_M$  values which are larger than the original values is sure to lead to reduced sensitivities across all recipes, and this is the case. The 2 dip BSAGA and 5 dip BSAGA LRS values are significantly reduced,  $p = 0.0003^{***}$  and  $p = 0.0279^*$  respectively. This is also the case for 2 and 5 dips of GA1.0%, which have significantly lower sensitivities,  $p = 0.0018^{**}$  and  $p = 0.0040^{**}$  respectively. Thus the use of a lower percentage concentration of PEI did not yield better results than the original designs either.

### 5.5.3 PEI 5% Included After Styrene

In a final effort to determine whether PEI could be of benefit the sensitivity of a DAAO based D-ser biosensor one last approach was considered. This was an approach which had been utilised before within the research group. It proved effective when other methods of including PEI did not. The premise of this method was to use a stronger solution of PEI for an initial interaction with the enzyme. Along with this a lower concentration of PEI was applied in the middle of the dipping process to help secure and interact with the outer layers of enzyme. Two variations of this approach were examined.

#### 5.5.3.1 PEI 5% Used In Conjunction with PEI 1.0%

The first approach was to use an initial PEI5.0% dip between the Sty and the 600UPBS on the first layer. The second dip of PEI was a dip into PEI1.0% on the fifth layer after the other dips of that layer had been applied. Thus the second dip of PEI had five layers of 600UPBS underneath and above it. The same four recipes from Section 5.4.4 were used as the basis for the new designs. They when modified became;  $Pt_D\text{-Sty-PEI5.0%-[600UPBSx5-BSAGA1.0%]x2-PEI1.0\%(5)}$ ,  $Pt_D\text{-Sty-PEI5.0%-[600UPBSx2-BSAGA1.0%]x5-PEI1.0\%(5)}$ ,  $Pt_D\text{-Sty-PEI5.0%-[600UPBSx5-GA1.0%]x2-PEI1.0\%(5)}$  and  $Pt_D\text{-Sty-PEI5.0%-[600UPBSx2-GA1.0%]x5-PEI1.0\%(5)}$ .

The calibration data for these recipes is listed in Table 10-15, the kinetic fit data in Table 5-17 and the results are depicted in Figure 5-23. Here again the colours and

symbols used in the figure are consistent with those previously used for the same general formulation.

Electrode Design	Pt <sub>D</sub> -Sty-PEI5.0%-[600UPBSx5-BSAGA1.0%]x2-PEI1.0%(5), n=4	Pt <sub>D</sub> -Sty-PEI5.0%-[600UPBSx2-BSAGA1.0%]x5-PEI1.0%(5), n=4	Pt <sub>D</sub> -Sty-PEI5.0%-[600UPBSx5-GA1.0%]x2-PEI1.0%(5), n=3	Pt <sub>D</sub> -Sty-PEI5.0%-[600UPBSx2-GA1.0%]x5-PEI1.0%(5), n=4
<b>Kinetics</b>	M-M, p = 0.6133	M-M, p = 0.2150	M-M-H, p = 0.0031	M-M-H, p = 0.3457
<b>R<sup>2</sup></b>	0.9675	1.000	0.9998	0.9984
<b>J<sub>max</sub>, μA.cm<sup>-2</sup></b>	22.51 ± 3.95	46.21 ± 0.21	73.99 ± 5.99	78.02 ± 2.33
<b>K<sub>M</sub>, μM</b>	6359 ± 2742	5513 ± 67	21348 ± 3478	7180 ± 451
<b>α</b>			0.8840 ± 0.0252	
<b>LRS, μA.cm<sup>-2</sup>.mM<sup>-1</sup></b>	3.540 ± 0.951	8.382 ± 0.066	3.466 ± 0.285	10.87 ± 0.38

Table 5-17

Kinetic parameters, fit, J<sub>max</sub> and K<sub>M</sub> values calculated from the calibration data in Table 10-15. J<sub>max</sub>, K<sub>M</sub>, α and LRS are presented as Mean ± SEM.

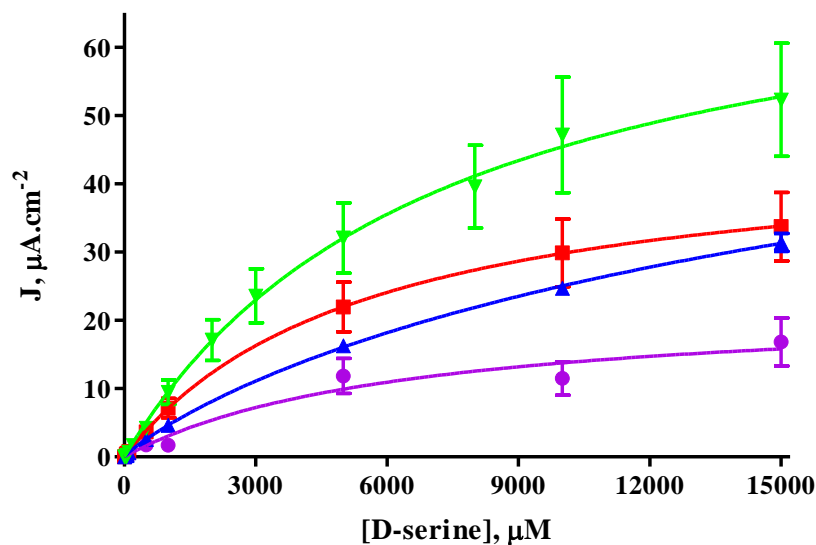


Figure 5-23

J-concentration plot of the four recipes selected for further investigation when modified with PEI5.0% and PEI1.0%. Represented are Pt<sub>D</sub>-Sty-PEI5.0%-[600UPBSx5-BSAGA1.0%]x2-PEI1.0%(5) (purple trace), Pt<sub>D</sub>-Sty-PEI5.0%-[600UPBSx2-BSAGA1.0%]x5-PEI1.0%(5) (red trace), Pt<sub>D</sub>-Sty-PEI5.0%-[600UPBSx5-GA1.0%]x2-PEI1.0%(5) (blue trace) and Pt<sub>D</sub>-Sty-PEI5.0%-[600UPBSx2-GA1.0%]x5-PEI1.0%(5) (green trace).

Unfortunately, as with the other recipes where PEI was utilised, it is quite clear that there has once again been a deterioration of the kinetic parameters of the various electrode types produced. The modification with PEI5.0% and PEI1.0% appear to have

been detrimental to all kinetic parameters, including the loss of M-M-H kinetic fit in all but one case.

Statistically, the  $J_{\max}$  value of the 2 dip BSAGA design has decreased,  $p = 0.0028^{**}$ . The 5 dip BSA and 2 dip GA recipes have also seen a decrease in their  $J_{\max}$  values,  $p = 0.0007^{***}$  and  $p = 0.0002^{***}$  respectively. There is no significant change in the  $J_{\max}$  of the 5 dip GA design,  $p = 0.1475$ . The  $K_M$  values describe a similar picture of decline. The 2 dip and 5 dip BSAGA biosensors show no significant change in the  $K_M$  concentration,  $p = 0.1366$  and  $p = 0.0902$  respectively. The 2 dip and 5 dip GA recipes on the other hand show significantly higher  $K_M$  values,  $p = 0.0429^*$  and  $p = 0.0002^{***}$  respectively.

Sensitivity, calculated from the combined  $J_{\max}$  and  $K_M$  figures, provides a clear summary of these statistics. All of the recipes show a significantly reduced LRS,  $p = 0.0002^{***}$ ,  $p = 0.0028^{**}$ ,  $p < 0.0001^{***}$  and  $p = 0.0054^{**}$  for 2 dip BSAGA, 5 dip BSAGA, 2 dip GA and 5 dip GA respectively. Thus again it is clear to see that the use of PEI has not improved the sensitivity of the biosensors. This is most likely due to an inhibitory interaction between the positive charges on the PEI and the groups that exist on the outside of the enzyme molecule. It could also be due, in part, to an increased diffusional barrier for the D-serine and  $H_2O_2$  to pass through.

### 5.5.3.2 PEI 5% Used In Conjunction with PEI 0.1%

In a final attempt to incorporate PEI within the biosensor designs the strong initial binding dip and weaker consolidation dip was attempted again. This time it was attempted with PEI5.0% and PEI0.1%. Thus the four recipes became; Pt<sub>D</sub>-Sty-PEI5.0%-[600UPBSx5-BSAGA1.0%]x2-PEI0.1%(5), Pt<sub>D</sub>-Sty-PEI5.0%-[600UPBSx2-BSAGA1.0%]x5-PEI0.1%(5), Pt<sub>D</sub>-Sty-PEI5.0%-[600UPBSx5-GA1.0%]x2-PEI0.1%(5) and Pt<sub>D</sub>-Sty-PEI5.0%-[600UPBSx2-GA1.0%]x5-PEI0.1%(5).

The calibration data for these recipes is presented in Table 10-16 and the kinetic fit information in Table 5-18. Plotted in Figure 5-24 is the information from both tables. As in the last three sections the colours and symbols used within the graph are consistent with those used for the unmodified recipes chosen in Section 5.4.4. It is clear that again the use of PEI has resulted in a deterioration of all of the relevant kinetic

parameters. This is borne out by the statistics. Comparison of the results is in relation to the recipes in Section 5.4.4, before alteration with PEI.

Electrode Design	Pt <sub>D</sub> -Sty-PEI5.0%-[600UPBSx5-BSAGA1.0%]x2-PEI0.1%(5), n=4	Pt <sub>D</sub> -Sty-PEI5.0%-[600UPBSx2-BSAGA1.0%]x5-PEI0.1%(5), n=4	Pt <sub>D</sub> -Sty-PEI5.0%-[600UPBSx5-GA1.0%]x2-PEI0.1%(5), n=3	Pt <sub>D</sub> -Sty-PEI5.0%-[600UPBSx2-GA1.0%]x5-PEI0.1%(5), n=4
<b>Kinetics</b>	M-M-H, p = 0.0012	M-M, p = 0.8846	M-M, p = 0.3743	M-M, p = 0.6904
<b>R<sup>2</sup></b>	1.000	0.9999	0.9986	0.9990
<b>J<sub>max</sub>, μA.cm<sup>-2</sup></b>	72.83 ± 1.89	50.66 ± 0.35	10.32 ± 0.63	77.11 ± 1.96
<b>K<sub>M</sub>, μM</b>	13257 ± 721	5842 ± 102	13089 ± 1461	7871 ± 407
<b>α</b>	0.9350 ± 0.0121			
<b>LRS, μA.cm<sup>-2</sup>.mM<sup>-1</sup></b>	5.494 ± 0.157	8.672 ± 0.096	0.7887 ± 0.0413	9.798 ± 0.275

Table 5-18

Kinetic parameters, fit, J<sub>max</sub> and K<sub>M</sub> values calculated from the calibration data in Table 10-16. J<sub>max</sub>, K<sub>M</sub>, α and LRS are presented as Mean ± SEM.

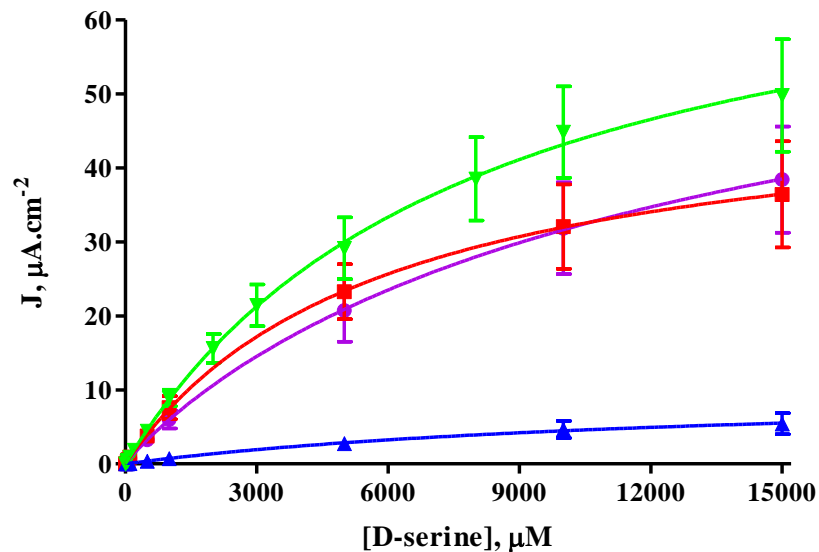


Figure 5-24

J-concentration plot of the four recipes selected for further investigation when modified with PEI5.0% and PEI0.1%. Represented are Pt<sub>D</sub>-Sty-PEI5.0%-[600UPBSx5-BSAGA1.0%]x2-PEI0.1%(5) (purple trace), Pt<sub>D</sub>-Sty-PEI5.0%-[600UPBSx2-BSAGA1.0%]x5-PEI0.1%(5) (red trace), Pt<sub>D</sub>-Sty-PEI5.0%-[600UPBSx5-GA1.0%]x2-PEI0.1%(5) (blue trace) and Pt<sub>D</sub>-Sty-PEI5.0%-[600UPBSx2-GA1.0%]x5-PEI0.1%(5) (green trace).

Statistically the J<sub>max</sub> of the 2 dip BSAGA is reduced, p = 0.0008\*\*\*, as it for the 5 dip BSAGA and 2 dip GA recipes, p = 0.0011\*\* and p = 0.0007\*\*\* respectively. The 5 dip GA design has a J<sub>max</sub> which is unchanged with the inclusion of PEI5.0% and PEI1.0%, p = 0.0761.

The  $K_M$  values have also deteriorated, with large increases to be seen in some cases. The 2 dip BSAGA has a significantly larger  $K_M$ ,  $p = 0.0004^{***}$ , but the 5 dip BSAGA recipe has a non-significantly different value,  $p = 2089$ . The 2 dip GA and 5 dip GA recipes also have increased  $K_M$  concentrations,  $p = 0.0327^*$  and  $p < 0.0001^{***}$  respectively.

Summarising these changes it can be seen that all the LRS values are lower than in the unmodified recipes. The sensitivity is lower for 2 dip BSAGA, 5 dip BSAGA, 2 dip GA and 5 dip GA,  $p = 0.0002^{***}$ ,  $p = 0.0037^{**}$ ,  $p = 0.0012^{**}$  and  $p = 0.0050^{**}$ . Having examined a range of options that endeavoured to include PEI in a productive manner it was decided to discontinue these efforts. After several attempts of changing the method of combination, the recipe within which it was combined and the concentration of the PEI utilised, it became clear that it was not likely to be a useful addition to a D-ser biosensor.

## 5.6 The Incorporation of FAD into Selected Designs

With the elimination of PEI as a potential method for increasing the sensitivity of the biosensors it was decided to pursue other interesting substances. One of particular interest was FAD. This vital cofactor was already present within the enzyme and was essential for substrate turnover. Thus inclusion of extra quantities of it held a substantial possibility for improving sensitivity. The inclusion of FAD in Section 4.8.2 had already shown promising signs that it would indeed produce a beneficial effect. Examined is the effect of placing the FAD before and after the application of the enzyme dip within that particular layer. This could alter the layer of enzyme that the particular dip of FAD interacts with. Placed before the enzyme dip the FAD might interact more with the bound enzyme of previous layers and minimally with the dip of enzyme that followed. Placed after the enzyme dip it is likely that the FAD interacts predominantly with the enzyme applied just previous and which had not yet been bound/ or dried onto previous layers.

### 5.6.1 FAD Included Before DAAO

The first approach considered was to include FAD at a concentration of 0.02 mM (FAD0.02). A dip of this was included on the same layers as either BSAGA1.0% or GA1.0% in their respective recipes. The dip into FAD occurred before the dip into

600UPBS, which itself was before the BSAGA1.0% or GA1.0%. The same four recipes used throughout the PEI study were used for the FAD study. When the FAD0.02 was included the recipes took the form of;  $Pt_D\text{-Sty-[600UPBSx5-FAD0.02(befE)-BSAGA1.0\%]x2}$ ,  $Pt_D\text{-Sty-[600UPBSx2-FAD0.02(befE)-BSAGA1.0\%]x5}$ ,  $Pt_D\text{-Sty-[600UPBSx5-FAD0.02(befE)-GA1.0\%]x2}$  and  $Pt_D\text{-Sty-[600UPBSx2-FAD0.02(befE)-GA1.0\%]x5}$ , where (befE) indicates the FAD dip occurred before the enzyme dip in that particular layer. The calibration data collected from these recipes is presented in Table 10-17. Some improvements in the kinetic parameters are found, when FAD0.02 is included in this manner, and other values are unchanged. But, in general, there is an undesirable change in the kinetic fits presented in Table 5-19.

The  $J_{max}$  of 2 dip BSAGA is significantly improved,  $p < 0.0001^{***}$ , but the  $J_{max}$  of 2 dip GA and 5 dip GA show a significant decrease, both  $p < 0.0001^{***}$ . The 5 dip BSAGA shows no change,  $p = 0.6898$ . The  $K_M$  concentration of the 2 dip BSAGA recipe is significantly increased,  $p = 0.0002^{***}$ , as is the 5 dip BSAGA value,  $p = 0.0305^*$ . The 2 dip GA  $K_M$  is unchanged,  $p = 0.0985$ , and the 5 dip GA concentration is significantly higher,  $p = 0.0007^{***}$ .

The sensitivities displayed by these new designs are not encouraging. The 2 dip BSAGA1.0% design and the 5 dip BSAGA1.0% design both show significant decreases in their LRS,  $p = 0.0003^{***}$  and  $p = 0.0112^*$  respectively. The 2 dip and 5 dip GA1.0% also, unfortunately, show significant decreases in their sensitivities relative to the recipes before FAD0.02 modification,  $p < 0.0001^{***}$  and  $p = 0.0042^{**}$  respectively. Thus overall it cannot be said that the inclusion of FAD 0.02mM benefitted the biosensor design.

Electrode Design	Pt <sub>D</sub> -Sty-[600UPBSx5-FAD0.02(befE)-BSAGA1.0%]x2, n=4	Pt <sub>D</sub> -Sty-[600UPBSx2-FAD0.02(befE)-BSAGA1.0%]x5, n=4	Pt <sub>D</sub> -Sty-[600UPBSx5-FAD0.02(befE)-GA1.0%]x2, n=3	Pt <sub>D</sub> -Sty-[600UPBSx2-FAD0.02(befE)-GA1.0%]x5, n=4
<b>Kinetics</b>	M-M-H, p = 0.0176	M-M-H, p = 0.0034	M-M, p = 0.3009	M-M, p = 0.4113
<b>R<sup>2</sup></b>	1.000	0.9998	0.9990	0.9999
<b>J<sub>max</sub>, μA.cm<sup>-2</sup></b>	113.5 ± 1.9	79.08 ± 2.96	51.29 ± 1.46	56.39 ± 0.65
<b>K<sub>M</sub>, μM</b>	8761 ± 331	8193 ± 737	5739 ± 418	7826 ± 201
<b>α</b>	0.9652 ± 0.0110	0.8998 ± 0.0224		
<b>LRS, μA.cm<sup>-2</sup>.mM<sup>-1</sup></b>	12.96 ± 0.27	9.652 ± 0.511	8.937 ± 0.419	7.205 ± 0.108

Table 5-19

Kinetic parameters, fit, J<sub>max</sub> and K<sub>M</sub> values calculated from the calibration data in Table 10-17. J<sub>max</sub>, K<sub>M</sub>, α and LRS are presented as Mean ± SEM.

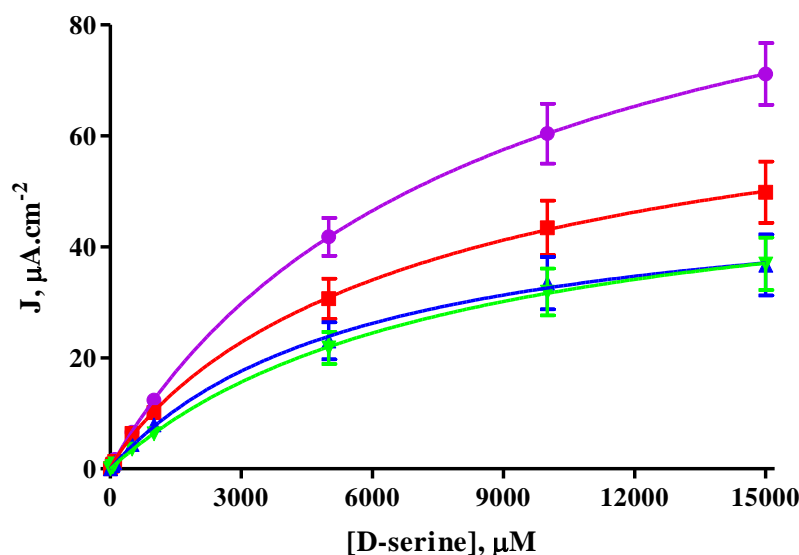


Figure 5-25

J-concentration plot of the four recipes selected for further investigation when modified with FAD0.02. Represented are PtD-Sty-[600UPBSx5-FAD0.02(befE)-BSAGA1.0%]x2 (purple trace), PtD-Sty-[600UPBSx2-FAD0.02(befE)-BSAGA1.0%]x5 (red trace), PtD-Sty-[600UPBSx5-FAD0.02(befE)-GA1.0%]x2 (blue trace) and PtD-Sty-[600UPBSx2-FAD0.02(befE)-GA1.0%]x5 (green trace).

### 5.6.2 FAD Included After dAAO

Taking into account the sometimes unchanged and improved values shown sporadically with FAD at 0.02 mM concentration, it was decided to examine its use again, this time at a concentration of 0.08 mM (FAD0.08). The same four recipes were used, except that this time around the FAD0.08 dip was applied after the 600UPBS dip and before the binding layer of BSAGA1.0% or GA1.0% was applied. Dips of FAD0.08 were only applied on layers that also have a binding layer applied.

Electrode Design	Pt <sub>D</sub> -Sty-[600UPBSx5-FAD0.08-BSAGA1.0%]x2 n = 4	Pt <sub>D</sub> -Sty-[600UPBSx2-FAD0.08-BSAGA1.0%]x5 n = 4	Pt <sub>D</sub> -Sty-[600UPBSx5-FAD0.08-GA1.0%]x2 n = 3	Pt <sub>D</sub> -Sty-[600UPBSx2-FAD0.08-GA1.0%]x5 n = 4
<b>Kinetics</b>	M-M-H, n/c	M-M-H, p = 0.0051	M-M-H, p = 0.0007	M-M-H, p = 0.0096
<b>R<sup>2</sup></b>	0.9882	0.9999	0.9997	0.9998
<b>J<sub>max</sub>, μA.cm<sup>-2</sup></b>	25.42 ± 4.52	49.15 ± 0.47	56.72 ± 0.5284	77.12 ± 0.98
<b>K<sub>M</sub>, μM</b>	9214 ± 1549	2654 ± 73	878.0 ± 27.8	1805 ± 71.54
<b>α</b>	2.717 ± 0.638	1.061 ± 0.015	1.207 ± 0.040	1.094 ± 0.028
<b>LRS, μA.cm<sup>-2</sup>.mM<sup>-1</sup></b>	2.759 ± 0.116	18.52 ± 0.34	64.61 ± 1.63	42.73 ± 1.21

Table 5-20

Kinetic parameters, fit, J<sub>max</sub> and K<sub>M</sub> values calculated from the calibration data in Table 10-18. J<sub>max</sub>, K<sub>M</sub>, α and LRS are presented as Mean ± SEM.

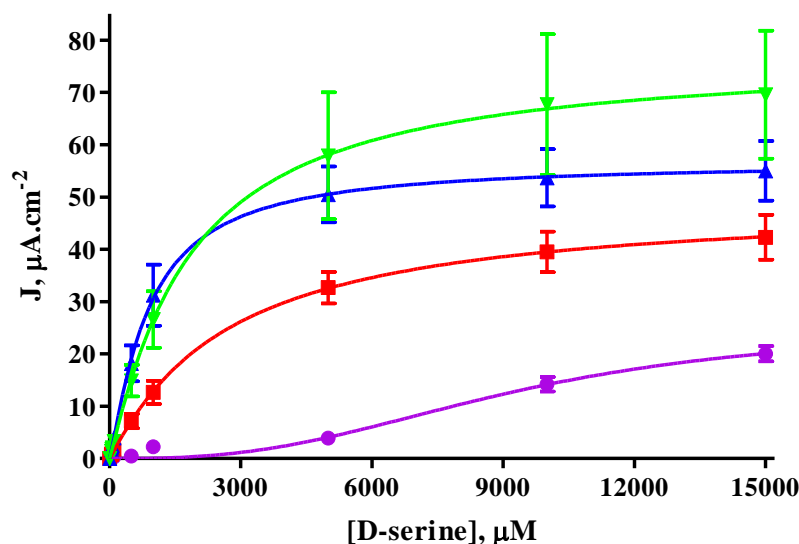


Figure 5-26

J-concentration plot of the four recipes selected for further investigation when modified with FAD0.02. Represented are Pt<sub>D</sub>-Sty-[600UPBSx5-FAD0.08-BSAGA1.0%]x2 (purple trace), Pt<sub>D</sub>-Sty-[600UPBSx2-FAD0.08-BSAGA1.0%]x5 (red trace), Pt<sub>D</sub>-Sty-[600UPBSx5-FAD0.08-GA1.0%]x2 (blue trace) and Pt<sub>D</sub>-Sty-[600UPBSx2-FAD0.08-GA1.0%]x5 (green trace).

The recipes to be examined were thus; Pt<sub>D</sub>-Sty-[600UPBSx5-FAD0.08-BSAGA1.0%]x2, Pt<sub>D</sub>-Sty-[600UPBSx2-FAD0.08-BSAGA1.0%]x5, Pt<sub>D</sub>-Sty-[600UPBSx5-FAD0.08-GA1.0%]x2 and Pt<sub>D</sub>-Sty-[600UPBSx2-FAD0.08-GA1.0%]x5. They were calibrated as before for their response to D-ser and the data collected is presented in Table 10-18. The kinetic fit information for the calibration data and a depiction of the resultant J-concentration curves are shown in Table 5-20 and Figure 5-26.

The kinetic parameters show that the results obtained with the use of FAD0.08 were quite mixed. On one hand the 2 dip BSAGA1.0% recipe appears to suffer, with unfavourable increases and decreases in the parameters and a very severe sigmoidal fit, but the other designs seem to have improved on the results obtained without the FAD0.08.

Beginning with the 2 dip BSAGA and 5 dip BSAGA recipes, the  $J_{\max}$  values have both significantly decreased,  $p = 0.0051^{**}$  and  $p = 0.0010^{**}$  respectively. The  $K_M$  values have reacted differently with the 2 dip BSAGA concentration increasing significantly,  $p = 0.0123^*$ , and the 5 dip BSAGA  $K_M$  decreasing,  $p = 0.0023^{**}$ . This results in the 2 dip BSAGA LRS being significantly decreased,  $p = 0.0002^{***}$ , and the 5 dip BSAGA design showing a significant increase in sensitivity,  $p < 0.0001^{***}$ .

The 2 dip GA1.0% recipe has a significant decrease in  $J_{\max}$ ,  $p = 0.0014^{**}$ , as does the 5 dip GA1.0% recipe,  $p = 0.0277$ . The  $K_M$  of 2 dip GA1.0% is significantly reduced,  $p = 0.0049^{**}$ , and the 5 dip GA1.0% concentration shows a non-significant change,  $p = 0.1587$ . The sensitivity of the 5 dip GA1.0% design is unchanged,  $p = 0.3976$ . However, the 5 dip design has an LRS that is significantly increased over the non FAD0.08 recipes,  $p = 0.0001^{***}$

## 5.7 Conclusion

With the conclusion in Chapter 4 that the initially proposed design was not fit for the purposes intended, a process of designing a new biosensor began. This process started from the very basic concept of adsorbing  $\alpha$ AAO onto the bare metal surface. From there it progressed to a simple study of how many layers of the enzyme could optimally be built up on the electrode surface using GA as a cross-linking agent, and then the introduction of an ‘immobilisation matrix’; styrene. Styrene was combined with some commonly used elements in the design of biosensors, GA, BSA and BSA/GA, and a further examination of the optimal build up of layers occurred. These studies yielded the observation that, overall, 10 layers of  $\alpha$ AAO, combined within the immobilisation matrix and some other agents, would likely yield the best results in the long run.

The second issue resolved was that of the formulation of the enzyme solution. This issue was initially raised in Section 4.7.1, and in Section 5.2.4 the matter was settled with a PBS solution with a pH of 8.5 and 600 U/mL of  $\alpha$ AAO definitively coming out

as the best all round choice. At this time it was also observed that BSA on its own did not produce any favourable sensitivity and was excluded from further study. Thus the basic structure of the evolving biosensor came to be; a bare Pt/Ir disk surface, an initial layer of the immobilisation matrix styrene, 10 layers of  $\alpha$ AAO PBS 600U and interspersed within these ten layers would be some combination of GA, BSA/GA or other substances.

The investigation into the use of GA within this general formula was the first thorough and very comprehensive study which moved the project forward to a definite design protocol. More than six concentrations of GA (although only six are reported for clarity and due to the poor results of other recipes) were tested, with 1, 2, 5 and 10 dips being interspersed among the enzyme dips for all concentrations. This process was repeated for a study using BSA/GA, where once again the concentration of GA used within this formula was up to 10 different concentrations. Overall these studies yielded a strong set of results which generally indicated that the use of 1% GA, dipped 2 or 5 times with the 10 layers of  $\alpha$ AAO produced the best results.

At this time the decision was taken to select the four most promising recipes and carry them forward to further studies. Utilising more recipes than this would have enormously increased the number of permutations and combinations to be examined. The four recipes selected were Pt<sub>D</sub>-Sty-[600UPBSx5-BSAGA1.0%]x2, Pt<sub>D</sub>-Sty-[600UPBSx2-BSAGA1.0%]x5, Pt<sub>D</sub>-Sty-[600UPBSx5-GA1.0%]x2 and Pt<sub>D</sub>-Sty-[600UPBSx2-GA1.0%]x5.

These selected protocols were then studied and examined in the context of the inclusion of PEI. Despite the beneficial effects shown in other biosensor designs, it was found that there was no combination involving PEI which improved on any of the vital kinetic parameters of the proposed biosensor. A further exploration involving FAD did however yield promising results under certain circumstances. When used in conjunction with, and only on those layers where GA 1.0% was present, and in between the enzyme and GA dip, the addition of 0.08 mM FAD was shown to maintain or increase the sensitivity of the biosensor when compared to the analogue biosensor without FAD. However, if the FAD was included before the enzyme and GA dip, or in conjunction with BSA/GA in any way, the result was a significantly decreased sensitivity in all cases.

Thus, in combination with the first four most promising protocols there were now two more recipes to consider in relation to any further improvements. These were; Pt<sub>D</sub>-Sty-[600UPBSx5-FAD0.08-GA1.0%]x2 and Pt<sub>D</sub>-Sty-[600UPBSx2-FAD0.08-GA1.0%]x5.

In summary, while it was considered that significant progress had been made towards a sensitive and reproducible biosensor it was hoped that further changes could be made which would provide superior sensitivity. It was encouraging that the enzyme solution was now being used continuously for multiple fabrication processes without changing the results.

References

- Andersson MM & Hatti-Kaul R. (1999). Protein stabilising effect of polyethyleneimine. *Journal of Biotechnology* **72**, 21-31.
- Aso C & Aito Y. (1962). Intramolecular-Intermolecular Polymerization of Glutaraldehyde. *Bulletin of the Chemical Society of Japan* **35**, 1426-1426.
- Avrameas S & Ternynck T. (1969). The cross-linking of proteins with glutaraldehyde and its use for the preparation of immunoadsorbernts. *Immunochemistry* **6**, 53-66.
- Bolger FB. (2007). The *in vitro* and *in vivo* characterisation and application of real time sensors and biosensors for neurochemical studies of brain energy metabolism. In *Department of Chemistry*. National University of Ireland, Maynooth.
- Broun GB. (1976). [20] Chemically aggregated enzymes. In *Methods in Enzymology*, ed. Klaus M, pp. 263-280. Academic Press.
- Gibson TD, Pierce BLJ, Hulbert JN & Gillespie S. (1996). Improvements in the stability characteristics of biosensors using protein-polyelectrolyte complexes. *Sensors and Actuators B: Chemical* **33**, 13-18.
- Goldstein L. (1976). Kinetic behavior of immobilized enzyme systems. In *Methods in Enzymology*, ed. Klaus M, pp. 397-443. Academic Press.
- Gregg RA & Mayo FR. (1947). Chain transfer in the polymerisation of styrene. III. The reactivities of hydrocarbons toward the styrene radical. *Discussions of the Faraday Society* **2**, 328-337.
- Gregg RA & Mayo FR. (1948). Chain transfer in the polymerisation of styrene. II. The reaction of styrene with carbon tetrachloride. *Journal of the American Chemical Society* **70**, 2373-2378.
- Gregg RA & Mayo FR. (1953). Chain transfer in the polymerisation of styrene. VII. Compounds containing halogens, oxygen and nitrogen. *Journal of the American Chemical Society* **75**, 3530-3533.
- Hardy PM, Nicholls AC & Rydon HN. (1969). The nature of glutaraldehyde in aqueous solution. *Journal of the Chemical Society D: Chemical Communications* **0**, 565-566.

- Haughton E. (pending publication). Real-time Neurochemical Analysis of Excitatory Amino Acids: Enzyme-modified Microelectrochemical Biosensors for Aspartate and Glutamate. In *Department of Chemistry*. National University of Ireland, Maynooth, (pending publication).
- Jansen EF & Olson AC. (1969). Properties and enzymatic activities of papain insolubilized with glutaraldehyde. *Arch Biochem Biophys* **129**, 221-227.
- Jansen EF, Tomimatsu Y & Olson AC. (1971). Cross-linking of  $\alpha$ -chymotrypsin and other proteins by reaction with glutaraldehyde. *Arch Biochem Biophys* **144**, 394-400.
- Johansson E, Marko-Varga G & Gorton L. (1993). Study of a reagent- and mediator-less biosensor for D-amino acids based on co-immobilized D-amino acid oxidase and peroxidase in carbon paste electrodes. *J Biomater Appl* **8**, 146-173.
- Kacaniklic V, Johansson K, Marko-Varga G, Gorton L, Jönsson-Pettersson G & Csöregi E. (1994). Amperometric biosensors for detection of L- and D-amino acids based on coimmobilized peroxidase and L- and D-amino acid oxidases in carbon paste electrodes. *Electroanalysis* **6**, 381-390.
- Kamath N, Melo JS & D'Souza SF. (1988). Urease immobilized on polyethyleneimine cotton cloth. *Applied Biochemistry & Biotechnology* **19**, 251-258.
- Kawahara J-i, Ohmori T, Ohkubo T, Hattori S & Kawamura M. (1992). The structure of glutaraldehyde in aqueous solution determined by ultraviolet absorption and light scattering. *Anal Biochem* **201**, 94-98.
- Korn AH, Fairheller SH & Filachoine EM. (1972). Glutaraldehyde: Nature of the reagent. *Journal of Molecular Biology* **65**, 525-529.
- Margel S & Rembaum A. (1980). Synthesis and Characterization of Poly(glutaraldehyde). A Potential Reagent for Protein Immobilization and Cell Separation. *Macromolecules* **13**, 19-24.
- Mayo FR. (1943). Chain transfer in the polymerization of styrene. I. The reaction of solvents with free radicals. *Journal of the American Chemical Society* **65**, 2324-2329.
- Mayo FR. (1948). Chain transfer in the polymerisation of styrene. IV. The effect of chain length on the reaction of styrene and carbon tetrachloride. *Journal of the American Chemical Society* **70**, 3689-3694.

- Mayo FR. (1953). Chain transfer in the polymerisation of styrene. VIII. Chain transfer with bromobenzene and mechanism of thermal initiation. *Journal of the American Chemical Society* **75**, 6133-6141.
- Mayo FR & Gregg RA. (1948). Effects of inhibitors on the polymerization of styrene. *Journal of the American Chemical Society* **70**, 1284-1286.
- Mayo FR, Gregg RA & Matheson MS. (1951). Chain transfer in the polymerisation of styrene. VI. Chain transfer with styrene and benzoyl peroxide; the efficiency of initiation and the mechanism of chain termination. *Journal of the American Chemical Society* **73**, 1691-1700.
- Migneault I, Dartiguenave C, Bertrand MJ & Waldron KC. (2004). Glutaraldehyde: behaviour in aqueous solution, reaction with proteins, and application to enzyme crosslinking. *BioTechniques* **37**, 790-802.
- Miller AA & Mayo FR. (1956). Oxidation of unsaturated compounds. I. The oxidation of styrene. *Journal of the American Chemical Society* **78**, 1017-1023.
- Monsan P, Puzo G & Mazarguil H. (1975). Study of the mechanism of glutaraldehyde-protein bond formation. *Biochimie* **57**, 1281.
- Okuda K, Urabe I, Yamada Y & Okada H. (1991). Reaction of glutaraldehyde with amino and thiol compounds. *Journal of Fermentation and Bioengineering* **71**, 100-105.
- Ottesen M & Svensson B. (1971). Modification of papain by treatment with glutaraldehyde under reducing and non-reducing conditions. *Comptes-rendus des travaux du Laboratoire Carlsberg* **38**, 171.
- Poyard S, Martelet C, Jaffrezic-Renault N, Cosnier S & Labbe P. (1999). Association of a poly(4-vinylpyridine-co-styrene) membrane with an inorganic/organic mixed matrix for the optimization of glucose biosensors. *Sensors & Actuators B: Chemical* **58**, 380-383.
- Priddy DB. (1994). Recent advances in styrene polymerization. In *Polymer Synthesis*, pp. 67-114. Springer Berlin Heidelberg.
- Rembaum A, Margel S & Levy J. (1978). Polyglutaraldehyde: A new reagent for coupling proteins to microspheres and for labeling cell-surface receptors. *Journal of Immunological Methods* **24**, 239-250.

- Richards FM & Knowles JR. (1968). Glutaraldehyde as a protein cross-linking reagent. *Journal of Molecular Biology* **37**, 231-233.
- Senthuran A, Senthuran V, Mattiasson B & Kaul R. (1997). Lactic acid fermentation in a recycle batch reactor using immobilized *Lactobacillus casei*. *Biotechnology & Bioengineering* **55**, 841-853.
- Shimizu M, Kanai Y, Uchida H & Katsube T. (1994). Integrated biosensor employing a surface photovoltage technique. *Sensors & Actuators B: Chemical* **20**, 187-192.
- Tashima T, Imai M, Kuroda Y, Yagi S & Nakagawa T. (1991). Structure of a new oligomer of glutaraldehyde produced by aldol condensation reaction. *The Journal of Organic Chemistry* **56**, 694-697.
- Tashima T, Kawakami U, Harada M, Sakata T, Satoh N, Nakagawa T & Tanaka H. (1987). Isolation and Identification of New Oligomers in Aqueous Solution of Glutaraldehyde (Analytical, Chemical). *Chemical & pharmaceutical bulletin* **35**, 4169-4180.
- Tomimatsu Y, Jansen EF, Gaffield W & Olson AC. (1971). Physical chemical observations on the  $\alpha$ -chymotrypsin glutaraldehyde system during formation of an insoluble derivative. *Journal of Colloid and Interface Science* **36**, 51-64.
- Volotovskiy V & Kim N. (1998). Cyanide determination by an ISFET-based peroxidase biosensor. *Biosensors & Bioelectronics* **13**, 1029-1033.
- Weetall HH. (1974). Immobilized enzymes. Analytical applications. *Analytical Chemistry* **46**, 602A-615a.
- Xu S & Han X. (2004). A novel method to construct a third-generation biosensor: Self-assembling gold nanoparticles on thiol-functionalized poly(styrene-co-acrylic acid) nanospheres. *Biosensors & Bioelectronics* **19**, 1117-1120.
- Zaborsky OR & Co CR. (1973). *Immobilized enzymes*, vol. 18901. CRC press Cleveland.

---

**6. CYLINDER ELECTRODES, METHYL  
METHACRYLATE AS AN IMMOBILISATION  
MATRIX AND *IN VITRO*  
CHARACTERISATION**

---

## 6.1 Introduction

Despite the discovery of two FAD recipes which displayed similar or better sensitivity than the originally proposed design it was still considered possible to improve on these recipes. An area of concern was to do with the actual live currents being measured, as opposed to the calculated current density (J) values. When the sensitivity was converted to the current change expected to be seen for a concentration change of 100  $\mu\text{M}$  in D-ser the results were not favourable. For Pt<sub>D</sub>-Sty-[600UPBSx5-FAD0.08-GA1.0%]x2, with a sensitivity of  $64.61 \pm 1.63 \mu\text{A}\cdot\text{cm}^{-2}\cdot\text{mM}^{-1}$ , the current flowing through an electrode at 100  $\mu\text{M}$  D-ser is  $0.7298 \pm 0.0200 \text{ nA}$ . For the LRS of Pt<sub>D</sub>-Sty-[600UPBSx5-BSAGA1.0%]x2,  $72.91 \pm 3.19 \mu\text{A}\cdot\text{cm}^{-2}\cdot\text{mM}^{-1}$ , the measured current would be  $0.8947 \pm 0.0391 \text{ nA}$ . These are two very low currents. While it is possible to monitor changes at this level it was decided it would be much more beneficial to explore possibilities for increasing this current.

Of primary concern was the knowledge that the interference from ascorbic acid (AA), which would react at the surface of the electrode *in vivo*, would generate a current of approximately 0.8 to 1.2 nA on 2 mm cylinder hydrogen peroxide biosensors (O'Brien *et al.*, 2007), 0.6 to 1.0 nA on 1 mm cylinder bare Pt/Ir electrodes (Rothwell *et al.*, 2008) and 0.25 nA for a bare Pt/Ir disk electrode (Rothwell *et al.*, 2009) (all at 400  $\mu\text{M}$  AA). This information led to the first attempted alteration, a change in the geometry of the electrode from a disk to a 0.5 mm cylinder surface. Although a change in the electrode geometry to a larger surface area was likely to increase the interference as demonstrated above, it was likely to increase the currents achieved to an even greater extent. This is due to the 'edge-effect' whereby the interference due to AA is reduced, when current densities are considered, by using a cylinder rather than a disk electrode (Rothwell *et al.*, 2009). This reduction in response is due to an edge density for a 1 mm cylinder which is 32 times smaller than the corresponding 125  $\mu\text{m}$  disk, which yields an AA current  $\sim 20$  times lower. Although it has previously been shown that it is difficult to achieve the same sensitivity when using a cylinder electrode (Zain *et al.*, 2010) the decrease should be not of the same magnitude as the change in AA sensitivity. It was hoped that overall an increase in the D-ser/AA current ratio likely to be encountered in the *in vivo* environment.

The basic configuration, of most biosensors discussed within this chapter, is as depicted in Figure 6-1. All alterations discussed in this chapter centre on this design with various layers being omitted or modified or added as detailed in each section.

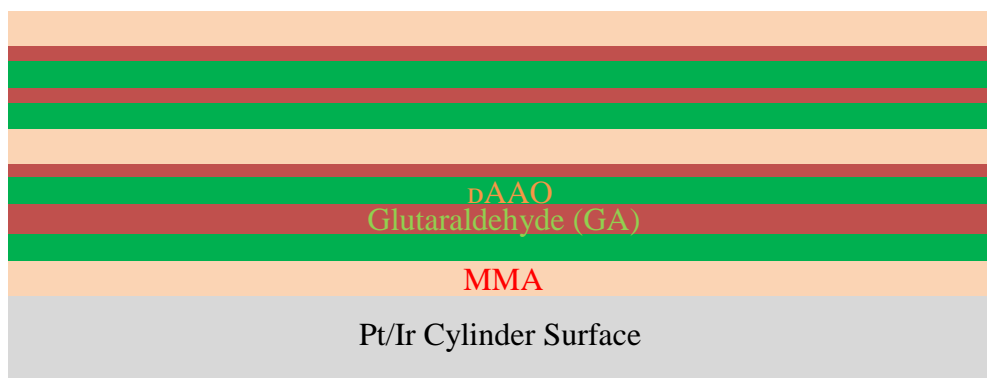


**Figure 6-1**

The basic configuration of biosensors discussed within Chapter 6.

## 6.2 Cylinder Electrodes and MMA – Protocol Improvements

### 6.2.1 The Use of Electrodes with a Cylindrical Surface

Having decided to embark on an inspection of the possibilities offered by a cylinder electrode it became necessary to choose the dimensions of this new electrode. A very important parameter that was necessary to consider was the intended end use of the biosensor. In this regard it was highly likely that the final electrode design could see use in mice, as a knockout strain lacking in dAAO has been indentified which would be very interesting in terms of future study (Miyoshi *et al.*, 2012). While 1 mm and 2 mm electrodes were suitable for use in rat brains, it was felt that these sizes of electrode were too large for use in a mouse. Thus considering the dimensions of a mouse brain it was decided to use only a 0.5 mm cylinder length. This meant that the cylinder surface was still the dominant surface, being 4 times longer than the electrode diameter, and the edge density (ratio of edge length to surface area, important parameter in AA rejection when PPD is being utilised) was reduced from  $319\text{ cm}^{-1}$  to  $1.88\text{ cm}^{-1}$ .

Even distribution of the various components of the biosensor on this new surface was considered to be a problem. This would be a cause for the reduction in sensitivity seen previously, along with the fact that the layers of substance applied would also be thinner. In an attempt to overcome this problem different mechanism for drying the electrodes were considered. The methods were; the normal method of hanging the

electrode so that the active disk surface pointed vertically down to the ground, an inverted method where the electrodes were placed standing with the disk surface pointing vertically upwards towards the sky, and a final method whereby the electrodes were spun horizontally about their axis using the equipment described in Section 3.4.1.

Lastly it was necessary to consider which biosensor recipe or recipes would be used to examine the properties of the cylinder electrode and drying methods. The decision was made to use Pt<sub>C</sub>-Sty-[600UPBSx5-GA1.0%]x2 (first seen in Section 5.3.3 as a disk electrode). The main considerations behind this were that it was similar to the two disk based recipes which provided the highest sensitivity, it had the largest  $J_{\max}$  of the recipes previously considered ( $178.8 \pm 4.5 \mu\text{A}\cdot\text{cm}^{-2}$ ), and that it had a relatively large  $K_M$  at  $\sim 5000 \mu\text{M}$ . It was hoped this combination of properties would allow an easier distinction to be drawn between the different cylinder drying methods.

The calibration data obtained when biosensors were constructed according to the recipe Pt<sub>C</sub>-Sty-[600UPBSx5-GA1.0%]x2 on 0.5 mm long cylinder electrodes is presented in Table 11-1. These electrodes were dried by three methods; normal, inverted and spun. The relevant kinetic data for the three variants is presented below in Table 6-1.

From the kinetic data and the J-concentration plot, Figure 6-2, it is quite clear that there are distinctly different results produced by the three drying methods. The method of spinning the electrodes as they dry immediately appears to produce the best results. This is borne out when considered statistically too. The spun electrodes have the largest  $J_{\max}$ ,  $14.78 \pm 0.55 \mu\text{A}\cdot\text{cm}^{-2}$ , which is significantly larger than both the normal and inverted electrodes,  $p = 0.0320^*$  and  $p = 0.0009^{***}$  respectively. The normal method produces a  $J_{\max}$  also significantly larger than the inverted electrodes,  $p = 0.0048^{**}$ . The  $K_M$  concentration for the spun electrodes is the smallest value. It is significantly smaller than the value for the normal electrodes,  $p = 0.0047^{**}$ , although it is not significantly different from the value of the inverted electrodes,  $p = 0.1482$ , owing to the large SEM associated with this drying method. The normal and inverted also have non-significantly different  $K_M$  concentrations,  $p = 0.4950$ .

Electrode Design	Pt <sub>C</sub> -Sty-[600UPBSx5-GA1.0%]x2, n = 4 Normal	Pt <sub>C</sub> -Sty-[600UPBSx5-GA1.0%]x2, n = 4 Inverted	Pt <sub>C</sub> -Sty-[600UPBSx5-GA1.0%]x2, n = 4 Spun
<b>Kinetics</b>	M-M, p = 0.9906	M-M, p = 0.0914	M-M-H, p = 0.0165
<b>R<sup>2</sup></b>	0.9930	0.9473	0.9935
<b>J<sub>max</sub>, μA.cm<sup>-2</sup></b>	12.72 ± 0.49	7.784 ± 1.020	14.78 ± 0.55
<b>K<sub>M</sub>, μM</b>	3082 ± 343.4	4210 ± 1415	1456 ± 141
<b>α</b>			1.359 ± 0.142
<b>LRS, μA.cm<sup>-2</sup>.mM<sup>-1</sup></b>	4.128 ± 0.324	1.849 ± 0.408	10.15 ± 0.71

Table 6-1

Kinetic parameters, fit, J<sub>max</sub> and K<sub>M</sub> values calculated from the calibration data in Table 11-1. J<sub>max</sub>, K<sub>M</sub>, α and LRS are presented as Mean ± SEM.

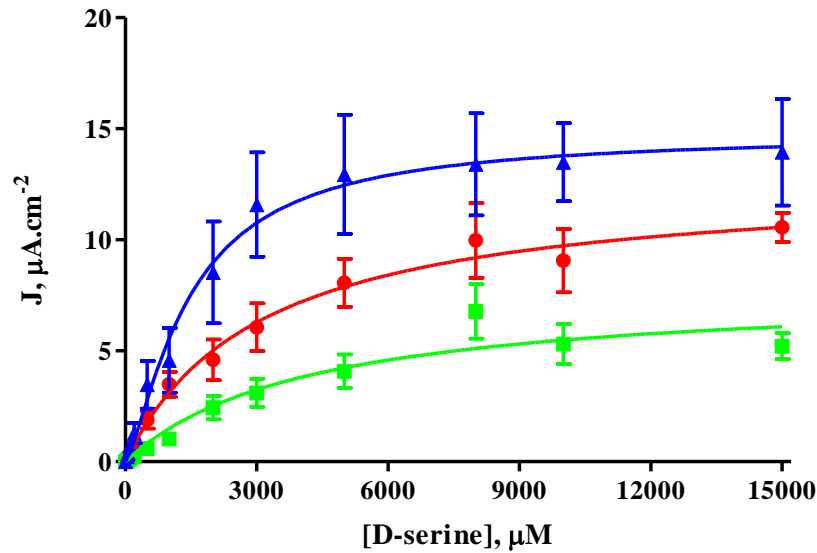


Figure 6-2

J-concentration plot of the Pt<sub>C</sub>-Sty-[600UPBSx5-GA1.0%]x2 recipe when made using three different drying methods. The normal method is depicted by the red trace, spun electrodes by the blue trace and inverted electrodes by the green trace.

When the sensitivity of the three drying methods is considered the stark difference seen in the plot comes to the fore. The spun electrodes have the largest LRS,  $10.15 \pm 0.71 \mu\text{A}\cdot\text{cm}^{-2}\cdot\text{mM}^{-1}$ . It is significantly larger than that of the normal or inverted biosensor designs,  $p = 0.0003^{***}$  and  $p < 0.0001^{***}$  respectively. The normal electrodes, in turn, have a significantly larger LRS than the inverted electrodes,  $p = 0.0047^{**}$ . Thus it is clear to see that there is a distinct advantage to be gained by spinning electrodes with a cylindrical geometry as the substituent solutions are drying on to the surface. Therefore, from this point forward, all biosensors fabricated using cylinder electrodes were spun horizontally, along the electrode axis, as they were drying.

Having determined the efficacy of the drying methods it was now important to examine whether a gain had been made in terms of the current achieved by the electrodes. Previously for the same recipe on a disk surface a sensitivity of  $35.41 \pm 1.19 \mu\text{A}\cdot\text{cm}^{-2}\cdot\text{mM}^{-1}$  had been obtained, 3.5 times larger than the cylinder electrode LRS. The ratio of surface area when comparing the cylinder surface to the disk surface is  $\sim 17:1$ . Therefore, in terms of current, the cylinder electrode has produced a current almost 5 times larger than the disk alternative. This is shown when the LRS is converted to a current response for  $100 \mu\text{M}$  D-ser; the result is now  $2.119 \pm 0.148 \text{ nA}$ . This is a much improved result, already significantly improved on any of the best recipes for a disk surface and as such the decision was made to continue using cylinder electrodes.

### 6.2.2 MMA as an Immobilisation Matrix

In the quest for continuing improvement in the sensitivity and stability of our biosensors, the group runs trials with different immobilisation methods. One of these methods involved the substitution of Sty with methyl methacrylate (MMA). This is a very interesting substance which unlike Sty has been approved for use, in its polymerised form, in a wide variety of life science technologies, such as hard contact lenses, as cement for and hip replacements, as replacement intraocular lens, dentures, cosmetic surgery and dental fillings. This would obviously be an advantageous material to use in the construction of biosensors, as long as it didn't reduce the sensitivity of the sensors. MMA has seen use in biosensing applications previously (Hall *et al.*, 1996; Bean *et al.*, 2005; Dai *et al.*, 2008; Hervás Pérez *et al.*, 2008), and has been successfully utilised within the group for sensor applications (Bolger *et al.*, 2011a), with its presence on the sensor surface confirmed by scanning electron microscopy, although the degree of polymerisation is unknown. Indeed, there was a US patent filed in regard to its use in biosensing application (Patent no: 5,284,140 Date: Feb 8<sup>th</sup> 1994). The monomer has a boiling point of  $100.5 \text{ }^\circ\text{C}$  and it, by a very similar mechanism to styrene, spontaneously polymerises when inhibitors are not present, with a multitude of factors affecting the rate of polymerisation (Lingnau *et al.*, 1980; Stickler & Meyerhoff, 1981; Lingnau & Meyerhoff, 1983, 1984b; Lingnau & Meyerhoff, 1984a; Srinivasan *et al.*, 2011; Liu *et al.*, 2012)

Electrode Design	Pt <sub>C</sub> -MMA-[600UPBSx5-GA1.0%]x2 n = 8	Pt <sub>C</sub> -Sty-[600UPBSx5-GA1.0%]x2 n = 4	Pt <sub>C</sub> -{MMA-[600UPBSx5-GA1.0%]x2}x2 n = 8	Pt <sub>C</sub> -{Sty-[600UPBSx5-GA1.0%]x2}x2 n = 8
<b>Kinetics</b>	M-M, p = 0.3800	M-M-H, p = 0.0165	M-M-H, p < 0.0001	M-M-H, p = 0.0002
<b>R<sup>2</sup></b>	0.9986	0.9935	0.9995	0.9996
<b>J<sub>max</sub>, μA.cm<sup>-2</sup></b>	14.94 ± 0.18	14.78 ± 0.55	28.30 ± 0.19	22.00 ± 0.23
<b>K<sub>M</sub>, μM</b>	1355 ± 62	1456 ± 141	627.0 ± 14.9	1275 ± 38
<b>α</b>		1.359 ± 0.142	1.368 ± 0.035	1.144 ± 0.028
<b>LRS, μA.cm<sup>-2</sup>.mM<sup>-1</sup></b>	11.02 ± 0.40	10.15 ± 0.71	45.14 ± 0.90	17.25 ± 0.37

Table 6-2

Kinetic parameters, fit, J<sub>max</sub> and K<sub>M</sub> values calculated from the calibration data in Table 11-2. J<sub>max</sub>, K<sub>M</sub>, α and LRS are presented as Mean ± SEM.

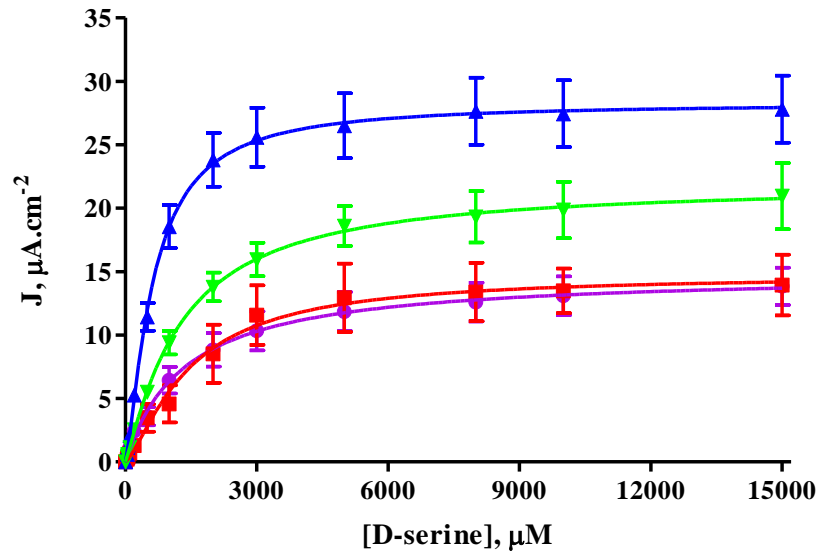


Figure 6-3

J-concentration plot of the Pt<sub>C</sub>-Sty-[600UPBSx5-GA1.0%]x2 (red trace), Pt<sub>C</sub>-{Sty-[600UPBSx5-GA1.0%]x2}x2 (green trace), Pt<sub>C</sub>-MMA-[600UPBSx5-GA1.0%]x2 (purple trace) and Pt<sub>C</sub>-{MMA-[600UPBSx5-GA1.0%]x2}x2 (blue trace).

Combined with an examination of MMA as an immobilisation matrix there was also an interest in examining how a second application would affect sensitivity. Another approach which had been previously explored it had shown a benefit in a limited number of circumstances (Haughton, pending publication). As explained in Section 3.5.5, a second application would be applied one hour after the initial application, resulting in a doubling of the layers within the complete protocol. The recipes to be utilised to explore both of these possible advancements were; Pt<sub>C</sub>-Sty-[600UPBSx5-GA1.0%]x2, Pt<sub>C</sub>-{Sty-[600UPBSx5-GA1.0%]x2}x2, Pt<sub>C</sub>-MMA-[600UPBSx5-

GA1.0%]x2 and Pt<sub>C</sub>-{MMA-[600UPBSx5-GA1.0%]x2}x2. The calibration results for these designs are listed in Table 11-2.

A striking aspect of the calibration results and the kinetic data, shown in Table 6-2, is the similarity between the Sty and MMA recipes with one application. The  $J_{\max}$  values are not significantly different,  $p = 0.8010$ , and neither are the  $K_M$  concentrations,  $p = 0.4557$ . As a consequence there is also no statistical difference in their sensitivities,  $p = 0.2758$ . The only difference between them is the shape of their kinetic curve, with the Sty design conforming to M-M-H and the MMA design best described by a M-M curve.

There is however a marked difference in both the case of Sty and MMA when comparing the one application protocol with the two application protocol. For Sty, the two application method has a significantly higher  $J_{\max}$  than the single application,  $p < 0.0001^{***}$ , but the  $K_M$  value is not different,  $p = 0.3031$ . The overall result is a significantly better LRS,  $p < 0.0001^{***}$ . Upon increasing the MMA design to two applications within the protocol there is also an increase in the  $J_{\max}$ ,  $p < 0.0001^{***}$ , and, unlike Sty, a significantly lower  $K_M$ ,  $p < 0.0001^{***}$ . Together the result is a significantly increased sensitivity,  $p < 0.0001^{***}$ .

Finally, there are significant differences between the Sty and MMA double applications protocols. They both conform to M-M-H kinetics but that is where the similarities end. The MMA recipe with two applications shows a significantly higher  $J_{\max}$  and a significantly lower  $K_M$ ,  $p < 0.0001^{***}$  for both. Combined together the two values result in a significantly higher LRS,  $p < 0.0001^{***}$ , for the MMA 2 application recipe. It is quite clear that this is a far superior recipe, in terms of sensitivity and current, to any formulations examined previously. Not only is it a cylinder electrode, but it has a sensitivity which is at least twice as large as any other cylinder recipe considered. The LRS is also less than half that of the most sensitive disk electrode design, despite it having a surface area 17 times larger. Thus for a concentration of 100  $\mu\text{M}$  D-ser it is returning a current of  $9.425 \pm 0.188$  nA.

The difference between the Sty and MMA is likely due to their structure. The Sty, with its benzene ring, will form a denser and less porous polymer which might be advantageous in retaining enzyme but a hindrance to the permeability of species into and out of the active site of the DAAO. The polymeric form of MMA will contain,

instead of benzene rings, flexible side chains, which could be less successful at retain enzyme but allow greater quantities of substrate and product to circulate at the biosensor surface. I suggest this is the reason that the two application MMA protocol is significantly more sensitive than the Sty two application protocol or either single application design.

## 6.3 Further Examination of MMA Based Recipes

### 6.3.1 Previous Best Recipes Re-Examined

Having seen the benefits of MMA, with regard to sensitivity improvements, it was deemed necessary to explore again the recipes which had yielded the best results for disk electrodes and Sty (Section 5.4.4). These recipes were not modified to include MMA, instead of Sty, and a second application was added to results in four new protocols; Pt<sub>C</sub>-{MMA-[600UPBSx5-GA1.0%]x2}x2, Pt<sub>C</sub>-{MMA-[600UPBSx2-GA1.0%]x5}x2, Pt<sub>C</sub>-{MMA-[600UPBSx5-BSAGA1.0%]x2}x2 and Pt<sub>C</sub>-{MMA-[600UPBSx2-BSAGA1.0%]x5}x2. The calibration data collected for these protocols is displayed in Table 11-3 with the accompanying kinetic data in Table 6-3. All four designs are graphically represented in Figure 6-4.

Upon first glance it is clear to see that the 2 dip BSAGA1% is no longer the recipe which performs best, in fact it is now the worst of the four recipes. The two 5 dip recipes appear to be identical and the 2 dip GA1% recipe from the previous section appears to offer the best performance. Statistically the 2 dip BSAGA design has the lowest  $J_{\max}$ , it is significantly smaller than the 2 dip GA, 5 dip GA and 5 dip BSAGA recipes,  $p = 0.0006^{***}$ ,  $p = 0.0008^{***}$  and  $p < 0.0001^{***}$  respectively. It also has the largest mean  $K_M$  value but due to the large SEM also associated with it is only significantly larger than the 2 dip GA recipe,  $p = 0.0435^*$ . It is not significantly different from the 5 dip GA and 5 dip BSAGA recipes,  $p = 0.0628$  and  $p = 0.0655$  respectively. The LRS value is however significantly smaller than the 2 dip and 5 dip GA,  $p < 0.0001^{***}$  for both, and the 5 dip BSAGA protocols,  $p = 0.0005^{***}$ .

Electrode Design	Pt <sub>C</sub> -{MMA-[600UPBSx5-GA1%]x2}x2 n = 8	Pt <sub>C</sub> -{MMA-[600UPBSx2-GA1%]x5}x2 n = 4	Pt <sub>C</sub> -{MMA-[600UPBSx5-BSAGA1%]x2}x2 n = 4	Pt <sub>C</sub> -{MMA-[600UPBSx2-BSAGA1%]x5}x2 n = 4
<b>Kinetics</b>	M-M-H, p < 0.0001	M-M, p = 0.4378	M-M, p = 0.2785	M-M, p = 0.6220
<b>R<sup>2</sup></b>	0.9995	0.9997	0.9934	0.9985
<b>J<sub>max</sub>, μA.cm<sup>-2</sup></b>	28.30 ± 0.19	26.07 ± 0.29	7.365 ± 1.338	26.45 ± 0.65
<b>K<sub>M</sub>, μM</b>	627.0 ± 14.9	3264 ± 118	19407 ± 5578	3532 ± 272
<b>α</b>	1.368 ± 0.035			
<b>LRS, μA.cm<sup>-2</sup>.mM<sup>-1</sup></b>	45.14 ± 0.90	7.989 ± 0.213	0.3795 ± 0.041	7.488 ± 0.418

Table 6-3

Kinetic parameters, fit, J<sub>max</sub> and K<sub>M</sub> values calculated from the calibration data in Table 11-3. J<sub>max</sub>, K<sub>M</sub>, α and LRS are presented as Mean ± SEM.

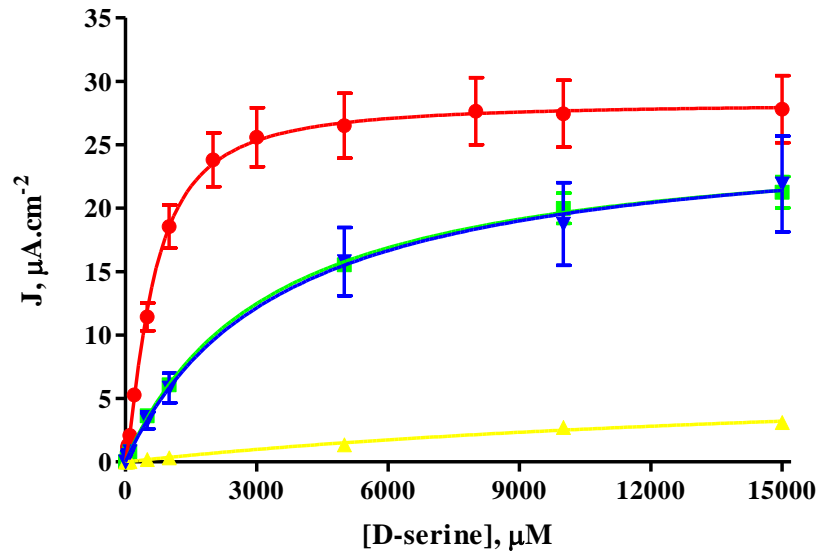


Figure 6-4

J-concentration plot of the four recipes selected in Section 5.4.4 when modified to utilise MMA and with a second application in the protocol. Displayed are Pt<sub>C</sub>-{MMA-[600UPBSx5-GA1.0%]x2}x2 (red trace), Pt<sub>C</sub>-{MMA-[600UPBSx2-GA1.0%]x5}x2 (green trace), Pt<sub>C</sub>-{MMA-[600UPBSx5-BSAGA1.0%]x2}x2 (yellow trace) and Pt<sub>C</sub>-{MMA-[600UPBSx2-BSAGA1.0%]x5}x2 (blue trace).

Considering now the two 5 dip recipes it is possible to see how similar they are. The J<sub>max</sub>, K<sub>M</sub>, and LRS for the two recipes are all non-significantly different, p = 0.6114, p = 0.4007 and p = 0.3270 respectively. They are both best described by M-M kinetic curves. The 2 dip GA recipe undoubtedly provides the best results of the four protocols. This becomes evident when it is statistically analysed against the 5 dip GA, 2 dip BSAGA and 5 dip BSAGA recipes. It has the largest J<sub>max</sub>, p < 0.0001\*\*\* for 5 dip GA, and p = 0.0005\*\*\* for 2 dip BSAGA, excepting the 5 dip BSAGA recipe, p = 0.0713. It also has the smallest K<sub>M</sub> concentration, p = 0.0002\*\*\*, p = 0.0435\* and p = 0.0018\*\*

respectively. As a result it has a far superior sensitivity when compared to the same recipes,  $p < 0.0001$ \*\*\* for all.

It was becoming clear that the  $Pt_C\text{-}\{MMA\text{-}[600UPBSx5-GA1.0\%]x2\}x2$  recipe was likely to be the most sensitive design that would be found. This is due to the two dips of GA providing a small amount of cross-linking that helps secure the dAAO in the MMA matrix without denaturing the enzyme as the five dip GA design appears to. In the case of the BSAGA recipe the opposite seems to be the case, with the smaller quantity of BSAGA dips have a very low sensitivity, likely due to insufficient quantities of GA being available due to it mainly linking the BSA. With increased levels of BSAGA it is seen that the sensitivity improves significantly.

### 6.3.2 Addition of FAD to the GA 1% Recipes

In order to ensure complete exploration of protocols that had previously yielded good results it was necessary however to re-examine how the incorporation of FAD would affect this new stand-out design. Previously, for the similar recipe based around Sty and with only one application, FAD had enhanced sensitivity significantly. To elucidate how it would react in a MMA matrix two new protocols were conceived;  $Pt_C\text{-}\{MMA\text{-}[600UPBSx5-FAD0.08-GA1.0\%]x2\}\text{-}x2$  and  $Pt_C\text{-}\{MMA\text{-}[600UPBSx5-GA1.0\%]x2\text{-}FAD0.08(5)\}x2$ . Thus, as in the previous advantageous arrangement it was first incorporated on the fifth and tenth layer, after the 600UPBS but before the GA1.0%, *i.e.* twice per application and four dips overall. Secondly it was incorporated into only the fifth layer, again after the 600UPBS and before the GA1.0%, two dips overall.

The calibration data for the two new recipes is displayed above in Table 11-4, with the original for comparison. Following, in Table 6-4, is the kinetic data obtained when the three recipes were analysed. From the calibration data and some of the kinetic calculations the three recipes look very similar. However, statistically the differences can be shown. As hinted at by Figure 6-5, the recipe with FAD emerges as the strongest protocol. This is quite different to the results seen in Section 5.6.2, where the influence of FAD is a positive one.

Electrode Design	Pt <sub>C</sub> -{MMA-[600UPBSx5-GA1%]x2}x2, n = 8	Pt <sub>C</sub> -{MMA-[600UPBSx5-GA1.0%]x2-FAD0.08(5)}x2, n = 4	Pt <sub>C</sub> -{MMA-[600UPBSx5-FAD0.08-GA1.0%]x2}-x2, n = 4
Kinetics	M-M-H, p < 0.0001	M-M, p = 0.1388	M-M-H, p = 0.0140
R <sup>2</sup>	0.9995	0.9996	0.9985
J <sub>max</sub> , μA.cm <sup>-2</sup>	28.30 ± 0.19	34.53 ± 0.64	29.87 ± 0.76
K <sub>M</sub> , μM	627.0 ± 14.9	1966 ± 122	1339 ± 110
α	1.368 ± 0.035		1.293 ± 0.103
LRS, μA.cm <sup>-2</sup> .mM <sup>-1</sup>	45.14 ± 0.90	17.56 ± 0.83	22.32 ± 1.38

Table 6-4

Kinetic parameters, fit, J<sub>max</sub> and K<sub>M</sub> values calculated from the calibration data in Table 11-4. J<sub>max</sub>, K<sub>M</sub>, α and LRS are presented as Mean ± SEM.

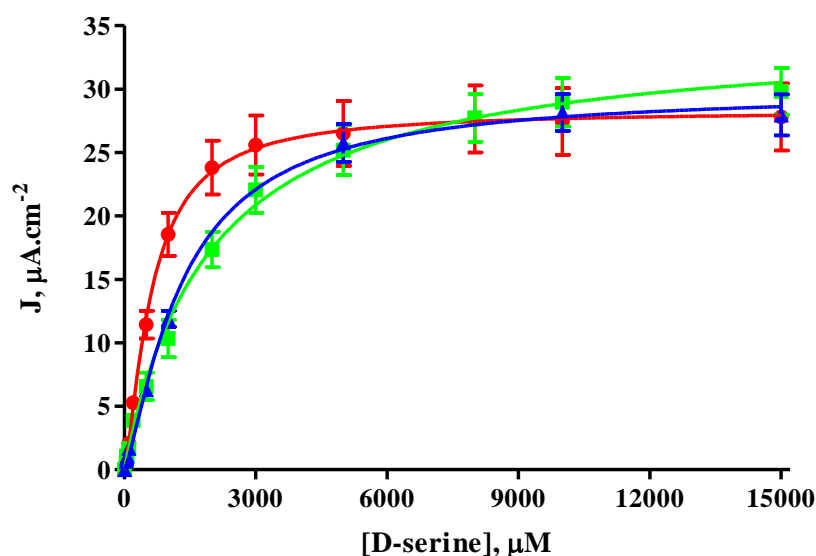


Figure 6-5

J-concentration plot of the data in Table 11-4 and Table 6-4. Pt<sub>C</sub>-{MMA-[600UPBSx5-GA1%]x2}x2 is red, Pt<sub>C</sub>-{MMA-[600UPBSx5-GA1.0%]x2-FAD0.08(5)}x2 is green and Pt<sub>C</sub>-{MMA-[600UPBSx5-FAD0.08-GA1.0%]x2}-x2 is the blue trace.

Between the two FAD recipes all parameters are quite different. The recipe with two dips of FAD overall (green trace) has a significantly higher J<sub>max</sub> than four dip FAD recipe (blue trace), p = 0.0003\*\*\*. The two dip FAD recipe also has a significantly higher K<sub>M</sub> concentration, p = 0.0017\*\*. Combined, this leads to a two dip FAD recipe with significantly lower LRS, p = 0.0103\*, than a four dip FAD recipe.

The design with no FAD has a lower J<sub>max</sub> than the two dip FAD protocol, p < 0.0001\*\*\*, but not the four dip FAD protocol, with which there is no significant difference, p = 0.0856. Not using FAD does however produce a significantly lower K<sub>M</sub> value than both the two dip and four dip FAD recipes, p < 0.0001\*\*\* and p = 0.0004\*\*\* respectively. It is this significantly lower K<sub>M</sub> which means that the design

without FAD has a significantly higher sensitivity than the protocols containing FAD,  $p < 0.0001^{***}$  in both cases. Thus in the case of cylinder recipes, formulated with MMA and not Sty and when two applications are applied within the protocol it is found that not using FAD produces a more sensitive biosensor than when using FAD. This is in direct contrast to some results for disk electrodes using single applications and Sty as an immobilisation matrix. A possible reason for this is that due to the increased surface area the quantity/concentration of FAD added is insufficient to be found in close enough proximity to the enzyme to be effective and could likely be occupying valuable cross-linking sites without providing any additional benefit.

### 6.3.3 An Additional Layer of MMA

At this time, before accepting the Pt<sub>C</sub>-{MMA-[600UPBSx5-GA1%]x2}x2 design as the preferred recipe, it was deemed necessary to briefly check the stability of the biosensors. A set of biosensors was fabricated, calibrated, and then calibrated again 1 and 4 days later, having been stored at 4°C between each calibration. The results are listed in the top half of Table 11-5 and Table 6-5. The results are also depicted in Figure 6-6, where the initial Day 0 calibration is plotted in red, the Day 1 calibration in orange and the Day 4 calibration in yellow.

Distinct differences were noticed between the results over the 5 days. One-way ANOVA of the  $J_{max}$  values for the Pt<sub>C</sub>-{MMA-[600UPBSx5-GA1%]x2}x2 results show that there is no difference between Day 0 and Day 1,  $p > 0.0500$ , there was a significant decrease between Day 0 and Day 4,  $p < 0.0010^{***}$ , and a significant decrease between Day 1 and Day 4,  $p < 0.0100^{**}$ . There are no significant differences when the  $K_M$  values are examined. All comparisons return a non-significant result of  $p < 0.0500$ . Finally the sensitivities also show a change. There is a significant decrease in the LRS from Day 0 to Day 1,  $p < 0.0100^{**}$ , and a significant decrease between Day 0 and Day 4,  $p < 0.0100^{**}$ . However there is no significant change in sensitivity between Day 1 and Day 4,  $p < 0.0500$ . Thus, after an initial decrease the LRS appears to reach a stable level.

Electrode Design	Pt <sub>C</sub> -{MMA-[600UPBSx5-GA1%]x2}x2 DAY 0, n = 4	Pt <sub>C</sub> -{MMA-[600UPBSx5-GA1%]x2}x2 DAY 1, n = 4	Pt <sub>C</sub> -{MMA-[600UPBSx5-GA1%]x2}x2 DAY 4, n = 4
<b>Kinetics</b>	M-M, p = 0.2807	M-M, p = 0.6172	M-M, p = 0.9574
<b>R<sup>2</sup></b>	0.9472	0.9386	0.9375
<b>J<sub>max</sub>, μA.cm<sup>-2</sup></b>	34.40 ± 1.217	31.59 ± 1.510	22.41 ± 1.007
<b>K<sub>M</sub>, μM</b>	727.6 ± 113.4	1581 ± 299	1261 ± 233.0
<b>α</b>			
<b>LRS, μA.cm<sup>-2</sup>.mM<sup>-1</sup></b>	47.27 ± 6.38	19.98 ± 3.10	17.76 ± 2.75
Electrode Design	Pt <sub>C</sub> -{MMA-[600UPBSx5-GA1%]x2}x2-MMA DAY 0, n = 4	Pt <sub>C</sub> -{MMA-[600UPBSx5-GA1%]x2}x2-MMA DAY 1, n = 4	Pt <sub>C</sub> -{MMA-[600UPBSx5-GA1%]x2}x2-MMA DAY 4, n = 4
<b>Kinetics</b>	M-M-H, p = 0.0008	M-M-H, p = 0.0175	M-M, p = 0.6348
<b>R<sup>2</sup></b>	0.9882	0.9989	0.9738
<b>J<sub>max</sub>, μA.cm<sup>-2</sup></b>	32.40 ± 0.48	42.09 ± 1.41	45.15 ± 1.25
<b>K<sub>M</sub>, μM</b>	635.4 ± 31.1	785.5 ± 74.7	1116 ± 131
<b>α</b>	1.315 ± 0.092	1.925 ± 0.437	
<b>LRS, μA.cm<sup>-2</sup>.mM<sup>-1</sup></b>	50.99 ± 2.12	53.58 ± 4.48	40.46 ± 4.01

Table 6-5

Kinetic parameters, fit, J<sub>max</sub> and K<sub>M</sub> values calculated from the calibration data in Table 11-5. J<sub>max</sub>, K<sub>M</sub>, α and LRS are presented as Mean ± SEM.

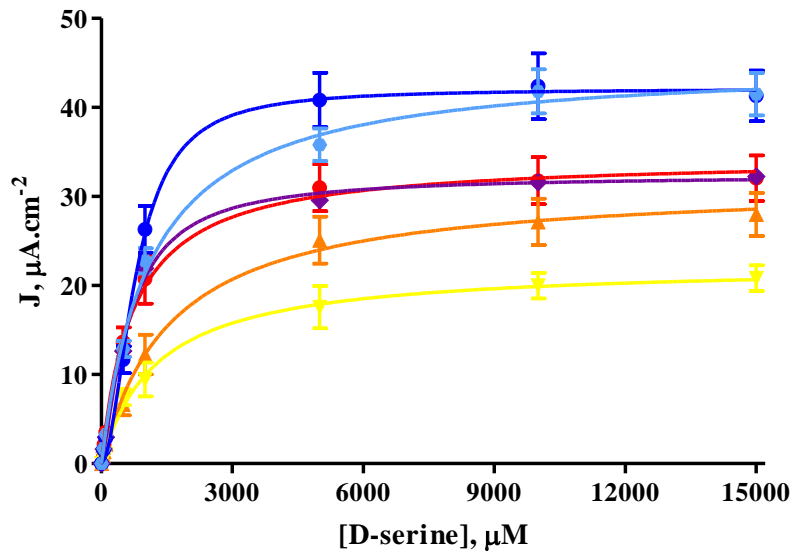


Figure 6-6

J-concentration plot of the Pt<sub>C</sub>-{MMA-[600UPBSx5-GA1%]x2}x2 and Pt<sub>C</sub>-{MMA-[600UPBSx5-GA1%]x2}x2-MMA biosensors calibrated over a period of 5 days. For Pt<sub>C</sub>-{MMA-[600UPBSx5-GA1%]x2}x2 Day 0 is depicted in red, Day 1 in orange and Day 4 in yellow. The Day 0 calibration of Pt<sub>C</sub>-{MMA-[600UPBSx5-GA1%]x2}x2-MMA is the purple trace, Day 1 is dark blue and Day 4 is light blue.

In an attempt to control the level of the decrease, which was significant and almost half of the starting value, it was decided to incorporate an extra layer of MMA. This layer would be applied as a single dip, after the second application had been allowed to dry

for an hour at 4 °C. The electrodes would then be stored in a fridge for at least 3 hours before being calibrated. The first important aspect to be considered with this change was to see if it would alter the initial kinetic parameters of the electrodes in any significant way. By comparing the two Day 0 sets of results it can be seen that there is no significant difference between the  $J_{\max}$ ,  $K_M$ , or LRS of the results,  $p = 0.1769$ ,  $p = 0.4902$  and  $p = 0.6186$  respectively. Thus having established that there is no significant difference between the Day 0 kinetic parameters it was then possible to consider how the electrodes with the extra MMA layer changed over the 5 day period. Firstly, the  $J_{\max}$  is significantly increased on Day 1 compared to Day 0,  $p < 0.0010^{***}$ , and significantly increased on Day 4 when compared to Day 0,  $p < 0.0010^{***}$ . There is no significant difference between Day 1 and Day 4,  $p > 0.0500$ . Contrastingly, there is no difference in the  $K_M$  concentration between Day 0 and Day 1,  $p > 0.0500$ .

Now considering the sensitivity of the protocol with the extra layer of MMA the full benefit of this layer can be determined. Using one-way ANOVA it is seen that there is no statistical difference between the sensitivity across the three calibrations and the 5 days,  $p < 0.0500$  for all comparisons. The extra MMA dip has stabilised the sensitivity of the electrodes. This stabilisation is further elucidated when the sensitivity of the two recipes is compared on the three calibration days. We have already seen that the Day 0 results are not significantly different. When we consider Day 1 and Day 4 we can see that the  $Pt_C\{-[MMA-[600UPBSx5-GA1\%]x2]x2\}$  recipe has a significantly lower sensitivity than the  $Pt_C\{-[MMA-[600UPBSx5-GA1\%]x2]x2\}$ -MMA protocol,  $p = 0.0008^{***}$  and  $p = 0.0034^{**}$  respectively. It was decided based on all previous data that  $Pt_C\{-[MMA-[600UPBSx5-GA1\%]x2]x2\}$ -MMA was going to be the optimal electrode design. Its sensitivity appeared to be stable and of a favourable magnitude,  $50.99 \pm 2.12 \mu A.cm^{-2}.mM^{-1}$  for a 0.5 mm cylinder electrode, is a very satisfactory result when compared to a starting point of  $63 \pm 2 \mu A.cm^{-2}.mM^{-1}$  for a disk electrode.

#### 6.4 Interference Rejection Strategies

Having discovered what was considered the optimal protocol for sensitivity there was now the issue of interference to be considered. Ascorbic acid is the most prevalent electroactive interferent in brain ECF, present at a concentration of 400  $\mu M$  (Miele & Fillenz, 1996). It is used as a benchmark with which to quantify the ability of biosensors to reject all interference from electroactive substances and only detect the target analyte. In

order to reject interferents two substances were employed which had been shown to be highly successful previously (see Section 1.3), *o*-PD and Naf. In order to quantify the success of these substances it was necessary to also examine how H<sub>2</sub>O<sub>2</sub> and AA are detected in the absence of these substances. It was also necessary to study how these substances would affect the sensitivity of the biosensors to D-ser.

#### 6.4.1 Hydrogen Peroxide and AA without Interference Rejection Layers

Firstly, it is necessary to state how H<sub>2</sub>O<sub>2</sub> and AA behave at the bare metal surface and without any interference rejection or other substances incorporated from the recipe. This will provide a basis for quantifying the effectiveness of the rejection layers once applied. Thus, Pt<sub>C</sub> and was calibrated for response to H<sub>2</sub>O<sub>2</sub> and AA up to 1000 μM. The results are presented below in Table 11-6, with the associated linear regression and fit data in Table 6-6. These results are then plotted in Figure 6-7.

It is very clear from the calibration that the AA has a far higher rate of reaction than H<sub>2</sub>O<sub>2</sub> at the Pt/Ir surface. The current from a 1000 μM solution of AA is more than twice as high as that of H<sub>2</sub>O<sub>2</sub>, it is a significantly larger difference,  $p < 0.0001^{***}$ . There is also a significant difference between the LRS values with the AA value again significantly higher,  $p = 0.0002^{***}$ .

	Pt <sub>C</sub> , H <sub>2</sub> O <sub>2</sub> n = 24	Pt <sub>C</sub> , AA n = 8
Slope, μA.cm <sup>-2</sup> .mM <sup>-1</sup>	170.0 ± 2.5	437.5 ± 3.8
R <sup>2</sup>	0.9980	0.9997
Y – intercept	-0.9536 ± 0.8829	2.992 ± 2.312
X - intercept	5.610	-6.838
J @ 1000 μM, μA.cm <sup>-2</sup>	170.8 ± 15.3	437.9 ± 30.2

Table 6-6

Linear regression fit data for Pt<sub>C</sub> when calibrated for response to AA and H<sub>2</sub>O<sub>2</sub>. Data is presented as Mean ± SEM where appropriate.

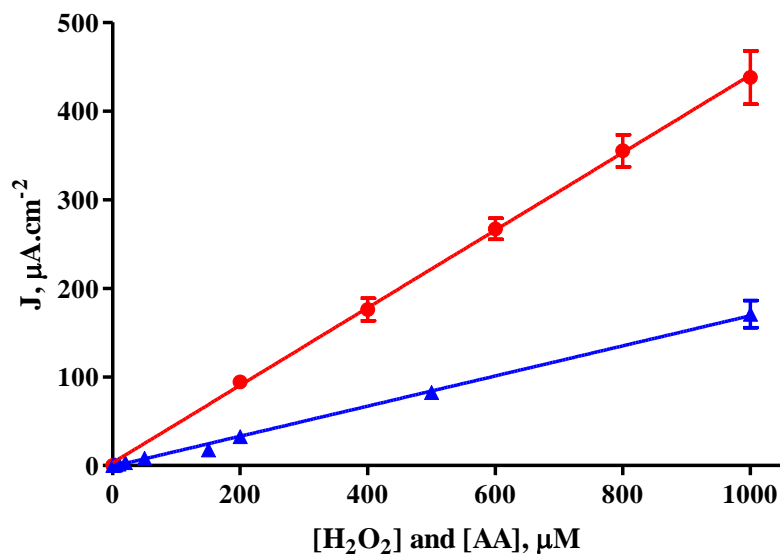


Figure 6-7

J-concentration plot for the calibration of Pt<sub>C</sub>. Depicted is the response to H<sub>2</sub>O<sub>2</sub> (blue trace) and AA (red trace. Data is drawn from Table 11-6 and Table 6-6.

#### 6.4.2 P-*o*-PD Grown by CV and CPA

To attempt to remove interference from electroactive species the first approach considered was the use of a polymer film created from *o*-PD. This polymerised *o*PD film (P-*o*-PD) has previously been grown by two methods, indeed both had been used in the early development of D-ser sensors by Z.M. Zain (see Section 4.2). These methods were: by CPA (PPD) and by CV (PPD<sub>CV</sub>). To investigate the interferent rejection properties of P-*o*-PD grown by both of these methods the following two recipes were fabricated and calibrated for response to AA: Pt<sub>C</sub>-PPD-{MMA-[600UPBSx5-GA1%]x2}x2-MMA and Pt<sub>C</sub>-PPD<sub>CV</sub>-{MMA-[600UPBSx5-GA1%]x2}x2-MMA. The results of these calibrations are presented in Table 11-7.

Inspecting the linear regression data for the PPD we can see a very large value for the x-intercept value, as well as a very poor R<sup>2</sup> value of 0.6957. Bearing these in mind and examining the calibration points plotted in Figure 6-8 it is clear that it is not possible to fit a linear regression to the PPD data. This is a positive outcome as it has been documented that when grown and functioning optimally P-*o*-PD should display a 'self-blocking' mechanism (Lowry & O'Neill, 1994; Craig & O'Neill, 2003). This mechanism demonstrates that not only is the polymer preventing AA from reaching the surface of the electrode but that when small quantities do react at the surface the products produced are blocking the pathways to the surface for other molecules of AA. The

observation of this effect is a satisfactory result. Subsequently the linear fit for the PPD curve was omitted from Figure 6-8 as it made no sense to include it and it does not appear to fit the points well (as indicated by the poor  $R^2$  value).

Polymerisation Method	PPD n = 16	PPD <sub>CV</sub> n = 4
Slope, $\mu\text{A}\cdot\text{cm}^{-2}\cdot\text{mM}^{-1}$	$0.2099 \pm 0.0694$	$0.1466 \pm 0.0062$
$R^2$	0.6957	0.9929
Y - intercept	$0.0756 \pm 0.0420$	$0.0070 \pm 0.0038$
X - intercept	-360.2	-47.65
J @ 1000 $\mu\text{M}$ , $\mu\text{A}\cdot\text{cm}^{-2}$	$0.236 \pm 0.017$	$0.152 \pm 0.087$

Table 6-7

Linear regression fit data when PPD and PPD<sub>CV</sub> are compared for response to AA while incorporated into Pt<sub>C</sub>-PoPD-[MMA-[600UPBSx5-GA1%]x2]x2-MMA. Data is presented as Mean  $\pm$  SEM where appropriate.

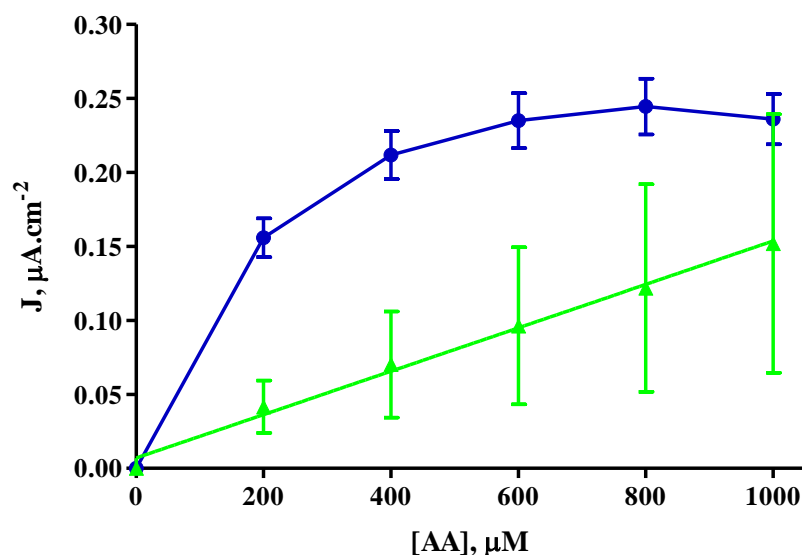


Figure 6-8

J-concentration plot for the calibration of Pt<sub>C</sub>-P-o-PD-[MMA-[600UPBSx5-GA1%]x2]x2-MMA, where the method of polymerisation of the P-o-PD was changed. Depicted are the CPA method (PPD) in blue and the CV method (PPD<sub>CV</sub>) in green. Data is drawn from Table 11-7 and Table 6-7.

On the other hand the PPD<sub>CV</sub> calibration displays a distinctly linear response. This is not a desirable result as it means that there will be no self-blocking of AA and as the concentration of it fluctuates in an *in vivo* environment the background current will also fluctuate. This will obscure current changes due to changing levels of D-ser. It thus appears that CV is not a favourable method to grow the P-o-PD layer.

Statistically it is not reasonable to compare the slopes of the linear fits. A better comparison is to compare the current density at particular concentrations. At 1000  $\mu\text{M}$  AA, which should be the plateau region of an ideally behaving self-blocking response,

there is no significant difference between the two responses,  $p = 0.4146$ . At  $400 \mu\text{M}$ , the physiological concentration, there is a significant difference, with the PPD value being the larger value,  $p = 0.0012^{**}$ . This difference, although it may appear better to have a lower response at physiological level, is not a good thing as it is more important to have a consistent response over different concentration levels. An attribute that can be seen when the  $400 \mu\text{M}$  and  $1000 \mu\text{M}$  responses are compared for PPD,  $p = 0.3127$ . Now, the same comparison for  $\text{PPD}_{\text{CV}}$  also yields no significant difference,  $p = 0.4202$ , but looking at the J values and the plot it is easy to see that for  $\text{PPD}_{\text{CV}}$  this non-significant result is due to the much larger error in its values, and that there is quite a large scope for the current to change.

### 6.4.3 Naf before CV and CPA Grown P-*o*-PD

In an effort to further improve interference rejection a second strategy was examined. This was the incorporation of Naf with a P-*o*-PD film. As previously stated in Section 4.4, Naf used after the application of a P-*o*-PD film can have a detrimental effect (Friedemann *et al.*, 1996). But, it has also been shown that Naf used in the correct manner can have significant interferent rejection properties (Pan & Arnold, 1996; Xu *et al.*, 2002; Brown & Lowry, 2003; López *et al.*, 2006; Hervás Pérez *et al.*, 2008; Brown *et al.*, 2009). Thus, it was decided to incorporate the Naf underneath the P-*o*-PD layer. This led to two new designs to be tested for AA response:  $\text{Pt}_{\text{C}}\text{-Naf-PPD-}\{\text{MMA-}[\text{600UPBSx5-GA1\%}]_{\text{x}2}\}_{\text{x}2}\text{-MMA}$  and  $\text{Pt}_{\text{C}}\text{-Naf-PPD}_{\text{CV}}\text{-}\{\text{MMA-}[\text{600UPBSx5-GA1\%}]_{\text{x}2}\}_{\text{x}2}\text{-MMA}$ . The Naf was applied by dipping into 1% Naf, five times with five minutes drying time between each layer. The results of these calibrations are presented in Table 11-8. As in the previous section, when the linear fit data in Table 6-8 is examined it is clear that neither set of data is suitable for a linear fit. This is a favourable result for reasons explained also in the last section. As such no fit is ascribed to either the Naf-PPD (blue) or Naf- $\text{PPD}_{\text{CV}}$  (green) in Figure 6-9.

Interference Layers	Naf-PPD n = 24	Naf-PPD <sub>CV</sub> n = 4
Slope, $\mu\text{A}\cdot\text{cm}^{-2}\cdot\text{mM}^{-1}$	$-0.0219 \pm 0.0170$	$0.1032 \pm 0.0255$
$R^2$	0.2927	0.8044
Y – intercept	$0.0196 \pm 0.0103$	$0.0258 \pm 0.0154$
X - intercept	894.3	-249.7
J @ 1000 $\mu\text{M}$ , $\mu\text{A}\cdot\text{cm}^{-2}$	$-0.011 \pm 0.030$	$0.106 \pm 0.018$

Table 6-8

Linear regression fit data when Naf-PPD and Naf-PPD<sub>CV</sub> are compared for response to AA while incorporated into Pt<sub>C</sub>-Naf-PoPD-{MMA-[600UPBSx5-GA1%]x2}x2-MMA. Data is presented as Mean  $\pm$  SEM where appropriate.

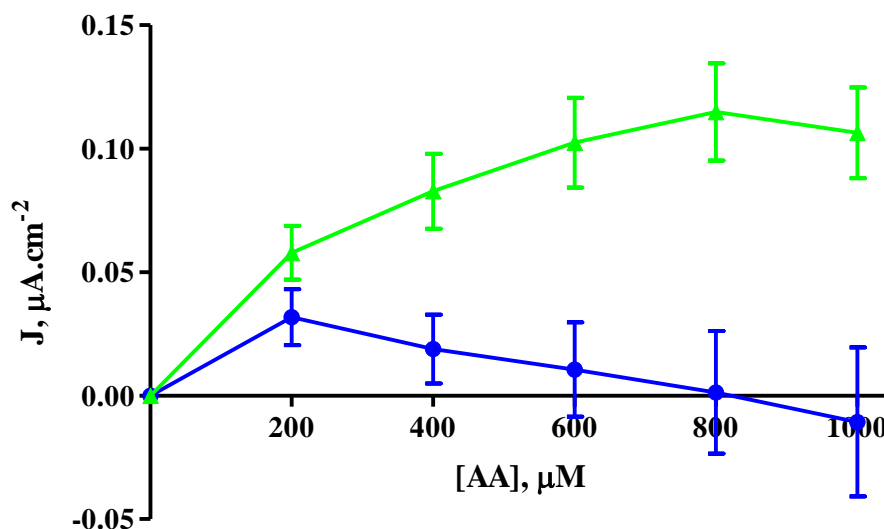


Figure 6-9

J-concentration plot for the AA calibration of sensors with combined Naf-P-o-PD interference layers. Depicted are the CPA method (Naf-PPD) in blue and the CV method (Naf-PPD<sub>CV</sub>) in green. Data is drawn from Table 11-8 and Table 6-8.

Comparison by concentration best illustrates the difference between the two protocols. At 400  $\mu\text{M}$  the Naf-PPD layers produce a response which is not significantly different from the Naf-PPD<sub>CV</sub> response,  $p = 0.0800$ . For 1000  $\mu\text{M}$ , there is a significant difference, with the Naf-PPD<sub>CV</sub> J value significantly higher than the Naf-PPD figure,  $p = 0.0033^{**}$ . Encouragingly there is no significant difference between the 400 and 1000  $\mu\text{M}$  J values for Naf-PPD,  $p = 0.3800$ , or for Naf-PPD<sub>CV</sub>,  $p = 0.3598$ .

The differences between the Naf-P-o-PD and P-o-PD protocols are also significant. The PPD response at 400  $\mu\text{M}$  is significantly higher than the Naf-PPD response,  $p < 0.0001^{***}$ , but the PPD<sub>CV</sub> value is not significantly different compared to the Naf-PPD<sub>CV</sub> value at 400  $\mu\text{M}$ ,  $p = 0.7575$ . At 1000  $\mu\text{M}$  there are also significant differences, Naf-PPD produces a significantly lower current than the PPD only protocol,  $p <$

0.0001\*\*\*. However, again there is no significant difference between Naf-PPD<sub>CV</sub> and PPD<sub>CV</sub>,  $p = 0.6285$ .

Overall the Naf-PPD protocol produces the best results. At 1000  $\mu\text{M}$ , the plateau value, its response is significantly lower than that for PPD and Naf-PPD<sub>CV</sub>, although it is not significantly lower than that of PPD<sub>CV</sub> due to the large error associated with this recipe,  $p = 0.569$ . In fact the response to AA at 1000  $\mu\text{M}$  can be said to be zero, which is a remarkable result. It was considered the preferred choice for use as an interference rejection solution.

#### 6.4.4 Effects on Electrode Sensitivity of Interferent Layers

An important consideration when choosing an interferent rejection strategy is also to consider the difference, if any, they will cause in sensitivity. It had been seen before within the group that the inclusion of PPD could in some cases enhance sensitivity. Thus it was necessary to calibrate various recipes, with the interferent layers incorporated, for response to D-ser. The recipes were: Pt<sub>C</sub>-{MMA-[600UPBSx5-GA1%]x2}x2-MMA, Pt<sub>C</sub>-Naf-PPD-{MMA-[600UPBSx5-GA1%]x2}x2-MMA, Pt<sub>C</sub>-PPD-{MMA-[600UPBSx5-GA1%]x2}x2-MMA and Pt<sub>C</sub>-PPD<sub>CV</sub>-{MMA-[600UPBSx5-GA1%]x2}x2-MMA. The results are displayed in Table 11-9. The associated calculated kinetic parameters are listed in Table 6-9 and all this information is summarised in Figure 6-10.

Unfortunately the most immediate and obvious effect of the interference rejection layers is the loss of a substantial amount of sensitivity to D-ser when the Naf-PPD combination is utilised. However, while this is not a desirable effect, it is not detrimental either. The most important properties of a biosensor are selectivity and sensitivity, both must be given equal consideration and it is essential to find an appropriate combination where a compromise is reached and one parameter is not sacrificed at the expense of the other.

Electrode Design	No interferent rejection layer n = 16	with Naf-PPD n = 52	with PPD n = 4	with PPD <sub>CV</sub> n = 4
<b>Kinetics</b>	M-M-H, p = 0.0003	M-M-H, p < 0.0001	M-M, p = 0.1036	M-M-H, p = 0.0016
<b>R<sup>2</sup></b>	0.9969	0.9999	0.9982	0.9994
<b>J<sub>max</sub>, μA.cm<sup>-2</sup></b>	34.63 ± 0.66	24.08 ± 0.14	42.88 ± 0.63	40.55 ± 0.43
<b>K<sub>M</sub>, μM</b>	649.4 ± 37.2	1462 ± 23	1122 ± 69	688.3 ± 24.7
<b>α</b>	1.417 ± 0.101	1.178 ± 0.016		1.199 ± 0.051
<b>LRS, μA.cm<sup>-2</sup>.mM<sup>-1</sup></b>	53.33 ± 2.47	16.47 ± 0.18	38.22 ± 1.99	58.91 ± 1.74

Table 6-9

Kinetic parameters, fit, J<sub>max</sub> and K<sub>M</sub> values calculated from the calibration data in Table 11-9. J<sub>max</sub>, K<sub>M</sub>, α and LRS are presented as Mean ± SEM.

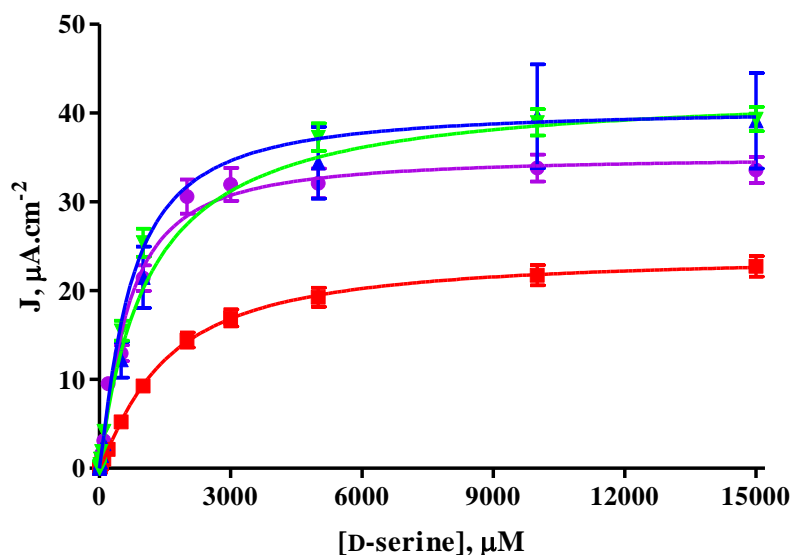


Figure 6-10

J-concentration plot of the data in Table 11-9 and Table 6-9 which elucidate the effect of interferent rejection layers on sensitivity. The purple trace is the full MMA recipe without any interferent rejection layers. The blue trace is PPD recipe, the green trace is PPD<sub>CV</sub> and the red trace is the Naf-PPD recipe.

From the J<sub>max</sub> attained by the basic recipe with no P-*o*-PD or Naf layers, there is a significant increase upon incorporation of PPD or PPD<sub>CV</sub>, p < 0.0001\*\*\* for both, as seen by the group with previous work. Conversely though, there is a significant decrease in the J<sub>max</sub> value when Naf-PPD is used, p < 0.0001\*\*\*, compared to the no interference layer, PPD and PPD<sub>CV</sub> recipes. Between the J<sub>max</sub> of the PPD protocol and the PPD<sub>CV</sub> recipe there is also a significant difference, p = 0.0012\*\*, with the PPD value the larger of the two.

There are also significant differences to be found in the K<sub>M</sub> values. There is no significant difference between the basic recipe and the PPD<sub>CV</sub> design, p = 0.3970. The

PPD protocols  $K_M$  is significantly higher than the basic and the PPD<sub>CV</sub> recipes,  $p < 0.0001^{***}$  and  $p = 0.0010^{**}$  respectively. Finally the Naf-PPD recipe has the highest  $K_M$  value of the four. It is significantly larger than the basic, PPD and PPD<sub>CV</sub> protocols,  $p < 0.0001^{***}$ ,  $p = 0.0002^{***}$  and  $p < 0.0001^{***}$  respectively. The LRS of the basic recipe is not significantly changed when PPD<sub>CV</sub> is incorporated,  $p = 0.2894$ . Both the basic and PPD<sub>CV</sub> designs has significantly higher sensitivities when compared to the recipe that has PPD included,  $p = 0.0087^{**}$  and  $p = 0.0002^{***}$  respectively. The lowest LRS is found with the Naf-PPD recipe. It is significantly lower than the basic, PPD and PPD<sub>CV</sub> designs,  $p < 0.0001^{***}$ ,  $p = 0.0016^{**}$  and  $p = 0.0002^{***}$  respectively.

This lower LRS of the Naf-PPD, as previously stated, is not a desirable result. It is possibly due to a number of reasons. The first is that the extra layers of Naf could be behaving as a diffusional barrier which is reducing the quantity of H<sub>2</sub>O<sub>2</sub>, produced in the enzymatic reaction, reaching the Pt/Ir surface of the electrode. The second possibility is that because of the charge on D-ser, its approach to the electrode and DAAO could be retarded by the anionic nature of the Naf. Thus the use of Naf proved to be a double edged sword. It was however, one that it was decided to accept. Due to the low concentrations reported for D-ser in the *in vivo* environment, the advantage of having almost no interference from AA and other electroactive species was outweighed by the loss in sensitivity associated with this advantage. Thus the decision was made that the final protocol for the design of the D-ser biosensor would be Pt<sub>C</sub>-Naf-PPD-{MMA-[600UPBSx5-GA1%]x2}x2-MMA.

## 6.5 *In Vitro* Characterisation – Stability

Having settled on a definite protocol it was now necessary to begin an extensive characterisation of the sensor and its behaviour under a variety of situations and after ‘treatments’. These treatments would hopefully reinforce the biosensor as a valid design capable of handling the *in vivo* environment and performing the task it was designed to do. Thus a range of *in vitro* treatments were devised and carried out on the biosensor design, the treatments were designed to exceed the severity of any environmental condition likely to be found *in vivo*. The first series of these tests to be devised were stability tests. These tests were designed to test how the biosensor sensitivity would be maintained over extended periods and uses.

### 6.5.1 Repeated Calibration Stability – Short Term

The first stability test was a very simple one, a repeated calibration test over a short time period, see Section 3.6.2. The calibration data for the six calibrations is listed in Table 11-10. The number of calibration points was increased to provide more concise information. Forthwith the full protocol will not be listed and only the treatment will be discussed. Below, in Table 6-10, the relevant kinetic data for the six consecutive calibrations is listed. Statistical analysis carried out on the six calibrations was one-way ANOVA in type, as the electrodes differed only by treatment.

Examining the  $J_{\max}$  values gives a first indication of the changes that occurred. Between Cal 1 and Cal 2, and Cal 1 and Cal 3 there was no significant change, both  $p > 0.0500$ . But between Cal 1 and Cal 4, 5 and 6 there was a significant decrease in  $J_{\max}$ ,  $p < 0.0010^{***}$  for all three comparisons. There was no significant change between Cal 2 and Cal 3 either,  $p < 0.0500$ . However, Cal 4, 5, and 6 all showed a significant decrease from Cal 2,  $p > 0.0010^{***}$  for all three. There was a significant drop in the  $J_{\max}$  for Cal 4, 5 and 6 compared to Cal 3,  $p < 0.0010^{***}$  in all cases. However, between Cal 4 and Cal 5 there was no significant change in the  $J_{\max}$ ,  $p > 0.0500$ . There were significant decreases to be seen between both Cal 4 and Cal 6, and Cal 5 and Cal 6,  $p < 0.0010^{***}$  for both comparisons. All of these changes are alluded to upon close examination of the  $J$  values at 15,000  $\mu\text{M}$  D-ser in Table 11-10.

The changes in the  $K_M$  concentrations are only infrequently significant. Comparing Cal 1 to the other five calibrations there is no significant change in any of them,  $p > 0.0500$ , except between Cal 1 and Cal 4, where Cal 4 is significantly higher,  $p < 0.0010^{***}$ . The  $K_M$  of Cal 2 is not significantly different from either Cal 3 or Cal 6,  $p > 0.0500$  in both cases, but Cal 4 and Cal 5 are both significantly higher,  $p < 0.0010^{***}$  and  $p < 0.0100^{**}$  respectively. The  $K_M$  concentration of Cal 3 is not significantly different from Cal 4, Cal 5 or Cal 6, all  $p > 0.0500$ . Cal 4 and Cal 5 are also non-significantly different,  $p > 0.0500$ , but the Cal 4  $K_M$  is significantly higher than the Cal 6 value,  $p < 0.0100^{**}$ . There is no significant change in the concentration between Cal 5 and Cal 6,  $p > 0.0500$ .

Calibration	Cal 1, n = 8	Cal 2, n = 8	Cal 3, n = 8
<b>Kinetics</b>	M-M, p = 0.1450	M-M-H, p = 0.0014	M-M, p = 0.4900
<b>R<sup>2</sup></b>	0.9965	0.9989	0.9979
<b>J<sub>max</sub>, μA.cm<sup>-2</sup></b>	21.54 ± 0.47	21.05 ± 0.42	20.41 ± 0.45
<b>K<sub>M</sub>, μM</b>	2114 ± 152	1927 ± 97	2502 ± 151
<b>α</b>		1.168 ± 0.047	
<b>LRS, μA.cm<sup>-2</sup>.mM<sup>-1</sup></b>	10.19 ± 0.55	10.93 ± 0.37	8.516 ± 0.339
Calibration	Cal 4, n = 8	Cal 5, n = 8	Cal 6, n = 8
<b>Kinetics</b>	M-M, p = 0.5511	M-M, p = 0.6772	M-M-H, p = 0.0047
<b>R<sup>2</sup></b>	0.9979	0.9980	0.9991
<b>J<sub>max</sub>, μA.cm<sup>-2</sup></b>	16.80 ± 0.33	17.00 ± 0.31	13.50 ± 0.27
<b>K<sub>M</sub>, μM</b>	3045 ± 174	2684 ± 148	2185 ± 111
<b>α</b>			1.131 ± 0.042
<b>LRS, μA.cm<sup>-2</sup>.mM<sup>-1</sup></b>	5.517 ± 0.223	6.336 ± 0.254	6.177 ± 0.205

Table 6-10

Kinetic parameters, fit, J<sub>max</sub> and K<sub>M</sub> values calculated from the calibration data in Table 11-10. J<sub>max</sub>, K<sub>M</sub>, α and LRS are presented as Mean ± SEM.

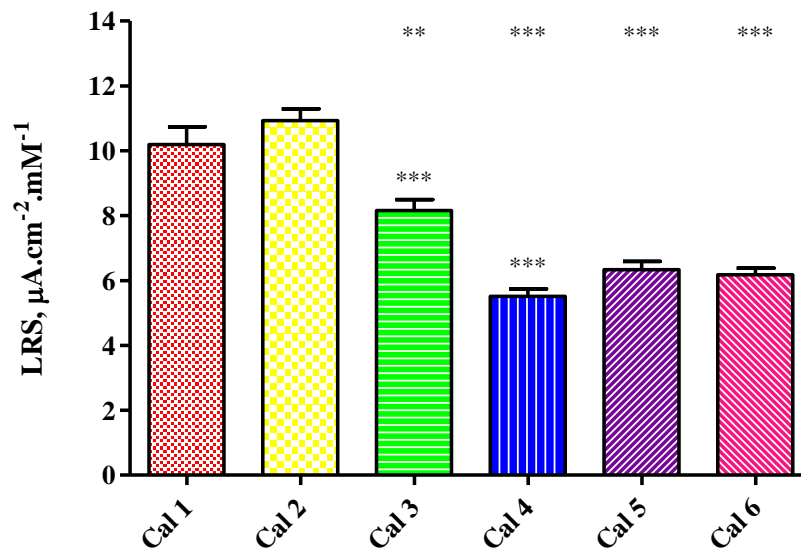


Figure 6-11

Bar chart of the sensitivities of the biosensor following repeated calibration. Stars at the top of the graph depict the significance of change compared Cal 1 and stars sitting at the top of the bar illustrate degree of change relative to the previous calibration.

The LRS values are depicted in Figure 6-11. The stars of significance at the top of the graph indicate change compared to Cal 1. The stars just at the top of the bars indicate change from the previous Cal, for example those on top of the bar for Cal 4 indicate the change relative to Cal 3. An absence of stars indicates there was no significant change. This convention will be maintained forthwith. There are significant changes to be seen in sensitivity, particularly in the range of Cal 2 to Cal 4. The LRS doesn't change between Cal 1 and Cal 2,  $p > 0.0500$ , there is a significant decrease from Cal 1 to Cal 3,

$p < 0.0100^{**}$ , and Cal 4, 5 and 6 are all also significantly lower in sensitivity compared to Cal 1,  $p < 0.0010^{***}$  for all three comparisons. Looking at Cal 2 it is found that all of Cal 3, 4, 5 and 6 result in a significantly lower LRS,  $p < 0.0010^{***}$  for all four calibrations. Cal 3 also produces a similar set of comparisons, with all of Cal 4, Cal 5 and Cal 6 significantly lower in sensitivity,  $p < 0.0010^{***}$ ,  $p < 0.0100^{**}$  and  $p < 0.0100^{**}$  respectively. Once Cal 4 has occurred there are no longer any significant changes, with Cal 4 and Cal 5, Cal 4 and Cal 6, and Cal 5 and Cal 6 not displaying any significant changes in LRS,  $p < 0.0500$  for all comparisons.

Considering the LRS results as percentages of the initial calibration the different calibrations read as follow: Cal 1 –  $100.0 \pm 5.4\%$ , Cal 2 –  $107.3 \pm 3.6\%$ , Cal 3 –  $80.0 \pm 3.3\%$ , Cal 4 –  $54.1 \pm 2.2\%$ , Cal 5 –  $62.2 \pm 2.5\%$  and Cal 6 –  $60.6 \pm 2.0\%$ . Thus after a period of initial decrease in sensitivity, the LRS appears to settle at approximately 60% of the initial value.

### 6.5.2 Repeated Calibration Stability – Long Term

The second part of the stability series was to repeat the six calibration process but over an extended period of time. The calibration data for this trial is displayed in Table 11-11 and the calculated kinetic parameters are listed in Table 6-11.

The changes that occur in the  $J_{\max}$  appear minimal when compared to Day 0 but some are significant and comparisons between other days are more often than not significant. From Day 0 there is no significant change in the  $J_{\max}$  when compared to Day 1, Day 7 or Day 21,  $p > 0.0500$  for all three. There is a significant increase, Day 0 to Day 3,  $p < 0.0500^{*}$ , and a significant decrease from Day 0 to Day 28,  $p < 0.0010^{***}$ . There are no significant changes in the  $J_{\max}$  from Day 1 to Day 3 or Day 1 to Day 7,  $p > 0.0500$  for both cases. There are, however, significant decreases from Day 1 to Day 21 and Day 1 to Day 28,  $p < 0.0100^{**}$  and  $p < 0.0010^{***}$  respectively. The  $J_{\max}$  does not change significantly between, Day 3 and Day 7,  $p > 0.0500$ , but decreases significantly from Day 3 to Day 21 and from Day 3 to Day 28,  $p < 0.0010^{***}$ . Examination of Day 21 and Day 28 also presents significantly lower  $J_{\max}$  values when compared to Day 7,  $p < 0.0010^{***}$  in both cases. Finally, there is significant change in the  $J_{\max}$  between Day 21 and Day 28,  $p > 0.0500$ .

The  $K_M$  concentrations change significantly after Day 0 and Day 1, but there after the changes are not significant. The  $K_M$  Day 0 and Day 1 do not differ significantly,  $p > 0.0500$ . But other days do differ, Days 3, 7, 21 and 28 all present concentrations that are significantly higher than Day 0,  $p < 0.0010^{***}$  for all four. Examining Day 1 it is found that there are again significant increases in the  $K_M$  values for Day 3, 7, 21 and 28,  $p < 0.0100^{**}$  for Days 3 and 7, and  $p < 0.0010^{***}$  for Days 21 and 28. However, when Day 3, Day 7, Day 21 and Day 28  $K_M$  concentrations are compared in any manner the result is a non-significant change,  $p > 0.0500$ , for all possible comparisons of  $K_M$ .

The main changes in the LRS values have been summarised in Figure 6-12. The changes are more pronounced than those for the first stability test. From the initial calibration on Day 0 all subsequent calibrations on later days display a significant reduction in sensitivity,  $p < 0.0010^{***}$  for all five days. The same is true for the Day 1 calibration, whereby the calibrations on Day 3, Day 7, Day 21 and Day 28 are all also affected by a significantly lower sensitivity,  $p < 0.0010^{***}$  for all four days. The first non-significant change comes between Day 3 and Day 7, where there is no significant difference in the LRS to be found,  $p > 0.0500$ . Day 21 has a significantly lower sensitivity than Day 3 though,  $p < 0.0100^{**}$ , as does Day 28,  $p < 0.0010^{***}$ . Days 21 and 28 also display a lower sensitivity than Day 7,  $p < 0.0010^{***}$  in both cases. Finally, there is no significant change in the LRS between Day 21 and Day 28.

In percentage terms, with Day 0 being  $100.0 \pm 1.7\%$ , the LRS of the other calibrations read as: Day 1 –  $76.9 \pm 1.6\%$ , Day 3 –  $33.1 \pm 0.8\%$ , Day 7 –  $36.6 \pm 0.8\%$ , Day 21 –  $22.3 \pm 0.6\%$  and Day 28 –  $19.8 \pm 1.3\%$ . Thus there appears to be a major decrease in sensitivity over the initial 3 days with it remaining stable for the rest of the first week and a further loss in sensitivity between week 1 and week 3.

Calibration	Day 0, n = 4	Day 1, n = 4	Day 3, n = 4
<b>Kinetics</b>	M-M-H, p < 0.0001	M-M-H, p < 0.0001	M-M, p = 0.3418
<b>R<sup>2</sup></b>	0.9996	0.9995	0.9992
<b>J<sub>max</sub>, μA.cm<sup>-2</sup></b>	19.60 ± 0.15	20.79 ± 0.24	22.99 ± 0.32
<b>K<sub>M</sub>, μM</b>	1128 ± 25	1558 ± 46	4000 ± 148
<b>α</b>	1.330 ± 0.032	1.225 ± 0.033	
<b>LRS, μA.cm<sup>-2</sup>.mM<sup>-1</sup></b>	17.37 ± 0.30	10.93 ± 0.37	5.747 ± 0.141
Calibration	Day 7, n = 4	Day 21, n = 4	Day 28, n = 4
<b>Kinetics</b>	M-M-H, p = 0.0011	M-M, p = 0.1570	M-M-H, p = 0.0415
<b>R<sup>2</sup></b>	0.9997	0.9988	0.9969
<b>J<sub>max</sub>, μA.cm<sup>-2</sup></b>	21.63 ± 0.35	18.31 ± 0.35	15.28 ± 0.91
<b>K<sub>M</sub>, μM</b>	3400 ± 128	4723 ± 220	4437 ± 553
<b>α</b>	1.091 ± 0.024		1.188 ± 0.087
<b>LRS, μA.cm<sup>-2</sup>.mM<sup>-1</sup></b>	6.363 ± 0.143	3.876 ± 0.115	3.443 ± 0.233

Table 6-11

Kinetic parameters, fit, J<sub>max</sub> and K<sub>M</sub> values calculated from the calibration data in Table 11-11. J<sub>max</sub>, K<sub>M</sub>, α and LRS are presented as Mean ± SEM.

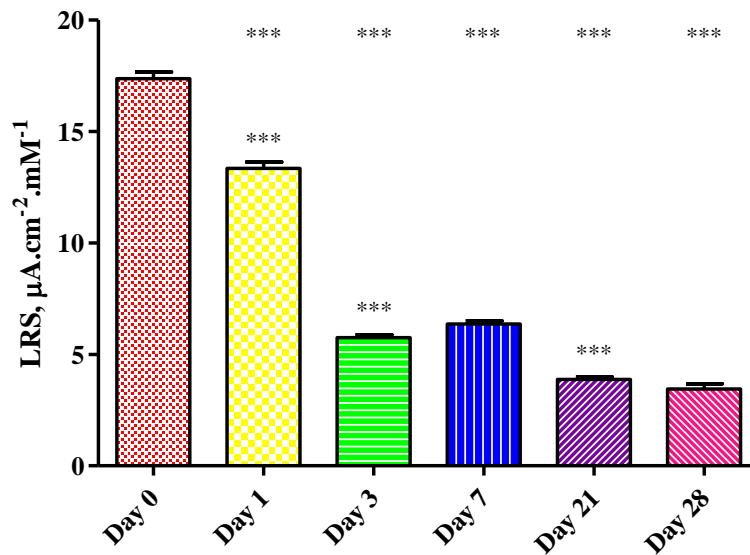


Figure 6-12

Bar chart of the sensitivities of the biosensor following repeated calibration of biosensors over a four week period. Stars at the top of the graph depict the significance of change compared Day 0 and stars sitting at the top of the bar illustrate degree of change relative to the previous calibration.

These results suggest that time between calibrations does affect the sensitivity displayed, as the closely spaced calibrations of the first stability test showed less of a decrease. However, another factor is also alluded to, that being the repeated cooling and reheating of the electrodes and dAAO when they are stored at 4 °C between calibrations. This factor is also hinted at in the short term stability testing whereby the largest decrease in sensitivity occurred between Cal 3 and Cal 4 when the electrodes were stored at 4 °C overnight before Cal 4, 5 and 6 were carried out the following day.

Indeed, the electrodes were stable over the course of the three calibrations on the second day. Thus not only does it appear that time affects the sensitivity but also a repeated cooling of the electrodes, below the temperature where the enzyme is designed to be active, and reheating to a temperature close to a physiological level for calibration, 25 °C.

### 6.5.3 Long Term Stability – Shelf Life Study

The final component of the stability testing was to test biosensors with only two calibrations – a shelf-life test. The results of the calibrations are displayed below in Table 11-12, with the corresponding kinetic fits detailed in Table 6-12.

Statistically there is no difference between the  $J_{\max}$  values of Day 0 and Day 21,  $p = 0.1384$ . A significant difference does appear between Day 0 and Day 28, with Day 28 displaying the larger value,  $p = 0.0098^{**}$ . There is also a significant increase in  $J_{\max}$  from Day 21 to Day 28,  $p = 0.0224^*$ . The  $K_M$  concentration of Day 0 is significantly lower than the Day 21 and Day 28 concentration,  $p = 0.0009^*$  and  $p = 0.0015^{**}$  respectively. Between Day 21 and 28 however there is no significant change in the  $K_M$  value,  $p = 0.0987$ .

The sensitivities decline significantly after the initial Day 0 calibrations. Both Day 21 and 28 are significantly lower,  $p < 0.0001^{***}$ . The Day 21 LRS is also significantly lower than the Day 28 value,  $p = 0.0050^{**}$ . In terms of percentage of the Day 0 calibration, the results are as follows: Day 0 –  $100.0 \pm 0.7 \%$ , Day 21 –  $43.0 \pm 1.3 \%$  and Day 28 –  $52.3 \pm 1.7 \%$ . The Day 21 and Day 28 LRS results are higher than those for the long term repeated calibration results for the same time between calibrations. This reinforces the theory that repeated calibration affects the sensitivity. They are also decreased compared to Cal 1 - 6 in the short term study, and Day 1 in the long term study, again reinforcing the theory that time and temperature fluctuations also affect the sensitivity. The significant increase in sensitivity between Day 21 and Day 28 could possibly indicate that given long enough, after the first calibration, the components of the biosensor are slowly interacting and arriving at a stable configuration.

Calibration	Day 0, n = 8	Day 21, n = 4	Day 28, n = 4
Kinetics	M-M-H, $p < 0.0001$	M-M, $p < 0.0001$	M-M, $p = 0.3418$
$R^2$	0.9996	0.9962	0.5406
$J_{\max}$ , $\mu\text{A}\cdot\text{cm}^{-2}$	$27.28 \pm 0.10$	$28.21 \pm 0.45$	$30.27 \pm 0.50$
$K_M$ , $\mu\text{M}$	$1489 \pm 14$	$3582 \pm 157$	$3160 \pm 149$
$\alpha$	$1.188 \pm 0.010$		
LRS, $\mu\text{A}\cdot\text{cm}^{-2}\cdot\text{mM}^{-1}$	$18.32 \pm 0.12$	$7.876 \pm 0.235$	$9.579 \pm 0.316$

Table 6-12

Kinetic parameters, fit,  $J_{\max}$  and  $K_M$  values calculated from the calibration data in Table 11-12.  $J_{\max}$ ,  $K_M$ ,  $\alpha$  and LRS are presented as Mean  $\pm$  SEM.

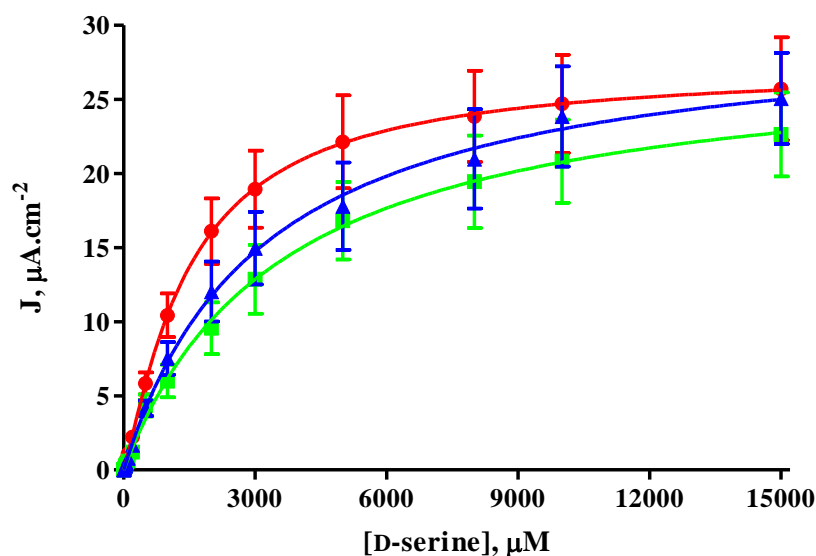


Figure 6-13

$J$ -concentration plot of the effect an extended period of storage would have on the biosensor. In red is the response at Day 0. The green trace depicts Day 21 and the blue trace Day 28.

## 6.6 *In Vitro* Characterisation – Bio-Compatibility

A second important set of characterisation tests carried out on the biosensors were designed to test the biocompatibility of the biosensors. This means attempting to determine how they would react in an *in vivo* environment and how that environment would react to them. Would the native constituents attack the biosensor components or encase it to protect the brain? To try to elucidate the influence of these factors a series of tests were carried out which would test the biosensor compatibility with protein, lipid and the brain tissue from a rat (Kane & O'Neill, 1998).

### 6.6.1 BSA 1% Treatment

The first bio-compatibility treatment used involved the protein BSA (as used previously in various biosensor protocols). This protein was made up as a 1 % solution and after an initial Day 0 calibration the sensors were stored in this solution at 4 °C, and calibrated again on Day 1, Day 3, Day 7, Day 10 and Day 14. The calibration data is listed in Table 11-13 and the associated kinetic fit and parameters are shown in Table 6-13.

It is immediately clear, both from the two tables of data and Figure 6-14, that the treatment with BSA 1% causes radical changes in all parameters of the biosensor. Beginning with the  $J_{\max}$  values, it can be seen that compared to Day 0 all other days have significantly reduced values,  $p < 0.0010^{***}$  for all. There is no significant change between Day 1 and Day 3,  $p > 0.0500$ . However, all of Day 7, 10 and 14 are significantly lower than both Day 1 and Day 3,  $p < 0.0010^{***}$  in all cases. The  $J_{\max}$  for Day 10 and 14 are also significantly lower than that shown by Day 7,  $p < 0.0010^{***}$  for both. There is no significant difference between the  $J_{\max}$  of Day 10 and Day 14,  $p > 0.0050$ .

The  $K_M$  values are also significantly affected by the treatment. From the initial low of Day 0, there is a significant increase observed when compared to Day 1,  $p < 0.0100^{**}$ , Day 3,  $p < 0.0010^{***}$ , Day 7,  $p < 0.0010^{***}$ , and Day 14,  $p < 0.0010^{***}$ . There is no significant difference between Day 0 and Day 10,  $p > 0.0500$ . Between Day 1 and Day 3 and Day 1 and Day 7 there are also significant increases in the  $K_M$  concentration to be observed,  $p < 0.0010^{***}$  in both cases. Again there is no significant difference between Day 1 and Day 10,  $p > 0.0500$ . However there is a significant increase between Day 1 and Day 14,  $p < 0.0010^{***}$ . There are no significant differences between Day 3 and 7, Day 3 and 14, or Day 7 and 14,  $p > 0.0500$  in all three cases. Day 10 is has a significantly lower concentration calculated for its  $K_M$  than either Day 3, Day 7 or Day 14,  $p < 0.0010^{***}$  in all instances.

Calibration	Day 0, n = 4	Day 1, n = 4	Day 3, n = 4
<b>Kinetics</b>	M-M-H, p < 0.0001	M-M-H, p = 0.0013	M-M, p = 0.1926
<b>R<sup>2</sup></b>	0.9996	0.9995	0.9992
<b>J<sub>max</sub>, μA.cm<sup>-2</sup></b>	23.26 ± 0.40	17.94 ± 0.38	19.25 ± 0.95
<b>K<sub>M</sub>, μM</b>	1536 ± 69	4287 ± 205	8069 ± 800
<b>α</b>	1.237 ± 0.052	1.108 ± 0.028	
<b>LRS, μA.cm<sup>-2</sup>.mM<sup>-1</sup></b>	15.15 ± 0.48	4.184 ± 0.113	2.386 ± 0.127
Calibration	Day 7, n=4	Day 10, n = 4	Day 14, n = 4
<b>Kinetics</b>	M-M, p = 0.1648	M-M-H, p = 0.0104	M-M, p = 0.1655
<b>R<sup>2</sup></b>	0.9997	0.9988	0.9969
<b>J<sub>max</sub>, μA.cm<sup>-2</sup></b>	11.63 ± 0.31	5.580 ± 0.417	7.231 ± 0.211
<b>K<sub>M</sub>, μM</b>	9524 ± 476	3329 ± 433	8992 ± 510
<b>α</b>		1.805 ± 0.318	
<b>LRS, μA.cm<sup>-2</sup>.mM<sup>-1</sup></b>	1.221 ± 0.031	1.676 ± 0.123	0.8041 ± 0.0235

Table 6-13

Kinetic parameters, fit, J<sub>max</sub> and K<sub>M</sub> values calculated from the calibration data in Table 11-13. J<sub>max</sub>, K<sub>M</sub>, α and LRS are presented as Mean ± SEM.

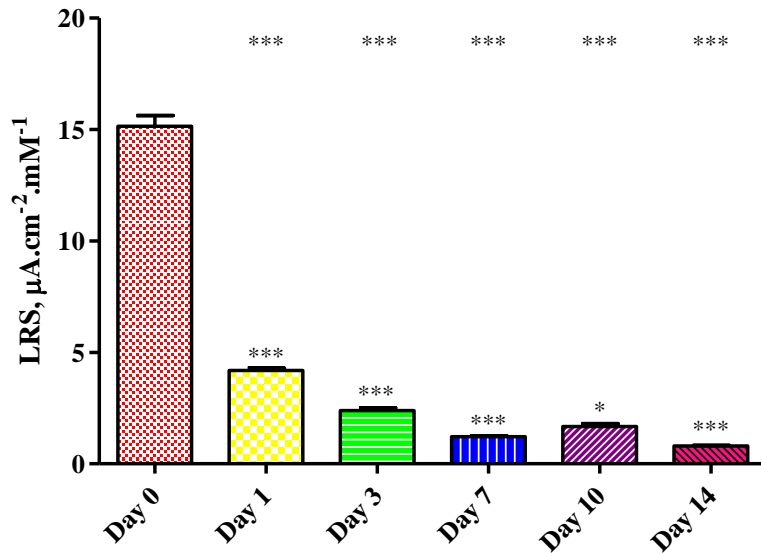


Figure 6-14

Bar chart of the sensitivities of the biosensor following storage in a BSA 1% solution over two weeks.

The changes that occur in the sensitivities of the electrodes are illustrated in Figure 6-14. It is easy to see that the changes are quite dramatic. From the initial high of Day 0, all other days in comparison are significantly less sensitive, p < 0.0010\*\*\* for all days. Day 3, 7, 10 and 14 also have significantly lower LRS values than Day 1, p < 0.0010\*\*\* in all instances. All sensitivities are again reduced when then compared to Day 3, p < 0.0010\*\*\* for Day 7 and Day 14 and p < 0.0100\*\* for Day 10. Between Day 7 and Day 10, there is a significant increase in the LRS, p < 0.0500\*, and there is a non-significant change between Day 7 and Day 14, p > 0.0500. There is, finally, a significant decrease from Day 10 to Day 14, p < 0.0010\*\*\*.

Converting the LRS values to a percentage of the initial Day 0 starting value the extent of the changes becomes clear. The percentages are: Day 0 –  $100.0 \pm 3.2\%$ , Day 1 –  $27.6 \pm 0.7\%$ , Day 3 –  $15.7 \pm 0.8\%$ , Day 7 –  $8.1 \pm 0.2\%$ , Day 10 –  $11.1 \pm 0.8\%$  and Day 14 –  $5.3 \pm 0.2\%$ . Thus in the first day of the treat over 70% of sensitivity is lost. From that point until Day 3 a further 30% of the remaining sensitivity is lost. By Day 14 there has been a loss of approximately 95% of the initial sensitivity.

As a rough guide to the amount of this decrease that has been caused by the BSA 1% and not the other factors previously discussed it is useful to use the percentage changes encountered in Section 6.5.2. The effects of the 4 °C storage conditions and subsequent heating and cooling of the electrodes, six calibrations on the same biosensors, and an extended time period (although not as long in the case of the BSA 1% treatment) are all built into the percentage changes obtained in that study. Thus, subtracting the percentage changes in that section from the changes in this section will give a guide to the effect of just the BSA 1%. When this is done the extra degradation caused by the BSA 1% treatment are as follows: Day 1 –  $49 \pm 2.4\%$ , Day 3 –  $17.3 \pm 1.7\%$ , Day 7 –  $28.6 \pm 1.0\%$ , Day 10 –  $11.3 \pm 1.5\%$ , Day 14 –  $14.5 \pm 1.5\%$ .

### 6.6.2 BSA 10% Treatment

In continuation of the bio-compatibility test a further protein treatment study was conducted. This time a BSA 10% solution was used. The same experimental protocol as for BSA 1% was followed with electrodes being calibrated six times from Day 0 – Day 14, with the same intervals. The data obtained from the calibration is listed in Table 11-14 and Table 6-14.

Each day after the Day 0 calibration has a significantly lower  $J_{\max}$  than the Day 0 value,  $p < 0.0010^{***}$  for Day 1, 3, 7, 10 and 14. Between Day 1 and Day 3 there is a significant decrease in  $J_{\max}$ ,  $p < 0.0100^{**}$ . Day 7, Day 10 and Day 14 all have a significantly lower  $J_{\max}$  than the Day 1 value,  $p < 0.0010^{***}$  for all comparisons. The same is true for Day 3, where again, the Day 7, 10 and 14 values of  $J_{\max}$  are significantly decreased,  $p < 0.0010^{***}$ . After the Day 7 calibration there is a significant decrease to Day 10,  $p < 0.0500^*$ , and Day 14,  $p < 0.0010^{***}$ . But there is no significant difference between Day 10 and Day 14 when the  $J_{\max}$  values are compared,  $p > 0.0500$ .

Calibration	Day 0, n = 4	Day 1, n = 4	Day 3, n = 4
<b>Kinetics</b>	M-M-H, p < 0.0001	M-M, p = 0.1118	M-M, p = 0.5193
<b>R<sup>2</sup></b>	0.9997	0.9995	0.9994
<b>J<sub>max</sub>, μA.cm<sup>-2</sup></b>	31.57 ± 0.31	23.08 ± 0.23	20.52 ± 0.29
<b>K<sub>M</sub>, μM</b>	1714 ± 45	3209 ± 92	5116 ± 173
<b>α</b>	1.147 ± 0.024		
<b>LRS, μA.cm<sup>-2</sup>.mM<sup>-1</sup></b>	18.42 ± 0.33	7.193 ± 0.144	4.010 ± 0.085
Calibration	Day 7, n = 4	Day 10, n = 4	Day 14, n = 4
<b>Kinetics</b>	M-M-H, p = 0.0254	M-M, p = 0.1488	M-M-H, p = 0.0459
<b>R<sup>2</sup></b>	0.9972	0.9929	0.9982
<b>J<sub>max</sub>, μA.cm<sup>-2</sup></b>	13.35 ± 0.64	10.80 ± 0.50	10.09 ± 0.59
<b>K<sub>M</sub>, μM</b>	3534 ± 372	4800 ± 545	5807 ± 702
<b>α</b>	1.184 ± 0.082		1.133 ± 0.065
<b>LRS, μA.cm<sup>-2</sup>.mM<sup>-1</sup></b>	3.778 ± 0.228	2.251 ± 0.162	1.737 ± 0.110

Table 6-14

Kinetic parameters, fit, J<sub>max</sub> and K<sub>M</sub> values calculated from the calibration data in Table 11-14. J<sub>max</sub>, K<sub>M</sub>, α and LRS are presented as Mean ± SEM.

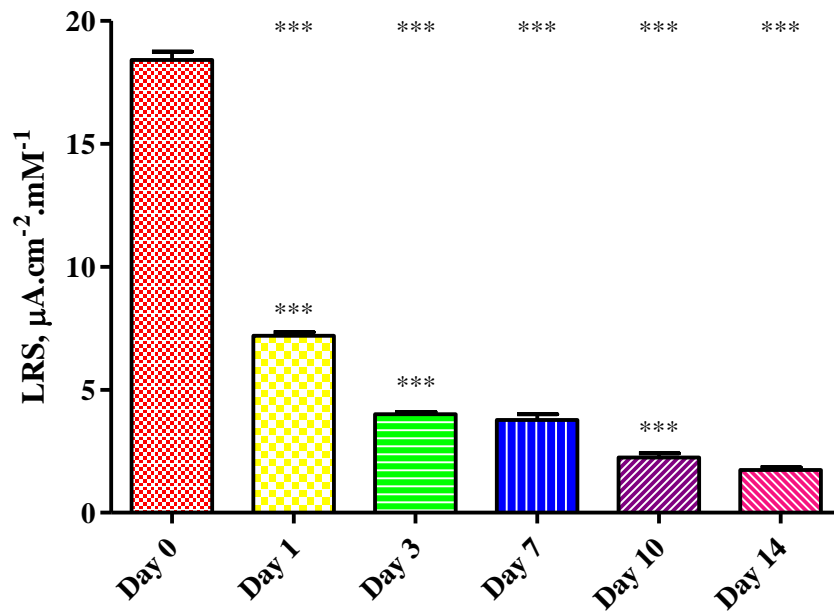


Figure 6-15

Bar chart of the sensitivities of the biosensor following storage in a BSA 10% solution over two weeks.

There are fewer significant changes in the K<sub>M</sub> concentrations that were calculated for the 6 calibrations. The K<sub>M</sub> of Day 0 and Day 1 do not vary significantly, p > 0.0500. But the concentrations for Day 3, 7, 10 and 14 are all significantly higher than that of Day 0, p < 0.0010\*\*\* for Day 3, 10 and 14 and p < 0.0500\* for Day 10. From the Day 1 value of K<sub>M</sub> there is a significant increase at Day 3 and Day 14, p < 0.0500\* and p < 0.0100\*\* respectively. But there is no significant difference between Day 1 and 7 or Day 1 and 10, p > 0.0500 for both. Following the Day 3 calibration there is no significant change

in the  $K_M$  concentration for any of Day 7, 10 or 14,  $p > 0.0500$  for all three. There is also no difference between the  $K_M$  of Day 7 and Day 10,  $p > 0.0500$ , but Day 14 shows a significant increase when compared to Day 7,  $p < 0.0100^{**}$ .

As per the previous section the changes in the LRS of the biosensors, when treated with BSA 10%, are displayed graphically in Figure 6-15. It can be seen that all subsequent days display a lower sensitivity than that for Day 0,  $p < 0.0010^{***}$  for all days (see the stars at the top of the bar chart). There is a similar picture when the LRS for Day 1 is considered and compared to the subsequent calibrations, again all are significantly lower,  $p < 0.0010^{***}$  for all comparisons. Between Day 3 and Day 7 however, there is no significant change in the sensitivity value,  $p > 0.0500$ . However, both Day 10 and 14 are significantly lower than not only the Day 3 LRS,  $p < 0.0010^{***}$  for both, but also when compared to the Day 7 sensitivity,  $p < 0.0010^{***}$  for both. Lastly, there is no significant change in the LRS when Day 10 is compared with Day 14,  $p > 0.0500$ .

As before, consideration of the LRS values in terms of percentage of the Day 0 value helps elucidate the changes that occurred. The percentages read as follows: Day 0 –  $100 \pm 1.8\%$ , Day 1 –  $39.1 \pm 0.8\%$ , Day 3 –  $21.8 \pm 0.5\%$ , Day 7 –  $20.5 \pm 1.2\%$ , Day 10 –  $12.2 \pm 0.9\%$ , Day 14 –  $9.4 \pm 0.6\%$ . Now, using the same analysis as was used for BSA 1% to eliminate the deterioration in sensitivity caused by other factors, the results for the long-term stability trials are subtracted. Application of this process results in values, which approximate the extra reduction in sensitivity solely to BSA 10%, they are: Day 1 –  $37.8 \pm 2.4\%$ , Day 3 –  $11.3 \pm 1.3\%$ , Day 7 –  $16.1 \pm 2.1\%$ , Day 10 –  $10.1 \pm 1.5\%$ , and Day 14 –  $10.4 \pm 1.9\%$ .

The BSA 10% treatment has less of an effect on sensitivity than the 1% treatment. This is not without precedent as an earlier biosensor design for D-serine also demonstrated this unusual characteristic. It is most likely due to the 1% solution being of the right concentration to bind to available sites in the biosensor matrix and block up the pores within the matrix as well as the enzyme channels and to remain firmly set there. However, with the 10% solution the greater quantity and mass of BSA being deposited onto the biosensor is more easily de-adsorbed from the surface once transferred to the calibration cell, due to the increased weight and thickness of the layer and the greater concentration difference with the bulk solution.

### 6.6.3 PEA 1% Treatment

The third component of the bio-compatibility study was to examine what would happen to the biosensor when it was exposed to a lipid. The lipid chosen was PEA, and it was made up as a 1% solution. The electrodes were stored in this solution over a two week period, during which six calibrations were carried out, again on Day 0, Day 1, Day 3, Day 7, Day 10 and Day 14. The calibration data for these tests is displayed in Table 11-15, along with the accompanying kinetic parameters in Table 6-15.

Similar to the results of the protein treatment trial, the electrodes show a deterioration in the vital kinetic parameters following treatment with the lipid PEA 1% solution. This is very evident when the  $J_{\max}$  values are considered. When comparing the value obtained for any day to the  $J_{\max}$  value of any day later in the trial, the later day always has a significantly reduced value,  $p < 0.0010^{***}$  for all cases where Days 0, 1, 3 and 7 are the first day chosen in the comparison. The only time this is not the case is when Day 10 is compared to Day 14, in this case there has been no significant change in the calculated  $J_{\max}$ ,  $p > 0.0500$ . Thus the  $J_{\max}$  undergoes a regular and consistently significant decrease until the very last day of the trial.

There are fewer significant changes in the concentrations calculated for the Michaelis-Menten constant,  $K_M$ . Initially there is a non-significant change between Day 0 and Day 1,  $p > 0.0500$ , followed by a significant increase on Day 3 compared to Day 0,  $p < 0.0500^*$ . Days 7, 10 and 14 all then have a significantly higher  $K_M$  compared to Day 1. When Day 1 is considered in comparison to Day 3 no significant change is found to have occurred,  $p > 0.0500$ . However, Day 7, Day 10 and Day 14 all display significantly higher  $K_M$  concentrations,  $p < 0.0100^{**}$ ,  $p < 0.0500^*$  and  $p < 0.0010^{***}$  respectively. Day 7 and Day 10 present no significant change compared to Day 3,  $p > 0.0500$  for both, but there is a significant increase when Day 14 is compared to Day 3,  $p < 0.0100^{**}$ . The concentrations calculated for Day 10 and Day 14 are not significantly different from that calculated for Day 7,  $p > 0.0500$  in both instances, and there is also a non significant change between Day 10 and Day 14,  $p > 0.0500$ .

Calibration	Day 0, n = 4	Day 1, n = 4	Day 3, n = 4
<b>Kinetics</b>	M-M-H, p < 0.0001	M-M-H, p < 0.0001	M-M, p = 0.9007
<b>R<sup>2</sup></b>	0.9994	0.9998	0.9992
<b>J<sub>max</sub>, μA.cm<sup>-2</sup></b>	26.32 ± 0.25	23.99 ± 0.24	17.44 ± 0.27
<b>K<sub>M</sub>, μM</b>	1141 ± 31	2465 ± 56	4709 ± 179
<b>α</b>	1.365 ± 0.040	1.233 ± 0.023	
<b>LRS, μA.cm<sup>-2</sup>.mM<sup>-1</sup></b>	23.07 ± 0.47	9.733 ± 0.138	3.704 ± 0.090
Calibration	Day 7, n =4	Day 10, n = 4	Day 14, n = 4
<b>Kinetics</b>	M-M, p = 0.9071	M-M, p = 0.5080	M-M, p = 0.0588
<b>R<sup>2</sup></b>	0.9972	0.9991	0.9870
<b>J<sub>max</sub>, μA.cm<sup>-2</sup></b>	10.56 ± 0.38	4.808 ± 0.090	4.610 ± 0.432
<b>K<sub>M</sub>, μM</b>	7049 ± 539	6282 ± 260	9139 ± 1647
<b>α</b>			
<b>LRS, μA.cm<sup>-2</sup>.mM<sup>-1</sup></b>	1.498 ± 0.064	0.7653 ± 0.0186	0.5044 ± 0.0466

Table 6-15

Kinetic parameters, fit, J<sub>max</sub> and K<sub>M</sub> values calculated from the calibration data in Table 11-15. J<sub>max</sub>, K<sub>M</sub>, α and LRS are presented as Mean ± SEM.

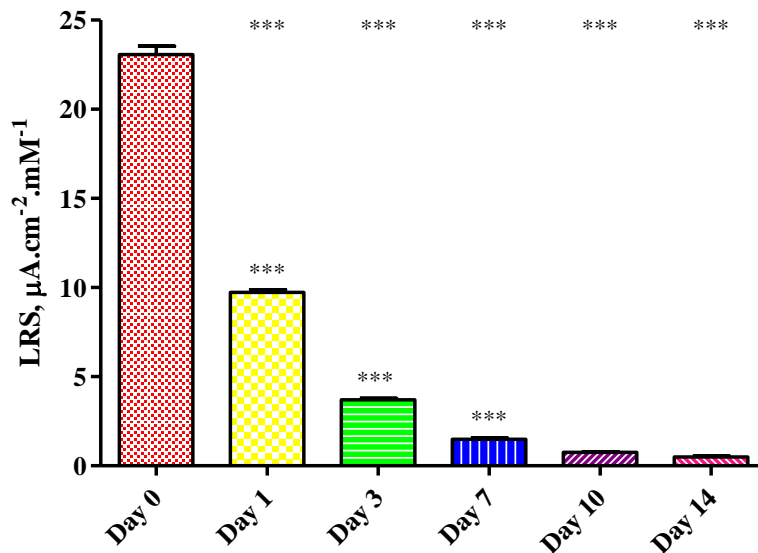


Figure 6-16

Bar chart of the sensitivities of the biosensor following storage in a PEA 1% solution over two weeks.

The bar chart in Figure 6-16 gives an indication of the changes that occur in the LRS values over the course of the treatment. In nearly all cases the changes are significant. The only two non-significant results are illustrated in the chart. Those comparisons are between Day 7 and Day 10, and Day 10 and Day 14, p > 0.0500. All other possible comparisons between the six days are significantly different, p < 0.0010\*\*\* in all cases, with the later Day or calibration resulting in a significantly lower sensitivity.

The LRS values as a percentage of the initial Day 0 value are as follows: Day 0 – 100 ± 2.1%, Day 1 – 42 ± 0.6%, Day 3 – 16.1 ± 0.4%, Day 7 – 6.5 ± 0.3%, Day 10 – 3.3 ±

0.1% and Day 14 –  $2.2 \pm 0.2\%$ . Removing the other factors which are involved in the degradation of the biosensor sensitivity gives an approximate quantification of the effect of the PEA 1% solution. The percentage extra degradation attributable to the PEA 1% solution is: Day 1 –  $34.7 \pm 2.2\%$ , Day 3 –  $17.0 \pm 1.2\%$ , Day 7 –  $30.1 \pm 1.1\%$ , Day 10 –  $19.0 \pm 1.7\%$  and Day 14 –  $17.6 \pm 1.5\%$ . Thus the PEA 1% solution contributed about a 25% extra loss in sensitivity at any particular time.

#### 6.6.4 PEA 10% Treatment

As with the BSA protein treatment, the PEA lipid treatment was repeated with the PEA concentration being increased to 10%. The calibration data is listed in Table 11-16, and the associated kinetic fits and parameters are shown in Table 6-16.

There are significant changes across all of the  $J_{max}$  values for this PEA 10% study. Every single value is significantly lower than those before it. Examining Day 0, all subsequent days show a significant fall in  $J_{max}$ ,  $p < 0.0010^{***}$  for all days when compared to Day 0. The same is true for Day 1, with Day 3, 7, 10 and 14 all significantly lower,  $p < 0.0010^{***}$  for all comparisons. From the  $J_{max}$  value of Day 3, there are significant decreases observed to Day 7, 10 and 11,  $p < 0.0100^{**}$ ,  $p < 0.0010^{***}$  and  $p < 0.0010^{***}$  respectively. At Day 7 the  $J_{max}$  is significantly larger than its value at Day 10 or Day 14,  $p < 0.0010^{***}$  in both instances. Lastly, the  $J_{max}$  at Day 14 is significantly lower than the  $J_{max}$  observed at Day 10.

Calibration	Day 0, n = 4	Day 1, n = 4	Day 3, n = 4
<b>Kinetics</b>	M-M-H, $p < 0.0001$	M-M-H, $p = 0.0072$	M-M-H, $p = 0.0235$
<b>R<sup>2</sup></b>	0.9996	0.9960	0.9915
<b>J<sub>max</sub>, <math>\mu\text{A}\cdot\text{cm}^{-2}</math></b>	$34.35 \pm 0.40$	$16.48 \pm 0.57$	$12.49 \pm 0.70$
<b>K<sub>M</sub>, <math>\mu\text{M}</math></b>	$1871 \pm 55$	$1929 \pm 163$	$2382 \pm 298$
<b><math>\alpha</math></b>	$1.193 \pm 0.030$	$1.282 \pm 0.102$	$1.332 \pm 0.158$
<b>LRS, <math>\mu\text{A}\cdot\text{cm}^{-2}\cdot\text{mM}^{-1}</math></b>	$18.36 \pm 0.36$	$8.534 \pm 0.480$	$5.245 \pm 0.411$
Calibration	Day 7, n =4	Day 10, n = 4	Day 14, n = 4
<b>Kinetics</b>	M-M, $p = 0.3242$	M-M, $p = 0.9936$	M-M, $p = 0.2480$
<b>R<sup>2</sup></b>	0.9992	0.9921	0.9943
<b>J<sub>max</sub>, <math>\mu\text{A}\cdot\text{cm}^{-2}</math></b>	$9.294 \pm 0.303$	$5.137 \pm 0.542$	$2.677 \pm 0.334$
<b>K<sub>M</sub>, <math>\mu\text{M}</math></b>	$15481 \pm 813$	$15357 \pm 2619$	$23416 \pm 4188$
<b><math>\alpha</math></b>			
<b>LRS, <math>\mu\text{A}\cdot\text{cm}^{-2}\cdot\text{mM}^{-1}</math></b>	$0.6004 \pm 0.0127$	$0.3345 \pm 0.0231$	$0.1143 \pm 0.0653$

Table 6-16

Kinetic parameters, fit,  $J_{max}$  and  $K_M$  values calculated from the calibration data in Table 11-16.  $J_{max}$ ,  $K_M$ ,  $\alpha$  and LRS are presented as Mean  $\pm$  SEM.

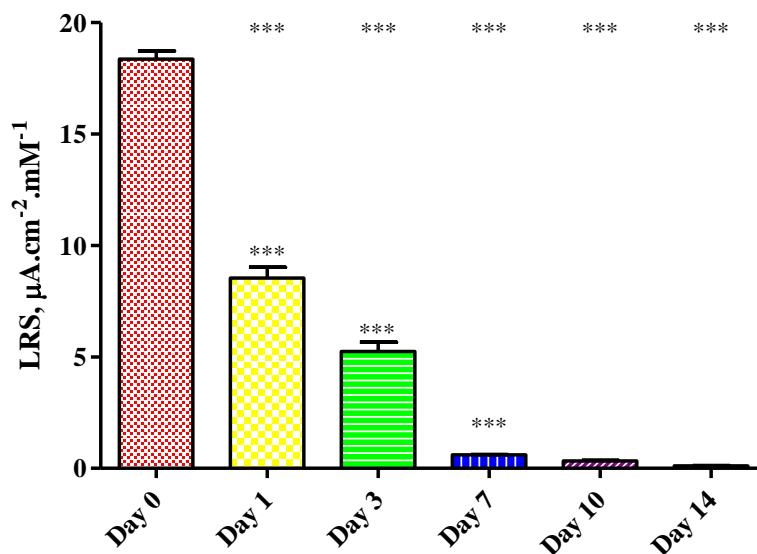


Figure 6-17

Bar chart of the sensitivities of the biosensor following storage in a PEA 10% solution over two weeks.

From Table 6-16 it should also be clear that there are some significant changes in the  $K_M$  concentrations observed over the two week trial period. Comparing Day 0 with Day 1 and Day 0 with Day 3, there is statically a non-significant difference between the concentrations,  $p > 0.0500$  for both. However, when compared to Day 0 there is a significant increase in the  $K_M$  for Day 7,  $p < 0.0100^{**}$ , Day 10,  $p < 0.0100^{**}$ , and Day 14,  $p < 0.0010^{***}$ . There is a non-significant change between Day 1 and Day 3,  $p > 0.0500$ . Taking the  $K_M$  of Day 1 and Day 3 it is found that there are significant increases to be observed when they are compared to Day 7,  $p < 0.0100^{**}$  for both, Day 10,  $p < 0.0100^{**}$  for both, and Day 14,  $p < 0.0010^{***}$  for both also. The  $K_M$  concentrations of Day 7 compared to Day 10 and 14, and Day 10 compared to Day 14 are all not significantly different,  $p > 0.0050$  in all three cases.

The illustration of the LRS values in Figure 6-17, demonstrates the size and significance of the changes that occurred over the two weeks the biosensors were treated with PEA 10%. When the Day 0 LRS is compared to any value that was observed afterwards there is a significant decrease associated with it,  $p < 0.0010^{***}$ . The same is true when the same comparisons are performed with either the Day 1 LRS or Day 3 LRS, where all subsequent values are significantly lower,  $p < 0.0010^{***}$  in all cases. Comparing the sensitivity of Day 7 to Day 10 or Day 14 and the sensitivity of Day 10 to Day 14, there are no significant differences to found,  $p > 0.0500$  for the three pairs of values.

The conversion of the LRS values to a percentage of the initial value yields: Day 0 –  $100.0 \pm 2.0\%$ , Day 1 –  $46.5 \pm 2.6\%$ , Day 3 –  $28.5 \pm 2.2\%$ , Day 7 –  $3.3 \pm 0.1\%$ , Day 10 –  $1.8 \pm 0.1\%$  and Day 14 –  $0.62 \pm 0.04\%$ . As in previous cases, removing the effects accumulated when the long-term stability test was run gives an approximate indication of the further degradation caused solely by the PEA 10%: Day 1 –  $30.3 \pm 4.2\%$ , Day 3 –  $4.5 \pm 3.0\%$ , Day 7 –  $33.4 \pm 0.9\%$ , Day 10 –  $20.5 \pm 0.8\%$  and Day 14 –  $19.2 \pm 1.4\%$ .

### 6.6.5 Brain Tissue Treatment

The final component of the bio-compatibility trials was an *ex vivo* trial. This involved the treatment of the electrodes with a segment of brain tissue from a Wistar rat, as it has been extensively shown that exposure to the brain can reduce the sensitivity of enzymatic biosensors by 70% (Garguilo & Michael, 1995; Wilson & Gifford, 2005), which was attributable solely to fouling caused by biological molecules. It is well known that implantation of a device into brain tissue and the associated brain injury triggers a foreign body response (FBR) (Morais *et al.*, 2010). This FBR results a cascade of acute responses for inflammatory and wound healing purposes. The substances released in this environment are responsible for the loss of sensitivity seen with implantation and the brain tissue test is an attempt to quantify its effects on the biosensor. These effects have also been shown for non-enzymatic sensors to varying degrees (Brown *et al.*, 2009; Bolger *et al.*, 2011a) and in particular for carbon paste electrodes (Ormonde & O'Neill, 1989, 1990; Bolger *et al.*, 2011b).

The brain was removed from a subject less than one hour post-mortem and immediately frozen without cleaning or preservation techniques. This ensured that as much of the natural substances found in the brain were retained in the sample. When the trial was to be conducted, a  $5 \text{ mm}^3$  segment was cut off the frozen brain and allowed to thaw. Once thawed the sample was placed into a container with 0.5 mL of water. This prevented the tissue from drying out and adhering to the electrode surface. If the sample dried out, removing or inserting the electrodes would lead to substantial amounts of damage to the electrodes. The electrodes were inserted into the tissue sample, so that the active surface was completely immersed into the tissue, after initial calibration. They were stored this way, at 4 °C, between subsequent calibrations. The calibration data for the trial, which took place over two weeks, is displayed in Table 11-17 with the associated kinetic fit and constants listed in Table 6-17.

It is quite apparent from the kinetic data that there are differences in the  $J_{\max}$  values over the course of the treatment. In fact, these differences are large enough to be significant in all cases. For each comparison possible, the later calibration has a significantly reduced  $J_{\max}$  compared to the earlier calibration,  $p < 0.0010^{***}$  for all instances except that of Day 3 compared to Day 7 where  $p < 0.0100^{**}$ . The  $K_M$  values also undergo change; however they are only significant when considering comparisons involving Day 0. From Day 0 the concentration increases significantly when compared to Day 1 and Day 3,  $p < 0.0500^*$  for both, Day 7,  $p < 0.0100^{**}$ , and Day 14,  $p < 0.0010^{***}$ . However, after Day 0, from Day 1 forward there are no more significant changes to be found. All comparisons involving solely Day 1, 3, 7 & 14 are non-significantly different,  $p > 0.0500$ . This is a positive result, demonstrating that, despite a decreasing  $J_{\max}$ , after an initial increase in the  $K_M$  the kinetic curve retains at least one constant parameter. This is despite the harsh treatment of repeated calibrations and long-term storage in brain tissue. Previous studies have only looked at the effect after a few hours of implantation (Ormonde & O'Neill, 1990; Garguilo & Michael, 1995) or for two calibrations over 3 days (Bolger *et al.*, 2011a).

Calibration	Day 0, n = 4	Day 1, n = 4	Day 3, n = 4	Day 7, n = 4	Day 14, n = 4
<b>Kinetics</b>	M-M-H, $p < 0.0001$	M-M, $p = 0.9706$	M-M-H, $p < 0.0001$	M-M, $p = 0.5680$	M-M-H, $p = 0.0427$
<b>R<sup>2</sup></b>	0.9996	0.9959	0.9963	0.9843	0.9962
<b>J<sub>max</sub>, μA.cm<sup>-2</sup></b>	14.80 ± 0.10	9.372 ± 0.228	7.126 ± 0.207	5.849 ± 0.297	3.299 ± 0.156
<b>K<sub>M</sub>, μM</b>	920.0 ± 19.7	2183 ± 172	2222 ± 136	2527 ± 396	2915 ± 312
<b>α</b>	1.331 ± 0.030		1.573 ± 0.123		1.202 ± 0.095
<b>LRS, μA.cm<sup>-2</sup>.mM<sup>-1</sup></b>	16.09 ± 0.27	4.293 ± 0.254	3.207 ± 0.130	2.315 ± 0.265	1.132 ± 0.072

Table 6-17

Kinetic parameters, fit,  $J_{\max}$  and  $K_M$  values calculated from the calibration data in Table 11-17.  $J_{\max}$ ,  $K_M$ ,  $\alpha$  and LRS are presented as Mean ± SEM.

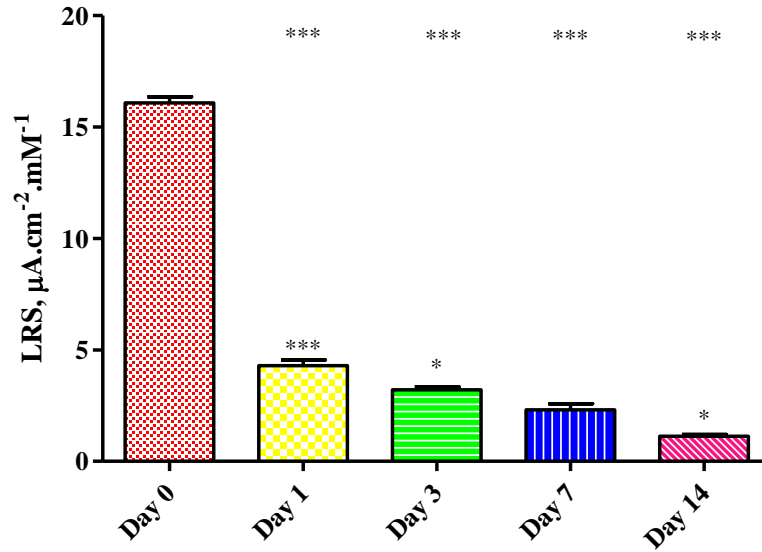


Figure 6-18

Bar chart of the sensitivities of the biosensor following storage in a brain tissue sample over two weeks.

Due to the decreasing  $J_{\max}$  there are significant changes to be found in the sensitivity values. The LRS values of Day 1, Day 3, Day 7 and Day 14 are all significantly reduced compared to Day 0,  $p < 0.0010^{***}$ . Between Day 1 and Day 3 there is also a significant reduction,  $p < 0.0500^*$ . Day 7 and 14 are further reduced compared to Day 0,  $p < 0.0010^{***}$ . There are no significant changes in sensitivity between Day 3 and Day 7,  $> 0.0500$ . Day 14, however, is significantly reduced in LRS compared to Day 3 and Day 7,  $p < 0.0010^{***}$  and  $p < 0.0500^*$  respectively.

To help quantify the changes in sensitivity it is useful to convert the LRS values to a percentage of the initial value: Day 0 –  $100.0 \pm 1.7\%$ , Day 1 –  $26.7 \pm 1.6\%$ , Day 3 –  $19.9 \pm 0.8\%$ , Day 7 –  $14.3 \pm 1.6\%$  and Day 14 –  $7.0 \pm 0.5\%$ . It is also useful again to compare these percentages to the decreases experienced over the course of the first 5 calibrations of the long-term stability study in order to elucidate the percentage decreases attributable solely to the brain tissue treatment: Day 1 –  $50.2 \pm 3.2\%$ , Day 3 –  $13.2 \pm 1.6\%$ , Day 7 –  $22.2 \pm 2.5\%$ , Day 14 –  $15.3 \pm 1.1\%$ . The decrease of 73.3% experienced between Day 0 and Day 1 (~ 15 hours in the brain tissue sample) is similar to the 70% decrease seen by Garguilo and Michael after 7 hours of exposure.

## 6.7 *In Vitro* Characterisation – pH and Temperature Effects

Following the stability and bio-compatibility testing it was also necessary to test how the biosensor would behave at extremes of pH and at physiological temperatures. The pH changes are akin to a stress test to see how changes in pH could affect the activity of the enzyme in particular. The temperature trial is necessary as the biosensor will be operating at 37 °C *in vivo* whereas all the testing has been carried out at 25 °C.

### 6.7.1 pH Changes

While it is not likely that the pH of the brain environment will vary significantly from 7.4 it is known to occur (Zimmerman & Wightman, 1991), it was decided to test what effect pH changes would produce on the biosensor sensitivity. It is likely the enzyme could lose activity if it is subject to extremes of pH (Burton, 1951; Dixon & Kleppe, 1965b; Brunori *et al.*, 1971; Horiike *et al.*, 1976) as DAAO is biologically designed to operate at 7.4. The pH values of 6.5 and 8.0 were chosen (Bolger *et al.*, 2011a) as the test values of pH and the standard PBS of pH 7.4 was altered to achieve these values. The calibration data obtained is presented in Table 11-18 with the relevant calculated kinetic data displayed in Table 6-18.

Calibration	pre pH 8.0 n = 4	pH 8.0 n = 4	pre pH 6.5 n = 4	pH 6.5 n = 4
<b>Kinetics</b>	M-M-H, p < 0.0001	M-M-H, p < 0.0001	M-M-H, p = 0.0132	M-M-H, p = 0.0025
<b>R<sup>2</sup></b>	0.9996	0.9966	0.9930	0.9947
<b>J<sub>max</sub>, μA.cm<sup>-2</sup></b>	28.94 ± 0.21	33.07 ± 0.67	19.23 ± 2.20	12.43 ± 1.03
<b>K<sub>M</sub>, μM</b>	903.9 ± 20.6	974.6 ± 74	4367 ± 1486	5823 ± 824
<b>α</b>	1.251 ± 0.028	1.435 ± 0.102	0.7667 ± 0.0754	1.445 ± 0.140
<b>LRS, μA.cm<sup>-2</sup>.mM<sup>-1</sup></b>	32.02 ± 0.57	33.93 ± 1.64	4.404 ± 1.002	2.135 ± 0.133

Table 6-18

Kinetic parameters, fit, J<sub>max</sub> and K<sub>M</sub> values calculated from the calibration data in Table 11-18. J<sub>max</sub>, K<sub>M</sub>, α and LRS are presented as Mean ± SEM.

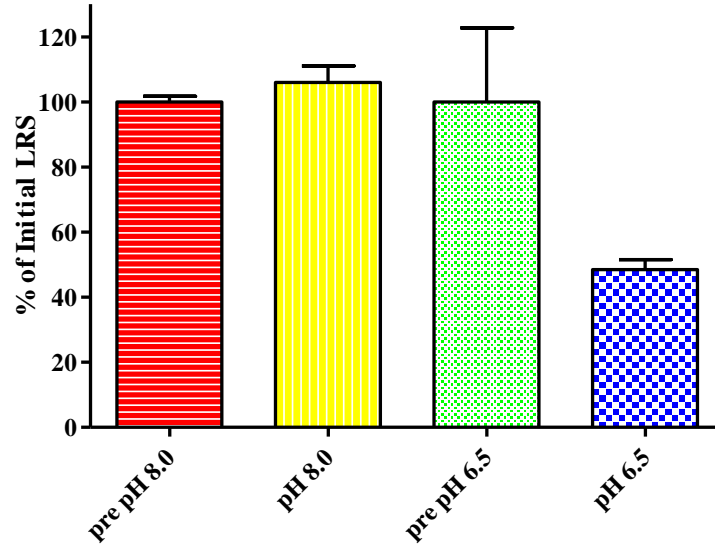


Figure 6-19

Comparison of the changes caused to the sensitivity of the biosensor by changing the pH of the calibration buffer. Shown in red is the pH 7.4 pre pH 8.0, pH is in yellow, the green trace is pH 7.4 pre pH 6.5 and the blue trace is pH 6.5.

There are contrasting results for the two pH trials. It appears that the pH 8.0 calibration has no effect on the sensitivity of the biosensor whereas the pH 6.5 calibration seems to have had a negative impact on sensitivity. When the  $J_{\max}$  values are considered there is no significant difference between the pre 8.0 and 8.0 value,  $p > 0.0500$ . But, contrastingly, there is a significant decrease found from the pre 6.5  $J_{\max}$  to the 6.5 value,  $p < 0.0500^*$ . Looking at the  $K_M$  concentrations, it is found that in the case of both the pH 8.0 and the pH 6.5 trials there are no significant differences between the pH 7.4 pre calibration and the altered pH calibrations,  $p > 0.0500$  in both cases.

Consideration of the LRS changes gives an overall indication of the changes within the two tests. Statistically it is discovered that between the pre pH 8.0 calibration and the pH 8.0 calibration there is a non-significant change in the sensitivity,  $p > 0.0500$ . The same is true for the pre pH 6.5 and pH 6.5 calibrations where no significant difference is found,  $p > 0.0500$ . Examining the percentages involved, illustrated in Figure 6-19 gives an alternative indication of how the two treatments affect the sensitivity of the biosensor. The pre pH 8.0 calibration returns  $100 \pm 1.8\%$  and the pH 8.0 calibration has a sensitivity of  $106.0 \pm 5.1\%$ . The pre pH 6.5 calibration yielded a sensitivity of  $100.0 \pm 22.8\%$  and the pH 6.5 calibration itself was  $48.5 \pm 3.0\%$  as sensitive. Comparing this result to the first two calibrations of the short-term repeated calibration trial, which were  $100.0 \pm 5.4\%$  and  $107.3 \pm 3.6\%$  sensitive respectively, further illustrates the point that there has been no significant change in the sensitivity for the pH 8.0 trial. However, it

does indicate that mean sensitivity value of the pH 6.5 trial had decreased by approximately half. This change may be due to the isoelectric point (IEP) of the enzyme, which has been determined to be pH 6.24 (Yagi & Ohishi, 1972). As a molecule approaches its IEP from a pH above the IEP it loses its net negative charge and becomes neutral. The changes which occur within the molecule at this point can be irreversible and may potentially affect the activity of an enzyme. Effects similar to this have been seen before, where as the pH approaches 6.0 the activity decreases, with peak activity in the region of pH 8.0 – 9.0 (Pernot *et al.*, 2008; Zain *et al.*, 2010).

### 6.7.2 Temperature Changes

It was not possible during the development of the biosensor to run all calibrations at the physiological temperature of 37 °C. This is the temperature at which the biosensor would be operating at *in vivo* and indeed the temperature that it is operates at in a natural environment. Thus, a trial was conducted whereby the experimental apparatus was heated up to  $37.0 \pm 0.2$  °C and maintained at this temperature throughout a calibration. The results of an initial calibration and a post 37 °C calibration, both at room temperature and the 37 °C calibration are displayed in Table 11-19 with the kinetic fit data listed in Table 6-19.

There are significant changes to be found across all of the  $J_{\max}$  values. The 37 °C value is significantly lower than the pre 37 °C  $J_{\max}$ ,  $p < 0.0500^*$ . The post 37 °C calibration also has a significantly decreased  $J_{\max}$  when compared to the pre 37 °C value,  $p < 0.0010^{***}$ . Lastly the post 37 °C is also significantly lower than the 37 °C result,  $p < 0.0010^{***}$ .

Calibration	pre 37 °C, n = 4	37 °C, n = 4	post 37 °C, n = 4
<b>Kinetics</b>	M-M, p = 0.2484	M-M, p = 0.7614	M-M, p = 0.1150
<b>R<sup>2</sup></b>	0.9978	0.9989	0.9966
<b>J<sub>max</sub>, <math>\mu\text{A}\cdot\text{cm}^{-2}</math></b>	$21.96 \pm 0.45$	$20.55 \pm 0.23$	$11.73 \pm 0.28$
<b>K<sub>M</sub>, <math>\mu\text{M}</math></b>	$3012 \pm 179$	$1829 \pm 72$	$2607 \pm 189$
<b>LRS, <math>\mu\text{A}\cdot\text{cm}^{-2}\cdot\text{mM}^{-1}</math></b>	$7.292 \pm 0.307$	$11.23 \pm 0.34$	$4.500 \pm 0.237$

Table 6-19

Kinetic parameters, fit,  $J_{\max}$  and  $K_M$  values calculated from the calibration data in Table 11-19.  $J_{\max}$ ,  $K_M$ ,  $\alpha$  and LRS are presented as Mean  $\pm$  SEM.

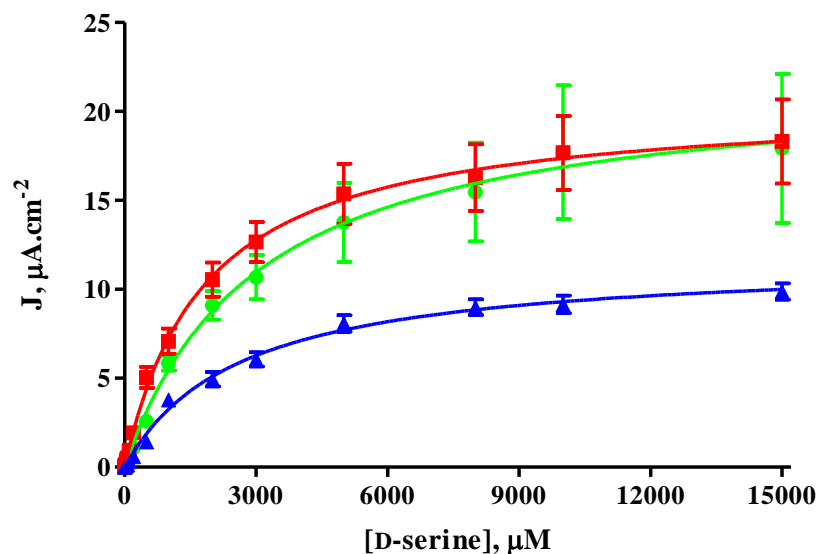


Figure 6-20

J-concentration plot of the pre 37 °C calibration (green trace), the calibration at 37 °C (red trace) and the post 37 °C calibration (blue trace).

Examining the  $K_M$  concentrations it is seen that a different pattern of significant changes were brought about the 37 °C treatment. From the initial concentration of the pre 37 °C calibration there is a significant decrease in the value for the 37 °C result,  $p < 0.0100^{**}$ . The post 37 °C result is then significantly increased when compared to the 37 °C calibration,  $p < 0.0500^*$ . Interestingly, the change between the pre 37 °C and post 37 °C  $K_M$  results is not significant,  $p > 0.0500$ .

The combination of the fluctuating  $J_{max}$  and  $K_M$  values results in significant changes in the sensitivities of the biosensors. The initial response of the pre 37 °C is increased significantly by the calibration at 37 °C,  $p < 0.0010^{***}$ . From this peak, the LRS decreases significantly with the post 37 °C calibration,  $p < 0.0010^{***}$ . There is also a significant decrease observed when the pre 37 °C and post 37 °C sensitivities are compared,  $p < 0.0010^{***}$ . In terms of percentage of the initial LRS result, the three values are: pre 37 °C –  $100.0 \pm 4.2\%$ , 37 °C –  $154.0 \pm 4.7\%$ , post 37 °C –  $61.7 \pm 3.3\%$ . These are favourable values when compared to the short-term repeated calibration values of: Cal 1 –  $100.0 \pm 5.4\%$ , Cal 2 –  $107.3 \pm 3.6\%$ , Cal 3 –  $80.0 \pm 3.3\%$ . It shows that when utilised in an environment at physiological temperature the  $\alpha$ AAO does turnover substrate at a higher rate, this is to be expected as it is closer to the environment within which the enzyme evolved to function in. But it also shows again that fluctuation in temperature can cause a reduction in sensitivity, similar to the effects

shown by the changes in pH and the effects of refrigeration during the short-term and long-term stability testing.

## 6.8 *In Vitro* Characterisation – Interference Studies

Having decided on an interference rejection mechanism, the combination of Naf and PPD, and tested it for its rejection of AA from the electrode surface it was now necessary to complete a more thorough examination of the interference characteristics of the biosensor. To do this a combination of three different studies were utilised. The first was a combined calibration where a range of amino acids were injected into the PBS in series to test the reaction of the immobilised DAAO to the presence of amino acids other than D-ser. Secondly, D-alanine, the most commonly occurring amino acid, by concentration other than D-ser, was calibrated in full for the biosensors response to it. Lastly the biosensor was calibrated for response to a range of other electroactive species found in the ECF and brain environment.

### 6.8.1 Amino-Acids and Glycine

There is a substantial range and variety of amino acids present in the brain, with both the D- and L- analogues commonly occurring. Due to the non-selective nature of DAAO (Ferraris *et al.*, 2008) it is necessary to quantify the level of reactivity of the biosensor to these other amino acids. It should be noted that the stereospecificity specific of DAAO is absolute, L-amino acids do not inhibit or act as substrates for it (Molla *et al.*, 2003). Despite this, for completeness and to be comparable to previously published data the calibration was carried out across a range of D- and L-amino acids as well as glycine. Glycine is also a co-agonist at the NR1 subunit of the NMDA glutamate receptor (Danysz & Parsons, 1998).

The amino acid substrates used were: the D- and L- isomers of serine (ser), alanine (ala), aspartic acid (asp), phenylalanine (phe), glutamic acid (glut), arginine (arg), proline (pro) and histidine (his) along with D-lysine (D-lys), D-tyrosine (D-tyr) and glycine (gly). Further amino acids appear in Section 6.8.3 as electroactive interferents.

The responses obtained during this trial are displayed in Table 6-20 and plotted in Figure 6-21. The responses were calculated using the settled level of the previous substrate as a new baseline. This in some cases lead to a negative response as the

levels settled further over an extended period of time, or the addition of another substrate diluted the quantity of active substrate reaching the enzyme. There is also the added factor of possible baseline drift occurring over such a long calibration, over 3 hours long.

As expected it is clear to see that the L-amino acids and glycine, when error is taken into account, produce no response from the biosensor. There is little or no response from D-glut, D-lys and D-tyr. The currents recorded for D-asp, D-arg and D-his are approximately half that of D-ser. D-phe and D-ala produce a response level similar to that of D-ser, while D-pro is approximately twice as reactive as these three D-amino acids. These are not unexpected results as an increased  $k_{cat}$ , catalytic rate, for D-pro has been widely reported along with similar levels of activity for D-ser, D-ala and D-phe (Dixon & Kleppe, 1965a; Molla *et al.*, 2006). The varying responses are also due to the different types of D-amino acids used: arg, his and lys have positively charged side chains, asp and glu have negatively charged side chains (at physiological pH), ser has polar uncharged side chains, ala, phe and tyr all contain hydrophobic side chains. Along with the charge differences gly, pro and ala are aliphatic compounds, phen and tyr are aromatic compounds, asp and glu are acidic, arg, his and lys are basic in nature and finally ser is hydroxylic. The combination of these characteristics as well as the differences in size and shape will all contribute to the varying response of the biosensor to the different amino acids. Perhaps most important of all is the varying substrate affinity and catalytic efficiency the different D-amino acids have for DAAO (Dixon & Kleppe, 1965a).

Substrate	J, 10 $\mu$ M, $\mu$ A.cm <sup>-2</sup> , n = 6		Substrate	J, 10 $\mu$ M, $\mu$ A.cm <sup>-2</sup> , n = 6	
	Mean	$\pm$ SEM		Mean	$\pm$ SEM
D-ser	0.065	0.005	L-ser	-0.003	0.003
D-ala	0.073	0.006	L-ala	-0.021	0.008
D-asp	0.034	0.008	L-asp	0.006	0.005
D-phe	0.083	0.009	L-phe	0.007	0.002
D-glut	0.008	0.004	L-glut	-0.011	0.005
D-pro	0.143	0.021	L-pro	-0.018	0.016
D-arg	0.030	0.012	L-arg	-0.002	0.007
D-his	0.035	0.005	L-his	0.009	0.008
D-lys	-0.009	0.003	Gly	-0.006	0.006
D-tyr	0.013	0.012			

Table 6-20

Calibration data for a range of amino acids. The indicated values are the response following to 10  $\mu$ M of the amino acid, having taken the resting value of the previous substrate as a new baseline.

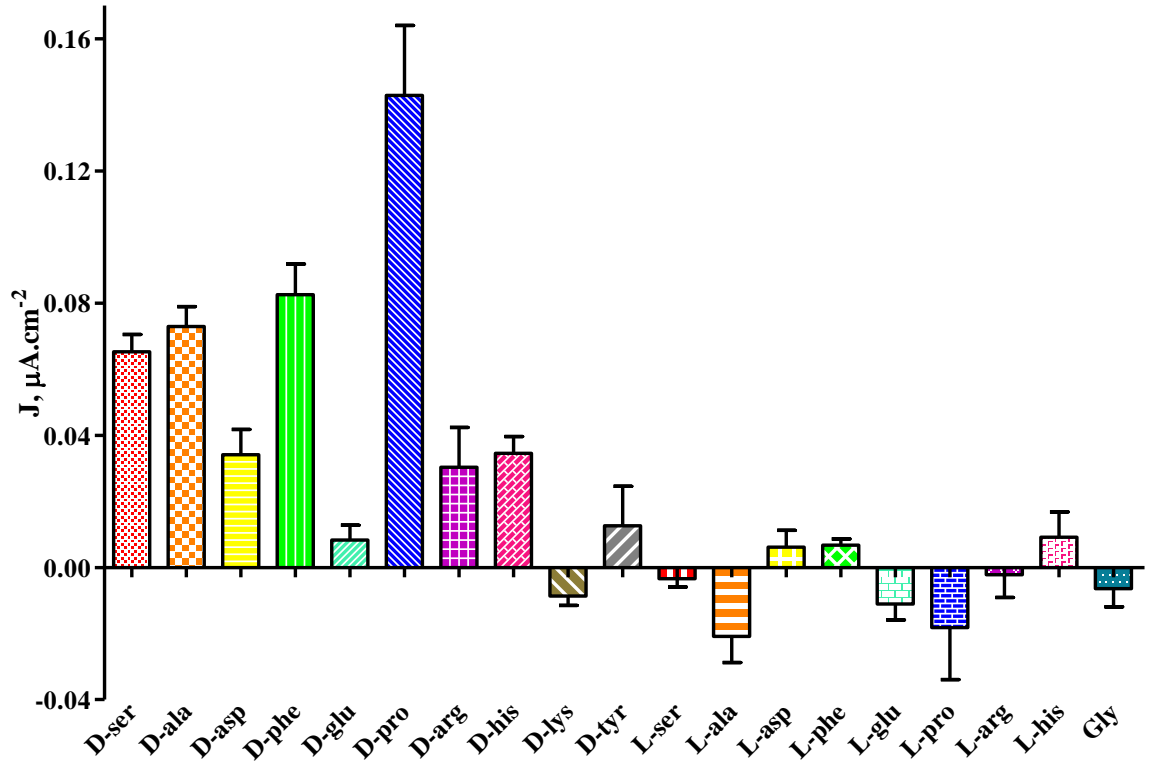


Figure 6-21

The 10  $\mu\text{M}$  response of the biosensor to various amino acids.

The large responses obtained for D-ala, D-phe and D-pro are not of any major significance as previously explained (Section 0). D-ser is, in general, the D-amino acid that is highest in concentration and two orders of magnitude greater than D-ala and D-asp, the next two most prolific amino acids (Hashimoto *et al.*, 1993; Morikawa *et al.*, 2001; Wolosker *et al.*, 2002; Hamase *et al.*, 2005). Thus even with equal sensitivity to these substrates the likely effect on the output signal would only be  $\sim 1\%$  of the changes in signal due to D-ser.

### 6.8.2 D-Alanine

Having identified that there was a significant response to D-ala and being aware that it was the most prolific D-amino acid apart from D-ser it was decided to conduct a full calibration to elicit better the response of the biosensor to this substrate. It was hoped that this would also allow a better quantification of the likely interference in signal from the other D-amino acids. Being able to put a definite figure on the sensitivity to D-ala along with the relative concentrations know by brain region would allow a finer resolution of the quantity of interference likely. Thus a full D-ala calibration was

conducted on biosensors previously calibrated for D-ser response. The results are displayed in Table 11-20.

The kinetic parameters are listed in Table 6-21, and contribute to the plot in Figure 6-22. Statistically, there is no significant difference between the  $J_{\max}$  values of the pre and post D-ser calibrations,  $p > 0.0500$ , but the D-ala calibration has a significantly higher  $J_{\max}$  value than either the pre or post calibration,  $p < 0.0010^{***}$  in both cases.

These statistical differences also hold true when the  $K_M$  concentration is examined. The pre and post calibrations are non-significantly different,  $p > 0.0500$ , and the D-ala calibration is significantly different to both the pre and post concentrations,  $p < 0.0010^{***}$ . In the case of the  $K_M$  however the D-ala value is significantly higher.

Not surprisingly, the LRS values also show the same statistical differences as the  $J_{\max}$  and  $K_M$ . The pre and post calibrations are equally as sensitive,  $p > 0.0500$ , and the D-ala shows a significantly higher sensitivity than both the D-ser calibrations,  $p < 0.0010^{***}$ . It is clear that without other amino acids present that DAAO has quite an affinity for D-ala, and is almost twice as sensitive to it as D-ser.

Calibration	pre D-alanine, n = 4	D-alanine, n = 4	post D-alanine, n = 4
<b>Kinetics</b>	M-M-H, $p < 0.0001$	M-M-H, $p = 0.0005$	M-M-H, $p = 0.0003$
<b><math>R^2</math></b>	0.9995	0.9984	0.9984
<b><math>J_{\max}</math>, <math>\mu\text{A}\cdot\text{cm}^{-2}</math></b>	$13.49 \pm 0.11$	$17.68 \pm 0.26$	$13.14 \pm 0.23$
<b><math>K_M</math>, <math>\mu\text{M}</math></b>	$1198 \pm 29$	$818.1 \pm 39.5$	$1238 \pm 62$
<b><math>\alpha</math></b>	$1.385 \pm 0.036$	$1.209 \pm 0.053$	$1.247 \pm 0.059$
<b>LRS, <math>\mu\text{A}\cdot\text{cm}^{-2}\cdot\text{mM}^{-1}</math></b>	$11.26 \pm 0.20$	$21.61 \pm 0.83$	$10.62 \pm 0.39$

Table 6-21

Kinetic parameters, fit,  $J_{\max}$  and  $K_M$  values calculated from the calibration data in Table 11-20.  $J_{\max}$ ,  $K_M$ ,  $\alpha$  and LRS are presented as Mean  $\pm$  SEM.

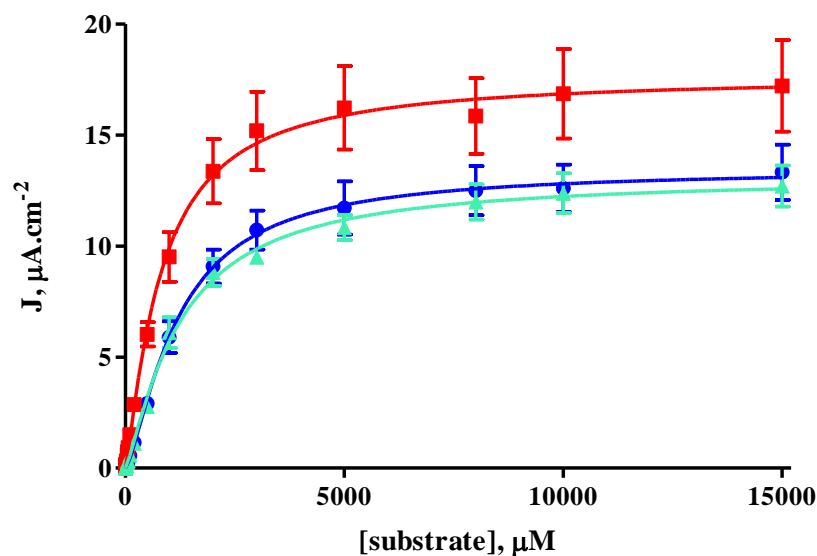


Figure 6-22

J-concentration plot of the D-ala calibration (red trace) with the pre (dark blue trace) and post (light blue trace) D-ser calibration.

However what is also shown in this set of tests is that exposure to D-ala appears to have maintained the sensitivity of the biosensors towards D-ser. If the short term repeated calibrations are re-examined it is seen that the LRS of Cal 1 and Cal 3 are  $100.0 \pm 5.4\%$  and  $80.0 \pm 3.3\%$  respectively. Here the first and second D-ser calibrations (Cal 1 and Cal 3 respectively) post sensitivities of  $100.0 \pm 1.8\%$  and  $94.3 \pm 3.5\%$  respectively. The D-ala calibration has a sensitivity of  $191.9 \pm 7.3\%$  compared to a Cal 2 value of  $107.3 \pm 3.6\%$ . If exposure to other D-amino acids improves or maintains the sensitivity of the enzyme and the biosensors towards D-ser then this can only be beneficial for *in vivo* applications. Finally the approximate ratio of D-ser to D-ala in the cerebellum as reported by Hamase is 35:1 (Hamase *et al.*, 2005; Miyoshi *et al.*, 2009; Miyoshi *et al.*, 2011) and with the biosensor almost twice as sensitive to D-ala the maximum signal due to D-ala is likely to be in the range of 5% of the D-ser signal. Although as seen in the long amino acid calibration, due to varying affinities of the different D-amino acids for DAAO it is possible that it could be much less, when other substrates are competing with each other for access to the DAAO.

### 6.8.3 Native Electroactive Species

Having already explored the interference from the primary electroactive interferent in the brain, AA, see Section 6.4, it was necessary to establish what the effect, if any, the other electroactive species in the ECF would have. Having shown that the combination

of the Naf and PPD layers could eliminate interference from the high concentrations of AA it was unlikely that any other electroactive species would produce a response, but its verification was still essential. Chosen for testing were AA and its oxidised form dehydroascorbic acid (DHAA), the amino acids, L-cysteine (L-cys), L-tryptophan (L-trp) and L-tyrosine, (L-tyr), the metabolite of purine nucleotides – uric acid (UA), the monoamine neurotransmitters dopamine (DA) and 5-hydroxytryptamine (serotonin) (5-HT), three of their metabolites – homovanillic acid (HVA), 5-hydroxyindoleacetic acid (5-HIAA) and 3,4-dihydroxyphenylacetic acid (DOPAC), and another anti-oxidant L-glutathione.

The experiment was conducted similar to the amino acid calibration except that it was conducted under an atmosphere of nitrogen and all solutions were nitrogen saturated. The substances were added as a standard aliquot, of 100  $\mu\text{L}$ , which contained an ECF concentration for the particular substrate. After an initial small increase in current due to convective effect the signal quickly settled back to, or below, baseline levels during the quiescent period and as the ‘self-blocking mechanism’ took effect. This can clearly be seen in Figure 6-23.

The concentration of L-gluta, L-cys, L-trp and L-tyr in the ECF are unknown, therefore relatively high  $\mu\text{M}$  values were chosen (O'Brien *et al.*, 2007), all other values were chosen to be at least the *in vivo* concentration of consensus. The only substance where the concentration to be used was difficult to determine was DA, as there is ongoing controversy over the proposed levels *in vivo* with values ranging from 0.05  $\mu\text{M}$  (Zetterström *et al.*, 1983) to 0.0005  $\mu\text{M}$  (Cartmell *et al.*, 2000). Thus, to cover all possibilities a high level of 0.5  $\mu\text{M}$  was chosen.

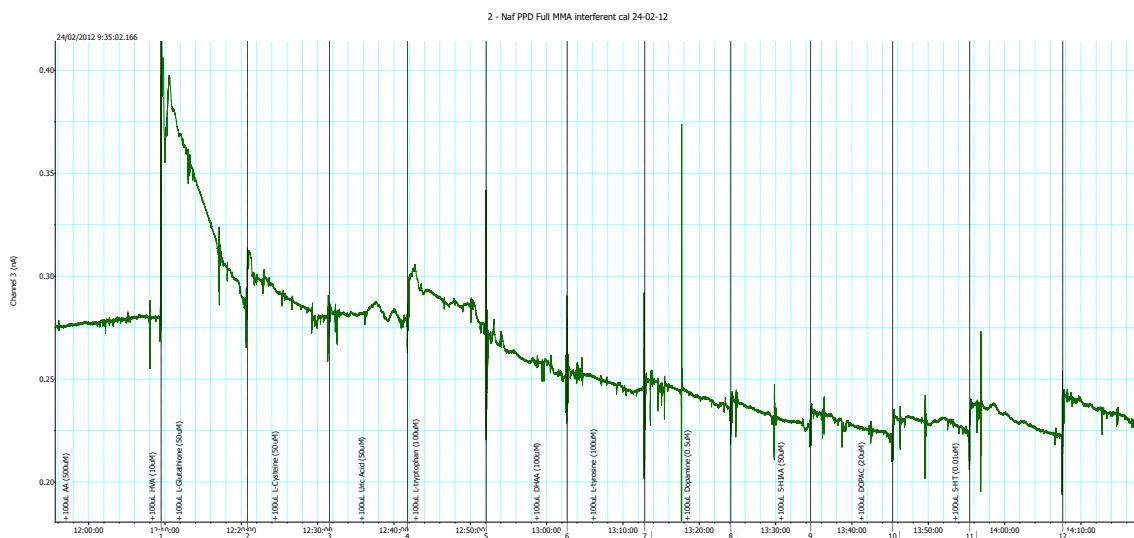


Figure 6-23

The raw data trace obtained for one electrode during the interferent calibration. Each dotted line indicated the addition of the next species.

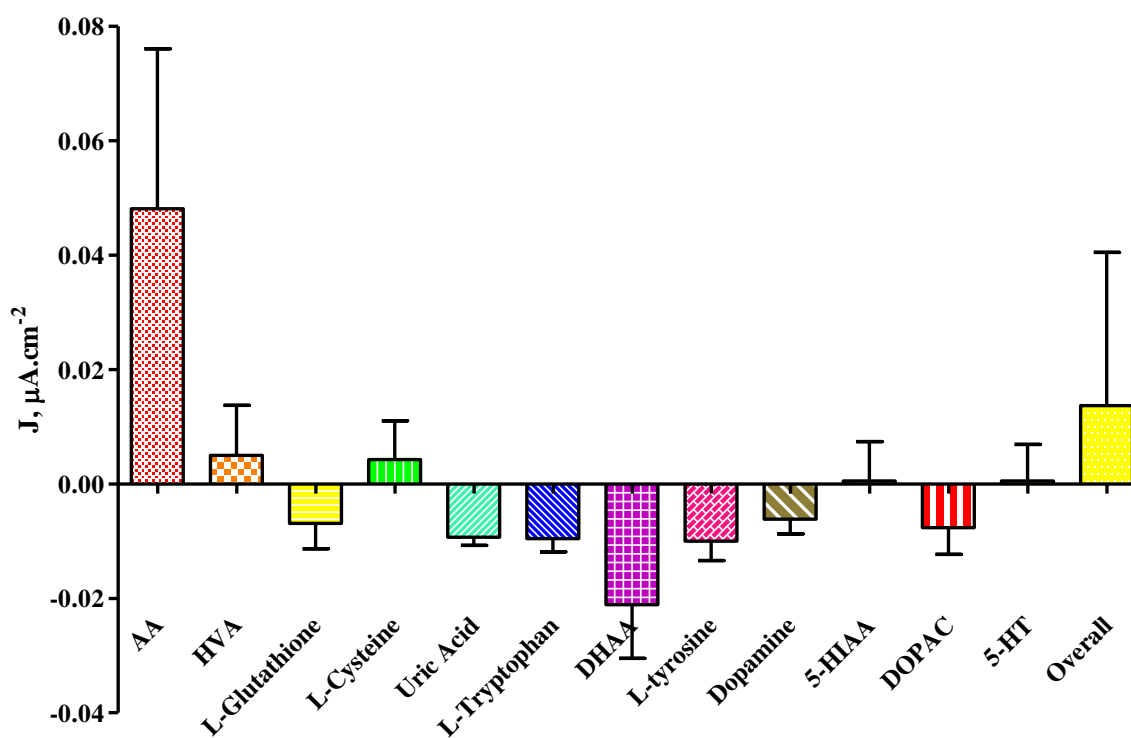


Figure 6-24

Bar chart of the sensitivity of the biosensor to various electroactive interferents.

Examining the data a number of interesting and satisfying points are illustrated. Firstly the large response to AA, the first substance injected is to be expected, as the ‘self-blocking mechanism’ in the polymer has not had time to establish. A similar, large, initial response was shown when the polymer layers were being characterised in Section 6.4.3 for only a 200  $\mu\text{M}$  AA concentration, yet after this the current decreases with time

as self-blocking occurs. Indeed this can be seen to occur in this instance in both Figure 6-23 and in the overall figures as a lot of the later injections display a negative response. Indeed the total overall response is similar to that shown in Section 6.4.3 for 400  $\mu\text{M}$  AA despite a substantially greater quantity and variety of electroactive species being present. These are encouraging results overall, and they show that once the biosensors have been allowed to settle in an *in vivo* environment, the milieu of different species present should not affect detection of D-ser beyond affecting the baseline current.

## 6.9 *In Vitro* Characterisation – Oxygen Dependency Studies

As ‘first generation’ biosensors, the D-ser sensors designed operate by oxidising the  $\text{H}_2\text{O}_2$  produced by an enzyme. DAAO is an oxidase enzyme, and as already detailed in Section 2.7 and 2.8.2, oxygen is required for it, in particular the FAD unit, to function correctly. Therefore, as with all oxidase based biosensors, it is necessary to determine if changes in the oxygen level of brain will affect the sensitivity of the sensor. Oxygen in the ECF is usually maintained at  $\sim 50 \mu\text{M}$  (Zimmerman & Wightman, 1991), with a drop below  $\sim 30 \mu\text{M}$  likely to lead to cell death. At atmospheric conditions, that all experiments have been carried out at so far, the PBS that the electrodes reside in will maintain an oxygen level of  $\sim 240 \mu\text{M}$  (Foster *et al.*, 1993).

The results of the oxygen dependence experiments are detailed in the following sections. The quantity of data involved in the graphs to follow is huge ( $\sim 7000$  points) and therefore will only be graphically represented.

### 6.9.1 Oxygen Dependence at 10 $\mu\text{M}$ D-serine

The first concentration of D-ser to be examined was 10  $\mu\text{M}$ , slightly above the accepted level *in vivo*. It would be unlikely under normal circumstances for levels in the ECF to exceed this level, unless a specific drug treatment or a direct local injection of D-ser were utilised to bring it about. Thus oxygen dependency at this concentration is very important. The results of the experiments carried out in the presence of 10  $\mu\text{M}$  D-ser are displayed in Figure 6-25:

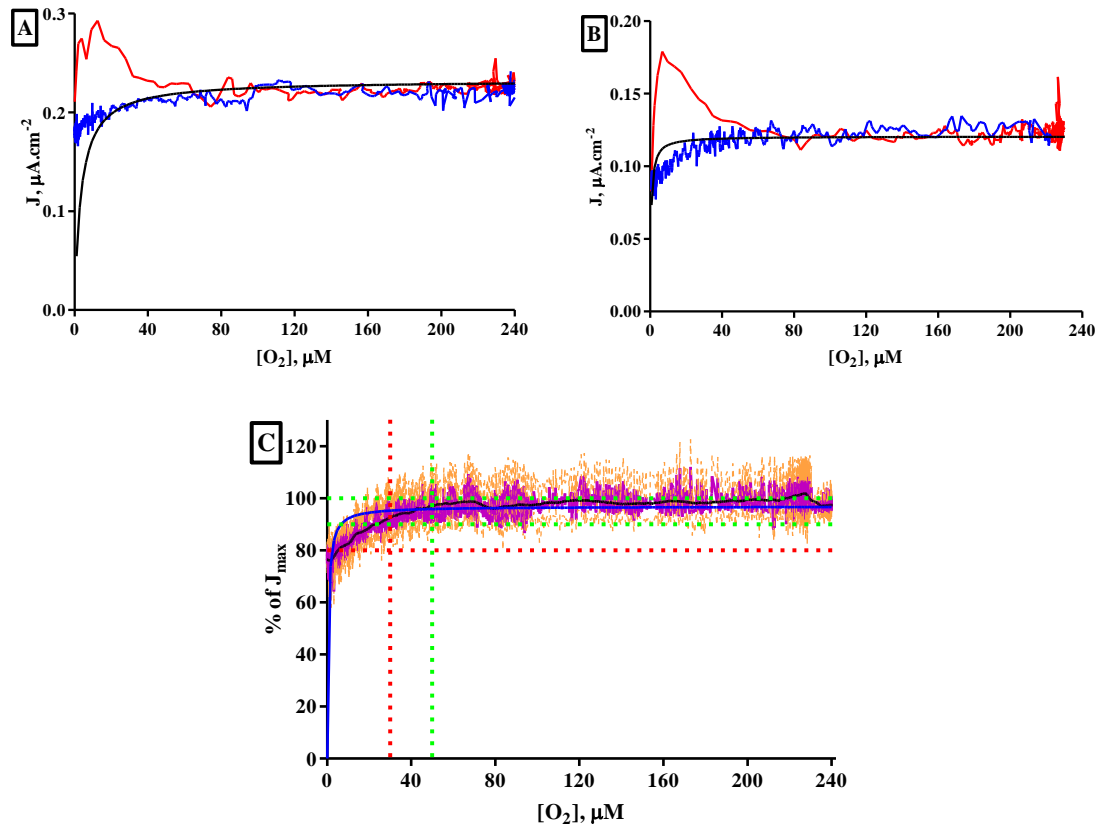


Figure 6-25

The oxygen dependence of the biosensor in the presence of 10  $\mu\text{M}$  D-ser. *A & B*: the raw data recorded for two sets of biosensors as the oxygen level was first decreased (blue trace) and then increased (red trace) with the accompanying M-M curve for the two sets of data in each case (black curve). *C*: the data from all four traces was combined. The mean  $\pm$  SEM are plotted in purple and orange respectively. The black line is the smoothed trace for all points. The blue curve is the M-M fit for this smoothed trace.

In Figure 6-25, graphs A and B are the raw data traces for two different sets of biosensors. Each trace is the mean of the data from the three biosensors used in that experiment. The blue trace is the data collected as the oxygen concentration was decreased by removing the air source and bubbling  $\text{N}_2$  through the PBS. Once the reading on the oxygen and D-ser sensors had reached a plateau, and remained there stable for 1 minute, the  $\text{N}_2$  was removed and air was bubbled into the cell again. This process lead to the production of the red trace as the dissolved  $\text{O}_2$  levels increased towards 240  $\mu\text{M}$  again. It is very clear that during the time at near zero dissolved  $\text{O}_2$  that D-ser was still finding its way into the active site of the enzyme and that decreased activity, caused by the lack of oxygen, was leading to a build up of substrate within the enzyme molecules. This is evidenced in the very large increase in current as air is again pumped into the cell. The red trace shows a large spike and overshoots the maximum current by some considerable amount. In A the current reaches 126% of  $J_{\text{max}}$ , and in B the values reaches 149% of the maximum current. These bursts of activity are short

lived however, as the time taken to reach 50  $\mu\text{M}$  from the zero point is approximately 18 and 20 seconds for A and B respectively. At this point the currents have returned to the  $J_{\text{max}}$  value again.

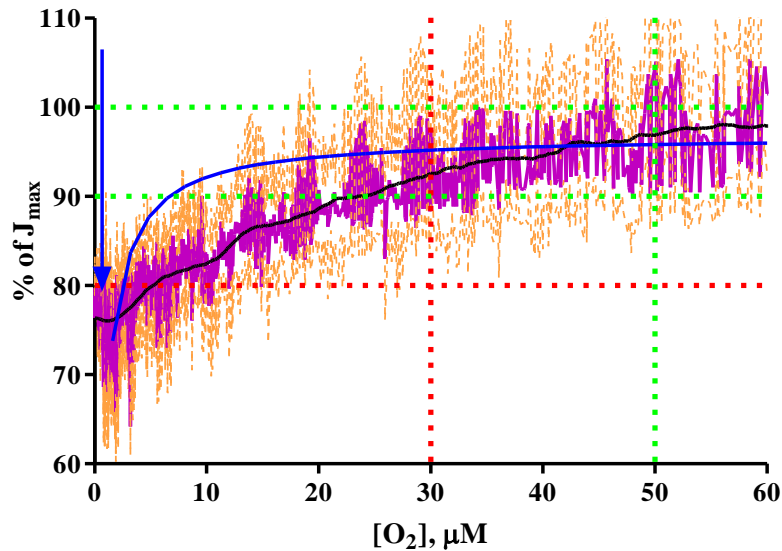


Figure 6-26

A detailed view of the oxygen dependence of the biosensor in the presence of 10  $\mu\text{M}$  D-ser. The mean  $\pm$  SEM are plotted in purple and orange respectively. The black line is the smoothed trace for all points. The blue curve is the M-M fit for this smoothed trace. The blue arrow indicates the calculated  $K_M(\text{O}_2)$ .

A closer examination of the behaviour of the biosensors in the lower oxygen level environment is afforded in Figure 6-26. The black trace is obtained with an in built smoothing function in Prism, the analysis and graphing software, where each point is smoothed with 30 neighbours on either side using a sixth degree polynomial. This is the most complex smoothing feature offered by the programme. This smoothed data, and even the raw means (in purple) show that the response of the biosensor is well above 90% of  $J_{\text{max}}$  levels. Indeed, the response has not reached 100% of  $J_{\text{max}}$  when the  $\text{O}_2$  level reaches 60  $\mu\text{M}$ , therefore the variance in the signal between 30 and 50  $\mu\text{M}$   $\text{O}_2$  is minimal. The accepted level of response for oxygen independence to be declared is 80% of  $J_{\text{max}}$ . Achieving this by 5  $\mu\text{M}$   $\text{O}_2$  demonstrates that the biosensor is oxygen independent for 10  $\mu\text{M}$  of D-ser.

The blue trace is a Michaelis-Menten Kinetic fit for the smoothed function of the data. Only an M-M fit was considered as the oxygen interaction occurs at a single site and does not produce cooperativity (it was not possible for Prism to fit a M-M-H curve to the data in some cases). The  $J_{\text{max}}$  of the fit was found to be  $96.79 \pm 0.19$  % of the value

calculated for the individual raw traces in Figure 6-25, due most likely to the smoothing process, where the effect of outliers is reduced, and the limited fall off in current observed as the dissolved O<sub>2</sub> approached 0 μM lead to an R<sup>2</sup> value of 0.2425. The K<sub>M</sub>(O<sub>2</sub>) was found to be 0.502 ± 0.025 μM O<sub>2</sub> (indicated by the blue arrow).

### 6.9.2 Oxygen Dependence at 20 μM D-serine

At approximately three times the proposed *in vivo* concentration of D-ser, 20 μM would be a stringent test of whether the biosensor design would be useful and successful in an *in vivo* environment. The raw traces in A and B of Figure 6-27 are quite similar to those observed for 10 μM of D-ser. As the dissolved O<sub>2</sub> levels increase from their zero level (red trace) there again is a large spike observed as the enzyme units all become active as the oxygen rapidly diffuses through the solution and into the active sites. In this instance for A the spike reaches a maximum value of 153% of the J<sub>max</sub> value approximately 5 seconds after the air supply is re-established. The spike lasts for approximately 17 seconds and returns to the level of the J<sub>max</sub> as the dissolved O<sub>2</sub> content reaches 55 μM. For B, the maximum J reached is 187% of the maximum value of the kinetic fit. This occurred 6 seconds after the reintroduction of air to the solution, and the spike lasted a total of 18 seconds before returning to the J<sub>max</sub> value as the dissolved O<sub>2</sub> concentration was approximately 60 μM.

In Figure 6-28 it can be seen that for 20 μM D-ser, similar to 10 μM, the recorded currents are over 90% of J<sub>max</sub> when the O<sub>2</sub> concentration is 30 μM, and has not yet reached the J<sub>max</sub> value by 60 μM O<sub>2</sub>. Thus once again there is little change in the signal when the O<sub>2</sub> concentration is varied between 30 and 50 μM. Oxygen independence, at least 80% of the J<sub>max</sub>, is achieved at just above 20 μM oxygen. The M-M fit of the smoothed data has a J<sub>max</sub> corresponding to 100.2 ± 0.20% of the individual calibrations. There is an associated K<sub>M</sub>(O<sub>2</sub>) of 1.460 ± 0.047 μM and an R<sup>2</sup> value of 0.5646.

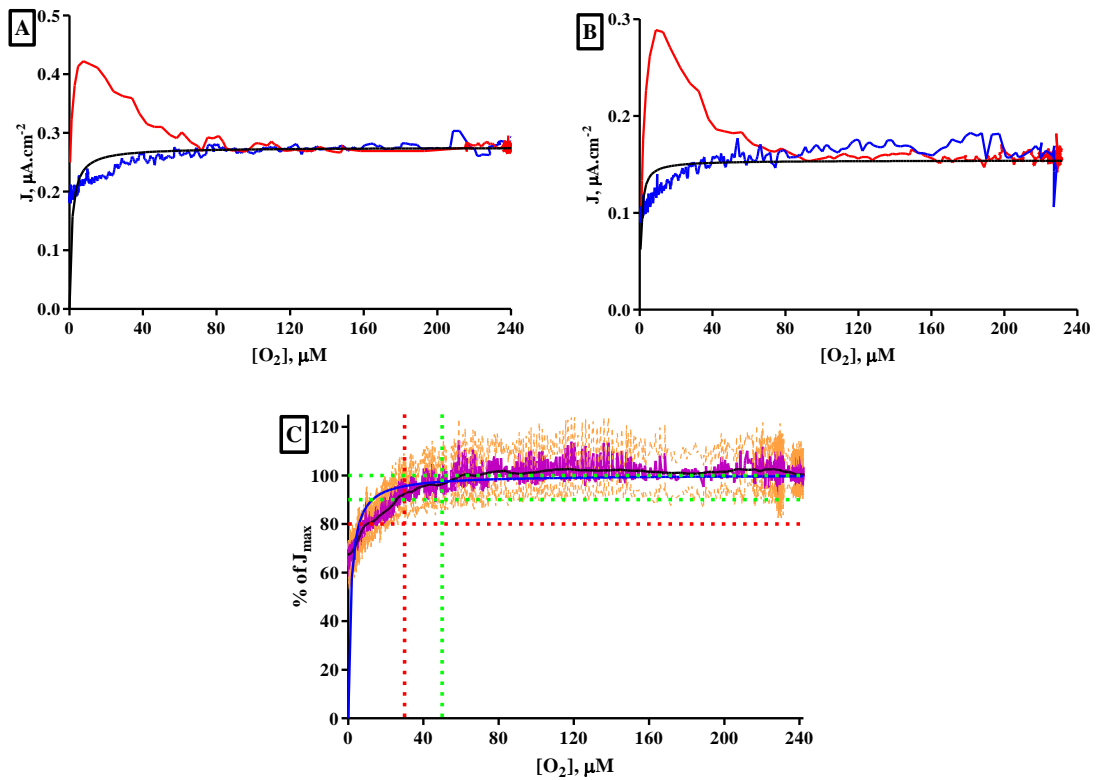


Figure 6-27

The oxygen dependence of the biosensor in the presence of 20  $\mu\text{M}$  D-ser. A & B: the raw data recorded for two sets of biosensors. C: the data from all four traces combined.

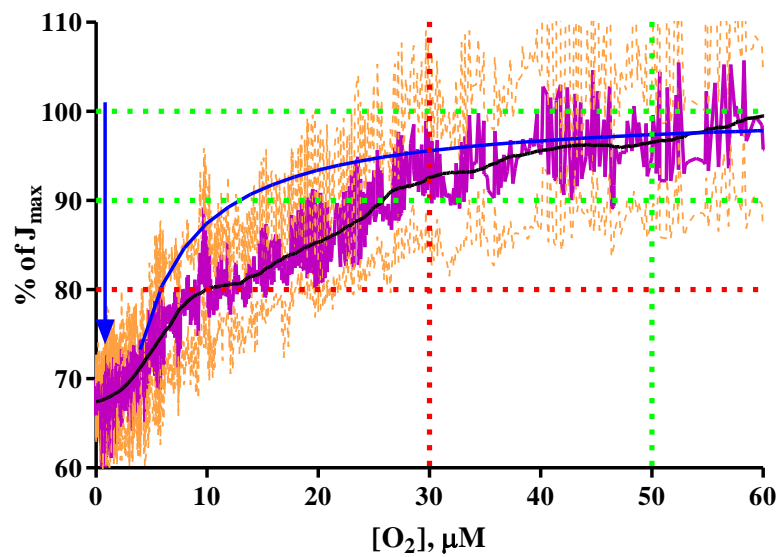


Figure 6-28

A detailed view of the oxygen dependence of the biosensor in the presence of 20  $\mu\text{M}$  D-ser.

### 6.9.3 Oxygen Dependence at 50 $\mu\text{M}$ D-serine

The testing of oxygen dependence at 50  $\mu\text{M}$  D-ser, 10 times the proposed physiological concentration was the third concentration of D-ser used to elucidate the characteristics of the biosensors. The results are displayed below in Figure 6-29:

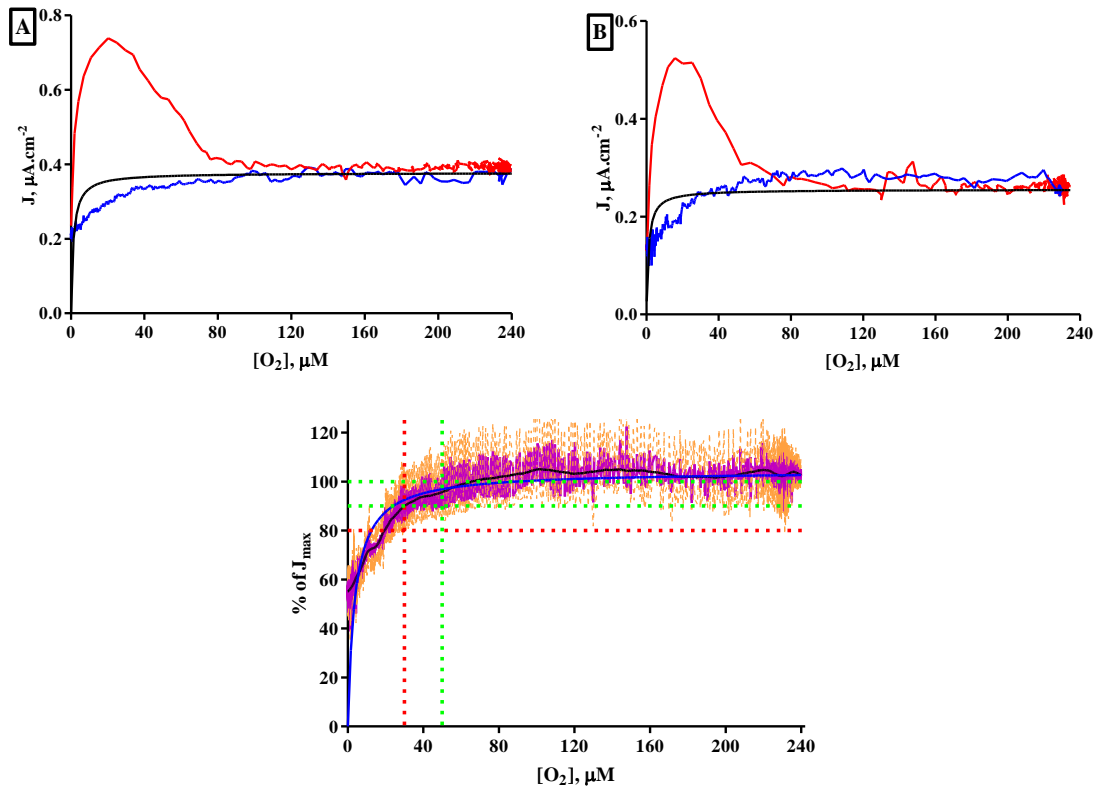


Figure 6-29

The oxygen dependence of the biosensor in the presence of 50  $\mu\text{M}$  D-ser. *A & B*: the raw data recorded for two sets of biosensors. *C*: the data from all four traces combined.

Once again, this time with 50  $\mu\text{M}$  D-serine, it is possible to see the large overshoot of the currents recorded during the increasing oxygen levels phase of the experiment (red traces in Figure 6-29, parts A and B). For calibration A the current reaches in excess of 195% of the maximum current calculated by the kinetic fit (black curve). This occurs after 8 seconds after the air supply has been reinstated. The period of increased activity lasts for 23 seconds overall and the signal returns to the  $J_{\text{max}}$  as the dissolved oxygen content passes 75  $\mu\text{M}$ . In the case of calibration B the overshoot peaks at 205% after 10 seconds. The increased activity period lasts 22 seconds in total and the  $J$  returns to the maximum level as the % concentration of  $\text{O}_2$  in solution passes 75  $\mu\text{M}$ .

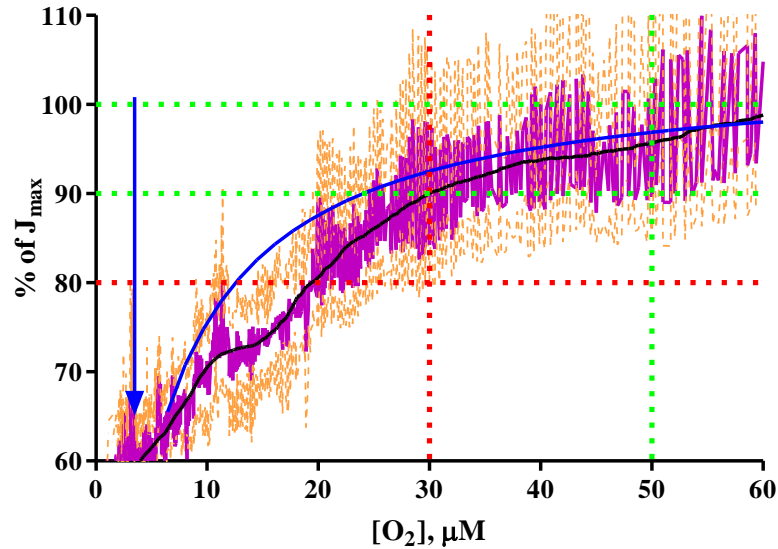


Figure 6-30

A detailed view of the oxygen dependence of the biosensor in the presence of 50  $\mu\text{M}$  D-ser.

The M-M kinetic fit curve (blue trace in Figure 6-30), modelled on the black trace of smoothed data, has a  $J_{\text{max}}$  equivalent to  $104.2 \pm 0.3\%$  of that calculated for the raw data in A and B. The  $K_M(\text{O}_2)$  of  $3.804 \pm 0.103 \mu\text{M}$  (blue arrow) is larger than that of the 20  $\mu\text{M}$  D-ser calibration, and the  $R^2$  value of 0.7797 shows a much closer fit to M-M kinetics. This is due to the steeper decrease in the recorded signal at lower  $\text{O}_2$  levels. Once again it is satisfactory to see that the response has reached at least 90% of  $J_{\text{max}}$  at 30  $\mu\text{M}$   $\text{O}_2$ , and that the variance between 30 and 50  $\mu\text{M}$  is minimal with the response still not reaching  $J_{\text{max}}$  by 60  $\mu\text{M}$   $\text{O}_2$ . The minimum acceptable level of signal response, 80%, is reached when the dissolved oxygen concentration is approximately 20  $\mu\text{M}$ .

#### 6.9.4 Oxygen Dependence at 100 $\mu\text{M}$ D-serine

To complete the set of oxygen dependence calibrations a concentration of 100  $\mu\text{M}$  D-ser was studied. This concentration is far in excess of any likely to be seen *in vivo* even with significant external manipulation. The results are presented below in Figure 6-31:

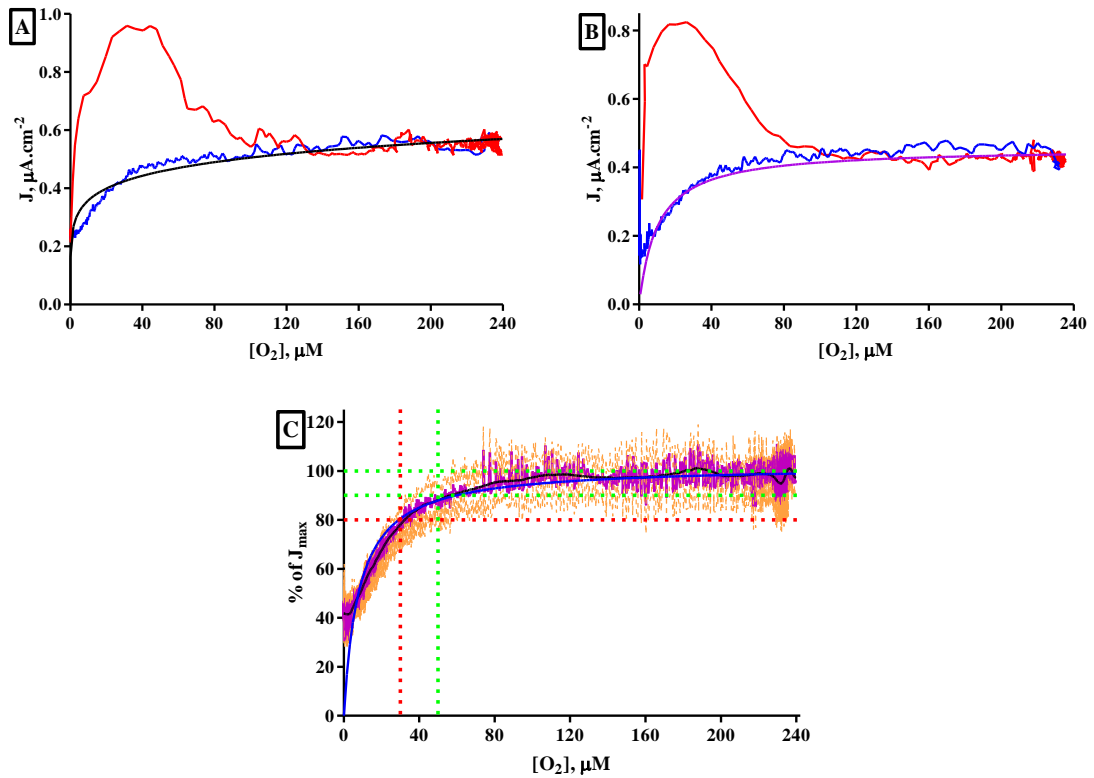


Figure 6-31

The oxygen dependence of the biosensor in the presence of 100 μM D-ser. A & B: the raw data recorded for two sets of biosensors. C: the data from all four traces combined.

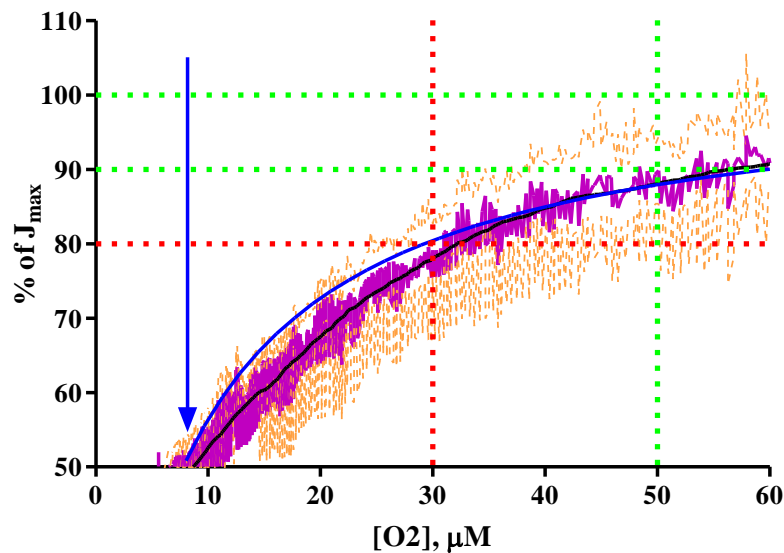


Figure 6-32

A detailed view of the oxygen dependence of the biosensor in the presence of 100 μM D-ser.

As with the three other concentrations of D-ser utilised in this study, there is a large overshoot in the  $J$  values as oxygen is resupplied to the system (red traces in A and B, Figure 6-31) for 100 μM D-ser. In experiment A the period of higher activity peaks at 176% of the  $J_{max}$  after 11 seconds. The period of activity lasts in total 27 seconds before

returning the  $J_{\max}$  value at approximately 90  $\mu\text{M O}_2$ . A peak J that is 180% of the  $J_{\max}$  is attained for calibration B after 10 seconds. The overshoot in current lasts for a total of 22 seconds and returns to the  $J_{\max}$  when the dissolved oxygen content reaches 80  $\mu\text{M}$ .

In Figure 6-32 it can be seen that the kinetic curve (blue trace) and the mean values (purple) and the smoothed values (black trace) all reach the 80% of  $J_{\max}$  mark between 30 and 32  $\mu\text{M}$  dissolved oxygen content. At 50  $\mu\text{M O}_2$  the J value is still less than 90% of the maximum and is only just reaching 90% as the oxygen content increases to 60  $\mu\text{M}$ . While this is on the limit of being called oxygen independent it is still satisfactory to observe that the variance in the signal size is less than 10% over the physiological range. This again is a more than satisfactory result - it would only be in very rare circumstances that the physiological concentration of D-ser could reach 100  $\mu\text{M}$ , such as severe manipulation by external forces or drugs. The M-M curve fitted to the data has an  $R^2$  value of 0.9015, a  $J_{\max}$  of  $102.3 \pm 0.3\%$  of the individually fitted  $J_{\max}$  values, and a  $K_M(\text{O}_2)$  of  $8.141 \pm 0.166 \mu\text{M O}_2$  (indicated by the blue arrow).

## 6.10 *In Vitro* Characterisation – Other Parameters

### 6.10.1 Limit of Detection

A very important characteristic for any sensor is its limit of detection (LOD). This value is the minimum concentration of a particular substrate that the sensor can be said to reliably detect. The main factor influencing the baseline or background signal and the quantity of noise associated with it. Thus the LOD is calculated as three times the standard deviation (SD) of the baseline values. Below this value the signal is determined to be compromised or unreliable due to the noise inherent in any detection system, and any changes smaller than this cannot be attributed to a change in the analyte levels. Thus the baseline data for the 52 biosensors used in 6.4.4, to calculate the final sensitivity, were analysed to determine the LOD. These sensors had a mean baseline of  $0.102 \mu\text{A.cm}^{-2}$ , with a SD of  $\pm 0.007 \mu\text{A.cm}^{-2}$ . The sensitivity of these sensors was calculated as  $16.47 \pm 0.18 \mu\text{A.cm}^{-2}.\text{mM}^{-1}$ . Thus the SD converts to a concentration of  $4.250 \pm 0.047 \times 10^{-4} \text{ mM}$ . The limit of detection of these biosensors is thus  $0.425 \pm 0.005 \mu\text{M}$ .



[D-serine]	5 - 10 $\mu\text{M}$				10 - 20 $\mu\text{M}$			
Electrode	E1	E2	E3	E4	E1	E2	E3	E4
Original Baseline, nA	0.784	0.956	0.502	0.421	0.896	1.008	0.610	0.476
New Baseline, nA	0.877	1.016	0.601	0.476	1.076	1.116	0.801	0.578
Difference, nA	0.093	0.060	0.099	0.055	0.181	0.108	0.191	0.102
90% of Difference, nA	0.084	0.054	0.089	0.049	0.163	0.097	0.172	0.092
90% Threshold, nA	0.868	1.010	0.591	0.470	1.058	1.105	0.782	0.568
Time Taken, s	9.125	8.500	9.125	10.500	1.375	3.875	5.750	7.750
[D-serine]	20 - 40 $\mu\text{M}$				40 - 50 $\mu\text{M}$			
Electrode	E1	E2	E3	E4	E1	E2	E3	E4
Original Baseline, nA	1.091	1.131	0.807	0.582	1.446	1.377	1.275	0.804
New Baseline, nA	1.447	1.362	1.245	0.802	1.645	1.503	1.480	0.921
Difference, nA	0.355	0.230	0.438	0.221	0.199	0.125	0.205	0.117
90% of Difference, nA	0.320	0.207	0.394	0.198	0.179	0.113	0.184	0.105
90% Threshold, nA	1.411	1.339	1.201	0.780	1.625	1.490	1.459	0.909
Time Taken, s	5.125	9.500	1.375	5.125	9.000	7.750	0.750	5.500
[D-serine]	50 - 60 $\mu\text{M}$				60 - 100 $\mu\text{M}$			
Electrode	E1	E2	E3	E4	E1	E2	E3	E4
Original Baseline, nA	1.773	1.562	1.462	0.932	1.849	1.775	1.690	1.035
New Baseline, nA	1.995	1.675	1.728	1.035	2.525	2.198	2.487	1.446
Difference, nA	0.222	0.113	0.266	0.103	0.676	0.423	0.796	0.411
90% of Difference, nA	0.200	0.102	0.239	0.092	0.608	0.380	0.717	0.370
90% Threshold, nA	1.973	1.664	1.701	1.025	2.457	2.155	2.407	1.405
Time Taken, s	10.250	5.875	11.250	1.000	1.500	1.250	10.500	1.125

Table 6-22

Data collected for the determination of the response time of the biosensor.

The red line indicates the mean level of the signal for 50  $\mu\text{M}$  D-ser. This was calculated as the mean of 20 seconds of recorded data previous to the point of injection. The yellow line indicates the new level which was recorded after the injection had occurred; again this was taken as the mean of 20 second period 30 seconds after the injection had taken place. The green line is the 90% threshold the current had to cross to be considered the end point of the response time. The vertical black line is the time-point where the injection occurred and the current began to climb above the previous baseline. The time between the black line and where the trace crosses the green line was calculated as the response time.

This analysis was performed on all four electrodes used in the calibration for 6 different concentration changes. The changes used were the in the range 5 to 100  $\mu\text{M}$ , chosen to reflect the range where changes might be expected to occur during *in vivo* experimentation. The data collected during this analysis is recorded in Table 6-22. From

this data the mean, standard deviation and standard error of mean were calculated. The mean  $\pm$  SEM was found to be  $5.95 \pm 0.75$  s with an SD of  $\pm 3.66$  s ( $n = 24$ ).

## 6.11 Conclusions

With the perceived need to improve the currents being detected, as opposed to the sensitivity as described by the J value, a new approach was considered. This involved firstly the alteration of the electrode surface to a 0.5 mm cylinder from the original disk, and secondly the exchange of the styrene for MMA as an immobilisation matrix. The new cylinder surface produced a marked increase in the currents being achieved at the proposed physiological levels. With MMA used in a two application process the sensitivity, as a function of surface area, was also improved four-fold.

Together these results were chosen as the best path forward for the biosensor protocol. The sensitivity of Pt<sub>C</sub>-{MMA-[600UPBSx5-GA1.0%]x2}x2 is  $45.14 \pm 0.90 \mu\text{A}\cdot\text{cm}^{-2}\cdot\text{mM}^{-1}$ , as compared to Pt<sub>D</sub>-Sty-[600UPBSx5-GA1.0%]x2 and Pt<sub>D</sub>-Sty-[600UPBSx5-FAD0.08-GA1.0%]x2 which have sensitivities of  $35.41 \pm 1.19 \mu\text{A}\cdot\text{cm}^{-2}\cdot\text{mM}^{-1}$  and  $64.61 \pm 1.63 \mu\text{A}\cdot\text{cm}^{-2}\cdot\text{mM}^{-1}$  respectively. This is especially impressive considering that the cylinder protocol had roughly 16 times the surface area of the disk electrodes. With this in mind, the reintroduction of FAD to the cylinder protocol was examined. However, it was found in this instance that the new formulation did not accept FAD very well and the sensitivities were significantly reduced. Thus it appeared that the best recipe had been discovered in Pt<sub>C</sub>-{MMA-[600UPBSx5-GA1.0%]x2}x2.

With this in mind a quick stability trial was performed. It was found that there was a significant loss of sensitivity over 5 days which was considered unacceptable. A solution was found in the application of a further layer of MMA which served to encapsulate and stabilise the substances already on the surface. This alternative, Pt<sub>C</sub>-{MMA-[600UPBSx5-GA1.0%]x2}x2-MMA provided a significantly better retention of sensitivity, and was selected as the best design to be used as long as interference rejection layers could successfully be incorporated within it. It has a sensitivity of  $53.33 \pm 2.47 \mu\text{A}\cdot\text{cm}^{-2}\cdot\text{mM}^{-1}$ .

The selection of the interference layer offered two possibilities. A P-*o*-PD layer, grown by CPA (PPD) which would block out the majority of interference and slightly decrease the sensitivity to  $38.22 \pm 1.99 \mu\text{A}\cdot\text{cm}^{-2}\cdot\text{mM}^{-1}$ , or a combination of PPD with 5 layers of

Naf applied before it which completely blocked out AA interference but significantly reduced the sensitivity further to only  $16.47 \pm 0.18 \mu\text{A}\cdot\text{cm}^{-2}\cdot\text{mM}^{-1}$ . In the context of the small currents that would be attainable *in vivo* the consensus was that a greater degree of interference rejection would provide the best overall solution. Thus, the Naf-PPD combination was chosen, yielding a final biosensor protocol of Pt<sub>C</sub>-Naf-PPD-{MMA-[600UPBSx5-GA1.0%]x2}x2.

Thus, the *in vitro* characterisation of the final biosensor design began. Firstly the stability was tested over a short period of time and with repeated calibrations. This provided a reference for the effects of repeated calibration, as opposed to time or treatment effects, for the remainder of the characterisation. The protocol was also tested for stability over multiple calibrations over a long period of time. It was found that repeated calibration could reduce sensitivity by between 40 and 45% over 4 to 6 calibrations in a short space of time and by up to 80% with repeated calibration over a long period of time. It appears that a major factor affecting this loss is the heating, cooling, wetting and drying processes that take place when the sensors are put into and out of storage. Single calibrations over an extended period of time also alluded to the effect time had on the sensors. This is possibly due to the continuing slow interaction of the molecule layers in the biosensor, which alters the composition or bonding between the substances present.

Bio-compatibility studies illustrated that the biosensors are affected to a greater degree by protein (BSA) than lipid (PEA) treatments. Unusually a low level of BSA, 1%, degraded the sensitivity further than a 10% BSA treatment, but this had been seen previously for the characterisation of an earlier D-ser biosensor design and is thus an expected result. Exposure to a brain tissue sample elicited drastic changes in the sensitivity, reducing it by 50% after one day when the repeated calibration effect was taken out. The effects noticed in these studies are possibly far greater than those that would be experienced in an *in vivo* environment and the constant flux of the sensors in and out of the respective solutions and tissue samples could expose the biosensing membrane to far greater damage than if it was only inserted once and then remained stationary.

Temperature and pH changes also produced some effect on the biosensor sensitivity. But it was no more than is to be expected following the repeated calibration procedures and the effect that both of these elements have on the functioning of an enzyme.

When tested for sensitivity towards other amino acids it is found that there is no significant sensitivity towards any of the L-amino acids or glycine. Some D-amino acids were detected while others were not. D-ser, D-ala and D-phe were all detected to the same degree, while the biosensor was twice as sensitive to D-pro as it was to the later three. When calibrated individually the biosensor was twice as sensitive to D-ala as it was to D-ser, but this is in-line with reported kinetic rates and affinities. As with the initial interference testing for AA, the design was found to be equally unresponsive to the 11 other common electroactive species.

The final, and vitally important, characteristic explored is the oxygen independence of the protocol. It is found that the design is oxygen independent up to a concentration of 100  $\mu\text{M}$  D-ser. Subsequent to this satisfactory result, the limit of detection was determined to be  $0.425 \pm 0.005 \mu\text{M}$  and the biosensor has a response time of  $5.95 \pm 0.75$  s. This biosensor was ultimately decided to be fit for chronic *in vivo* utilisation.

References

- Bean LS, Heng LY, Yamin BM & Ahmad M. (2005). The electrochemical behaviour of ferrocene in a photocurable poly(methyl methacrylate-co-2-hydroxyethyl methacrylate) film for a glucose biosensor. *Bioelectrochemistry* **65**, 157-162.
- Bolger FB, Bennett R & Lowry JP. (2011a). An *in vitro* characterisation comparing carbon paste and Pt microelectrodes for real-time detection of brain tissue oxygen. *Analyst* **136**, 4028-4035.
- Bolger FB, McHugh SB, Bennett R, Li J, Ishiwari K, Francois J, Conway MW, Gilmour G, Bannerman DM, Fillenz M, Tricklebank M & Lowry JP. (2011b). Characterisation of carbon paste electrodes for real-time amperometric monitoring of brain tissue oxygen. *Journal of Neuroscience Methods* **195**, 135-142.
- Brown FO, Finnerty NJ & Lowry JP. (2009). Nitric oxide monitoring in brain extracellular fluid: characterisation of Nafion-modified Pt electrodes *in vitro* and *in vivo*. *Analyst* **134**, 2012-2020.
- Brown FO & Lowry JP. (2003). Microelectrochemical sensors for *in vivo* brain analysis: An investigation of procedures for modifying Pt electrodes using Nafion ®. *Analyst* **128**, 700-705.
- Brunori M, Rotilio GC, Antonini E, Curti B, Branzoli U & Massey V. (1971). Oxidation-reduction potentials of D-amino acid oxidase. *Journal of Biological Chemistry* **246**, 3140-3144.
- Burton K. (1951). The stabilization of D-amino acid oxidase by flavin-adenine dinucleotide, substrates and competitive inhibitors. *The Biochemical Journal* **48**, 458-467.
- Cartmell J, Perry KW, Salhoff CR, Monn JA & Schoepp DD. (2000). The potent, selective mGlu2/3 receptor agonist LY379268 increases extracellular levels of dopamine, 3,4-dihydroxyphenylacetic acid, homovanillic acid, and 5-hydroxyindole-3-acetic acid in the medial prefrontal cortex of the freely moving rat. *Journal of Neurochemistry* **75**, 1147-1154.
- Craig JD & O'Neill RD. (2003). Comparison of simple aromatic amines for electrosynthesis of permselective polymers in biosensor fabrication. *Analyst* **128**, 905-911.

- Dai H, Wu X, Wang Y, Zhou W & Chen G. (2008). An electrochemiluminescent biosensor for vitamin C based on inhibition of luminol electrochemiluminescence on graphite/poly(methylmethacrylate) composite electrode. *Electrochimica Acta* **53**, 5113-5117.
- Danysz W & Parsons CG. (1998). Glycine and N-methyl-D-aspartate receptors: Physiological significance and possible therapeutic applications. *Pharmacological Reviews* **50**, 597-664.
- Dixon M & Kleppe K. (1965a). D-amino acid oxidase II: Specificity, competitive inhibition and reaction sequence. *Biochimica et Biophysica Acta (BBA):- Nucleic Acids and Protein Synthesis* **96**, 368-382.
- Dixon M & Kleppe K. (1965b). D-amino acid oxidase III. Effect of pH. *Biochimica et Biophysica Acta* **96**, 383-389.
- Ferraris D, Duvall B, Ko Y-S, Thomas AG, Rojas C, Majer P, Hashimoto K & Tsukamoto T. (2008). Synthesis and biological evaluation of D-amino acid oxidase inhibitors. *Journal of Medicinal Chemistry* **51**, 3357-3359.
- Foster TH, Hartley DF, Nichols MG & Hilf R. (1993). Fluence Rate Effects in Photodynamic Therapy of Multicell Tumor Spheroids. *Cancer Research* **53**, 1249-1254.
- Friedemann MN, Robinson SW & Gerhardt GA. (1996). *o*-Phenylenediamine-modified carbon fiber electrodes for the detection of nitric oxide. *Analytical Chemistry* **68**, 2621-2628.
- Garguilo MG & Michael AC. (1995). Optimization of amperometric microsensors for monitoring choline in the extracellular fluid of brain-tissue. *Analytica Chimica Acta* **307**, 291-299.
- Hall CE, Datta D & Hall EAH. (1996). Parameters which influence the optimal immobilisation of oxidase type enzymes on methacrylate copolymers as demonstrated for amperometric biosensors. *Analytica Chimica Acta* **323**, 87-96.
- Hamase K, Konno R, Morikawa A & Zaitzu K. (2005). Sensitive determination of D-amino acids in mammals and the effect of D-amino-acid oxidase activity on their amounts. *Biological & Pharmaceutical Bulletin* **28**, 1578-1584.
- Hashimoto A, Nishikawa T, Konno R, Niwa A, Yasumura Y, Oka T & Takahashi K. (1993). Free D-serine, D-aspartate and D-alanine in central nervous system and

serum in mutant mice lacking D-amino acid oxidase. *Neuroscience Letters* **152**, 33-36.

Haughton E. (pending publication). Real-time Neurochemical Analysis of Excitatory Amino Acids: Enzyme-modified Microelectrochemical Biosensors for Aspartate and Glutamate. In *Department of Chemistry*. National University of Ireland, Maynooth, (pending publication).

Hervás Pérez JP, López-Cabarcos E & López-Ruiz B. (2008). Encapsulation of glucose oxidase within poly(ethylene glycol) methyl ether methacrylate microparticles for developing an amperometric glucose biosensor. *Talanta* **75**, 1151-1157.

Horiike K, Shiga K, Nishina Y & Yamano T. (1976). pH dependence of catalysis of the monomer of hog kidney D-amino acid oxidase. *Medical Journal of Osaka University* **27**, 33-46.

Kane DA & O'Neill RD. (1998). Major differences in the behaviour of carbon paste and carbon fibre electrodes in a protein-lipid matrix: implications for voltammetry in vivo. *Analyst* **123**, 2899-2903.

Lingnau J & Meyerhoff G. (1983). The spontaneous polymerization of methyl methacrylate. 6. Polymerization in solution: participation of transfer agents in the initiation reaction. *Polymer* **24**, 1473-1478.

Lingnau J & Meyerhoff G. (1984a). The spontaneous polymerization of methyl methacrylate. 7. External heavy atom effect on the initiation. *Die Makromolekulare Chemie* **185**, 587-600.

Lingnau J & Meyerhoff G. (1984b). Spontaneous polymerization of methyl methacrylate. 8. Polymerization kinetics of acrylates containing chlorine atoms. *Macromolecules* **17**, 941-945.

Lingnau J, Stickler M & Meyerhoff G. (1980). The spontaneous polymerization of methyl methacrylate. 4. Formation of cyclic dimers and linear trimers. *European Polymer Journal* **16**, 785-791.

Liu S, Srinivasan S, Grady MC, Soroush M & Rappe AM. (2012). Computational study of cyclohexanone–monomer co-initiation mechanism in thermal homopolymerization of methyl acrylate and methyl methacrylate. *The Journal of Physical Chemistry A* **116**, 5337-5348.

- López MS-P, Mecerreyes D, López-Cabarcos E & López-Ruiz B. (2006). Amperometric glucose biosensor based on polymerized ionic liquid microparticles. *Biosensors & Bioelectronics* **21**, 2320-2328.
- Lowry JP & O'Neill RD. (1994). Partial characterization *in vitro* of glucose oxidase-modified poly(phenylenediamine)-coated electrodes for neurochemical analysis *in vivo*. *Electroanalysis* **6**, 369-379.
- Miele M & Fillenz M. (1996). *In vivo* determination of extracellular brain ascorbate. *Journal of Neuroscience Methods* **70**, 15-19.
- Miyoshi Y, Hamase K, Okamura T, Konno R, Kasai N, Tojo Y & Zaitzu K. (2011). Simultaneous two-dimensional HPLC determination of free D-serine and D-alanine in the brain and periphery of mutant rats lacking D-amino-acid oxidase. *Journal of Chromatography B, Analytical Technologies in the Biomedical Life Sciences* **879**, 3184-3189.
- Miyoshi Y, Hamase K, Tojo Y, Mita M, Konno R & Zaitzu K. (2009). Determination of D-serine and D-alanine in the tissues and physiological fluids of mice with various D-amino-acid oxidase activities using two-dimensional high-performance liquid chromatography with fluorescence detection. *Journal of Chromatography B, Analytical Technologies in the Biomedical Life Sciences* **877**, 2506-2512.
- Miyoshi Y, Konno R, Sasabe J, Ueno K, Tojo Y, Mita M, Aiso S & Hamase K. (2012). Alteration of intrinsic amounts of D-serine in the mice lacking serine racemase and D-amino acid oxidase. *Amino Acids*.
- Molla G, Motteran L, Piubelli L, Pilone MS & Pollegioni L. (2003). Regulation of D-amino acid oxidase expression in the yeast *rhodotorula gracilis*. *Yeast* **20**, 1061-1069.
- Molla G, Sacchi S, Bernasconi M, Pilone MS, Fukui K & Pollegioni L. (2006). Characterization of human D-amino acid oxidase. *FEBS Letters* **580**, 2358-2364.
- Morais J, Papadimitrakopoulos F & Burgess D. (2010). Biomaterials/tissue interactions: Possible solutions to overcome foreign body response. *The AAPS Journal* **12**, 188-196.
- Morikawa A, Hamase K, Inoue T, Konno R, Niwa A & Zaitzu K. (2001). Determination of free D-aspartic acid, D-serine and D-alanine in the brain of mutant mice lacking D-amino acid oxidase activity. *Journal of Chromatography B, Biomedical Sciences & Applications* **757**, 119-125.

- O'Brien KB, Killoran SJ, O'Neill RD & Lowry JP. (2007). Development and characterization *in vitro* of a catalase-based biosensor for hydrogen peroxide monitoring. *Biosensors & Bioelectronics* **22**, 2994-3000.
- Ormonde DE & O'Neill RD. (1989). Altered response of carbon paste electrodes after contact with brain tissue: Implications for modified electrode use *in vivo*. *Journal of Electroanalytical Chemistry and Interfacial Electrochemistry* **261**, 463-469.
- Ormonde DE & O'Neill RD. (1990). The oxidation of ascorbic acid at carbon paste electrodes: Modified response following contact with surfactant, lipid and brain tissue. *Journal of Electroanalytical Chemistry and Interfacial Electrochemistry* **279**, 109-121.
- Pan S & Arnold MA. (1996). Selectivity enhancement for glutamate with a Nafion/glutamate oxidase biosensor. *Talanta* **43**, 1157-1162.
- Pernot P, Mothet J-P, Schuvailo O, Soldatkin A, Pollegioni L, Pilone M, Adeline M-T, Cespuoglio R & Marinesco S. (2008). Characterization of a yeast D-amino acid oxidase microbiosensor for D-serine detection in the central nervous system. *Analytical Chemistry* **80**, 1589-1597.
- Rothwell SA, Killoran SJ, Neville EM, Crotty AM & O'Neill RD. (2008). Poly(*o*-phenylenediamine) electrosynthesized in the absence of added background electrolyte provides a new permselectivity benchmark for biosensor applications. *Electrochemistry Communications* **10**, 1078-1081.
- Rothwell SA, Kinsella ME, Zain ZM, Serra PA, Rocchitta G, Lowry JP & O'Neill RD. (2009). Contributions by a novel edge effect to the permselectivity of an electrosynthesized polymer for microbiosensor applications. *Analytical Chemistry* **81**, 3911-3918.
- Srinivasan S, Lee MW, Grady MC, Soroush M & Rappe AM. (2011). Computational evidence for self-initiation in spontaneous high-temperature polymerization of methyl methacrylate. *The Journal of Physical Chemistry A* **115**, 1125-1132.
- Stickler M & Meyerhoff G. (1981). The spontaneous thermal polymerization of methyl methacrylate. 5. Experimental study and computer simulation of the high conversion reaction at 130°C. *Polymer* **22**, 928-933.
- Wilson GS & Gifford R. (2005). Biosensors for real-time *in vivo* measurements. *Biosensors & Bioelectronics* **20**, 2388-2403.

- Wolosker H, Panizzutti R & Miranda JD. (2002). Neurobiology through the looking-glass: D-serine as a new glial-derived transmitter. *Neurochemistry International* **41**, 327-332.
- Xu J-J, Yu Z-H & Chen H-Y. (2002). Glucose biosensors prepared by electropolymerization of *p*-chlorophenylamine with and without Nafion. *Analytica Chimica Acta* **463**, 239-247.
- Yagi K & Ohishi N. (1972). Structure and function of D-amino acid oxidase: IV. Electrophoretic and ultracentrifugal approach to the monomer equilibrium. *Journal of Biochemistry* **71**, 993-998.
- Zain ZM, O'Neill RD, Lowry JP, Pierce KW, Tricklebank M, Dewa A & Ab Ghani S. (2010). Development of an implantable D-serine biosensor for in vivo monitoring using mammalian D-amino acid oxidase on a poly (*o*-phenylenediamine) and Nafion-modified platinum-iridium disk electrode. *Biosensors & Bioelectronics* **25**, 1454-1459.
- Zetterström T, Sharp T, Marsden CA & Ungerstedt U. (1983). *In vivo* measurement of dopamine and its metabolites by intracerebral dialysis: Changes after D-amphetamine. *Journal of Neurochemistry* **41**, 1769-1773.
- Zimmerman JB & Wightman RM. (1991). Simultaneous electrochemical measurements of oxygen and dopamine in vivo. *Analytical Chemistry* **63**, 24-28.

---

---

**7. A PRELIMINARY *IN VIVO* STUDY OF  
THE BIOSENSOR FUNCTIONALITY**

---

---

## 7.1 Introduction

The overall aim of this thesis was to produce a D-amino acid oxidase based biosensor capable of detecting D-serine, and the changes in its concentration, in the mammalian brain. Having completed the *in vitro* development and characterisation of such a biosensor, and being satisfied with the results, it was deemed necessary to perform a preliminary investigation of the performance of the biosensor *in vivo*. Without this it is not possible to quantify the success of the biosensor design as physiological circumstances are uniquely challenging.

Previously Pernot *et al.* had demonstrated the performance of their D-ser biosensor in the frontal cortex of a rat (strain unknown) (Pernot *et al.*, 2008). However, the rat was anaesthetised with a ketamine/xylazine mixture during the procedure. It is known that ketamine acts on the NMDA receptor (Hirota & Lambert, 1996), and hence influences the glutamatergic system, as well as influencing NO synthesis (Aroni *et al.*, 2009). Both of these systems are highly implicated in the regulation of D-ser levels physiologically, see Section 1.4. Their work demonstrated an increasing level of D-ser in the brain over 3 hours, following an intraperitoneal (i.p.) injection of 1 g D-ser/kg body weight.

Zain has also demonstrated the functioning of a DAAO biosensor in the striatum of Sprague-Dawley rats (Zain *et al.*, 2010). The rats were also anaesthetised, this time with a chloralose/ethyl carbamate mixture. It was found possible to demonstrate a brief response, about three seconds, to a high concentration, 5  $\mu$ L of a 100 mM solution, of D-ser. The D-ser was delivered by microinjection beside the implanted biosensor. It was discovered that there appeared to be a highly effective uptake system removing the injected D-ser, as the signal dropped back below baseline in less than 1 second, and a high concentration of D-ser was required to elicit a response.

With both of these studies demonstrating results obtained under anaesthetic, it was decided to try to obtain results from an awake and freely moving animal. To do this two different devices would need to be implanted into a subject; a microdialysis probe, for the delivery of substances into the brain, and the DAAO biosensor, to monitor any changes that were elicited. The results are all taken from one animal, where a biosensor was co-implanted into the right striatum with a microdialysis probe and a second biosensor implanted into the left striatum. This was due to time constraints on further experimentation, and that this study was meant to be only a preliminary investigation

into the correct functioning of the final biosensor design. The striatum was chosen as it is a large, and surgically easy to find, area of the cerebrum which forms part of the basal ganglia in the subcortical region of the telencephalon (see Section 1.1).

## 7.2 aCSF Perfusion

The first effect to be studied was the effect that an aCSF perfusion would have on the response of the biosensors as this would be the vehicle for all other perfused substances. Thus it was administered into the right striatum of the subject and the response monitored on the biosensor in the right and left striatum.

<b>n = 6</b>	<b>Mean</b>	<b>± S.D.</b>	<b>± S.E.M.</b>
<b>Initial Baseline Current (I, nA)</b>	0.851	0.473	0.193
<b>Maximum/Minimum Current (I, nA)</b>	0.609	0.340	0.139
<b>Time to max/min Current (hrs)</b>	00:54:43	00:19:21	00:07:54
<b>Overall Current Change (I, nA)</b>	-0.242	0.145	0.059
<b>% Current change from Baseline</b>	-28.1	5.9	2.4
<b>Post Baseline (I, nA)</b>	0.752	0.440	0.180
<b>Time to Post Baseline (end perfusion) (hrs)</b>	01:16:10	00:23:17	00:09:30
<b>Post Baseline % Change</b>	-12.1	9.2	3.8

Table 7-1

Data collected from perfusions of aCSF into the right striatum of a rat

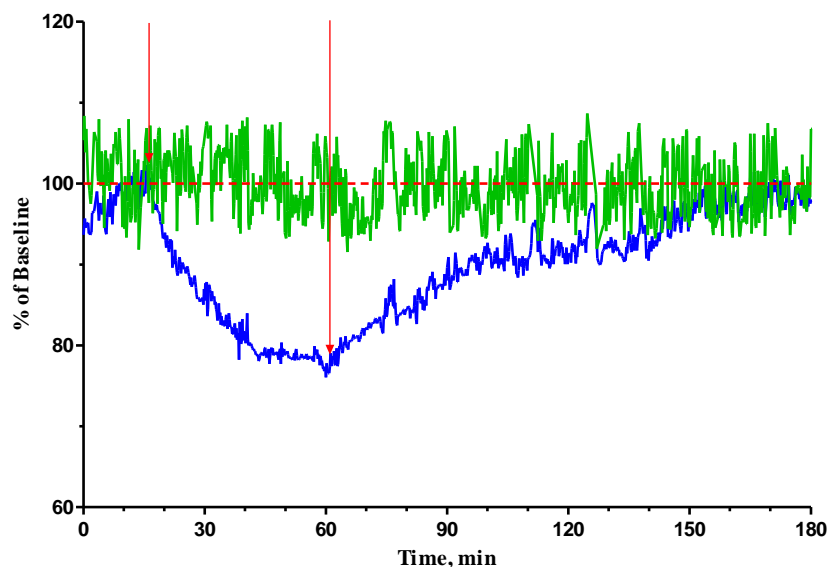


Figure 7-1

An aCSF perfusion from day 14 of the experiment period. The red arrows indicate the start and end of the perfusion. The blue line is the trace from the electrode in the right striatum next to the microdialysis probe, the green trace is the biosensor in the left striatum.

### 7.3 Serine Perfusions

Having established how the vehicle affected the signal, it was possible to examine using both stereoisomers of serine in the perfusate. It was hoped that different concentrations of D-ser would elicit different quantities of change in the signal with some producing decreases in the signal and others increases. It was also necessary to look at the effect L-ser would have on the current. It would be hoped that there would be a similar response as that elicited for aCSF, as L-ser is not a substrate for DAAO and does not inhibit its function (Figure 6-21)(Pollegioni *et al.*, 2007). Taken together these results would be verifiable evidence that the sensor was functioning as intended.

#### 7.3.1 D-serine perfusions

Thus a range of D-serine concentrations were chosen in the hope of returning a range of responses. This began at 10  $\mu$ M and increased up to 1000  $\mu$ M. The same protocol was followed as with aCSF perfusions.

##### 7.3.1.1 10 $\mu$ M D-serine

D-ser perfusions began with a 10  $\mu$ M concentration of D-ser made up in an aCSF solution. The perfusion was performed in the same manner as before. However a problem did occur during the experiment. In order to keep the subject calm and relaxed human presences were avoided, as much as possible, within the experimental room while perfusions were in progress. To this end, and bearing in mind that the aCSF perfusions took, on average, nearly 55 minutes to reach a baseline, after an initial 5 minute observation period the subject was left alone until the 40<sup>th</sup> minute. At this time it was found that the perfusion tube had come away from the probe inlet.

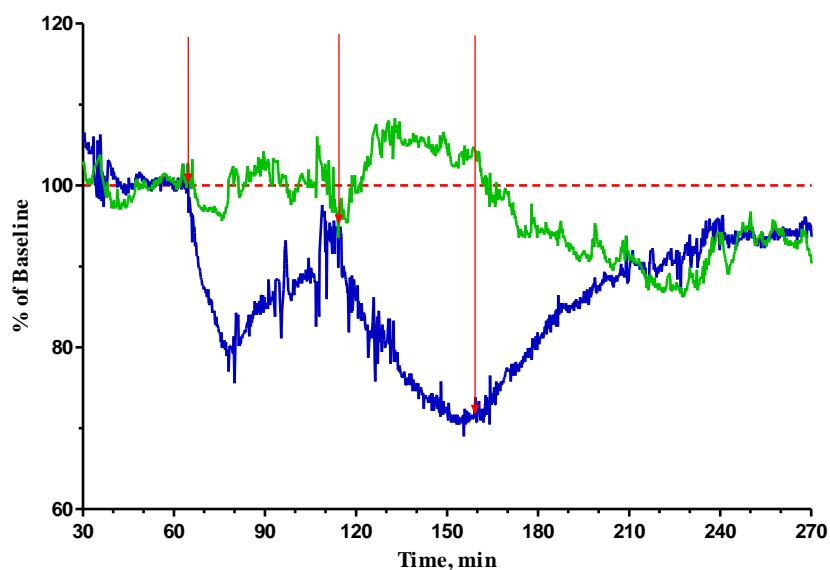


**Figure 7-2**  
Perfusion of D-ser.

Examination of the data, presented in Figure 7-2, clearly displays the occurrence of this after approximately 15 minutes after the commencement of the experiment (first red arrow). Following this, the recorded signal (blue trace) for the biosensor next to the probe, begins to increase again. This continues until the tubing is re-attached in the 50<sup>th</sup> minute, second red arrow) whereby the current then returns to a decreasing trend. After a baseline is reached the perfusion is stopped, the third red arrow, and the signal is allowed to find its new baseline.

Taking account of the break in the perfusion the results overall are as follows: it took 46:40 minutes to reach the perfusion response level, the current decreasing from 0.414 nA to 0.295 nA, a decrease of 0.119 nA or 28.8% less than the pre-perfusion level. It took 1:12:20 hours for the current to return to a stable level after the perfusion was ended. The current at this point was 0.388 nA, 6.4% below the pre-perfusion level.

### 7.3.1.2 20 $\mu$ M D-serine

A perfusion of 20  $\mu$ M D-ser yielded similar results to the 10  $\mu$ M perfusion.

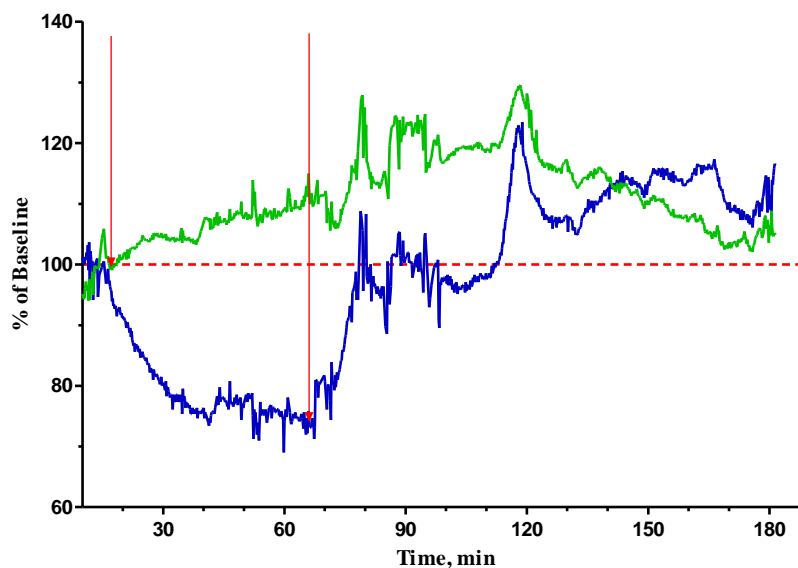


**Figure 7-3**  
Perfusion of D-ser.

The pre-perfusion current was 0.415 nA. After 40:15 minutes the current reached its stable in-perfusion level of 0.310 nA. This was 0.105 nA or 25.4 % below the pre-perfusion level. Following the ending of the perfusion it took 1:22:10 hours for the signal to reach a stable post-perfusion level of 0.465. This was 12.0% higher than the pre-perfusion level.

It is interesting to note that against the background of the response to the perfusion some global signal changes on both sensors are visible. At approximately the 80, 90 and 120 minute marks in Figure 7-3 it is possible to see three different and similar, in time, size and shape, current changes. Unfortunately there are no records of any physical activity or any other occurrences at those times. It does, however, illustrate that the biosensors are detecting the chemical changes occurring within the *in vivo* environment, with the local effect of the perfusions and global changes both detectable.

### 7.3.1.3 100 $\mu$ M D-serine

Having failed to illicit an increase in current for either 10 or 20  $\mu$ M D-ser, both of which are more concentrated than the proposed *in vivo* levels, it was decided to increase the perfusate concentration to 100  $\mu$ M D-ser in the hope of producing a higher response. Unfortunately, as can be seen in Figure 7-4, this response failed to materialise. Instead, from a pre-perfusion value of 0.447 nA, the current decreased to 0.340 nA after 42:25

minutes. This represented a decrease in current of 23.9%, or 0.107 nA, from the pre-perfusion level.

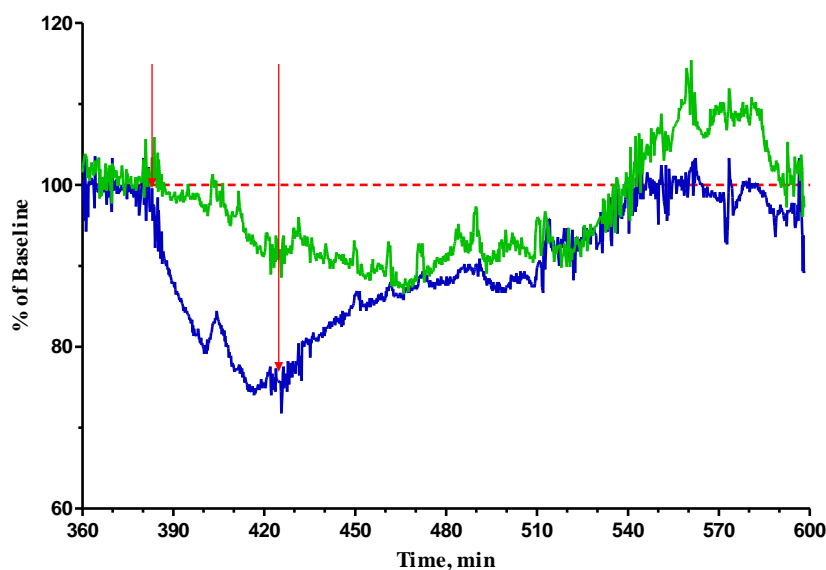


**Figure 7-4**  
Perfusion of D-ser.

From when the perfusion was ceased it took 2:00:00 hours for the current to reach a new stable post-perfusion level of 0.448 nA, an increase of 0.2% over the original pre-perfusion response. It is interesting to note the depression of the signal in the left hemisphere (green trace). This could be a global response to the sudden influx of large quantities of D-ser, where the systems in the brain are trying to remove excess quantities of D-ser. This in turn has depressed the levels in areas away from the microdialysis probe. Several hours after the perfusion has ended it is seen that the responses stabilise, to approximately their original values.

#### 7.3.1.4 1000 $\mu$ M D-serine

In a final attempt to produce an increase in the signal a very concentrated perfusate solution of 1000  $\mu$ M D-ser was used. Based on previous results there was little confidence that this would result in any significant difference from the responses to D-ser perfusions carried out previously. Indeed, observation of the results obtained, see Figure 7-5, shows that result was very similar to those already achieved. Per-perfusion the current was 0.435 nA. After 49:40 minutes of perfusion it reached a stable in-perfusion level of 0.341 nA, 0.094 nA or 21.6% below the pre-perfusion value.

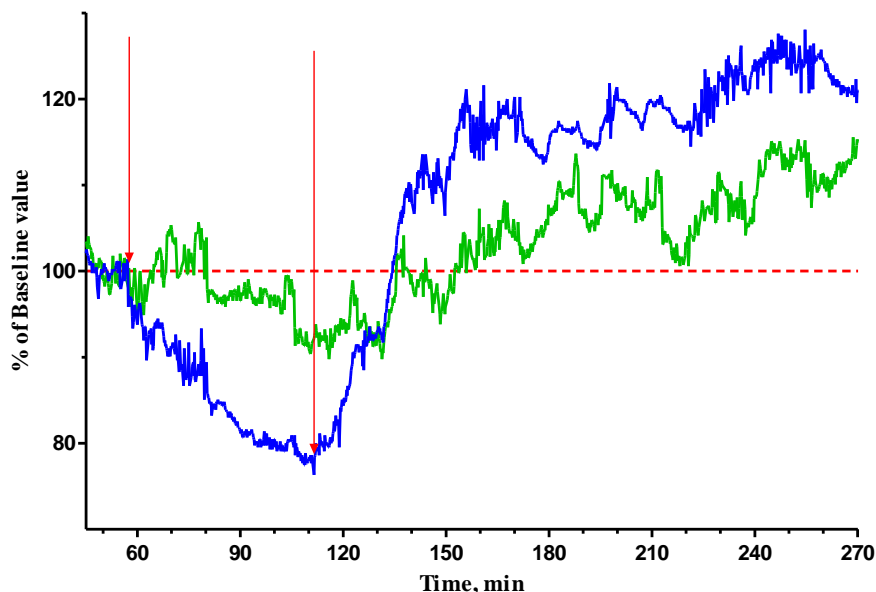


**Figure 7-5**  
Perfusion of D-ser.

Once the perfusion was stopped the current rose for 43:20 minutes to a new post-perfusion baseline of 0.513 nA, this was 18.1% above the pre-perfusion level. As seen with the 100  $\mu$ M perfusion, the 1000  $\mu$ M perfusion appears to produce some sort of a global response, where the biosensor in the left hemisphere also experiences a decrease in current. Post-perfusion, both biosensors register increases in current above the pre-perfusion baseline level for several hours.

### 7.3.1.5 *D-serine Perfusions Conclusions*

Overall the D-ser perfusions have not produced the desired results to confirm that the biosensor is functioning correctly. It is possible however to observe some interesting global and local changes that indicate that the biosensors are indeed detecting D-ser. However, the complex system, outlined in Section 1.6, which is responsible for the D-ser concentration in the ECF, appears to be very efficient at removing excess quantities of the amino acid and at keeping the concentration constant to prevent any excitotoxicity occurring (Shleper *et al.*, 2005). In order to produce categorically different responses, by perfusion, it was decided to look at interrupting these endogenous processes.

This is not an unprecedented situation as similar observations were made during the characterisation of a glutamate biosensor by other members of our group (data currently

unpublished), where perfusion of various concentrations of glutamate continually resulted in a decreased response. Indeed, increases in current were only achieved by the introduction of uptake blockers in combination with stimulated release. Considering that glutamate and D-ser are inextricably linked parts of the same neurotransmission system (Schell *et al.*, 1995) it could be expected that they would both be regulated in a similarly strict manner.

Further evidence for this tightly regulated system is evident from the *in vivo* work carried out with a D-ser biosensor previously (Zain *et al.*, 2010). Here it was demonstrated that an increase of only about 0.020 nA, and lasting only 2 or 3 s, was achievable using a 5  $\mu$ L microinjection of 100 mM D-ser. This concentration is two orders of magnitude higher than any used during this perfusion study. Following this increase a decrease of similar magnitude for less than 1 s was also noted as the removal systems over-compensated for a brief period.

### 7.3.2 L-serine perfusion

As a further clarification of the functioning of the biosensor it was necessary to show that it did not respond increased levels of an L-amino acid. L-ser was chosen, which is a known precursor to D-ser in combination with serine racemase (Wolosker *et al.*, 1999). However, an increase in production of D-ser would only be found if the serine racemase mechanism was activated. Since no stimuli for this system are being provided there should be no issue with a perfusion of L-ser resulting in an increase in D-ser concentration.

When the 1000  $\mu$ M perfusion of L-ser was conducted, see Figure 7-6, it was, as expected, found that there was no increase in the D-ser concentration, this is in agreement with Figure 6-21. Indeed the biosensor response to the perfusion was similar to that expected from an aCSF perfusion, the vehicle in all the perfusions. The pre-perfusion current was 0.459 nA. After 27:50 minutes of perfusion the current reached a new in-perfusion level of 0.352 nA. This was 0.107 nA or 23.3% below the pre-perfusion response. Once the perfusion was stopped it took 28:00 minutes for the signal to reach its post-perfusion level of 0.457 nA, just 0.4% below the pre-perfusion level.

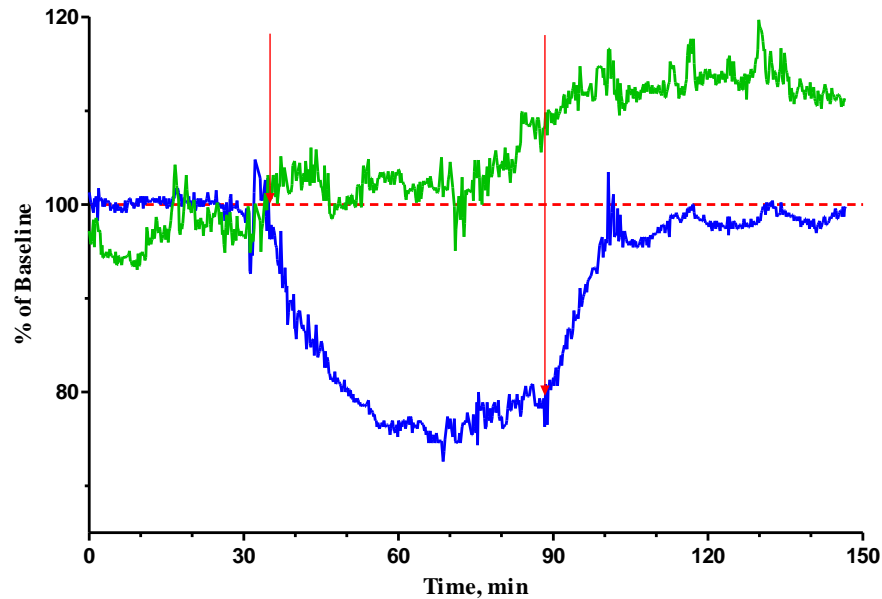


**Figure 7-6**  
A perfusion of L-ser.

It is clear that the response for the L-ser perfusion is very similar to that for either the aCSF or D-ser perfusions. The only major difference is the short time taken for the in-perfusion and post perfusion levels to be reached. Less than half an hour was required in both cases, as opposed to between 45 minutes and 1 hour 20 minutes for the previously mentioned experiments.

#### 7.4 Veratridine Perfusion

When it was realised that it was necessary to stimulate the endogenous release and production or block the clearance systems in order to witness a positive change in the current an exploration of work conducted by others began. A chemical which immediately provoked interest was Veratridine. A voltage-dependant sodium channel activator (Catterall, 1975; Catterall & Coppersmith, 1981; Romei *et al.*, 2011), it keeps these channels open for a long time (Bönisch *et al.*, 1983), actively preventing inactivation. This has the potential to cause neurotoxicity, and has been shown to cause cell death (Jordan *et al.*, 2000; Koike & Ninomiya, 2000; Koike *et al.*, 2000) through overstimulation of the second intra-membrane receptor site, and is thus classed as very toxic. It has, however, been shown to have a beneficial property in staving off cell death by apoptosis (Tanaka & Koike, 1997). More importantly to our purposes it has been shown to evoke the release of D-serine and glucose (Lowry *et al.*, 1998; Rosenberg *et al.*, 2010). Interestingly, it has also been reported that a 200  $\mu\text{M}$  perfusion of

Veratridine has also been shown to lower the concentration of D-ser (Hashimoto *et al.*, 2000). For the experiments carried out 100  $\mu$ M Veratridine in aCSF was utilised, the same concentration as used in the Rosenberg *et al.* D-serine study, and twice that used in the Lowry *et al.* glucose study. The first result obtained is shown below in Figure 7-7. Here two perfusions carried out in close proximity are shown. The rapid return to baseline after the first perfusion allowed the second to be undertaken, and the results mirror each other quite closely.

Over the two perfusions the average decrease from the baseline was 25.4%, which occurred  $27:55 \pm 00:20$  minutes after the start of the perfusion. Following cessation of the perfusion, the post-perfusion level was reached in  $22:10 \pm 05:00$  minutes and was on average  $2.2 \pm 1.0\%$  higher than the pre-perfusion level. Apart from the rapid return to a stable post-perfusion current the response is quite similar to that already demonstrated for the D-ser, L-ser and aCSF perfusions. The rapid return to baseline levels could be indicative of an effect of the Veratridine; however the lack of evidence for an effect during the perfusion means it is not possible to draw any conclusions from this data.

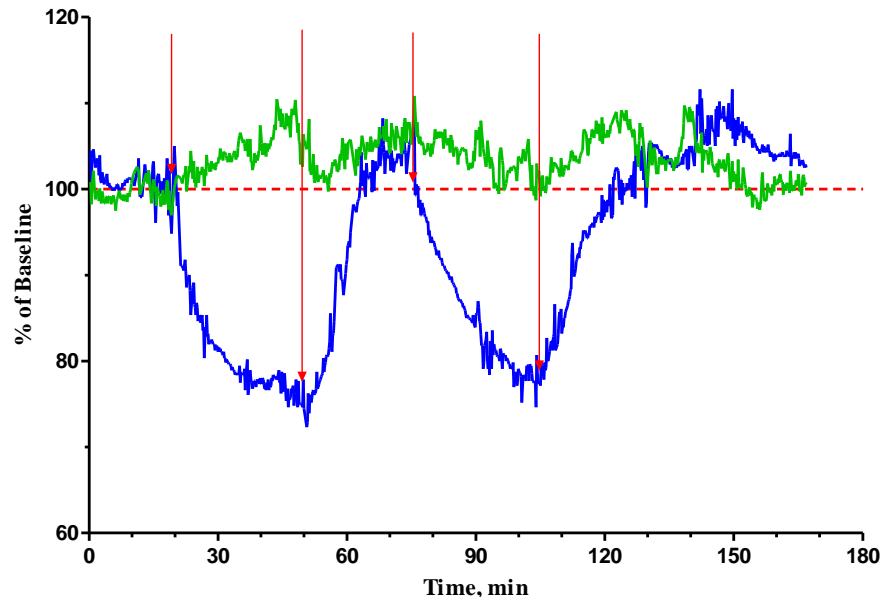


**Figure 7-7**  
A perfusion of Veratridine.

In an attempt to see if this possibility could be further clarified a more complex experiment was carried out. Using a liquid swivel, to switch between perfusion solutions, aCSF was perfused followed by Veratridine, before returning to an aCSF perfusion. The results are displayed in Figure 7-8.

While it is not conclusive this experiment does appear to offer some indication that the Veratridine is producing an increase in the signal. Initially with the perfusion of aCSF the current decreases by 24.6% over 01:19:15 hours. From the point where the Veratridine reaches the probe (first thick red arrow) until the point where the second perfusion of aCSF reaches the probe (second thick red arrow) the current increases by 3.9% over 01:21:35 hours. This occurs after an initial decrease in the response as the Veratridine takes effect. With the commencement of the second perfusion of aCSF, the current proceeds to decrease by 2.7% from its Veratridine level to almost exactly the same level as for the first aCSF perfusion. However, these changes are minimal and larger more definite changes are required to say that an increase in the signal was produced.

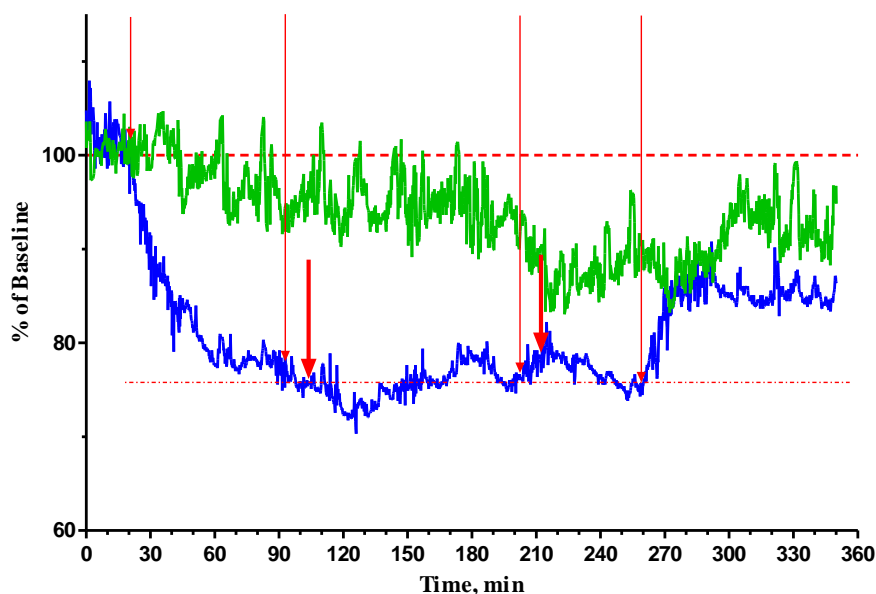


Figure 7-8

The compound perfusion sequence of aCSF, Veratridine and aCSF again. The first thin arrow indicates the start of the first aCSF perfusion. The second thin arrow indicates the switch-over to Veratridine, with the thicker arrow marking the point where the Veratridine would have reached the probe. The third thin arrow marks the switch-back to aCSF. The second thicker arrow marks the point where the solution would have filled the tubing and reaches the probe. The final thin arrow marks the end of the perfusion sequence. Thick arrows allow for the dead volume.

## 7.5 Mg.ATP Perfusion

Having failed to illicit any definitive, positive response from simple D-ser perfusions or the blanket stimulation approach of the glutamate pathway by Veratridine, the decision was taken to look at a more focus, D-ser specific approach. This meant looking at the mechanisms by which D-ser levels are regulated within the brain environment. While it

is capable of degrading D-ser, the distribution of DAAO does not locally correspond to that of D-ser (Schell *et al.*, 1995), and if any blockers of its action were utilised then the biosensor would also cease to function. There are also no transporters which are selective to D-ser only, instead there are a few low-affinity non-specific transporters thought to be involved in its re-uptake (Pollegioni & Sacchi, 2010). Thus action in this direction appeared to be a futile exercise. This left one major point in the proposed metabolic pathway of D-ser where action could be taken: the serine racemase (SR) pathway. It has been shown that SR distribution is similar to that of D-ser (Wolosker *et al.*, 1999) and that it is inextricably linked to the levels of D-ser in the brain environment. There is substantive evidence (de Miranda *et al.*, 2002; Strisovsky *et al.*, 2003; Foltyn *et al.*, 2005) that both  $Mg^{2+}$  and ATP are physiological co-factors which activate SR and promote higher activity. A full discussion of all the above issues can be found in Sections 1.4 and 1.5.

Thus in an attempt to promote the conversion of L-ser to D-ser by SR an Mg.ATP complex was obtained. A 1000  $\mu$ M solution of the Mg.ATP complex was formulated in aCSF for perfusion. Initially, two perfusions were conducted to ascertain the effectiveness of this type of treatment in an awake animal. The first was a short perfusion, lasting only 15 minutes. The second was a longer perfusion, continued until a stable response was achieved; this took 50 minutes to be confirmed. The results of both perfusions are displayed in Figure 7-9 **A** and **B** respectively. Both perfusions took place on the same day, and as can be seen from the time axes, the second perfusion began two and half hours after the ending of the first perfusion.

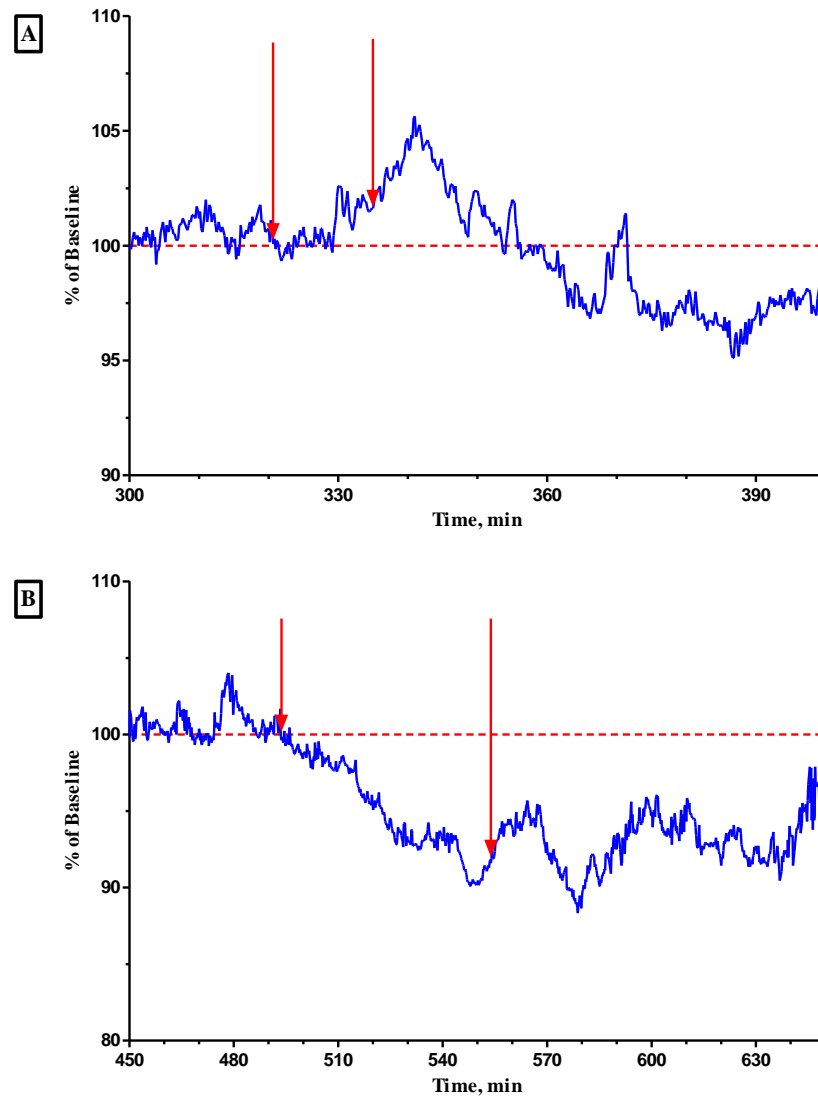


Figure 7-9

**A:** A short perfusion lasting only 15 minutes of 1mM Mg.ATP. **B:** A 1 hour perfusion of Mg.ATP until a stable response was achieved.

It is a satisfying result to see that initially the 15 minute perfusion of Mg.ATP produces an increase in the signal. By the end of the perfusion the signal has only increased 0.7% above the pre-perfusion level. Post-perfusion the signal continues to increase reaching a peak of 5.2% higher than the pre-perfusion current 21:20 minutes after the perfusion began and 6 minutes after it ended. The signal then decreases rapidly, finally settling at a post-perfusion response 47:20 minutes later that is 4.2% below the initial value.

The second, longer perfusion depicts a different, but similar response. This time there is no increase above baseline, and the current reaches a stable in-perfusion level, that is 7.1% below the initial value, after 40:00 minutes. However, similar to the short perfusion there is a period where, over the first 20 minutes, there is little change in the signal, with the current only 1.5% below the initial value. After this point the current

decreases more rapidly. The post-perfusion response is quite similar to the in-perfusion response, 6.8% below the pre-perfusion current 01:03:45 hours after the perfusion has ended.

A possible explanation for the differences in the signals obtained is that for the first perfusion the SR mechanism initially responds positively, producing D-ser from L-ser. Then after the initial 20 minute period where the levels increase, the brain finds a mechanism to either remove the excess D-ser or prevent it being produced, thereby protecting it from neurotoxic damage. This mechanism is evidenced also by the second perfusion where, for about a 20 minute period again, the signal does not change to any large degree, and then begins to decrease much more rapidly. The reason that an increase was not evident in the second perfusion is possibly that this protective system had already been primed and activated only two hours previously and thereby held the level of D-ser constant before beginning to decrease it again. It was also possible that a certain amount of the store of L-ser had already been utilised and was not available to the same extent to be converted to D-ser.

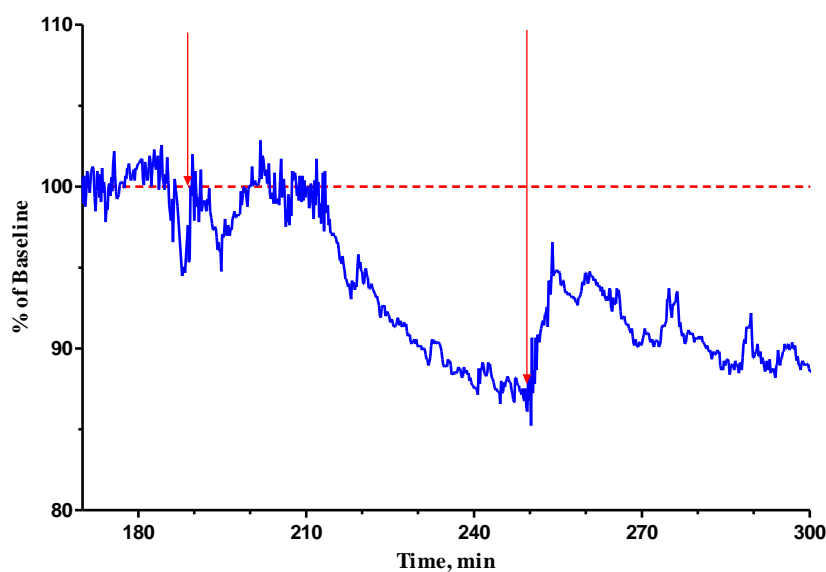


**Figure 7-10**

**A 1 hour perfusion of 1mM L-ser and 1mM Mg.ATP.**

Taking stock of these results a further experiment was planned and conducted. This involved the perfusion of 1000  $\mu$ M of L-ser along with the 1000  $\mu$ M of Mg.ATP for a period of 1 hour. It was hoped that this combination could further elucidate what was happening in the previous two experiments and confirm a signal increase. The perfusion is depicted in Figure 7-10. The results are similar to those experienced for the 1 hour

perfusion of 1 mM Mg.ATP. The signal reaches a minimum, during the perfusion, after 58:45 minute which is 12.2% below the pre-perfusion level. Once the perfusion has ceased, it takes 35:15 minutes to reach a stable post-perfusion level which is 10.7% below the pre-perfusion current. However, within this there are two interesting features. Similar to the two Mg.ATP only perfusions there is an initial period where little change occurs. In this case, after 19:05 minutes the current has only decreased by 0.1%, after which point it decreases rapidly. There is also an initial increase in the current after the perfusion has ceased. This peaks after 05:40 minutes at a current that is only 4.9% below the pre-perfusion baseline.

Given the similarities between the Mg.ATP and Mg.ATP & L-ser perfusions over 1 hour, it was decided to also conduct an Mg.ATP & L-ser perfusion over 15 minutes to investigate if this would also produce similarities with the 15 minute Mg.ATP experiment.

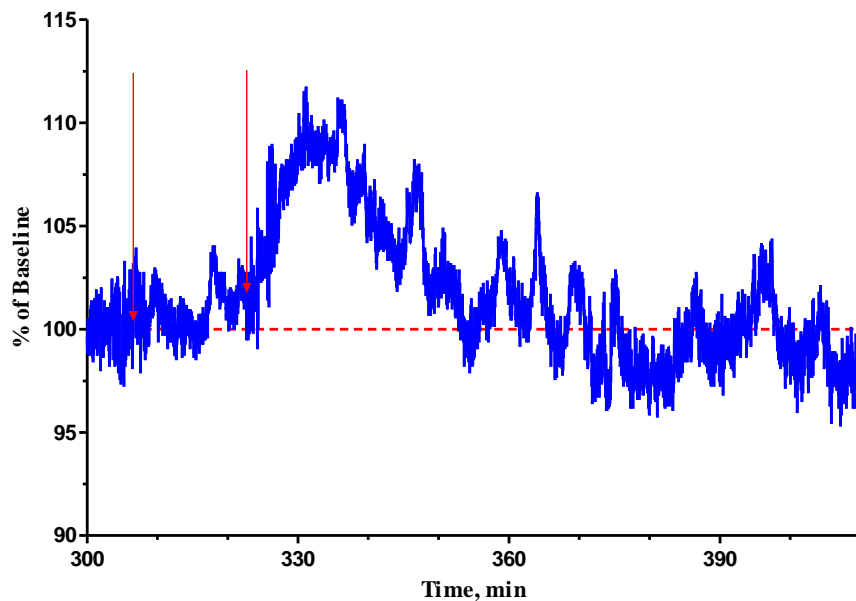


**Figure 7-11**

**A 15 minute perfusion of 1mM L-ser and 1mM Mg.ATP.**

This experiment, depicted in Figure 7-11, did bear striking similarities with the previous experiment, Figure 7-9 A. Initially, during the perfusion the current increases by 1.7% after the 15 minutes have elapsed, then for 13:15 minutes after the end of the perfusion the current continues to increase up to a level 9.9% above the pre-perfusion baseline. The current eventually settles at a post-perfusion baseline 56:35 minutes after the end of the perfusion with a current that is 2.2% below the starting value. The addition of the L-

ser to the perfusate seems to have augmented the increases in current achieved both during and after the perfusion, as well as the length of time that the current increases for. It also appears to have retarded the decrease in current post-perfusion. This backs up the possibility that a lowering in the concentration of available L-ser, during the first two Mg.ATP only perfusions, had an effect on the results.

## 7.6 EDTA Perfusions

A vital component in the SR pathway for the formation of L- and D-ser, EDTA is responsible for the regulation of its  $\alpha,\beta$  elimination process. This process is responsible for the conversion of D-ser to pyruvate and ammonia, which is a constant process that is fast enough to regulate D-ser levels in intact cells (Wolosker, 2011).

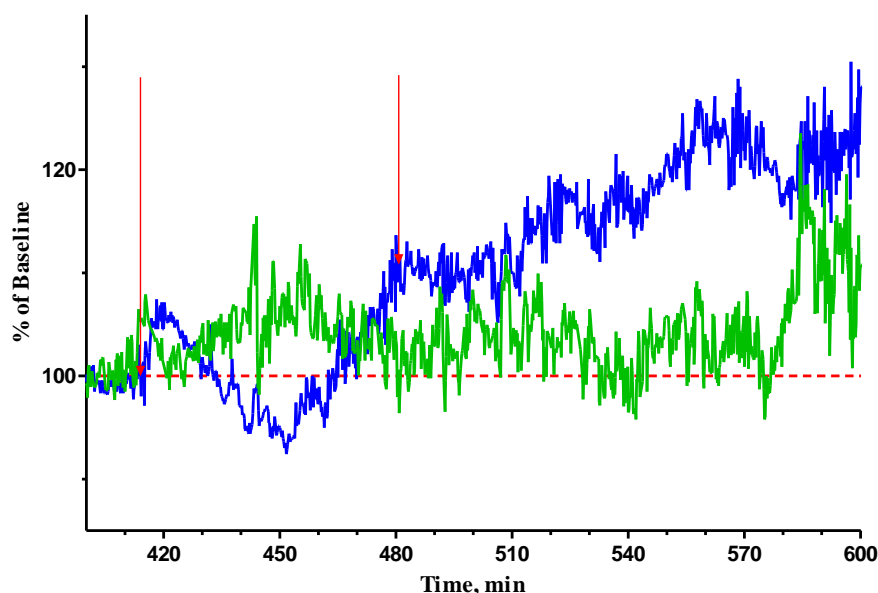
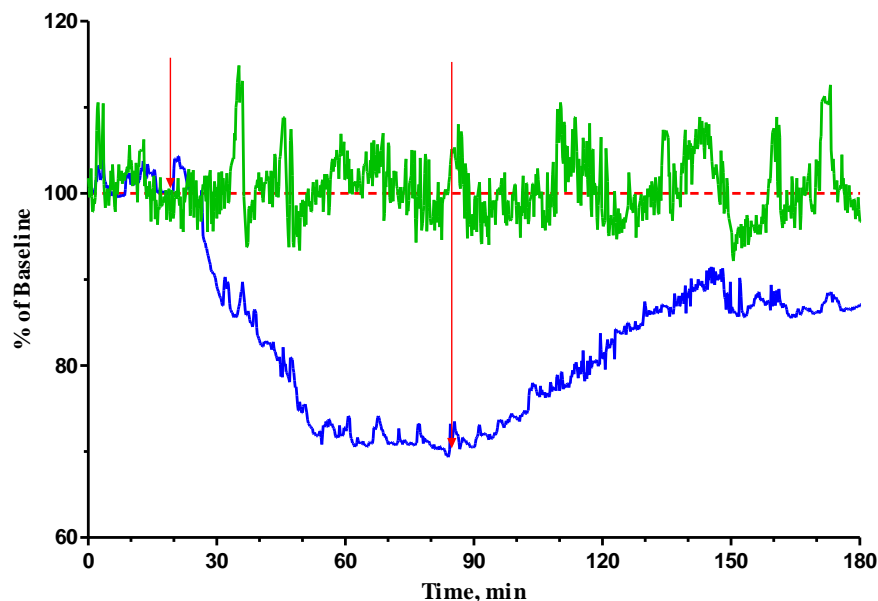


Figure 7-12

A 1 mM EDTA perfusion.

EDTA can act by complexing available  $Mg^{2+}$  and  $Ca^{2+}$ , thereby reducing the activity of SR and stabilising the levels of D-ser by preventing its elimination. Thus it could be used to artificially increase the amounts of D-ser by decreasing the turnover rate and extending its lifetime. This method, while completely different to the action of Mg.ATP, which not only dramatically increases the production but also elimination of D-ser, is the other side of the mechanism of SR.

The perfusion of 1 mM EDTA, Figure 7-12, confirmed this mechanism and was reinforced by the similarities with the *in vitro* results obtained with transfected HEK 293 cells (Foltyn *et al.*, 2005). Initially during the perfusion there was an increase to approximately 6% above the pre-perfusion level, and then a decrease in the signal to 6% below the initial value. This was then followed by a period of sustained increase, whereby at the end of the hour-long perfusion the current had increased to an in-perfusion level of 8.5% above the starting baseline. This increase continued for the almost 12 hours, whereby after 11:42:20 the post-perfusion current was 93.8% higher than the pre-perfusion level. The transfected cell study displayed an increase in D-ser concentration over 6 hours, the total length of time readings were taken for (Foltyn *et al.*, 2005).



**Figure 7-13**

**A perfusion of 1mM D-ser and 1mM EDTA.**

As an analogue to the L-ser and Mg.ATP perfusion, and to investigate further the mechanism of D-ser regulation a 1 mM EDTA with 1 mM D-ser perfusion was also conducted, see Figure 7-13. Overall after the hour long perfusion there was a 30.9% decrease in the current from the pre-perfusion level. The post-perfusion baseline was attained 01:06:35 minutes after the end of the perfusion and the signal was 14.0% less than the initial value. What is significant about this is that the current decrease is larger than that for an aCSF or D-ser perfusion. This could indicate that, due to the large quantity of D-ser being perfused that the removal mechanisms have activated. But, now

with the EDTA complexing available  $Mg^{2+}$  and  $Ca^{2+}$  there is also no D-ser being produced in the astrocytes, further reducing the *in vivo* concentration.

## 7.7 NO Perfusion

A further mechanism which is proposed to regulate the action of SR is a feedback control instigated by NMDAr's. The activation NMDAr's in turn activates neuronal nitric oxide synthase (Kuriyama & Ohkuma, 1995; Dawson & Dawson, 1996). This post-synaptic NO feeds back into pre-synaptic cells where it S-nitrosylates SR, inactivating it, and thereby decreases the concentration of D-ser (Mustafa *et al.*, 2007). This correlates with data suggesting that presence NO and D-ser regulate the activity of SR (Shoji *et al.*, 2006b, a) NMDAr activation also promotes translocation of SR to dendritic membranes which leads to prolonged inhibition of SR, however, this mechanism is not mediated by the associated production of NO (Balan *et al.*, 2009).

To determine if NO could have any effect on the D-ser signal produced by the biosensor it was decided to perfuse a high concentration of NO. Despite the possible danger posed by this, as NO is a highly reactive free radical liable to cause neurotoxicity, it is also necessary as its half-life *in vivo* is only 2 – 6 seconds (Wilson, 2002). The NO was produced by a previously described method (Brown *et al.*, 2005), at the time of production and immediate concentration determination by UV-Vis the NO was present in solution at ~ 700  $\mu$ M. However, this solution of NO is unstable and degrades by up to 20% in an hour. Thus it was possible that the concentration decreased to 500  $\mu$ M both during the time that it took to purge the lines with the solution and set up the experiment as well as the time taken to perform the experiment. Two perfusions were carried out, the first of which was 15 minutes long and is depicted in Figure 7-14.

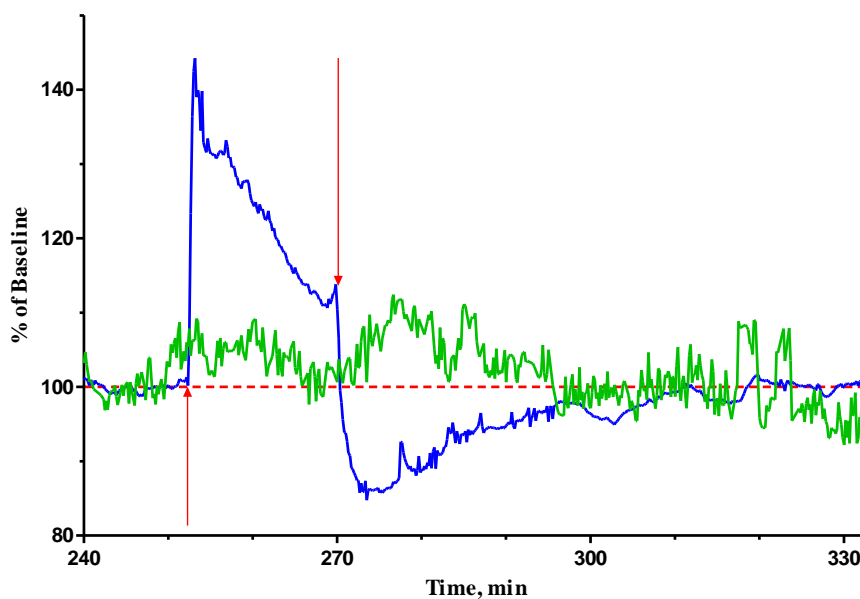


Figure 7-14

A 15 minute perfusion of NO.

The perfusion of NO produced some unusual but, upon reflection, entirely expected features. The primary one is the drastic spike in the signal immediately after the perfusion begins. This is due to the detection of NO at the surface of the electrode. NO is similar in size to  $O_2$  and  $H_2O_2$  and thus it can penetrate the interference rejection layer, and can be oxidised between + 600 mV and + 900 mV vs. SCE. This is normally not an issue as the *in vivo* concentration of NO is less than 1  $\mu\text{M}$ . With a perfusion of 500 – 700  $\mu\text{M}$  however there is a noticeable current produced. Initially at the start of the perfusion this produces an increase of 29.7% in the current compared to the pre-perfusion reading. Post-perfusion with the removal of the supply of NO there is decrease of 26.5% in the current, when compared to the pre-perfusion level. These changes are similar and do indicate that it is solely the oxidation of the NO at the Pt surface which is responsible for these features. Aside from this, it is noticeable that within the perfusion the signal decreases by 18.1% of the pre-perfusion current over 15 minutes, and post-perfusion it increases by 14.8% to settle 0.1% below the initial current 50:20 minutes after the perfusion has ended.

To investigate if these effects were reproducible the perfusion was repeated, this time extending over 30 minutes. The results are graphed in Figure 7-15:

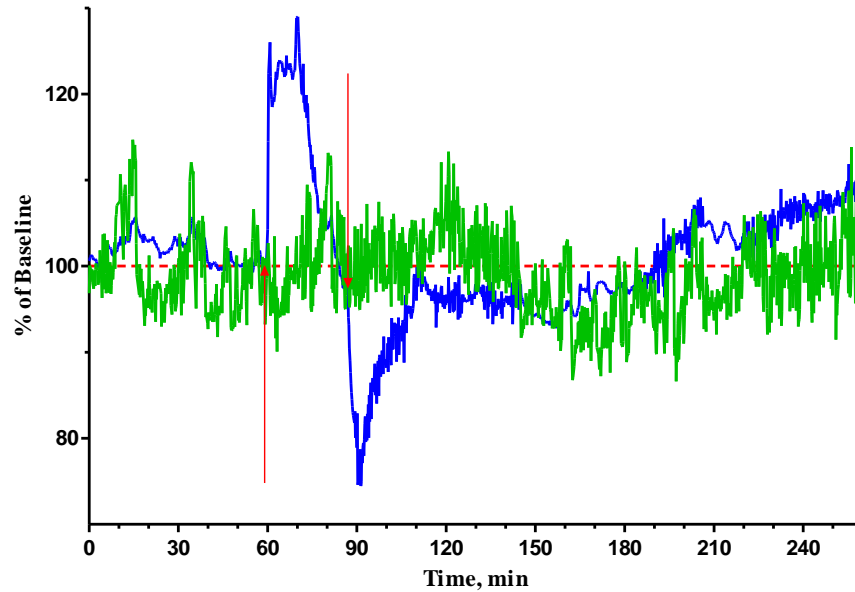


Figure 7-15

A 30 minute perfusion of NO.

It is clear to see that the same NO detection effects are present again, producing a large increase in the signal at the start of the perfusion and a large decrease in current at the end of the perfusion. However, with the increased perfusion time the changes during and after the perfusion are more pronounced. As a percentage of the initial pre-perfusion current, the signal decreases by 26.1% during the perfusion and proceeds to increase by 22.2% post-perfusion to what appears to be a stable level after 27:10 minutes. This post-perfusion signal is 2.9% below the pre-perfusion current. Interestingly though, it can be seen that after approximately one hour of a stable signal the current then begins to increase, this increase continues until 3:16:45 hours after the perfusion has ended with the signal rising to a level 8.7% above the pre-perfusion current. It remains at the level for four hours before decreasing slowly back to a current similar to the initial post-perfusion current. It is difficult to say if this effect is due to the NO perfusion, or to what it may be attributable and further experimentation is required to investigate if it is reproducible.

## 7.8 L-NAME Perfusion

N $\omega$ -Nitro-L-arginine methyl ester hydrochloride (L-NAME) has been shown to prevent the production of NO by inhibiting the function of all forms of nitric oxide synthase (NOS) (Alderton et al., 2001). Having shown that NO perfusions could reduce the concentration of D-ser it was decided that L-NAME could be used to examine whether

the reverse process also occurred. Thus a perfusion of 100  $\mu\text{M}$  L-NAME was carried out, the results of which are illustrated in Figure 7-16:

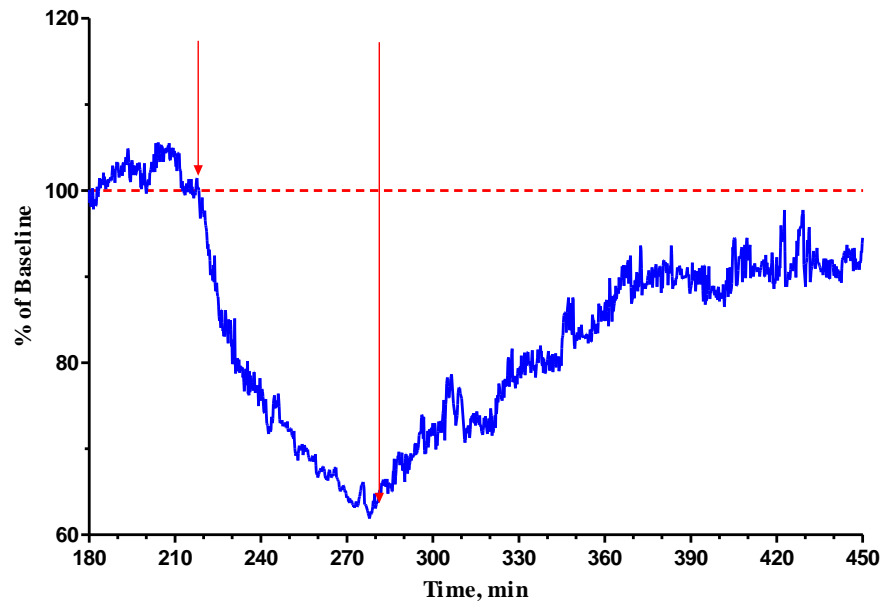


**Figure 7-16**

**A perfusion of L-NAME.**

It is quite clear that L-NAME produced only a decrease in current. This decrease bottomed out at a level 36.8% below the pre-perfusion current 55:10 minutes after the perfusion began. This was the largest decrease observed during any perfusion. After the perfusion ended, 01:39:45 hours elapsed before a stable post-perfusion signal was attained. This signal was 9.8% less than the pre-perfusion current. The larger than previously seen decrease could be due to any number of factors; an unusually elevated D-ser level to begin with, L-NAME producing no effect on the D-ser metabolic pathway and thus behaving no different to an aCSF perfusion, a reduction in the background signal due to the loss of NO interference, an undetermined effect of L-NAME which adversely effects the release or production of D-ser. It is not possible to say what causes this decrease and further experimentation would be required to elucidate and provide insight into this issue.

## **7.9 AA Perfusion**

All of the previous perfusions and results were examined in the light of complete interference rejection. It was felt that after 16 days of implantation that it was necessary

to test this assumption. As a result, an aCSF solution containing 1000  $\mu\text{M}$  AA was perfused, and the results can be seen in Figure 7-17.

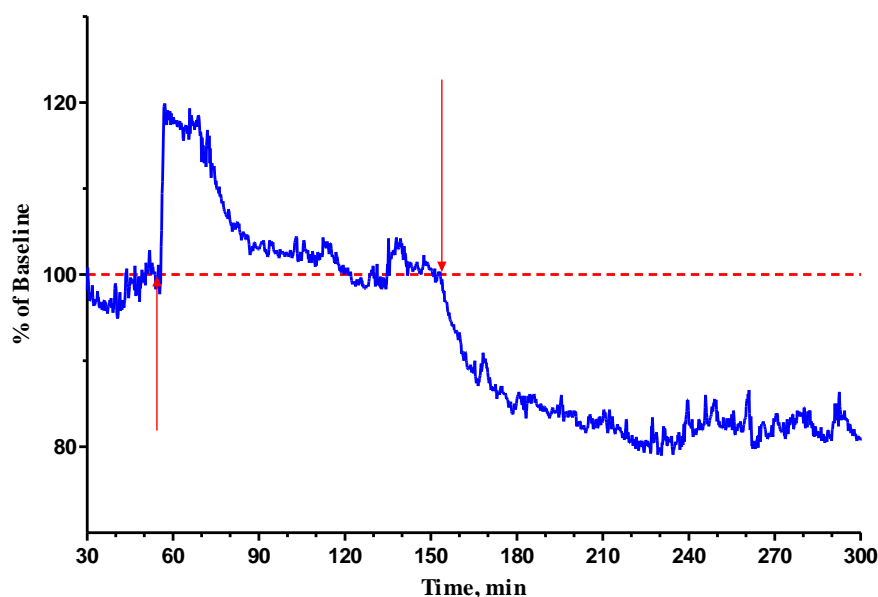


**Figure 7-17**

**A perfusion of 1 mM AA.**

While there is no doubt that the large concentration of AA did initially increase the signal current, an 18.5% increase after 3:45 minutes, it was not a long lived effect. After 38:00 minutes the current had reduced back to a level only 2.1% above the pre-perfusion response. Given that the ‘self-blocking’ mechanism would have 30 minutes to react and form against this concentration of AA, from the 400  $\mu\text{M}$  typical *in vivo* level (Miele & Fillenz, 1996), during an *in vitro* calibration this is a very satisfactory result. It would be expected that the complete constantly changing environment *in vivo* would lengthen this settling time. Just before the cessation of the perfusion, 1:35:55 hours, the current was only 0.5% higher than the initial value. Following the ending of the perfusion the current proceeds to decrease rapidly, eventually finding a post-perfusion level, 17.5% below the initial pre-perfusion response, after 49:50 minutes. The similarity of the initial increase and final decrease, coupled with the in-perfusion activation of the ‘self-blocking’ mechanism coincide to provide evidence that the interference rejection layers are functioning as desired even after 16 days exposure to the *in vivo* environment.

### 7.10 Saline Injection

Before any experiments could be carried out by s.c. injection it was necessary to determine what effect or artefact would be visible, see Figure 7-18.

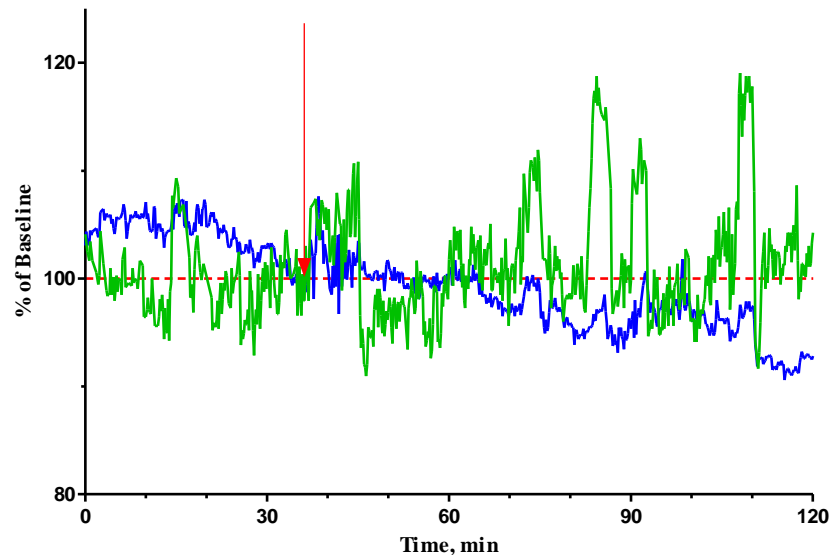


Figure 7-18

An s.c. injection of 1 mL saline.

These effects could be due to either the stress of receiving the injection or the vehicle itself. In this case an injection of 1 mL of normal saline solution was the vehicle. It is immediately clear that vehicle produces no effect at all, and that the injection is almost negligible for either biosensor when compared to the general signal changes and noise. This is a satisfactory and expected result.

### 7.11 MK-801 Injection

With the considerable interest in D-ser due to its hypothesised role in the pathology of schizophrenia, it made sense to briefly explore this possibility. Probably the most common ways to induce schizophrenic stereotypy, in accordance with the glutamate hypothesis, is by the administration of MK-801 (Tsai & Coyle, 2002), a non-competitive antagonist of the NMDA receptor. It acts by binding to the interior ion channel of an activated NMDAR and prevent the passage of  $\text{Ca}^{2+}$  (Huettner & Bean, 1988). Thus although the binding sites for glutamate and D-serine are available, the receptor cannot carry out its function once activated.

The use of MK-801 has illustrated the involvement of D-ser in NMDAR induced neurotoxicity (Shleper *et al.*, 2005), the regulation of CREB phosphorylation in Müller glia of the retina (Lamas *et al.*, 2007; Chavira-Suárez *et al.*, 2008) and the up-regulation of SR and DAAO mRNA expression (Yoshikawa *et al.*, 2004a; Yoshikawa *et al.*, 2004b). Furthermore, DAAO<sup>-/-</sup> mice, which have elevated levels of D-ser, display an attenuation of MK-801 induced schizophrenic-like symptoms (Hashimoto *et al.*, 2005). With this in mind it was considered highly likely that a systemic administration of 0.3 mg/kg MK-801 would produce some effect on the D-ser levels recorded in the striatum. The results obtained are displayed in Figure 7-19.

There is an effect on D-ser levels in both the left (green trace) and right (blue trace) striatum. However, they do differ. In the left striatum the signal increases from the pre-injection level by a maximum of 12.9% after 25 minutes. The current then begins to decrease, reaching a minimum level of 19.6% below the baseline after 5 hours. At this point the levels increase for a period of an hour, but stabilise back to the lower level and this low level is maintained until at least 10 hours after the injection took place. At this point the current is still 20.1% below the pre-injection value.

The right striatum appears to be affected differently by the injection. After 25 minutes the current has increased by 8.9% from its pre-injection level. It continues to increase until 160 minutes after the injection at which point it is 21.6% above the baseline value. This elevated level is then maintained until approximately 7 hours have elapsed, at which point the response is 16.4% above the initial value, before it begins to decrease. By the time 10 hours have passed since the injection, the current has fallen back to 4.3% below the initial value and appears stable at this level.

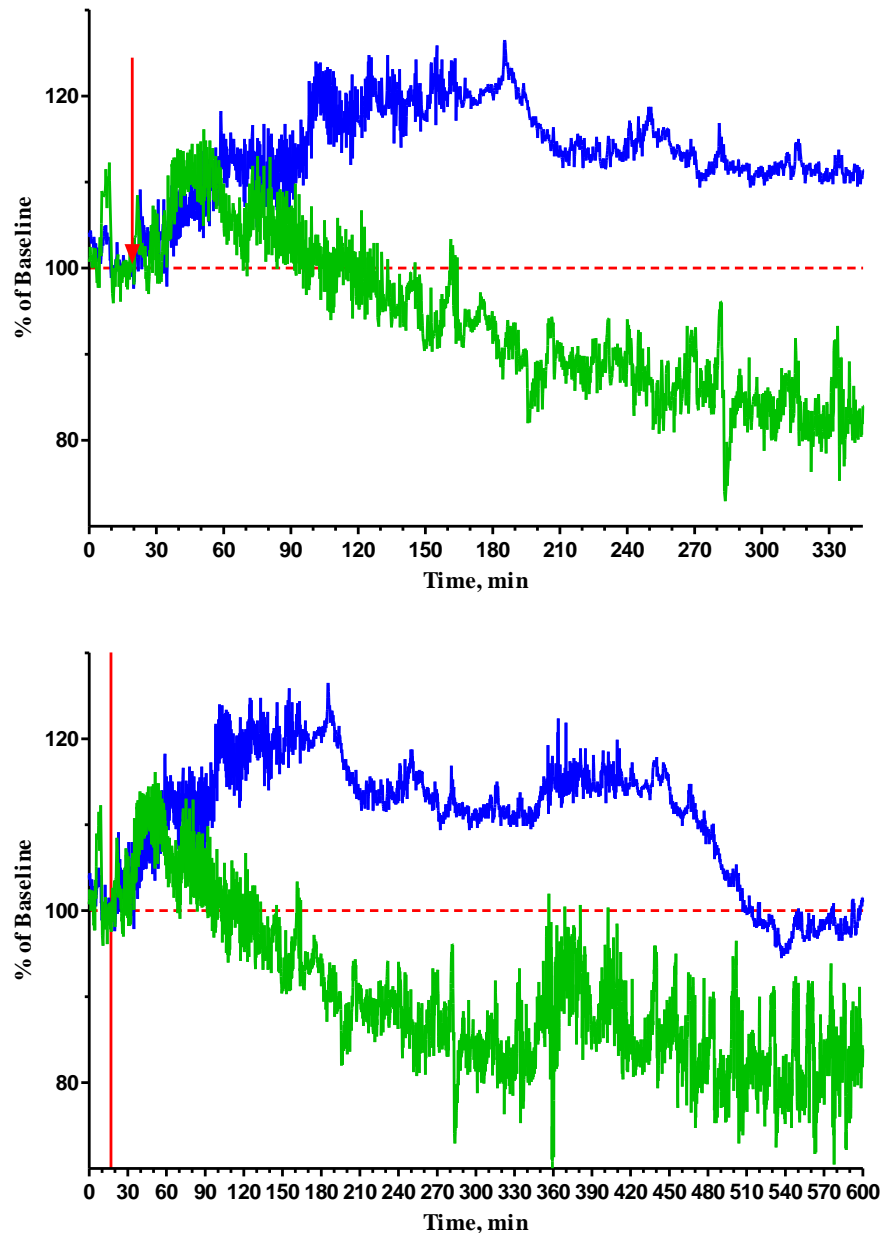


Figure 7-19

An MK-801 s.c. injection, 0.3 mg/kg in 1 ml saline. The top graph depicts the first 5 hours after the injection and the bottom graph a total of 10 hours.

In summary the systemic administration of MK-801 produces an increase in D-ser levels. This is possibly due to the fact that the NMDA<sub>r</sub>'s have become inactive, and in an effort to restore normal signalling processes the brain has elevated the concentration of D-ser, one of the coagonists of the NMDA receptor. That the two different hemispheres respond differently could be due to a number of reasons, but it is felt that it could mainly be due to the fact that a large number of experiments over 16 days have been carried out on the right striatum, and that the combined microdialysis probe and biosensor have, due to their size, induced a greater degree of damage and subsequent gliosis in the right hemisphere (Jaquins-Gerstl & Michael, 2009), leading it to appear to

behave differently in this instance. The extent of gliosis has been shown to alter the apparent concentration of substances within the ECF (Jaquins-Gerstl *et al.*, 2011).

## 7.12 Conclusions

With the stated aim of this thesis being the development of a D-ser biosensor capable of detecting endogenous changes *in vivo* it was important to demonstrate that the final protocol was capable of doing exactly that. As such, biosensors were implanted into the right and left striatum of a rat, with a microdialysis probe co-implanted in the right striatum to allow the delivery of desired substances into the vicinity of the electrode in the right striatum. It is necessary to demonstrate both an increase and decrease in the response of the electrodes due to imposed changes, via microdialysis, that are most likely only attributable to D-ser.

Initially this was attempted by perfusing different concentrations of D-ser in aCSF, the vehicle was also perfused to provide a reference. When this was done it was found that there was no conclusive difference found between any concentration used, with aCSF, 10  $\mu$ M, 20  $\mu$ M, 100  $\mu$ M and 1000  $\mu$ M D-ser producing decreases in current of 28.1%, 28.8%, 25.4%, 23.9% and 21.6% from the initial baseline. Given the concentration of D-ser perfused, these changes were not of a magnitude which indicated that D-ser was being detected. It is evident that there is a very effective internal mechanism present which maintains and tightly regulates the concentration of D-ser *in vivo*. Similar results to this have been observed for the *in vivo* detection of glutamate, the signalling partner of D-ser. A perfusion of L-ser producing a decrease in current that was similar to that of an aCSF perfusion. This was an expected result.

Bearing these results in mind targeting the release, uptake, production and destruction mechanisms are other methods available to elicit a change in the D-ser concentration. The first target was the release mechanism, and the drug Veratridine was utilised. A substance which opens and locks open sodium channels, it has been shown previously to elicit positive and negative changes in the concentration of D-ser and other substances. In this study it produced a decrease of 25.4% when perfused on its own and when perfused between two aCSF perfusions it failed to produce any conclusive change at all.

The production and degradation mechanism was the next to be targeted. The transport and uptake mechanisms are complex and not fully determined for D-ser. This means that the action of SR was probed. Initially with Mg.ATP to induce an increased rate of forward reaction for the conversion of L-ser to D-ser and secondly by EDTA to stabilise the D-ser level against  $\alpha,\beta$ -elimination by SR. Perfusing both of these substances produced very similar responses. For short 15 minute perfusions a short increase in current was observed, and for longer hour long perfusions the level was maintained for the first 20 minutes before beginning a slow decrease. These were positive results which indicate that it is possible to both induce and detect increases in the D-ser concentration *in vivo*.

A further point that was targeted for analysis was the S-nitrosylation and thereby inactivation of SR by NO. A perfusion of NO, while detecting the high level of NO itself, observed a decrease in D-ser current. A perfusion of L-NAME, which is a non-selective NOS inhibitor that reduces NO levels also produced a decrease in the D-ser current. This decrease was at least 36% below the baseline which, when taken with the data for multiple aCSF perfusions and the NO perfusion data makes this data difficult to interpret, and further investigation is required.

Interference rejection was confirmed on the 16<sup>th</sup> day after implantation by perfusion of 1000  $\mu$ M of AA. The result confirmed that the Naf-PPD layer was standing up to the complex *in vivo* environment and ensuring an interference free signal. Finally an MK-801 s.c. injection demonstrated altered D-ser concentration in both hemispheres of the brain, producing first an increase and then a decrease in the observed currents.

Overall, the biosensor developed is suitable for *in vivo* chronic monitoring of D-ser concentrations. However, extensive further study is required to fully characterise the biosensor, particularly in the *in vivo* environment.

## References

- Alderton WK, Cooper CE & Knowles RG. (2001). Nitric oxide synthases: structure, function and inhibition. *The Biochemical Journal* **357**, 593-615.
- Aroni F, Iacovidou N, Dontas I, Pourzitaki C & Xanthos T. (2009). Pharmacological aspects and potential new clinical applications of ketamine: reevaluation of an old drug. *Journal of Clinical Pharmacology* **49**, 957-964.
- Balan L, Foltyn VN, Zehl M, Dumin E, Dikopoltsev E, Knoh D, Ohno Y, Kihara A, Jensen ON, Radzishovsky IS & Wolosker H. (2009). Feedback inactivation of D-serine synthesis by NMDA receptor-elicited translocation of serine racemase to the membrane. *Proceedings of the National Academy of Sciences* **106**, 7589-7594.
- Bönisch H, Graefe K & Keller B. (1983). Tetrodotoxin-sensitive and-resistant effects of veratridine on the noradrenergic neurone of the rat vas deferens. *Naunyn-Schmiedeberg's Archives of Pharmacology* **324**, 264-270.
- Brown FO, Finnerty NJ, Bolger FB, Millar J & Lowry JP. (2005). Calibration of NO sensors for in-vivo voltammetry: laboratory synthesis of NO and the use of UV-visible spectroscopy for determining stock concentrations. *Analytical & Bioanalytical Chemistry* **381**, 964-971.
- Catterall WA. (1975). Activation of the action potential Na<sup>+</sup> ionophore of cultured neuroblastoma cells by veratridine and batrachotoxin. *Journal of Biological Chemistry* **250**, 4053-4059.
- Catterall WA & Coppersmith J. (1981). Pharmacological properties of sodium channels in cultured rat heart cells. *Molecular Pharmacology* **20**, 533-542.
- Chavira-Suárez E, Ramírez M & Lamas M. (2008). D-Serine/N-methyl-D-aspartate receptor signaling decreases DNA-binding activity of the transcriptional repressor DREAM in Müller glia from the retina. *Neuroscience Letters* **432**, 121-126.
- Dawson TM & Dawson VL. (1996). Nitric oxide synthase: Role as a transmitter/mediator in the brain and endocrine system. *Annual Review of Medicine* **47**, 219-227.
- de Miranda J, Panizzutti R, Foltyn VN & Wolosker H. (2002). Cofactors of serine racemase that physiologically stimulate the synthesis of the N-methyl-D-

aspartate (NMDA) receptor coagonist D-serine. *Proceedings of the National Academy of Sciences* **99**, 14542-14547.

Foltyn VN, Bendikov I, De Miranda J, Panizzutti R, Dumin E, Shleper M, Li P, Toney MD, Kartvelishvily E & Wolosker H. (2005). Serine racemase modulates intracellular D-serine levels through an  $\alpha,\beta$ -elimination activity. *Journal of Biological Chemistry* **280**, 1754-1763.

Hashimoto A, Kanda J & Oka T. (2000). Effects of N-methyl-D-aspartate, kainate or veratridine on extracellular concentrations of free D-serine and L-glutamate in rat striatum: an in vivo microdialysis study. *Brain Research Bulletin* **53**, 347-351.

Hashimoto A, Yoshikawa M, Niwa A & Konno R. (2005). Mice lacking D-amino acid oxidase activity display marked attenuation of stereotypy and ataxia induced by MK-801. *Brain Research* **1033**, 210-215.

Hirota K & Lambert DG. (1996). Ketamine: its mechanism(s) of action and unusual clinical uses. *British Journal of Anaesthesia* **77**, 441-444.

Huettner JE & Bean BP. (1988). Block of N-methyl-D-aspartate-activated current by the anticonvulsant MK-801: selective binding to open channels. *Proceedings of the National Academy of Sciences* **85**, 1307-1311.

Jaquins-Gerstl A & Michael AC. (2009). Comparison of the brain penetration injury associated with microdialysis and voltammetry. *Journal of Neuroscience Methods* **183**, 127-135.

Jaquins-Gerstl A, Shu Z, Zhang J, Liu Y, Weber SG & Michael AC. (2011). Effect of dexamethasone on gliosis, ischemia, and dopamine extraction during microdialysis sampling in brain tissue. *Analytical Chemistry* **83**, 7662-7667.

Jordan J, Galindo MF, Calvo S, Gonzalez-Garcia C & Cena V. (2000). Veratridine induces apoptotic death in bovine chromaffin cells through superoxide production. *British Journal of Pharmacology* **130**, 1496-1504.

Koike T & Ninomiya T. (2000). Alteration of veratridine neurotoxicity in sympathetic neurons during development in vitro. *Neuroreport* **11**, 151-155.

Koike T, Tanaka S, Oda T & Ninomiya T. (2000). Sodium overload through voltage-dependent Na<sup>+</sup> channels induces necrosis and apoptosis of rat superior cervical ganglion cells in vitro. *Brain Research Bulletin* **51**, 345-355.

- Kuriyama K & Ohkuma S. (1995). Role of nitric oxide in central synaptic transmission: Effects on neurotransmitter release. *The Japanese Journal of Pharmacology* **69**, 1-8.
- Lamas M, Lee-Rivera I, Ramírez M & López-Colomé AM. (2007). D-Serine regulates CREB phosphorylation induced by NMDA receptor activation in Müller glia from the retina. *Neuroscience Letters* **427**, 55-60.
- Lowry JP, O'Neill RD, Boutelle MG & Fillenz M. (1998). Continuous monitoring of extracellular glucose concentrations in the striatum of freely moving rats with an implanted glucose biosensor. *Journal of Neurochemistry* **70**, 391-396.
- Miele M & Fillenz M. (1996). *In vivo* determination of extracellular brain ascorbate. *Journal of Neuroscience Methods* **70**, 15-19.
- Mustafa AK, Kumar M, Selvakumar B, Ho GPH, Ehmsen JT, Barrow RK, Amzel LM & Snyder SH. (2007). Nitric oxide S-nitrosylates serine racemase, mediating feedback inhibition of D-serine formation. *Proceedings of the National Academy of Sciences* **104**, 2950-2955.
- Pernot P, Mothet J-P, Schuvailo O, Soldatkin A, Pollegioni L, Pilone M, Adeline M-T, Cespuglio R & Marinesco S. (2008). Characterization of a yeast D-amino acid oxidase microbiosensor for D-serine detection in the central nervous system. *Analytical Chemistry* **80**, 1589-1597.
- Pollegioni L, Piubelli L, Sacchi S, Pilone M & Molla G. (2007). Physiological functions of D-amino acid oxidases: from yeast to humans. *Cellular and Molecular Life Sciences* **64**, 1373-1394.
- Pollegioni L & Sacchi S. (2010). Metabolism of the neuromodulator D-serine. *Cellular and Molecular Life Sciences* **67**, 2387-2404.
- Romei C, Di Prisco S, Raiteri M & Raiteri L. (2011). Glycine release provoked by disturbed Na<sup>+</sup>, K<sup>+</sup> and Ca<sup>2+</sup> homeostasis in cerebellar nerve endings: roles of Ca<sup>2+</sup> channels, Na<sup>+</sup>/Ca<sup>2+</sup> exchangers and GlyT2 transporter reversal. *Journal of Neurochemistry* **119**, 50-63.
- Rosenberg D, Kartvelishvily E, Shleper M, Klinker CMC, Bowser MT & Wolosker H. (2010). Neuronal release of D-serine: a physiological pathway controlling extracellular D-serine concentration. *The FASEB Journal* **24**, 2951-2961.

- Schell MJ, Molliver ME & Snyder SH. (1995). D-Serine, an endogenous synaptic modulator: Localization to astrocytes and glutamate-stimulated release. *Proceedings of the National Academy of Sciences* **92**, 3948-3952.
- Shleper M, Kartvelishvily E & Wolosker H. (2005). D-Serine Is the dominant endogenous coagonist for NMDA receptor neurotoxicity in organotypic hippocampal slices. *The Journal of Neuroscience* **25**, 9413-9417.
- Shoji K, Mariotto S, Ciampa AR & Suzuki H. (2006a). Mutual regulation between serine and nitric oxide metabolism in human glioblastoma cells. *Neuroscience Letters* **394**, 163-167.
- Shoji K, Mariotto S, Ciampa AR & Suzuki H. (2006b). Regulation of serine racemase activity by D-serine and nitric oxide in human glioblastoma cells. *Neuroscience Letters* **392**, 75-78.
- Strisovsky K, Jiraskova J, Barinka C, Majer P, Rojas C, Slusher BS & Konvalinka J. (2003). Mouse brain serine racemase catalyzes specific elimination of L-serine to pyruvate. *FEBS Letters* **535**, 44-48.
- Tanaka S & Koike T. (1997). Veratridine delays apoptotic neuronal death induced by NGF deprivation through a Na<sup>+</sup>-dependent mechanism in cultured rat sympathetic neurons. *International Journal of Developmental Neuroscience* **15**, 15-27.
- Tsai G & Coyle JT. (2002). Glutamatergic mechanisms in schizophrenia. *Annual Review Pharmacology & Toxicology* **42**, 165-179.
- Wilson GS. (2002). *Encyclopedia of Electrochemistry, Volume 9: Bioelectrochemistry*. Wiley - VCH, Weinheim.
- Wolosker H. (2011). Serine racemase and the serine shuttle between neurons and astrocytes. *Biochimica et Biophysica Acta* **1814**, 1558-1566.
- Wolosker H, Blackshaw S & Snyder SH. (1999). Serine racemase: A glial enzyme synthesizing D-serine to regulate glutamate-N-methyl-D-aspartate neurotransmission. *Proceedings of the National Academy of Sciences* **96**, 13409-13414.
- Yoshikawa M, Kobayashi T, Oka T, Kawaguchi M & Hashimoto A. (2004a). Distribution and MK-801-induced expression of serine racemase mRNA in rat brain by real-time quantitative PCR. *Brain Research Molecular Brain Research* **128**, 90-94.

Yoshikawa M, Oka T, Kawaguchi M & Hashimoto A. (2004b). MK-801 upregulates the expression of D-amino acid oxidase mRNA in rat brain. *Brain Research Molecular Brain Research* **131**, 141-144.

Zain ZM, O'Neill RD, Lowry JP, Pierce KW, Tricklebank M, Dewa A & Ab Ghani S. (2010). Development of an implantable D-serine biosensor for in vivo monitoring using mammalian D-amino acid oxidase on a poly (*o*-phenylenediamine) and Nafion-modified platinum-iridium disk electrode. *Biosensors & Bioelectronics* **25**, 1454-1459.

---

## **8. GENERAL CONCLUSIONS**

---

## 8.1 General Conclusions

The stated aim of this thesis was to design and characterise a DAAO based biosensor capable of detecting endogenous changes in D-ser *in vivo*. This desire stemmed from the recent determination of D-ser as an important neurotransmitter, with responsibility for involving many process and implication is the pathology of multiple major diseases. Thus a device which could reliably monitor its concentration *in vivo* and therefore be usable as a tool to elucidate the complicated pathways and mechanism by which it acted and was controlled is viewed as an important technological advance. It would also have further implications in the development of new treatments and drugs, as well as diagnosis for disease states. At the offset, it appeared that there was a functional biosensor available that could be characterised and utilised in the *in vivo* environment in a short space of time. However, this did not turn out to be the case.

Multiple and extensive efforts were made to reproduce the biosensor with the properties described by Z. M. Zain. It was discovered that this was only possible when each set of sensors was fabricated using completely fresh solutions. Even under these conditions it was not guaranteed that the desired sensitivity would be attained, with the possibility of achieving a success rate of 1 in 4 or less even with new solutions. An extensive and thorough investigation into the proposed biosensor design was conducted. This examined each individual component in order to determine its effects and decipher any problems that were inherent in the manufacturing protocol. It was discovered that the high concentration of glutaraldehyde that was utilised was responsible for the degradation of the enzyme solution, resulting in it losing its activity after only a few uses. There also appears to be an issue with the interaction of the Nafion<sup>®</sup> layers and the P-*o*-PD layer. It has been shown that application of Naf after P-*o*-PD degrades the P-*o*-PD layer, resulting in lower interference rejection. The Naf layer also provided a further complication whereby it appears to form such a solid matrix with the P-*o*-PD that the adherence of the subsequent GA and DAAO layers are little better than that observed at a bare metal surface. This is not the case with Naf free designs. Many alterations and process changes were investigated and undertaken to remedy these issues, but no satisfactory resolution was found. The information gleaned however was quite useful and with this in mind the decision was made to explore brand new protocols and design a new biosensor.

This process began in Chapter 5 with the basic adsorption, cross-linking and immobilisation techniques being examined. These processes evolved and got increasingly more complex as more information was gleaned. Some results of this are; the utilisation of 600UPBS enzyme solution instead of 600UH<sub>2</sub>O, BSA and PEI not being utilised in the basic design, GA only being utilised on specific layers of the protocol, and additional amounts of FAD being of benefit under a particular set of circumstances. This exploration into a new model of biosensor for D-ser ended with a styrene-based immobilisation matrix which contained the sensing element DAAO and the cross-linking component GA. Several promising recipes were discovered. However, it was felt that a problem remained with the physical currents being achieved, despite what was considered good levels of sensitivity in comparison to other biosensor designs. This meant that some basic changes would have to be made to these designs to seek improvements and finally settle on a single recipe for manufacturing the biosensor.

Chapter 6 saw the culmination of these efforts. The major changes undertaken were; the alteration of the Pt/Ir electrode geometry from a 125 µm disk surface to a 500 µm long cylinder with a 125 µm diameter, and the changing of the immobilisation matrix substance to methyl methacrylate and the discontinuation of styrene. Both solutions brought substantial increases in the basic currents being recorded. With a final design of the sensing elements settled upon it then became necessary to examine interference rejection solutions and how they would fit in with or alter the sensing properties of the biosensor. A combination, involving an initial five layers of Naf followed by a PPD layer that was electro-polymerised onto the surface via CPA, was chosen. These two processes were completed before the application of the sensing layer elements. Subsequent to the issues of sensitivity and selectivity being resolved a thorough and often harsh examination of the characteristics of the biosensor was conducted. Stability is affected by time - repeated short-term and long-term use affects the sensitivity of the biosensor but not in a manner which is a cause for major concern. Exposure to protein, lipid and brain tissue also reduced the sensitivity, but only in a manner consistent with expectations from other biosensor designs. Also in line with expectations are the effects that changes in temperature and pH produce on the biosensor.

A comprehensive study on the interference rejection properties of the design illustrate that there is no interference to be found from either L-amino acids or electroactive species. Any interference from D-amino acids is minimal and not likely to be

problematic *in vivo* due to their relative concentrations; D-ser is by far the most prolific. Oxygen independence was established up to 100  $\mu\text{M}$  D-ser and with a limit of detection which is one tenth of the proposed *in vivo* concentration and with a 6 second response time the biosensor was determined to be suitable for *in vivo* use following its extensive *in vitro* characterisation.

*In vivo* implantation highlighted possible issues that may occur with any experiment or treatment that relates to D-ser concentration alteration, as it appears to be very tightly regulated. It was not possible to increase the response of the sensor by perfusion D-ser alone, or by blanket stimulation of the ion dependant signalling system. Nevertheless, through focused and specific pharmacological alteration of the systems that control the production and destruction of D-ser it was possible to show increases and decreases in D-ser concentration, long and short-term effects and some of the complex interplay that exists between these systems. However, a lot more extensive work is required to determine any specific attributes and draw any definite conclusions.

With the usefulness of the biosensor demonstrated with the experiments conducted already a clear direction for the use of the biosensor has been shown. Further experimentation on the action of SR, to include the substances indentified in this thesis which appear to affect and more novel inhibitors or activators would be a very useful and highly informative exercise. There is a large scope for examining what changes substances like MK-801, and other NMDAr and glutamatergic system activators, inhibitors, competitive and non-competitive agonists and antagonists, produce on D-ser levels in the long and short term and with different levels of exposure.

The most exciting possibilities are in the pairing of this technology with other sensing technologies. Already identified as targets of interest are glutamate, NO and pyruvate. Studying the interplay between all of these systems, not only under the manipulations alluded to in the previous paragraph but especially in animal models of disease would be a thoroughly exciting prospect that could yield many important discoveries in relation to the pathology of degenerative brain disorders. Finally, if the proposed work is conducted in the near future, this technology could see its finest moment as it is used to monitor the effectiveness and clinical development of new and novel treatments for these disease states.



## 8.2 Publications, Conferences and Funding Acknowledgements

### 8.2.1 Publications

- i. Pierce, K.W., Zain, Z.M., Lowry, J.P., O'Neill, R.D., Dewa, A., Ab Ghani, S. (2009) "Development of a D-amino acid oxidase-based biosensor for Long-Term In-Vivo Electrochemistry (LIVE) studies of D-serine in the mammalian brain" – Poster Presentation, *DRHEA Module: Electroanalytical Chemistry Modern Techniques and Applications*. National University of Ireland, Maynooth, Co. Kildare, Ireland.
- ii. Zain, Z.M., O'Neill, R.D., Lowry, J.P., Pierce, K.W., Tricklebank, M., Dewa, A., Ab Ghani, S. "Development of an implantable D-serine biosensor for *in vivo* monitoring using mammalian D-amino acid oxidase on a poly (*o*-phenylenediamine) and Nafion-modified platinum-iridium disk electrode", *Biosensors and Bioelectronics*, 25 (2010) pp 1454-1459.
- iii. Pierce, K.W., Dalton, M., O'Neill, R.D., Lowry, J.P. (2010) "Development of Polystyrene Based D-serine Biosensor" – Oral Presentation, 62<sup>nd</sup> Irish Universities Chemistry Research Colloquium, Queens University Belfast; pp .
- iv. Pierce, K.W., Dalton, M., Lowry, J.P. (2010) "Development and characterisation of a polystyrene based D-serine biosensor for neurochemical detection and analysis" – Poster Presentation, In *Monitoring Molecules in Neuroscience*, Westerink, B., Clinckers, R., Smolders, I., Sarre, S. and Michotte, Y. (Eds.) Vrije Universiteit Brussel, Brussels, Belgium; pp 169-171.
- v. Pierce, K.W., Dalton, M., Lowry, J.P. (2011) "Development and Characterisation of an MMA based D-Serine Biosensor for Neuro-chemical Detection and Analysis" – Oral Presentation, In *Conference on Analytical Sciences Ireland 2011 - 6<sup>th</sup> CASi*, Dublin City University Dublin 9, Ireland; pp 24.
- vi. Pierce, K.W., Dalton, M., Lowry, J.P. (2011) "An MMA based D-Serine Biosensor for Neurochemical Detection and Analysis" – Poster Presentation, In *Neuroscience Ireland*, Coogan A., Commins S., Roche R., Lowry J.P. National University of Ireland, Maynooth, Co. Kildare, Ireland; pp 44.

### 8.2.2 Conferences Attended

- i. Bioengineering '08 Symposium, Imperial College London, London, United Kingdom.
- ii. 60<sup>th</sup> Irish Universities Chemistry Research Colloquium 2008, University College Cork, Cork, Co. Cork, Ireland.
- iii. Irish Neurosciences Discussion Group 2009, The Tullamore Court Hotel, Tullamore, Co. Offaly, Ireland.
- iv. 61<sup>st</sup> Irish Universities Chemistry Research Colloquium 2009, Dublin Institute of Technology, Aungier St., Dublin 2, Ireland.
- v. 63<sup>rd</sup> Irish Universities Chemistry Research Colloquium 2011, University College Dublin, Belfield, Dublin 4, Ireland.

### 8.2.3 Awards

Best Presentation Award – 6<sup>th</sup> CASi, Dublin City University, Dublin, 2011.

### 8.2.4 Funding Acknowledgements

We would like to gratefully acknowledge financial support from Science Foundation Ireland 03/IN3/B376 & 03/IN3/B376S, Dr. Mark Tricklebank and Eli Lilly & Company, and the Centre of Applied Science for Health which is funded by the Higher Education Authority under the Programme for Research in Third Level Institutions (PRTL) Cycle 4.

### 8.2.5 In Preparation

“The influence of glutaraldehyde and charged substances on the enzyme loading and sensitivity of a biosensor.”

“A methyl methacrylate based D-amino acid oxidase biosensor for the *in vivo* detection of D-serine.”

---

---

**9. APPENDIX 1: MEAN AND SEM DATA  
FOR CHAPTER 4**

---

---

Electrode Design	Pt <sub>D</sub> -PPD-Naf1% $\times$ 5-GA25% $\times$ 1-600UH <sub>2</sub> O $\times$ 10, n=13		Pt <sub>D</sub> -PPD-Naf1% $\times$ 3-GA25% $\times$ 3-600UH <sub>2</sub> O $\times$ 10, n=7		Pt <sub>D</sub> -PPD-Naf1% $\times$ 3-GA25% $\times$ 3-600UH <sub>2</sub> O $\times$ 5, n=4	
	[D-Serine] $\mu$ M	Mean, J, $\mu$ A.cm <sup>-2</sup>	$\pm$ SEM, J, $\mu$ A.cm <sup>-2</sup>	Mean, J, $\mu$ A.cm <sup>-2</sup>	$\pm$ SEM, J, $\mu$ A.cm <sup>-2</sup>	Mean, J, $\mu$ A.cm <sup>-2</sup>
0	0	0	0	0	0	0
10	0.088	0.014	0.081	0.012	0.070	0.009
20	0.161	0.024	0.157	0.021	0.145	0.022
50	0.334	0.045	0.368	0.036	0.276	0.057
100	0.647	0.101	0.670	0.072	0.435	0.118
200	1.080	0.142	1.288	0.128	0.753	0.212
500	2.222	0.308	2.869	0.303	1.711	0.448
1000	4.151	0.507	5.224	0.570	4.206	1.070
2000	7.360	0.835	9.301	0.981	5.200	1.367
3000	9.493	1.083	12.378	1.128	7.033	1.734
5000	13.626	1.399	16.499	1.715	9.541	2.422
7000	15.552	1.471	19.469	1.883	11.227	2.755

Table 9-1

D-ser calibration data for the 3 variations of sensor design. Data presented as J values with Mean  $\pm$  SEM.

[D-Serine], $\mu$ M	E1, J, $\mu$ A.cm <sup>-2</sup>	E2, J, $\mu$ A.cm <sup>-2</sup>	E3, J, $\mu$ A.cm <sup>-2</sup>	E4, J, $\mu$ A.cm <sup>-2</sup>	E5, J, $\mu$ A.cm <sup>-2</sup>	E6, J, $\mu$ A.cm <sup>-2</sup>	E7, J, $\mu$ A.cm <sup>-2</sup>	E8, J, $\mu$ A.cm <sup>-2</sup>
0	0	0	0	0	0	0	0	0
10	0.500	0.020	0.070	0.085	0.101	0.059	0.099	0.114
20	0.918	0.165	0.187	0.193	0.180	0.121	0.170	0.231
50	2.140	0.301	0.398	0.420	0.359	0.255	0.262	0.469
100	4.310	0.501	0.724	0.834	0.681	0.489	0.425	0.851
200	9.655	2.014	1.710	2.882	1.257	0.960	0.713	1.649
500	16.777	3.088	2.875	3.415	3.023	2.115	1.298	3.866
1000	38.753	6.077	7.331	16.071	8.040	3.717	2.111	8.752
2000	39.528	8.415	10.184	13.023	8.237	7.076	3.370	12.431
3000	40.917	9.467	12.948	20.647	11.544	9.262	4.451	15.752
5000	41.456	17.052	19.716	27.017	16.119	12.278	6.000	18.043
8000	38.144	13.148	22.100	30.076	18.504	15.685	8.317	22.219
10000	38.101	15.589	25.523	33.902	18.797	14.933	8.224	33.581

Table 9-2

D-ser calibration data for the 8 electrodes prepared by Pt<sub>D</sub>-PPD-Naf1% $\times$ 3-GA25% $\times$ 3-600UH<sub>2</sub>O $\times$ 10 with freshly prepared solutions. Data presented as J values with Mean  $\pm$  SEM

[D-Serine], $\mu\text{M}$	E1, J, $\mu\text{A}\cdot\text{cm}^{-2}$	E2, J, $\mu\text{A}\cdot\text{cm}^{-2}$	E3, J, $\mu\text{A}\cdot\text{cm}^{-2}$	E4, J, $\mu\text{A}\cdot\text{cm}^{-2}$	E5, J, $\mu\text{A}\cdot\text{cm}^{-2}$	E6, J, $\mu\text{A}\cdot\text{cm}^{-2}$	E7, J, $\mu\text{A}\cdot\text{cm}^{-2}$	E8, J, $\mu\text{A}\cdot\text{cm}^{-2}$
0	0	0	0	0	0	0	0	0
10	0.366	0.050	0.038	0.072	0.024	0.034	0.019	0.035
20	0.539	0.128	0.072	0.091	0.044	0.063	0.061	0.069
50	1.608	0.176	0.232	0.367	0.101	0.143	0.158	0.141
100	2.599	0.385	0.334	0.361	0.190	0.277	0.293	0.253
200	4.435	0.552	0.588	0.579	0.348	0.519	0.574	0.479
500	11.305	1.767	1.499	1.653	0.744	1.119	1.276	1.053
1000	18.926	2.809	2.560	2.551	1.313	2.037	2.397	1.927
2000	24.137	4.256	4.107	4.587	2.165	3.616	4.171	3.241
3000	29.782	5.571	5.996	8.203	2.947	4.833	5.725	4.665
5000	32.919	7.351	8.186	12.072	3.942	6.528	8.035	6.424
8000	42.911	10.944	14.290		4.856	12.196	14.195	9.563
10000	42.128	11.699	15.444		5.386	13.631	16.009	8.730

Table 9-3

D-ser calibration data for the 8 electrodes prepared by Pt<sub>D</sub>-PPD-Naf1% $\times$ 3-GA25% $\times$ 3-600UH<sub>2</sub>Ox10 with freshly prepared solutions after 7 days of storage at 4°C. Data presented as J values with Mean  $\pm$  SEM

Electrode Design	Pt <sub>D</sub> -Naf1% $\times$ 3-GA25% $\times$ 3-600UH <sub>2</sub> Ox5, n=4		Pt <sub>D</sub> -GA25% $\times$ 3-600UH <sub>2</sub> Ox5, n=4		Pt <sub>D</sub> -Naf1% $\times$ 3-600UH <sub>2</sub> Ox5, n=4	
	Mean, J $\mu\text{A}\cdot\text{cm}^{-2}$	SEM, J $\mu\text{A}\cdot\text{cm}^{-2}$	Mean, J $\mu\text{A}\cdot\text{cm}^{-2}$	SEM, J $\mu\text{A}\cdot\text{cm}^{-2}$	Mean, J $\mu\text{A}\cdot\text{cm}^{-2}$	SEM, J $\mu\text{A}\cdot\text{cm}^{-2}$
[D-Serine] $\mu\text{M}$						
0	0	0	0	0	0	0
10	0.112	0.014	0.049	0.013	0.160	0.038
20	0.249	0.020	0.126	0.039	0.356	0.080
50	0.700	0.078	0.320	0.105	0.797	0.183
100	1.241	0.255	0.538	0.159	1.369	0.311
200	2.407	0.472	0.947	0.274	2.493	0.586
500	4.946	0.472	1.726	0.459	5.830	1.309
1000	9.784	1.004	2.867	0.731	10.792	1.923
2000	22.108	3.517	4.773	1.125	17.047	4.321
3000	23.645	3.606	6.492	1.511	25.396	5.727
5000	33.934	5.107	8.818	1.988	31.964	8.443
7000	39.518	6.343	11.117	2.480	39.975	9.970

Table 9-4

D-ser calibration data for the 4 alterations of prepared Pt<sub>D</sub>-PPD-Naf1% $\times$ 3-GA25% $\times$ 3-600UH<sub>2</sub>Ox5 to explore the influence of the Naf1% $\times$ 3 dips on the sensitivity of the electrode. The values for Pt<sub>D</sub>-PPD-Naf1% $\times$ 3-GA25% $\times$ 3-600UH<sub>2</sub>Ox5 have been omitted for clarity but can be found in Table 9-1. Data presented as J values with Mean  $\pm$  SEM.

%GA used	0.5%, n = 4		1%, n = 3		2%, n = 8	
[D-Serine], $\mu\text{M}$	Mean, J, $\mu\text{A}\cdot\text{cm}^{-2}$	$\pm$ SEM, J, $\mu\text{A}\cdot\text{cm}^{-2}$	Mean, J, $\mu\text{A}\cdot\text{cm}^{-2}$	$\pm$ SEM, J, $\mu\text{A}\cdot\text{cm}^{-2}$	Mean, J, $\mu\text{A}\cdot\text{cm}^{-2}$	$\pm$ SEM, J, $\mu\text{A}\cdot\text{cm}^{-2}$
0	0	0	0	0	0	0
10	0.002	0.001	0.102	0.021	0.047	0.011
20	0.003	0.001	0.215	0.027	0.082	0.017
50	0.007	0.002	0.533	0.033	0.164	0.035
100	0.009	0.002	1.116	0.053	0.435	0.117
200	0.019	0.003	2.247	0.063	0.751	0.157
500	0.039	0.006	5.316	0.158	1.298	0.297
1000	0.059	0.008	9.517	0.203	2.255	0.490
2000	0.088	0.012	18.077	0.518	4.147	0.871
3000	0.108	0.013	23.715	0.204	5.938	1.185
5000	0.142	0.018	32.615	0.756	9.412	2.059
8000	0.181	0.023	43.282	1.433	10.776	2.354
10000	0.202	0.025	46.796	2.247	12.426	2.343
%GA used	5%, n = 3		10%, n = 3		25%, n = 4	
[D-Serine], $\mu\text{M}$	Mean, J, $\mu\text{A}\cdot\text{cm}^{-2}$	$\pm$ SEM, J, $\mu\text{A}\cdot\text{cm}^{-2}$	Mean, J, $\mu\text{A}\cdot\text{cm}^{-2}$	$\pm$ SEM, J, $\mu\text{A}\cdot\text{cm}^{-2}$	Mean, J, $\mu\text{A}\cdot\text{cm}^{-2}$	$\pm$ SEM, J, $\mu\text{A}\cdot\text{cm}^{-2}$
0	0	0	0	0	0	0
10	0.008	0.004	0.006	0.005	0.014	0.008
20	0.018	0.010	0.011	0.008	0.048	0.017
50	0.042	0.023	0.028	0.012	0.146	0.035
100	0.084	0.043	0.059	0.020	0.303	0.071
200	0.154	0.080	0.119	0.029	0.601	0.128
500	0.346	0.181	0.268	0.061	1.215	0.241
1000	0.624	0.320	0.449	0.105	1.990	0.365
2000	1.100	0.566	0.775	0.182	2.998	0.520
3000	1.482	0.758	1.030	0.240	3.910	0.651
5000	2.099	1.077	1.445	0.330	5.405	0.854
8000	2.820	1.426	1.911	0.437	7.253	1.227
10000	3.144	1.635	2.100	0.478	8.339	1.404

Table 9-5

D-ser calibration data for the 6 variations of prepared Pt<sub>D</sub>-PPD<sub>CV</sub>-3xNaf1%-3xGA25%-5x600UH<sub>2</sub>O to investigate the influence of GA% on the sensitivity of the biosensor. Listed is the data obtained when 0.5%, 1%, 2%, 5%, 10% and 25% GA were utilised.

Enzyme soln. used	200 U.mL <sup>-1</sup> soln, 1.9 U.g <sup>-1</sup> solid, Fluka, n = 8		100 U.mL <sup>-1</sup> soln, 2.3 U.g <sup>-1</sup> solid, Sigma, n = 8		250 U.mL <sup>-1</sup> soln, 2.3 U.g <sup>-1</sup> solid, Sigma, n = 8		600 U.mL <sup>-1</sup> soln, 2.3 U.g <sup>-1</sup> solid, Sigma, n = 3	
[D-Serine] $\mu$ M	Mean, J, $\mu$ A.cm <sup>-2</sup>	$\pm$ SEM, J, $\mu$ A.cm <sup>-2</sup>	Mean, J, $\mu$ A.cm <sup>-2</sup>	$\pm$ SEM, J, $\mu$ A.cm <sup>-2</sup>	Mean, J, $\mu$ A.cm <sup>-2</sup>	$\pm$ SEM, J, $\mu$ A.cm <sup>-2</sup>	Mean, J, $\mu$ A.cm <sup>-2</sup>	$\pm$ SEM, J, $\mu$ A.cm <sup>-2</sup>
0	0	0	0	0	0	0	0	0
10	0.072	0.020	0.085	0.031	0.285	0.082	0.454	0.107
20	0.157	0.027	0.129	0.057	0.620	0.144		
50	0.298	0.052	0.304	0.091	0.777	0.180	0.651	0.179
100	0.408	0.089	0.568	0.124	1.264	0.278		
200	1.514	0.170	1.001	0.183	0.968	0.408	1.012	0.333
500	3.769	0.329	1.958	0.254	3.625	1.043	3.100	0.732
1000	6.526	0.966	3.322	0.363	5.712	1.106	5.100	1.017
1500	8.371	1.170	4.464	0.441	7.898	1.182	7.544	1.917
2000	10.155	1.423	5.409	0.523	9.993	1.438	10.360	2.665
3000	12.561	2.044	6.995	0.688	14.666	2.075	18.026 <sub>1</sub>	1.373 <sup>1</sup>
5000	17.237	2.927	10.317	0.938	21.180	3.064	21.898 <sub>2</sub>	2.382 <sup>2</sup>
7000			12.423	1.123	25.869	3.574		
8000			14.307	0.734			24.171	2.680

Table 9-6

D-ser calibration data for the 4 variations of Pt<sub>5</sub>-PPD-Naf1% $\times$ 5-GA25%-Enzymex10. Listed is the data obtained when using enzyme solids supplied by Fluka Chemic and Sigma. Different calibration steps were used as they were sourced over a period of time (<sup>1</sup>4000  $\mu$ M, <sup>2</sup> 6000  $\mu$ M), this does not affect the fitting of kinetic curves or comparative analysis.

Electrode Design	Naf1% $\times$ 5-GA25%-600U+Ax10, n=4		Naf1% $\times$ 3-GA25% $\times$ 3-600U+Ax10, n=3		Naf1% $\times$ 3-GA25% $\times$ 3-600U+Ax5, n=7	
[D-ser] $\mu$ M	Mean, J, $\mu$ A.cm <sup>-2</sup>	$\pm$ SEM, J, $\mu$ A.cm <sup>-2</sup>	Mean, J, $\mu$ A.cm <sup>-2</sup>	$\pm$ SEM, J, $\mu$ A.cm <sup>-2</sup>	Mean, J, $\mu$ A.cm <sup>-2</sup>	$\pm$ SEM, J, $\mu$ A.cm <sup>-2</sup>
0	0	0	0	0	0	0
10	0.049	0.064	0.309	0.068	0.069	0.010
20	0.136	0.055	0.588	0.157	0.199	0.014
50	0.299	0.096	1.169	0.352	0.311	0.038
100	0.507	0.239	2.075	0.576	0.662	0.058
200	0.938	0.242	4.051	0.716	1.101	0.127
500	2.476	0.473	7.036	0.235	2.432	0.287
1000	4.256	0.754	11.724	0.685	4.421	0.549
1500	5.579	0.931			6.179	0.745
2000	6.865	1.119	19.963	2.378	7.592	0.969
3000	9.904	1.851	26.725	2.332	9.893	1.129
5000	13.117	2.162	33.451	3.080	13.913	1.549

Table 9-7

D-ser calibration data for the 3 variations of the biosensors in Table 9-1 where the enzyme solutions have been changed to include stabilising additives.

Electrode Design	Pt <sub>D</sub> -PPD-Naf1% $\times$ 3-GA25% $\times$ 3-600H <sub>2</sub> O $\times$ 3 n = 4		Pt <sub>D</sub> -PPD-Naf1% $\times$ 3-GA25% $\times$ 3-600U+A $\times$ 3 n = 4	
	[D-Serine], $\mu$ M	Mean, J, $\mu$ A.cm <sup>-2</sup>	$\pm$ SEM, J, $\mu$ A.cm <sup>-2</sup>	Mean, J, $\mu$ A.cm <sup>-2</sup>
0	0	0	0	0
10	0.053	0.023	0.018	0.008
20	0.053	0.021	0.031	0.014
50	0.196	0.066	0.072	0.031
100	0.381	0.122	0.127	0.057
200	0.741	0.234	0.220	0.105
500	1.939	0.596	0.477	0.235
1000	3.635	1.100	0.844	0.425
1500			1.144	0.586
2000	6.400	1.954	1.410	0.723
3000	9.021	2.628	1.884	0.984
5000	11.974	3.496	2.680	1.402

Table 9-8

D-ser calibration data for the recipe Pt<sub>D</sub>-PPD-Naf1% $\times$ 3-GA25% $\times$ 3-Enzymex3 using two different enzyme solutions. The first is the 600UH<sub>2</sub>O solution standardly used and the second is the 600U+A solution where the enzyme solution has been changed to include stabilising additives.

Electrode Design	GA 2%, 600UH <sub>2</sub> O, n = 4		GA 2%, 600UPBS, n = 3		GA 25%, 600UH <sub>2</sub> O, n = 4		GA 25%, 600UPBS, n = 7	
	[D-Serine] $\mu$ M	Mean, J, $\mu$ A.cm <sup>-2</sup>	SEM, J, $\mu$ A.cm <sup>-2</sup>	Mean, J, $\mu$ A.cm <sup>-2</sup>	SEM, J, $\mu$ A.cm <sup>-2</sup>	Mean, J, $\mu$ A.cm <sup>-2</sup>	SEM, J, $\mu$ A.cm <sup>-2</sup>	Mean, J, $\mu$ A.cm <sup>-2</sup>
0	0	0	0	0	0	0	0	0
10	0.026	0.015	0.062	0.005	0.070	0.009	0.078	0.012
20	0.045	0.025	0.109	0.011	0.145	0.022	0.178	0.013
50	0.116	0.055	0.238	0.023	0.276	0.057	0.352	0.031
100	0.239	0.104	0.437	0.037	0.435	0.118	0.644	0.065
200	0.461	0.192	0.835	0.066	0.753	0.212	1.598	0.274
500	1.120	0.449	1.936	0.169	1.711	0.448	2.811	0.323
1000	2.094	0.819	3.554	0.273	4.206	1.070	7.443	1.695
2000	3.767	1.536	6.292	0.461	5.200	1.367	8.962	1.251
3000	5.130	2.082	8.584	0.696	7.033	1.734	12.010	1.957
5000	6.617	2.626	12.301	0.989	9.541	2.422	16.604	2.448
7000					11.227	2.755		
8000	9.525	3.762	15.992	1.156			18.578	2.677
10000	10.729	4.215	18.013	1.467			21.507	3.708

Table 9-9

D-ser calibration data for the recipe Pt<sub>D</sub>-PPD-Naf1% $\times$ 3-GAx3-Enzymex5. Two different enzyme solutions were utilised, the first is the 600UH<sub>2</sub>O solution standardly used and the second is the 600UPBS solution where the enzyme solution has been made in PBS with a pH 8.5. Also utilised were two concentrations of GA, 2% and 25%.

Electrode Design	PPD <sub>a</sub> , 2% GA, 600UH <sub>2</sub> O, n = 4		PPD <sub>a</sub> , 2% GA, 600UPBS, n = 4		PPD <sub>cv</sub> , 2% GA, 600UH <sub>2</sub> O, n = 8		PPD <sub>cv</sub> , 2% GA, 600UPBS, n = 4	
	Mean, J, $\mu\text{A}\cdot\text{cm}^{-2}$	$\pm$ SEM, J, $\mu\text{A}\cdot\text{cm}^{-2}$	Mean, J, $\mu\text{A}\cdot\text{cm}^{-2}$	$\pm$ SEM, J, $\mu\text{A}\cdot\text{cm}^{-2}$	Mean, J, $\mu\text{A}\cdot\text{cm}^{-2}$	$\pm$ SEM, J, $\mu\text{A}\cdot\text{cm}^{-2}$	Mean, J, $\mu\text{A}\cdot\text{cm}^{-2}$	$\pm$ SEM, J, $\mu\text{A}\cdot\text{cm}^{-2}$
<b>0</b>	0	0	0	0	0	0	0	0
<b>10</b>	0.070	0.019	0.099	0.021	0.047	0.011	0.089	0.006
<b>20</b>	0.119	0.030	0.140	0.039	0.082	0.017	0.176	0.015
<b>50</b>	0.278	0.073	0.316	0.089	0.164	0.035	0.339	0.020
<b>100</b>	0.502	0.129	0.637	0.181	0.435	0.117	0.712	0.053
<b>200</b>	0.937	0.244	1.248	0.354	0.751	0.157	1.299	0.083
<b>500</b>	2.114	0.536	3.152	0.903	1.298	0.297	2.986	0.197
<b>1000</b>	3.716	0.950	5.870	1.634	2.255	0.490	5.435	0.381
<b>2000</b>	6.633	1.700	10.286	2.721	4.147	0.871	9.637	0.850
<b>3000</b>	9.152	2.390	13.357	3.667	5.938	1.185	12.541	1.192
<b>5000</b>	12.879	3.375	17.160	4.204	9.412	2.059	17.657	1.734
<b>8000</b>	17.187	4.556	22.118	4.803	10.776	2.354	23.437	2.251
<b>10000</b>	19.246	5.151	23.778	4.955	12.426	2.343	26.315	2.481

Table 9-10

**d-ser calibration data for the recipe Pt<sub>D</sub>-PPD-Naf1% $\times$ 3-GA2% $\times$ 3-Enzymex5. Two different enzyme solutions were utilised, the first is the 600UH<sub>2</sub>O solution standardly used and the second is the 600UPBS solution where the enzyme solution has been made in PBS with a pH 8.5. The PPD formulation was also changed between PPD (normal N<sub>2</sub> saturated solution, CPA), PPD<sub>a</sub> (CPA, exposed to atmosphere during polymerisation) and PPD<sub>cv</sub> (normal N<sub>2</sub> saturated solution, CV).**

Electrode Design	Pt <sub>D</sub> -PPD-Naf1% $\times$ 3-[GA2% $\times$ 3-600UH <sub>2</sub> Ox5] $\times$ 2, n = 4		Pt <sub>D</sub> -PPD-Naf1% $\times$ 3-GA2%-600UH <sub>2</sub> Ox5, n = 4	
	[D-serine], $\mu\text{M}$	Mean, J, $\mu\text{A}\cdot\text{cm}^{-2}$	$\pm$ SEM, J, $\mu\text{A}\cdot\text{cm}^{-2}$	Mean, J, $\mu\text{A}\cdot\text{cm}^{-2}$
<b>0</b>	0	0	0	0
<b>10</b>	0.030	0.012	0.026	0.015
<b>20</b>	0.073	0.022	0.045	0.025
<b>50</b>	0.183	0.051	0.116	0.055
<b>100</b>	0.322	0.091	0.239	0.104
<b>200</b>	0.648	0.174	0.461	0.192
<b>500</b>	1.602	0.417	1.120	0.449
<b>1000</b>	3.058	0.810	2.094	0.819
<b>2000</b>	5.329	1.427	3.767	1.536
<b>3000</b>	7.832	2.030	5.130	2.082
<b>5000</b>	11.561	2.948	6.617	2.626

Table 9-11

**The d-ser calibration data for the recipes Pt<sub>D</sub>-PPD-Naf1% $\times$ 3-GA2% $\times$ 3-600UH<sub>2</sub>Ox5 and Pt<sub>D</sub>-PPD-Naf1% $\times$ 3-[GA2% $\times$ 3-600UH<sub>2</sub>Ox5] $\times$ 2.**

Electrode Design	Pt <sub>D</sub> -PPD-Naf1% $\times$ 3-GA25% $\times$ 3-PEI1%-600UH <sub>2</sub> Ox5, n = 4	
[D-serine], $\mu$ M	Mean J, $\mu$ A.cm <sup>-2</sup>	$\pm$ SEM J, $\mu$ A.cm <sup>-2</sup>
0	0	0
10	0.006	0.001
20	0.012	0.002
50	0.026	0.007
100	0.058	0.012
200	0.111	0.023
500	0.242	0.052
1000	0.413	0.098
2000	0.662	0.187
3000	0.876	0.244
5000	1.282	0.376
8000	1.776	0.572
10000	2.037	0.679

Table 9-12

The D-ser calibration data for the recipes Pt<sub>D</sub>-PPD-Naf1% $\times$ 3-GA25% $\times$ 3-PEI1%-600UH<sub>2</sub>Ox5.

Electrode Design	Pt <sub>D</sub> -PPD-Naf1% $\times$ 3-600UH <sub>2</sub> Ox5-PEI1%-BSAGA, n = 4		Pt <sub>D</sub> -PPD-Naf1% $\times$ 3-GA25%-600UH <sub>2</sub> Ox5-PEI1%-BSAGA, n = 4	
[D-serine], $\mu$ M	Mean, J, $\mu$ A.cm <sup>-2</sup>	$\pm$ SEM, J, $\mu$ A.cm <sup>-2</sup>	Mean, J, $\mu$ A.cm <sup>-2</sup>	$\pm$ SEM, J, $\mu$ A.cm <sup>-2</sup>
0	0	0	0	0
10	0.008	0.002	1.007	0.915
20	0.011	0.005	1.193	1.067
50	0.023	0.008	0.999	0.775
100	0.063	0.016	1.323	0.845
200	0.098	0.025	1.479	0.756
500	0.143	0.031	2.817	1.155
1000	0.260	0.049	5.274	1.379
2000	0.401	0.081	8.029	1.569
3000	0.533	0.103	12.126	2.929
5000	0.698	0.143	18.525	2.892
8000	0.915	0.182	20.343	2.888

Table 9-13

The D-ser calibration data for the recipes Pt<sub>D</sub>-PPD-Naf1% $\times$ 3-600UH<sub>2</sub>Ox5-PEI1%-BSAGA and Pt<sub>D</sub>-PPD-Naf1% $\times$ 3-GA25%-600UH<sub>2</sub>Ox5-PEI1%-BSAGA.

Electrode Design	PtD-PPD-Naf1% $\times$ 3-GA-PEI1%-600UH <sub>2</sub> Ox5-FAD, n = 4		PtD-PPD-Naf1% $\times$ 3-PEI1%-600UH <sub>2</sub> Ox5-FAD, n = 4	
	[D-serine], $\mu$ M	Mean, J, $\mu$ A.cm <sup>-2</sup>	$\pm$ SEM, J, $\mu$ A.cm <sup>-2</sup>	Mean, J, $\mu$ A.cm <sup>-2</sup>
<b>0</b>	0	0	0	0
<b>10</b>	0.059	0.012	0.007	0.001
<b>20</b>	0.085	0.021	0.009	0.001
<b>50</b>	0.168	0.030	0.013	0.002
<b>100</b>	0.320	0.044	0.016	0.003
<b>200</b>	0.508	0.081	0.023	0.005
<b>500</b>	0.958	0.179	0.036	0.010
<b>1000</b>	1.461	0.254	0.055	0.017
<b>2000</b>	2.305	0.405	0.081	0.027
<b>3000</b>	3.091	0.623	0.098	0.035
<b>5000</b>	4.334	0.592	0.132	0.048
<b>8000</b>	5.738	0.784	0.168	0.062
<b>10000</b>	6.376	0.810	0.184	0.068

Table 9-14

The D-ser calibration data for the recipes Pt<sub>D</sub>-PPD-Naf1% $\times$ 3-600UH<sub>2</sub>Ox5-PEI1%-BSAGA and Pt<sub>D</sub>-PPD-Naf1% $\times$ 3-GA25%-600UH<sub>2</sub>Ox5-PEI1%-BSAGA.

---

---

**10. APPENDIX 2: MEAN AND SEM DATA  
FOR CHAPTER 5**

---

---

Electrode Design	Pt <sub>D</sub> -600UH <sub>2</sub> O n = 4		Pt <sub>D</sub> -600UH <sub>2</sub> Ox5 n = 3		Pt <sub>D</sub> -600UH <sub>2</sub> Ox10 n = 4		Pt <sub>D</sub> -600UH <sub>2</sub> Ox15 n = 4	
	Mean, J, $\mu\text{A}\cdot\text{cm}^{-2}$	$\pm$ SEM, J, $\mu\text{A}\cdot\text{cm}^{-2}$	Mean, J, $\mu\text{A}\cdot\text{cm}^{-2}$	$\pm$ SEM, J, $\mu\text{A}\cdot\text{cm}^{-2}$	Mean, J, $\mu\text{A}\cdot\text{cm}^{-2}$	$\pm$ SEM, J, $\mu\text{A}\cdot\text{cm}^{-2}$	Mean, J, $\mu\text{A}\cdot\text{cm}^{-2}$	$\pm$ SEM, J, $\mu\text{A}\cdot\text{cm}^{-2}$
0	0	0	0	0	0	0	0	0
100	0.066	0.576	0.088	0.040	0.026	0.005	0.020	0.005
200	-0.010	0.529	0.166	0.065	0.053	0.021	0.030	0.013
400	-0.118	0.471	0.269	0.096	0.112	0.059	0.056	0.026
600	-0.108	0.345	0.332	0.121	0.145	0.080	0.069	0.031
800	-0.277	0.346	0.353	0.155	0.186	0.096	0.089	0.039
1000	-0.343	0.306	0.447	0.184	0.206	0.108	0.100	0.045
1500	-0.330	0.246	0.547	0.212	0.307	0.172	0.139	0.058
2000	-0.346	0.180	0.610	0.238	0.364	0.214	0.169	0.073
3000	-0.129	0.131	0.819	0.279	0.500	0.309	0.227	0.094
4000	-0.024	0.047	0.946	0.307	0.597	0.373	0.270	0.110
5000	0.019	0.008	1.050	0.332	0.681	0.422	0.305	0.124
6000	0.031	0.081	1.109	0.358	0.749	0.461	0.338	0.137

Table 10-1

The D-ser calibration data for the recipes Pt<sub>D</sub>-600UH<sub>2</sub>O, Pt<sub>D</sub>-600UH<sub>2</sub>Ox5, Pt<sub>D</sub>-600UH<sub>2</sub>Ox10 and Pt<sub>D</sub>-600UH<sub>2</sub>Ox15.

Electrode Design	Pt <sub>D</sub> -[GA1%-600UH <sub>2</sub> O]x1, n=4		Pt <sub>D</sub> -[GA1%-600UH <sub>2</sub> O]x5, n=4		Pt <sub>D</sub> -[GA1%-600UH <sub>2</sub> O]x10, n=4		Pt <sub>D</sub> -[GA1%-600UH <sub>2</sub> O]x15, n=4	
	Mean, J, $\mu\text{A}\cdot\text{cm}^{-2}$	$\pm$ SEM, J, $\mu\text{A}\cdot\text{cm}^{-2}$	Mean, J, $\mu\text{A}\cdot\text{cm}^{-2}$	$\pm$ SEM, J, $\mu\text{A}\cdot\text{cm}^{-2}$	Mean, J, $\mu\text{A}\cdot\text{cm}^{-2}$	$\pm$ SEM, J, $\mu\text{A}\cdot\text{cm}^{-2}$	Mean, J, $\mu\text{A}\cdot\text{cm}^{-2}$	$\pm$ SEM, J, $\mu\text{A}\cdot\text{cm}^{-2}$
0	0	0	0	0	0	0	0	0
100	0.312	0.153	1.276	0.324	1.108	0.248	1.162	0.400
200	0.616	0.283	2.474	0.626	2.233	0.452	2.400	0.755
400	1.160	0.572	4.692	1.183	4.335	0.855	4.703	1.454
600	1.693	0.858	6.827	1.727	6.629	1.147	7.298	2.099
800	2.148	1.080	8.754	2.249	9.307	1.388	10.505	2.409
1000	2.603	1.315	10.812	2.785	11.990	1.592	12.531	3.563
1500	3.679	1.812	15.067	3.865	18.617	2.418	19.754	4.862
2000	4.706	2.352	19.003	4.872	24.958	2.666	24.651	6.550
3000	6.146	3.045	26.294	6.697	35.100	3.751	32.105	8.883
4000	7.528	3.780	32.183	8.146	41.566	4.128	38.370	9.905
5000	8.322	4.135	36.844	9.351	45.744	4.549	41.728	10.139
6000	9.385	4.713	40.900	10.550	48.394	4.778	45.152	8.891

Table 10-2

The D-ser calibration data for the recipes Pt<sub>D</sub>-[GA1%-600UH<sub>2</sub>O]x1, Pt<sub>D</sub>-[GA1%-600UH<sub>2</sub>O]x5, Pt<sub>D</sub>-[GA1%-600UH<sub>2</sub>O]x10 and Pt<sub>D</sub>-[GA1%-600UH<sub>2</sub>O]x15.

Electrode Design	Pt <sub>D</sub> -[600UH <sub>2</sub> O-GA1%]x1, n=3		Pt <sub>D</sub> -[600UH <sub>2</sub> O-GA1%]x5, n=4		Pt <sub>D</sub> -[600UH <sub>2</sub> O-GA1%]x10, n=3		Pt <sub>D</sub> -[600UH <sub>2</sub> O-GA1%]x15, n=3	
D-Serine, $\mu\text{M}$	Mean, J, $\mu\text{A}\cdot\text{cm}^{-2}$	$\pm$ SEM, J, $\mu\text{A}\cdot\text{cm}^{-2}$	Mean, J, $\mu\text{A}\cdot\text{cm}^{-2}$	$\pm$ SEM, J, $\mu\text{A}\cdot\text{cm}^{-2}$	Mean, J, $\mu\text{A}\cdot\text{cm}^{-2}$	$\pm$ SEM, J, $\mu\text{A}\cdot\text{cm}^{-2}$	Mean, J, $\mu\text{A}\cdot\text{cm}^{-2}$	$\pm$ SEM, J, $\mu\text{A}\cdot\text{cm}^{-2}$
0	0	0	0	0	0	0	0	0
100	11.282	9.555	0.321	0.093	0.412	0.085	0.329	0.067
200	32.727	29.511	0.528	0.059	0.829	0.152	0.639	0.129
400	35.710	29.273	1.154	0.255	1.741	0.307	1.192	0.297
600	81.993	37.267	1.468	0.169	2.630	0.406	1.709	0.340
800	77.739	33.124	1.776	0.185	3.445	0.513	2.169	0.496
1000	75.096	30.248	2.135	0.179	4.381	0.523	2.649	0.639
1500	75.707	27.856	2.995	0.212	6.319	0.764	3.830	0.936
2000	69.449	26.844	3.780	0.225	8.149	0.961	4.784	1.039
3000	71.964	22.584	5.321	0.307	11.494	1.278	6.677	1.620
4000	68.731	23.861	7.199	0.538	14.360	1.468	8.313	1.871
5000	92.747	61.589	8.232	0.463	16.786	1.492	9.769	2.312
6000	100.256	67.989	9.439	0.475	15.246	1.748	10.349	2.258

Table 10-3

The D-ser calibration data for the recipes Pt<sub>D</sub>-[600UH<sub>2</sub>O-GA1%]x1, Pt<sub>D</sub>-[600UH<sub>2</sub>O-GA1%]x5, Pt<sub>D</sub>-[600UH<sub>2</sub>O-GA1%]x10 and Pt<sub>D</sub>-[600UH<sub>2</sub>O-GA1%]x15.

Electrode Design	Pt <sub>D</sub> -Sty-600UH <sub>2</sub> Ox5, n=4		Pt <sub>D</sub> -Sty-600UH <sub>2</sub> Ox10, n=4		Pt <sub>D</sub> -Sty-600UH <sub>2</sub> Ox15, n=4		Pt <sub>D</sub> -Sty-600UH <sub>2</sub> Ox20, n=4	
D-Serine, $\mu\text{M}$	Mean, J, $\mu\text{A}\cdot\text{cm}^{-2}$	$\pm$ SEM, J, $\mu\text{A}\cdot\text{cm}^{-2}$	Mean, J, $\mu\text{A}\cdot\text{cm}^{-2}$	$\pm$ SEM, J, $\mu\text{A}\cdot\text{cm}^{-2}$	Mean, J, $\mu\text{A}\cdot\text{cm}^{-2}$	$\pm$ SEM, J, $\mu\text{A}\cdot\text{cm}^{-2}$	Mean, J, $\mu\text{A}\cdot\text{cm}^{-2}$	$\pm$ SEM, J, $\mu\text{A}\cdot\text{cm}^{-2}$
0	0	0	0	0	0	0	0	0
40	0.194	0.059	0.135	0.018	0.223	0.106	0.062	0.032
50	0.569	0.231	0.141	0.037	0.247	0.117	0.083	0.056
60	0.560	0.253	0.219	0.033	0.358	0.173	0.140	0.087
100	1.272	0.479	0.256	0.075	0.493	0.232	0.238	0.135
200	2.572	0.946			0.995	0.479	0.399	0.141
500	6.256	1.225	1.181	0.195	2.849	1.279	0.749	0.166
1000	5.021	1.301	1.733	0.224	4.793	2.405	1.245	0.210
2000	7.809	1.661	2.121	0.294	8.566	4.682	1.430	0.418
3000	13.524	3.072			11.803	6.868	1.545	0.638
5000	22.394	4.697	4.351	0.599	17.024	9.028	2.411	0.685
8000	24.925	3.459			21.744	12.251	2.779	0.523
10000	17.158	3.390	6.558	1.228	25.495	13.841	2.615	0.510
15000	23.536	3.837	8.474	2.014	27.894	15.626	3.404	0.553

Table 10-4

The D-ser calibration data for the recipes PtD-Sty-600UH<sub>2</sub>Ox5, PtD-Sty-600UH<sub>2</sub>Ox10, PtD-Sty-600UH<sub>2</sub>Ox15 and PtD-Sty-600UH<sub>2</sub>Ox20.

Electrode Design	Pt <sub>D</sub> -Sty-[600UH <sub>2</sub> O-GA1%]x10 n = 3		Pt <sub>D</sub> -Sty-[600UH <sub>2</sub> O-BSA1%]x10 n = 4		Pt <sub>D</sub> -Sty-[600UH <sub>2</sub> O-BSAGA]x10 n = 4		Pt <sub>D</sub> -Sty-[600UH <sub>2</sub> O-BSAGA0.1%]x10 , n = 6	
	Mean, J, $\mu\text{A.cm}^{-2}$	$\pm$ SEM, J, $\mu\text{A.cm}^{-2}$	Mean, J, $\mu\text{A.cm}^{-2}$	$\pm$ SEM, J, $\mu\text{A.cm}^{-2}$	Mean, J, $\mu\text{A.cm}^{-2}$	$\pm$ SEM, J, $\mu\text{A.cm}^{-2}$	Mean, J, $\mu\text{A.cm}^{-2}$	$\pm$ SEM, J, $\mu\text{A.cm}^{-2}$
0	0	0	0	0	0	0	0	0
40	0.413	0.123	0.016	0.005	0.116	0.007	0.014	0.005
50	0.540	0.167	0.020	0.007	0.443	0.039	0.018	0.006
60	0.674	0.217	0.023	0.007	0.578	0.021	0.023	0.008
100	1.058	0.357	0.034	0.013	1.478	0.135	0.031	0.012
200	1.745	0.531			3.244	0.430		
500	3.866	0.754	0.100	0.045	7.450	1.410	0.102	0.042
1000	7.756	0.687	0.158	0.073	11.775	3.559	0.158	0.064
2000	12.241	1.789	0.256	0.121	19.892	5.609	0.256	0.097
3000	17.179	2.015			25.311	7.212		
5000	22.636	2.925	0.446	0.215	35.472	9.599	0.428	0.137
8000	30.797	3.636	0.542	0.261	48.159	11.565		
10000	32.632	4.372	0.616	0.293	54.745	11.598	0.641	0.196
15000	33.524	5.230	0.745	0.357	56.961	12.547	0.792	0.235
Electrode Design	Pt <sub>D</sub> -Sty-[600UPBS-GA1%]x10 n = 8		Pt <sub>D</sub> -Sty-[600UPBS-BSA1%]x10 n = 4		Pt <sub>D</sub> -Sty-[600UPBS-BSAGA]x10 n = 4		Pt <sub>D</sub> -Sty-[600UPBS-BSAGA0.1%]x10 , n = 4	
	Mean, J, $\mu\text{A.cm}^{-2}$	$\pm$ SEM, J, $\mu\text{A.cm}^{-2}$	Mean, J, $\mu\text{A.cm}^{-2}$	$\pm$ SEM, J, $\mu\text{A.cm}^{-2}$	Mean, J, $\mu\text{A.cm}^{-2}$	$\pm$ SEM, J, $\mu\text{A.cm}^{-2}$	Mean, J, $\mu\text{A.cm}^{-2}$	$\pm$ SEM, J, $\mu\text{A.cm}^{-2}$
0	0	0	0	0	0	0	0	0
40	1.059	0.117	0.012	0.003	0.461	0.079	0.141	0.058
50	1.363	0.179	0.024	0.012	0.802	0.086	0.240	0.117
60	1.615	0.232	0.026	0.013	1.198	0.129	0.278	0.139
100	2.554	0.339	0.040	0.019	2.061	0.214	0.414	0.205
200	3.706	0.323			3.633	0.413		
500	11.501	1.310	0.279	0.209	7.862	0.871	1.428	0.683
1000	20.259	2.128	0.327	0.215	15.254	1.941	2.504	1.208
2000	31.242	1.722	0.494	0.317	25.044	2.460	4.241	2.003
3000	35.752	2.342			31.282	3.507		
5000	61.669	6.792	0.840	0.535	42.030	5.363	4.800	0.699
8000	64.132	8.105	1.068	0.687	48.061	5.096		
10000	65.104	2.974	1.128	0.717	50.088	5.616	7.178	1.585
15000	71.378	3.628	1.388	0.884	52.639	6.014	8.363	1.711

Table 10-5

The D-ser calibration data for the recipes devised to examine the difference in sensitivity when 600UPBS is used in place of 600UH<sub>2</sub>O.

Electrode Design	Pt <sub>D</sub> -Sty-[600UPBS-GA0.1%]x10, n = 3		Pt <sub>D</sub> -Sty-[600UPBS-GA0.2%]x10, n = 4		Pt <sub>D</sub> -Sty-[600UPBS-GA0.5%]x10, n = 4	
[D-Serine], $\mu\text{M}$	Mean, J, $\mu\text{A}\cdot\text{cm}^{-2}$	$\pm$ SEM, J, $\mu\text{A}\cdot\text{cm}^{-2}$	Mean, J, $\mu\text{A}\cdot\text{cm}^{-2}$	$\pm$ SEM, J, $\mu\text{A}\cdot\text{cm}^{-2}$	Mean, J, $\mu\text{A}\cdot\text{cm}^{-2}$	$\pm$ SEM, J, $\mu\text{A}\cdot\text{cm}^{-2}$
0	0	0	0	0	0	0
40	0.128	0.052	0.105	0.023	1.077	0.228
50	0.156	0.063	0.131	0.028	1.318	0.254
60	0.199	0.079	0.157	0.034	1.376	0.289
100	0.319	0.128	0.263	0.056	2.386	0.386
500	1.445	0.582	1.214	0.259	9.706	0.649
1000	2.711	1.095	2.303	0.493	17.039	0.594
5000	9.975	3.956	8.408	1.779	47.084	5.087
10000	15.096	5.894	12.973	2.733	57.512	7.593
15000			15.669	3.260	60.056	7.964
Electrode Design	Pt <sub>D</sub> -Sty-[600UPBS-GA1.0%]x10, n = 8		Pt <sub>D</sub> -Sty-[600UPBS-GA1.5%]x10, n = 3		Pt <sub>D</sub> -Sty-[600UPBS-GA2.0%]x10, n = 4	
[D-Serine], $\mu\text{M}$	Mean, J, $\mu\text{A}\cdot\text{cm}^{-2}$	$\pm$ SEM, J, $\mu\text{A}\cdot\text{cm}^{-2}$	Mean, J, $\mu\text{A}\cdot\text{cm}^{-2}$	$\pm$ SEM, J, $\mu\text{A}\cdot\text{cm}^{-2}$	Mean, J, $\mu\text{A}\cdot\text{cm}^{-2}$	$\pm$ SEM, J, $\mu\text{A}\cdot\text{cm}^{-2}$
0	0	0	0	0	0	0
40	1.059	0.117	1.343	0.365	0.892	0.280
50	1.363	0.179	1.651	0.454	1.205	0.370
60	1.615	0.232	1.572	0.504	1.486	0.464
100	2.554	0.339	2.804	0.851	2.332	0.697
500	11.501	1.310	9.088	2.681	10.827	3.137
1000	20.259	2.128	15.089	4.366	18.802	5.284
5000	61.669	6.792	31.184	4.142	31.215	7.849
10000	65.104	2.974	34.235	3.586	31.428	7.409
15000	71.378	3.628	35.431	3.530	32.067	7.117

Table 10-6

The D-ser calibration data for the general recipe Pt<sub>D</sub>-Sty-[600UPBS-GA]x10. There were 6 difference percentages of GA used, 0.1%, 0.2%, 0.5%, 1%, 1.5% and 2%.

Electrode Design	Pt <sub>D</sub> -Sty-[600UPBSx2-GA0.1%]x5, n = 3		Pt <sub>D</sub> -Sty-[600UPBSx2-GA0.2%]x5, n = 3		Pt <sub>D</sub> -Sty-[600UPBSx2-GA0.5%]x5, n = 3	
[D-Serine], $\mu\text{M}$	Mean, J, $\mu\text{A}\cdot\text{cm}^{-2}$	$\pm$ SEM, J, $\mu\text{A}\cdot\text{cm}^{-2}$	Mean, J, $\mu\text{A}\cdot\text{cm}^{-2}$	$\pm$ SEM, J, $\mu\text{A}\cdot\text{cm}^{-2}$	Mean, J, $\mu\text{A}\cdot\text{cm}^{-2}$	$\pm$ SEM, J, $\mu\text{A}\cdot\text{cm}^{-2}$
0	0	0	0	0	0	0
40	0.048	0.010	1.799	1.394	0.291	0.059
50	0.053	0.008	1.942	1.419	0.365	0.077
60	0.083	0.010	2.061	1.421	0.442	0.090
100	0.141	0.019	2.470	1.452	0.720	0.162
500	0.570	0.043	5.562	1.322	3.073	0.550
1000	0.921	0.055	8.641	1.261	5.569	0.955
5000	2.951	0.138	25.399	2.792	18.033	2.044
10000	4.458	0.306	35.208	3.956	26.056	2.764
15000	5.661	0.803	40.048	4.380	28.974	1.637
Electrode Design	Pt <sub>D</sub> -Sty-[600UPBSx2-GA1.0%]x5, n = 3		Pt <sub>D</sub> -Sty-[600UPBSx2-GA1.5%]x5, n = 4		Pt <sub>D</sub> -Sty-[600UPBSx2-GA2.0%]x5, n = 4	
[D-Serine], $\mu\text{M}$	Mean, J, $\mu\text{A}\cdot\text{cm}^{-2}$	$\pm$ SEM, J, $\mu\text{A}\cdot\text{cm}^{-2}$	Mean, J, $\mu\text{A}\cdot\text{cm}^{-2}$	$\pm$ SEM, J, $\mu\text{A}\cdot\text{cm}^{-2}$	Mean, J, $\mu\text{A}\cdot\text{cm}^{-2}$	$\pm$ SEM, J, $\mu\text{A}\cdot\text{cm}^{-2}$
0	0	0	0	0	0	0
40	1.043	0.109	0.177	0.081	0.439	0.079
50	1.545	0.175	0.219	0.112	0.556	0.099
60	1.789	0.205	0.254	0.136	0.657	0.118
100	2.935	0.339	0.435	0.220	1.099	0.198
500	12.058	2.079	1.902	1.041	5.166	1.101
1000	21.545	3.556	3.609	2.072	9.792	2.047
5000	65.100	17.933	12.200	6.584	30.439	5.323
10000	74.314	20.277	17.740	8.186	41.681	7.246
15000	77.684	21.290	19.792	8.904	46.945	8.301

Table 10-7

The D-ser calibration data for the general recipe Pt<sub>D</sub>-Sty-[600UPBSx2-GA]x5. There were 6 difference percentages of GA used, 0.1%, 0.2%, 0.5%, 1%, 1.5% and 2%.

Electrode Design	Pt <sub>D</sub> -Sty-[600UPBSx5-GA0.1%]x2, n = 4		Pt <sub>D</sub> -Sty-[600UPBSx5-GA0.2%]x2, n = 4		Pt <sub>D</sub> -Sty-[600UPBSx5-GA0.5%]x2, n = 3	
[D-Serine], $\mu\text{M}$	Mean, J, $\mu\text{A}\cdot\text{cm}^{-2}$	$\pm$ SEM, J, $\mu\text{A}\cdot\text{cm}^{-2}$	Mean, J, $\mu\text{A}\cdot\text{cm}^{-2}$	$\pm$ SEM, J, $\mu\text{A}\cdot\text{cm}^{-2}$	Mean, J, $\mu\text{A}\cdot\text{cm}^{-2}$	$\pm$ SEM, J, $\mu\text{A}\cdot\text{cm}^{-2}$
0	0	0	0	0	0	0
40	0.055	0.024	0.329	0.181	0.155	0.035
50	0.089	0.027	0.320	0.035	0.185	0.040
60	0.108	0.038	0.375	0.066	0.221	0.046
100	0.161	0.050	1.086	0.378	0.384	0.083
500	0.424	0.096	3.212	1.185	1.736	0.364
1000	0.682	0.139	5.518	1.996	3.265	0.672
5000	1.918	0.289	20.835	8.449	12.272	1.387
10000	2.741	0.564	36.437	13.804	18.018	1.505
15000	2.916	0.614	41.699	16.408	20.846	1.432
Electrode Design	Pt <sub>D</sub> -Sty-[600UPBSx5-GA1.0%]x2, n = 3		Pt <sub>D</sub> -Sty-[600UPBSx5-GA1.5%]x2, n = 3		Pt <sub>D</sub> -Sty-[600UPBSx5-GA2.0%]x2, n = 4	
[D-Serine], $\mu\text{M}$	Mean, J, $\mu\text{A}\cdot\text{cm}^{-2}$	$\pm$ SEM, J, $\mu\text{A}\cdot\text{cm}^{-2}$	Mean, J, $\mu\text{A}\cdot\text{cm}^{-2}$	$\pm$ SEM, J, $\mu\text{A}\cdot\text{cm}^{-2}$	Mean, J, $\mu\text{A}\cdot\text{cm}^{-2}$	$\pm$ SEM, J, $\mu\text{A}\cdot\text{cm}^{-2}$
0	0	0	0	0	0	0
40	1.445	0.227	0.265	0.075	0.025	0.005
50	1.839	0.290	0.402	0.078	0.032	0.007
60	2.223	0.351	0.491	0.081	0.042	0.008
100	3.843	0.677	0.663	0.183	0.066	0.014
500	12.970	0.974	5.238	1.450	0.267	0.056
1000	24.393	1.684	9.232	2.645	0.469	0.100
5000	89.386	3.351	33.581	3.296	1.676	0.348
10000	121.585	7.145	43.259	6.206	2.639	0.549
15000	137.583	9.136			3.206	0.675

Table 10-8

The D-ser calibration data for the general recipe Pt<sub>D</sub>-Sty-[600UPBSx5-GA]x2. There were 6 difference percentages of GA used, 0.1%, 0.2%, 0.5%, 1%, 1.5% and 2%.

Electrode Design	Pt <sub>D</sub> -Sty-[600UPBS]x10-GA0.1%, n = 4		Pt <sub>D</sub> -Sty-[600UPBS]x10-GA0.2%, n = 3		Pt <sub>D</sub> -Sty-[600UPBS]x10-GA0.5%, n = 4	
	[D-Serine], $\mu\text{M}$	Mean, J, $\mu\text{A}\cdot\text{cm}^{-2}$	$\pm$ SEM, J, $\mu\text{A}\cdot\text{cm}^{-2}$	Mean, J, $\mu\text{A}\cdot\text{cm}^{-2}$	$\pm$ SEM, J, $\mu\text{A}\cdot\text{cm}^{-2}$	Mean, J, $\mu\text{A}\cdot\text{cm}^{-2}$
0	0	0	0	0	0	0
40	0.014	0.003	0.132	0.066	0.126	0.062
50	0.018	0.003	0.166	0.060	0.171	0.081
60	0.028	0.003	0.202	0.050	0.206	0.095
100	0.048	0.007	0.496	0.208	0.316	0.159
500	0.094	0.006	0.963	0.146	1.338	0.728
1000	0.148	0.013	1.362	0.164	2.395	1.323
5000	0.329	0.039	3.483	0.436	9.056	5.073
10000	0.490	0.063	4.871	0.676	12.195	6.816
15000	0.534	0.068	6.040	0.850	13.625	7.598
Electrode Design	Pt <sub>D</sub> -Sty-[600UPBS]x10-GA1.0%, n = 4		Pt <sub>D</sub> -Sty-[600UPBS]x10-GA1.5%, n = 4		Pt <sub>D</sub> -Sty-[600UPBS]x10-GA2.0%, n = 4	
	[D-Serine], $\mu\text{M}$	Mean, J, $\mu\text{A}\cdot\text{cm}^{-2}$	$\pm$ SEM, J, $\mu\text{A}\cdot\text{cm}^{-2}$	Mean, J, $\mu\text{A}\cdot\text{cm}^{-2}$	$\pm$ SEM, J, $\mu\text{A}\cdot\text{cm}^{-2}$	Mean, J, $\mu\text{A}\cdot\text{cm}^{-2}$
0	0	0	0	0	0	0
40	0.130	0.068	0.572	0.058	0.529	0.092
50	0.168	0.091	0.703	0.075	0.697	0.114
60	0.197	0.104	0.853	0.088	0.855	0.140
100	0.333	0.168	1.376	0.143	1.425	0.237
500	1.556	0.711	6.011	0.708	6.813	1.319
1000	2.973	1.350	11.001	1.252	12.786	2.606
5000	11.668	4.709	34.085	5.885	32.744	4.633
10000	16.859	5.797	39.001	6.104	38.999	4.522
15000	18.846	6.357	39.441	5.816	56.629	6.452

Table 10-9

The D-ser calibration data for the general recipe Pt<sub>D</sub>-Sty-[600UPBS]x10-GA. There were 6 difference percentages of GA used, 0.1%, 0.2%, 0.5%, 1%, 1.5% and 2%.

Electrode Design	Pt <sub>D</sub> -Sty-[600UPBS-BSAGA0.005%] x10, n = 3		Pt <sub>D</sub> -Sty-[600UPBS-BSAGA0.01%] x10, n = 4		Pt <sub>D</sub> -Sty-[600UPBS-BSAGA0.02%] x10, n = 4		Pt <sub>D</sub> -Sty-[600UPBS-BSAGA0.05%] x10, n = 4	
[D-Serine], μM	Mean, J, μA.cm <sup>-2</sup>	± SEM, J, μA.cm <sup>-2</sup>	Mean, J, μA.cm <sup>-2</sup>	± SEM, J, μA.cm <sup>-2</sup>	Mean, J, μA.cm <sup>-2</sup>	± SEM, J, μA.cm <sup>-2</sup>	Mean, J, μA.cm <sup>-2</sup>	± SEM, J, μA.cm <sup>-2</sup>
0	0	0	0	0	0	0	0	0
40	0.006	0.003	0.099	0.042	0.025	0.007	0.114	0.042
50	0.011	0.003	0.069	0.022	0.032	0.009	0.139	0.055
60	0.007	0.005	0.057	0.017	0.034	0.010	0.163	0.064
100	0.015	0.005	0.055	0.013	0.054	0.016	0.240	0.096
500	0.039	0.030	0.096	0.018	0.175	0.048	0.682	0.268
1000	0.073	0.052	0.146	0.027	0.289	0.075	1.057	0.407
5000	0.242	0.210	0.333	0.065	0.804	0.200	2.723	0.963
10000	0.446	0.315	0.444	0.090	1.044	0.254	3.622	1.227
15000	0.472	0.368	0.504	0.106	1.141	0.278	3.819	1.189
Electrode Design	Pt <sub>D</sub> -Sty-[600UPBS-BSAGA0.1%]x10, n = 4		Pt <sub>D</sub> -Sty-[600UPBS-BSAGA0.2%]x10, n = 4		Pt <sub>D</sub> -Sty-[600UPBS-BSAGA0.5%]x10, n = 3			
[D-Serine], μM	Mean, J, μA.cm <sup>-2</sup>	± SEM, J, μA.cm <sup>-2</sup>	Mean, J, μA.cm <sup>-2</sup>	± SEM, J, μA.cm <sup>-2</sup>	Mean, J, μA.cm <sup>-2</sup>	± SEM, J, μA.cm <sup>-2</sup>		
0	0	0	0	0	0	0		
40	0.084	0.006	0.151	0.027	0.351	0.126		
50	0.122	0.011	0.200	0.042	0.373	0.163		
60	0.147	0.011	0.238	0.048	0.470	0.189		
100	0.220	0.014	0.437	0.078	0.724	0.308		
500	0.769	0.053	1.850	0.293	3.025	1.347		
1000	1.351	0.075	3.445	0.581	5.036	2.183		
5000	5.157	0.616	12.221	1.963	16.935	7.410		
10000	7.771	1.225	17.916	2.989	24.603	10.044		
15000	9.281	1.650	21.262	3.659	29.890	10.525		
Electrode Design	Pt <sub>D</sub> -Sty-[600UPBS-BSAGA1.0%]x10, n = 3		Pt <sub>D</sub> -Sty-[600UPBS-BSAGA1.5%]x10, n = 4		Pt <sub>D</sub> -Sty-[600UPBS-BSAGA2.0%]x10, n = 4			
[D-Serine], μM	Mean, J, μA.cm <sup>-2</sup>	± SEM, J, μA.cm <sup>-2</sup>	Mean, J, μA.cm <sup>-2</sup>	± SEM, J, μA.cm <sup>-2</sup>	Mean, J, μA.cm <sup>-2</sup>	± SEM, J, μA.cm <sup>-2</sup>		
0	0	0	0	0	0	0		
40	0.409	0.135	0.139	0.022	0.322	0.019		
50	0.582	0.158	0.184	0.030	0.415	0.036		
60	0.721	0.198	0.212	0.033	0.500	0.043		
100	1.117	0.322	0.353	0.054	0.802	0.062		
500	4.313	1.245	1.503	0.199	3.294	0.273		
1000	8.653	2.401	2.392	0.298	5.917	0.565		
5000	27.743	9.555	10.111	1.344	20.232	2.588		
10000	41.858	14.278	15.408	1.736	27.158	3.593		
15000	50.849	17.153	18.335	1.988	30.760	4.522		

Table 10-10

The D-ser calibration data for the general recipe Pt<sub>D</sub>-Sty-[600UPBS-BSAGA]x10. Presented are the ten different solutions of BSAGA used.

Electrode Design	Pt <sub>D</sub> -Sty-[600UPBSx2-BSAGA0.1%]x5, n = 3		Pt <sub>D</sub> -Sty-[600UPBSx2-BSAGA0.2%]x5, n = 3		Pt <sub>D</sub> -Sty-[600UPBSx2-BSAGA0.5%]x5, n = 3	
	Mean, J, $\mu\text{A}\cdot\text{cm}^{-2}$	$\pm$ SEM, J, $\mu\text{A}\cdot\text{cm}^{-2}$	Mean, J, $\mu\text{A}\cdot\text{cm}^{-2}$	$\pm$ SEM, J, $\mu\text{A}\cdot\text{cm}^{-2}$	Mean, J, $\mu\text{A}\cdot\text{cm}^{-2}$	$\pm$ SEM, J, $\mu\text{A}\cdot\text{cm}^{-2}$
[D-Serine], $\mu\text{M}$						
0	0	0	0	0	0	0
40	0.001	0.006	-0.023	0.023	0.035	0.006
50	0.006	0.009	-0.024	0.026	0.045	0.009
60	0.008	0.012	-0.022	0.028	0.053	0.011
100	0.018	0.010	-0.012	0.031	0.081	0.014
500	0.085	0.010	0.100	0.053	0.293	0.058
1000	0.153	0.030	0.196	0.067	0.471	0.087
5000	0.508	0.193	0.958	0.218	1.413	0.214
10000	0.771	0.309	1.489	0.282	2.061	0.311
15000	0.957	0.408	2.002	0.389	2.521	0.384
Electrode Design	Pt <sub>D</sub> -Sty-[600UPBSx2-BSAGA1.0%]x5, n = 4		Pt <sub>D</sub> -Sty-[600UPBSx2-BSAGA1.5%]x5, n = 4		Pt <sub>D</sub> -Sty-[600UPBSx2-BSAGA2.0%]x5, n = 3	
	Mean, J, $\mu\text{A}\cdot\text{cm}^{-2}$	$\pm$ SEM, J, $\mu\text{A}\cdot\text{cm}^{-2}$	Mean, J, $\mu\text{A}\cdot\text{cm}^{-2}$	$\pm$ SEM, J, $\mu\text{A}\cdot\text{cm}^{-2}$	Mean, J, $\mu\text{A}\cdot\text{cm}^{-2}$	$\pm$ SEM, J, $\mu\text{A}\cdot\text{cm}^{-2}$
[D-Serine], $\mu\text{M}$						
0	0	0	0	0	0	0
40	0.280	0.074	0.703	0.160	0.544	0.122
50	0.391	0.108	0.905	0.205	0.663	0.160
60	0.510	0.142	1.093	0.247	0.794	0.198
100	0.915	0.269	1.829	0.413	1.403	0.357
500	4.573	1.398	7.787	1.780	6.438	1.662
1000	8.544	2.628	14.765	3.384	12.138	3.072
5000	33.724	8.880	46.143	8.438	36.261	7.157
10000	47.266	11.450	53.937	8.252	43.151	6.209
15000	55.720	13.598	57.448	8.421	45.804	6.208

Table 10-11

The D-ser calibration data for the general recipe Pt<sub>D</sub>-Sty-[600UPBSx2-BSAGA]x5. There were 6 difference percentages of GA used within the BSAGA solution, 0.1%, 0.2%, 0.5%, 1.0%, 1.5% and 2.0%.

Electrode Design	Pt <sub>D</sub> -Sty-[600UPBSx5-BSAGA0.1%]x2, n = 3		Pt <sub>D</sub> -Sty-[600UPBSx5-BSAGA0.2%]x2, n = 3		Pt <sub>D</sub> -Sty-[600UPBSx5-BSAGA0.5%]x2, n = 3	
	Mean, J, $\mu\text{A}\cdot\text{cm}^{-2}$	$\pm$ SEM, J, $\mu\text{A}\cdot\text{cm}^{-2}$	Mean, J, $\mu\text{A}\cdot\text{cm}^{-2}$	$\pm$ SEM, J, $\mu\text{A}\cdot\text{cm}^{-2}$	Mean, J, $\mu\text{A}\cdot\text{cm}^{-2}$	$\pm$ SEM, J, $\mu\text{A}\cdot\text{cm}^{-2}$
[D-Serine], $\mu\text{M}$						
0	0	0	0	0	0	0
40	0.112	0.106	0.039	0.009	0.885	0.161
50	0.007	0.007	0.055	0.013	1.311	0.157
60	0.087	0.078	0.076	0.012	1.550	0.270
100	0.106	0.089	0.111	0.024	2.309	0.305
500	0.083	0.016	0.445	0.067	10.748	1.675
1000	0.246	0.085	0.822	0.116	18.928	2.571
5000	0.793	0.188	2.528	0.354	46.271	5.435
10000	1.181	0.182	3.686	0.466	66.646	23.226
15000	1.130	0.176	4.475	0.521	74.560	28.064
Electrode Design	Pt <sub>D</sub> -Sty-[600UPBSx5-BSAGA1.0%]x2, n = 4		Pt <sub>D</sub> -Sty-[600UPBSx5-BSAGA1.5%]x2, n = 4		Pt <sub>D</sub> -Sty-[600UPBSx5-BSAGA2.0%]x2, n = 4	
	Mean, J, $\mu\text{A}\cdot\text{cm}^{-2}$	$\pm$ SEM, J, $\mu\text{A}\cdot\text{cm}^{-2}$	Mean, J, $\mu\text{A}\cdot\text{cm}^{-2}$	$\pm$ SEM, J, $\mu\text{A}\cdot\text{cm}^{-2}$	Mean, J, $\mu\text{A}\cdot\text{cm}^{-2}$	$\pm$ SEM, J, $\mu\text{A}\cdot\text{cm}^{-2}$
[D-Serine], $\mu\text{M}$						
0	0	0	0	0	0	0
40	2.032	0.102	1.307	0.248	1.203	0.276
50	2.588	0.125	1.694	0.322	1.630	0.348
60	3.130	0.141	2.042	0.391	1.912	0.448
100	4.852	0.209	3.266	0.623	3.470	0.757
500	19.949	0.703	14.602	2.813	13.299	2.347
1000	33.700	1.619	25.747	4.410	24.934	4.793
5000	55.316	6.393	53.520	2.778	57.345	9.037
10000	56.598	7.632	59.377	3.005	69.739	10.001
15000	57.162	7.520	62.018	3.390	74.886	10.971

Table 10-12

The D-ser calibration data for the general recipe Pt<sub>D</sub>-Sty-[600UPBSx5-BSAGA]x2. There were 6 difference percentages of GA used within the BSAGA solution, 0.1%, 0.2%, 0.5%, 1.0%, 1.5% and 2.0%.

Electrode Design	Pt <sub>D</sub> -Sty-PEI1.0%- [600UPBSx5-BSAGA1.0%]x2, n=4		Pt <sub>D</sub> -Sty-PEI1.0%- [600UPBSx2-BSAGA1.0%]x5, n=4		Pt <sub>D</sub> -Sty-PEI1.0%- [600UPBSx5-GA1.0%]x2, n=4		Pt <sub>D</sub> -Sty-PEI1.0%- [600UPBSx2-GA1.0%]x5, n=4	
	d-Serine, μM	Mean, J, μA.cm <sup>-2</sup>	± SEM, J, μA.cm <sup>-2</sup>	Mean, J, μA.cm <sup>-2</sup>	± SEM, J, μA.cm <sup>-2</sup>	Mean, J, μA.cm <sup>-2</sup>	± SEM, J, μA.cm <sup>-2</sup>	Mean, J, μA.cm <sup>-2</sup>
<b>0</b>	0	0	0	0	0	0	0	0
<b>40</b>	0.237	0.064	0.136	0.019	1.449	0.956	0.281	0.069
<b>50</b>	0.291	0.067	0.183	0.026	1.853	1.216	0.340	0.083
<b>60</b>	0.431	0.093	0.229	0.033	2.238	1.477	0.439	0.102
<b>100</b>	0.736	0.145	0.353	0.048	3.617	2.409	0.694	0.172
<b>500</b>	3.598	0.617	1.530	0.226	5.253	0.326	3.080	0.755
<b>1000</b>	6.254	1.031	2.739	0.399	13.744	4.497	5.597	1.328
<b>5000</b>	24.177	3.960	9.259	1.378	36.973	4.930	18.771	4.096
<b>10000</b>	33.920	5.611	13.429	1.687	52.171	8.021	28.821	5.453
<b>15000</b>	39.755	6.570	15.837	1.846	60.183	9.254	33.138	6.408

Table 10-13

The D-ser calibration data for the recipes which included PEI1.0% after the dip into Sty and before a dip into 600UPBS.

Electrode Design	Pt <sub>D</sub> -Sty-PEI0.1%- [600UPBSx5-BSAGA1.0%]x2, n=4		Pt <sub>D</sub> -Sty-PEI0.1%- [600UPBSx2-BSAGA1.0%]x5, n=3		Pt <sub>D</sub> -Sty-PEI0.1%- [600UPBSx5-GA1.0%]x2, n=4		Pt <sub>D</sub> -Sty-PEI0.1%- [600UPBSx2-GA1.0%]x5, n=4	
	d-Serine, μM	Mean, J, μA.cm <sup>-2</sup>	± SEM, J, μA.cm <sup>-2</sup>	Mean, J, μA.cm <sup>-2</sup>	± SEM, J, μA.cm <sup>-2</sup>	Mean, J, μA.cm <sup>-2</sup>	± SEM, J, μA.cm <sup>-2</sup>	Mean, J, μA.cm <sup>-2</sup>
<b>0</b>	0	0	0	0	0	0	0	0
<b>40</b>	0.431	0.056	0.905	0.088	0.344	0.078	0.216	0.015
<b>50</b>	0.561	0.077	0.965	0.064	0.442	0.100	0.277	0.017
<b>60</b>	0.669	0.090	1.123	0.071	0.539	0.123	0.363	0.024
<b>100</b>	1.100	0.151	1.507	0.106	0.863	0.199	0.574	0.038
<b>500</b>	4.936	0.711	13.802	7.253	3.539	0.831	2.567	0.629
<b>1000</b>	8.934	1.248	17.870	7.338	6.258	1.434	4.903	0.999
<b>5000</b>	27.165	3.349	40.386	5.066	19.959	4.488	16.958	2.169
<b>10000</b>	41.419	4.924	47.745	3.267	28.320	6.128	24.101	2.484
<b>15000</b>	47.871	5.381	54.600	1.682	31.950	6.770	27.098	2.925

Table 10-14

The D-ser calibration data for the recipes which included PEI0.1% after the dip into Sty and before a dip into 600UPBS.

Electrode Design	Pt <sub>D</sub> -Sty-PEI5.0%- [600UPBSx5-BSAGA1.0%]x2- PEI1.0%(5), n=4		Pt <sub>D</sub> -Sty-PEI5.0%- [600UPBSx2-BSAGA1.0%]x5- PEI1.0%(5), n=4		Pt <sub>D</sub> -Sty-PEI5.0%- [600UPBSx5-GA1.0%]x2- PEI1.0%(5), n=3		Pt <sub>D</sub> -Sty-PEI5.0%- [600UPBSx2-GA1.0%]x5- PEI1.0%(5), n=4		
	d-Serine, $\mu\text{M}$	Mean, J, $\mu\text{A}\cdot\text{cm}^{-2}$	$\pm$ SEM, J, $\mu\text{A}\cdot\text{cm}^{-2}$	Mean, J, $\mu\text{A}\cdot\text{cm}^{-2}$	$\pm$ SEM, J, $\mu\text{A}\cdot\text{cm}^{-2}$	Mean, J, $\mu\text{A}\cdot\text{cm}^{-2}$	$\pm$ SEM, J, $\mu\text{A}\cdot\text{cm}^{-2}$	Mean, J, $\mu\text{A}\cdot\text{cm}^{-2}$	$\pm$ SEM, J, $\mu\text{A}\cdot\text{cm}^{-2}$
<b>0</b>	0	0	0	0	0	0	0	0	0
<b>40</b>	0.146	0.036	0.344	0.083	0.186	0.016	0.020	0.012	0.012
<b>50</b>	0.187	0.045	0.405	0.086	0.224	0.025	0.189	0.055	0.055
<b>60</b>	0.242	0.051	0.519	0.099	0.279	0.029	0.260	0.064	0.064
<b>100</b>	0.402	0.087	0.791	0.152	0.632	0.134	0.718	0.175	0.175
<b>500</b>	1.771	0.406	3.683	0.773	2.568	0.155	4.230	0.772	0.772
<b>1000</b>	1.710	0.364	7.154	1.436	4.618	0.201	9.453	1.772	1.772
<b>5000</b>	11.846	2.563	21.960	3.642	16.283	0.453	32.061	5.149	5.149
<b>10000</b>	11.488	2.443	29.890	4.959	24.728	0.463	47.140	8.466	8.466
<b>15000</b>	16.819	3.521	33.718	5.014	31.408	1.314	52.292	8.261	8.261

Table 10-15

The D-ser calibration data for the recipes which included PEI5.0% after the dip into Sty and before a dip into 600UPBS and a dip into PEI1.0% on the fifth layer after the other dips had been applied.

Electrode Design	Pt <sub>D</sub> -Sty-PEI5.0%- [600UPBSx5-BSAGA1.0%]x2- PEI0.1%(5), n=4		Pt <sub>D</sub> -Sty-PEI5.0%- [600UPBSx2-BSAGA1.0%]x5- PEI0.1%(5), n=4		Pt <sub>D</sub> -Sty-PEI5.0%- [600UPBSx5-GA1.0%]x2- PEI0.1%(5), n=3		Pt <sub>D</sub> -Sty-PEI5.0%- [600UPBSx2-GA1.0%]x5- PEI0.1%(5), n=4		
	d-Serine, $\mu\text{M}$	Mean, J, $\mu\text{A}\cdot\text{cm}^{-2}$	$\pm$ SEM, J, $\mu\text{A}\cdot\text{cm}^{-2}$	Mean, J, $\mu\text{A}\cdot\text{cm}^{-2}$	$\pm$ SEM, J, $\mu\text{A}\cdot\text{cm}^{-2}$	Mean, J, $\mu\text{A}\cdot\text{cm}^{-2}$	$\pm$ SEM, J, $\mu\text{A}\cdot\text{cm}^{-2}$	Mean, J, $\mu\text{A}\cdot\text{cm}^{-2}$	$\pm$ SEM, J, $\mu\text{A}\cdot\text{cm}^{-2}$
<b>0</b>	0	0	0	0	0	0	0	0	0
<b>40</b>	0.309	0.063	0.363	0.077	0.032	0.009	0.344	0.050	0.050
<b>50</b>	0.419	0.091	0.456	0.088	0.040	0.010	0.475	0.064	0.064
<b>60</b>	0.500	0.101	0.571	0.110	0.051	0.013	0.511	0.068	0.068
<b>100</b>	0.759	0.154	0.929	0.177	0.076	0.019	0.908	0.109	0.109
<b>500</b>	3.268	0.660	3.780	0.694	0.382	0.080	4.428	0.538	0.538
<b>1000</b>	6.004	1.233	7.586	1.564	0.710	0.144	8.909	1.111	1.111
<b>5000</b>	20.729	4.214	23.270	3.717	2.748	0.685	29.147	4.158	4.158
<b>10000</b>	31.840	6.194	32.071	5.697	4.660	1.160	44.843	6.177	6.177
<b>15000</b>	38.424	7.179	36.423	7.185	5.418	1.426	49.801	7.614	7.614

Table 10-16

The D-ser calibration data for the recipes which included PEI5.0% after the dip into Sty and before a dip into 600UPBS and a dip into PEI0.1% on the fifth layer after the other dips had been applied.

Electrode Design	Pt <sub>D</sub> -Sty- [600UPBSx5- FAD0.02(befE)- BSAGA1.0%]x2, n=4		Pt <sub>D</sub> -Sty- [600UPBSx2- FAD0.02(befE)- BSAGA1.0%]x5, n=4		Pt <sub>D</sub> -Sty- [600UPBSx5- FAD0.02(befE)- GA1.0%]x2, n=3		Pt <sub>D</sub> -Sty- [600UPBSx2- FAD0.02(befE)- GA1.0%]x5, n=4		
	d-Serine, μM	Mean, J, μA.cm <sup>-2</sup>	± SEM, J, μA.cm <sup>-2</sup>	Mean, J, μA.cm <sup>-2</sup>	± SEM, J, μA.cm <sup>-2</sup>	Mean, J, μA.cm <sup>-2</sup>	± SEM, J, μA.cm <sup>-2</sup>	Mean, J, μA.cm <sup>-2</sup>	± SEM, J, μA.cm <sup>-2</sup>
<b>0</b>	0	0	0	0	0	0	0	0	0
<b>40</b>	0.513	0.162	0.501	0.050	0.648	0.155	0.371	0.071	
<b>50</b>	1.065	0.170	0.694	0.075	0.630	0.142	0.463	0.093	
<b>60</b>	1.177	0.124	0.853	0.094	0.739	0.151	0.447	0.100	
<b>100</b>	1.673	0.116	1.331	0.140	1.139	0.189	0.914	0.179	
<b>500</b>	6.586	0.490	6.393	0.743	4.401	0.504	3.583	0.712	
<b>1000</b>	12.397	0.861	10.162	0.806	7.926	0.869	6.347	1.063	
<b>5000</b>	41.804	3.401	30.663	3.618	23.062	3.333	21.794	2.910	
<b>10000</b>	60.417	5.403	43.458	4.898	33.462	4.708	31.867	4.215	
<b>15000</b>	71.160	5.558	49.850	5.540	36.742	5.494	36.950	4.709	

Table 10-17

The d-ser calibration data for the recipes which included FAD0.02 before the dip into 600UPBS on the same layers that BSAGA or GA were to be applied.

Electrode Design	Pt <sub>D</sub> -Sty- [600UPBSx5- FAD0.08- BSAGA1.0%]x2 n = 4		Pt <sub>D</sub> -Sty- [600UPBSx2- FAD0.08- BSAGA1.0%]x5 n = 4		Pt <sub>D</sub> -Sty- [600UPBSx5- FAD0.08- GA1.0%]x2 n = 3		Pt <sub>D</sub> -Sty- [600UPBSx2- FAD0.08- GA1.0%]x5 n = 4		
	d-Serine, μM	Mean, J, μA.cm <sup>-2</sup>	± SEM, J, μA.cm <sup>-2</sup>	Mean, J, μA.cm <sup>-2</sup>	± SEM, J, μA.cm <sup>-2</sup>	Mean, J, μA.cm <sup>-2</sup>	± SEM, J, μA.cm <sup>-2</sup>	Mean, J, μA.cm <sup>-2</sup>	± SEM, J, μA.cm <sup>-2</sup>
<b>0</b>	0	0	0	0	0	0	0	0	0
<b>40</b>	0.162	0.028	0.720	0.148	1.716	0.360	1.392	0.276	
<b>50</b>	0.159	0.027	0.853	0.172	2.168	0.461	1.774	0.346	
<b>60</b>	0.244	0.026	1.018	0.188	2.497	0.525	2.102	0.412	
<b>100</b>	0.323	0.042	1.644	0.314	3.961	0.873	3.293	0.657	
<b>500</b>	0.485	0.058	7.183	1.379	18.193	3.424	14.896	3.010	
<b>1000</b>	2.259	0.319	12.660	2.222	31.241	5.833	26.588	5.394	
<b>5000</b>	3.894	0.459	32.676	2.999	50.500	5.368	57.888	12.118	
<b>10000</b>	14.213	1.394	39.511	3.875	53.707	5.487	67.694	13.442	
<b>15000</b>	20.040	1.464	42.301	4.299	55.013	5.691	69.579	12.254	

Table 10-18

The d-ser calibration data for the recipes which included FAD0.08 after the dip into 600UPBS and before the BSAGA or GA dip was applied. It was only used on the same layers that BSAGA or GA was to be applied.

---

---

**11. APPENDIX 3: MEAN AND SEM DATA  
FOR CHAPTER 6**

---

---

Electrode Design	Pt <sub>C</sub> -Sty-[600UPBSx5-GA1.0%]x2, n = 4 Normal		Pt <sub>C</sub> -Sty-[600UPBSx5-GA1.0%]x2, n = 4 Inverted		Pt <sub>C</sub> -Sty-[600UPBSx5-GA1.0%]x2, n = 4 Spun	
	d-Serine, $\mu\text{M}$	Mean, J, $\mu\text{A}\cdot\text{cm}^{-2}$	$\pm$ SEM, J, $\mu\text{A}\cdot\text{cm}^{-2}$	Mean, J, $\mu\text{A}\cdot\text{cm}^{-2}$	$\pm$ SEM, J, $\mu\text{A}\cdot\text{cm}^{-2}$	Mean, J, $\mu\text{A}\cdot\text{cm}^{-2}$
0	0	0	0	0	0	0
40	0.189	0.037	0.030	0.007	0.224	0.080
50	0.208	0.036	0.049	0.012	0.333	0.112
60	0.265	0.040	0.070	0.024	0.382	0.131
100	0.359	0.073	0.124	0.040	0.693	0.237
200	0.616	0.136	0.219	0.048	1.282	0.451
500	1.885	0.387	0.590	0.163	3.466	1.077
1000	3.485	0.555	1.026	0.258	4.568	1.458
2000	4.591	0.920	2.434	0.528	8.524	2.291
3000	6.056	1.075	3.099	0.635	11.582	2.348
5000	8.058	1.076	4.076	0.752	12.943	2.684
8000	9.971	1.689	6.771	1.220	13.400	2.300
10000	9.056	1.426	5.297	0.898	13.492	1.757
15000	10.557	0.657	5.207	0.584	13.944	2.402

Table 11-1

The d-ser calibration data returned when the recipe Pt<sub>C</sub>-Sty-[600UPBSx5-GA1.0%]x2 was examined under different drying conditions.

Electrode Design	Pt <sub>C</sub> -MMA-[600UPBSx5-GA1.0%]x2, n = 8		Pt <sub>C</sub> -Sty-[600UPBSx5-GA1.0%]x2, n = 4		Pt <sub>C</sub> -{MMA-[600UPBSx5-GA1.0%]x2}x2 n=8		Pt <sub>C</sub> -{Sty-[600UPBSx5-GA1.0%]x2}x2 n=8	
	d-Serine, $\mu\text{M}$	Mean, J, $\mu\text{A}\cdot\text{cm}^{-2}$	$\pm$ SEM, J, $\mu\text{A}\cdot\text{cm}^{-2}$	Mean, J, $\mu\text{A}\cdot\text{cm}^{-2}$	$\pm$ SEM, J, $\mu\text{A}\cdot\text{cm}^{-2}$	Mean, J, $\mu\text{A}\cdot\text{cm}^{-2}$	$\pm$ SEM, J, $\mu\text{A}\cdot\text{cm}^{-2}$	Mean, J, $\mu\text{A}\cdot\text{cm}^{-2}$
0	0	0	0	0	0	0	0	0
40	0.422	0.144	0.224	0.080	0.609	0.079	0.414	0.047
50	0.562	0.119	0.333	0.112	1.154	0.109	0.582	0.068
60	0.730	0.184	0.382	0.131	1.331	0.147	0.611	0.074
100	1.131	0.254	0.693	0.237	2.096	0.180	1.124	0.147
200	2.428	0.535	1.282	0.451	5.271	0.350	2.551	0.316
500	3.600	0.714	3.466	1.077	11.434	1.095	5.516	0.497
1000	6.433	1.050	4.568	1.458	18.556	1.700	9.399	0.928
2000	8.842	1.327	8.524	2.291	23.811	2.120	13.788	1.132
3000	10.332	1.535	11.582	2.348	25.598	2.326	15.958	1.308
5000	11.855	1.531	12.943	2.684	26.502	2.549	18.595	1.568
8000	12.603	1.530	13.400	2.300	27.647	2.635	19.323	2.033
10000	13.089	1.528	13.492	1.757	27.452	2.640	19.861	2.228
15000	13.845	1.469	13.944	2.402	27.808	2.644	20.954	2.614

Table 11-2

The d-ser calibration data returned when MMA and Sty were compared over one and two applications for the general recipe Pt<sub>C</sub>-{X-[600UPBSx5-GA1.0%]x2}x1/x2.

Electrode Design	Pt <sub>C</sub> -{MMA-[600UPBSx5-GA1%]x2}x2 n = 8		Pt <sub>C</sub> -{MMA-[600UPBSx2-GA1%]x5}x2 n = 4		Pt <sub>C</sub> -{MMA-[600UPBSx5-BSAGA1%]x2}x2 n = 4		Pt <sub>C</sub> -{MMA-[600UPBSx2-BSAGA1%]x5}x2 n = 4	
	Mean, J, $\mu\text{A.cm}^{-2}$	$\pm$ SEM, J, $\mu\text{A.cm}^{-2}$	Mean, J, $\mu\text{A.cm}^{-2}$	$\pm$ SEM, J, $\mu\text{A.cm}^{-2}$	Mean, J, $\mu\text{A.cm}^{-2}$	$\pm$ SEM, J, $\mu\text{A.cm}^{-2}$	Mean, J, $\mu\text{A.cm}^{-2}$	$\pm$ SEM, J, $\mu\text{A.cm}^{-2}$
<b>0</b>	0	0	0	0	0	0	0	0
<b>40</b>	0.609	0.079	0.319	0.020	0.021	0.001	0.350	0.089
<b>50</b>	1.154	0.109	0.406	0.024	0.022	0.002	0.417	0.091
<b>60</b>	1.331	0.147	0.523	0.031	0.032	0.003	0.505	0.105
<b>100</b>	2.096	0.180	0.817	0.054	0.042	0.004	0.818	0.173
<b>500</b>	11.434	1.095	3.641	0.231	0.190	0.019	3.281	0.661
<b>1000</b>	18.556	1.700	6.083	0.394	0.332	0.036	5.826	1.165
<b>5000</b>	26.502	2.549	15.540	0.422	1.361	0.123	15.795	2.690
<b>10000</b>	27.452	2.640	19.991	1.195	2.733	0.282	18.754	3.252
<b>15000</b>	27.808	2.644	21.256	1.233	3.105	0.322	21.915	3.778

Table 11-3

The D-ser calibration data returned when MMA replaced Sty and a second application was incorporated into the four best designs from Section 5.4.4.

Electrode Design	Pt <sub>C</sub> -{MMA-[600UPBSx5-GA1%]x2}x2 n = 8		Pt <sub>C</sub> -{MMA-[600UPBSx5-GA1.0%]x2-FAD0.08(5)}x2, n = 4		Pt <sub>C</sub> -{MMA-[600UPBSx5-FAD0.08-GA1.0%]x2}x2, n = 4	
	Mean, J, $\mu\text{A.cm}^{-2}$	$\pm$ SEM, J, $\mu\text{A.cm}^{-2}$	Mean, J, $\mu\text{A.cm}^{-2}$	$\pm$ SEM, J, $\mu\text{A.cm}^{-2}$	Mean, J, $\mu\text{A.cm}^{-2}$	$\pm$ SEM, J, $\mu\text{A.cm}^{-2}$
<b>0</b>	0	0	0	0	0	0
<b>40</b>	0.609	0.079	0.638	0.090	0.673	0.046
<b>50</b>	1.154	0.109	1.073	0.081	0.908	0.076
<b>60</b>	1.331	0.147	0.990	0.093	1.084	0.083
<b>100</b>	2.096	0.180	1.684	0.150	1.692	0.108
<b>200</b>	5.271	0.350	3.883	0.410		
<b>500</b>	11.434	1.095	6.565	1.082	6.305	0.410
<b>1000</b>	18.556	1.700	10.347	1.479	11.892	0.634
<b>2000</b>	23.811	2.120	17.353	1.402		
<b>3000</b>	25.598	2.326	22.058	1.808		
<b>5000</b>	26.502	2.549	25.190	1.960	25.768	1.488
<b>8000</b>	27.647	2.635	27.735	1.882		
<b>10000</b>	27.452	2.640	28.971	1.914	28.151	1.449
<b>15000</b>	27.808	2.644	29.817	1.833	27.962	1.617

Table 11-4

The D-ser calibration data returned when MMA replaced Sty and a second application was incorporated into the four best designs from Section 5.4.4.

Electrode Design	Pt <sub>C</sub> -{MMA-[600UPBSx5-GA1%]x2}x2 DAY 0, n = 4		Pt <sub>C</sub> -{MMA-[600UPBSx5-GA1%]x2}x2 DAY 1, n = 4		Pt <sub>C</sub> -{MMA-[600UPBSx5-GA1%]x2}x2 DAY 4, n = 4	
	[D-Serine], μM	Mean, J, μA.cm <sup>-2</sup>	± SEM, J, μA.cm <sup>-2</sup>	Mean, J, μA.cm <sup>-2</sup>	± SEM, J, μA.cm <sup>-2</sup>	Mean, J, μA.cm <sup>-2</sup>
0	0	0	0	0	0	0
40	1.224	0.158	0.895	0.142	0.393	0.087
50	1.540	0.194	1.362	0.134	0.505	0.118
60	2.162	0.163	1.338	0.288	0.653	0.154
100	3.526	0.258	2.161	0.377	1.069	0.249
500	13.650	1.648	6.656	1.231	7.455	0.901
1000	20.724	2.744	12.243	2.226	9.445	1.908
5000	30.996	2.652	25.088	2.635	17.563	2.381
10000	31.778	2.648	27.149	2.598	19.991	1.437
15000	32.053	2.564	27.983	2.433	20.836	1.440
Electrode Design	Pt <sub>C</sub> -{MMA-[600UPBSx5-GA1%]x2}x2-MMA DAY 0, n = 4		Pt <sub>C</sub> -{MMA-[600UPBSx5-GA1%]x2}x2-MMA DAY 1, n = 4		Pt <sub>C</sub> -{MMA-[600UPBSx5-GA1%]x2}x2-MMA DAY 4, n = 4	
	[D-Serine], μM	Mean, J, μA.cm <sup>-2</sup>	± SEM, J, μA.cm <sup>-2</sup>	Mean, J, μA.cm <sup>-2</sup>	± SEM, J, μA.cm <sup>-2</sup>	Mean, J, μA.cm <sup>-2</sup>
0	0	0	0	0	0	0
50	1.649	0.102	1.539	0.093	1.706	0.112
100	2.995	0.103	2.889	0.193	3.317	0.132
500	12.654	0.618	11.682	1.500	12.886	0.902
1000	21.932	0.620	26.313	2.608	22.782	1.418
5000	29.607	0.638	40.837	3.043	35.815	1.825
10000	31.625	0.697	42.387	3.692	41.805	2.483
15000	32.261	0.664	41.306	2.844	41.507	2.387

Table 11-5

The D-ser calibration data from for the general recipe Pt<sub>C</sub>-{MMA-[600UPBSx5-GA1%]x2}x2 and Pt<sub>C</sub>-{MMA-[600UPBSx5-GA1%]x2}x2-MMA over 4 days.

Electrode Design	Pt <sub>C</sub> n = 24		Electrode Design	Pt <sub>C</sub> n = 8	
[H <sub>2</sub> O <sub>2</sub> ], μM	Mean, J, μA.cm <sup>-2</sup>	± SEM, J, μA.cm <sup>-2</sup>	[AA], μM	Mean, J, μA.cm <sup>-2</sup>	± SEM, J, μA.cm <sup>-2</sup>
0	0	0	0	0	0
1	0.168	0.016	200	94.334	6.620
2	0.351	0.037	400	176.127	12.642
5	0.942	0.065	600	267.090	11.766
10	1.833	0.158	800	355.075	18.079
20	3.421	0.318	1000	437.895	30.164
50	8.352	0.702			
150	17.838	1.399			
200	32.751	2.984			
500	82.505	7.277			
1000	170.793	15.341			

Table 11-6

Calibration responses obtained for H<sub>2</sub>O<sub>2</sub> and AA on Pt<sub>C</sub>.

Polymerisation Method	PPD n = 16		PPD <sub>CV</sub> n = 4	
[AA], μM	Mean, J, μA.cm <sup>-2</sup>	± SEM, J, μA.cm <sup>-2</sup>	Mean, J, μA.cm <sup>-2</sup>	± SEM, J, μA.cm <sup>-2</sup>
0	0	0	0	0
200	0.156	0.013	0.042	0.018
400	0.212	0.016	0.070	0.036
600	0.235	0.019	0.096	0.053
800	0.245	0.019	0.122	0.070
1000	0.236	0.017	0.152	0.087

Table 11-7

Calibration responses obtained for AA on Pt<sub>C</sub>-PPD-[MMA-[600UPBSx5-GA1%]x2]x2-MMA and Pt<sub>C</sub>-PPD<sub>CV</sub>-[MMA-[600UPBSx5-GA1%]x2]x2-MMA.

Interference Layers	Naf-PPD n = 24		Naf-PPD <sub>CV</sub> n = 4	
[AA], μM	Mean, J, μA.cm <sup>-2</sup>	± SEM, J, μA.cm <sup>-2</sup>	Mean, J, μA.cm <sup>-2</sup>	± SEM, J, μA.cm <sup>-2</sup>
0	0	0	0	0
200	0.032	0.011	0.058	0.011
400	0.019	0.014	0.083	0.015
600	0.011	0.019	0.102	0.018
800	0.001	0.025	0.115	0.020
1000	-0.011	0.030	0.106	0.018

Table 11-8

Calibration responses obtained for AA on Pt<sub>C</sub>-Naf-PPD-[MMA-[600UPBSx5-GA1%]x2]x2-MMA and Pt<sub>C</sub>-Naf-PPD<sub>CV</sub>-[MMA-[600UPBSx5-GA1%]x2]x2-MMA.

Electrode Design	No interferent rejection layer n = 16		with Naf-PPD n = 52		with PPD n = 4		with PPD <sub>CV</sub> n = 4	
	Mean, J, $\mu\text{A.cm}^{-2}$	$\pm$ SEM, J, $\mu\text{A.cm}^{-2}$	Mean, J, $\mu\text{A.cm}^{-2}$	$\pm$ SEM, J, $\mu\text{A.cm}^{-2}$	Mean, J, $\mu\text{A.cm}^{-2}$	$\pm$ SEM, J, $\mu\text{A.cm}^{-2}$	Mean, J, $\mu\text{A.cm}^{-2}$	$\pm$ SEM, J, $\mu\text{A.cm}^{-2}$
<b>0</b>	0	0	0	0	0	0	0	0
<b>1</b>	0.062	0.006	0.018	0.002	0.047	0.008	0.043	0.002
<b>2</b>	0.125	0.009	0.032	0.003	0.097	0.016	0.099	0.006
<b>5</b>	0.233	0.013	0.052	0.004	0.217	0.037	0.221	0.020
<b>10</b>	0.409	0.020	0.085	0.007	0.407	0.074	0.453	0.047
<b>20</b>	0.707	0.040	0.154	0.015	0.728	0.130	1.049	0.133
<b>50</b>	1.628	0.113	0.490	0.032	1.447	0.229	1.901	0.151
<b>100</b>	3.126	0.247	1.040	0.071	2.775	0.451	4.191	0.463
<b>200</b>	9.518	0.751	2.136	0.161				
<b>500</b>	12.955	0.889	5.232	0.335	12.223	2.005	15.494	1.123
<b>1000</b>	21.422	1.429	9.275	0.582	21.515	3.439	25.408	1.580
<b>2000</b>	30.605	1.908	14.439	0.845				
<b>3000</b>	31.960	1.855	16.935	0.969				
<b>5000</b>	32.091	1.669	19.267	1.063	34.411	4.045	37.293	1.541
<b>10000</b>	33.812	1.520	21.750	1.140	39.643	5.848	38.955	1.473
<b>15000</b>	33.584	1.465	22.745	1.163	39.135	5.374	39.333	1.383

Table 11-9

The D-ser calibration data returned when calibrations were performed to elucidate the effect upon sensitivity of the interferent rejection layers.

Calibration	Cal 1, n = 8		Cal 2, n = 8		Cal 3, n = 8	
[D-Serine], $\mu\text{M}$	Mean, J, $\mu\text{A.cm}^{-2}$	$\pm$ SEM, J, $\mu\text{A.cm}^{-2}$	Mean, J, $\mu\text{A.cm}^{-2}$	$\pm$ SEM, J, $\mu\text{A.cm}^{-2}$	Mean, J, $\mu\text{A.cm}^{-2}$	$\pm$ SEM, J, $\mu\text{A.cm}^{-2}$
0	0	0	0	0	0	0
1	0.012	0.004	0.018	0.010	0.017	0.006
2	0.025	0.008	0.031	0.012	0.022	0.006
5	0.044	0.015	0.062	0.016	0.045	0.011
10	0.075	0.025	0.073	0.019	0.072	0.020
20	0.162	0.051	0.111	0.028	0.125	0.025
50	0.282	0.092	0.225	0.068	0.212	0.043
100	0.367	0.109	0.327	0.088	0.414	0.103
200	0.459	0.133	0.484	0.086	0.422	0.082
500	0.761	0.238	0.711	0.166	0.750	0.154
1000	1.659	0.664	1.416	0.337	1.414	0.298
2000	3.492	1.094	3.551	0.863	3.912	0.708
3000	6.610	1.811	6.612	1.414	5.120	0.933
5000	11.228	2.920	11.008	2.357	9.281	1.521
8000	13.456	3.168	12.978	2.386	10.955	1.817
10000	14.450	3.234	15.531	2.626	14.104	2.079
15000	17.069	3.123	18.547	2.288	15.669	2.319
Calibration	Cal 4, n =8		Cal 5, n = 8		Cal 6, n = 8	
[D-Serine], $\mu\text{M}$	Mean, J, $\mu\text{A.cm}^{-2}$	$\pm$ SEM, J, $\mu\text{A.cm}^{-2}$	Mean, J, $\mu\text{A.cm}^{-2}$	$\pm$ SEM, J, $\mu\text{A.cm}^{-2}$	Mean, J, $\mu\text{A.cm}^{-2}$	$\pm$ SEM, J, $\mu\text{A.cm}^{-2}$
0	0	0	0	0	0	0
1	0.012	0.003	0.008	0.003	0.000	0.005
2	0.015	0.003	0.016	0.004	-0.005	0.012
5	0.027	0.004	0.028	0.006	0.025	0.006
10	0.044	0.007	0.089	0.027	0.036	0.010
20	0.087	0.017	0.118	0.026	0.056	0.009
50	0.161	0.028	0.245	0.048	0.129	0.035
100	0.231	0.044	0.309	0.058	0.158	0.038
200	0.242	0.043	0.376	0.071	0.210	0.033
500	0.400	0.068	0.669	0.107	0.431	0.085
1000	1.406	0.317	0.940	0.175	0.820	0.174
2000	2.670	0.555	2.140	0.430	1.833	0.377
3000	3.788	0.595	4.935	0.839	4.157	0.812
5000	6.323	1.084	7.651	1.408	6.586	1.262
8000	8.267	1.454	9.039	1.686	7.859	1.450
10000	10.941	1.955	10.595	2.026	9.667	1.896
15000	12.516	1.899	12.467	2.228	10.919	2.196

Table 11-10

The D-ser calibration data from obtained when biosensors were calibrated 6 times over a 2 day period.

Calibration	Day 0, n = 4		Day 1, n = 4		Day 3, n = 4	
[D-Serine], $\mu\text{M}$	Mean, J, $\mu\text{A}\cdot\text{cm}^{-2}$	$\pm$ SEM, J, $\mu\text{A}\cdot\text{cm}^{-2}$	Mean, J, $\mu\text{A}\cdot\text{cm}^{-2}$	$\pm$ SEM, J, $\mu\text{A}\cdot\text{cm}^{-2}$	Mean, J, $\mu\text{A}\cdot\text{cm}^{-2}$	$\pm$ SEM, J, $\mu\text{A}\cdot\text{cm}^{-2}$
0	0	0	0	0	0	0
1	0.026	0.014	0.015	0.003	0.014	0.001
2	0.030	0.008	0.023	0.003	0.018	0.001
5	0.052	0.003	0.053	0.011	0.029	0.004
10	0.109	0.020	0.063	0.012	0.048	0.003
20	0.177	0.003	0.088	0.013	0.111	0.008
50	0.492	0.055	0.358	0.059	0.260	0.023
100	0.950	0.122	0.783	0.111	0.506	0.055
200	1.914	0.243	1.668	0.233	0.943	0.114
500	4.967	0.316	4.189	0.632	2.171	0.321
1000	8.641	1.112	7.279	1.174	5.006	0.908
2000	13.534	1.405	12.396	1.954	7.482	1.115
3000	15.481	1.997	14.130	1.987	9.897	1.526
5000	17.399	1.745	17.000	2.284	12.716	1.743
8000	18.238	1.548	18.092	2.309	15.710	2.017
10000	18.675	1.348	18.749	2.248	16.129	1.996
15000	18.702	1.510	19.728	2.151	18.141	2.401
Calibration	Day 7, n = 4		Day 21, n = 4		Day 28, n = 4	
[D-Serine], $\mu\text{M}$	Mean, J, $\mu\text{A}\cdot\text{cm}^{-2}$	$\pm$ SEM, J, $\mu\text{A}\cdot\text{cm}^{-2}$	Mean, J, $\mu\text{A}\cdot\text{cm}^{-2}$	$\pm$ SEM, J, $\mu\text{A}\cdot\text{cm}^{-2}$	Mean, J, $\mu\text{A}\cdot\text{cm}^{-2}$	$\pm$ SEM, J, $\mu\text{A}\cdot\text{cm}^{-2}$
0	0	0	0	0	0	0
1	-0.007	0.005	0.014	0.002	0.002	0.001
2	0.002	0.008	0.010	0.001	0.009	0.001
5	0.009	0.007	0.015	0.000	0.016	0.004
10	0.017	0.008	0.037	0.004	0.039	0.011
20	0.036	0.010	0.067	0.005	0.078	0.025
50	0.283	0.040	0.158	0.014	0.157	0.023
100	0.489	0.059	0.260	0.037	0.291	0.040
200	0.999	0.132	0.679	0.020	0.578	0.061
500	2.202	0.254	1.529	0.070	1.236	0.124
1000	4.614	0.517	3.198	0.319	2.239	0.210
2000	7.710	0.871	5.619	0.730	4.227	0.462
3000	10.156	1.116	6.773	0.748	5.325	0.530
5000	13.048	1.439	9.771	0.592	8.812	1.200
8000	15.284	1.631	11.742	0.707	9.917	0.799
10000	16.835	1.579	12.078	0.793	11.351	0.504
15000	17.980	1.687	13.954	0.646	12.195	0.736

Table 11-11

The D-ser calibration data from obtained when biosensors were calibrated repeatedly over an extended period of time.

Calibration	Day 0, n = 8		Day 21, n = 4		Day 28, n = 4	
	Mean, J, $\mu\text{A}\cdot\text{cm}^{-2}$	$\pm$ SEM, J, $\mu\text{A}\cdot\text{cm}^{-2}$	Mean, J, $\mu\text{A}\cdot\text{cm}^{-2}$	$\pm$ SEM, J, $\mu\text{A}\cdot\text{cm}^{-2}$	Mean, J, $\mu\text{A}\cdot\text{cm}^{-2}$	$\pm$ SEM, J, $\mu\text{A}\cdot\text{cm}^{-2}$
<b>0</b>	0	0	0	0	0	0
<b>1</b>	0.026	0.014	0.015	0.003	0.014	0.001
<b>2</b>	0.030	0.008	0.023	0.003	0.018	0.001
<b>5</b>	0.052	0.003	0.053	0.011	0.029	0.004
<b>10</b>	0.109	0.020	0.063	0.012	0.048	0.003
<b>20</b>	0.177	0.003	0.088	0.013	0.111	0.008
<b>50</b>	0.492	0.055	0.358	0.059	0.260	0.023
<b>100</b>	0.950	0.122	0.783	0.111	0.506	0.055
<b>200</b>	1.914	0.243	1.668	0.233	0.943	0.114
<b>500</b>	4.967	0.316	4.189	0.632	2.171	0.321
<b>1000</b>	8.641	1.112	7.279	1.174	5.006	0.908
<b>2000</b>	13.534	1.405	12.396	1.954	7.482	1.115
<b>3000</b>	15.481	1.997	14.130	1.987	9.897	1.526
<b>5000</b>	17.399	1.745	17.000	2.284	12.716	1.743
<b>8000</b>	18.238	1.548	18.092	2.309	15.710	2.017
<b>10000</b>	18.675	1.348	18.749	2.248	16.129	1.996
<b>15000</b>	18.702	1.510	19.728	2.151	18.141	2.401

Table 11-12

The D-ser calibration data from obtained when biosensors were calibrated once after an extended period of time in storage.

Calibration	Day 0, n = 4		Day 1, n = 4		Day 3, n = 4	
[D-Serine], $\mu\text{M}$	Mean, J, $\mu\text{A}\cdot\text{cm}^{-2}$	$\pm$ SEM, J, $\mu\text{A}\cdot\text{cm}^{-2}$	Mean, J, $\mu\text{A}\cdot\text{cm}^{-2}$	$\pm$ SEM, J, $\mu\text{A}\cdot\text{cm}^{-2}$	Mean, J, $\mu\text{A}\cdot\text{cm}^{-2}$	$\pm$ SEM, J, $\mu\text{A}\cdot\text{cm}^{-2}$
0	0	0	0	0	0	0
1	0.021	0.012	0.004	0.001	0.014	0.013
2	0.035	0.010	0.007	0.002	0.003	0.001
5	0.043	0.012	0.016	0.004	0.005	0.003
10	0.055	0.017	0.032	0.008	0.012	0.005
20	0.101	0.068	0.067	0.012	0.013	0.004
50	0.387	0.137	0.149	0.030	0.071	0.013
100	0.837	0.254	0.305	0.057	0.213	0.049
200	1.832	0.566	0.632	0.121	0.468	0.121
500	4.652	1.207	1.548	0.326	1.090	0.189
1000	8.464	2.439	2.829	0.612	1.933	0.387
2000	13.532	3.922	5.350	1.266	4.623	0.829
3000	16.471	4.892	7.356	1.725	5.329	0.652
5000	18.220	5.472	9.799	2.548	7.074	1.237
8000	21.559	6.284	12.001	3.039	8.903	1.921
10000	20.846	5.940	12.591	3.195	10.879	2.056
15000	21.765	6.117	14.509	3.765	12.770	2.272
Calibration	Day 7, n = 4		Day 10, n = 4		Day 14, n = 4	
[D-Serine], $\mu\text{M}$	Mean, J, $\mu\text{A}\cdot\text{cm}^{-2}$	$\pm$ SEM, J, $\mu\text{A}\cdot\text{cm}^{-2}$	Mean, J, $\mu\text{A}\cdot\text{cm}^{-2}$	$\pm$ SEM, J, $\mu\text{A}\cdot\text{cm}^{-2}$	Mean, J, $\mu\text{A}\cdot\text{cm}^{-2}$	$\pm$ SEM, J, $\mu\text{A}\cdot\text{cm}^{-2}$
0	0	0	0	0	0	0
1	0.007	0.004	-0.006	0.001	-0.003	0.001
2	0.009	0.003	-0.001	0.001	-0.008	0.002
5	0.030	0.012	0.004	0.001	-0.010	0.003
10	0.049	0.024	0.007	0.002	-0.005	0.004
20	0.032	0.004	0.018	0.003	0.003	0.004
50	0.048	0.007	0.049	0.007	0.028	0.007
100	0.116	0.015	0.100	0.015	0.069	0.010
200	0.241	0.030	0.197	0.030	0.172	0.024
500	0.568	0.096	0.467	0.071	0.407	0.068
1000	1.101	0.194	0.907	0.126	0.661	0.104
2000	2.005	0.320	1.541	0.236	1.198	0.205
3000	3.024	0.463	2.006	0.357	1.819	0.330
5000	3.920	0.758	4.088	1.145	2.754	0.265
8000	5.168	1.019	5.212	1.140	3.341	0.417
10000	5.913	1.251	4.460	1.070	3.796	0.544
15000	7.211	1.566	5.127	1.191	4.519	0.784

Table 11-13

The D-ser calibration data from obtained when biosensors were calibrated repeatedly, over a two week period, and were stored in BSA 1% between calibrations.

Calibration	Day 0, n = 4		Day 1, n = 4		Day 3, n = 4	
[D-Serine], $\mu\text{M}$	Mean, J, $\mu\text{A}\cdot\text{cm}^{-2}$	$\pm$ SEM, J, $\mu\text{A}\cdot\text{cm}^{-2}$	Mean, J, $\mu\text{A}\cdot\text{cm}^{-2}$	$\pm$ SEM, J, $\mu\text{A}\cdot\text{cm}^{-2}$	Mean, J, $\mu\text{A}\cdot\text{cm}^{-2}$	$\pm$ SEM, J, $\mu\text{A}\cdot\text{cm}^{-2}$
0	0	0	0	0	0	0
1	0.009	0.019	0.005	0.002	0.000	0.001
2	0.021	0.041	0.019	0.003	0.002	0.001
5	0.037	0.042	0.028	0.005	0.011	0.003
10	0.060	0.044	0.074	0.009	0.029	0.006
20	0.110	0.037	0.118	0.017	0.062	0.011
50	0.449	0.033	0.326	0.031	0.182	0.030
100	1.084	0.059	0.689	0.058	0.325	0.052
200	2.483	0.106	1.285	0.107	0.706	0.121
500	6.240	0.463	2.861	0.233	1.714	0.304
1000	11.263	0.493	5.529	0.455	3.553	0.402
2000	17.131	1.243	8.700	0.578	5.612	0.880
3000	20.445	1.710	11.442	0.513	7.490	1.285
5000	24.188	2.133	14.075	0.365	10.449	1.482
8000	27.342	1.914	16.215	0.463	12.212	1.766
10000	28.271	1.990	17.869	0.581	13.762	1.455
15000	28.731	2.037	18.808	0.823	15.252	1.563
Calibration	Day 7, n = 4		Day 10, n = 4		Day 14, n = 4	
[D-Serine], $\mu\text{M}$	Mean, J, $\mu\text{A}\cdot\text{cm}^{-2}$	$\pm$ SEM, J, $\mu\text{A}\cdot\text{cm}^{-2}$	Mean, J, $\mu\text{A}\cdot\text{cm}^{-2}$	$\pm$ SEM, J, $\mu\text{A}\cdot\text{cm}^{-2}$	Mean, J, $\mu\text{A}\cdot\text{cm}^{-2}$	$\pm$ SEM, J, $\mu\text{A}\cdot\text{cm}^{-2}$
0	0	0	0	0	0	0
1	0.005	0.001	0.005	0.002	0.005	0.000
2	0.001	0.002	0.006	0.002	0.008	0.003
5	-0.003	0.017	0.007	0.001	0.015	0.008
10	-0.002	0.017	0.026	0.007	0.030	0.015
20	0.042	0.023	0.042	0.010	-0.006	0.028
50	0.108	0.026	0.098	0.022	0.042	0.022
100	0.237	0.044	0.184	0.038	0.133	0.027
200	0.496	0.084	0.373	0.077	0.250	0.039
500	1.209	0.200	0.801	0.148	0.585	0.101
1000	2.238	0.382	1.697	0.372	1.108	0.208
2000	5.035	0.459	3.384	0.804	2.226	0.486
3000	5.648	0.542	4.007	0.862	3.587	0.833
5000	7.727	1.129	5.221	0.976	4.369	1.220
8000	10.164	1.377	7.604	1.362	5.931	1.194
10000	10.362	1.296	7.159	1.153	6.637	1.327
15000	11.120	1.005	7.869	1.182	7.509	1.354

Table 11-14

The D-ser calibration data from obtained when biosensors were calibrated repeatedly, over a two week period, and were stored in 10% BSA between calibrations.

Calibration	Day 0, n = 4		Day 1, n = 4		Day 3, n = 4	
	Mean, J, $\mu\text{A}\cdot\text{cm}^{-2}$	$\pm$ SEM, J, $\mu\text{A}\cdot\text{cm}^{-2}$	Mean, J, $\mu\text{A}\cdot\text{cm}^{-2}$	$\pm$ SEM, J, $\mu\text{A}\cdot\text{cm}^{-2}$	Mean, J, $\mu\text{A}\cdot\text{cm}^{-2}$	$\pm$ SEM, J, $\mu\text{A}\cdot\text{cm}^{-2}$
0	0	0	0	0	0	0
1	0.014	0.003	0.016	0.011	-0.003	0.001
2	0.028	0.005	0.027	0.014	-0.001	0.004
5	0.045	0.009	0.052	0.024	-0.016	0.006
10	0.096	0.023	0.071	0.023	0.003	0.009
20	0.186	0.040	0.135	0.040	0.008	0.009
50	0.621	0.140	0.347	0.082	0.093	0.035
100	1.244	0.291	0.658	0.142	0.236	0.064
200	2.677	0.623	1.211	0.282	0.603	0.149
500	6.062	1.401	2.850	0.662	1.487	0.401
1000	11.646	2.855	5.865	1.035	3.443	1.353
2000	18.152	3.924	10.329	1.704	5.164	1.581
3000	21.303	4.199	13.536	2.608	6.785	1.684
5000	23.091	4.296	16.984	3.552	8.896	2.461
8000	24.309	4.379	19.638	3.930	10.818	2.729
10000	24.999	4.307	20.162	3.927	12.035	2.928
15000	25.632	4.332	21.635	4.086	13.274	3.304
Calibration	Day 7, n = 4		Day 10, n = 4		Day 14, n = 4	
	Mean, J, $\mu\text{A}\cdot\text{cm}^{-2}$	$\pm$ SEM, J, $\mu\text{A}\cdot\text{cm}^{-2}$	Mean, J, $\mu\text{A}\cdot\text{cm}^{-2}$	$\pm$ SEM, J, $\mu\text{A}\cdot\text{cm}^{-2}$	Mean, J, $\mu\text{A}\cdot\text{cm}^{-2}$	$\pm$ SEM, J, $\mu\text{A}\cdot\text{cm}^{-2}$
0	0	0	0	0	0	0
1	-0.002	0.002	-0.010	0.010	0.014	0.015
2	-0.002	0.001	-0.007	0.010	0.019	0.029
5	-0.001	0.003	0.027	0.028	0.021	0.034
10	0.002	0.003	0.001	0.010	0.017	0.032
20	0.019	0.007	-0.002	0.013	0.018	0.034
50	0.056	0.015	0.017	0.011	0.021	0.033
100	0.104	0.029	0.047	0.013	0.020	0.006
200	0.258	0.059	0.112	0.025	0.062	0.005
500	0.641	0.144	0.342	0.098	0.185	0.025
1000	1.234	0.268	0.682	0.169	0.404	0.048
2000	2.234	0.460	1.208	0.285	0.802	0.109
3000	3.598	1.044	1.575	0.367	1.014	0.168
5000	4.259	0.878	2.123	0.462	1.689	0.223
8000	5.418	1.132	2.670	0.529	2.070	0.363
10000	6.141	1.286	2.869	0.637	2.775	0.339
15000	7.313	1.573	3.460	0.767	2.657	0.527

Table 11-15

The D-ser calibration data obtained when biosensors were calibrated repeatedly, over a two week period, and were stored in PEA 1% between calibrations.

Calibration	Day 0, n = 4		Day 1, n = 4		Day 3, n = 4	
[D-Serine], $\mu\text{M}$	Mean, J, $\mu\text{A}\cdot\text{cm}^{-2}$	$\pm$ SEM, J, $\mu\text{A}\cdot\text{cm}^{-2}$	Mean, J, $\mu\text{A}\cdot\text{cm}^{-2}$	$\pm$ SEM, J, $\mu\text{A}\cdot\text{cm}^{-2}$	Mean, J, $\mu\text{A}\cdot\text{cm}^{-2}$	$\pm$ SEM, J, $\mu\text{A}\cdot\text{cm}^{-2}$
0	0	0	0	0	0	0
1	0.016	0.002	-0.003	0.002	-0.003	0.003
2	0.038	0.006	0.012	0.009	-0.003	0.006
5	0.069	0.010	0.022	0.010	0.004	0.013
10	0.096	0.014	0.058	0.024	0.019	0.022
20	0.177	0.013	0.077	0.021	0.047	0.023
50	0.439	0.046	0.070	0.023	0.097	0.025
100	0.629	0.063	0.136	0.033	0.092	0.028
200	0.782	0.076	0.192	0.030	0.145	0.014
500	1.293	0.109	0.160	0.023	0.251	0.014
1000	2.383	0.211	0.958	0.123	0.580	0.064
2000	5.832	0.531	2.596	0.204	1.240	0.102
3000	10.516	0.800	4.356	0.389	2.846	0.385
5000	18.541	1.750	9.459	0.772	6.415	1.947
8000	21.506	2.315	9.971	1.076	6.261	0.841
10000	26.265	2.689	12.683	0.807	8.840	1.168
15000	29.297	2.783	14.390	1.080	10.918	1.370
Calibration	Day 7, n = 4		Day 10, n = 4		Day 14, n = 4	
[D-Serine], $\mu\text{M}$	Mean, J, $\mu\text{A}\cdot\text{cm}^{-2}$	$\pm$ SEM, J, $\mu\text{A}\cdot\text{cm}^{-2}$	Mean, J, $\mu\text{A}\cdot\text{cm}^{-2}$	$\pm$ SEM, J, $\mu\text{A}\cdot\text{cm}^{-2}$	Mean, J, $\mu\text{A}\cdot\text{cm}^{-2}$	$\pm$ SEM, J, $\mu\text{A}\cdot\text{cm}^{-2}$
0	0	0	0	0	0	0
1	0.012	0.005	-0.003	0.002	-0.006	0.001
2	0.007	0.002	0.002	0.012	-0.026	0.024
5	0.007	0.001	0.003	0.012	-0.020	0.012
10	0.011	0.002	0.005	0.011	-0.018	0.009
20	0.023	0.002	0.004	0.013	-0.019	0.005
50	0.031	0.008	0.010	0.016	-0.018	0.005
100	0.038	0.009	0.003	0.017	-0.013	0.002
200	0.043	0.008	0.004	0.016	-0.012	0.003
500	0.084	0.009	0.010	0.005	0.006	0.012
1000	0.146	0.025	0.043	0.006	0.028	0.014
2000	0.230	0.042	0.157	0.031	0.076	0.016
3000	0.568	0.101	0.301	0.063	0.127	0.005
5000	1.063	0.197	0.592	0.126	0.246	0.045
8000	1.439	0.247	0.839	0.174	0.291	0.043
10000	2.299	0.412	1.284	0.296	0.458	0.068
15000	3.272	0.566	1.928	0.511	0.719	0.090

Table 11-16

The D-ser calibration data obtained when biosensors were calibrated repeatedly, over a two week period, and were stored in PEA 10% between calibrations.

Cal	Day 0, n = 4		Day 1, n = 4		Day 3, n = 4		Day 7, n = 4		Day 14, n = 4	
	Mean, J, $\mu\text{A}\cdot\text{cm}^{-2}$	$\pm$ SEM, J, $\mu\text{A}\cdot\text{cm}^{-2}$								
<b>0</b>	0	0	0	0	0	0	0	0	0	0
<b>1</b>	0.008	0.003	-0.003	0.002	0.004	0.004	0.001	0.002	0.002	0.001
<b>2</b>	0.038	0.010	0.003	0.002	-0.001	0.001	-0.004	0.001	0.003	0.000
<b>5</b>	0.072	0.011	0.015	0.009	0.005	0.001	0.025	0.011	0.006	0.001
<b>10</b>	0.079	0.013	0.024	0.008	0.012	0.002	0.005	0.004	0.013	0.003
<b>20</b>	0.026	0.026	0.022	0.007	0.045	0.018	0.011	0.003	0.026	0.006
<b>50</b>	0.365	0.024	0.115	0.018	0.080	0.013	0.060	0.002	0.061	0.016
<b>100</b>	0.802	0.035	0.291	0.032	0.168	0.017	0.144	0.027	0.111	0.030
<b>200</b>	1.747	0.031	0.612	0.073	0.356	0.025	0.426	0.056	0.207	0.056
<b>500</b>	4.429	0.144	1.526	0.123	0.854	0.065	0.883	0.123	0.317	0.092
<b>1000</b>	7.919	0.167	3.390	0.519	1.615	0.131	1.510	0.217	0.744	0.192
<b>2000</b>	10.854	0.553	4.630	0.296	2.817	0.180	2.403	0.348	1.233	0.311
<b>3000</b>	12.132	0.677	5.515	0.558	4.618	0.604	3.998	0.471	1.590	0.339
<b>5000</b>	13.524	0.890	6.049	0.815	5.704	0.966	3.511	0.252	2.285	0.341
<b>8000</b>	14.229	0.958	7.160	0.965	6.415	0.939	4.275	0.156	2.673	0.298
<b>10000</b>	14.298	0.865	7.734	0.914	6.530	0.967	4.497	0.193	2.545	0.294
<b>15000</b>	14.140	0.813	8.481	0.959	6.581	1.056	5.252	0.222	2.889	0.288

Table 11-17

The D-ser calibration data obtained when biosensors were calibrated repeatedly, over a two week period, and were stored in brain tissue between calibrations.

Calibration	pre pH 8.0 n = 4		pH 8.0 n = 4		pre pH 6.5 n = 4		pH 6.5 n = 4	
	Mean, J, $\mu\text{A}\cdot\text{cm}^{-2}$	$\pm$ SEM, J, $\mu\text{A}\cdot\text{cm}^{-2}$						
<b>0</b>	0	0	0	0	0	0	0	0
<b>1</b>	0.029	0.006	0.007	0.005	0.019	0.011	0.014	0.010
<b>2</b>	0.051	0.008	0.023	0.010	0.017	0.004	0.016	0.010
<b>5</b>	0.044	0.009	0.034	0.012	0.033	0.008	0.022	0.012
<b>10</b>	0.066	0.013	0.044	0.014	0.059	0.012	0.028	0.012
<b>20</b>	0.307	0.087	0.083	0.022	0.083	0.018	0.042	0.013
<b>40</b>	0.474	0.097	0.129	0.034	0.304	0.077	0.039	0.015
<b>50</b>	0.786	0.154	0.968	0.152	0.450	0.100	0.084	0.020
<b>60</b>	1.082	0.199	1.068	0.161	0.469	0.109	0.088	0.019
<b>100</b>	1.934	0.393	1.964	0.243	0.882	0.196	0.117	0.021
<b>200</b>	3.927	0.867	4.651	0.802	1.447	0.282	0.200	0.025
<b>500</b>	9.065	1.764	8.473	1.545	4.185	1.148	0.468	0.065
<b>1000</b>	15.342	2.547	15.815	2.340	4.105	0.490	1.015	0.131
<b>2000</b>	21.224	2.654	25.057	2.958	6.635	0.765	1.954	0.260
<b>3000</b>	24.160	2.884	27.633	2.792	8.584	0.828	3.834	0.680
<b>5000</b>	25.316	2.910	31.568	2.881	10.335	0.850	4.878	1.064
<b>8000</b>	26.968	2.774	31.071	2.915	11.754	0.910	8.193	2.080
<b>10000</b>	27.923	2.704	32.855	2.944	11.712	0.966	8.497	2.097
<b>15000</b>	28.088	2.747	30.681	3.175	14.421	1.624	9.758	2.182

Table 11-18

The D-ser calibration data returned when calibrations were performed to elucidate the effect of pH changes on the sensitivity of the biosensor.

Calibration	pre 37 °C, n = 4		37 °C, n = 4		post 37 °C, n = 4	
D-Serine, $\mu\text{M}$	Mean, J, $\mu\text{A}\cdot\text{cm}^{-2}$	$\pm$ SEM, J, $\mu\text{A}\cdot\text{cm}^{-2}$	Mean, J, $\mu\text{A}\cdot\text{cm}^{-2}$	$\pm$ SEM, J, $\mu\text{A}\cdot\text{cm}^{-2}$	Mean, J, $\mu\text{A}\cdot\text{cm}^{-2}$	$\pm$ SEM, J, $\mu\text{A}\cdot\text{cm}^{-2}$
<b>0</b>	0	0	0	0	0	0
<b>1</b>	0.014	0.007	0.031	0.003	0.019	0.015
<b>2</b>	0.031	0.005	0.040	0.004	0.023	0.009
<b>5</b>	0.056	0.007	0.068	0.014	0.031	0.008
<b>10</b>	0.091	0.012	0.092	0.017	0.070	0.022
<b>20</b>	0.141	0.022	0.168	0.009	0.060	0.021
<b>40</b>	0.201	0.016	0.340	0.017	0.117	0.037
<b>50</b>	0.253	0.041	0.432	0.030	0.143	0.038
<b>60</b>	0.332	0.050	0.515	0.041	0.145	0.040
<b>100</b>	0.531	0.058	0.930	0.150	0.313	0.061
<b>200</b>	1.085	0.077	1.922	0.194	0.602	0.067
<b>500</b>	2.574	0.187	5.046	0.592	1.429	0.118
<b>1000</b>	5.842	0.412	7.074	0.718	3.785	0.354
<b>2000</b>	9.094	0.804	10.549	0.958	4.940	0.409
<b>3000</b>	10.682	1.240	12.660	1.134	6.063	0.400
<b>5000</b>	13.764	2.223	15.364	1.691	8.082	0.467
<b>8000</b>	15.471	2.771	16.280	1.873	8.998	0.439
<b>10000</b>	17.709	3.759	17.672	2.084	9.150	0.499
<b>15000</b>	17.923	4.192	18.319	2.362	9.878	0.453

Table 11-19

The D-ser calibration data for calibrations which were performed at room temperature and 37 °C.

Calibration [substrate], $\mu\text{M}$	pre D-alanine, n = 4		D-alanine, n = 4		post D-alanine, n = 4	
	Mean, J, $\mu\text{A}\cdot\text{cm}^{-2}$	$\pm$ SEM, J, $\mu\text{A}\cdot\text{cm}^{-2}$	Mean, J, $\mu\text{A}\cdot\text{cm}^{-2}$	$\pm$ SEM, J, $\mu\text{A}\cdot\text{cm}^{-2}$	Mean, J, $\mu\text{A}\cdot\text{cm}^{-2}$	$\pm$ SEM, J, $\mu\text{A}\cdot\text{cm}^{-2}$
0	0	0	0	0	0	0
1	0.015	0.005	0.047	0.008	0.007	0.003
2	0.024	0.006	0.079	0.020	0.013	0.003
5	0.034	0.005	0.154	0.021	0.028	0.004
10	0.040	0.007	0.164	0.019	0.050	0.007
20	0.059	0.009	0.325	0.026	0.113	0.011
40	0.107	0.019	0.599	0.068	0.249	0.032
50	0.222	0.034	0.742	0.047	0.317	0.032
60	0.294	0.042	0.912	0.048	0.333	0.029
100	0.571	0.060	1.504	0.094	0.592	0.062
200	1.152	0.125	2.862	0.207	1.132	0.106
500	2.911	0.260	6.025	0.548	2.785	0.279
1000	5.899	0.708	9.512	1.119	6.108	0.692
2000	9.085	0.760	13.381	1.446	8.811	0.608
3000	10.726	0.880	15.198	1.766	9.509	0.299
5000	11.719	1.202	16.234	1.877	10.840	0.568
8000	12.505	1.107	15.860	1.704	11.988	0.796
10000	12.606	1.070	16.867	2.013	12.385	0.893
15000	13.332	1.241	17.221	2.064	12.713	0.926

Table 11-20

The calibration data for a D-ala calibration, and a pre and post D-ser calibration.

Substrate	J, $\mu\text{A}\cdot\text{cm}^{-2}$ , n = 8		Substrate Concentration, $\mu\text{M}$
	Mean	$\pm$ SEM	
AA	0.048	0.028	500
HVA	0.005	0.009	10
L-gluta	-0.007	0.004	50
L-cys	0.004	0.007	50
UA	-0.009	0.001	50
L-trp	-0.010	0.002	100
DHAA	-0.021	0.009	100
L-tyr	-0.010	0.003	100
DA	-0.006	0.003	0.5
5-HIAA	0.001	0.007	50
DOPAC	-0.008	0.005	20
5-HT	0.001	0.006	0.01
Overall	0.014	0.027	> 1000

Table 11-21

Calibration data for electroactive species found in the ECF.